XLVI OSI SYMPOSIUM

INTERNATIONAL CONFERENCE ON OPTICS, PHOTONICS & QUANTUM INFORMATION

OPTIQ-2023

DECEMBER 11-13, 2023

ABSTRACTS

Organized by,

International School of Photonics
Cochin University of Science and Technology
Kerala 682 022

PREFACE

Physics encompasses a multitude of fascinating branches. Optics and photonics stand out as a particularly captivating domain, unveiling the secrets of light and its behaviour.

The Optical Society of India (OSI) was founded in the year 1965. This organisation born from the passion of a few, blossomed into a vibrant group testament to the enduring power of shared purpose and steadfast dedication. The society always take deliberate efforts to promote and diffuse knowledge in the field of optics and photonics. For achieving this goal, OSI encourages to conduct research activities in pure and applied optics and also promotes coordination between designers, manufacturers and users of optical technology. Moreover, OSI publishes books, journals, reports and transactions relating to the field of optics. OSI has been hosting annual national /international symposia for the last four decades.

International School of Photonics, Cochin University of Science and Technology is privileged to host the XLVI OSI Annual Symposium- International Conference on Optics, Photonics & Quantum Information (OPTIQ-2023) from December 11 – 13, 2023 in God's own country. Cochin University, cradled by the serene shores of the Arabian Sea stands as a beacon of scientific and technological excellence in our nation. International School of Photonics has garnered a distinguished reputation in the field of applied optics and photonics research recognised for its significant contributions.

Prominent figures from optics community across the globe will deliver illuminating talks on diverse aspects of photonics and quantum information with their expertise in respective disciplines. Emerging researchers will present their promising research findings through insightful oral and poster presentations.

CONTENTS

OPTIQ-2023 Committee 1
Session Plan 5
Plenary Talk 9
Invited Talk 15
Contributory Papers 55
Category 01 : Artificial-Intelligence and Machine-Learning in Photonics (AMP) 56
Category 02 : Biophotonics & Medical Optics (BPM) 61
Category 03 : Diffractive, Free-form and Adaptive Optics (DFA) 66
Category 04 : Fiber Optic Devices, Sensors and Instrumentation (FIB) 70
Category 05 : Guided Wave and Nonlinear Optics (GNO) 101
Category 06 : Green Photonics (GPH) 110
Category 07 : Integrated Optic Circuits and Devices (IOC) 113
Category 08 : Imaging and Super-resolution (ISR 114
Category 09 : Lasers Applications & Beam Optics (LSB 120
Category 10 : Microwave and THz Photonics (MWT 130
Category 11 : Nano-photonics & Plasmonics (NPH) 132
Category 12 : Optical Data Storage & Display Devices (DSD) 154
Category 13 : Optical Interferometry and Holography (HOL) 155
Category 14 : Optical Instrumentation, Fabrication and Metrology (IFM) 177
Category 15 : Optical Materials (MAT) 190
Category 16 : Optical System Design (DES) 205
Category 17 : Optical Sources and Illumination Engineering (SIE) 213
Category 18 : Optoelectronic Devices (OED) 218
Category 19 : Photonic Crystals & Metamaterials (PHC) 227
Category 20 : Photonic Networks, Switching Interconnects & Access (NET) 237
Category 21 : Quantum Information (QI) 239
Category 22 : Quantum Optical Technologies (QOT) 243
Category 23 : Singular Optics & Laser Speckles (SIN) 264
Category 24 : Theory, Modelling & Simulation (THM) 279
Category 25 : Ultrafast Optics (UFO) 290
Category 26 : Any other topics related to Optics and Photonics (OTH) 293
Theses 303

OPTIQ - 2023 COMMITTEE

PATRONS

Prof. C S Narayanamurthy, President, Optical Society of India (OSI)

Prof. (Dr.) P G Sankaran, Vice Chancellor, Cochin University of Science and Technology (CUSAT)

Dr. Ajith Kumar K, Director, Naval Physical and Oceanographic Laboratory (NPOL)

CORE COMMITTEE

Chair	Pramod Gopinath, CUSAT
Co-Chair	M Kailasnath, CUSAT T. Santhanakrishnan, NPOL
Convenor	Saji K J, CUSAT
Co-Convenor	Priya Rose T, CUSAT Mohamed Ameen P, CUSAT R Rajesh, NPOL

NATIONAL ADVISORY COMMITTEE

Achanta Venu Gopal, CSIR – NPL, India

Ajay Kumar, IRDE, Dehradun, India

Ajoy K Ghatak, NASI Allahabad, India

Alika Khare, IIT Guwahati, India

Anurag Sharma, IIT Delhi, India

B D Gupta, IIT Delhi, India

Bishnu P Pal, Mahindra École Central, India

Balpreet Singh Ahluwalia, UiT, The Arctic University of Norway

Carmen Menoni, Colorado State University, USA

Chennupati Jagadish, Australian National University, Australia

C P Girijavallabhan, CUSAT, India

C Vijayan, IIT Madras, India

Dag Hanstorp, University of Gothenburg, Sweden

D Narayana Rao, University of Hyderabad, India

Enakshi Sharma, University of Delhi South Campus, India

G Ravindra Kumar, TIFR Mumbai, India

Govind P Agrawal, University of Rochester

Hitesh Mehta, Fiber Optica, India

Jagannath Nayak, DRDO-CHESS, Hyderabad, India

James C Wyant, University of Arizona, USA

Joby Joseph, IIT Delhi, India

Kallol Bhattacharya, University of Calcutta, India

Kehar Singh, IIT Delhi, India

K R Suresh Nair, Amara Raja Design Alpha Pvt Ltd, India

K V Sriram, LEOS Bengaluru, India

L N Hazra, University of Calcutta, Kolkata, India

M Senthil Kumar, Space Application Centre, Ahmedabad, India

M R Shenoy, IIT Delhi, India

Murukeshan Vadakke Matham, NTU Singapore

N V Unnikrishnan, Mahatma Gandhi University, India

Pierre Chavel, CNRS Institut d Optique, France

P Radhakrishnan, CUSAT, India

Prasad A Naik, BITS Pilani, India

Prem Kumar, Northwestern University, USA

Rajpal S Sirohi, Alabama University, USA

Ramanand Tewari, One Silicon Chip Photonics, Canada

Ranjan Sen, CGCRI Kolkata, India

Ranjan Singh, Nanyang Technological University, Singapore

Renaud Bachelot, University of Troyes, France

R K Shevgaonkar, IIT Bombay, India

R K Thareja, IIT Kanpur, India

R K Varshney, IIT Delhi India

Rupamanjari Ghosh, Shiv Nadar University, India

R Vijaya, IIT Kanpur, India

S Anantha Ramakrishna, CSIR-CSIO, India

S Dutta Gupta, TIFR Hyderabad, India

S K Bhadra, IACS Kolkata, India

Sushil Mujumdar, TIFR Mumbai, India

T Srinivas, IISc Bangalore, India

V M Nandakumaran, CUSAT, India

V N Mahajan, University of Arizona, USA

V P N Nampoori, CUSAT, India

V Unnikrishnan Nayar, University of Kerala, India

Vipul Rastogi, IIT Roorkee, India

Wolfgang Freude, KIT, Germany

TECHNICAL PROGRAM COMMITTEE

A R Ganeshan, IIT Madras, India
Akhilesh Kumar Mishra, IIT Roorkee, India
Amarendra K Sarma, IIT Guwahati, India
Amit Rai, Jawaharlal Nehru University New Delhi, India
Amol Choudhary, IIT Delhi, India
Anchal Srivastava, University of Lucknow, India
Anil Prabhakar, IIT Madras, India
Arijit Sharma, IIT Tirupati, India
Ankur Gupta, IIT Jodhpur, India
Anoop K K, CUSAT, India
Arti Agrawal, University of Technology Sydney, Australia
Arup Lal Chakraborty, IIT Gandhinagar, India
Asima Pradhan, IIT Kanpur, India
Ayan Banerjee, IISER-Kolkata, India
Balaji Srinivasan, IIT Madras, India
Bhargab Das, CSIR-CSIO, India
Bijoy Krishna Das, IIT Madras, India
Biswanath Chakraborty, IIT Jammu, India
Bodhaditya Santra, IIT Delhi, India
C K Jayasankar, Sri Venkateshwara University, India
Dalip S Mehta, IIT Delhi, India
Debabrata Goswami, IIT Kanpur, India
Deepa Venkitesh, IIT Madras, India
Dibakar Roy Chowdhury, Mahindra Ecole Centrale Hyderabad, India
Dinesh N Naik, IIST, India
G Vijaya Prakash, IIT Delhi, India
G V Pavan Kumar, IISER Pune, India
Goutam K Samanta, PRL Ahemdabad, India
Harshwardhan Wanare, IIT Kanpur, India
Jasleen Lugani, IIT Delhi, India
Jolly Xavier P, IIT Delhi, India
Joseph John, IIT Bombay, India
K Nithyanandan, IIT Hyderabad, India
Kamal P Singh, IISER Mohali, India
Kedar B Khare, IIT Delhi, India
Maruthi Manoj Brundavanam, IIT Kharagpur, India
Mukesh Jewariya, CSIR-NPL, India
Naveen K Nischal, IIT Patna, India
Nimish Dixit, IRDE Dehradun, India
P Nandakumar, BITS Pilani, Goa, India
P K Dutta, IIT Kharagpur, India
P Senthil Kumaran, IIT Delhi, India
Pabitra Nath, Tezpur University, India
Parinada Vasa, IIT Bombay, India
Prasanta K Panigrahi, IISER Kolkata, India
Raj Kumar, CSIO, Chandigarph, India
Rajan Jha, IIT Bhubaneshwar, India
Rajesh Kumar, IIT Indore, India
Rajesh V Nair, IIT Ropar, India
Rajib Chakraborty, University of Calcutta, India
Rakesh K Singh, IIT BHU, India
Reji Philip, RRI, Bangalore, India
Renu John, IIT Hyderabad, India
Riju C Issac, CUSAT, India
Ritwick Das, NISER Bhubaneshwar, India
S Chaitanya Kumar, TIFR, Hyderabad, India
Sai Santosh K Raavi, IIT Hyderabad, India
Sajan D George, Manipal, India
Samir K Mondal, CSIR-CSIO, India
Sanjay K Mishra, IRDE, Dehradun, India
Sanjay Kumar Srivastava, Banaras Hindu University, India
Sanket Goel, BITS-Pilani, Hyderabad, India
Saptarshi Ghosh, IIT Indore, India
Saurabh Mani Tripathi, IIT Kanpur, India
Saurabh Raj, IIT Delhi, India
Shailendra K Varshney, IIT Kharagpur, India
Shankar K Selvaraja, IISc Bengaluru, India
Shanti Bhattacharya, IIT Madras, India
Shivkiran Bhakta B N, IIT Kharagpur, India
Sivarama Krishnan, IIT Madras, India
Somak Bhattacharya, IIT BHU, India
Sriganesh Prabhu, TIFR Mumbai, India
Sudhir Khare, IRDE Dehradun, India
Suhas Jejurikar, University of Mumbai, India
Surajit Dhara, University of Hyderabad, India
Tapajyoti Das Gupta, IISc Bengaluru, India
Tarak Nath Dey, IIT Guwahati, India
Unnikrishnan Gopinathan, IRDE Dehradun, India
Varun Raghunthan, IISc Bengaluru, India
Venugopal Rao Soma, University of Hyderabad, India

LOCAL ORGANIZING COMMITTEE

Pramod Gopinath, CUSAT
Saji K J, CUSAT
M Kailasnath, CUSAT
Sheenu Thomas, CUSAT
Muhammad Rishad K P, CUSAT
Priya Rose T, CUSAT
Praveen C S, CUSAT
Mohamed Ameen P, CUSAT
T Santhanakrishnan, NPOL
R Rajesh, NPOL
Sreehari C V, NPOL

SUB COMMITTEE

Amrutha Thomas
Anila Thomas
Anita Mary Peter
Anjaly T R
Anugop B
Arpitha Sunny
Arun Pappachan
Arun R Chandran
Athira T Das
Betsy Susan Abraham
Cicily Rigi V J
Dency John
Devika Raja
Hajara P
Irene Rose
Jijo George
Jose Antony V J
Karthika Sankar
Ananthakrishnan V
Keerthana S H
Lakshmi R
Lakshmi Srinivasan
Linsa G J
Maneesha M
Mitty George
Mubeena Rafi
Praveen P
Priya Mary N J
Safna Saif
Sathe Mayur Anil
Shanto T A
A K Sooraj Viswam
Soumya S
Syammohan V
Titu Thomas
Vijoy K V
Vinod P
Abishek Nair

Session Plan

All times in IST (+5.30 GMT)

DAY 1 (11 December 2023)				
Registration starts at 08:00 AM				
Inaugural Session (Venue: Seminar Complex Auditorium, CUSAT)				
09:30 - 10:30 AM	**Inauguration**			
10:30 - 10:45 AM	**High Tea**			
10:45 - 11:30 AM	**Plenary 1** (Speaker: K. V. Sriram)			
11:30 - 12:15 AM	**Plenary 2** (Speaker: Murukeshan Vadakke Matham)			
12:15 - 01:00 PM	**Techno – Commercial Session** **1. ATOS** **2. BIS**			
01:00 - 02:00 PM	***Lunch (Venue: Seminar Complex, CUSAT)***			
Technical Session- 1				
	Hall A (Auditorium)	**Hall B (Seminar Hall)**	**Hall C (ISP Auditorium)**	**Hall D (Executive Hall)**
02:00 - 03:30 PM	**Optical Interferometry and Holography (HOL)**	**Photonic works, Switching Interconnects & Access (NET) & Photonic Crystals & Metamaterials (PHC)**	**Quantum Optical Technologies (QOT) / Quantum Information (QI)**	**Diffractive, Free-form and Adaptive Optics (DFA)**
02:00 - 02:30 PM	A.R Ganesan	Enakshi Sharma (NET)	Ashok Kumar	C. S. Narayanamurthy
02:30 - 03:00 PM	Harshwardhan Wanare	R. Vijaya	Arijit Sharma	Bosanta R. Boruah
03:00 - 03:30 PM	HOL: 118, 119, 120	PHC:140, 141	QOT: 142,143,146	Sanjay K. Mishra
03:30 - 03:45 PM	***Tea Break***			
Technical Session- 2				
03:45 - 05:15 PM	**Nano-photonics & Plasmonics (NPH)**	**Green Photonics (GPH) & Ultrafast Optics (UFO)**	**Lasers Applications & Beam Optics (LSB)**	**Fiber Optic Devices, Sensors and Instrumentation (FIB)**
03:45 - 04:15 PM	Shanti Bhattacharya	Animesh Jha (GPH)	Venugopal Rao Soma	Bishnu P. Pal
04:15 - 04:45 PM	Subhasish Duttagupta	Chaitanya Kumar Suddapalli	Reji Philip	Arup Lal Chakraborty
04:45 - 05:15 PM	Harish Krishnamoorthy	Smijesh N.	LSB:128	R. Rajesh
05:15 - 06:45 PM	**Poster Session 1**			
06:45 - 07:45 PM	**OSI General Body Meeting** (Venue: Seminar Complex Auditorium, CUSAT)			
07:30 - 09:00 PM	***Dinner** (Venue: Seminar Complex, CUSAT)*			

All times in IST (+5.30 GMT)

DAY 2 (12 December 2023)				
09:00 - 09:45 AM	**Plenary 3** (Speaker: Prem Kumar)			
Technical Session- 3				
	Hall A (Auditorium)	**Hall B (Seminar Hall)**	**Hall C (ISP Auditorium)**	**Hall D (Executive Hall)**
09:45 - 11:15 AM	**Singular Optics & Laser Speckles (SIN)**	**Quantum Optical Technologies (QOT) / Quantum Information (QI) – II**	**Any other topics related to Optics and Photonics (OTH) & Optical Materials (MAT)**	**Biophotonics & Medical Optics (BPM)**
09:45 - 10:15 AM	Maruthi Manoj Brundavanam	Sadiq Rangwala	Kehar Singh	D. S. Mehta
10:15 - 10:45 AM	Goutam K. Samanta	Rakesh K. Singh	Deepa Venkitesh	Santhosh Chidangil
10:45 - 11:15 AM	Nirmal K. Viswanathan	Rajesh V. Nair	Sivarama Krishnan (MAT)	Renu John
11:15 - 11:30 AM	***Tea Break***			
Technical Session- 4				
11:30 - 01:00 PM	**Optoelectronic Devices (OED)**	**Optical Instrumentation, Fabrication and Metrology (IFM)**	**Contributory Talks**	**Artificial-Intelligence and Machine-Learning in Photonics (AMP)**
11:30 - 12:00 PM	Aloka Sinha	Kallol Bhattacharya	HOL: 121, 122, 147 IFM:123,124, 125, 126 SIN:144	R. Prasanth
12:00 - 12:30 PM	Narayanan Unni K. N.	Sajan D. George		T. Srinivas
12:30 - 01:00 PM	Stephane Treabol	Rajan Jha		AMP:101,102,103
01:00 - 02:00 PM	***Lunch*** *(Venue: Seminar Complex, CUSAT)*			
02:00 - 02:45 PM	**Plenary 2** (Speaker: Dag Hanstorp)			
Technical Session- 5				
02:45 - 03:45 PM	**Theory, Modelling & Simulation (THM)**	**Contributory Talks**	**Contributory Talks**	**Lasers Applications & Beam Optics (LSB) – II & Nano-photonics & Plasmonics (NPH) - II**
02:45 - 03:15 PM	Akhilesh Kumar Mishra	BPM: 105 GNO:115,116, 117, 145	DES: 106,107 DFA: 108,109 DSD:110	Jagannath Nayak (LSB)
03:15 - 03:45 PM	Anurag Sharma			NPH: 132, 133, 134
03:45 - 05:15 PM	***Tea Break*** **+ Poster Session 2**			
05:15 - 06:00 PM	**Distinguished Evening Lecture** (Speaker: C. P. Girijavallabhan)			
06:00 - 07:00 PM	**Cultural events**			
07:00 - 09:00 PM	***Conference Dinner***			

All times in IST (+5.30 GMT)

DAY 3 (13 December 2023)				
09:00 - 09:45 AM	**Plenary 4** (Speaker: Andreone Antonello)			
Technical Session- 6				
	Hall A (Auditorium)	**Hall B (Seminar Hall)**	**Hall C (ISP Auditorium)**	**Hall D (Executive Hall)**
09:45 - 10:45 AM	**Integrated Optic Circuits and Devices (IOC) & Optoelectronic Devices (OED)**	**Microwave and THz Photonics (MWT)**		**Fiber Optic Devices, Sensors and Instrumentation (FIB) - II**
09:45 - 10:15 AM	L. N. Hazra	Ranjan Singh	Thesis 1-5	Vipul Rastogi
10:15 - 10:45 AM	OED: 135, 136, 137, 148	Rajeev N. Kini		FIB: 111,112,113
10:45 - 12:15 PM	**Tea Break + Poster Session 3**			
Technical Session- 7				
12:15- 1:15 PM	**Nano-photonics & Plasmonics (NPH) - III & Ultrafast Optics (UFO) - II**	**Optical Materials (MAT) & Any other topics related to Optics and Photonics (OTH)**		**Contributory Talks**
12:15 - 12:45 PM	Gautam Das (NPH)	P. R. Biju	Thesis 6-9	FIB: 114, 149 NPH: 129, 130, 131
12:45 - 01:15 PM	Joakim Bood (UFO)	OTH:138,139		
01:15 - 02:15 PM	***Lunch*** *(Venue: Seminar Complex, CUSAT)*			
Technical Session- 8				
02:15 - 3:15 PM	**Optical Interferometry and Holography (HOL) - II**	**Ultrafast Optics (UFO)**	**Imaging and Super-resolution (ISR)**	**Any other topics related to Optics and Photonics (OTH) - II**
02:15 - 02:45 PM	Raj Kumar	Riju Issac	P. Nandakumar	Suhas M. Jejurikar
02:45 - 03:15 PM	Dinesh N. Naik		Joby Joseph	Sunil S.
03:15 - 04:15 PM	**Concluding Session**			
04:15 - 04:30 PM	***Tea***			

Plenary Talks

Indian Lunar Missions: Lessons Learnt and the Triumph of CHANDRAYAAN-3

Dr. K.V.Sriram,
Director, Laboratory for Electro-Optics Systems (LEOS), ISRO
I Cross, I Stage, Peenya Industrial Estate,
Peenya, Bengaluru 560058
E-mail: drkvs@leos.gov.in & directorleos@leos.gov.in

It is indeed, an incredible journey for the Indian Space Research Organization (ISRO) having ventured into interplanetary missions and the arduous lunar space missions taught us some important lessons. CHANDRAYAAN-1, the first of the interplanetary missions through which how to carry out space manoeuvers, reach lunar space and place a spacecraft in the intended orbit is successfully demonstrated. The science outcome from its few scientific payloads also created a renewed interest even for the global community to reconsider lunar expeditions. The next Indian lunar mission of CHANDRAYAAN-2 comprising of an orbiter and a lander, though a partial success rendered unfulfilled tasks and many technical challenges to overcome independently. The lander missed by a whisker to have soft landing on the lunar surface whereas the orbiter is still live and facilitated creation of lunar atlas as well as mineralogical mapping of the moon. The third venture viz., CHANDRAYAAN-3, a well-conceived and meticulously planned mission underwent several special tests, which ensured that it is going to be a sure-shot success much before its launch. Most importantly hardware in-loop tests, refined navigation guidance and control algorithms and the hot or cold redundancies built for vital subsystems helped to resolve the technical glitches faced during CHANDRAYAAN-2 landing, yielding a fail-proof spacecraft system.

Sensors play a crucial role in aiding the lander for a safe and soft landing on any planetary surface. A suite of electro-optical sensors such as the star sensor, laser inertial reference gyro with accelerometer, laser altimeter, laser doppler velocimeter, Lunar horizontal velocity camera and the lander hazard avoidance camera have been deployed in CHANDRAYAAN-3 whose immaculate performances have been the key to successful lunar landing. It is important to mention that many of these sensors have been designed and characterized at the laboratory for electro-optics systems (LEOS), Bengaluru. The talk will encompass a briefing on CHANDRAYAAN missions of ISRO, details on the sensors with their performances onboard and some typical science experiments carried out with rover instruments such as the seismometer and the laser induced breakdown spectroscope. Some ambitious additional experiments carried out with lander and the propulsion module shall also be described.

Optical juggling

Dag Hanstorp
University of Gothenburg
dag.hanstorp@gu.se

Optical levitation and optical tweezers, two techniques for manipulation of microscopic particles, were invented by the 2018 Nobel prize laureate Arthur Ashkin. In optical levitation [Ashkin and Dziedzic APL 19 (1971) 283], a focused, vertically aligned laser beam is used to trap micrometer-sized transparent particles where the photon pressure from the light is balancing gravity. I will in this presentation review how optical levitation can be used as an advanced research tool and well as an instrument for teaching experimental physics.

First, it will be shown how a pair of optically levitated particles execute a dance where the motion resembles the orbits of the balls of a carnival juggler. The motion can be ascribed by a mechanism by which the dominant force on each particle alternates between radiation pressure and gravity as the particles takes turns to eclipse each other [Bae A. J.*et al.* PRL **12** (2019) 043902]. This research was part in a project where we study collisions and coalescence of liquid droplets. This is of relevance in many applications, such as in atmospheric science to model rain drop formation or in combustion research to study fuel mixing.

Second, I will present a recent study of light scattering from trapped droplets where we observed rich Mie spectra of overlapping resonances. We show that the directional Mie spectrum of evaporating water droplets can be explained by a quantum analogy turning the droplet into an “optical atom" with angular momentum, tunnelling, and excited states [Marmolejo *et al.* PRL, **130** (2023) 043804].

Finally, I will describe how optical levitation can be used in physics education to demonstrate physical phenomena such as radiation pressure, light diffraction, the motion of a charged particles in electric fields, and the interaction of ionizing radiation with matter. I will, for example, present how optical levitation can be used to demonstrate a damped driven harmonic oscillator [Marmolejo *et al.* AJP, **88** (2020)490] and how the removal of a single electron from a trapped droplet can be observed using the bare eye as the only detector [Marmolejo *et al.* Scient. Rep. **11** (2021) 10703] |.

Engineering Challenges for the Emerging Quantum Networks

Prem Kumar
Northwestern University
Center for Photonic Communication and Computing, ECE Department
2145 Sheridan Road, Evanston, IL 60208, USA
kumarp@northwestern.edu

Quantum internet of the future will require device functionalities that implicitly respect the fundamental facts such as quantum information cannot be copied and cannot be measured precisely. A quantum repeater, for example—analog of an optical amplifier that enabled global reach of the ubiquitous Internet connectivity we enjoy today—is yet to be demonstrated, although recent years have seen tremendous progress. Many other device functionalities—switches, routers, format converters, etc.—would also be needed that do not unnecessarily disturb or corrupt the quantum information as it flows from one node of the internet to another. In recent years, my group has engineered many quantum tools and techniques that fulfill the requirements for distributing quantum information in a networked environment. In this talk, I will present our motivation, design, construction, characterization, and utilization of some example techniques for near-term networked quantum applications.

Micro-nanoscale patterning: Impact of interferometric and random optics, and their industrial applications

Murukeshan Vadakke Matham, Centre for Optical and Laser Engineering, School of MAE, Nanyang Technological University, SINGAPORE 639798
e-mail: mmurukeshan@ntu.edu.sg address

Optics technology that focuses on semiconductor, biomedical, and energy sectors in the recent past has seen the impact of micro-and nanoscale patterning and its dimension control, a challenging trend to achieve smaller features or devices with micro- or nano-scale features. This automatically demanded the need for achieving much smaller features beyond the forecasted sub 30nm fabrication methodologies. Hence, there is significant push for smaller dimension recently that has posed many challenges. In this context, a new branch of conventional and nearfield optical concepts started emanating for improving patterning resolution has started developing. These approaches have been receiving considerable attention for its ability to produce high-density sub-wavelength features at the micro- and nano-scale levels for their applications in a variety of fields ranging from engineering, semiconductor to healthcare. This plenary talk will be covering the above-mentioned aspects focussing on the in house developed concepts and technologies in the related areas by the author's group.

The talk will initially detail the need for using visible or near UV wavelengths for patterning and explore how interferometric concepts can enable such approaches. It will then detail the development and instrumentation details of a multi-beam laser interferometric lithography system for conventional and near field optics assisted patterning at the micro- and nanoscale. These patterned structures are then demonstrated for semiconductor applications detailing the challenges faced in meeting the forecasted technology nodes of sub-30nm features. This will then be followed by novel nanoscale patterning approaches using random optics such as the recently proposed and innovative speckle lithography. This has proven to make reliable hydrophobic, hydrophilic surfaces, and black or white silicon structures for potential industrial applications. The talk will conclude by highlighting the current and future research challenges using periodic and aperiodic patterns obtained by interferometric approaches for high resolution imaging and the use of random optics concepts for high contrast high resolution imaging.

Majority of the research results presented in this talk were financially supported through COLE-EDB Funding and by the Ministry of Education, Singapore, under its Academic Research Fund Tier 1 (RG119/21).

Probing solids, liquids, and meta-devices by THz Time Domain Ellipsometry

Antonello Andreone
Department of Physics, University of Naples Federico II, and
National Institute for Nuclear Physics (INFN), Naples Unit
Naples, 80126 ITALY
andreone@unina.it

Ellipsometry is extensively used in the optical regime to investigate the properties of many materials as well as to evaluate with high precision the surface roughness and thickness of thin films and multilayered systems. Due to the inherent *non-coherent detection* technique, data analyses in optical ellipsometry tend to be complicated and require the use of a predetermined model, therefore indirectly linking the sample properties to the measured ellipsometric parameters. Time-domain techniques recently developed in the THz region make possible instead ellipsometry based on a *coherent* detection approach that provides in a simple and direct way the measurement of the material response. In this talk, I will give an overview of the emerging field of THz time domain ellipsometry. After a brief description of the THz spectroscopy, the general features of a ellipsometric setup designed and manufactured in-house and operating in time domain will be introduced, putting in evidence similarities and differences with respect to the classical optical counterpart. To back up and validate the study, results of ellipsometric measurements carried out on different systems in the frequency range 0.1-2 THz will be presented. I will first show experiments performed on semiconducting Silicon samples with different doping level. With the ever-increasing demand for semiconductors with widely tunable carrier concentrations, there is a renewed interest for non-destructive and fast characterization techniques that are capable of measuring very high carrier concentrations. Then, I will focus on experiments probing the THz dynamics - at a mesoscopic level - of different aliphatic alcohols and the corresponding aqueous solutions. Recently, H-bonding mechanisms and the competing effects produced by the amphipathic nature of the solute in water-based mixtures are catching a great deal of attention in many different biological, chemical, and engineering applications such as biosensing, solution chemistry, aquametry and aquaphotomics, agri-food, energy, protein hydrolysis. Finally, I will present preliminary results on the use of variable angle spectroscopic polarimetry for the characterization of digital metasurfaces, a first step towards the fruitful exploitation of THz time domain ellipsometry for testing RIS (Reconfigurable Intelligent Surfaces) in new generation telecommunications systems.

Invited Talks

Emerging Trends in Machine Learning for Solar PV Energy Prediction: A Comparative Analysis of Linear Regression, SVM, and MLP

R.Prasanth, UNESCO Madanjeet School of Green Energy Technology, Pondicherry University, Kalapet, Pondicherry 605014, India
prasanth.get@pondiuni.edu.in, prasanth.ravindran@gmail.com

Machine learning techniques have witnessed remarkable growth and innovation in recent years, driven by emerging trends in the field. One of the promising applications of machine learning is the prediction of solar photovoltaic (PV) energy generation, which is crucial for efficient grid management and renewable energy integration. This abstract provides an overview of the relevance and significance of using machine learning methods such as Linear Regression, Support Vector Machines (SVM), and Multilayer Perceptron (MLP) for solar PV energy prediction within the context of emerging trends in machine learning.

Accurate prediction of solar PV energy generation is essential for grid stability, energy management, and the integration of renewable energy sources. Traditional methods based on weather data and historical patterns often need to catch up in capturing the dynamic nature of solar energy generation. Machine learning techniques offer a data-driven approach to address these challenges, allowing for more precise and real-time predictions. Solar PV energy prediction aids in optimizing energy distribution, reducing operational costs, and mitigating the intermittency of solar power.

This abstract compares the performance of three machine learning techniques - Linear Regression, Support Vector Machines (SVM), and Multilayer Perceptron (MLP) - for solar PV energy prediction. Linear Regression is a simple and interpretable model that forms a baseline for comparison. SVM is known for its ability to handle non-linear data and robustness to noise. MLP, as a neural network architecture, can capture complex relationships in the data.

The analysis considers prediction accuracy, model complexity, scalability, and adaptability to changing conditions. Moreover, the study discusses the importance of feature selection and engineering in enhancing the predictive power of these models. It also considers the impact of real-time data and the role of ensemble methods in improving the reliability of predictions.

In conclusion, using machine learning techniques in solar PV energy prediction aligns with emerging trends in machine learning, offering a data-driven, adaptive, and accurate approach to address the challenges posed by renewable energy integration. The comparative analysis of Linear Regression, SVM, and MLP sheds light on the strengths and limitations of each method, providing valuable insights for researchers and practitioners in the field of solar energy prediction and energy management.

Inverse Design Techniques for Photonic Integrated Circuits

T Srinivas and Preetam Kumar
ECE Dept, Indian Institute of Science
tsrinu@iisc.ac.in

Computational techniques are necessary to design and analyse complex photonic integrated circuits. Funcitonal approach based on AI/ML techniques are emerging as powerful methods to design photonic integreted circuits. Given a function, such as demultiplexing, direct approach involves taking a standard structure like a directional coupler and tracking whether it meets the required functionality. In the inverse

design techniques (IDT), specific structure is not assumed but by using AI/ML techniques arbitrary structures are tested for their functionality. Due to iterative and deep learning approach there is good possibly for quick convergence, along with possibility to include several design parameters. In this talk various aspects of functional design approach and IDT are described and applied to specific functional cases, such as a mux/demux, and spectral characteristics of a TiO2 − SiO2 based multilayer thin film device.

Optical Biopsy - Multimodal and Multispectral Optical Point-of-Care Devices for Early Cancer Screening and Diagnosis

Dalip Singh Mehta

Bio-Photonics and Green Photonics Laboratory, Department of Physics

Indian Institute of Technology Delhi, Hauz Khas, New Delhi 110016, India

E-mail: mehtads@physics.iitd.ac.in

Recently variety of optical techniques have been developed for cancer screening and diagnosis. These include optical imaging, microscopy, and various spectroscopic techniques. Among imaging and microscopy; polarization imaging and microscopy, quantitative phase microscopy, and optical coherence tomography have been used for cancer screening and diagnosis. Optical spectroscopic techniques include diffuse reflectance spectroscopy, auto-fluorescence, fluorescence spectroscopy and Raman spectroscopy which have great potential for in-vivo cancer screening and diagnosis in real-time with high specificity and sensitivity. Most of these techniques are not-contact, non-invasive and can be implemented in-vivo leading to real time cancer screening and diagnosis. So far most of these techniques are implemented individually therefore the accuracy of cancer diagnosis is less. Hence invasive histopathology is still dominant for cancer diagnosis and is treated as the gold standard. But histopathology requires long process, takes long time for diagnosis and subjective.

We report convergence of multimodal and multispectral optical imaging and spectroscopic techniques for early cancer screening and diagnosis [1-7]. These are point-of-care devices leading to real-time /in-vivo optical biopsy. We have developed multimodal and multispectral optical devices for tumour margin detection during breast cancer surgery and in-vivo fast oral cancer screening and diagnosis of cancer. Auto-fluorescence and fluorescence spectroscopy and imaging are most important techniques for cancer screening which have been developed indigenously by our group. Auto-fluorescence spectroscopy provides information about native fluorescence, and which is molecular specific and provides important information about cancerous and precancerous state of molecular composition compared to normal tissue. Fluorescence spectroscopy and imaging is mainly used for contrast enhancement during intra-operative procedure to guide complete removal of tumour margin detection. But we found significant spectral changes in fluorescence spectra of cancerous and non-cancerous tissues [1-5]. Experimental results spectral changes of pre-cancerous and cancerous cases will be discussed. We have implemented machine learning and AI based methods to classify the results of cancerous, pre-cancerous, and normal tissues. We have also implemented surface enhanced Raman spectroscopy-based technique for molecular finger printing to validate our results. Microstructural features of tissues and cells is important for diagnosis of cancer [7]. We have developed micro-spectro-endoscopic device of simultaneous microscopy and fluorescence spectroscopy of cancerous and non-cancerous tissues during intra-operative procedure and in-vivo. Both auto-fluorescence and fluorescence spectroscopy and microscopy have been demonstrated.

The main outcome of the developed point-of-care devices is the use optical technologies in hospitals and clinics for the benefit of mankind. In low resource setting developing world, moving cancer treatments out of specialized centres and into local clinics or small hospitals could significantly lower healthcare costs,

travel time and leading to early diagnosis and treatment. We have developed a field-portable multi-spectral and multi-modal devices, which are point-of-care devices for the consistent and cost-effective screening of oral, cervical and breast cancer patients. These techniques are non-contact and non-invasive and are reliable methods. Prototypes developed and installed at AIIMS Hospital New Delhi. The novelty and innovation is non-contact and non-invasive/minimally invasive technology based on field-portable multi-modal high-resolution fluorescence spectroscopy and imaging for in-vivo diagnosis of breast and oral cancer. Leading to label-free, fast screening and diagnosis of cancer without staining.

References

1. Dalip Singh Mehta, Pramila Thapa, Veena Singh, Himanshu Joshi, Dibya Jyoti Sarangi, Deepika Mishra, Anurag Srivastava, Multimodal and multispectral diagnostic devices for oral and breast cancer screening in low resource settings, Current Opinion in Biomedical Engineering, Pages 100485 (2023).
2. Pramila Thapa, Veena Singh, Sunil Bhatt, Kiran Maurya, Virendra Kumar, Vivek Nayyar, Kiran Jot, Deepika Mishra, Anurag Srivastava, Dalip Singh Mehta, Multimodal Fluorescence Imaging and Spectroscopic Techniques for Oral Cancer Screening: A Real-time Approach, Methods and Applications in Fluorescence 2023
3. Pramila Thapa, Veena Singh, Komal Gupta, Anurag Shrivastava, Virendra Kumar, Kamal Kataria, Piyush Ranjan Mishra, and Dalip Singh Mehta, Point-of-care devices based on fluorescence imaging and spectroscopy for tumour margin detection during breast cancer surgery: Towards breast conservation treatment, Accepted for publication in Lasers in Surgery and Medicine 2023.
4. Pramila Thapa, Veena Singh, Sunil Bhatt, Shilpa Tayal, Priyanka Mann, Kiran Maurya, Deepika Mishra, Dalip Singh Mehta, Development of multimodal micro-endoscopic system with oblique illumination for simultaneous fluorescence imaging and spectroscopy of oral cancer, Journal of Biophotonics e202100284 (2022).
5. Ankit Butola, Dilip K Prasad, Azeem Ahmad, Vishesh Dubey, Darakhshan Qaiser, Anurag Srivastava, Paramasivam Senthilkumaran, Balpreet Singh Ahluwalia, Dalip Singh Mehta, Deep learning architecture "LightOCT" for diagnostic decision support using optical coherence tomography images of biological samples, Biomedical Optics Express 11 (9), 5017-5031 (2020).
6. Ankit Butola, Azeem Ahmad, Vishesh Dubey, Vishal Srivastava, Darakshan Qaiser, Anurag Srivastava, P. Senthilkumaran, Dalip Singh Mehta, "Volumetric analysis of breast cancer tissue using machine learning and swept source optical coherence tomography", Applied Optics 58 (5), (2019).
7. Vishesh Dubey, Azeem Ahmad, Ankit Butola, Darakshan Qaiser, Anurag Srivastava, Dalip Singh Mehta, "Low coherence quantitative phase microscopy with machine learning model and Raman spectroscopy for the study of breast cancer cells and their classification," Applied Optics 58 (5), (2019).

Recent developments in diagnostic technologies for oral cancer screening

Santhosh Chidangil

Centre of Excellence for Biophotonics, Department of Atomic and Molecular Physics, Manipal Academy of Higher Education, Manipal-576104

Email: santhosh.cls@manipal.edu

Newer methods for cancer diagnosis are mostly based on biophotonics technologies which deal with the

study of the interaction of light with living systems. It is a continuously growing field, where the properties of electromagnetic radiation are utilized to address biomedical problems. Among several biophotonics technologies, Laser spectroscopy is popular in medical research to probe molecular structure-function and interaction mechanisms to detect, diagnose, and treat diseases in cheaper, faster, and non-invasive ways. Laser Induced Fluorescence techniques combined are found to be easily extendable for the in vivo screening and detection of oral cancer. The biophotonics team at MAHE has developed a portable oral cancer screening device based on autofluorescence characteristics of tissues for in vivo applications. The system was tested for more than 350 volunteers which includes normal, premalignant, and malignant conditions, and found that the sensitivity and specificity are more than 90% each. Salivary protein analysis using locally assembled high-performance chromatography combined with laser-induced fluorescence technique is another non-invasive method developed and tested by the team for the detection and screening of oral lesions. The talk will cover the recent developments in oral cancer diagnosis technologies and details of the biophotonics devices developed by the research team at MAHE, Manipal.

Holographic generation of complex light beams for communication and metrological applications

Bosanta Ranjan Boruah, Computer generated holography and Optical imaging Laboratory,
Department of Physics, IIT Guwahati, Assam-781039
e-mail: brboruah@iitg.ac.in

Computer generated holography realised with a dynamically reconfigurable device can be used to generate laser beams with user defined phase [*American Journal of Physics*: **77** 331 (2009)] and amplitude profiles [Optics Communications: 515 , 128201 (2022)], which together are called complex amplitude profile. In this talk I will discuss dynamic control of the complex amplitude profile of a laser beam using binary holograms written on fast spatial light modulators. We are thus able to modulate both the phase and amplitude of a laser beam and reconfigure them at a rate much higher than the standard video rate. We extend holographic beam control technique to design novel wavefront sensing schemes [*Optics Letters* : **41** (23), 5600-5603 (2016), *JOSA A*: **36** (5), 741-750 (2019)] for state of the art metrological applications [Optics Letters: 47(21), 5509 (2022), Optics Letters: 47 (16) 4151 (2022)]. We also further use the technique to develop novel free space communication systems [Communications Physics: 3 203(2020)]. Results from some demonstration experiments will also be presented and discussed in this talk.

Investigations on turbulence impacted light beams for free-space optical communications

*S R Lekshmi, Dinesh N Naik and *C S Narayanamurthy*
Applied and Adaptive Optics Laboratory, Dept. Of Physics, Indian Institute of Space Science and Technology(IIST), Valiamala, Trivandrum - 695547
**C S Narayanamurthy: murthy@iist.ac.in*

There is a renewed interest in wave propagation analysis through atmospheric turbulence and turbid media because of its wide range of applications ranging from astronomical to biomedical imaging. Researchers have been constantly trying to optimise the free space optical communication systems without or with the minimal use of adaptive optics system. Some of optimization techniques are altering their degree of coherence, and degree of polarization, or using different classes of beam shapes. In this lecture, we demonstrate that by passing different classes of light beams through a laboratory level turbulence simulator to see their potential to be used in free space communication systems. In the first part, the Fried coherence

length which is an important parameter of atmospheric turbulence is measured using the rotating pseudo random phase plate which mimics atmospheric turbulence. The autocorrelation function generated from the quantitative properties of a rotating PRPP in one of the arms of a Mach-Zehnder interferometer is used in this new method for finding Fried parameter. Then the wave propagation analysis of partially coherent Gaussian-Schell model beams, zero order Bessel-Gaussian beams and partially coherent Gaussian vortex beams through a rotating pseudo random phase plate are extensively analyzed for the suitability of them for free space optical communications with minimum or no adaptive optics. In all these analysis, the effect of turbulence is quantitatively characterized by calculating their scintillation index, beam wandering and Zernike polynomials and qualitatively by finding the intensity line profiles at the laboratory level. The experimental results are further extended and verified using simulations. It is found that certain classes of beams under certain criteria show more resilience to the impact of turbulence making them desirable for free space optical communication. Further, the phenomenon of enhanced backscattering is studied using Laguerre Gaussian and Bessel-Gaussian beams. These beams are focused onto a detector after passing through a rotating dynamic turbulence twice. After passing through, the backscattered light beams are examined. When a beam is reflected off from a retro-reflector, it exhibits enhanced backscattering and with a typical Gaussian beam, the amplification factor approaches two, and it decreases as the topological charge increases. The Bessel Gaussian beam also exhibits enhanced backscattering, with an enhancement factor comparable to that of Gaussian beam. Along with the increased backscatter, the endurance of the BG beams is also preserved as compared to the other incident beams.

References

1. Lekshmi S.R., Dinesh N. Naik, C.S. Narayanamurthy “Fried’s coherence length measurement of dynamic Kolmogorov type turbulence using the autocorrelation function”, Journal of Optics, IOP, 24, (2022)

2. Lekshmi S.R., Dinesh N. Naik & C.S. Narayanamurthy (2023) Insensitivity of partially coherent Gaussian -Schell model beams to the impact of dynamic Kolmogorov type turbulence, Journal of Modern Optics, 70:3, 161-169, (2023)

3. Lekshmi S.R., C.S. Narayanamurthy, The resilience of zero order Bessel–Gaussian Beams to the impact of dynamic Kolmogorov type of turbulence, Optics Communications, Volume 532, 129243 (2023)

Performances of Electro-optical Sensors in Turbulence

SK Mishra
Instruments Research and Development Establishment, Dehradun-248008
skmishra.irde@gov.in

Electro-optical sensors when used in various type of random media such as Atmospheric, Seawater and Aero dynamic turbulences [1], their performance significantly compromised as per the uses scenario. This need to be properly studied for providing remedial solutions or specifying the performance limitations. Adaptive optics [2] is a one hardware based solution but it is costlier affair.
The talk includes the effect of non-homogeneous turbulence [3-4] on the performance of Adaptive Optical Sensors and their uses for various Defence Applications. Comparison of well-known Kolmogorov and Non-Kolmogorov models and their uses will be presented in detail with an example scenario.

References

1. Tyson, RK et al., *Taylor & Francis Press* (2022).
2. Zeeshan, F, et al., *Opt. Eng.* 61, 03611 (2022).
3. Andrews, L, et al., 2nd Ed., *SPIE Press* (2005).
4. Toselli, I, et al., *Opt Express* 28, 17347-17361 (2020).

Optical fiber designs tailored for specialty applications

Somnath Ghosh[1], Ajanta Barh[2], Sonali Dasgupta[3], R.K. Varshney[4], M.R. Shenoy[4], Kamna Pande[5] and Bishnu Pal[,5]*
[1]Physics Department IIT Jodhpur, [2]DTU Lyngby Denmark, [3]STEMMonsters Bangalore, [4]Physics Department IIT Delhi, [5]Mahindra University Ecole Centrale School of Engineering Hyderabad 50043
[*]e-mail: bishnu.pal@mahindrauniversity.edu.in

Optical fiber telecommunications have revolutionized long-distance communication in the last century, and have enabled the current internet-driven information technology revolution. Today, one billion plus Internet users worldwide exchange over 2,000 Petabytes of data every month, most of which is carried by undersea optical fiber cables. One Terabyte transmission implies transmission of almost 15,625,000 simultaneous telephone conversation. Fiber-to-the-home continues to expand its footprint, bringing high-quality and low-cost voice, video, and data services to our doorsteps at high speed. Both these developments have significantly impacted the lives of people all over the globe. Equally important is the quiet revolution that took place with the diversification of optical fiber technology into allied fields like sensing, imaging, high-power lasers, lighting, displays, etc. Fiber optic sensors have found wide-ranging applications from structural health monitoring of civil structures like buildings, bridges, aircrafts to securing perimeters sensitive defence installations and airports, sensing hazardous chemicals and biomedical markers. Fiber-based sensors are a multi-billion-dollar industry today. Endoscopes, example of earliest uses of fiber optics in biomedical instrumentation, are extensively used for *in vivo* imaging of biological tissue within e.g. stomach of a human body. Today, fibers are used for imaging as well as for drug delivery, photodynamic therapy, laser-assisted surgery, etc.

Rare-earth doped fiber amplifiers are one of the early success stories of high-capacity, broadband fiber-optic networks. These developments also paved the way for development of industrial grade kW power fiber lasers (lasers are essentially optical amplifiers converted to an oscillator through optical feedback), which now compete with conventional lasers in peak power and beam quality, while being more compact, energy-efficient, and offering greater ease of operation. Today, both single-mode (~ 10 kW) and multi-mode fiber lasers emitting (~ 100 kW) when combined outputs of several individual lasers are used to maximizing output power.

In this talk we will attempt to show that besides signal carrying legacy fibers like SMF-28/G-652, NZDSF/ G655 fibers, there exist a big demand for application-specific specialty fibers. Several examples can be cited like dispersion compensating fibers for telecom networks, rare-earth doped fibers for signal amplification/fiber lasers, highly non-linear microstructured fibers for Supercontinuum light generation, or Chalcogenide/plastic fibers for Mid-IR/THz generations and transmission through wavelength translation, hollow core fibers for extremely low loss propagation, multicore fibers for space division multiplexed high volume signal transmission and so on.

Emerging trends in wavelength-modulated tunable diode laser spectroscopy

Arup Lal Chakraborty
Electrical Engineering, IIT Gandhinagar, Gandhinagar 382055
arup@iitgn.ac.in

Trace gas sensing in outdoor settings has assumed special significance in the Indian context due to the alarming deterioration of air quality in several major cities. It is necessary to develop city-wide, mobile air quality monitoring systems that can track emissions in real-time. The biggest challenge in this kind of work is to ensure that the measurements are not restricted to fixed ground locations but are carried out in vehicle -mounted and airborne systems so that high spatial-temporal resolution of measurement is achieved. The need to deliver highly reliable measurements despite the harsh outdoor conditions is also a very challenging problem that can only be effectively addressed through a blend of advanced photonic techniques, robust engineering of systems and clever data processing algorithms.
The vibrant field of tunable diode laser absorption spectroscopy (TDLAS) for trace gas sensing received a shot in the arm thanks to the development of frequency-agile quantum cascade lasers (QCLs) that emit very deep in the mid-infrared region of the spectrum that is known as the finger print region because molecules have their unique absorption signatures there, and the absorption is very strong. This talk will provide an overview of the emerging trends in this area and then describe our efforts towards the development of high-sensitivity mid-infrared (and near-infrared) TDLAS systems that have been trialled extensively in Ahmedabad, Gandhinagar and Mount Abu. The talk will first introduce the principle of wavelength modulation spectroscopy (WMS), and then compare the two popular regimes namely, 1f WMS and 2f WMS, to bring out the merits and demerits of the two approaches. The focus will then shift to a recently developed 1f WMS technique [2] that has been shown to have significantly lower detection limit compared to the 2f WMS technique. The engineering aspects will then be described with specific focus on this robust calibration-free 1f WMS technique that makes the system extremely resilient to large, small, slow and rapid signal variations that arise due to inevitable opto-mechanical instabilities. The talk will conclude with a set of results from various measurement campaigns that we have been undertaken by the Photonic Sensors Lab at IITGN.

References

1. G. B. Rieker et. al., *Appl. Opt*. 48, 5546-5560 (2009).
2. S. De et. al., *Appl. Opt*. 62, 3160-3168, (2023).

Few-Mode and OAM Mode Optical Fibers for Mode Division Multiplexing Communication Systems

Vipul Rastogi[1,2], Ishani De[1]*
[1]Department of Physics, Indian Institute of Technology Roorkee, Roorkee- 247 667
[2]Center of Photonics and Quantum Communication Technology, Indian Institute of Technology Roorkee, Roorkee-247 667
**vipul.rastogi@ph.iitr.ac.in*

The transmission capacity in single-mode fiber is soon approaching the Shannon limit of 100 (~Tbit/s) [1]. With all the degrees of multiplexing, like wavelength, polarization, amplitude, and phase exhausted, space

division multiplexing (SDM) is the solution to the forecasted upcoming capacity crunch. Mode division multiplexing is a subset of SDM in which orthogonal spatially overlapping modes are employed as distinct data routes. Depending on the number of modes utilized, the transmission fibers in MDM can be classified into few-mode and multimode fibers [2].

The erbium-doped fiber amplifier (EDFA) is an integral component in fiber-based optical communication systems. We have designed an annulus core few-mode fiber amplifier for the amplification of the LP_{01}, $LP_{11,}$ $LP_{21,}$ and LP_{31} mode groups [3]. For amplifiers in MDM communications, gain equalization is very important, i.e., differential modal gain (DMG) should be very low. Using single trench ring core FM-EDFA, we included amplification of LP_{41} mode and decreased the DMG to 0.45 dB while having the modal gain of more than 20 dB [4].

In our recent work, we have used orbital angular momentum (OAM) modes as an orthogonal modal basis set for MDM systems. OAM modes allowed us to increase the information carrying capacity by more than 5 fold due to orthogonality between OAM modes with different topological charges *l*. With OAM modes, we were able to reduce the DMG of OAM-EDFA substantially to below 0.2 dB. We have proposed an OAM EDFA based on index guiding circular photonic crystal fiber amplifying 20 OAM modes with a gain excursion of less than 2 dB and noise figure of less than 4.2 dB [5]. We have also designed transmission fiber for 42 OAM modes across the C band and studied the characteristics of the supported modes in the fiber [6].

References

1. P. P Mitra and J.B Stark*, Nature* 441, 1027-1030 (2001)
2. D. J Richardson et al., *Nat*. *Photonics* **7**, 324-362 (2009).
3. A. Gaur and V. Rastogi, *IEEE Photon. Technol. Lett.,* 28, 1057-1060 (2016)
4. A. Gaur and V. Rastogi, *J. Opt. Soc. Am. B*, 25, 2211-2216 (2018)
5. A. Mehta, M. Rehan and V. Rastogi, *J. Opt. Soc. Am. B*, 38, F138-F143 (2021)
6. I. De and V. Rastogi, 6th Workshop on Optics and Photonics: Theory and Computational Techniques – *OPTCT 2022*, IIT Delhi, India, December 26-27, 2022.

Design and development of fiber optic acoustic sensor, polarizing beam splitter, and flexoelectric generator

Aloka Sinha
Department of Physics, Indian Institute of Technology Delhi, New Delhi, India
Email ID: aloka@physics.iitd.ac.in

Optical device devices are an indispensable part of our day-to-day life, including electro-optic devices, sensors, displays, and acousto-optic devices. Integration of liquid crystals (LCs) with optical devices makes them tunable, which makes it a promising device for advanced optics. In the recent decade, we have successfully developed LC-based optical waveguides [1], beam steering devices [2], and sensors [3]. In the most recent work, we developed an LC-based active beam splitter, optical fiber cantilever-based acoustic sensors, and an LC polymer film-based flexoelectricity generator. A brief description of these works is explained as follows:

We demonstrated a polymer film-integrated optical fiber cantilever-based low-frequency acoustic sensor with a significantly high sensitivity [4]. The laser light is coupled from an input fiber to an output cantilever fiber where the input fiber is kept fixed, and the cantilever is free to vibrate under the acoustic

pressure, resulting in variation in the transmitted light as shown in Fig.1. We achieved a large signal-to-noise ratio of 70 dB with a high sensitivity of 958 mV/Pa at its resonance frequency. This sensor is advantageous over the previous investigations in terms of its high sensitivity, large signal-to-noise ratio, and low minimum detectable pressure using simple fabrication methods.

We have also developed and fabricated an LC-based active polarization beam splitter (PBS) using the principle of total internal reflection [5]. The fabricated LC-PBS is operated in two different modes: non-splitting mode and polarization splitting mode. The externally applied voltage can switch the mode of the PBS, which makes the device active and flexible (see Fig. 2). The device exhibits fascinating advantages, which include bistability with highly stable modes, a large splitting angle along with wider operating range.

Currently, we have successfully introduced LCs in the field of energy harvesting applications to study the flexoelectric effect. The LC molecules were successfully embedded inside the polymer composite matrix to enhance the dielectric properties and the flexoelectric coefficient of the composite film.

References

1. V. Sharma, and A. Sinha, *Optics & Laser Technology,* 159, 108987 (2023).
2. R. Panchal, and A. Sinha. *JOSA B*, 40, 1189-1195 (2023).
3. S. Chakraborty, R. Panchal and A. Sinha, *Applied Optics*, 62, 627-634 (2023).
4. R. Panchal and A. Sinha, *IEEE Sensors Journal* (2023) DOI: 10.1109/JSEN.2023.3322719.
5. V. Sharma, A. Sinha, *Optics Letters,* 48, 2357-2360 (2023).

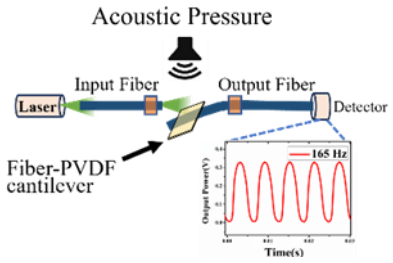

Fig. 1. Fiber optic acoustic-optic sensor.

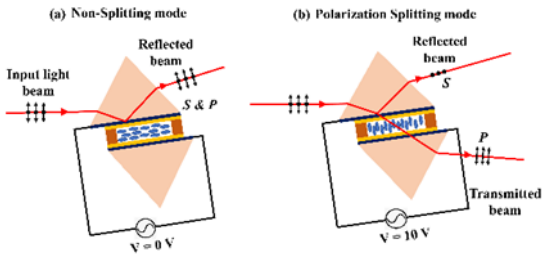

Fig. 2. LC-based polarization beam splitter.

Semiconductor Quantum Dot Glass Engineering for Photothermal, Photocatalytic, and Photoluminescence Applications using Solar Energy

*M. Al-Murish[1], V. Autade[2], Y Liu[1], R P. Panmand[2], S W. Gosavi[3], B B. Kale[2], A. J. Scott[1], E K Barimah[1] and A. Jha[1]**

[1] School of Chemical and Process Engineering, University of Leeds, Leeds, LS2 9JT, UK.

[2] Centre for Materials for Electronics Technology (C-MET), Off Pashan Road, Panchawati, Pune–411008, India.

[3]Department of Physics, Savitribai Phule Pune University (SPPU), Pune -411007, India.

**Corresponding and participating author: a.jha@leeds.ac.uk*

The importance of quantum dot materials for optoelectronic and light-emitting applications was recognized more than 40 years ago, culminating in the Nobel Prize in Chemistry in 2023[1]. Although the semiconduc-

tor divalent chalcogenides have been extensively researched for catalysis and photoluminescence[1], the photo-induced degradation has remained a major barrier for much wider applications in adverse environment. In this presentation, the mechanisms of photothermal, photocatalysis, and photoluminescence properties of CdS/MnS dispersed Q-dots in a silicate glass matrix are explained. The importance of controlling the Q-dot size and size distribution in maximizing the energy transfer from solar spectrum to physico-chemical and photothermal process is explained by analysing the UV-visible, Raman, heat transfer, catalysis efficiency data.

The results of solar energy harvesting for photothermal, photocatalytic[2], and photoluminescence applications are exemplified in Figures 1a to 1c, respectively.

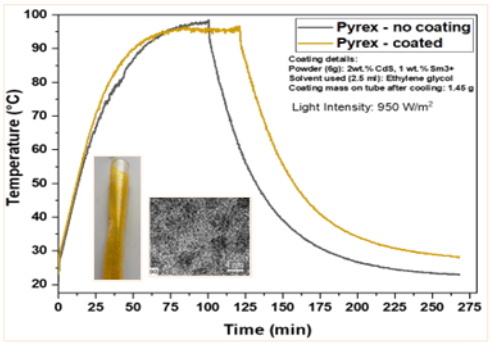

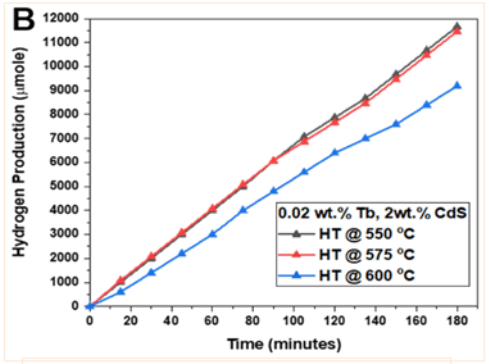

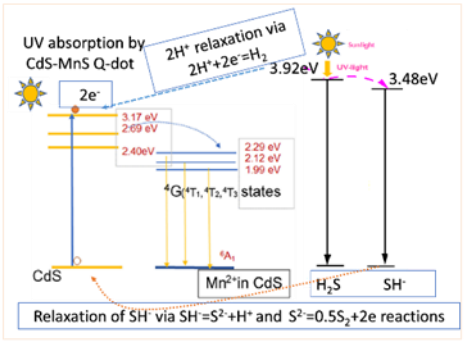

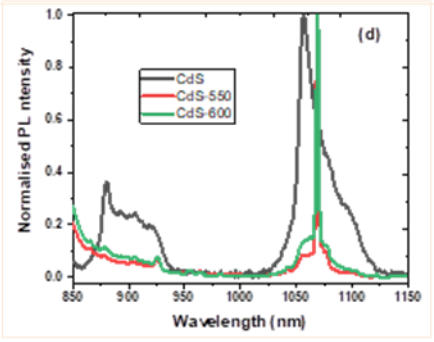

References

1. L. E. Brus, *Appl. Phys. A* 53, 465 (1991).
2. M Al-Murish et al: *ACS Appl. Energy Mater*. 2023, 6, 17, 8875–8888.

Improved Interferometric Configurations for Tilt Measurement at Nanoscale

A R Ganesan
Department of Physics, Indian Institute of Technology Madras,
Chennai,600036, India.
**arg@iitm.ac.in*

Interferometric methods serve as a convenient tool for the measurement of tilt with high sensitivity. The applications of the measurement of small tilt angle range from leveling devices to planetary measurement, coordinate measurement methods etc. The Michelson interferometer is most commonly used to measure tilt angle where any one of the mirrors or both mirrors are rotated to obtain the fringe pattern [1]. However, the lower limit of measurable tilt is limited by the beam size and associated optics. As the fringe width increases with decrease of tilt angle, one would reach a limit where the width of the bright fringe equals the

beam size. Below this tilt, we cannot distinguish between a bright fringe of width greater than the beam size and a fringe free field. This can be overcome if we increase the sensitivity so that we obtain some fringes within the beam and thereby could measure the fringe width.
We present some improved interferometric configurations where the sensitivity of measurement is highly enhanced and thereby the lower limit of tilt measurement is pushed down. The modified configurations of Michelson interferometer and Cyclic interferometer presented here would provide double or manifold sensitivity. The Michelson Interferometer has been modified by incorporating a mirrored right angled prism for doubling the sensitivity[2]. The improvised Cyclic Interferometer uses a Double Sided Mirror (DSM) and two parallel mirrors to introduce multiple reflections between DSM and mirrors and thereby increasing the sensitivity several fold [3]. Tilts as low as 500 nano radian have been measured accurately. The incorporation of polarization in these interferometers would further enhance the sensitivity and tilts at nanoscele could be measured which could not be achieved by existing interferometric methods. The various existing methods of tilt measurement along with the proposed novel method shall be presented.

References

1. R. S. Sirohi, Introduction to Optical Metrology (Taylor & Francis Group, New York, 2016), pp. 91-92
2. Laxman Mandal, Jaspal Singh, A R Ganesan, “Michelson Interferometer with mirrored right-angled prism for measurement of tilt with double sensitivity”, Journal of Optics, https://doi.org/10.1007/s12596-023-01327-2 (2023)
3. Laxman Mandal, Jaspal Singh, A R Ganesan, “Modified Cyclic Interferometer for measurement of nanoradian tilt with multifold sensitivity”. Optics Communications, 546, 129815, https://doi.org/10.1016/j.optcom.2023.129815 (2023)

Interferometry: a continuing saga of surprises

Harshawardhan Wanare

Department of Physics, Indian Institute of Technology Kanpur, Kanpur 208016

hwanare@iitk.ac.in

I will dwell on two interferometric arrangements that are counter-intuitive, and yet full of promise. One involves interferometric arrangement to quantify Quantum tunnelling, wherein the arms of the interferometer are dominated by evanescent fields - tunnelling - and has the potential to accurately measure the Hartman effect – both in the temporal and the spectral domain. The second one involves polarization-based interferometer wherein the phase differences between the arms of the interferometer are mapped on to the polarization content of light and little occurs in the intensity of the light. The second interferometer has the potential to invoke the geometric Pancharatnam phase to sieve out information about sub-wavelength features.

Nonlinearity in phase accumulation in optical interference

Dinesh N. Naik

Applied and Adaptive Optics Laboratory, Department of Physics,

Indian Institute of Space Science and Technology, Thiruvananthapuram, Kerala, 695547

dineshnnaik@iist.ac.in

In optical metrology, the phase difference between interfering fields is analysed through the recorded intensity, interferogram. The techniques to enhance the sensitivity of the phase detection in optical interferometry will be presented with an emphasis on the recent progress achieved in the field of optical metrology. In many amplified sensing schemes such as weak measurements and spectral switches, the out-of-phase interference or the orthogonal projection of the field is shown to induce large shifts in the centroid of the measured intensity distributions. In this talk, we relate those effects to the non-linearity in the phase of interference or phase accumulated by the superposed fields upon interference. The phase of the resultant field is recently shown to vary non-linearly for a linear variation of phase difference between the interfering fields. The detection of phase of interference can have potential application in sensing very small phase differences through amplification. Experimental demonstration using a modified Michelson interferometer will be discussed where the phase shift introduced by one of the beams in a tilted three-beam interference is shown to induce amplification in phase of two beam interference when measured with respect to the third beam acting as reference. The phase of interference exhibiting non linearity is applied to the low coherence interferometry in which case, the nonlinearity in the accumulation of spectral phase of two beam spectral interference as function of path delay is observed.

Holographic Optics for High Functional AR/ VR Displays

Raj Kumar

CSIR – Central Scientific Instruments Organisation, Chandigarh 160030, India

e-mail address: raj.optics@csio.res.in

Augmented reality (AR) and virtual reality (VR) displays are attracting great interest due to their wide range of applications including education, entertainment, training, gaming, healthcare etc. These displays are head worn and therefore demand smallest possible size and minimum weight of the system. AR displays need to have see-through capability so that the virtual information from the display source could be seamlessly merged with the real environment information. This makes design and manufacturing of AR displays more challenging as compared with the VR displays. In AR displays an optical beam combiner is required to combine the virtual information with the real information, while VR displays uses a reflector only to steer the virtual information towards the eyes of the viewer. Parameters of the beam combiner in AR displays need to be optimized so that it does not distort the information of real scene passed through it as well as the virtual information reflected by it towards the viewer. Different technologies such as conventional optics, freeform optics, segmented mirrors, diffractive optics, metasurfaces and holographic optics etc. are being explored and used to improve functionality of the AR/VR displays.

The information of display source guided through an optical waveguide result in compact systems with wearable form as compared to the displays realized with free space optics. Use of conventional optical elements as in-coupler and out-coupler of the waveguide increase size and weight apart from decreased photometric performance. Holographic optical elements also known as holographic optics are very thin, light weight and provide high photometric performance compared with conventional optics. Holographic optics selectively diffracts desired wavelength towards the viewer with high efficiency and allow high transmittance at other wavelengths without introducing any additional aberration in the transmitted light.

Thus, holographic optics provides high functionality for wearable AR/VR displays. We have developed a model based on Bragg degenerate condition for designing and fabrication of high-performance holographic waveguide couplers. Effect of the properties of the display source and the photopolymer materials on the waveguide-based displays are also studied. The fabricated holographic waveguide-based displays and their performance parameters are presented and discussed.

Decoding reflected light for optical metrology

Kallol Bhattacharya

Department of Applied Optics and Photonics, University of Calcutta,JD-2, Sector III, Salt Lake, Kolkata 700106

E-mail: khattacharya@gmail.com

Reflected light from a dielectric or metallic surface contains a host of information related to the reflecting interface. In total internal reflection (TIR) the phase of the reflected amplitude for TE and TM components of polarization are a function of the angle of incidence and the refractive indices of the pair of media involved in the process. It is therefore possible possible to determine the refractive index and its variations of the reflecting interface. Combined with a suitable microscopic imaging system, the evaluation of refractive indices of biological samples are therefore possible. Unlike interferometric methods this technique is nearly independent of the thickness variations of the sample provided that the thickness of the sample greater than a few microns. It will also be shown that transmission and non-TIR reflection measurements can lead to evaluation of the same physical parameters of the reflecting interface including the roughness of metal surfaces with a resolution of tens of nanometers and the complex refractive index of metals. Utilizing normal reflection (instead of TIR) it is possible to achieve the same results. The principles behind these methods will be presented and will be substantiated by experimental results.

Interface engineering materials for Photonics Applications

Sajan D. George, Centre for Applied Nanosciences, Department of Atomic and Molecular Physics, Manipal Academy of Higher Education, Manipal, Karnataka, India – 576 104

sajan.george@manipal.edu

Interface engineering to tailor the properties has been now finding applications in diverse areas including photonics. One of the important surface properties that are currently being exploited is surface wettability which is normally quantified in terms of an equilibrium water contact angle. Inspired by naturally occurring surfaces that exhibit extreme wettability behaviour, researchers are currently employing various physical and chemical methods to create surfaces of desired wettability properties and explore their photonics applications. By replicating the rose-petal inspired surfaces created on the polymer (PMMA) via femtosecond laser patterning onto a flexible soft elastomer (PDMS) using the soft lithographic technique, we demonstrated the surfaces that exhibit superhydrophobicity and underwater superhydrophobicity for the first time [1-2]. Upon incorporating plasmonic nanoparticles via in-situ reduction, we achieved superhydrophobic surface-enhanced Raman scattering substrates [3]. These photonic substrates provide the advantage of concentration enrichment while providing a large Raman scattering enhancement factor that allows the detection of the femtomolar. In pursuit of creating a cost-effective plasmonic droplet analytic assay platform, we demonstrated by exploiting a water contact angle difference of 180^0, it is possible to self-partition a sliding microliter droplet into picoliter droplets [4]. Further, we developed a strategy to optically print the plasmonic particles along with the analyte via optothermal forces and finger-printed molecules via SERS technique [5-6]

References

1. J. E. George. V. M. Rodriguez, D. Mathur, S. Chidangil, S. D. George, Mater. Design 100, 8-18 (2016)
2. J. E. George, C. S. Chidangil, S. D. George, Advanced Materials and Interfaces, 1601088 (2017)
3. J. E. George, V. K. Unnikrishnan, D. Mathur, C. Santhosh, S. D. George Sens. Actuators B: Chem., 272, 485-493 (2018)
4. Peethan, Aravind. M, S. Chidangil, S. D. George, Lab-on-a-Chip, 22, 4110-4117 (2022)
5. K. Monisha, K. Suresh, S. D. George, Laser & Photonics Reviews, 2300303 (2023)
6. K. Monisha, K. Suresh, A. Bankapur, S. D. George, Sensors and Actuator B: Chemical 377, 133047 (2023).

A prophylactic strategy for Global synthesis of Optical and Photonic Systems

Lakshminarayan Hazra

Department of Applied Optics and Photonics, University of Calcutta, JD 2 Sector III Salt Lake, Kolkata 700 106 INDIA

lnhaphy@caluniv.ac.in, lnhazra@yahoo.com

lakshminarayanhazra@gmail.com

Most optical or photonic systems used in practice constitute a lens subsystem that carries out the core optical functions of the system. The term ‘lens’ is used in an extended sense to indicate all refracting, reflecting, and diffractive elements used in the system. In practice, optimal design of these elements pertaining to specific requirements of different applications poses a major challenge in optical system design, except for the trivial cases. Despite the ready availability of powerful optical design software, real success in optical system design calls for the experience and ingenuity of the designer in working out the structural design layout for specific problems.

To facilitate the same, a prophylactic strategy to obtain globally or quasi-globally optimum solutions for the nondeterministic polynomial (NP) time-hard problem of lens design optimization has been developed. The inherent “curse of dimensionality” associated with this problem can be circumvented by taking recourse to a synergistic combination of top-down and bottom-up approaches. The strategy leads to a systematic approach to the global synthesis of optical and electro-optical systems, obviating thereby the need for the use of suboptimal makeshift solutions often used in practice.

The essential point in the whole approach is to realize that a “good” optical system can only be obtained by a combination of “bad” components. However, the defects of these bad components cannot be arbitrary; a good system for a given configuration calls for specific defects in its components or modules. The strategy advocated in this talk does not only lead to globally or quasi-globally optimum solutions for conventional optical systems, but it also provides cues for the efficient use of unconventional optical elements, e.g., aspheric, gradient index (GRIN), diffractive or freeform elements in emerging applications.

For a complex system consisting of several modules or components, our strategy enables optimal modification of part/parts of the system or the system as a whole. Globally optimum values of desirable defects for each of the modules to be modified are determined first with the help of evolutionary programming. Next, a combination of semi-analytical procedures and global optimization techniques are utilized for synthesizing each of the defective modules. At each stage, appropriate measures are incorporated to

prevent undesirable occurrence of higher order aberrations in the system. Lastly, the overall system obtained thereby is re-optimized again with the help of a local optimization algorithm by using the available degrees of freedom.

Our prophylactic strategy, briefly enunciated above, does not only reduce significantly the role of heuristics in optical design, but it also enables a better understanding of the behaviour of modules comprising the optical system. The strategy is based on aberration theory, local optimization algorithms, and evolutionary programming. Some illustrative examples are presented.

References

1. Structural design of multicomponent lens systems, L. N. Hazra, Appl. Opt., Vol.23, 4440 (1984).
2. Simulated Annealing with constrained random walk in structural design of doublet lenses, S. Banerjee and L. N. Hazra, Opt. Eng., Vol. 37, No.12, 3260 (1998).
3. A prophylactic strategy for global synthesis in lens design, L. N. Hazra and S. Chatterjee, Optical Review (Japan), Vol.12, No.3 247 (2005).
4. A novel approach for structural synthesis of zoom systems, L. N. Hazra and S. Pal, Proc. SPIE, Vol. 7786, 778607-1/11 (2010).
5. Foundations of Optical System Analysis and Design, Lakshminarayan Hazra, CRC Press, Taylor & Francis, Boca Raton, Florida, Chapter 21, 711 – 731 (2022).

An in-house constructed confocal fluorescence microscope and its applications

P. Nandakumar and Geetha K. Varier*

Department of Physics, BITS Pilani K. K. Birla Goa campus, Goa 403 726

**Corresponding author: nandan@goa.bits-pilani.ac.in*

Confocal fluorescence microscopy is an indispensable tool widely popular in biology research due to its capability to acquire cross-sectional images of cells and tissues noninvasively. However, the commercial confocal microscopes available today have an inflexible design and are prohibitively expensive for individual laboratories and research groups. Here, we report on the design and development of a cost-effective dual-channel confocal laser scanning fluorescence microscope [1] and its applications in different research areas. In particular, we will discuss the application of the microscope in studying biomolecular transport through nuclear membranes and present results on the nuclear transport of dextran molecules, graphene quantum dots, and gold nanoparticles. We will also show how the same microscope design can be used to carry out photothermal and multiphoton imaging with minimal modifications to the setup [2]. Applications of the microscope in detecting single photon emission from colloidal quantum dots will also be discussed briefly.

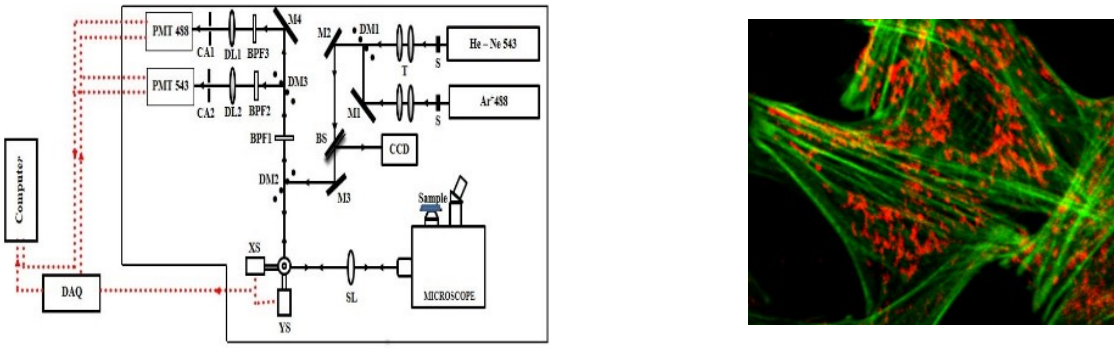

(Left) Optical layout of dual fluorescence channel confocal microscope using lasers having wavelengths 488nm and 543nm. (Right) Image of fluorescently labeled Muntjac skin fibroblast cells (Alexa Fluor 488 phalloidin labeled actin filaments and Alexa Fluor 555 tagged Mitochondria) acquired using a dual fluorescence channel confocal microscope

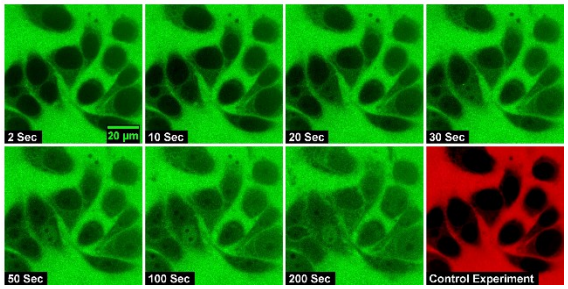

Time-lapse confocal images depicting passive nuclear import of FITC-labeled dextran molecules having a molecular weight of 20 kDa across the HeLa cell nucleus. The frames show an increase in fluorescence intensity inside the nucleus with time.

References

1. P. K. Shakhi, M. M. Bijeesh, Geetha K. Varier, and P. Nandakumar, "An in-house constructed dual-channel confocal fluorescence microscope for biomolecular imaging," OSA Continuum 4, 2177-2192 (2021)
2. Confocal imaging of single BaTiO3 nanoparticles by two-photon photothermal microscopy, M.M. Bijeesh, P.K. Shakhi, S. Arunkarthick, Geetha.K. Varier, P. Nandakumar, Scientific Reports. 7 (2017) 1643

Evolution of a laser-produced Tungsten plasma in the early stages

Amogh M.S., Sebin Sebastian Xavier, Cyril Benny, Pranitha Sankar, Nancy Verma, Reji Philip

Raman Research Institute, C.V Raman Avenue, Sadashivanagar, Bangalore 560080, India

reji@rri.res.in

In this work, a nanosecond pulsed laser (1064 nm, 7 ns) is used to generate laser-produced plasma (LPP) from a Tungsten target, which is then analysed using several techniques such as optical emission spectroscopy, laser plasma interferometry, imaging, and shadowgraphy. The ambient pressure range is set between 10-400 Torr. Measurements show that plasma temperature and number density are significantly affected by the ambient pressure. The plume expansion dynamics is analysed using linear, shockwave, and drag models (measured using time-resolved imaging). Spectral analysis reveals a strong correlation between the number densities obtained from Saha-Boltzmann and Stark broadening of the H-alpha line (Balmer series). The interferometric method yields number density measurements even when strong continuum emission is present from free electrons. Shadowgraphy is used to observe and measure

shockwave expansion at atmospheric pressure. Interferometric and imaging results imply that the plasma does not conform to the two-layer model, with radial electron density and plasma emission inhomogeneities arising beyond 75 Torr due to shockwave formation. Despite the inhomogeneities, the plasma remains in Local Thermodynamic Equilibrium (LTE) during the observed time window up to 1 μs. Since for Tungsten the electron impact parameters are unknown, H-alpha is recommended for a more straightforward estimation of number densities, in consideration of the strong linear relationship between the number densities obtained from the Saha-Boltzmann method and Stark broadening of the H-alpha line.

Semiconductor LIPSS: New Insights and Applications

*Venugopal Rao Soma**

*Advanced Centre of Research in High Energy Materials **(ACRHEM),***

DRDO Industry Academia – Centre of Excellence (DIA-COE),

University of Hyderabad, Hyderabad 500046, Telangana, India

**soma_venu@uohyd.ac.in*

Laser-induced periodic surface structures (LIPSS) on semiconductors are a fascinating and developing field with potential applications, for example, in the fields of antireflective interfaces, anti-counterfeiting, self-cleaning, anti-fog, and anti-bacterial applications [1-6]. Typically, femtosecond (fs)/picosecond (ps) laser pulses are utilized to create these nanostructures. Herein we discuss the formation of LIPSS achieved using fs/ps pulses irradiation on GaAs and Silicon. Ensuing applications [7-12] from these exotic nanostructures [e.g., sensing hazardous molecules using the surface-enhanced Raman spectroscopy (SERS) technique] will be discussed in the presentation.

Acknowledgments: DRDO is acknowledged for support through ACRHEM [ERIP/ER/1501138/M/01/319/D (R&D)]. Venugopal Rao Soma also thanks the University of Hyderabad for support through the Institute of Eminence (IoE) project UOH/IOE/RC1/RC1-2016. The IoE grant was gotten through notification F11/9/2019-U3(A) from MHRD, India.

References

1. J. Bonse, S. Gräf, *Nanomaterials,* 11(12), art. no. 3326 (2021).
2. J. Bonse, *Nanomaterials*, 10(10), art. no. 1950 (2020).
3. J. Bonse, S. Gräf, *Laser and Photonics Reviews*, 14(10), art. no. 2000215 (2020).
4. C. Florian et al. *Journal of Laser Applications*, 32(2), art. no. 022063 (2020).
5. J. Bonse et al., *IEEE J. Selected Topics in Quant. Electronics*, 23(3), 7581030, pp. 109-123 (2016).
6. J. Bonse et al., *Journal of Laser Applications*, 24(4), art. no. 042006 (2012).
7. A. Mangababu et al., *Applied Surface Science*, 589, art. no. 152802 (2022).
8. A. Mangababu, et al. *Surfaces and Interfaces,* 36, 102563 (2023).
9. K.R. Kumar et al. *J. Phys. D: Appl. Phys.,* 55, 405103 (2022).
10. A. Mangababu, et al. *Optics Letters,* 48(21), 5539-5542 (2022)

Phosphor materials for lighting and security application

P R Biju

Mahatma Gandhi University, India

Phosphor-converted white LEDs caught the attention of researchers in the field of solid-state lighting because of their remarkable properties. A commonly acceptable way of fabrication of pc-WLEDs is by combining YAG: Ce^{3+} yellow phosphor and InGaN blue LED chip using organic binders for white light generation but it suffers chromaticity shift and reduction of luminous efficacy due to thermal and chemical degradation which adversely affect the longevity of WLEDs. Also, the lack of red component in Ce-YAG phosphor results in poor colour rendering index (CRI) and high correlated colour temperature (CCT). Phosphor in Glass (PiG), an inorganic colour converter with excellent heat resistance have been proposed. Several PiG systems with the combination of YAG:Ce^{3+} phosphor with tellurite and silicate glasses for lighting applications with appreciable luminescent properties have been reported. The excellent chemical stability, luminescent properties, heat resistance and high transparency of PiG establish the potential as an inorganic colour converter in WLEDs and other lighting devices.

The development of luminescent security ink for anti-counterfeiting applications is one of the most significant application of phosphors. Tagging anti-counterfeiting labels using luminescent materials to the products that need to be safeguarded its market challenges. When compared to standard fluorescent inks, which generally yield visible emission when excited to UV irradiation, there are numerous potential advantages to using RE doped luminescent security inks for anti-counterfeiting applications. Furthermore, when compared to commercial fluorescent dyes, RE doped luminescent inks exhibit both down conversion and upconversion processes in a single host lattice, making them intrinsically more difficult to copy. Another advantage of RE doped inks over commercially available fluorescent dyes is that the former offer sharper transitions without photo bleaching. Furthermore, RE doped inks can be designed to give the right colour rendering index only at specified excitation power densities, making authentic read conditions even more difficult to replicate.

Ultrafast emergence of an e-h quantum liquid phase in photoexcited low-dimensional MoS_2

Sivarama Krishnan[1,2], Pritha Dey[1], Vikash Mishra[1], Tejendra Dixit[3] and Anubhab Sahoo[1]*

[1]Department of Physics, Indian Institute of Technology Madras, Chennai, Tamil Nadu

[2] Quantum Center for Diamond and Emerging Materials group, Indian Institute of Technology Madras, Chennai, Tamil Nadu

[3]Optoelectronics and Quantum Devices Group, Department of Electronics and Communication Engineering, Indian Institute of Information Technology Design and Manufacturing, Kancheepuram, Chennai, Tamil Nadu

Email: srkrishnan@iitm.ac.in*

In transition metal dichalcogenides (TMDCs) family, MoS_2 is a physically and chemically stable and excellent material due to strong spin orbit coupling and large exciton binding energy. In this system, photo-induced dynamics has mostly been studied from the perspective of individual quasi-particles – excitons, bi-excitons or, even, trions - their formation, evolution and decay. The role of multi-body and exciton dynamics, the associated collective behaviour, condensation and inter-excitonic interactions remain intriguing and seek attention, especially in room-temperature scenarios which are relevant for device applications [1]. In this work, we show evidence for the formation and decay of an unexpected electron-

hole quantum liquid phase at room-temperature on ultrafast picosecond timescales in multi-layer MoS_2 nanoparticles through femtosecond broadband transient absorption spectroscopy. Unlike monolayer MoS_2, nanoparticles synthesized via femtosecond laser ablated in liquid (fs-PLAL) shows these features at room temperature. Our studies reveal the complete dynamical picture: the initial electron-hole plasma (EHP) condenses into an quantum electron-hole liquid (EHL) phase which typically lasts as long as 10 ps, revealing its robustness, whereafter the system decays through phonons. The formation of the EHL phase has an important consequence: the strong interaction between the excitons decreases Coulomb screening leading to a renormalization of single exciton energies. Our measurements capture this essential bandgap renormalization (BGR) in transient absorption spectra over a wide range of pump fluences; the BGR can be as high as 50 meV, as discerned from the time-dependent shift in excitonic resonances [2]. Although the total BGR is a cumulative effect of the quantum EHL phase along with the EHP phase and phonons, we employ a successful physical model to extract each of these contributions using a set of coupled nonlinear rate equations governing the individual population of these constituent phases.

References

1. Pritha Dey, Tejendra Dixit, Vikash Mishra, Anubhab Sahoo, Cheriyanath Vijayan and Sivarama Krishnan, "Emergence and relaxation of an e-h quantum liquid phase in photoexcited MoS2 nanoparticles at room temperature", Advanced optical materials, accepted (2023)
2. G. Beni and T. M. Rice, " The Electron-Hole Liquid in Semiconductors: Theoretical Aspects" Solid State Phys - Adv Res Appl. 32(C):1-86, (1978).

THz Acoustic Phonon Amplification in Quantum Wells

Rajeev N Kini

Indian Institute of Science Education and Research Thiruvananthapuram, Kerala, India

Email ID: rajeevkini@iisertvm.ac.in

An intense source of coherent phonons, a SASER similar to a laser, is useful for various applications like modulation of light at THz frequencies, generation of high-frequency electric signals, and non-destructive evaluation of nanostructures. For such applications, electrical methods for phonon generation are preferred over optical methods owing to the convenience electrical methods provide. Acoustic phonon generation and amplification can be achieved by a Cerenkov process in a semiconductor structure when the electron drift velocity exceeds the velocity of sound. This process can lead to large amplification factors and this process has been studied theoretically.[1] However, experimental studies on high-frequency phonon generation using the Cerenkov process are scarce. The amplification of $\approx$ 0.4 THz acoustic phonons in a superlattice (SL) has been previously reported using electrical current in the ampere range, and gain coefficients of $\approx 10^4$ cm^{-1} were achieved.[2] In this talk, we demonstrate the amplification of $\approx$ 0.45 THz coherent acoustic phonons in a double quantum well structure embedded in an acoustic phonon cavity. Acoustic phonons generated by the impulsive excitation of an SL by near-IR femtosecond pulses are amplified in a 2λ acoustic phonon cavity. The cavity encloses a double quantum well (DQW), and the DQW is placed such that the maximum phonon displacement of the cavity phonon mode occurs at the center of the quantum wells. This ensures strong coupling between the drifting electrons and the confined phonons. The strong coupling facilitates the amplification of the cavity phonon mode when electrical current flows along the propagation direction of the phonons. Since the 2λ cavity is thin ($d \approx 23$ nm), it is easy to achieve electron drift velocity, $v_d = \mu V/d$ exceeding that of the phonon velocity even for modest applied voltages ($V \approx 0.5$ V) , which results in small electric currents in the structure ($\approx$ mA). We demonstrate phonon gains of the order of $\approx 10^6$ cm^{-1} for currents in the mA range.

References

1. Komirenko, S. M., Kim, K. W., Demidenko, A. A., Kochelap, V. A. & Stroscio, M. A. Generation and amplification of sub-THz coherent acoustic phonons under the drift of two-dimensional electrons. *Phys. Rev. B* **62**, 7459–7469 (2000).
2. Shinokita, K. *et al.* Strong Amplification of Coherent Acoustic Phonons by Intraminiband Currents in a Semiconductor Superlattice. *Phys. Rev. Lett.* **116**, 075504 (2016).

On-Chip THz Topological Photonics for 6G to XG Wireless

Ranjan Singh[1,2,*]

[1]*Division of Physics and Applied Physics, School of Physical and Mathematical Sciences, Nanyang Technological University, 21 Nanyang Link, Singapore 637371, Singapore.*

[2]*Centre for Disruptive Photonic Technologies, The Photonics Institute, Nanyang Technological University, 50 Nanyang Avenue, Singapore 639798, Singapore.*

[*]*E-mail: ranjans@ntu.edu.sg*

Global digitalization and the recent rise of artificial intelligence-based data-driven applications have directed their vectors towards terabits per second (Tbps) communication links. The fast-evolving 5G communication network cannot fulfill this demand due to several technological challenges, including bandwidth scarcity, which has stimulated innovative technologies with a vision of 6G communication. Semiconductor and emerging quantum material-based Terahertz (THz) micro-nanotechnologies have been identified as critical candidates for the emerging 6G communication with the potential to provide ubiquitous connectivity and remove the barrier between the physical, digital, and biological worlds. Nonetheless, the existing THz silicon photonic communication devices suffer from backscattering, bending loss, free space path loss and limited data speed. Here, I will describe a new class of quantum-inspired on-chip THz photonic topological devices consisting of low-loss, broadband single channel 160 Gbit/s interconnect and 100 Gbps wireless devices. Silicon topological photonics will pave the path for augmentation of CMOS-compatible hybrid electronic-photonic driven terahertz technologies, vital for accelerating the development of future 6G to XG communications that would empower societies with real-time terabits per second wireless connectivity for network sensing, holographic communication, cognitive internet of everything, and massive digital cloning of the physical and the biological world.

Compact Multiplexers/ De-multiplexers for On Chip Optical Interconnects

Enakshi Khular Sharma

Formerly at Department of Electronic Science,

University of Delhi South Campus, New Delhi-110021

enakshi54@yahoo.co.in

The physical barrier of the transistor dimension has led the technology towards multicore processors. Such multicore processors require a large electrical interconnect network which consumes ~80% of the microprocessor power and cannot meet the rapidly growing bandwidth requirement. Hence, Silicon-on-insulator (SOI) optical waveguide interconnects are emerging as a replacement to the on-chip and inter-chip copper electrical interconnects. CMOS technology has enabled the integration of SOI photonic

circuits with electronic circuits on the same substrate. The compact and high-density photonic device integration provides a compact optical interconnect system with large bandwidth and low power consumption [1]. To increase the bandwidth further and decrease the footprint, a multi-mode SOI trunk waveguide can be used with each mode connecting an individual data channel and multiplexers/de-multiplexers to couple/de-couple each channel and the shared multimode bus waveguide. The operation of the multiplexer/de-multiplexer is based on evanescent coupling between the fundamental mode of an input single mode waveguide and the selected mode of the trunk waveguide [2].

It is possible to couple into two modes of a trunk waveguide simultaneously in a single section by using two input waveguides collaterally arranged with the trunk waveguide instead of sequential coupling [3]. This enables the design of compact multi-channel (de) multiplexers. Further, as the silicon waveguide can support two orthogonally polarized modes, TE and TM, it is possible to double the channel capacity of an interconnect by using both the polarized modes [4]. To achieve a further increase in the bandwidth wavelength division multiplexing technique can also be added, employing different wavelengths (1.55 μm and 2 μm) as individual information carriers. [5].

References

1. D. A. B. Miller, "Rationale and challenges for optical interconnects to electronic chips", *Proc. IEEE*, 88(6), 728–749 (2000).
2. E. K. Sharma, J. P. Nath, N. Dhingra, "Coupled mode theory and coupled mode photonic devices: a review", *Asian Journal of Physics*, vol. 30, 1-18 (2021).
3. J. P. Nath, N. Dhingra, G. J. Saxena, and E. K. Sharma, "Compact Mode Division (de)Multiplexer Based on Collaterally Coupled SOI Waveguides", *IEEE Photon. Technol. Lett.,* 32(10), 595–598 (2020).
4. J. P. Nath, N. Dhingra, G. J. Saxena and E. K. Sharma, "SOI based compact mode- and polarization-division multiplexer for on-chip optical interconnects: design and simulation", *Applied Optics*, Vol. 61, 4195-4203 (2022).
5. J. P. Nath, G. J. Saxena, and E. K. Sharma, ""Silicon-based compact eight channel wavelength and mode division (de)multiplexer for on-chip optical interconnects", *Applied Optics*, vol. 62, 6380-6388 (2023).

3D Plasmonic structure on the surface of a tapered optical fiber for the detection of trace chemicals

Gautam Das

Lakehead University, Department of Physics

955 Oliver Road, Thunder Bay, Ontario P7B 5E1, Canada

gdas@lakeheadu.ca

We manufactured a 3-dimensional plasmonic structure using gold nanorods (GNRs) on a tapered optical fiber surface, known as an optical fiber probe, to detect and quantify chemicals at a lower concentration. GNRs were deposited using Optical Tweezing, forming a unique grating-like structure on the surface of the tapered fiber. The distribution of the GNRs can be manipulated by tweezing process. Surface Enhanced Raman spectroscopy (SERS) technique was used to obtain the spectrum of a chemical adsorbed on the probe.

The presentation includes the manufacturing process of the probe and its uses to detect chemicals such as (i) Crystal Violet - widely used to prevent diseases and infections in fish; (ii) Rhodamine 6G (R6G)

– widely used as a food colourant in spices, candies, and sweets, (iii) Xanthohumol – a compound present in hops, which is an essential ingredient in the brewery industry, and (iv) Glyphosate – a herbicide used to control and eliminate weeds. I will also present the characteristics of the substrate, stability, sensitivity and repeatability. The developed technology can be extended in detecting other chemicals of interest, most importantly, chemicals responsible for climate change and affecting human health.

The plasmonic structure can be used to develop a portable photonic device for detecting chemicals, which will be compact and cost-effective.

Funding: I want to acknowledge the financial support of the Natural Sciences and Engineering Research Council of Canada (NSERC) and the Canada Foundation for Innovation (CFI).

Acknowledgement: I would also like to acknowledge all present and past postdoctoral fellows and graduate and undergraduate students in the research group for their assistance in the lab activities. More importantly, Ms. Navneet Kaur, Ph.D. candidate and Dr. Joshua Trevisanutto for their contributions.

Combining Metaoptics and Optics for Microendoscopy

Shanti Bhattacharya

Department of Electrical Engineering, IIT Madras, Chennai 600036

shanti@ee.iitm.ac.in

Miniaturisation of optics is required for a variety of applications. In many cases, micro-optics could be used. However, as systems shrink in size, it becomes harder to achieve the desired optical transformation with refractive optics. Metaoptics has the advantage of being both compact, as well as being able to carry out tasks not possible with conventional optics. Multi-level phase elements are simpler to fabricate than diffractive optical elements. In this talk, I will present the basic ideas of metaoptics and how they can be fabricated. This will be followed by a discussion on the challenges of designing optics for a system with limited space, such as a microendoscope. The talk will end with a means by which to design a system with tight constraints that combines metaoptics and conventional optics to achieve imaging.

Reflectionless propagation of beams through a stratified medium

Sounak Sinha Biswas[1], Subhasish Dutta Gupta[1,2]

[1]Indian Institute of Science Education and Research, Kolkata

[2]Tata Institute of Fundamental Research, Hyderabad, email: sdg@tifrh.res.in

Since the pioneering work of Kay and Moses [1] on reflectionless potentials, there have been interesting demonstrations of total transmission of wave packets through their two-parameter realization [2], otherwise known as the Poschl-Teller ($sech^2$) potential. The quantum mechanical interpretation ensures the total transparency of the potential with respect to an incoming particle irrespective of the initial kinetic energy. The optical analogue was studied in detail both theoretically and experimentally keeping in view the practical applications [3, 4] as antireflection coatings. It was shown that a stratified medium with reflectionless potential profile can ensure omnidirectional and broadband near-complete transmission of plane waves for both TE and TM polarizations.

The omnidirectional character of the reflectionless profile motivated us to look at the scattering (reflection and transmission) of a finite beam (retaining its vector character) through the inhomogeneous film representing the profile with or without substrate. Recall that by virtue of the angular spectrum decomposition a beam can be considered as a collection of plane waves with wave vectors on and around the central wave vector direction. Recently such an approach was applied to show giant Goos-Hänchen

shift in a stratified medium supporting bound states in continuum [5]. We show that Gaussian and Laguerre-Gaussian beams can be transmitted through the film with <1% reflective losses in most scenarios (see Figure 1). We also discuss the superlative performance of our proposed profile in preserving the beam shape during transmission, and compare these results to a conventional $\lambda/2$ antireflection coating. Furthermore, we demonstrate large lateral and transverse shift of the beam for beams carrying orbital angular momentum, while linearly polarized beams exhibited only Goos-Hänchen shift.

Figure 1. Intensity distribution of incident (a), reflected (b) and transmitted (c) beams, for TE-polarized Gaussian beams incident at 30^0 on a reflectionless potential. The same results for a Laguerre-Gaussian beam (d, e, f) incident at 60^0. The red dot indicates the beam centroid.

References

1. Kay and H. E. Moses, Reflectionless Transmission through Dielectrics and Scattering Potentials, *Journal of Applied Physics,* 27(12):1503-1508, 1956.
2. N. Kiriushcheva and S. Kuzmin, Scattering of a Gaussian wave packet by a reflectionless potential, *American Journal of Physics,* 66(10):867-872, 1998.
3. S. D. Gupta and G. S. Agarwal, A new approach for broad-band omnidirectional antireflection coatings, *Opt. Express,* 15(15):9614-9624, 2007.
4. L. V. Thekkekara, V. G. Achanta, and S. D. Gupta, Optical reflectionless potentials for broadband, omnidirectional antireflection, *Opt. Express,* 22(14):17382--17386, 2014.
5. S. S. Biswas, G. Remesh, V. G. Achanta, A. Banerjee, N. Ghosh, and S. D. Gupta, Enhanced beam shifts mediated by bound states in continuum, *J. Opt.,* 25(9): 095401, 2023.

Reconfigurable Indefinite Nanophotonics

Harish N S Krishnamoorthy[1]

[1]*Tata Institute of Fundamental Research Hyderabad*

email: harishk@tifrh.res.in

Indefinite media supporting electromagnetic states with large wavevectors and featuring a hyperbolic isofrequency surface have been shown to exhibit a variety of peculiar properties such as negative refraction, broadband Purcell enhancement as well as nanoscale confinement of light. In this talk, I will discuss how the use of phase change materials in the nanostructure is a very effective strategy to tune these properties on-demand. Specifically, I will give examples of volatile and non-volatile hyperbolic metamaterials where the topology of the optical isofquency surface can be reconfigured to harness effects such as toggling between negative and positive refraction as well as dynamic control of emission rate of quantum emitters.

White Organic Light Emitting Diodes: Role of excimer, electromer and exciplex

K. N. Narayanan Unni

Centre for Sustainable Energy Technologies (C-SET)

CSIR-National Institute for Interdisciplinary Science and Technology

Thiruvananthapuram-695 019

unni@niist.res.in

Although information displays using Organic Light Emitting Diodes (OLEDs) have become a commercial reality, solid state lighting using OLEDs is yet to make a substantial market penetration. Cost is the main concern and the expensive luminescent dopants and complicated multilayer structures are the factors contributing to the high cost. Hence alternative device structures which are cost-effective are required. In the present talk, details of investigations using excimer, electromer and exciplex structures are presented.

Thermal evaporation technique is used to fabricate organic thin films and blends thereof where excimer, electromer and exciplex emission can be expected. It is further shown that the rate of evaporation and dipolar nature of the constituent layers influence excimer and electromer emissions respectively leading to near-white emission while proper management of exciplex excitons can lead to the same in exciplex structures.

References:

1. Reversible Shift from Excitonic to Excimer Emission in Fluorescent Organic Light-Emitting Diodes: Dependence on Deposition Parameters and Electrical Bias, Anjaly Soman, Anjali K. Sajeev, Kavya Rajeev and Narayanan Unni K. N., ACS Omega 2020, 5, 3, 1698–1707
2. White Organic Light-Emitting Diodes from Single Emissive Layers: Combining Exciplex Emission with Electromer Emission, C. K. Vipin, Atul Shukla, Kavya Rajeev
3. Monirul Hasan, Shih-Chun Lo, Ebinazar B. Namdas, Ayyappanpillai Ajayaghosh, and
4. K. N. Narayanan Unni, J. Phys. Chem. C 2021, 125, 41, 22809–22816
5. Blue Emitting Exciplex for Yellow and White Organic Light-Emitting Diodes, Kavya Rajeev, Chenusseri Kavalan Vipin, Anjali K. Sajeev, Atul Shukla, Sarah K. M. McGregor, Shih-Chun Lo, Ebinazar B. Namdas, K. N. Narayanan Unni, Frontiers of Optoelectronics 2023 (in press)

LIGO-India: A route to innovation

Sunil S

Institute for Plasma Research, Bhat, Gandhinagar, Gujarat. 382428

sunil@ipr.res.in

The acronym of Laser Interferometer Gravitational wave Observatory is LIGO. LIGO is an instrument to detect signal capable of distorting the space resulting due to cataclysmic event which occurred billions of years ago [1]. The principle behind LIGO is a modified Michelson interferometer which has been made so sensitive that it can measure a distance of 10^{-18}m [2]. To make the detector so sensitive, efforts are made and being made to reach the fundamental limits of science and technology [3].

LIGO is a multi-faceted discipline. It deals with the marvels of engineering like fabrication of large volume vacuum vessel to hold pressure less than 10^{-9}mbar [4] to, alignment of optical components to the precision of few millimeters kept few kilometers away. High power lasers making round trips in the interferometer cavity tends to deform the optical components which causes instabilities and dysfunction the operation of detector, mitigating techniques are applied so that LIGO operations are smooth [5]. Control systems provide active feedback to make the instrument stable and working.

LIGO-India will play an important role in trying to understand the place where we live and also supplement us with lots of new ideas.

References

1. https://www.ligo.caltech.edu/
2. https://dcc.ligo.org/public/0036/G070474/000/G070474-00.pdf
3. https://www.ligo.org/science/Publication-O1Noise/flyer.pdf
4. https://dcc.ligo.org/public/0141/G1700589/001/SocalAVS%20Talk_rev.003.pdf
5. https://arxiv.org/ftp/arxiv/papers/1411/1411.4547.pdf

A Nonlinear Image Authentication System Based on Double Fractional Mellin Transform

*Sachin[1], Phool Singh[2], Kehar Singh[3]**

[1]Department of Mathematics, IITHS, Kurukshetra University, Kurukshetra 136119

[2]Department of Mathematics, SoET, Central University of Haryana, Mahendergarh 123031

[3]Optics and Photonics Center, Indian Institute of Delhi, New Delhi 110016

**Kehar Singh: e-mail, keharsiitd@gmail.com*

A dual-user image authentication algorithm is proposed, based on the double Fractional Mellin Transform (FrMT). A security analysis of the nonlinear cryptosystem based on the single FrMT shows its vulnerability. In the proposed system, polar decomposition and sparse multiplexing are additionally applied to generate a ciphertext. Due to sparsification, the decryption does not reveal sufficient information regarding the plain-text, and an authentication step is required for validating the retrieved images. During the encryption process, polar decomposition generates two private keys that are used for authentication. The system has a large key space and is robust against several attacks such as noise-, occlusion-, brute force -, plain-text-, and special iterative attacks. A comparison is carried out with a similar existing scheme. Simulation results carried out using MATLAB^{TM} 2020a demonstrate the robustness and efficacy of the proposed algorithm. and may be extended to color images, audio, and video in future. The system can be a potent system for use in corporate offices, banks, hospitals, and government agencies. etc.

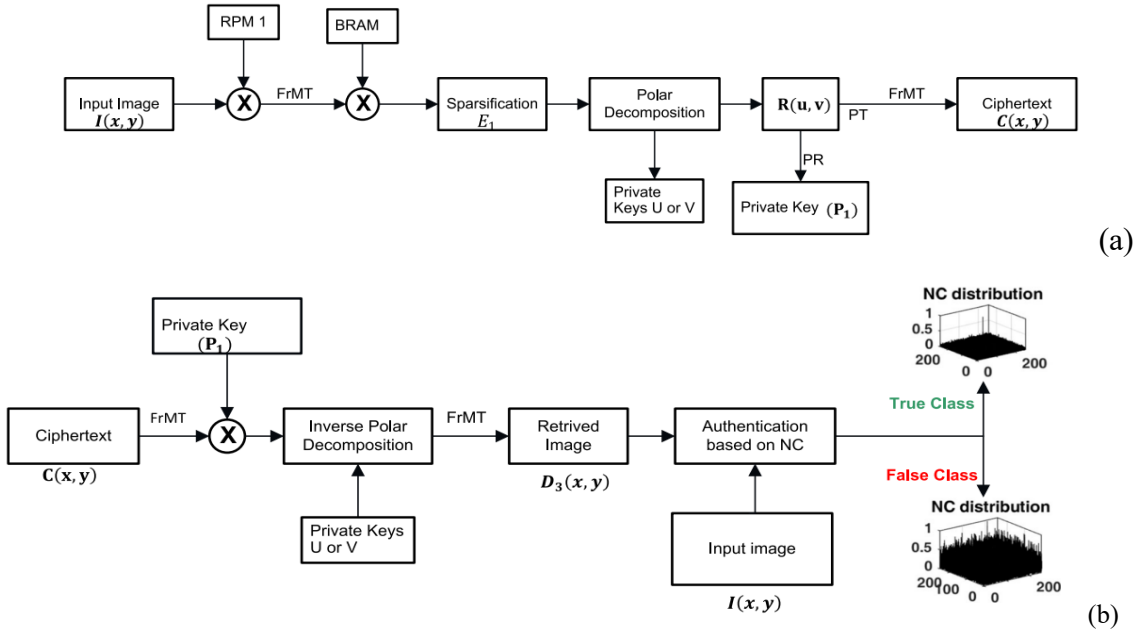

Fig: (a) Encryption process, BRAM (Binary Random Amplitude Mask, (b) Decryption-cum-authentication process, NC (Nonlinear Correlation) (Ref.1)

References

1. Sachin, Phool Singh, Kehar Singh, *Nonlin. Dynamics,* 111, 13579-13600 (2023).

Moving towards Pb/s transmission links

Deepa Venkitesh
IIT Madras, India

Proliferation of wireless technologies and the internet has led to an unprecedented demand in capacity in the backbone optical communication networks. Optical communication links have transitioned from intensity modulated direct detection systems to coherent communication in the long-haul links, and similar trends are observed in the recent years even in short distance links.
In this talk, we will review the progression of methods and schemes to achieve very high-capacity transmission, challenges faced in such implementations and some mitigation strategies. We will also discuss the prospects from the Advanced Optical Communication Testbed project, funded by the Department of Telecommunication, Govt. of India.

Understanding the optical materials for optoelectronic applications

Dr. Suhas M. Jejurikar,

National Centre for Nanosciences and Nanotechnology, University of Mumbai,

Kalina Campus, Santacruz (E), Mumbai 400092

e-mail: suhas.j@nano.mu.ac.in

Zinc oxide is one of the important materials for several optoelectronic applications. Hence the material is explored not only for the applications point of view but also to in rich the fundamental understanding of

materials. Concerning zinc oxide the defect related intrinsic optical behavior is of interest since from the past, where the assignment of emission (optical) properties to particular the defect is a controversial matter since the identification of crystal defects is not an easy task. Thus the first part of the talk covers deals with two types of ZnO microstructures with different defect morphologies by measuring their temperature dependent photoluminescence properties to quantify the contribution of the defects on observed optical emissions via theoretical modelling of the experimental observations. The second part of the talk discusses the epistructures of Ga_2O_3/ZnO/Ga_2O_3 (modified by changing the ZnO layer thickness) grown on c-Al_2O_3 substrate using pulsed laser deposition to understand the adequate UV photoemission observed from these epistructures. Both the observations are highly encouraging considering use of ZnO to be considered especially when the optoelectronic applications are considered.

Patterned Surfaces for Photonic Sensing and Imaging

R. Vijaya

Department of Physics and Centre for Lasers and Photonics

Indian Institute of Technology Kanpur, Kanpur 208016, Uttar Pradesh, India

rvijaya@iitk.ac.in

Surface-based optical functionalities are gaining traction due to the multiple advantages they can provide, such as smaller size, lighter weight, wider field of view and options for choosing wider/narrower wavelength sensitivity. The type of functionality is decided by the patterns present on the surface, in terms of their size, shape, spacing and refractive index. While some patterned surfaces are made quite easily by soft imprint lithography, there are other options as well for their fabrication.

This seminar is confined to the discussion on patterned surfaces and metasurfaces, specifically designed for the two functionalities of sensing and optical imaging. The type of unit cell chosen, and its size and role in providing the advantages of sensing small changes in refractive index will be discussed using distinctly different designs. When it comes to imaging applications, glass-based lenses that are commonly used for this purpose are superior in quality. However, they cannot be reconfigured for a specific purpose, such as imaging over a curved surface or to obtain multiple images over a small area. Patterned surfaces made with innovative shapes can enable such applications. One design from our work will be discussed in this context.

References

1. D. De and R. Vijaya, Dielectric Metasurfaces for Refractive Index Sensing towards Anemia Detection, *Front. Photonics*, 4, 1234060 (2023).
2. V. Biswas and R. Vijaya, Plasmonic metasurface with hexagonal nanobumps on flexible substrate for sensing, *Workshop on Recent Advances in Photonics (WRAP)-2023*, Allahabad, 7-9 Dec 2023.
3. G. Joshi and R. Vijaya, Millimeter-sized lens array on polymer surface, *Workshop on Recent Advances in Photonics (WRAP)-2023*, Allahabad, 7-9 Dec 2023.

Holographic imaging with quantum and classical light

*Rakesh Kumar Singh**

Laboratory of Information Photonics and Optical Metrology, Department of Physics, Indian Institute of Technology (Banaras Hindu University), Varanasi, 221005, Uttar- Pradesh, India

**Corresponding author: krakeshsingh.phy@iitbhu.ac.in*

Holography uses an interferometric approach to record and reconstruct the complex field. Availability of high-quality sensors and computational facilities have revolutionized the area through digital holography (DH) where the recorded hologram is reconstructed digitally rather than using optical means. DH reconstructs complex information and performs digital depth focusing [1]. Usually, holograms are recorded with interference of the two beams and it relies on the second order field correlation of the interfering sources. Recently, quantum-correlated light is used to exhibits peculiar interference effect and overcome certain limitations of the conventional imaging and the holography [2-4]. In particular, the intensity interferometers have been demonstrated with variety of quantum and classical sources for optical imaging. Such trends have inspired researchers to explore interference with higher order correlations. Here, we discuss holography with higher order correlations, particularly the fourth order field correlation with the quantum and classical light. Some of our recent works on the holography with higher order correlations will be discussed. These imaging systems with fourth order field correlations offers new opportunity for imaging through turbulence and in the low light condition such as imaging of target with low radar cross section (RSC).

Acknowledgment: RKS thanks the SERB (CORE/2019/000026) for support.

References

1. U. Schnars and W. Jueptner, *Springer* 2005
2. G. Thekkadath et.al., *Science Advan.* 9, eadh1439 (2023)
3. R. V. Vinu et.al., *Optica* 7,1697-1704 (2020)
4. T. Sarkar et. al., *Progress in Optics* 68, 101-181 (Ed. T. D. Visser) 2023

Quantum Technologies with Bright Squeezed Light

Ashok Kumar

Department of Physics

Indian Institute of Space Science and Technology (IIST), Thiruvananthapuram, Kerala, India

e-mail: ashokkumar@iist.ac.in

Quantum technologies harnessing squeezed light have emerged as powerful tools for revolutionizing quantum communication, sensing, and computation. This talk will explore our efforts to utilize two-mode bright squeezed light states for information encoding and quantum-enhanced sensing. It will delve into the generation of squeezed light in the laboratory through a nonlinear optical process involving lasers and hot atoms. Subsequently, we will demonstrate the EPR paradox using these beams to show their entanglement. The talk will then elaborate on the critical role of these entangled beams in information encoding through manipulation of their spatial correlations. Finally, we will highlight some advancements in quantum-

enhanced sensing, including a demonstration of sensitivity enhancement in plasmonic sensors employed in transmission-based measurements. These sensors hold immense potential for biological and chemical sensing, offering a unique opportunity to translate these advancements into practical applications.

Towards a trapped ion-based all-optical portable atomic clock

Arijit Sharma[1,2,*]

[1]*Department of Physics, Indian Institute of Technology Tirupati, Yerpedu-517619, A.P., India*

[2]*Center for Atomic, Molecular, and Optical Sciences and Technologies, Indian Institute of Technology Tirupati, Yerpedu-517619, A. P., India*

**Corresponding author: arijit@iittp.ac.in*

Optical clocks are the epitome of precise timekeeping. The efficiency and reliability of a clock have always been associated with periodicity (precision) and the ability to tell the correct time (accuracy). The key components of a clock are the oscillator, counter and frequency reference. Optical atomic clocks provide the highest level of sensitivity based on optical transitions in neutral atoms or trapped atomic ions. Such clocks define international timescales, provide a basis for testing the time invariance of fundamental constants and lead to the search for new physics beyond the Standard Model. Optical clocks have the potential to surpass their microwave counterparts in performance due to higher Q-factor ($\nu_0/\Delta\nu$, where ν_0 is the central frequency and $\Delta\nu$ is the linewidth of the transition) which ensures higher stability.
Portable atomic clocks have revolutionized applications in GPS (Global Positioning System) and navigation systems, civil and strategic communication [1,2], power grids and radar synchronization, etc. With the increasing use of field-deployable atomic clocks and frequency standards, many commercial and strategic applications including sensing, communications and navigation, are getting a tremendous technological boost. It is imperative to develop technologies to enable the development of next-generation portable atomic clocks utilising optical transitions in trapped cooled ions/atoms for superior performance in positioning, navigation and timing applications compared to warm atomic vapor based clocks.

At IIT Tirupati, we are engaged in developing the next generation all-optical trapped ion based portable frequency standards using optical transition in $^{40}Ca^{+}$ (calcium ion) for positioning, sensing and precision timing applications. We are working towards development of compact laser sources, electronics, and miniaturized vacuum systems for the development of an all-optical trapped ion-based portable frequency standard. We shall present a brief overview of our research activities at IIT Tirupati in this domain and discuss some of the challenges and opportunities related to a host of quantum technology applications using such portable all-optical atomic clocks. Arijit Sharma expresses gratitude for financial support from CAMOST and IIT Tirupati for the trapped ion atomic clock project.

References

1. Marlow et al., *IEEE Transactions on Ultrasonics, Ferroelectrics, and Frequency Control* 68, 2007-2022 (2021).
2. N. Poli et. al., *La Rivista del Nuovo Cimento* 36, 555-624 (2013).

Exploring the emission dynamics of cavity coupled quantum emitters

Rajesh V Nair

Laboratory for Nanoscale Optics and Meta-materials (LaNOM), Department of Physics,

Indian Institute of Technology Ropar, Rupnagar, Punjab 140001 India

e-mail: rvnair@iitrpr.ac.in

Quantum emitters (QEs) are pivotal in developing cutting-edge quantum technologies, including quantum computing, imaging, and sensing. The building blocks of quantum technologies require exceptional properties of QEs, such as brightness, stable photoluminescence (PL), optical addressability, and coherent manipulation. The NV centers in diamonds have emerged as promising QE with stable emission dynamics, long spin coherence time, and reproducibility even at room temperature, making NV ideal for single-photon sources. The most remarkable feature of NV center's is their ability to emit single photons with high reproducibility when transitioning between their electronic spin states, making NV centers ideal single-photon sources. Additionally, the long spin coherence times, on the order of milliseconds, allow for precise control and manipulation of quantum information. However, along with pure electronic transition (zero phonon line (ZPL)), the broad phonon sidebands (PSB) are also present in the NV spectra, responsible for dephasing and reducing the indistinguishability of photons.

One of the methods to increase the probability of transition through ZPL is to modify the density of states by means of resonant cavities. When QEs, such as NVs, are coupled to such optical cavities, their interaction with confined photons can be precisely controlled, creating a hybrid quantum system with enhanced properties. The metal-insulator-metal cavity can cope with this issue by coupling NV with them. We experimentally analyse the optical properties and investigate the effect of coupling strength on the emission and lifetime dynamics of the coupled NVs. The cavity-coupled NVs show a high decay rate and PL enhancement along with high tunability of cavity, thus offering a platform to couple a variety of QEs. The cavity-coupled NVs are at the forefront of quantum technology due to their unique properties, and strong interactions with optical cavities offer exciting prospects for the second quantum revolution, paving the way for cutting-edge applications in science and technology.

Structured beams for the experimental realization of Hilbert Hotel paradox

G. K. Samanta

Photonic Sciences Lab., Physical Research Laboratory, Navarangpura, Ahmedabad 380009, Gujarat, India

gsamanta@prl.res.in

Full Poincare beams are a special kind of vector vortex beams carrying all possible polarization states represented by the surface of the Poincare sphere in a single beam. Typically, the full Poincare beams are generated through the superposition of Gaussian beam and vortex beams having orthogonal polarization. Such beams have attracted a great deal of attention due to their wide range of applications for high-resolution microscopy, quantum information, material processing, particle micro-manipulation, and lithography.

On the other hand, historically, infinity was long considered a vague concept—boundless, endless, larger than the largest—without any quantifiable mathematical foundation. This view changed in the 1800s through the pioneering work of Georg Cantor, who showed that infinite sets follow their own seemingly paradoxical mathematical rules. In 1924, David Hilbert highlighted the strangeness of infinity through a

thought experiment now referred to as the Hilbert Hotel paradox, or simply Hilbert's Hotel. The paradox describes a "fully" occupied imaginary hotel having an infinite number of single-occupancy rooms. The manager can always find a room for new guests by simply shifting current guests to the next highest room, leaving the first room vacant.

In the current talk, we will discuss some of our recent results on fractional scalar and vector vortex beams representing the Hilbert Hotel paradox. Using full Poincare Bessel beams (FPB), we showed that one can create an infinite series of C-point polarization singularities. We have also devised a novel method to measure the polarization coverage of Poincare beams and showed that the FPBs are the superposition of an infinite number of Poincare beams.

Common Optical Components, Uncommon Optical Phenomena

Nirmal K. Viswanathan

School of Physics, University of Hyderabad, Hyderabad 500046, India

nirmalsp@uohyd.ac.in

Almost all optical experiments involving either a laser beam or a photon source interact with a variety of optical components before detection. These optical components include mirrors, lenses, polarizers-waveplates, and fibers / waveguides. While these common optical components faithfully do what they are expected to, there are some unintended consequences, which have been largely overlooked so far. With significant improvements in measurement techniques and sensitivities developed over the past decade, some of the very small unintended effects can be measured and quantified. Surprisingly, such measurements in the phase-polarization domain led to unravelling of uncommon optical phenomena, which can broadly be categorized as due to *spin-orbit interaction* (SOI) of light. The effects include first-order reciprocal and non-reciprocal spin-to-orbital angular momentum conversion, spin (orbital)-Hall effect of light and higher-order effects. In this talk, after a brief introduction to the SOI of light, I will present some recent experimental results and our understanding of these in the emerging context of SOI of light.

Topological transformation of fractional optical vortex beams

Maruthi Manoj Brundavanam

Department of Physics, IIT Kharagpur, Kharagpur-721302, West Bengal, India

bmmanoj@phy.iitkgp.ac.in

In this talk, the generation of optical vortex beams by the diffraction of a Gaussian beam from computer generated holograms with mixed edge-screw dislocation and their topological characteristics will be discussed. The beams thus generated are called fractional optical vortex (FOV) beams in literature and such beams exhibit some unique topological features not shared by their integer counter-parts. The fine structure of the singularity hosted in the FOV beams for different fractional orders is investigated experimentally. The topological transformations are found to greatly rely upon the wavefront curvature of the input beam via the evolved Gouy phase shift of component integer order vortex beams. Birth and evolution of different critical points, their transformation on orbital Poincaré sphere, transverse energy flow and vorticity distributions are found to be crucial in understanding the topology of such FOV beams. Further, the investigation of resultant vector polarization singularity due to unfolding of a FOV beam inside a birefringent uniaxial crystal reveals a novel way to control the Pancharatnam-Berry geometric phase associated with the generated partial Poincaré beams.

References

1. M. V. Berry, J. Opt. A: Pure Appl. Opt. **6,** 259 (2004).
2. S. Maji and M. M. Brundavanam, Opt. Lett. **42**, 2322 (2017).
3. S. Maji and M. M. Brundavanam, J. Opt. **20**, 045607 (2018).
4. S. Maji, A. Mondal and M. M. Brundavanam, Opt. Lett. **44,** 2286 (2019).
5. S. Maji, P. Jacob and M. M. Brundavanam, Phy. Rev. Applied, **12**, 054053 (2019).
6. S. Maji, A. K. Pattanayak and M. M. Brundavanam, J. Opt. **22**, 035401 (2020).
7. S. Maji and M. M. Brundavanam, Asian J. Phy. 30, 899 (2021).

Beam Propagations Methods: Recent Contributions

Anurag Sharma

Optics & Photonics Centre and Department of Physics,

Indian Institute of Technology Delhi, New Delhi – 110016

asharma@iitd.ac.in

Modelling and simulation of wave propagation through optical waveguides and devices based on them has been a central theme in the theory of guided wave photonics. It basically entails solving the wave equation (obtained from Maxwell's equations) for the boundary conditions represented by the waveguide/device. Photonic structures can be divided in two classes: low index contrast structures, such as optical fibers, and high contrast structures, such as silicon photonic waveguides. In the former case, one can use the simplifying assumption of scalar wave propagation and solve the much simpler Helmholtz equation or the scalar wave equation. However, in the latter case, one must consider the vectorial wave propagation and solve Maxwell's equations or the vector wave equation. In both these directions we have recently made some progress and we will discuss these developments and present some examples.

Optical fibers are azimuthally symmetric structures. There are several components such as tapers, Bragg and long period gratings and single-multimode-single (SMS) sensors, which also retain the azimuthal symmetry. In such cases, the fields can be decomposed in different azimuthal symmetries and each field of specific symmetry can be treated separately. This reduces the 3-D propagations problem to a 2-D propagation problem (in radial, r, and longitudinal, z, coordinates). However, finite difference or finite element methods work in Cartesian coordinates only. The collocation method, on the other hand, is suitable for this kind of problems. We have used the same and developed a propagation method for propagation of LP_{lm} modes in fibers tapers, FBGs and LPGs, etc [1,2]. We will discuss the method and present some examples.

Silicon photonics involves waveguides with high index contrast and one needs to consider the vector wave equation for propagation. We have recently developed a finite difference method for non-paraxial vector wave propagation. The method is a marching type of algorithm in which an incident field is propagated directly [3]. We will discuss its advantages and limitation and present some example.

References

1. Ramesh Kumar and Anurag Sharma, Opt. Fiber Technol. 53, 102017 (pp. 1-5) (2019).
2. Ajay Kumar and Anurag Sharma, International Workshop on Optical Wave & Waveguide Theory and Numerical Modelling (OWTNM-2023), Marseille, France, May 4-5, 2023.

3. Pratiksha Choudhary and Anurag Sharma, International Workshop on Optical Wave & Waveguide Theory and Numerical Modelling (OWTNM-2023), Marseille, France, May 4-5, 2023.

SPASER: Effects of pump and gain medium

Akhilesh Kumar Mishra

Department of Physics, Indian Institute of Technology Roorkee, Roorkee- 247667, Uttarakhand, India

Centre for Photonics and Quantum Communication Technology, Indian Institute of Technology Roorkee, Roorkee- 247667, Uttarakhand, India

akhilesh.mishra@ph.iitr.ac.in

The acronym *Spaser* refers to *Surface Plasmon Amplification by Stimulated Emission of Radiation*. A laser emits coherent photons and analogously a *spaser* system is supposed to provide coherent plasmons. The idea of *spaser* was first proposed by the Stockman and Bergmann in 2003 for the coherent amplification of the localized surface plasmon (LSP) mode [1, 2]. Later, surface plasmon polariton (SPP) mode lasers have also been suggested and demonstrated successfully [3]. *Spaser* efficiency hinges on three key components- pump, gain medium, and plasmon mode. Depending on the plasmon cavity, several types of nanolasers have been proposed such as plasmon nanowire laser, nanopatch laser, nanodisk laser, metal-coated nanolaser among others [3]. The efficiency of *spaser* is further enhanced by employing suitable gain medium and pumping scheme. However, setting aside the design complexity, a simple *spaser* geometry has a spherical metal nanoparticle that is surrounded by a large number of quantum dots (QDs) gain medium. These QDs support dipolar LSP mode. In the talk, I will present our resent results on theoretical investigation of the influence of pump and gain medium on the number of LSPs. In particular, I will discuss the characteristics of a four-level *spaser* when it is excited coherently and incoherently independently [4]. Further, the importance of electron-phonon interaction on the number of LSP will be talked about [5]. This process also generates a steady-state phonon number, which has potential applications in phonon lasers. Furthermore, at the end of my talk, results on the effects of chirped pulse on the excitation of the semiconductor quantum dots gain medium will be presented.

References

1. D. J. Bergman & M. I. Stockman, “Surface plasmon amplification by stimulated emission of radiation: quantum generation of coherent surface plasmons in nanosystems” Phy. Rev. Lett., 2003.
2. Stockman, Mark I. "Brief history of spaser from conception to the future." *Advanced Photonics* 2, no. 5 (2020): 054002-054002.
3. Ma, Ren-Min, and Rupert F. Oulton. "Applications of nanolasers." *Nature nanotechnology* 14, no. 1 (2019): 12-22.
4. A. Purohit and A. K. Mishra, “A comparative study of coherent and incoherent drives in four-level QD-based spaser”, https://arxiv.org/abs/2309.04451.
5. A. Purohit, V.S. Poonia, and A. K. Mishra, “Effect of electron-phonon interactions on three-level QD -based spaser: linear and quadratic potential” https://arxiv.org/abs/2309.04448.

Novel mid-infrared nonlinear materials for frequency conversion

Chaitanya Kumar Suddapalli
Tata Institute of Fundamental Research Hyderabad,
36/P Gopanpally, Hyderabad 500046, Telangana, India
chaitanya.suddapalli@tifrh.res.in

The advent of novel nonlinear optical materials over the past decade, together with progress in solid-state and fiber laser technology, have had a major impact on frequency conversion sources, enabling their advancement to new spectral and temporal domains. These developments have led to the realization of a new generation of advanced solid-state sources of tunable coherent radiation, now providing wavelength coverage in the mid-infrared with high output power and efficiency, along with good spatial, spectral and temporal quality. In this lecture, I will discuss state-of-the-art mid-infrared nonlinear materials and frequency conversion sources overcoming the limitation posed by conventional lasers.

New strategies for coherent Raman spectroscopy in reactive flows

Meena Raveesh[1], Ali Hoseinnia[1,2], Maria Ruchkina[1], Pengji Ding[1,3], Per-Erik Bengtsson[1], Mark Linne[2], and Joakim Bood[1]*

[1]Dep. of Physics, Lund University, Box 118, 221 00 Lund, Sweden

[2]School of Engineering, The University of Edinburgh, Edinburgh EH8 3JL, Scotland, UK

[3]School of Nuclear Science and Technology, Lanzhou University, 730000 Lanzhou, China

**joakim.bood@fysik.lu.se*

Rotational coherent anti-Stokes Raman spectroscopy (RCARS) is a powerful laser-based technique for non-intrusive measurements of temperature and species concentrations in gases, often considered to be the gold-standard for thermometry in reactive flows. However, the accuracy of the method for thermometry drops steeply for temperatures above ~1000 K. Furthermore, the technique is limited to detection of species present in concentrations higher than ~1%. The present talk will discuss new coherent Raman scattering concepts that may overcome these restrictions.

One of the techniques that will be presented is hybrid fs/ns RCARS, in which the rotational Raman coherences are driven with a broadband fs laser pulse (800 nm) and probed by a narrowband (single-mode) laser pulse (532 nm). This method has the ability to measure all coherence lifetimes simultaneously, which constitute a breakthrough for CARS thermometry, as it allows all Raman linewidths to be measured in a single-shot recording, offering single-shot thermometry based on experimental, instead of theoretical, linewidths.

The other newly developed concept that will be presented is Interferometric Quantum Control Rotational CARS, IQC-RCARS. This method relies on the fact that even with a weak non-resonant field, below the field strength needed for molecular alignment, the nonlinear polarization of the gas created by the rotational-Raman response to an fs laser pulse generates a rotational wave packet exhibiting revivals. Since the revival period is directly linked to the rotational constant, B, the revival structure constitutes a unique fingerprint for each molecular species. Using two fs laser pulses, called pump and control, two interfering wave packets are created, and a strong third-order polarization, i.e., the rotational-CARS signal, is generated while interacting with a single-mode ns laser pulse. Figure 1 shows a measured interferogram for pure N_2. The delay time between the pump and control pulse is along the horizontal axis and Raman shift is along the vertical axis. As can be seen, the spectral shape varies significantly with pump-control delay time. Hence, by exploiting the time domain while varying the delay between the pump and control pulses, the shape of the resulting spectra can be manipulated, optimizing the diagnostic for a specific application.

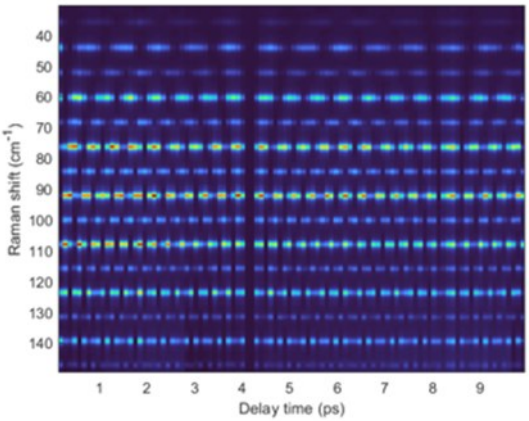

Fig. 1 *Interferogram of pure N_2 recorded with IQC-RCARS*

High-intensity attosecond beamline for XUV pump–XUV probe measurements with photon energies up to 150 eV

Dr. Smijesh N

School of Pure and Applied Physics

Mahatma Gandhi University,

Kottayam, Kerala - 686 560, India

E-mail: smijeshn@mgu.ac.in

Experimental strong-field physics is a fast-growing area of nonlinear optics triggered by the development of attosecond (10^{-18} s) pulses. These pulses exhibit laser-like properties, providing exceptional spatio-temporal resolution, and are promising candidates for investigating a broad class of atomic and molecular ultra-fast processes. In this talk, a newly constructed beamline capable of performing XUV-XUV pump-probe studies with attosecond pulses will be described. This source delivers up to 55 nJ of pulse energy in the Zr window (65 eV – 150 eV) via the up-scaling of high harmonic generation in a gas medium. In addition, it provides very high energy stability of typically 5%, and enables nonlinear temporal investigations by utilizing a reliable, stable split and delay-stage and different types of focusing geometries.

Machine Learning Approaches in Quantitative Phase Microscopy

*Ashwini S. Galande, Vikas Thapa, Aswathy Vijay, and Renu John**

Medical Optics and Sensors Laboratory

Department of Biomedical Engineering, Indian Institute of Technology Hyderabad

Telangana, India 502 284

**renujohn@bme.iith.ac.in*

Optical microscopy is one of the indispensable tools in hospitals for various diagnostic imaging a pplications like imaging biological cells and tissues for disease diagnosis. The important characteristics of the biological sample under imaging such as refractive index, optical thickness, absorption, reflection, etc. can be revealed through microscopy. The basic challenge with these microscopes is imaging transparent and weekly absorbing biological samples, which results in low-contrast images. Quantitative phase imaging

of biological samples without the use of additional contrast agents has been one of the topics of research among microscopists. Deep learning techniques have emerged as excellent tools for phase reconstruction, but the requirement of large datasets and lack of interpretability on unknown samples limits its commercial use. Recent developments in untrained deep models hold a promising approach as it leverage high-fidelity physical image formation models to provide state-of-the-art reconstruction algorithms.
In this talk, we discuss various deep-learning approaches in quantitative phase microscopy. We discuss the traditional iterative phase retrieval approaches and compare them with the recent algorithms involving trained and untrained models. We have explored the use of learned priors to reconstruct more complex biological samples such as cervical cells with a limited training dataset. We have observed in this research that combining capabilities of trained as well as physics-aware untrained deep networks can significantly improve the reconstruction without getting stuck in local minima. We use the lensless digital holographic microscope as a platform for recording experimental holograms and explore various single-shot phase retrieval techniques.

Cavity QED with Atoms and Molecules

Arun Bahuleyan, V. I. Gokul, V. R. Thakkar, S. P. Dinesh and S. A. Rangwala

Raman Research Institute, C. V. Raman Avenue, Sadashivanagar, Bengaluru 560080, India

email: sarangwala@rri.res.in

One of the foundational constructs in physics is the interaction between an atom and the electromagnetic field. In the quantum domain, this translates to the interaction between a single, two level atom and a near resonant photon occupying an atomic field mode. The most efficient way to experimentally study this system is when a single, approximately two level atom is coupled to a near resonant cavity. Such a system is called a Cavity QED system.
In our experiments, we preserve the conditions of a weak light field but include multiple atoms in the cavity. This leads to collective strong coupling of the atoms to the cavity and this system exhibits some remarkable properties. In this talk I will discuss the results of our experiments, for detection of molecular processes using atoms and cavities. In addition, I will focus on the coupling of the driven atomic oscillator with the cavity and show how the system can be made to lase or absorb light, with small changes.

Fiber Optic Sensing for Underwater Applications: Present and Future

Dr. R. Rajesh, Sc.G

Naval Physical & Oceanographic Laboratory (NPOL), Thrikkakara, Kochi, PIN - 682021

rajeshr.npol@gov.in

With the rapid technology advances in telecommunication industry, the field of Fiber Optic Sensors (FOS) is also developing equally and undergoing tremendous growth and advancement. In addition to the sensing of ocean parameters like salinity, temperature and depth, the acoustic and vibration sensing in maritime environment is widely used in both civilian and defence applications. Compared with the conventional measurement techniques, fiber optic sensing helps to avoid requirement of wet-end electronics, provides easy multiplexing of many and variant sensors in a single lead fiber, large data transfer through telemetry etc. This in turn reduces vulnerability in frequent failures, increased lifetime and gives a cost effective and

less complex solution for measurement and deployments in challenging ocean conditions.
Fiber optic based salinity, temperature and depth sensor in a single package was realized in recent time and effectively used for underwater explorations. The fiber optic based accelerometers, vector sensors, temperature sensors, salinity sensors, depth sensors and hydrophones are now available for field applications and satisfy the stringent requirements of underwater applications. Fiber mandrel type sensors were used for underwater acoustic and vibration sensing from many decades. These historic mandrel-type fiber sensors got relooked in the recent years with the addition of advanced laser sources since they can be used effectively in multiple scenarios. Further, the Fiber Bragg Grating (FBG) based sensors were also packaged in suitable schemes and used for various underwater parameters. With the inclusion of fiber grating laser based interferometric sensors, very high sensitive and compact hydrophone configurations were realized and utilized even as thin towed arrays for UUVs and lightweight platforms. With different packaging schemes and structures, simple fiber, FBGs and FBG laser sensors are realized and utilized for acceleration, seismic sensing, acoustic pressures, temperature, salinity and depth of water etc.
In the recent time, simple fiber cable based Distributed Acoustic Sensing (DAS) techniques utilizing Coherent OTDR concepts are also found to be highly potential for underwater acoustic and temperature sensing. Through already laid submarine telecommunication fiber cables, the above technique is proved to be highly potential for underwater seismic sensing, thereby detect earthquake and its epicentre. Its capability in underwater target detection is also being currently explored as an advanced area of research. Today, optical fibers or fiber based sensors can satisfy the requirements of monitoring most of the underwater parameters which are useful for underwater surveillance and maritime monitoring.

Near-ultraviolet and visible coherent light sources

Stéphane Trebaol

Univ Rennes, CNRS, Institut FOTON – UMR 6082, F-22305 Lannion, France

stephane.trebaol@enssat.fr

Nowadays, laser diodes are essential elements for the development of compact photonic devices. They offer the opportunity of combining good performances in terms of linewidth, optical power and frequency noise. The needs in the field of optical telecommunications have enabled the development of compact laser diodes mainly in the telecom C-band. The implementation of compact laser diodes with low-frequency noise at visible wavelengths covering the near-ultraviolet to infrared spectral range is a technological challenge recently addressed by several research groups. The objective is to provide laser diodes capable of meeting several application requirements in the fields of classical and quantum sensors and the metrology of optical frequencies for the production of compact optical clocks.
This talk will present laser architectures in the visible range designed to reach narrow linewidth single-mode emission. In particular, approach based on compact external cavity InGaN semiconductor laser diode will be discussed. To improve the laser coherency, stabilization schemes are implemented using versatile and compact optical references based on high quality factor optical resonators. The noise reduction performances are demonstrated on an external cavity diode laser by analyzing its frequency noise.

Optical microscopy beyond diffraction limit through structured illumination

Joby Joseph

Optics and Photonics Centre, IIT Delhi

Microscopy is an important tool for studying the structure and properties of materials, and for identifying

and characterizing small objects or organisms. However, the resolution we can achieve from optical microscopes is limited by diffraction. However recent years, many new optical techniques have come up with higher resolutions that break this diffraction limit. These microscopy techniques are called super-resolution microscopy or nanoscopy. There are several super-resolution microscopy techniques such as Structured Illumination microscopy (SIM), Stimulated Emission Depletion (STED) microscopy, Single molecule localization microscopy (SMLM) etc.

SIM even though gives a modest resolution enhancement, it stands out from others in many ways due to its practical usages. The biggest limitation of SIM is that even though it is faster than other super resolution microscopy technique, it is still limited to two times resolution enhancement. The talk will focus on the development of a novel Transillumination -SIM [TSIM] that circumvents this two times resolution enhancement limit and has high space bandwidth product. TSIM decouples the imaging and illuminating part by using mirrors. A multi-mirror setup generates illumination patterns with higher spatial frequencies than can be achieved from the imaging objective lens.

Sub-picosecond Density Evolution in Femtosecond Laser Produced Plasma Channels in air

Riju C Issac
Department of Physics
Cochin University of Science & Technology
Kochi 682 022, Kerala, India

Spatio-temporal evolution of electron density of plasma formed by the interaction of ultrafast laser with gas has been investigated using time-resolved Nomarski interferometry. Plasma channels are produced using 35 fs laser pulses from a 7mJ laser with 1kHz repetition frequency with focused intensity of $10^{16}\ W\ cm^{-2}$. A low-energy laser beam split from the main beam acts as the probe when passed through a delay line. A Nomarski interferometer utilizing a Wollaston prism is set up on the probe beam, with a temporal resolution of 100 fs. Dimensions of the observed plasma channel were about 100μm diameter and 1mm in length. Time and space-resolved measurements on the evolution and decay of the electron density were done. A 16-bit CCD camera and a 2X magnifier objective were used to record time-resolved interferograms. The phase data have been retrieved from the recorded interferogram and Abel inverted assuming cylindrical symmetry, using the open-source software IDEA. A stable plasma channel having dimensions (200μm diameter × 2 mm length) many times the Rayleigh length was formed behind th self-guided femtosecond laser pulses. A stable, long plasma channel can be used as an optical waveguide for applications like laser wakefield acceleration, and X-ray lasers.

Advancements of lasers in space applications

Jagannath Nayak & S Veerabuthiran

Centre for High Energy System and Science

Vignayana Kancha, Hyderabad-500069.

e-mail: jnayakdr@gmail.com & director.chess@gov.in

The advent of lasers has revolutionized various fields of science and technology, including space applications. In recent years, there has been a significant increase in the use of lasers for space applications such as communication, ranging, propulsion, space debris removal, etc. Laser technology offers numerous advantages in space applications, such as high data transmission rates, satellite ranging capabilities, and the

ability to deliver energy over long distances. Large number of space debris present in the orbit around earth poses a great threat to active satellites. By employing high-powered lasers, the laser directed energy system (LDES) can target and disintegrate the space debris of various sizes, thereby reducing the risk of collision with operational satellites and space stations. LDES configuration comprises of various subsystems and components. In this paper, technological areas such as high-power high energy laser, high accurate positioning and tracking system, sensitive detector, high resolution optical trans-receivers, thermal management system, etc. are discussed.

Cavity Interferometry using Processed Optical Micro-Nanostructures

Rajan Jha
Nanophotonics and Plasmonics Laboratory, School of Basic Sciences
IIT Bhubaneswar
Email id: rjha@iitbbs.ac.in

Optical inline systems with high resolution, integrability, and reconfigurability have been central to the development of advanced and futuristic systems. High-resolution cavity interferometers based on excitation of fundamental and higher order modes of processed fiber/microfiber and their combinations have been developed and demonstrated for static and dynamic magnetometry, hydrophone for mapping the underwater and Optical Profilometer [1-2]. On the other hand, optical nanowire integrated with different type of Quantum Emitters like Nitrogen vacancy in asymmetric elliptical faceted Diamond nanowire (ELFA) [3] and nanophotonic cavity formed by etching periodic rectangular through-holes on an optical nanowire [4] have been designed to realize strong light-matter interaction. The cavities not only maximize the coupling of spontaneous emission from a quantum emitter into optical nanowire guided modes but facilitates in demonstrating efficient unidirectional and/or bidirectional coupling of single photon from these Quantum Emitters [5] with coupling efficiencies as high as 90% can be realized by optimally placing the dipole. Such inline system may attract various quantum photonic applications in the area of quantum communication and metrology.

Acknowledgement

RJ acknowledges the support of SERB STAR Fellowship (Physical Science) and DST FIST.

References

1. K. Chatterjee, S. K. Pal & R. Jha, “Reconfigurable Optical Magnetometer for Static and Dynamic Fields”, Advanced Optical Materials, 9 (3), 2001574,(2021).

2. S. Dass, S. Kachhap, & R. Jha, “Hearing the Sounds of Aquatic Life Using Optical Fiber Micro-tip based Hydrophone, IEEE Transactions on Instrumentation and Measurement, 69 (7), 4015-4020 (2019).

3. S. Murmu, A. Kumar, & R. Jha, “Bidirectional coupling of diamond emitters to optical nanowire: tunable and efficient”, JOSA B 38 (12), F170-F177 (2021).
4. S. Sahu, K. P. Nayak, & R. Jha, “Optimization of nanofiber gratings for efficient single-photon collection”, Journal of Optics (2022).
5. S. Murmu, A. Kumar, & R. Jha, “Unidirectional Photon Coupling Using Asymmetric Diamond Emitters with Enhanced Spontaneous Emission” Advanced Quantum Technologies, 5 (7), 2100160, (2022).

Contributory Papers

Category 1

Artificial-Intelligence and Machine-Learning in Photonics (AMP)

AMP101 AI-Driven OAM Demultiplexing using Nanostructures

Chayanika Sharma, Purnesh Singh Badavath, P Supraja, Rakesh Kumar R, Vijay Kumar;*
National Institute of Technology Warangal, Hanamkonda, Telangana- 506004, India;
**Corresponding author: vijay@nitw.ac.in*

Light's fundamental degrees of freedom include space, time, wavelength, and polarization. These properties are utilized in optical multiplexing to modulate various information channels within distinct aspects of light, maximizing the communication bandwidth. The bulky size of traditional information optics presents substantial hurdles in terms of scalability and integration. To overcome that, nanophotonics has emerged as a beacon of hope by providing unparalleled manipulation of light at the nanoscale [1]. Artificial Intelligence strategies aid efficient demultiplexing of OAM beams using speckles facilitated by macro-structures [2], enhancing non-line-of-sight communication [3] and many other applications.

To fully leverage OAM in integrated photonics, we experimentally demonstrated the interaction of structured light with ZnO nanosheets grown on an aluminum substrate. The intensity speckle images of the $LG_{p,l}$ ($p = 0$; $l = \pm2, \pm4, \pm6, \pm8$) beams have been captured using a 4f imaging system and fed to the customized deep convolutional neural network. The trained CNN achieved >96% classification accuracy across propagation direction (from near-field to far-field) for vortex beams and their intensity degenerate counterparts. This method eases the rigorous focusing requirements, offering vast potential for easy implementation. This study validates the potential for speckle patterns, from macro to nanostructures, to achieve compact OAM demultiplexing in integrated photonics.

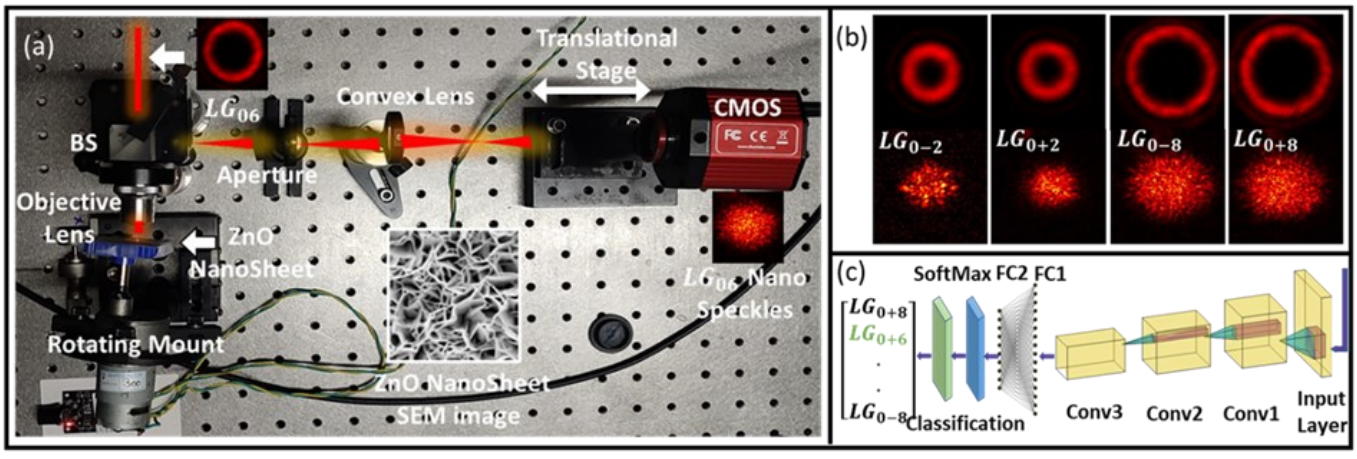

Fig.1.(a) Experimental set-up for nanostructure-based demultiplexing. (b) Structured light and corresponding speckles, (c) Convolutional neural network for demultiplexing LGp,l beams from captured speckle patterns.

Acknowledgment: SERB India funding (SRG/2021/001375)

References

1. Xinyuan Fang et al., "Nanophotonic manipulation of optical angular momentum for high-dimensional

information optics," Adv. Opt. Photon. 13, 772-833 (2021)
2. V. Raskatla et al., "Speckle-Based Deep Learning Approach for OAM Modes Classification," JOSA A 39, 759-765 (2022).
3. P. S. Badavath et al., "Speckle-based structured light shift-keying for non-line-of-sight optical communication," Appl. Opt. 62, G53-G59 (2023).

AMP102 Inverse design of metasurfaces for narrow-band absorption using Quantum Generative Adversarial Networks

*Sreeraj Rajan Warrier[1], Jayasri Dontabhaktuni[1]**
[1]Department of Physics, Mahindra University, Bahadurpally, Hyderabad-500043;
**Corresponding author: jayasri.d@mahindrauniversity.edu.in*

Metasurfaces are 2D periodic structures of metallic or dielectric constituents in the sub-wavelength regime and exhibit novel light-matter interactions. The development of these materials has resulted in a plethora of applications such as perfect absorption, perfect transmission, etc. Achieving the inverse design of such metasurfaces with specific electromagnetic responses however is not straight forward. Recently, with the advent of machine learning methods such as generative adversarial networks (GAN's), physics informed neural networks (PINN's), etc, the inverse design of metasurfaces for specific applications has become possible and increasingly being explored by the scientific community. Classical machine learning methods, however require large datasets for accurate prediction of metasurface designs. Very recently, with the advent of quantum computing for NISQ era, it is possible to explore application of hybrid quantum machine learning (QML) methods for such inverse design. Hybrid methods require smaller datasets and are very time efficient as compared to classical machine learning methods. In the current work, we show the results of application of hybrid QGAN method to inverse design of metasurfaces for narrow-band absorption in the infrared frequencies.

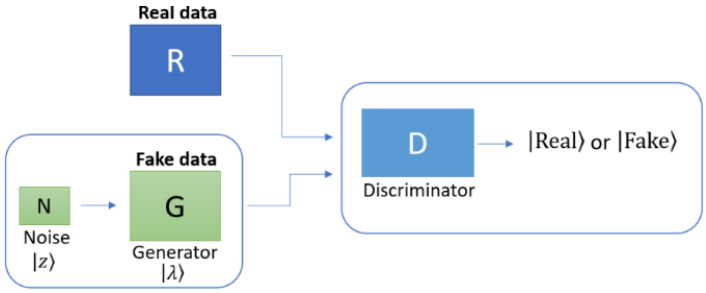

Fig 1. Schematic of Quantum Generative Adversarial Network.

References

1. I. Goodfellow et al., *Advances in neural information processing systems, 2672–2680 (2014).*
2. Pierre-Luc Dallaire-Demers and Nathan Killoran. *Phys. Rev. A 98, 012324.*
3. Christopher Yeung et al., *Advanced Optical Materials 9, 20, 2170079 (2021).*

AMP103 Machine Learning Assisted Structured Light Demultiplexing

Vijay Kumar; Department of Physics*
National Institute of Technology Warangal, Telangana - 506004;
**Corresponding author: vijay@nitw.ac.in*

Structured light with a spatial degree of freedom has emerged as a conceivable candidate for increasing the spectral efficiency of optical communication links. Basis sets like Hermite–Gaussian ($HG_{m,n}$), Laguerre–Gaussian ($LG_{p,l}$) and their superposition modes have been used for information encoding and multiplexing. There are many structured light demultiplexing techniques, but all of them are very sensitive to alignments and noise. Even artificial intelligent (AI) based structured light demultiplexing techniques require capturing the structured light's whole mode to identify them. The recent machine learning-assisted speckle-based structured light demultiplexing has shown to be noise and alignment-free by recognizing structured light through a small region of captured speckle field [1 – 3].

The key idea of machine learning-assisted speckle-based structured light is to identify the structured light not by using the mode but instead using the corresponding speckle pattern. Structured light's speckle patterns had the hidden information of the corresponding structured light and using the supervised deep learning model one can easily perform the structured light classification. The existing AI-based structured light demultiplexing used the intensity of the modes and failed to classify intensity degenerate modes. The speckle-based Structured light demultiplexing uses the speckle patterns therefore it can classify intensity degenerate structured light as well [4].

Optical communication is generally restricted to line-of-sight communication only. Since speckle-based demultiplexing uses the speckle patterns and performs the classification using a small portion of the speckle pattern, it can also be used to perform non-line-of-sight optical communication [5].

Acknowledgment: SERB India funding (SRG/2021/001375)

References

1. Venugopal Raskatla et. al., *JOSA A 39, 759-765 (2022).*
2. Venugopal Raskatla, et. al., *Optics and Photonics News, 51, (December 2022).*
3. Venugopal Raskatla, et. al., *Opt. Eng. 61, 036114 (2022).*
4. Venugopal Raskatla, et. al., *Opt. Eng. 62, 036104 (2023).*
5. Purnesh Singh Badavath, et. al., *Appl. Opt. 62, G53-G59 (2023).*

AMP201 Image Encryption and Enhancement Using Convolution Long Short Term Memory Model Based on Fractional Fourier Transform

Bhavana Sharma [1], Hukum Singh[2], Mehak Khurana[1],*
[1]Department of Computer science and Engineering, The NorthCap University, Gurugram, India,
[2] Department of Applied science, The NorthCap University, Gurugram, India.
**Corresponding author: bhavanasharma@ncuindia.edu*

This paper is mainly based on ConvLSTM model of recurrent convolutional neural network for denoising the decrypted image to improve the robustness of image. In this paper, first an optical cryptosystem based on pixel scrambling along with fractional Fourier transform is proposed to secure the image from various type of attacks, the most common of which is noise attack. The deep ConvLSTM improves the resolution of the reconstructed image and secures the images from not only noise attack but also occlusion attack, blur attack. Image parameters such as structural similarity index matrix (SSIM), Peak signal to noise ratio (PSNR) are used in comparing with various existing models. The obtained simulation results demonstrate that the proposed cryptosystem outperforms the existing state- of-the-art denoising methods. The proposed method can be used in secure image transmission in healthcare, multimedia transmission etc.

References

1. P. Refregier and B. Javidi, "Optical-image encryption based on input plane and Fourier plane random encoding," Opt. Lett., 20, 767-769, (1995).
2. G. Unnikrishnan, J. Joseph, and K. Singh, "Optical encryption by double-random phase encoding in the fractional Fourier domain," Opt. Lett., 25,887-889, (2000).
3. A. Buades, B. Coll, and J.-M. Morel, "A non-local algorithm for image denoising,'' in Proc. IEEE Comput. Soc. Conf. Comput. Vis. Pattern Recognit.",**2**,60–65, (2005).
4. K. Zhang, W. Zuo, S. Gu, and L. Zhang, "Learning deep CNN denoiser prior for image restoration," in Proc. IEEE Conf. Comput. Vis. Pattern Recognit.", 2808-2817, (2017).
5. K. Cho, B. van Merrienboer, C. Gulcehre, F. Bougares, H. Schwenk, and Y. Bengio., "Learning phrase representations using RNN encoder-decoder for statistical machine translation". 1724– 1734, (2014).
6. Chen, Jing, Li, Xiaowei and Wang Qiong-Hua. "Deep Learning for Improving the Robustness of Image Encryption" IEEE Access. **7**. 181083-181091, (2019).

AMP202 Data driven simulation of pulse propagation in the femtosecond region of the nonlinear fiber using physics-informed neural network

Gautam Kumar Saharia, Sagardeep Talukdar, Riki Dutta, Sudipta Nandy;*
Department of Physics, Cotton University, Guwahati, India, 781001 ;
**Corresponding author: phy2091011_gautam@ cottonuniversity.ac.in*

The Fokas-Lenells equation (FLE) describes the stable propagation of ultrashort pulses in nonlinear media. In this study, we simulated the pulse propagation in the femtosecond region of a nonlinear fiber described by the FLE using physics-informed neural networks (PINNs). PINNs are a new approach for numerically solving nonlinear partial differential equations that leverage the fast calculating speed and high precision of modern computing systems. We improved the PINN by adding multiple conserved quantities to the loss function to obtain both the bright and dark soliton solutions of the FLE. We found that the proposed scheme of conserved quantities informed PINN has a better convergence rate and generalizability than the basic PINN algorithm. We believe that the PINN approach to solving partial differential equations in nonlinear optics would be useful in studying various optical phenomena.

References

1. Raissi, Maziar, et al. "Physics-informed neural networks: A deep learning framework for solving forward and inverse problems involving nonlinear partial differential equations." *Journal of Computational Physics 378 (2019): 686-707.*
2. Wu, Gang-Zhou, et al. "Prediction of optical solitons using an improved physics-informed neural network method with the conservation law constraint." *Chaos, Solitons & Fractals 159 (2022): 112143.*
3. Matsuno, Yoshimasa. "A direct method of solution for the Fokas–Lenells derivative nonlinear Schrödinger equation: II. Dark soliton solutions." *Journal of Physics A: Mathematical and Theoretical 45.47 (2012): 475202.*
4. Saharia, Gautam Kumar, et al. "Data driven localized wave solution of the Fokas-Lenells equation using modified PINN." *arXiv preprint arXiv:2306.03105 (2023).*

AMP203

Analyzing MMF Specklegrams for Temperature Recognition using a Deep-Learning Model

*Nikhil Vangety and Sourabh Roy **
Dept. of Physics, National Institute of Technology Warangal, India
**sroy@nitw.ac.in*

In recent times with the advent of the machine and deep learning, there have been many works that utilize multimode fiber (MMF) specklegrams for the simple and efficacious recognition of different parameters [1-3]. In this study, we analyze specklegrams from the MMF for the recognition of different temperatures using deep learning. The experimental setup shown in Fig. 1 comprises a He-Ne laser (632.8 nm), whose light passes through MMF (plastic optical fiber of core diameter: 980 µm, NA:0.52) via a microscope objective, forming specklegrams at its end, captured by a CCD camera. We apply temperatures (30-50 ºC with 1 ºC step-size) using an oven and dimmerstat, capturing specklegrams for a total of 21,000 images (1000 images per temperature) which are split into 80%-10%-10% as the train-validation-test dataset. We train and validate the data using the deep learning AlexNet model and achieve 100% accuracy for both. The model gives 100% prediction accuracy on the test dataset. The individual recognition per temperature class is visualized by the Confusion matrix as shown in Fig. 2, demonstrating consistent 100% accuracy which proves the effectiveness of our deep-learning approach.

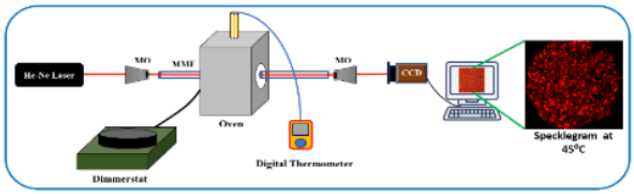

Fig 1. Experimental setup schematic

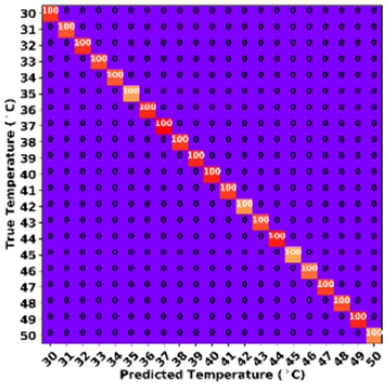

Fig 2. Confusion Matrix

References

1. Nikhil Vangety, Koustav Dey, Surya K. Ghosh, Sourabh Roy, "Analyzing specklegrams of plastic optical fiber using convolutional neural network for weight recognition," Opt. Eng. 61, 126112 (2022).
2. Nikhil Vangety, Koustav Dey, Sourabh Roy, "Weight-location recognition in a plastic optical fiber using a convolutional neural network," Optical Fiber Technology 75, 103166 (2023).
3. Yan Liu, Guangde Li, Qi Qin, Zhongwei Tan, Muguang Wang, Fengping Yan, "Bending recognition based on the analysis of fiber specklegrams using deep learning," Opt Laser Technol. 131, 106424 (2020).

Category 2

Biophotonics & Medical Optics (BPM)

BPM435 Label-free Multi-modal Optical Techniques for Early-stage Oral Cancer Screening

Pramila Thapa[1#], Sunil Bhatt[1], Himanshu Joshi[1], Veena Singh[1], Deepika Mishra[2] and Dalip Singh Mehta[1]*
[1]Bio-photonics and Green-photonics Laboratory, Department of Physics, Indian Institute of Technology Delhi, Hauz-Khas, New Delhi 110016, India
[2]Oral Pathology, Center for Dental Education & Research (CDER), AIIMS New Delhi, India;
Email- [#]pramilathapa643@gmail.com ; Correspondence - [*]mehtads@physics.iitd.ac.in

To combat the significant mortality and morbidity associated with cancer, there is a critical need for early-stage cancer screening methods. Conventional methods like histopathology are time-consuming and invasive, which can detect cancer at advanced stages. Therefore, there is an urgent need for alternative methods that can identify and diagnose cancer in its early stages, which can be accomplished by means of applying multimodal the application of optical techniques that are non-contact and non-invasive. Among these techniques, autofluorescence (AF) and quantitative phase microscopy (QPM) stand out as label-free optical methods that can be employed for early-stage cancer screening. The present manuscript deals with QPM and AF for early-stage cancer screening. QPM provides precise data regarding the morphological aspects of cancer progression, such as cell structures, dry mass, and optical thickness. These parameters vary at different stages of cancer as it advances at the cellular level. In addition to QPM, AF offers insights into cancer progression at the molecular level by investigating various endogenous fluorophores. In this study, we have done QPM, AF imaging, and AF spectroscopy for three classes of 9 oral cancer patients: oral squamous cell carcinoma, hyperplasia/dysplasia, and normal. A significant change in the optical phase of the three classes is observed. In AF imaging, there is variation in the intensity in three classes with the spectral changes in AF spectra of these three classes. By combining all these techniques, one can screen or diagnose the cancer at early-stages.

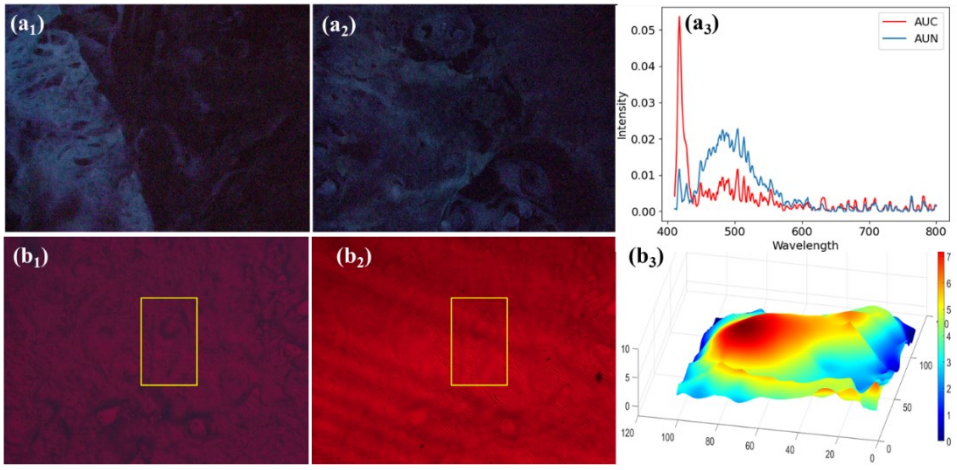

Figure 1. Autofluorescence images and quantitative imaging of oral squamous cell carcinoma and normal. (a_1-a_3) AF microscopic images and AF spectra of OSCC and normal, respectively. (b_1-b_3) brightfield, interferometric, and phase images of the OSCC tissue, respectively. AUC and AUN in (a_3) represent the AF spectra of OSCC and normal patients, respectively.

BPM105 Spherulites as nanophotonic building blocks

Venkata Jayasurya Yallapragada[1,], Benjamin Palmer[2], and Dan Oron[3];*
[1]Department of Physics, Indian Institute of Technology Kanpur, Kanpur 208016 India;
[2]Department of Chemistry, Ben-Gurion University of the Negev, Beer-Sheva 8410501, Israel;
[3]Department of Molecular Chemistry and Materials Science, Weizmann Institute of Science, Rehovot 7610001, Israel;
**Corresponding author: jayasurya@iitk.ac.in*

Recent studies of the visual system in several decapod crustaceans have revealed dense assemblies of spherical nanoparticles which function as efficient reflectors [1]. Each nanoparticle is made of highly birefringent material organized in such a way that light polarized tangential to the surface of the sphere experiences a large refractive index (~1.9) and light polarized normal to the surface experiences a small index (~1.4). Such particles are termed spherulites, and the spherulites in the crustacean eyes have typical diameters 300 - 400 nm. These subwavelength spherulites possess the same rotational symmetries as an optically isotropic sphere, while incorporating birefringent material. This is a novel route to optimally utilizing birefringent material in photonic structures.

Mie scattering calculations show that the backward scattering efficiency is enhanced in comparison to an optically isotropic sphere of similar size and refractive index. In addition, due to the larger tangential index, the scattering is dominated by the transverse electric (TE) modes, and prominent resonances appear in dark-field optical scattering spectra of single scatterers [2]. Extended ordered assemblies of spherulites exhibit photonic band structures that are markedly different from their isotropic counterparts. New band gaps open in regions of the irreducible Brillouin zone, and existing gaps may broaden or contract, while preserving the symmetry and degeneracy of each band. The changes in the photonic band structure caused by the large optical anisotropy can be very large, in the deep non-perturbative regime [3]. This leads to enhanced reflectance at wavelengths physiologically relevant for the marine crustaceans. Newer studies have also shed light on how the optical properties of spherulite assemblies can be dynamically tuned [4].

In my presentation, I will summarize the basic calculations and results and discuss the potential utility of spherulites in constructing photonic structures that realize novel optical responses.

References

1. B. A. Palmer et al, *Nature Nanotechnology 15, 138–144 (2020).*
2. L. M. Beck, et al, *Opt. Express 29, 20863–20871 (2021).*
3. V. J. Yallapragada and D. Oron, *Opt. Lett. 44, 5860–5863 (2019).*
4. K. Shavit, et al, *Science 379, 695–700 (2023).*

BPM204 In-vivo Imaging of the Human Tympanic Membrane for diagnosis of Otitis Media using low-cost Spectral -domain Optical Coherence Tomography

*Denny Melkay M George[*1], Hari Nandakumar[1], Prajal Chettri[1], R.N. Mahesh[2], Gopikrishna Muddu[2], and Shailesh Srivastava[1];*
[1]Department of Physics, Sri Sathya Sai Institute of Higher Learning, Prasanti Nilayam, Sri Sathya Sai District, Andhra Pradesh – 515134
[2] Sri Sathya Sai General Hospital, Prasanti Nilayam, Sri Sathya Sai District, Andhra Pradesh – 515134
**Corresponding author: dennymmgeorge@sssihl.edu.in*

In middle ear ailments such as otitis media, the thickness and curvature of the human tympanic membrane (TM) changes due to bio-film depositions. Any device that can estimate the thickness and visualize the curvature would aid in evaluating treatment outcomes as well as diagnosis. Optical coherence tomography (OCT) employing galvano-mirror and high-speed line-scan camera has been used for this purpose but the cost is prohibitively high. We show that the use of a much lower-cost custom-made line field spectral domain optical coherence tomography (SD-OCT) device using CMOS camera for imaging, can be used to visualize the curvature and evaluate the thickness of the human TM in-vivo. The OCT has an axial resolution of 18 µm and lateral resolution of 18 µm 50 µm, with an imaging depth range of 3 mm. Our optical setup built over a conventional camera tripod stand provides the manoeuvrability and flexibility to guide the light into the ear canal using a conventional speculum. Another CMOS viewport camera provides a view of the region being imaged. The custom-written Open CV software automates image acquisition and data processing to provide live averaged images at video rate. In spite of the challenges due to involuntary motion for interferometric imaging, we demonstrate the potential to measure the thickness and curvature of the TM using 10 averaged B-scans for each visualization that update at over 50 times per second.

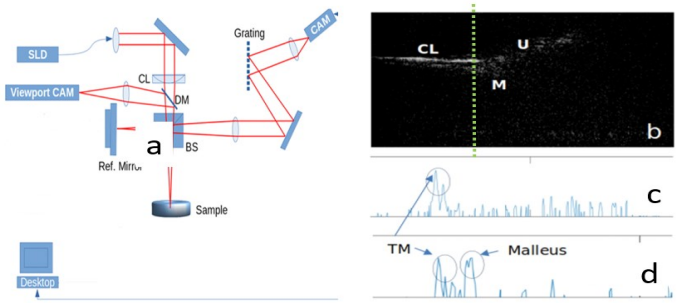

References

1. D. Huang et. al., *Science. 254(5035), 1178-81 (1991).*
2. J. F. de Boer et. al., *Biomed. Opt. Express. 8(7), 3248-80 (2017).*
3. D. M. M. George et. al., *Results in Optics. 5, 100144 (2021).*

BPM205 Detection of Adulteration in milk using a portable Raman Spectrometer

*Meenakshi[1#], Sathi Das[1], Anjika Kumari[1], Kanchan Saxena[2], Dalip Singh Mehta[1]**
[1]Bio-photonics and Green photonics laboratory, Department of Physics, Indian Institute of Technology Delhi, Huz-Khas, New Delhi-110016, India,
[2]Amity Institute of Renewable and Alternative Energy, Amity University, Sector 125, Noida, UP, India
**mehtads@physics.iitd.ac.in, [#]meenakshisingh2997@gmail.com*

Food adulteration is very common, recently. For example, milk is adulterated with melamine, and it also has very serious effects on health like kidney failure and much more these adulterants in milk are also very difficult to observe by the naked eye because of their white colour and their ease of mixing in milk. Raman Spectroscopy is an effective tool in detecting adulterations. It acts as a non-destructive, powerful technique for the chemical analysis of molecules giving the unique fingerprints of each molecule. The inherently low Raman signal of the molecule was enhanced using a colloidal solution of Ag NPs. As examined, the SERS spectra of samples were enhanced compared to Normal Raman and helped to achieve further trace-level detection of milk adulterants. For the detection of melamine in milk different samples were prepared from fresh buffalo milk, one is fresh milk and the remaining are adulterated milk solutions of melamine in pure milk were prepared by dissolving the appropriate amount of powdered adulterant in milk to make it 0.1M

concentration solution and all spectrum was taken at same integration time and same laser power with portable Raman spectrometer.

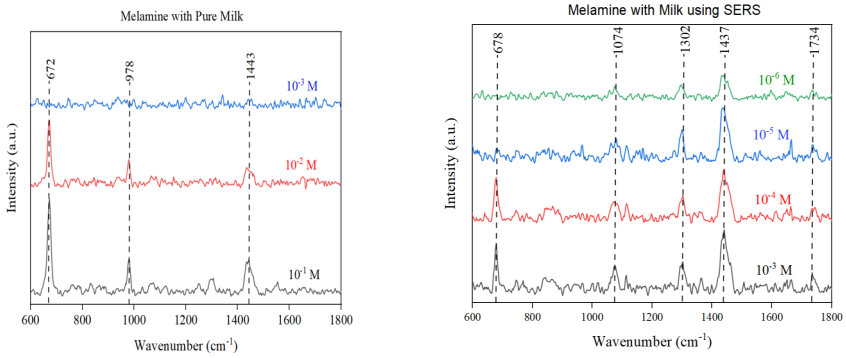

(a) *(b)*

Fig. 1 (a) shows the Raman peaks of melamine in pure milk with a limit of detection of millimolar concentration and (b) shows the SERS peaks of melamine in milk with a limit of detection of micromolar concentration.

References

1. Lenz, R., Enders, K., Stedmon, C.A., Mackenzie, D.M. and Nielsen, T.G., 2015. A critical assessment of visual identification of marine microplastic using Raman spectroscopy for analysis improvement. Marine Pollution Bulletin, 100(1), pp.82-91.

BPM206 Improved quantitative phase imaging via an optimization based transport of intensity equation

*Shubham Tiwari[1,2], Himanshu Joshi[2], Sunil Bhatt[2] , Harpreet Kaur[1,2], Shivam Trivedi[2], Dalip Singh Mehta[1,2]**

[1] Centre for Sensors, Instrumentation and Cyber Physical System Engineering (SeNSE), Indian Institute of Technology, Delhi, Hauz Khas, 110016;

[2]Biophotonics Lab, Department of Physics, Indian Institute of Technology, Delhi, Hauz Khas, 110016

** mehtads@physics.iitd.ac.in*

Transport of intensity equation(TIE) is a non-interferometry based technique for quantitative phase imaging (QPI). It has certain advantages over interferometry based techniques such as, speckle-free measurement, less vibration sensitivity due to a common path geometry and unwrapped phase retrieval however, the resolution and sensitivity with which the phase is measured in TIE is still limited due to various factors such as noise, boundary conditions, conditions on auxiliary function[1]. The TIE phase obtained can be improved using an optimization based approach. In TIE we have three intensity measurements at different planes of focus, we propose an amplitude based cost minimization method by minimizing the difference of measured amplitude(square-root of measured intensity) and theoretically expected amplitude in the three planes of focus.

The measured intensity at focus and phase obtained via TIE is used to create a field at focus. The field at defocussed planes are obtained via a defocus kernel. Cost function is created for different planes of focus by taking the difference of amplitudes at each plane. The cost is minimized using a gradient descent method and, in each iteration, for any plane, the field at focus is updated. Using this method, we also, simultaneously, recover the pupil function. The obtained pupil phase can provide information related to

aberrations present in the system. We have obtained high resolution QPI maps of RBCs and U2OS cells with significant improvements over phase obtained via TIE. Figure 1 below shows the comparison between phase map of RBCs(using a 40x, 0.65NA objective) obtained via TIE(fig. 1(a)) and the phase after applying the proposed algorithm(fig. 1(b)) clearly showing an improved phase sensitivity and resolution.

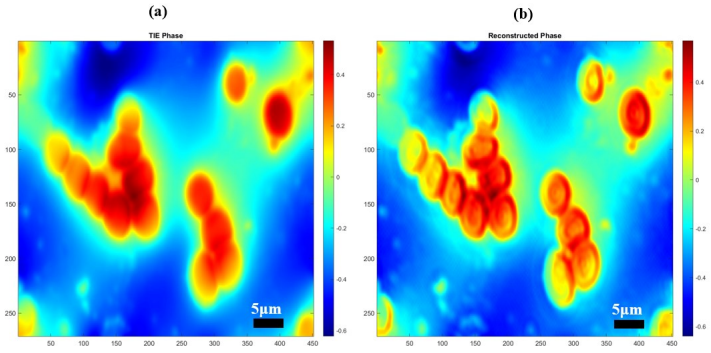

Fig. 1 Comparison of RBCs phase image via (a) TIE and (b) Proposed algorithm.

References

1. C. Zuo, J. Li, J. Sun, Y. Fan, J. Zhang, L. Lu, et al., 'Transport of intensity equation: a tutorial' Opt. Lasers Eng, 135 (2020), Article 106187, 10.1016/j.optlaseng.2020.106187

Category 3

Diffractive, Free-form and Adaptive Optics (DFA)

DFA108 Study of angular anisoplanatism using a pseudo-random phase plate

Jaspal Singh[1], Laxman Mandal[1], Biswajit Pathak[2], C.S. Narayanamurthy[2], AR Ganesan[1]*
[1]Applied Optics Laboratory, Indian Institute of Technology Madras, Chennai, 600036, India
[2]Applied and Adaptive Optics Laboratory, Indian Institute of Space Science and Technology, Thiruvananthapuram, Kerala, 695547, India
**Corresponding author: ph20d032@smail.iitm.ac.in*

In the present work, we have studied the angular anisoplanatism in a laboratory environment by generating two beams, one, a reference beam (mimicking a laser-guided star) and the other, an object beam (as a target object) and by employing a pseudo-random phase plate (PRPP) to mimic the atmospheric turbulence. Preliminary experimental results are presented that demonstrate the variation of different important parameters, such as, Zernike coefficient correlation, mean square error and beam centroid movement, as a function of angular separation between both the beams. This study is important for Adaptive Optics correction for imaging as well as free space optical communications.

Experimental Setup and Result: The schematic diagram of the experimental arrangement to study the angular anisoplanatism [1, 2] is shown in Fig. 1(a) where two beams were generated by using a cyclic interferometer type arrangement, which are then allowed to pass through the PRPP with controlled angular separation between both the beams. The Shack-Hartmann wavefront sensor (SH-WFS) finally records the turbulence impacted spots, from which different important parameters were evaluated using the intensity and slope information. Figure 1(b) shows one representative result that demonstrates the variation of wavefront mean-square error (MSE) as a function of angular separation (θ) between both the beams.

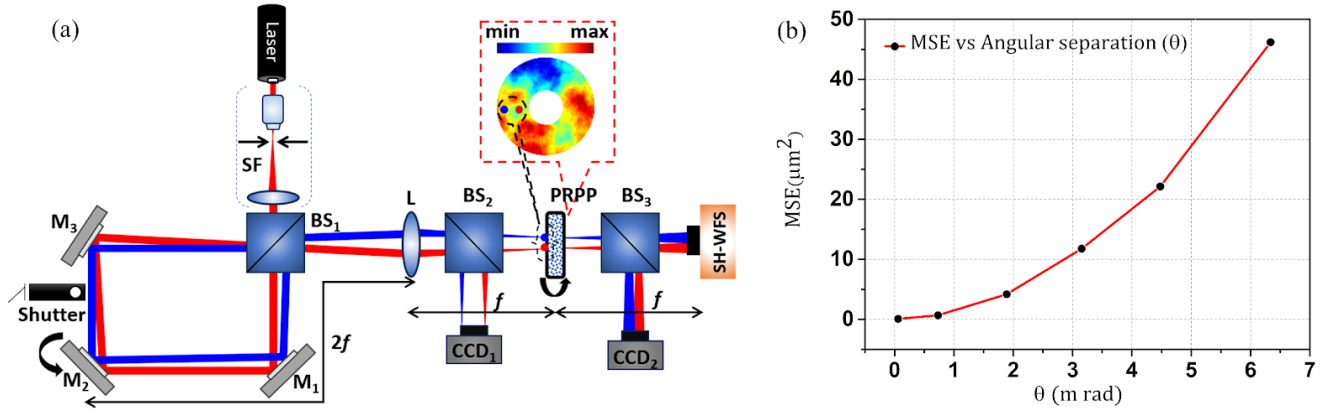

Figure 1 (a) cyclic type configuration to study anisoplanatism, SF: spatial filter; BS_1, BS_2, BS_3: beam splitter; M_1, M_2, M_3: mirrors; L: Lens; f: focal length of lens (L); CCD_1, CCD_2: charge coupled device; SH-WFS: Shack Hartmann wavefront sensor and (b) shows MSE as a function of angular separation between two beams.

References

1. D. L. Fried, *J Opt Soc Am 72 (1), 52 (1982).*

2. M. Moradi, *Optical Review 15 (2), 125 (2008).*

DFA109 Investigation of Coherent Beam Combining Efficiency in Diffractive Element-based Filled Aperture Approach

*M. S. Sooraj, Satyajit Maji, C. L. Linslal, S. Viswanathan, Balaji Srinivasan**
Dept of Electrical Engineering, IIT Madras 600036
**Corresponding author: balajis@ee.iitm.ac.in*

As the demand for high power lasers are increasing in different areas such as space exploration, material processing, defence, etc., coherent beam combination (CBC) based on diffractive optical elements (DOEs) has wide potential considering its high spectral and spatial purity with high efficiency [1, 2]. The use of binary phase elements for beam splitting and efficiency limitations has been analytically investigated well in the past with optimized grating parameters [3]. This work basically focuses on modelling of DOE phase profiles for beam splitting and simulation of beam combining with band-limited angular spectrum method (BLASM) propagation [4]. This investigation will give us a practical perspective of DOE based systems in terms of their implementation challenges and their limitations.

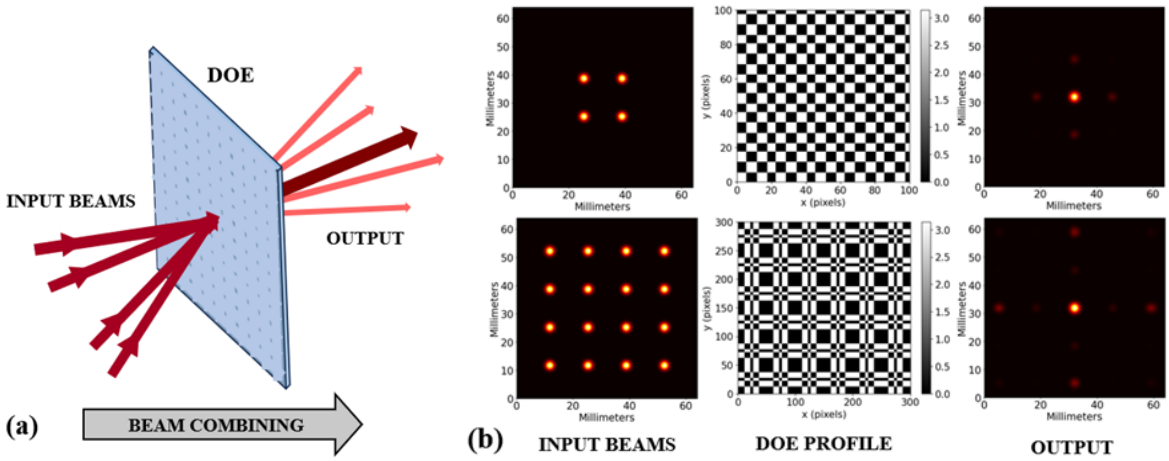

Figure 1: (a) Schematic diagram of DOE based 4 beam combination (b) DOE phase profiles and input/output beam profiles for both 4 beam and 16 beam combinations.

Figs. 1(a) and 1(b) show a schematic representation of 4 beam CBC and the phase profiles along with simulated beam combining inputs/outputs for 2x2 and 4x4 CBC. The 2D phase profiles for the above cases are generated by the addition of two orthogonal 1D phase profiles of 1x2 and 1x4 respectively and the beams are propagated in specific angles for combining. Simulations performed under identical beam parameters in phase locked state for 2x1, 4x1, 2x2 and 4x4 beam combinations result in efficiencies of 81%, 68.6%, 65.6%, and 47% respectively, limited by the diffraction efficiency of the DOEs. In our ongoing work, we are exploring multi-level phase gratings to improve the efficiency of the DOEs.

Acknowledgement: The authors would like to thank DRDO for funding this work.

References

1. A. Brignon, "Coherent laser beam combining". ISBN: 9783527652778 (2013)
2. C. L. Linslal. et al., ISSS Journal of Micro and Smart Systems. 11 pp-277 (2022)
3. Z. Hua, et al., Symposium on Photonics and Optoelectronics, *Chengdu, China. (2010).*
4. Kyoji Matsushima and Tomoyoshi Shimobaba, Opt. Express 17, 19662-19673 (2009)

DFA213 Optical Wireless Communication in Air-Underwater Channel

*Vikash Porwal, J. S. Rawat, and S.K. Mishra**
Instruments R&D Establishment, Dehradun-248008;
**skmishra.irde@gov.in*

Optical Wireless Communication technology can solve the problem of submarine vulnerability in existing airborne platform-submarine communication methods. The objective of the study is to explore the feasibility of such communication, develop the laboratory prototypes based on the outcome of feasibility study, and demonstrate optical wireless communication in the laboratory.

The laboratory prototypes including Laser Transmitter, Optical Receiver and Turbulence Cell are developed and characterized. A test setup is conceptualized and implemented to demonstrate the wireless communication in laboratory. A laser transmitter (Fig.1) uses the power of 3mW at 532 nm with 1.2 mrad divergence. The On Off Keying (OOK) scheme is used to modulate the laser beam. The PMT based optical receiver (Fig.2) with aperture 50 mm and field of view of less than 2^0 is used. The receiver sensitivity is measured as 100 nW. A Turbulence cell (Fig. 3) is used to introduce the channel loss of 0.16 m^{-1}. The channel loss introduced is estimated as 35 dB, which is accomplished by multiple and diffused reflections.

The developed laboratory prototypes are used to demonstrate optical wireless communication, in laboratory with data rate greater than 100 kbps against 35 dB air-water channel losses with the transfer of text, files and images successfully. The improvised prototypes can be used for outdoor experiments.

Fig.1: Laser transmitter

Fig. 2: Optical Receiver

Fig. 3: Turbulence Cell

References

1. A. Dixit et. al., *MAPAN-Journal of Metrology Society of India 35(2), 221-232 (2020).*
2. Jiemei et. al., *Optics Express 27(9), 12171-12181 (2019).*
3. S. Subramaniyam et. al., *Proceedings of ICOL, 141-144 (2019).*
4. SK Mishra et. al., *OSA Technical Digest/ Photonics, Th 3A.19 (2016).*
5. Sunita Sahani et. al., *Proceedings of INTOPMA, IIST Trivandrum (2017)*

DFA127 Phase Modulation Optical Communication through Kolmogorov type Turbulence

Shouvik Sadhukhan[1], Dinesh N. Naik[1] and C. S. Narayanamurthy[1]*

[1]Applied and Adaptive Optics Laboratory, Department of Physics, Indian Institute of Space Science and Technology (IIST), P.O: Valiamala, Trivandrum - 695547, State: Kerala; India
**Corresponding author: shouvikphysics1996@gmail.com*

Abstract: The present work deals with the phase modulation based optical communication through laboratory simulated Kolmogorov type turbulence. The comparison between the retrieved phases before and after turbulence impact has been done to justify the efficiency of our technique in optical communication systems.

Methodology and Results: The phase modulation is done in Michelson interferometer before turbulence impact plane. We have designed the experimental setup such that the two output beams of the interferometer propagate through collinear trajectories. The phases have been retrieved using single shot phase retrieval algorithms before and after the turbulence impact. We have used Hilbert transformation algorithm, Fourier Transformation algorithm, Continuous wavelet transform algorithm, Stockwell transform algorithm and Empirical wavelet transform algorithm for retrieving the phases.

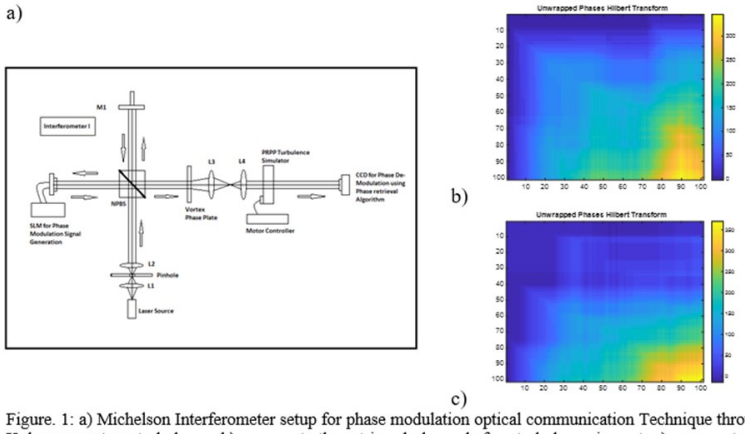

Figure. 1: a) Michelson Interferometer setup for phase modulation optical communication Technique through Kolmogorov type turbulence. b) represents the retrieved phases before turbulence impact. c) represents the retrieved phases after turbulence impact.

References

1. Gröger, A., Pedrini, G., Claus, D., Alekseenko, I., Gloeckler, F. and Reichelt, S., 2023. Advantages of holographic imaging through fog. Applied Optics, 62(10), pp.D68-D76.
2. Panchal, P., Naik, D.N. and Narayanamurthy, C.S., 2021. Insensitivity of higher order topologically charged Laguerre–Gaussian beams to dynamic turbulence impact. Optics Communications, 495, p.127023.

Category 4

Fiber Optic Devices, Sensors and Instrumentation (FIB)

FIB111 Ultra-sensitive detection of triethylamine (TEA) using LMR/LSPR based fiber optic probe

Jyoti[1,2], *R. K.Verma* [1,2]*

[1]*Central University of Rajasthan, Bandersindri, Ajmer, India, 305817*
[2]*University of Allahabad, Prayagraj, Uttar Pradesh, 211002*
**Corresponding author: rkverma@allduniv.ac.in*

From the literature survey, it has been analyzed that excessive intake and inhalation of TEA can cause health hazards such as blue haze, blurry vision, nausea, headache, and faintness and to prevent us from these hazards TEA detection has become essential [1,2]. For the detection of TEA, ZnO nanorods and porphyrin have been synthesized in this experiment and the topography, composition and morphology have been confirmed with FESEM, EDX and NMR characterization techniques. The fusion of both compounds (forms a hybrid material) was used to detect the performance parameter of fiber optic probes. The sensitivity of this hybrid material-based probe has been measured which was 7-fold to the sensitivity of the metal oxide (ZnO nanorods) based fiber optic probe. The selectivity study has also been performed and it has been measured that TEA has 83.495 nm shift in peak wavelengths which is 4.5 times the ethanol. This hybrid material-based fiber optic probe focuses on both better selectivity and sensitivity results for TEA and provides a very quick response time of a few seconds.

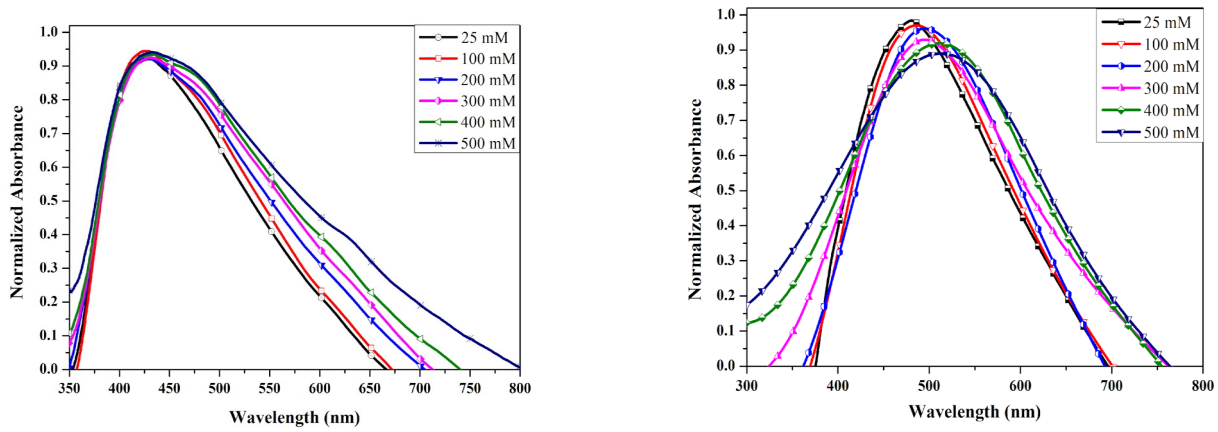

Figure 1 (a). Absorbance spectra for different concentrations of TEA on ZnO nanorods-coated probe, (b) porphyrin + ZnO nano-rods-based probe

References

1. Page et. al., *Occupa and Environ. Med. 60, 69-75, (2003).*
2. Liu et. al., *Small 18, 2104984 (2022).*

FIB112 Edge Filters for Optical Sensing Applications

Naveen Kumar M[1], Loraien Raju Kalathil[2], Kavyasree A.K[2], E.S. Shivaleela[1]*

[1]Department of Electrical Communication Engineering, IISc Bangalore, Karnataka - 56001
[2]International School of Photonics, CUSAT, Kerala - 682022
**Corresponding author: naveenkumarm@iisc.ac.in*

This work has identified promising edge filter components, Erbium-doped fibers (EDF) and a demultiplexer, which converts wavelength shifts into intensity changes, offering cost effectiveness for Fiber Bragg Grating (FBG) based strain sensing applications. DeMUX characterization identifies a negative slope edge filter in the 1540-1545 nm range as in Fig. 1.

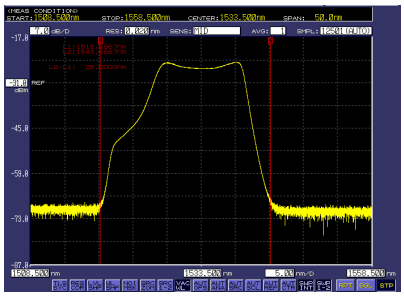

Fig. 1: Reference spectrum obtained for DeMUX output at the 1530 nm port

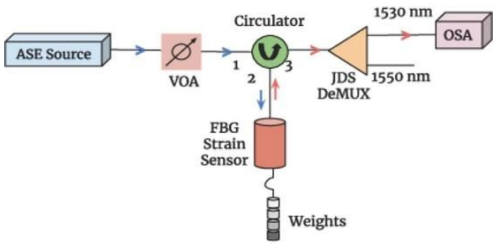

Fig. 2: Schematic illustration of DeMUX as strain sensor with FBG

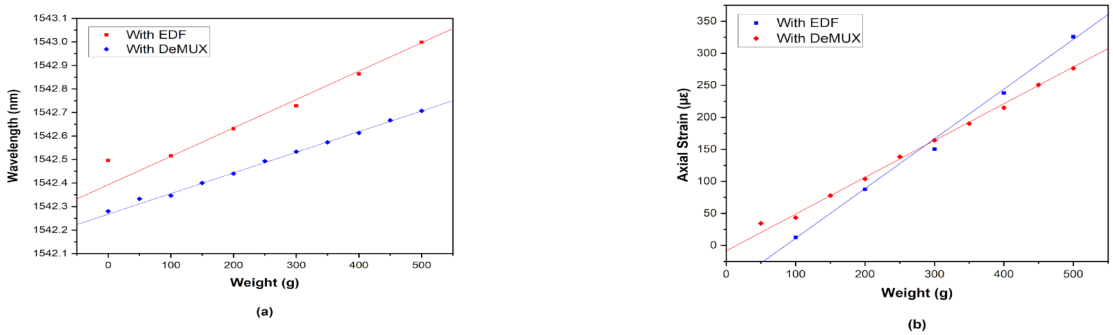

The strain sensing setup, as shown in Fig. 2, uses an Amplified spontaneous emission (ASE) source connected to port1 of a circulator and port 2 to a packaged FBG strain sensor, subjected to varying weights, at port 3 DeMUX (replaced with 9 m EDF) is connected. A sensitivity of wavelength shift of 19.3 pm/100g with 9 m EDF and 66.7 pm/100g for DeMUX, both utilizing the 1542 nm FBG strain sensor, was observed, which concludes that, the DeMUX exhibits higher sensitivity, thereby making it a more suitable choice as an edge filter.

References

1. Tiwari, et. al., "EDF-based edge-filter interrogation scheme for FBG sensors", IEEE Sensors Journal

13(4), 1315–1319 (2012).

FIB113 Detection of Phosphate using Different Geometries of Optical Fiber Sensor

Mohd.Ashraf[1], Mainuddin[1], M.T.Beg[1], Fiza Moin[1], R Rajesh[2]*
[1]Department of ECE, Jamia Millia Islamia, New Delhi-110025, India
NPOL, DRDO, Kochi, Kerala-682021, India
**Corresponding author: mainuddin@jmi.ac.in*

Fig.1. Photograph of the experimental setup

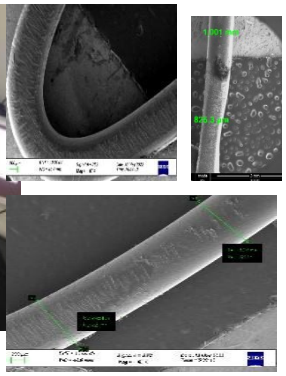

Fig.2.CCD images of developed sensor probe

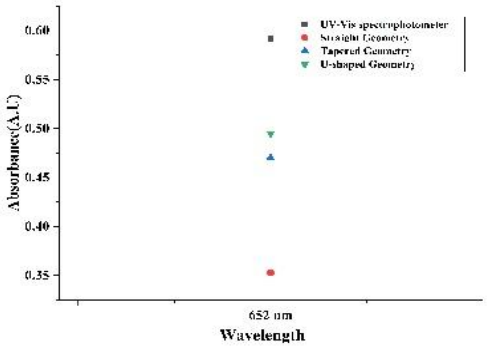

Fig.3. Absorbance of 10 ppm phosphate sample solutions

Water contamination is a significant threat to the environment and public health, requiring the development of efficient detection systems. Phosphate, a common contaminant in natural water sources, can pose health risks at both deficiency and excess levels. The WHO recommends a maximum limit of 1 mg/L for phosphate in drinking water [1]. Traditional detection methods like ion selective techniques, colorimetry, and spectrophotometry are expensive and bulky [2]. Recently, evanescent wave absorption-based fiber optic sensors (EWFS) have gained attention due to their simplicity, light weight, and accuracy. In this study, we present an EWFS with straight, tapered, and U-shaped probe geometries for phosphate ion detection in water. Evanescent wave (EW) absorption spectroscopy involves light traveling through an optical fiber, with some of it escaping through the cladding, creating an evanescent wave of wavelength λ. When the sensor's sensing region is immersed in the sample solution, this evanescent wave of wavelength λ is absorbed, as described in the literature [3,4]

$$P_t(z)=P_0e^{-\gamma z} \qquad (1)$$

Where, $P_t(z)$ specifies the power of light transmitted through the fiber at a certain distance "z," when sample is present, whereas γ represents the evanescent absorption coefficient. We have developed an experimental setup (Fig.1) to detect phosphate ions in water using three different sensor probes geometries made from multimode polymer optical fiber (OMPF1000). These probes were shaped into straight, tapered and U-shaped by de-cladding a 1 cm section from a 12 cm fiber length as shown in Fig.2.

The result of developed sensor (Fig.3) shows that U-shape exhibit the highest sensitivity of 0.0991O.D./ ppm followed by tapered geometry in comparison to straight geometry for detecting contaminants in water. This is due to the better EW interaction with impurities.

References

1. Lawal, et.al., *Talanta, 114 (2013).*
2. Pandikudy, et.al., Journal of optics, 42 (2013).
3. M. Ashraf et. al., *IEEE Sensors Journal, vol. 22, no. 15, pp. 14921-14928(2022).*

4. M. Ashraf et.al., *IEEE Sensors Journal, vol. 23, no. 10, pp. 10444-10451 (2023).*

FIB114 Optimized laser inscribed fibre Bragg gratings into fluoride fibres

Gayathri Bharathan[1], Alex Fuerbach[2]*

[1]Optics and Photonics Centre (OPC), Indian Institute of Technology Delhi (IITD), Delhi 110016, India
[2]MQ Photonics Research Centre, Macquarie University, NSW 2109, Australia
**Corresponding author: gayathrib@iitd.ac.in*

Fibre gratings, particularly fibre Bragg gratings (FBGs), were first exhibited over four decades ago and have since become important and ubiquitous components inside fibre laser cavities, optical communication networks, and sensor systems. Because of their widespread usage, the majority of published work has focused on silica-based glass fibres, which become essentially opaque at wavelengths over 2 µm, i.e., in the technically crucial mid-infrared (mid-IR) region of the electromagnetic spectrum. Soft glass fluoride fibres, on the other hand, particularly those made of ZBLAN (ZrF_4-BaF_2-LaF_3-AlF_3-NaF) and InF_3, provide low-loss transmission out to wavelengths of about 6 µm. However, while fluoride fibre manufacturing has advanced to a high level of maturity, with passive fibre attenuation levels as low as 1 dB/km, grating fabrication in these fibres remains challenging, and studies into ideal inscription techniques are still an active and ongoing scientific field.

Here we discuss the use of femtosecond laser technology to directly inscribe type-I FBGs into the core of fluoride optical fibres. We investigate and compare different fabrication techniques, including single-pass (line-by-line), double-pass, and stacking (plane-by-plane) methods (see Fig. 1), aiming to achieve the highest possible reflectivity FBGs suitable for mid-IR applications without using an expensive phase mask. In order to attain the optimum conditions for fabricating FBGs, a range of microscope objectives with varying numerical apertures and working distances were employed to meticulously manage the dimensions and appearance of the created grating layers. While exploring different parameter settings, we experimented with different pulse energies and inscription speeds to achieve a seamless refractive index modification characteristic of Type-I FBGs within the fluoride fibre. This systematic study allowed us to fabricate FBGs in fluoride fibres with highest reflectivity (99.98%) and ultra-low losses (<0.5 dB/cm) using direct fs laser inscription.

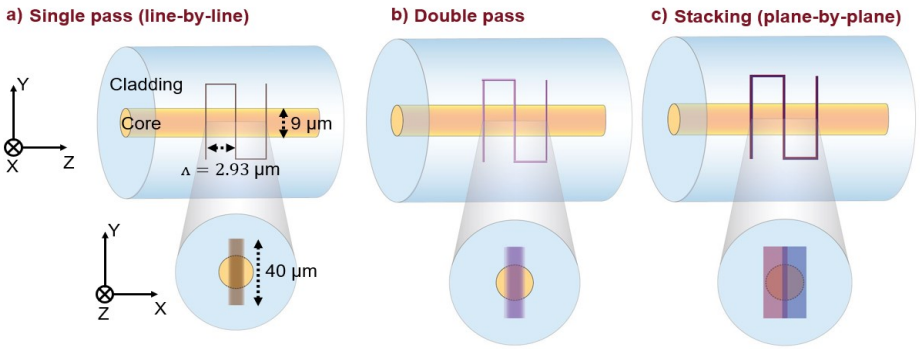

Figure 1. Longitudinal and transverse cross sections of various inscription techniques.

FIB214 Super Fluorescent Source for Fibre Optic Systems

Adwait Dawane[1], Lekshmi S Rajan[1], Yagya Malik[1], Praveena D[1], M N Srinivasa[1], Syeeda Nuzhath Zamani[1]*

[1]Laboratory of Electro Optic Systems (LEOS) – Indian Space Research Organisation, Peenya, Bengaluru, India 560058
**Adwait Dawane: adwait.dawane@leos.gov.in*

The phenomenon of generating photons when an excited state atom decays back to the ground state is called fluorescence. In conducive conditions the radiation field of the generated fluorescent photons couples itself with to the next photon to create a collective emission of such photons [1]. We report the design and development of a robust super fluorescent source with redundancy as shown in Figure 1 wherein starting from the left we have a pumping scheme with a 980 nm pump laser diode for generation of fluorescent photons of 1550 nm followed by an amplifying stage with the help of rare earth doped (Er^{3+}) fibre and finally the polarisation stage where we extract four outputs. The developed source module has low coherence length and broadband mode of operation with the spectral width observed experimentally to be 10-15 nm with the central wavelength ~ 1559.9 nm. We have incorporated double pass configuration [2] for our source module. The optical power performance of the four output ports as compared to the input pump power is shown in Figure 2. The source module is assembled in a mechanical housing and the spectrum stability has been experimentally observed to be <10ppm/ºC which is better than a semiconductor based broadband source with stability around 400ppm/ºC. The module can cater to four different fibre optic sensor heads if needed with only a single pump laser diode. Broadband operation and polarised output light along with spectrum stability can be utilised in fibre optic systems such as fibre optic gyroscopes, current sensors and fibre Bragg grating interrogators.

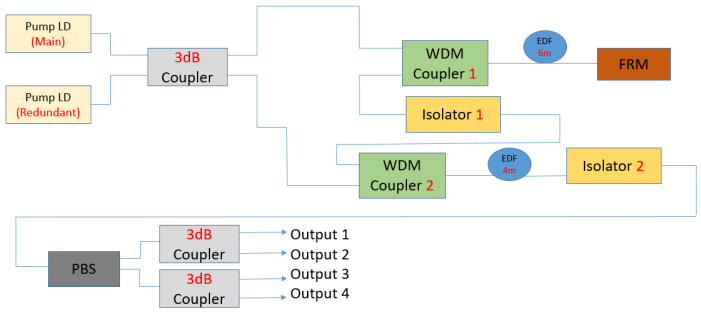

Figure 1 Design Configuration

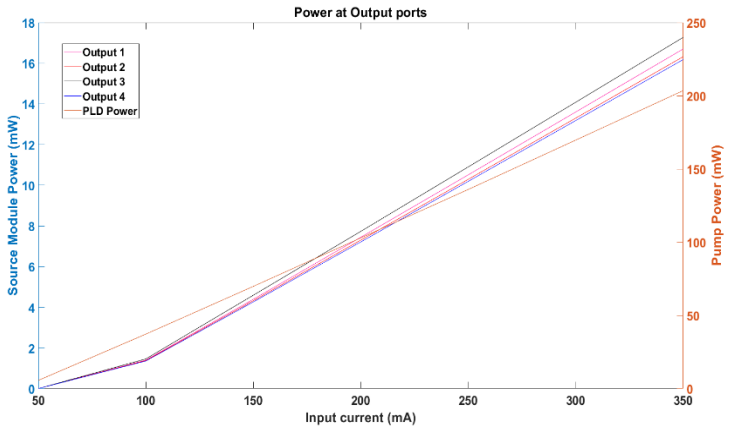

Figure 2 Optical Power Output

References

1. Dicke, R. H., PhysRev. 93.99, 1954, doi: 10.1103/PhysRev.93.99
2. Yan Li et. al., IEEE, 2013, doi: 10.1109/LPT.2013.2250948

FIB215 Optical study of Dye doped Polymer and its application in sensing

Akanksha Mishra[1], Roli Verma[1]*

University of Lucknow, Lucknow, 226007
**verma_r@lkouniv.ac.in*

This research examines the optical properties of Rhodamine6G (Rh6G) doped polyvinylpyrrolidone (PVP) and explores its potential for sensing applications. Rh6G is a well-known fluorescent dye with remarkable photophysical characteristics[1]. PVP is an excellent polymer matrix for hosting and capping such dyes[2], making this combination an interesting candidate for various sensing platforms.

The experimental approach begins with synthesising Rh6G-doped PVP samples with varying dye concentrations to investigate their optical behaviour. UV-Vis and fluorescence spectroscopy are employed to study dye's absorption and emission spectra in the absence and presence of polymer. This study aims to gain insight into the fluorescence quenching or enhancement mechanism when Rh6G-doped PVP encounters different types of anions. The study highlights the stability of Rh6G-doped PVP composites and observes shifts in their fluorescence emission intensity and wavelength over time, as well as in response to various anion species. The research shows the optical behaviour of Rh6G-doped PVP and demonstrates its versatility in sensing applications.

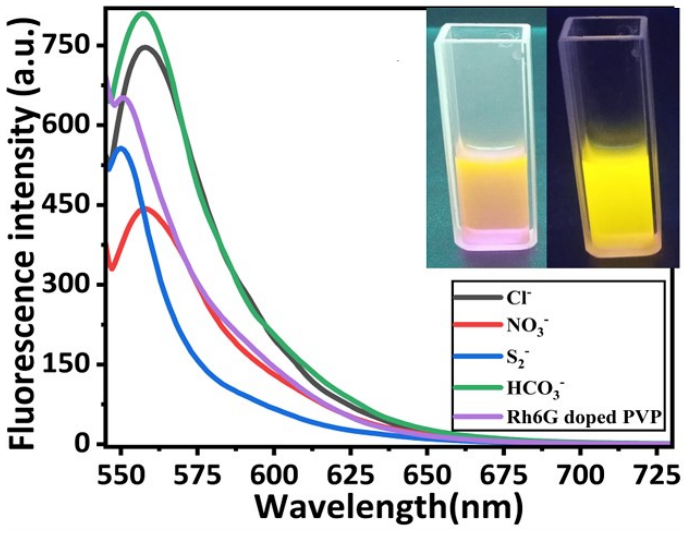

Fig.1 Fluorescence spectra of Rh6G doped PVP with different anions. Inset: colorimetric image of probe in visible and UV light.

References

1. Sivaraman G. et al., *Journal of Materials Chemistry B. 1 (42), 5768–5772 (2013).*
2. Basha M. A. et al., *Polymer Journal. 42(9), 728–734 (2010).*

FIB216 Effect of Lithium Niobate on the Sensing Performance of the Surface Plasmon Resonance Biosensor

*M. Muthumanicam[1], G. Alagu vibisha[2], M.C.L. Prabhakar[1], P. Suresh[1], K.B. Rajesh[2]**

[1]Department of ECE, Vel Tech Rangarajan Dr Sagunthala R & D Institute of Science and Technology, Chennai– 600025, TN, India
[2] Department of Physics, Chikkanna Govt. Arts College, Tiruppur 641602, TN, India
**Corresponding author: rajeskb@gmail.com*

We proposed a high-performance surface plasmon resonance biosensor with a novel structure of SiO_2 prism -Cu-$LiNbO_3$-BP based on angular interrogation Kretschmann configuration. This theoretical study exposes the vital contribution of SiO_2 prism, copper (Cu), Lithium Niobate ($LiNbO_3$), and black phosphorus (BP) to enhance the performance of the suggested SPR sensor. The perovskite material ($LiNbO_3$) sandwiched between Cu and BP layers provide superior sensing performance. The proper Cu and $LiNbO_3$ layer thickness optimized, which assists in achieving zero-closer minimum reflection (R_{min}), larger resonance angle shift, and small FWHM. Here, a monolayer of BP is used as a covering layer for the purposes of biomolecule absorption. The proposed biosensor optimized structure achieves ultra-high sensitivity (606°/RIU) as well as high FOM (177.19RIU^{-1}). The simple configuration of the suggested sensor offers accurate and rapid detection, making it appropriate for biomolecule detection.

The surface plasmon resonance (SPR) biosensor is an effective optical technology for sensing because of its special qualities, including high sensitivity, extremely precise, fast detection, long-term reliability [1]. The transfer matrix method is applied to calculate the suggested sensor's reflectance (Rp), which is a beneficial, easy, and accurate technique for multilayer structures [2]. First, we analysed the vital role of Cu, $LiNbO_3$, and Bp in enhancing the performance of the present sensor. The next phase is optimizing the thickness of the proposed layers in order to attain maximum sensitivity, lowest minimum reflectance (R_{min}), and smallest FWHM of the resonance curve. Here, it is noted that the proposed biosensor with a 60nm Cu layer only coated on SiO_2 prism exhibits sensitivity as 148°/RIU. Furthermore, it is observed that 10nm $LiNbO_3$ layer with monolayer BP placed on 46nm Cu attains sensitivity as high as 606°/RIU. Here, the inclusion and thickness optimization of the $LiNbO_3$ layer contribute more to enhancing the sensor sensitivity.

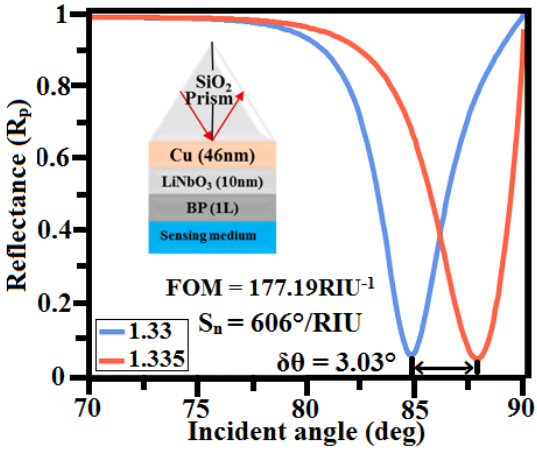

Fig 1.

References

1. H. Xu, L. Wu, X. Dai, Y. Gao, Y. Xiang, J. Appl. Phys. 120, (2016) 053101.
2. M. Yamamoto, Rev. Polarogr. 48, (2002) 209–237.

FIB217 Enhance Performance of SPR Biosensor Using Al-Co Bimetallic Layer Covered by $PbTiO_3$-BlueP/WS_2

*G. Alagu vibisha[1], R. Priyakalyani[1], K.B. Rajesh[1]**

[1] Department of Physics, Chikkanna Govt. Arts College, Tiruppur 641602, TN, India
**Corresponding author: rajeskb@gmail.com*

This numerical research work suggests a new configuration of a surface plasmon resonance (SPR) biosensor with enhanced sensing performance. The proposed modified Kretschmann model is composed of CaF_2 prism, Aluminium (Al), Cobalt (Co), Lead titanate ($PbTiO_3$), and BlueP/WS_2 under the angular introgation method. The thin layer of cobalt coated on Al film not only increases the sensitivity to a higher degree but also makes the Al-Co bimetallic layer cost-effective. The proposed sensor performance has improved with the inclusion of the $PbTiO_3$ layer owing to its high dielectric constant. Here, BlueP/WS_2 is suggested as an exterior coating due to its antioxidation capabilities and outstanding biomolecule-absorbing ability, which increase the long-term durability and sensitivity of the proposed biosensors. The thickness of the Al, Co, and $PbTiO_3$ layers has been carefully optimized to attain sensitivity and FOM as high as 536°/RIU and 117.06 RIU^{-1}, respectively. This SPR structure's excellent functionality has possible applications in biological detection and medical diagnostics, as well as the convenience of label-free sensing and real-time detection.

The prism based Kretschmann configuration is utilized in this SPR biosensor due to the advantages of not having an intermediary (air) between the base of the prism and the metal layer and the use of monochromatic light to obtain a high single-to-noise ratio [1]. The performance of the suggested SPR sensor design has been evaluated via the transfer matrix. Aluminium offers a narrower SPR spectrum and is more inexpensive than gold and silver [2]. Additionally, using a 2D material as a protective layer helps address the Al layer oxidation problem [2]. Al-Co bimetal combination is employed in the suggested biosensor, which contributes to improving sensitivity and reducing the FWHM of the SPR curve. Here, $PbTiO_3$ more supports increasing the sensing performance of the proposed structure to a great level through its optimized thickness. The well-optimized structure composed of 32nm Al, 1nm Co, 9nm $PbTiO_3$, and monolayer BlueP/WS_2 based proposed biosensor achieves FWHM as small as 4.57° and sensitivity as high as 536°/RIU.

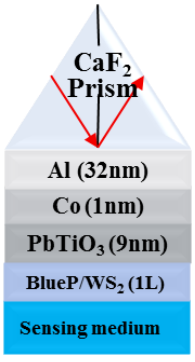

Fig.1 Schematic diagram of the proposed SPR biosensor

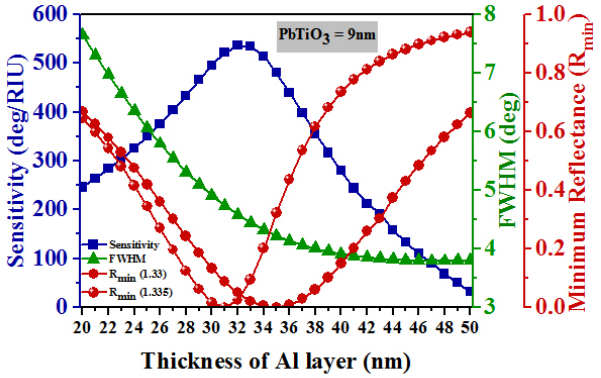

Fig. 2: ***Al layer thickness optimization***

References

1. E. Kretschmann, H. Raether, Z. Naturf. a, 23(12) (1968) 2135–2136.
2. P. K. Maharana, T. Srivastava, R. Jha, Plasmonics 9(5), (2014) 1113-1120.

FIB218 Effect of Porosity of Porous Silicon on the Performance of Fiber Optic SPR Sensor in NIR Region

*Anupam Kushwahar[1], Roli Verma[1,]**

[1]Department of Physics, University of Lucknow, Lucknow, India 226007.
**Corresponding author: roliverma10@gmail.com*

Optical sensors are important for the monitoring of environment, Agriculture production, public safety and for medical diagnostics. Herein, we have proposed a Fiber optic Surface Plasmons Resonance (FOSPR) based on Copper (Cu) and Porous Silicon (PSi) layers. PSi provide a high surface area and has abundant pores. Size of the PSi pore can be altered by controlling doping level, etching current density. Through the theoretical simulation, we have evaluated the effect of Porosity of PSi on the sensor Performance in Near Infra-Red (NIR) spectrum range [1]. Sensitivity and Figure of merit (FOM) has been calculated for different values of Porosity (0.3,0.4,0.5,0.6,0.7). The optimized structure produced a maximum sensitivity of 23800 nm/RIU for 0.3 porosity at 1.37 RIU. While, we get the maximum FOM of 240 RIU^{-1} for 0.7 porosity at 1.33 RIU. Due to advantage of alteration of pore size, it can be used as a good absorbent for different biological elements and gases. FOM of the probe can be tuned with porosity for high resolution of biological sensors as well.

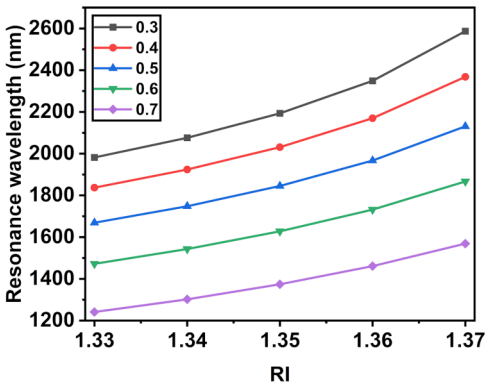

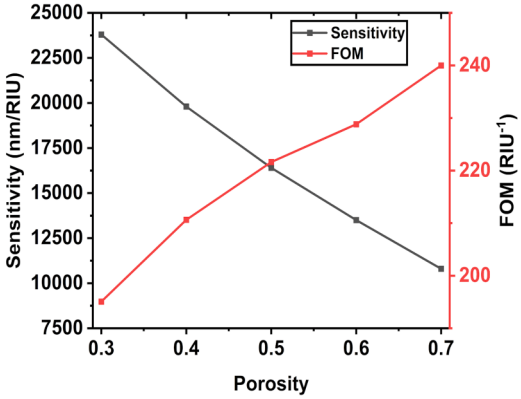

References

1. Zaky A. Zaky et al., *Scientific Reports 12, 1: 13777 (2022).*

FIB219 Time-Resolved Monitoring of Disturbance Propagation with Autocorrelation-Based Fiber Interferometry

Arvind Kumar Maurya[1], Ritesh Kumar[2], Venugopal Arumuru[3], and Rajan Jha[1]*
[1]NAPL, School of Basic Sciences IIT Bhubaneswar, Bhubaneswar India, 752050
[2]Shri Phanishwar Nath Renu Engineering College Araria, Bihar-854318
[3]Applied Fluids Group, School of Mechanical Sciences, IIT Bhubaneswar, India
**Corresponding Author -rjha@iitbbs.ac.in*

Accurate observation and analysis of disruptions within dynamic systems have significance in diverse scientific and engineering studies. Investigating the propagation rate of disturbances and their impact on various systems is crucial for enhancing the systems' efficiency, security, and reliability. The fiber interferometry-enabled autocorrelation technique offers an advanced monitoring platform for effective analysis of disturbance propagations [1]. To create inline-fiber-based Mach-Zehnder interferometers, a combination of single-mode fiber (SMF) and photonic crystal fiber or SMF-based structures is used. [2]. In

this study, SMF and PCF-based MZI structure is fabricated and characterized, which is sensitive to external vibration. Further, the combination of the developed interferometer unit is studied in the influence of a continuous disturbance to both sensing arms, and the impact is recorded simultaneously. In addition, the pace of this disturbance's spread was determined by an autocorrelation technique. The frequency and rate of propagation of this disturbance depend on the separation between these two interferometers which is subjected to the application and type of disturbance. The schematic of a combination of interferometers and disturbance propagation time estimation via autocorrelation technique is shown in Fig.1 (a) and (b). The proposed study has diverse applications, including acoustic wave monitoring in materials and structures, fluid dynamics analysis in pipelines and channels, seismic event tracking, and biomedical applications such as tissue vibration analysis. Real-time monitoring of disturbance velocity enables a deeper understanding of system dynamics and improves system engineering.

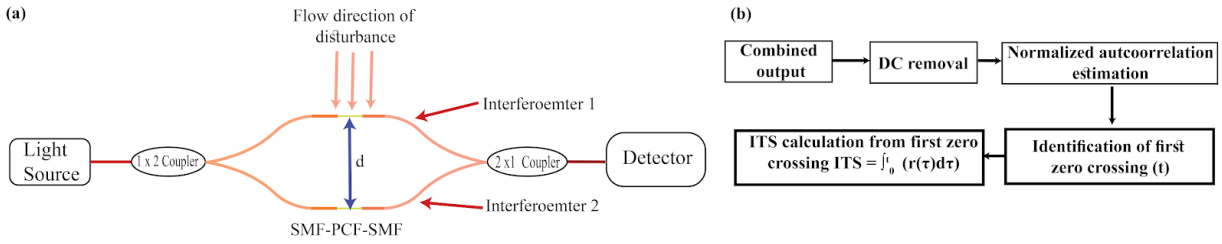

Fig. 1 (a) Schematic illustration of the typical experimental setup (b) Flow chart.

References

1. Lazo M. Manojlović, et. al., *Optics and Lasers in Engineering 48, 486-490 (2010).*
2. Chatterjee, K, et. al., *Scientific Reports 12, 3798 (2022)*

FIB220 Ultrasensitive whispering gallery mode biosensors

Arya Kumar Siddharth[1] and Venkata Ramanaiah Dantham[1]*
[1]Department of Physics, Indian Institute of Technology Patna, Bihar – 801106, India
**Corresponding author: dantham@iitp.ac.in*

At the very early stage of infection and disease, protein markers (at ultralow concentration) circulate throughout the body and may indicate infection or the reemergence of disease [1]. Therefore, the presence of infection or disease at an early stage would be elucidated through the detection of protein molecules at ultralow concentration within the bodily fluids. This detection is also helpful for environmental monitoring, emergency response, and homeland security [2]. Recently, the whispering gallery mode (WGM) biosensors have been found efficient for the real-time detection and sizing of protein molecules [3]. The WGM biosensor is nothing but transparent dielectric microparticles that act as high-quality factor (Q) optical microresonators upon suitable excitation with the help of tapered optical fibers. Recently, we have fabricated high Q optical microresonators and detected different types of protein molecules. The theoretical simulations based on the reactive sensing principle explain the experimental results. All the experimental and theoretical results will be presented at the conference. In addition, the different ways to boost the sensitivity of the WGM biosensors for the real-time detection and sizing of single protein molecules will be presented.

References

1. F. Vollmer et. al., *Appl. Phys. Lett. 80 (21), 4057–4059(2002).*
2. V.R. Dantham et. al., *Nano Lett. 13, 3347−3351(2013)*

3. J.Á. Freile et. al., *Sensors and Actuators B: Chemical, 346, 130512(2021).*

FIB221 Process Optimization of 4x1 Pump Combiner

Debparna Majumder, Atasi Pal*
CSIR-Central Glass & Ceramic Research Institute, Kolkata, India, 700032
Academy of Scientific & Innovative Research (AcSIR), Ghaziabad, India, 201002
**Corresponding author: dmdeb66@gmail.com*

Tapered fiber bundle (TFB)-based combiners play a vital role in the power scaling of fiber lasers. To obtain symmetricity in TFB structure, input fiber numbers are generally 7, 19,. or in asymmetric combiners, customized input and output fibers are applied [1,2]. In this work, the process of obtaining a near circular symmetrical TFB structure in 4x1 pump combiner has been presented using conventional four input pump fibers having core/cladding diameter of 105/125 µm, NA of 0.22. Two combiners have been developed to couple with output fibers having cladding diameter of 250 µm, NA of 0.46 and core diameter of 200 µm, NA of 0.22. The TFBs are prepared by tightly stacking the input fibers inside a pre-tapered silica capillary, followed by rotation implemented multiple fusing under vacuum pressure, further tapering down to OD/ID of 335/240 µm and OD/ID of 269/195 µm, maintaining the TR at 1.062 and 1.3. The taper length is set 10 mm for adiabaticity. Finally, the outer silica layer thickness of the TFBs are reduced to <12 µm through etching to obtain an outer diameter matched splicing region.

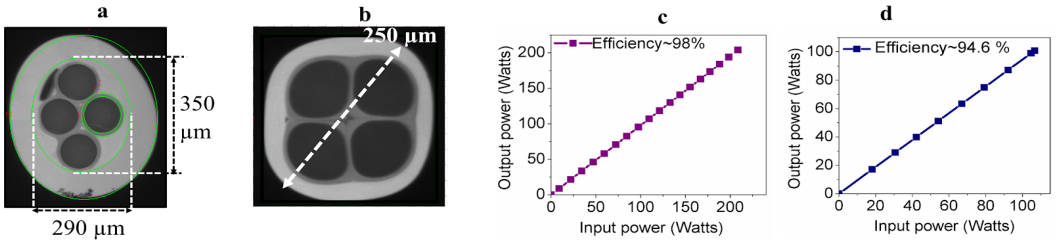

Fig.1 (a) Ellipticity in fiber bundle (b) processed near circular symmetric TFB (c) transmission efficiency of pump combiner with output fiber having cladding diameter 250 µm and (d) core diameter 200 µm, NA of 0.22

The implemented fusing process prevents the elliptical asymmetry in the fiber bundle (as shown in fig.1 (a)). The ellipticity results in a 3-7 deg. cleave angle which distorts the splicing region. Instead, a near-circular symmetrical TFB structure has been obtained along with outer diameter matching (shown in fig.1(b)) to maintain a cleave angle <0.5 degree and distortion-less uniform splicing region. Symmetricity, adiabaticity and brightness conservation maintaining TR<2 helps to obtain transmission efficiency of 98%, cumulative power handling >200 W maintaining an operating temperature <30 deg. C for the first combiner (as depicted in fig. 1(c)). However, conservation fails for the latter as TR is set at >1, and the obtained transmission efficiency is 94.6%, with cumulative power 100 W and operating temperature 50 deg. C (shown in fig. 1(d)). Hence it proves, that bundle symmetricity, brightness conservation, adiabaticity, and distortion-less uniform splicing region are essential to obtain high transmission efficiency along with high output power in the fabricated 4x1 pump combiners.

References

1. D. Stachowiak et.al., Opt. Laser Technol., 93, 33–40, (2017)
2. S. Zou et al., IEEE J. Light. Technol., 39, 7, 2130-2135, (2021)

FIB222 Ultra-selective enzyme and ultra-sensitive TCPP-based fiber optic probes for tyramine detection in wine

*R.K.Verma[1,2]*and Jyoti[1,2]*
[1]Central University of Rajasthan, Bandersindri, Ajmer, India, 305817
[2]University of Allahabad, Prayagraj, Uttar Pradesh, 211002
**Corresponding author: rkverma@allduniv.ac.in*

Spoiled, fermented, pickled food and stale beer and wines have a higher level of tyramine that cannot be metabolized in the intestine or liver [1]. The excess of tyramine in the body might lead to a hypertensive crisis and dangerously high blood pressure [2]. Titanium nanoparticles coated fiber optic probes with an additional layer of enzyme and 5,10,15,20 tetrakis(4-carboxyphenyl)porphyrin (TCPP) have been used to detect the tyramine in wine samples and the topology, morphology, and chemical composition have been confirmed with FESEM, EDX, and NMR characterization techniques. The performance parameters i.e. sensitivity, full width half maxima, figure of merit, limit of detection and limit of quantification have been calculated using both enzyme and TCPP-based fiber optic probes. The optimum value of sensitivity i.e. 0.572 nm/mM and other performance parameters have been obtained for the enzyme-coated probe. Selectivity and very quick response time of 3-6 seconds have been measured in this experimental work.

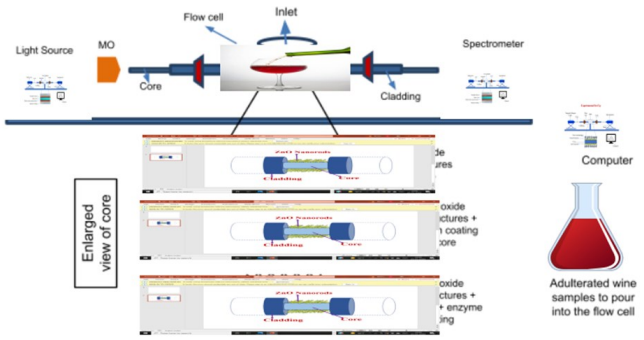

Figure1. Schematic diagram of fiber optic based bio-sensor for tyramine detectionin wine

References

1. Gaberniget. al.,*Eur. Food Res. Tech.235, 209-220 (2012).*
2. Flockhartet. al, (2012). *The Jour. of clini. Psychi. 73(suppl 1),4461 (2012).*

FIB223 All-Fiber Electric Field Sensing Using Cobalt-Doped Bismuth Ferrite Nanoparticles in a Three-Mirror Fabry-Perot Configuration

*Isha Sharma[1], Partha Roy Chaudhuri[1]**

[1]Department of Physics, Indian Institute of Technology, Kharagpur, 721302, India
**Corresponding author: roycp@phy.iitkgp.ac.in*

We present an experimental demonstration of an all-fiber electric field sensing configuration based on a three-mirror Fabry-Perot arrangement. The proposed approach utilizes a cantilever-beam deflection scheme.

In this configuration, we have coated an optimized composition of $BiFe_{0.9}Co_{0.1}O_3$ on the tip of an optical fiber, serving as a transducer [1]. The fiber tip is placed like a cantilever, with its coated end remains freely suspended (Fig. 1 (a)). We incorporated a 15 cm long single mode fiber positioned head-on with respect to

the coated fiber. This arrangement resulted in the formation of a micro-cavity between the two fibers. A thin layer of silver was deposited onto the surface of the fiber end using the evaporation deposition technique to create the reflecting mirror (reflectivity 80%). The detection of electric fields in our experimental scheme relies on the phenomenon that when the coated fiber is placed in an electric field, the induced polarization of the probe material leads to a bending effect, thereby resulting in the modulation of the cavity length. This modulation is utilized as a sensitive measure of the applied electric field. Furthermore, we have presented a theoretical model that accurately predicts the experimentally obtained results, considering the multiple reflection-transmission processes occurring within the Fabry-Perot circuit integrated with the beam-deflection based cavity [2]. The output transmitted profile of our scheme is illustrated in Fig. 1(b).

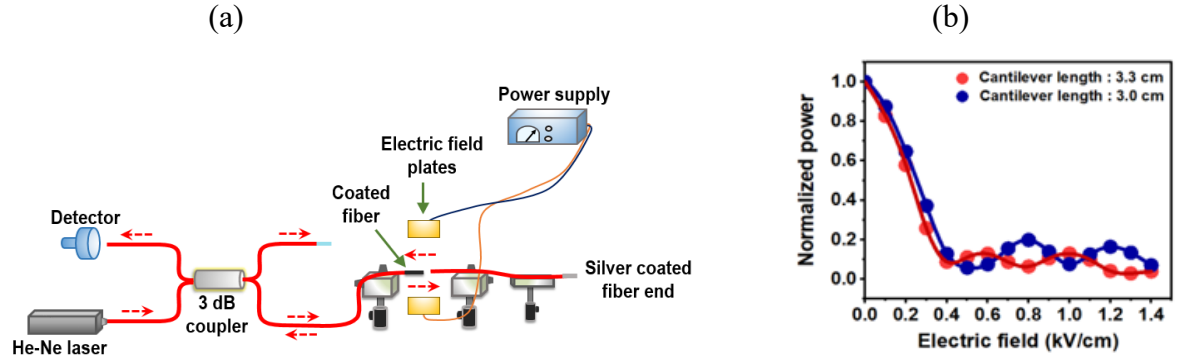

Fig. 1. (a) Schematic of the experimental setup (b) Output response with applied electric field for varying cantilever lengths.

References:

1. I. Sharma *et. al, Opt. Fiber Technol., 62, 102472 (2021).*
2. P. Simon *et. al, Appl. Opt., 51(19), 4536-4541 (2012).*

FIB224 Experiments on Phase-OTDR based Underwater Acoustic Sensing using 6mm fiber cable loop

Joseph Abraham Thomas, Malu Balachandran, C A Khansa, C V Sreehari, T V Praveen, T Santhanakrishnan and R Rajesh,*
Naval Physical Oceanographic Laboratory (NPOL), DRDO, Kochi, 682021, India
**Email: rajeshr.npol@gov.in*

Fiber optic sensing techniques based on Coherent Rayleigh backscattering have been widely used in many applications such as earthquake detection, perimeter security, railway track monitoring, underwater pipeline, submarine cable monitoring etc. [1]. In recent years, the concept has attracted by the research community due to their advantages like long-distance remote detection and cost effectiveness distributed sensing. Fiber optic cables have been extensively explored for vibration detections (land-based intrusion) employing Coherent Rayleigh backscattering based Phase-OTDR [2, 3]. Knowledge on acoustic sensitivity of fiber optic cables is very significant in the field of underwater sensing. Extensive studies on existing land and submarine cables for underwater fiber optic acoustic detection is required for sensing systems.

In this study, we demonstrate acoustic sensing on telecommunication cable using coherent Rayleigh backscattering based phase-OTDR. A semiconductor DFB laser with an exceptionally low narrow line width [<1kHz] and low phase noise was used as the light source. A semiconductor optical amplifier (SOA) to convert the continuous light into a pulsed probe signal. The backscattered light signal from Fiber Under Test (FUT) is received at probe side and separated using a circulator. A 6 mm diameter and 50m long conventional fiber optic telephonic cable wound into a spiral coil of ~ 40cm diameter was used as the

FUT, immersed in attest tank at 10m depth. The light is launched into the FUT through a 2 km long lead fiber optic cable. The probe pulse width is set as 200ns and 24 kHz pulse repetition rate, resulting in a spatial resolution of 20 meter. Phase of backscattered light at each position of the optical fiber cable is obtained by analyzing the electrical signal output from the Photodiode. The offline data is recorded and processed using MATLAB.The frequency response of the fiber optic cable is evaluated from 500Hz to 3kHz, the acoustic signatures were recorded. Herein, we found that a conventional telecommunication FO cables can be used for underwater acoustic detection effectively.

References

1. Juan C. Juarez et. al., Journal of Lightwave Technology, Vol. 23, No. 6, 2081-2087 (2006)
2. Petr Dejdar et. al., Sci Rep, 13, Article number: 7068 (2023)
3. Jason Johan et. al., Proc. SPIE 10680, Optical Sensing and Detection V, 106801B (2018)

FIB225 Ultra-high numerical aperture for dispersion compensation in chalcogenide based Photonic Crystal Fiber

*Jyoti Chauhan[1], Yogita Kalra1,Ravindra Kumar Sinha[1]**

[1]Delhi Technological University, Shahbad Daulatpur, Bawana Road, Delhi-110042
**dr_rk_sinha@yahoo.com*

We report a chalcogenide (As2Se3) based photonic crystal fiber having ultra-high numerical aperture value greater than 0.75 for wavelength 1.8-10 μm in Mid-IR range. The fiber acts as a dispersion compensating fiber with negative dispersion as low as approx -2000 ps/km-nm at 4.8 micrometers. The value of dispersion is significantly less due to the regular variation in the size of the holes in the transverse direction Also, confinement loss is appreciably less.

FIB226 Infrared - Visible – Ultraviolet Light Photo-detection Based on Nano-crystalline Metal Sulfide / Oxide Thin Films

Kashinath A. Bogle[1,]*

[1]Thin Films and Devices Laboratory, School of Physical Sciences, Swami Ramanand Teerth Marathwada University, Nanded – 431606
e-mail: kashianth.bogle@gmail.com

In this study, we present the creation of a high-quality photo-detector capable of detecting visible light. This detector relies on the utilization of consistent nano-crystalline metal sulfide/oxide thin films deposited onto a glass substrate using the spray pyrolysis method. An in-depth analysis of the film's structure, morphology, and chemical composition confirms the nano-crystalline properties of the thin film and its uniform coverage on the glass substrate. The photo-detection capabilities of these nano-crystalline thin films were assessed under illumination by visible light. To evaluate photodetection, we monitored the response of incident light in the form of photo-current when the films were exposed to light at different wavelengths, spanning from 420 to 700 nanometers. Notably, the fabricated device exhibited remarkable photo-detection characteristics even when operating at low voltage and with low-intensity illumination.

Time response measurements at various wavelengths revealed an ultra-fast response and decay time, along with high photosensitivity even at low bias voltage.

References

1. M. Choi, Y. J. Park, B. K. Sharma, S.-R. Bae, S. Y. Kim and J.-H. Ahn, Science Advances, 4, 8721 (2018)
2. S. Munde, N. Shinde, P. Khanzode, M. Budrukkar, P. Lahane, J. Dadge, S. Jejurikar, M. Mahabole, R. Khairnar and K. Bogle, Material Research Express, 5, 066203 (2018)
3. B. S. Chen, G. W. Meng, Q. L. Xu, X. G. Zhu, M. G. Kong, Z. Q. Chu, F. M. Han and Z. Zhang, ACS Nano, 4, 7105 (2010)
4. I. E. Morales-Fernández, M. I. Medina-Montes, L. A. González, B.Gnade, M. A. Quevedo-López and R. Ramírez-Bon, Thin Solid Films, 519, 512 (2010)

FIB227 Cost-effective Optical Comb Frequency Generation

Naveen Kumar M[1], Loraien Raju Kalathil[2], Kavyasree A.K[2], E.S. Shivaleela[1]*

[1]Department of Electrical Communication Engineering, IISc Bangalore, Karnataka - 56001
[2]International School of Photonics, CUSAT, Kerala - 682022
**Corresponding author: naveenkumarm@iisc.ac.in*

Optical frequency combs, akin to precisely spaced pulses of light, have revolutionized frequency measurements by leveraging the repetition rate of these pulses. Originally designed for ultra-precise timekeeping and spectroscopy, they have found widespread use across diverse fields. However, their generation typically involves complex setups. This paper introduces off-the-shelf components and cost-effective methods to generate optical frequency combs, specifically tailored for passive optical networks and short-reach communication systems. Our approach simplifies comb generation, while facilitating integration into emerging technologies. As such, it paves the way for a new era of cost-effective, high-performance optical communications, benefiting a multitude of applications.

Our design configuration, Fig.1, consists of a Sagnac loop that contains Polarization Maintaining Fibers (PMF) and Polarization Controllers (PC) and a Variable Optical Attenuator (VOA), with ASE source, VOA, PM circulator, coupler and an OSA. For slightly varying values of VOA thereby changing the path lengths, we obtained comb wavelength spacing of 0.7 nm and 0.6667 nm, as shown in Fig 2.

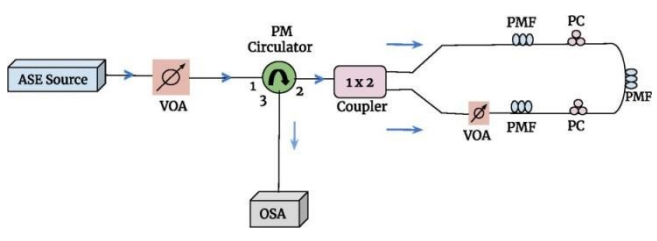

Fig. 1: Schematic for generating optical comb frequency using a PM circulator and a VOA in the Sagnac loop.

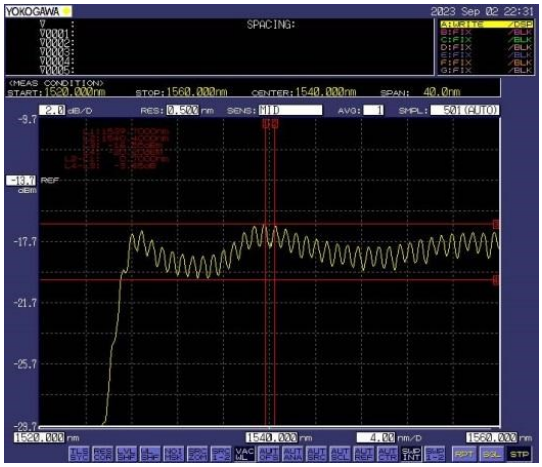

References

1. Zifei et al., Optical Frequency Comb Generation Using CMOS Compatible Cascaded Mach-Zehnder Modulators. IEEE Journal of Quantum Electronics (2019).
2. Xie et al., Wide-Spaced Optical Frequency Comb With Programmable Spacing. IEEE Photonics Technology Letters (2018).
3. Li, Meifeng et al., Flexible Tuning Optical Frequency Combs via Parametric Seeding in Microresonators with Normal Dispersion. IEEE Photonics Journal: 1-7 (2015).

FIB228 Beam self-cleaning multimode fiber under different conditions

Love Kumar Sharma[1], Vishwa Pal[1]*

[1]Dept. of Physics, Indian Institute of Technology Ropar, Rupnagar, Punjab, 140001, India
vishwa.pal@iitrpr.ac.in

The multimode optical fibers (MMFs) are being extensively reconsidered for their potential applications in spatial division multiplexing systems, upscaling the output power from fiber based lasers and more importantly as an accessible experimental platform for the study of complex spatiotemporal nonlinear dynamics. In particular, the Kerr beam self-cleaning (KBSC) has attracted a lot of research attention since it involves the evolution of the speckled output intensity pattern at low powers to a bell shaped beam that is similar to the fundamental mode (LP_{01}) or any other lower order mode of a multimode fiber at higher pump powers [1]. The nonlinear mechanism at the origin of such a peculiar self-organization of the beam can be understood as a parametric four wave mixing process, which breaks the orthogonality among the guided modes, and facilitates an energy transfer towards the lower-order modes. In particular, the refractive index of the fiber core undergoes a periodic longitudinal modulation as a result of the interaction between spatial self-induced periodic imaging and Kerr nonlinearity [2]. In our work, we adopted a 6 m long GRIN fiber with parabolic index profile supporting 20 modes and used different initial energy distributions among the guided modes from those previously reported and found that the power threshold for beam self-cleaning is different for different cases of initial energy distribution and not all the initial energy distribution leads to the phenomenon of KBSC. In the first case, we analysed the KBSC process with equal fractions (9%) of total peak pump power to the first 10 modes, and 1% each to the remaining 10 modes whereas in the second case, we distributed the total input peak power equally among the guided modes. The evolution of near-field spatial patterns for the two cases considered has been depicted in Figs. 1(a-f) and 1(a1-f1) respectively. It is observed that the output beam profile evolves from a speckle pattern at lower input power levels, into a well-defined bell-shaped profile at higher pump powers. The Fig. 1(g) shows that the intensity correlation parameter increases monotonically with the increasing pump power.

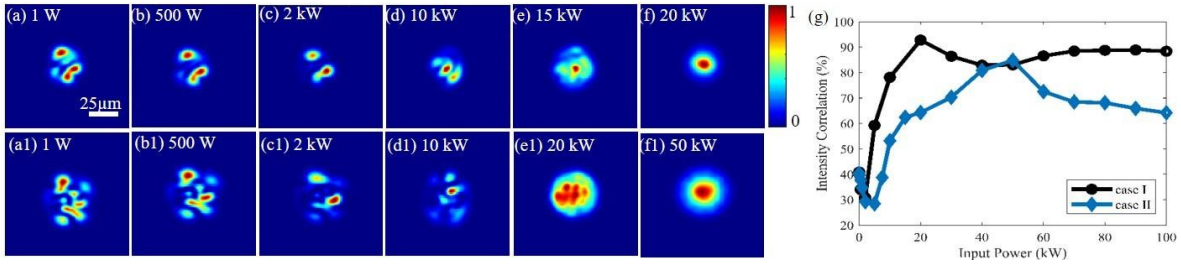

Fig.1. Evolution of near field beam profile upon increasing peak pump powers (a-f) for the case I, and (a1-f1) for the case II. (g) The variation of the intensity correlation parameter with the input peak power for the two cases.

References

1. Krupa et. al., *Nature Photon. 11, 237-241 (2017).*
2. Yuhang Wu et. al., *Opt. Lett. 46, 3312-3315 (2021).*

FIB229 Simulation of Acoustic Sensing Capabilities in Fiber Optic Communication Cables Using COMSOL Multi-Physics

*Malu Balachandran, Joseph Abraham Thomas, Praveen T.V, Sreehari C.V, Khansa C A, T. Santhanakrishnan and R. Rajesh**

Naval Physical and Oceanographic Laboratory, Kochi, India-682021

**email: rajeshr.npol@gov.in*

Fiber optic cables have emerged as versatile platforms for acoustic sensing applications, encompassing a broad spectrum of fields such as structural health monitoring, underwater surveillance, and seismic detection using different type of detection techniques. Fiber optic cables can be utilized as acoustic sensors based on Coherent Rayleigh Back scattering technique, where they can be set as distributed acoustic sensors (DAS). In DAS concept, the fiber optic cable is required to efficiently couple the acoustic field interaction with the fiber in it for an efficient detection. It is also proposed to use conventional underwater FO cables for acoustic detection and use the existing cables for surveillance purpose or seismic detection. However, the acoustic sensitivity of such cables is dependent on various design factors of the cables and unknown. Therefore an understanding of the influence of mechanical properties of different materials used in manufacturing the cables, along with the dimensions and geometry of the structures are very much important to predict the acoustic sensitivity and an attempt is made here to study this through simulation [1].

This paper presents a comprehensive study on acoustic sensitivity capability of certain fiber optic cables using the COMSOL Multi physics simulation platform. Simulations are performed to investigate the strain/ acoustic sensitivity of the cable under different conditions viz. external forces by varying material properties, geometric parameters to see the influence in optical performance of these cables [2]. Studies were initially done with bare fiber along with conventional protection coatings of different materials and properties. Then the study is extended to analyzing the acoustic sensing capabilities of different types of communication cables. Finite element model analysis of the cable properties has been done using the structural mechanics module in COMSOL Multi-physics for understanding how different parameters affect the cable performance [3]. The key contribution of this paper lies in understanding the effects of cable geometries in the strain sensitivity of a conventional jacketed patch cable was analyzed using FEM for strain analysis and studies were conducted, and the results will be discussed.

References

1. Bing Han et. al., *IEEE SENSORS JOURNAL, VOL. 21, NO. 4, (2021).*
2. Mohd Fahmi et. al., *IEEE 8th International Conference on Photonics (ICP), (2020).*
3. Joachim Hofmann et. al., *Proc. of SPIE, Vol. 9491, 94910E, (2015).*

FIB230 Human Footstep Detection using Rayleigh Backscattered Light in Underground Optical Fiber

Amarendra Pratap Singh[1], Neelam Verma[1], Ravinder Reddy M[1], Balaji Srinivasan[2] [1]Centre of Excellence, Bharat Electronics Limited 560013
[2]Dept. of Electrical Engineering, IIT Madras 600036
**Corresponding author: apratap@bel.co.in*

Despite multiple perimeter protection solutions such as electrical fences and PTZ cameras, a covert solution which can detect and locate intruders near the perimeter is a vital requirement. Rayleigh Backscattering light from underground laid optical fiber will be very apt for realizing such sensor system. This backscattered light picks up essential phase information if the light propagating through fiber is highly coherent. Forward propagating pulse and backscattered light interfere and provide us phase information spatially along the fiber. Such backscattered information stacked in slow time allows us to observe patterns due to any disturbances occurring near the fiber. Underground Test Bed was established to record various intrusion signals such as running and stamping of human. This paper presents the optical block diagram, intensity-based signal processing algorithm involved and reveals the signatures of stamping and running near the fiber.

ϕ-OTDR setup as shown in Fig 1(a) was established with a narrow linewidth laser with 40 mW CW power. AOM was used to generate 400 ns pulses with 5 kHz repetition rate. Further, EDFA was used to amplify the pulse power. ASE was filtered using reflective Bragg grating. Amplified pulse was sent to 3 km fiber length, part of which was laid underground. Backscattered light was collected sent to coherent receiver for mixing the signal with local power. Human weighing around 80 kg was running/stamping near the laid fiber and 2500 traces from one of the I/Q channel data was captured and stacked in slow time after mean subtraction. Fast Fourier transform was taken along the slow time. Waterfall obtained via such process contains spurious frequencies, not directly related with intrusion frequencies. Further processing is required to separate out the intrusion signal. After thresholding and low pass filtering with 500 Hz cut-off frequency, inverse Fourier transform was applied to convert back the data in time domain. Fig 1(b) shows the waterfall plot after the signal processing.

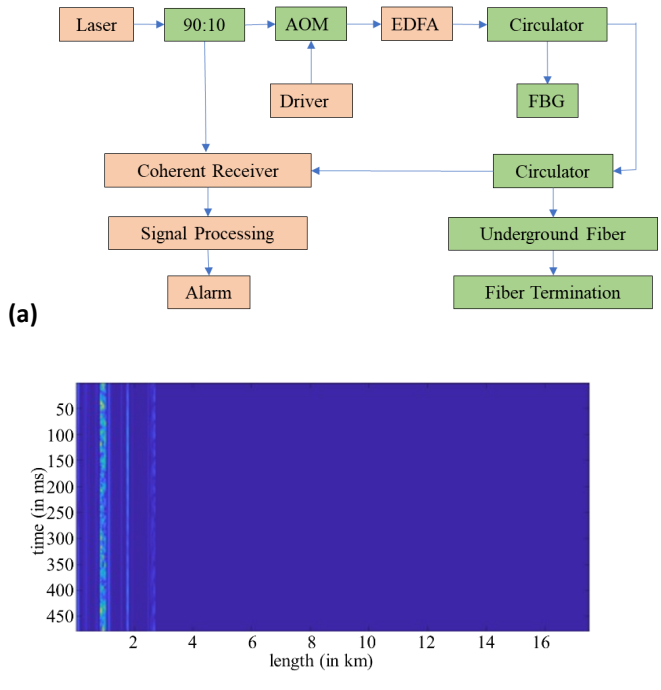

Fig 1. (a) Optical Block Diagram (b) Waterfall representation of post-processed vibration signal

References

1. True Phase Measurement of Distributed Vibration Sensors Based on Heterodyne ϕ-OTDR Huanhuan Liu ,Member, IEEE, Fufei Pang, Longbao Lv, Xuanwei Mei, Yingxiong Song, Jian Chen, and Tingyun Wang DOI:10.1109/JPHOT.2018.2791101 1943- 0655C 2018 IEEE.

FIB231 Highly Sensitive Refractometer utilising Plasmonic Mode Interference

*Neha[1] and Saurabh Mani Tripathi[1,2,3]**
[1]Optics and Photonics Centre, IIT Delhi, New Delhi-110016, India
[2]Centre for Lasers and Photonics, IIT Kanpur, U.P.-208016, India
[3]Department of Physics, IIT Kanpur, U.P.-208016, India
**Corresponding author: smt@iitd.ac.in*

An extremely sensitive plasmonic sensor utilizing a degenerate semiconductor core region, replacing conventionally used metallic region [1] sandwiched between two dielectric media, is proposed and analysed. We observe that the sensor supports symmetric as well as antisymmetric plasmonic modes, with a large propagation constant difference between those. The symmetric plasmonic mode can be easily excited by the core mode coupling technique, by axially splicing a conventional dielectric waveguide to the plasmonic waveguide. This technique, however, is not suitable to excite the antisymmetric plasmonic mode since the modal coupling coefficient [2] would vanish owing to the antisymmetric nature of the plasmonic field (see Fig.1(b)). We have, therefore, considered a suitable axial offset between the all-dielectric waveguide and the plasmonic waveguide as shown in Fig.1(a).

In our study, we considered the core width as d=200 nm and the plasmonic region length as L=0.3 mm. The transmission spectra at two different analyte refractive indices is shown in Fig.1(c), showing a sensitivity of ~4960 nm/RIU. An added advantage of the proposed sensor is that, in contrast to the conventional plasmonic sensors, the proposed sensor exhibits multiple resonances, which can be used for the simultaneous detection of a number of parameters.

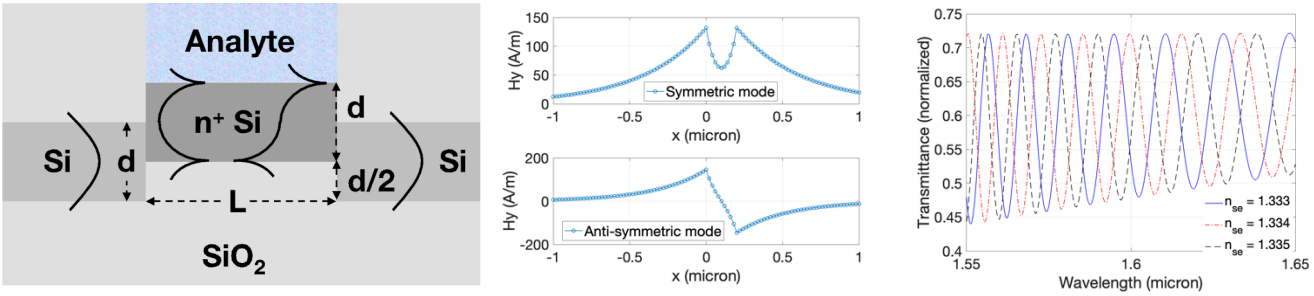

Figure 1 (a) Schematic diagram of sensor, (b) modal filed distribution of plasmonic waveguide, and (c) transmission spectra at different analyte refractive indices.

References

1. Kazanskiy, N. L., Khonina, S. N., & Butt, M. A. (2020). Plasmonic sensors based on Metal-insulator-metal waveguides for refractive index sensing applications: A brief review. Physica E: Low-dimensional systems and nanostructures, 117, 113798.
2. Optical Electronics, 2nd Ed., A. Ghatak and K. Thyagarajan, Cambridge University Press, 1989.

FIB232 Efficiency of MIP receptor SPR probe with and without GO for different pH samples of Sodium Benzoate

*Pratiksha Maurya[1], Roli Verma[1]**

[1]Department of Physics, University of Lucknow, Lucknow, Uttar Pradesh, India (226007)
**Corresponding author: roliverma10@gmail.om*

We report an experimental study of fabricated SPR-based Ag/MIP /SB sensor at different pH of Sodium Benzoate (SB) and checked the efficiency of Molecularly Imprinted (MIP) receptor with and without Graphene Oxide (GO). Figure 1(a) demonstrates the bar graph of various samples of SB at different pH after performing an SPR study of the probe. The present sensor shows a maximum shift in resonance wavelength of 70 nm at pH 7.4 while at other pH 4 and 8.4, it has only 10.03 nm and 7 nm shifts respectively [1]. Figure 1 (b) shows the effect of GO on the fabricated MIP receptor SPR probe for sensing of SB at pH 7.4 for both probes Ag/MIP/GO/SB and Ag/MIP /SB [2]. The total shift in resonance wavelength for probe Ag/MIP/SB is calculated to be 70 nm because the MIP probe has binding sites of the same size, shape, and functional group of SB while for the probe Ag/MIP/GO/SB is 11.59 nm. In Fig. b(i). there are minute shifts in SPR spectra recorded for Ag/MIP/GO/SB is smaller because GO, which is present in the MIP receptor interacts strongly with SB. So, after the first interaction with GO and SB, all the created cavities filled . Henceforth, no further shift was recorded after the first measurement because the bound SB molecules cannot be washed out of the sensing surface.

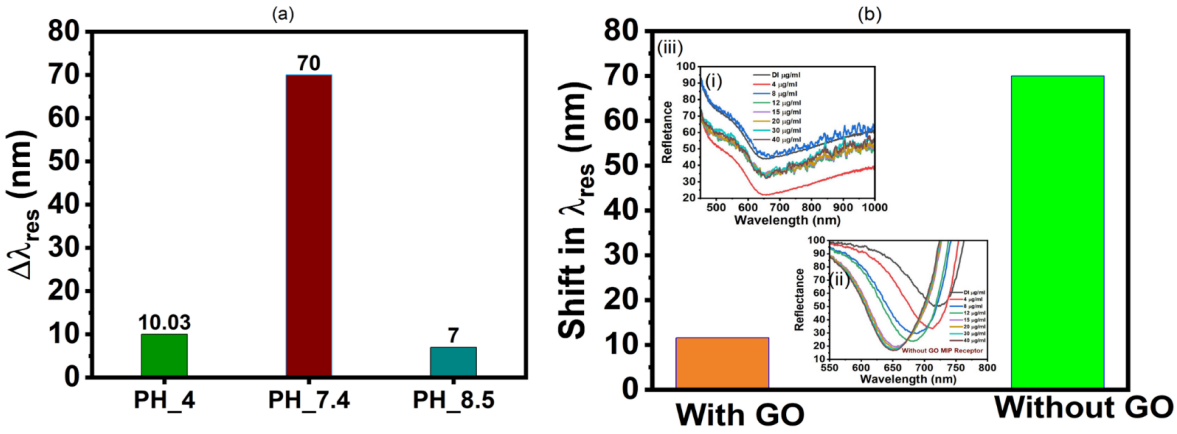

References

1. Shahmohammadi et.al., *Biotechnology and Health Sciences 3.3 7-11 (2016).*
2. Praphailong, W., and G. H. Fleet. Et.al., *Food Microbiology 14, 5 459-468 (1997).*

FIB233 PZT Based Frequency Modulation of DFB Fiber Lasers for PGC Based Interrogation of Interferometric Acoustic Sensors with TDM Architecture

*Praveen T V, C.V. Sreehari, Khansa C A, T. Santhanakrishnan and R. Rajesh**

Naval Physical and Oceanographic Laboratory, Kochi, India, PIN-682021
**email: rajeshr.npol@gov.in*

Among underwater acoustic sensors, interferometric fiber optic sensors have several advantages over the

conventional piezoelectric hydrophones due to its flexibility in realizing large sensor arrays of electrically passive nature. Hybrid TDM-DWDM multiplexing schemes are proven to be an efficient method for making large arrays with minimum hardware. Further, Phase Generated Carrier (PGC) technique is used for effective phase demodulation of interferometric fiber optic mandrel hydrophone with high dynamic range and better phase resolution operation. However, in such interrogator techniques, PGC modulation using the laser source at a known, higher frequency is the prime requirement and plays crucial role in the interrogator performance. In the present work, Distributed Feedback Fiber Laser (DFB-FL) is used as the master laser source and phase modulation is achieved by frequency modulation of the laser emission along with interferometer architecture. The frequency modulation of the laser is achieved by mounting the laser on a PZT slab controlled by a power module. The generated phase shifts in laser pulse for a carrier frequency is given $\delta\Delta\phi = -(2\pi n\Delta\imath/\lambda^2)\times(1- Pe)\times\varepsilon$ and it depends on refractive index *(n),* optical path difference *(Δι),* optical wavelength *(λ),* the axial strain *(ε)* on PZT slab due to modulation and the photo-elastic coefficient (*Pe*) of fiber laser. The experiment set up and generated phase modulations are shown in Fig. 1 & 2.

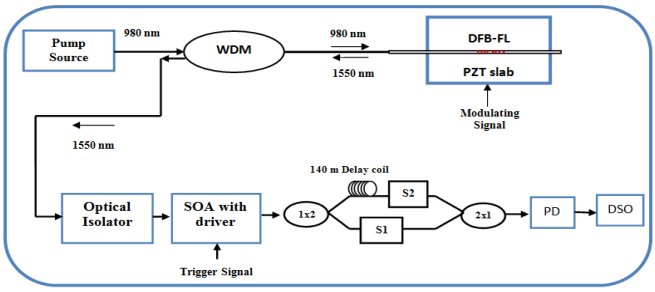

Fig.-1: Experiment set up

Fig.-2: 3π phase modulation on Laser Pulse

The PGC based TDM demodulation technique demands 3π phase shift over the interfered optical pulse for obtaining stable demodulated signal with better demodulation noise floor. The crucial elements for sustaining the 3π phase shift over the desired pulse duration and frequency is analyzed. The concern of modulation depth, PZT slab resonant states, locking of zero point of modulation with pulse center and strain distribution on PZT slab in the optimum phase shift generation through PZT based laser source modulation are also discussed in detail.

FIB234 Acoustic Low-Pass Filter for a Compact Fiber Optic Mandrel Hydrophone

*Praveena P.V., C.V. Sreehari, R. Rajesh and T. Santhanakrishnan**
Naval Physical and Oceanographic Laboratory, Kochi, India, PIN-682021
**e-mail: tsanthan.npol@gov.in*

Fibre optic mandrel hydrophones (FOH) convert acoustic signals falling on it into phase variations on the optical signal passing through an optical fibre wound on the mandrel. The dynamic range of optical phase demodulators is inversely proportional to the frequency of phase variation. High-frequency and high-amplitude acoustic signals can destabilize the demodulation of low-frequency signals. It is impractical to filter out such high-frequency variations before demodulation, especially in a time division multiplexed FOH array. Hence, an acoustic low-pass filter integrated with the FOH is essential to remove such high-frequency variations. In this paper, a compact FOH having a length of 50 mm, a diameter of 16 mm and an

acoustic low-pass filter based on small orifices having a diameter of 1.8 mm as shown in Fig. 1 is fabricated and tested[1]. Initially, the FOH is designed to get a flat frequency response up to 10 kHz and an acoustic low pass filter with a cylinder and orifices is designed to give acoustic attenuation above 5 kHz. Performance of the fabricated FOH is evaluated experimentally as shown in Fig. 2 for three cases namely (i) FOH alone, (ii) FOH placed inside the cylinder and (iii) FOH with cylinder and acoustic low-pass filter. The acoustic receiving sensitivity was obtained by comparing the compact FOH output with that of a standard hydrophone.

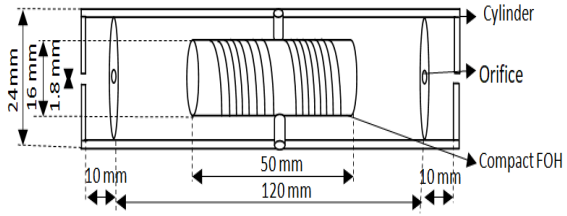

Fig. 1: Acoustic low-pass filter with compact FOH.

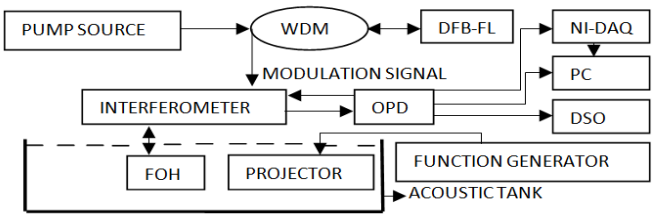

Fig. 2: Experimental setup.

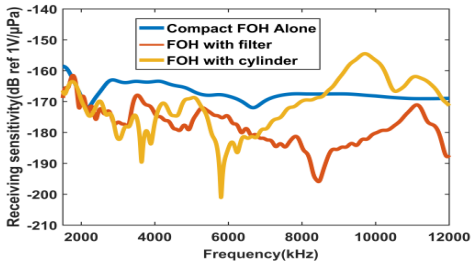

Fig. 3: Sensitivity of FOH for various frequencies with and without acoustic low-pass file

The results shown in Fig. 3 reveal a reduction of 5–15 dB in acoustic sensitivity above 5 kHz for the case of FOH with cylinder and acoustic low-pass filter. However, it was observed that the sensitivity response curve is not flat over bandwidth for cases (ii) and (iii) compared to (i). This could be due to the multiple reflections of the acoustic signal inside the cylinder.

References

1. Z. Wang et al., *Optics Lett.33(11), pp. 1267–1269 (2008).*

FIB235 An FBG-based throat microphone - influence of the placement of the FBG on the intelligibility of recorded speech

*Rituparna Jana[1], Nithin V. George[1] and Arup Lal Chakraborty[1]**
[1]Electrical Engineering, Indian Institute of Technology Gandhinagar, Gandhinagar-382355, India
**Corresponding author: arup@iitgn.ac.in*

Fiber Bragg grating (FBG)-based microphones can record speech with excellent background noise suppression [1] owing to the FBG's high strain-sensitivity. However, as this paper shows, the placement of the FBG on the throat has a pronounced effect on the quality and intelligibility of the recorded speech. The FBG microphone shown in Fig 1(a) was designed using a prestrained FBG with center wavelength of 1529.9 nm. The microphone was placed in the lower part of the throat near the thyroid gland and at the upper part near the thyroid cartilage, as shown in Fig 1(b). A 1531.52 nm distributed feedback tunable diode laser was used to perform intensity-based FBG interrogation. The vibration of the vocal cords

induces spectral shifts of the FBG's reflection spectrum that in turn translate to intensity changes recorded by the photodetector [2]. The block diagram of the experimental setup is shown in Fig 1(c). An adult female participant read 10 phonetically balanced sentences (Harvard lines) 10 times for each microphone placement. The speech was recorded simultaneously by the FBG microphone, and a reference condenser microphone was placed 5 cm away from her mouth. The FBG microphone's output was denoised using spectral subtraction. The signals from the FBG microphone and the reference microphone shown in Fig 1 (d) are similar over the same time intervals. The intelligibility of the speech recorded by the FBG microphone was assessed by non-intrusive speech intelligibility (SI) metrics. There is a statistically significant difference in speech intelligibility between the lower and upper throat recordings. This work will now be expanded to study the potential effect of the speaker's gender and age on the recorded speech intelligibility.

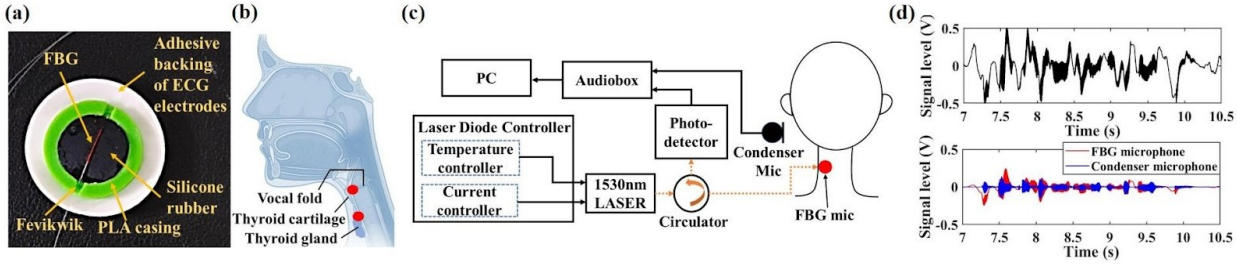

Fig 1: (a) The FBG microphone and (b) its placement on the throat. (c) Block diagram of the experimental setup. (d) Raw speech signal recorded by FBG microphone (black). Comparison of a speech signal recorded by the condenser microphone (blue) and the FBG microphone after denoising (red).

References

1. C. K. Jha et. al., *OFS Conference, Washington, DC: OSA, W4.44 (2021).*
2. D. Tosi et. al., *Appl. Opt. 47, 5123–5129 (2008).*

FIB236 Designing Polycarbonate coated FBG for High-performance Temperature Sensing

*Saikat Mondal[1], Partha Roy Chaudhuri[1]**

[1]Department of Physics, Indian Institute of Technology, Kharagpur, India, 721302
**Corresponding author: roycp@phy.iitkgp.ac.in*

Introduction: We proposed a high-performance fiber Bragg grating (FBG) based temperature sensor coated with elastomeric polymer. In order to enhance the temperature sensitivity, polycarbonate (Makrolon polycarbonate and Bayflex polyurethane) layer is coated on the FBG (Gaussian apodized), as it has a high thermal expansion coefficient (~70×10^{-6}/0C) which could effectively increase the sensitivity by 2.5 times higher than the typical conventional bare-FBG based sensor.

Analysis and Result: To analyse the temperature dependency of Bragg resonance wavelength (b=$2n_{eff}$, where n_{eff} is the effective refractive index, is the grating period), we have investigated the wavelength shifting of the proposed structure using Matlab simulation platform for the shift of b with increasing temperature (ΔT). The resulting the Bragg wavelength b is altered due to thermal expansion when temperature increases, consequently affects the λ_b. The expression of b due to ΔT temperature variation is as [2]:

$$\Delta\lambda_b = \{(1-\rho)\varepsilon + (\alpha_f + \eta)\ \Delta T\}\lambda_b \qquad (1)$$

Where ρ is the photo-elastic coefficient (~0.22) of the fiber material, α_f is the thermal expansion coefficient (~$0.55\times10^{-6}/^0$C) and is the thermo-optic coefficient (~$8.6\times10^{-6}/^0$C) of the FBG, ε [3] is the axial strain due to thermal expansion and we take the cross-section area of the polymer coating is 100 mm^2. Figure-1 shows the simulated reflected spectrum from the FBG in the temperature span of 20°C to 100°C and figure-2 illustrates the correlation between the $\Delta\lambda_b$(in nm) and the change of temperature (in °C)

Conclusion: The presented analytical model demonstrates notable temperature sensitivity owing to the incorporation of a polycarbonate-coated Fiber Bragg Grating (FBG). This model has successfully achieved an enhanced temperature sensitivity of 0.0365 nm/°C (where the conventional bare-FBG has temperature sensitivity ~0.0142 nm/°C)

References

1. F. Liu et. al., *Optik. 289, 171257 (2023).*
2. F.V Carreon et. al., *Opt. Fiber Technol. 77, 103257 (2023).*
3. Y. Feng et. al., *Applied Sciences. 9(2), 286 (2019).*

FIB237 Size dependent emission tuning in coupled dye doped step index polymer optical fibers

*Sathe Mayur Anil[1], M. Kailasnath [1]**

[1] International School of Photonics, Cochin University of Science and Technology, Cochin-22, India.

Corresponding author: kailas@cusat.ac.in

The whispering gallery modes [WGMs] in microcavities significantly enhance the light-matter interactions [1]. The organic dye-doped polymer fibers have been reported as WGM resonators [2, 3]. A coupled fiber laser was reported for single-mode lasing by using the Vernier effect [4, 5]. However, in the previously reported works, few-mode fibers were used, and the coupled fiber laser with multimode fibers needed to be explored more. The multimode dye-doped uncladded step-index fibers were fabricated [3], and lasing from fibers was observed separately and by coupling the two fibers. The coupled fiber laser system consists of two dye doped step index polymer optical fibers with unequal diameters 250µm and 350µm. One of the fibers was excited using a 532nm Q switched Nd:YAG laser and the emission was collected from the other using a CCD Spectrometer. The smaller diameter fiber was transversely excited, and emission (peak emission wavelength a) was collected from the surface of larger diameter fiber. Similarly, while exciting the larger diameter fiber, the emission (peak emission wavelength b) was collected from the fiber with smaller diameter. With the same pump pulse energy, it is observed that a is considerably smaller than b with a shift in the peak emission wavelength of approximately 22nm.

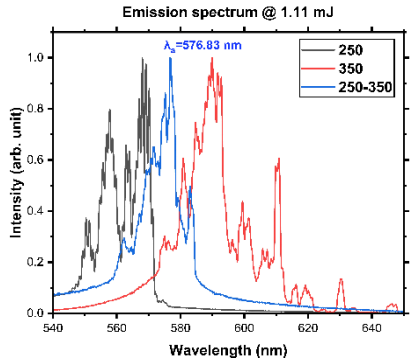

Fig. 1-Emission spectrum from single and coupled fibers (excitation fiber size 250µm – emission fiber size 350µm) at a pump pulse energy of 1.11 mJ

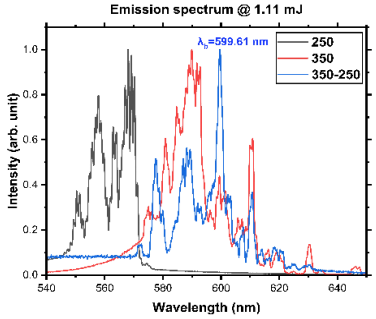

Fig. 2- Emission spectrum from single and coupled fibers (excitation fiber size 350µm – emission fiber size 250µm) at a pump pulse energy of 1.11 mJ.

References

1. K. Vahala, "Optical microcavities," *Nature, vol. 424, pp. 839-846, 2003.*
2. M Kailasnath, et. al., *PRAMANA - journal of physics , vol. 75, no. 5, p. 923–927, 2010.*
3. J. Peter, et.al., *Optics & Laser Technology, vol. 63, pp. 34-38, 2014.*
4. Van Duong Ta, et. al., *Adv. Optical Materials, vol. 2, pp. 220-225, 2014.*
5. Kun Ge, et. al., *Optics Express , vol. 30, no. 16, p. 28752, 2022.*

FIB238 Fano line-shaped transmission and photon coupling emission in hybrid optical nanowire structure

*Satyajit Murmu[1], Avijit Kumar[2] & Rajan Jha[1]**

[1] *Nanophotonics and Plasmonics Laboratory, School of Basic Sciences*
Indian Institute of Technology, Bhubaneswar-752050, Odisha, India.
[2] *Low-Dimensional Physics Laboratory, School of Basic Sciences*
Indian Institute of Technology, Bhubaneswar-752050, Odisha, India.
**Corresponding author: rjha@iitbbs.ac.in*

Advanced light-matter interface configurations like nano waveguides[1], ring resonators[2], and quantum electrodynamic (QED) cavities[3] exhibit reliable and efficient fluorescent photon coupling as well as photon channeling. Here we have designed a Bragg cavity-based hybrid waveguide system (shown in Fig. 1(a)) which exhibits a Fano line shape in the transmission spectra. The photon coupling and the emission rate of the dipole placed in the hybrid cavity exhibit a Fano line shape (shown in Fig. 1(b)). Further, the coupling efficiency of this cavity is found to be 80% at the largest Purcell factor of 100/265. The Purcell factor for the emitter located at the interface of the diamond nanowire and the optical nanofiber is found to be ~85% of the Purcell factor for the dipole positioned at the center of the diamond nanocavity.

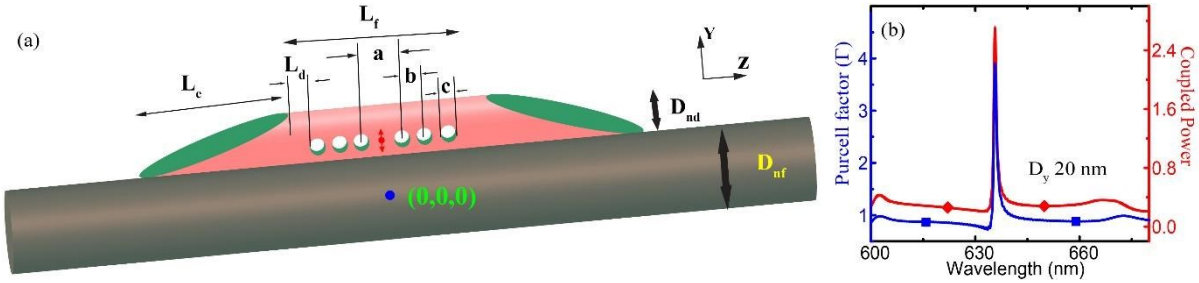

Fig. 1. (a) Schematic picture of the designed hybrid cavity with D_{nf}, D_{nd}, L_e, L_f, a, b, and c indicating the diameter of the optical nanowire, the diameter of the diamond nanowire, the etched length, the free length, cavity length, periodicity, and air groove diameter respectively. L_d denotes the distance between the starting point of the etched part and the closest air groove. The red dot with a double side arrow and the blue dot represent the dipole and the center of the coordinate system, respectively. (b) Dipole emission from the dipole in the proposed structure in position (D_x/D_y/D_z)=(0/20/102 nm).

References

1. Y. Yonezu, et al., *Sci. Rep., vol. 7, no. 1, p. 12985, (2017).*
2. Ł. Dusanowski, egt al., *Nano Lett., vol. 20, no. 9, pp. 6357–6363, Sep. (2020).*
3. R. Yalla, et al., *Phys. Rev. Lett., vol. 113, no. 14, pp. 1–5, (2014).*

FIB239 Embedding of FBG sensors in electromagnetic coils for temperature studies during high current pulse discharges

S.D.V.S. Jagannadha Raju[*1], P.P. Rahulnath[2], Pradeep K Maurya[2], M. Sukant[2], S. Pradhan[1]*
[1]Photonics and Quantum Optics Section, AMPD, BARC, Visakhapatnam-531011
[2]Electromagnetic Experimental Section, CAD, BARC, Visakhapatnam-531011
**Email: sdvsjr@barc.gov.in*

Fiber Bragg Gratings (FBGs) are passive optical fiber sensors [1] and are unaffected by high electromagnetic (EM) fields. Their thin (250 micron with coating) form factor [2] makes it easy to embed them in composite material within the electromagnetic (EM) coil. Solenoid EM coils are made of copper conductor winding which is reinforced with insulating fiber/epoxy composite material. The ID and OD of the cylindrical EM coil used are 24.6 mm and 70mm. So within this EM coil (yellow cylinder mounted between two nylon C-blocks as shown in fig. 1(a)) of thickness of 23 mm, two FBGs at central wavelengths 1548.040nm and 1562.051nm were embedded by inserting protective sleeves during fabrication.

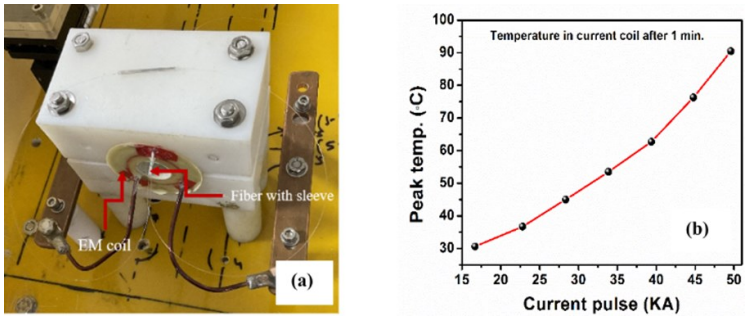

Fig. 1. (a) Current coil under testing with fiber embedded in sleeves (b) Temperature measured using FBG

Pulsed (underdamped) high current with peaks ranging from 16.7 kA to 49.61 kA were passed through the

coil. The duration of each pulse is 2 to 4 milliseconds. One minute after every pulse the peak temperature is attained due to ohmic heating in the coil and then then it slowly reaches room temperature by natural cooling. Peak temperatures attained at different current peaks is plotted in fig. 1(b). Repetitive experiments confirmed the same temperature values from 31 °C at 16.7 kA to 90.5 °C at 49.61 kA. However there was a shift of 50 to 100 picometers in the characteristic wavelength of FBGs (at room temperature) after several trials, which might be because the composite material has slightly readjusted itself adding to some residual stress on the FBGs. Further studies can help in delineating the effect of temperature and strain, designing current coils with long life and with higher duty cycle.

References

1. CVN Bhaskar et al., 'Recent advancements in fiber bragg gratings based temperature and strain measurement', Results in Optics, 100130 (2021).
2. B. Lee, 'Review of the present status of optical fiber sensors', Optical fiber technology, 9(2), 57-79 (2003).

FIB241 Fostering green synthesis for the detection of food preservative based on Molecular Imprinting Polymer

Shivani Maurya[1], Roli Verma[1#]

[1]Department of Physics, University of Lucknow, India, 226007

Roli Verma: [#]roliverma10@gmail.com

The present study aims to blend the decency of natural resources in the synthesis of metal nanoparticles which can exhibit the transducing mechanism of LSPR. The basic idea is to propose a cost-effective, portable LSPR-MIP-based probe as shown in Fig. 1 for the selective detection of formalin in food products like milk, soft drinks, and water bodies. Formalin is looked upon as a food preservative and is widely used to increase the shelf-life of consumable products. Ingesting formalin above the recommended amount can be carcinogenic to humans in the same way as it can provoke detrimental effects on water bodies and harm the existence of aquatic life. To date, many analytical studies [1][2] along with experimental studies [3] have been reported that suggest our proposed theme of combining selectivity (MIP), economical factor and eco-friendly (green synthesis approach) might be more work efficient.

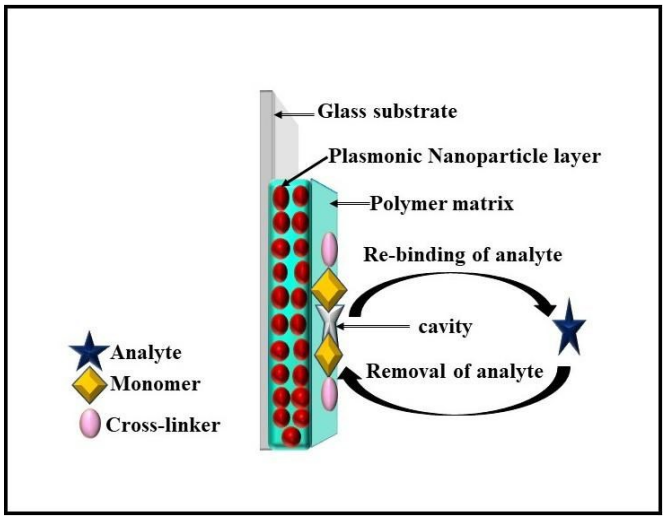

Fig. 1. Schematic of the proposed LSPR-MIP probe

References

1. Bhishma Karki et al., *Optical Engineering. 61, 017101-1 (2022).*
2. Md. Moznuzzaman et al., *Sensing and Bio-Sensing Research. 32, 100419 (2021).*
3. Hemant Ramakant Hegde et al., RSC Adv.11, 8042–8050 (2021)

FIB242 In-situ monitoring of nitric oxide in vehicle exhaust using a robust 1f wavelength modulation spectroscopy technique

*Shruti De[1], Malavika P D[2], Arup Lal Chakraborty[1]**

[1] Electrical Engineering, Indian Institute of Technology Gandhinagar, Gandhinagar-382355, India

[2] Integrated MSc Photonics, Cochin University of Science and Technology, Kochi-682022, India

**Corresponding author: arup@iitgn.ac.in*

The main challenge in laser spectroscopic outdoor trace gas sensing applications [1] is the need to ensure that the systems are immune to mechanical vibrations and dust that cause fluctuations in the received light intensity. This paper presents a robust, highly specific and highly sensitive $R_{1f}/\Delta I_l$ *wavelength modulation spectroscopy (WMS) [2]* technique that can overcome this seemingly simple problem. Figure 1a shows outdoor measurements of nitric oxide (NO) from the exhaust of a car running on petrol using a portable WMS system. The system was designed with a 10 mW mid-infrared 5257 nm quantum cascade laser (Alpes Lasers, HHL-1154). The absorption line of 5262.92 nm with line strength 2.32×10^{-20} $cm^{-1}/(mol\ cm^{-2})$ was chosen. The NO concentration extracted by fitting a simulated $R_{1f}/\Delta I_l$ to the experimental $R_{1f}/\Delta I_l$ obtained was 152 ppm at 0.3 bar as shown in Fig 1b. Figure 1c shows the raw quantity R_{1f} with vibration intentionally introduced in the system. The $R_{1f}/\Delta I_l$ WMS algorithm successfully extracts the NO concentration despite the significant variation in the quantity R_{1f} as shown in Fig 1d. The extracted mole fraction turns out to be 660 ppm in each case. The Allan deviation analysis of NO shown in Fig 1e establishes the minimum detection limit as 1.97 ppm for a path length of 28 cm. This corresponds to a pathlength normalized sensitivity of 551 ppb-m. Figure 4f shows the excellent long-term stability of the detection limit of our system over 8 h.

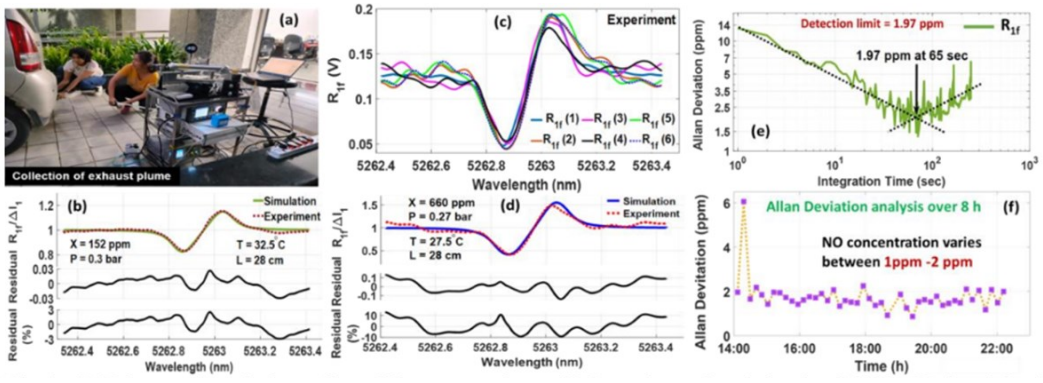

Fig. 1: (a) Exhaust plume being collected from a petrol car, (b) Experimental and simulated 1f WMS signal for 152 ppm NO and the residuals, (c) The random fluctuations in the experimentally obtained R_{1f} signal due to vibration, and (d) The good fit obtained between the 660 ppm NO experimental and simulated 1f WMS signal (e) Allan deviation shows the detection limit is 1.97 ppm for an optimum integration time of 65 s, (f) The low system drift is evident from the Allan deviation computed over 8 h.

References

1. K. Sun et. al., *Meas. Sci. Technol. 24, 125203 (2013).*

2. S. De et. al., *Appl. Opt. 62, 3160-3168, (2023).*

FIB243 Slotted Photonic Crystal Optical Nanofiber for Cavity QED

*Subrat Sahu[1], Kali P. Nayak[2], and Rajan Jha[1]**

[1] *Nanophotonics and Plasmonics Laboratory, School of Basic Sciences, IIT Bhubaneswar, Argul, Khordha 752050, India*

[2] *Department of Engineering Science, University of Electro-Communications, Chofu-Shi, Tokyo 182-8585, Japan*

**Corresponding author: rjha@iitbbs.ac.in*

Light-matter interaction with nano-waveguides has become a platform for various contemporary research fields typically in quantum photonics [1]. Cavity creation on nano-waveguides is a crucial requirement for enhancing the interaction strength to utilize in the field of cavity quantum electrodynamics (QED) [2,3]. In this prospect, an optical nanofiber (ONF, a subwavelength diameter fiber) based cavity is a promising candidate due to its ability to automatically coupling to single-mode fiber (SMF) in the fiber networks [2]. The spontaneous emissions from a quantum emitter (QE) can be enhanced by introducing a cavity structure on the ONF to facilitate the longitudinal confinement and realize cavity QED. Another interest of the ONF-based cavity is that the guided field can be transmitted over long distances for communication [2].

Here, we propose a slotted photonic crystal cavity (SPCC) structure on the ONF for cavity QED. Figure (a) shows the schematic diagram of the proposed device. The structure has been designed by assuming a QE emission wavelength of around 800 nm using FDTD simulations [3]. Here, two sets of Bragg mirrors with a defect region and a slot in the middle have been considered on an ONF. Introducing the slot not only facilitates QE to be housed in the strongest intensity field but also significantly enhances the spontaneous emission rate of QE. Figure (b) shows the spontaneous emission characteristics [Purcell factor (P_f) and coupling efficiency (η)] of QE with SPCC structure. We have achieved Purcell factor enhancement ~ 120 and a high single-photon coupling efficiency of ~ 90% into the fiber-guided modes in the presence of a slot, at N = 25. Thus, the presently designed SPCC structure with a single QE may open new possibilities in quantum information science [1].

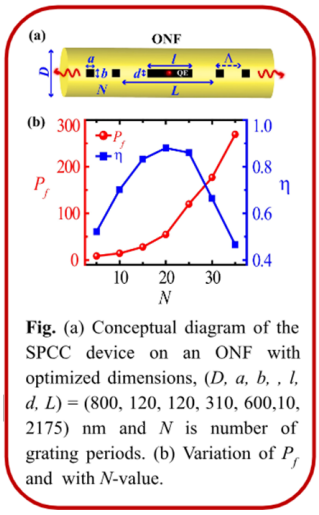

Fig. (a) Conceptual diagram of the SPCC device on an ONF with optimized dimensions, (D, a, b, , l, d, L) = (800, 120, 120, 310, 600,10, 2175) nm and N is number of grating periods. (b) Variation of P_f and with N-value.

References

1. Kimble, Nature 453, 1023 (2008).
2. Nayak et. al., J. Opt. 20, 73001 (2018).

3. Sahu et. al., J. Opt. 24(11), 115401 (2022)

FIB244 Methods for Slope Efficiency Optimization in an All Fiber Thulium Doped Laser

Vincent Akash Gomes[1,2], Atasi Pal[1,2]*

[1] CSIR-Central Glass and Ceramics Research Institute, Kolkata- 700032
[2] Academy of Scientific and Innovative Research, Ghaziabad- 201002
**Corresponding author: gomesvincent12@gmail.com*

Operating in wavelength range of 1800-2100 nm, thulium doped fiber lasers (TDFL) find applications in numerous areas of medical, industrial and academics. In the past decades, TDFLs have achieved high power and high optical-to-optical slope efficiency (OSE) (>50%) beyond the quantum efficiency limit of ~40%, possible due to cross-relaxation process available under 793 nm pumping [1]. In this work, an experimental study to improve the OSE for an all-fiber thulium doped fiber laser operating at 1940 nm is presented. The experimental setup consisted of six pump laser diodes (PLD), which were combined with a (6+1) pump combiner (PC) followed by a high reflective fiber Bragg grating (HR-FBG), thulium doped active fiber (TDAF), low reflective FBG (LR-FBG) and a cladding mode stripper (CMS); as shown in fig.1 (a). For method 1: length optimization of the TDAF was performed using cutback method with an initial length of 5 m using cutback step size of 0.5 m. Intrinsic lasing (around 2000 nm) was observed up to 4 m of TDAF. The highest OSE of 61% for length in the range of 3-3.5 m with circular-spiral routing and 10% LR-FBG configuration was observed. For method 2: circular-spiral routing of the TDAF was compared with elliptical-spiral routing. The Elliptical-spiral routing improved the OSE as by 4 % and, also reduced the optimum length of TDAF to ~3 m. The comparison OSE with respect to the length of the TDAF and routing diagram is shown in fig.1(b) and (c) respectively. In method 3: the LR-FBG reflectivity was changed between 5,10 and 50%. Reflectivity of 10% resulted in the highest OSE of 65%, with 52% and 48 % for reflectivity of 5% and 50% respectively. In conclusion, the most optimal resonator configuration was achieved using 3 m length of TDAF, elliptical-spiral routing, and LR-FBG with reflectivity of 10% which resulted in OSE of ~65% against a total pump power of 36 W. Such OSE optimization methods can also be used for fiber lasers at other wavelengths.

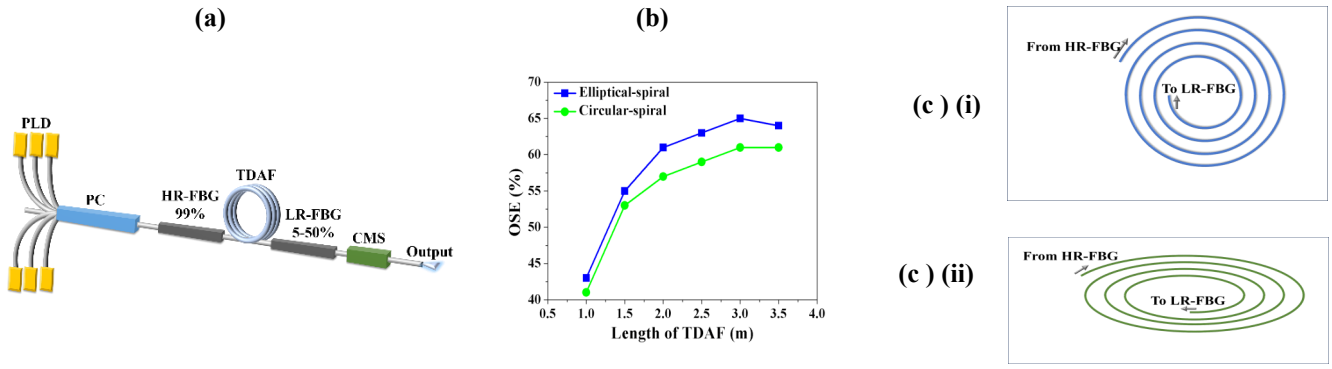

Fig.1 a)Experimental set up; b)OSE compare between circular and elliptical spiral routings c) i) circular and ii) elliptical spiral routing diagrammatic representation

References

1. A.Sincore et. al., IEEE JSTQE, 24, 1-8 (2018).

FIB149 Switchable Vector-Mode Generation Using a Mode-Selective Coupler Designed with a Standard Step-Index Fiber

Shankar Pidishety[1,3], P. Sampathi[2], Shaik Ahmed[1], Ram Soorat[1], D. Karuna Sagar[2]*

[1]School of Technology, Woxsen University, Telangana-502345, India.
[2]Department of Physics, Osmania University, Hyderabad, Telangana, 500 007, India.
[3]Optoelectronics Research Centre, University of Southampton, SO171BJ, UK.
**Corresponding author: pd.shankara@gmail.com.*

We present an all-fiber method for efficient switchable vector-modes generation using a mode-selective coupler (MSC) designed with a standard step-index fiber. Modulating the wavelength achieves both switching and phase matched selectivity of desired vector modes.

Optical beams with the vector characteristics provide access to manipulate the polarization, exhibiting high purity of quantum characteristics, enhance their applications by fully exploiting the degree of freedom related to polarization, particularly in high dimensional quantum systems [1,2]. While vector modes offer a full spectrum of benefits, they crucially relies on specialty fibers with complicated refractive index profile (RIP) [3]. However, designing MSC with such fiber is complicated, efficiency limited and requires high precision setups [4]. In this context, design of MSC using a standard step-index fibers via simplified fabrication technique while providing standard performance is highly desirable as demonstrated here.

In this work, we present the design of a MSC using standard step-index (25/125 μm, NA 0.12, OFS Inc. supporting 4 modes at 1550nm) fiber via a special cascaded weakly fusing technique that enables not only selective mode coupling via phase matching but also wavelength-modulated switching of the generated modes with polarization control, thereby preserving the vector characteristics in the generated modes, as shown the setup and results in figure 1.

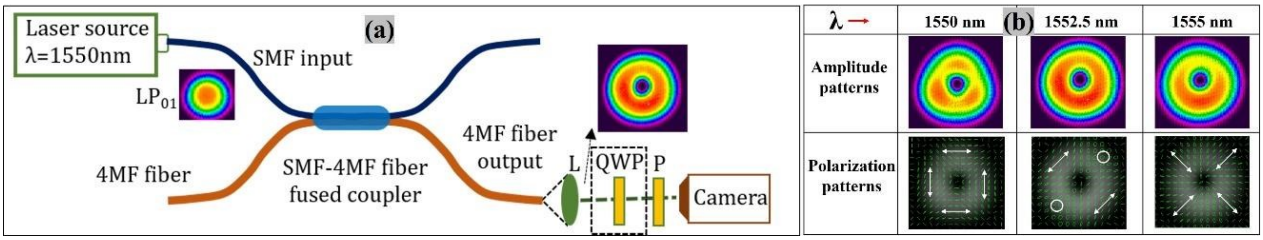

Figure 1: (a): Experimental characterization setup for MSC. (b): Amplitude (upper) and polarization patterns (lower-arrow lines) of generated modes at different wavelengths.

By leveraging the inherent vector properties of higher order modes (HOMs) of the fiber, ~96% device efficiency is demonstrated. More details will be presented during the conference. Such simple and highly efficient all-fiber based devices, with outstanding performance of preserving vector characteristics of generated modes are highly potential for various application such as quantum communication, quantum technology, particle manipulation and modes switching.

Authors thank Prof. Gilbetro Brambilla, University of Southampton, UK for laboratory access.

References

1. I. Nape, B. Sephton, P. Ornelas, C. Moodley, and A. Forbes, APL Photonics 8, 051101 (2023).
2. J. Wang, Q. Wang, J. Liu, and D. Lyu, AVS Quantum Science 4, 031701 (2022).
3. P. Gregg, P. Kristensen, et all, Nat Commun 10, 4707 (2019).
4. S. Pidishety, B. Srinivasan, and G. Brambilla, IEEE Photonics Technology Letters 29, 31 (2017).

Category 5

Guided Wave and Nonlinear Optics (GNO)

GNO115 Study of phase sensitivities of single layer and double layer Guided Mode Resonance structures.

Neethu Baburaj[1], Shereena Joseph[1] , Joby Joseph[1]*

[1]Photonics Research Lab, Department of Physics, Indian Institute of Technology, New Delhi-110016,India
**Corresponding author: bneethubaburaj@gmail.com*

Guided Mode Resonance (GMR) is an optical phenomenon occurring in nanostructures consisting of a grating layer and a waveguide layer on a substrate. Light incident on the grating layer gets diffracted into many orders, and one of the orders gets coupled to the waveguide mode on specific phase matching conditions, and a resonance condition occurs. This effect manifests as a peak in the reflection spectrum or a dip in the transmission spectrum. For a GMR with specified structure parameters, the resonance condition is sensitive to the refractive index (ri) of the surrounding medium and incident light conditions, including the polarization state, wavelength, and angle of incidence. Different interrogation techniques, namely wavelength, angular, intensity, and phase-detection methods, are employed for detecting the GMR signal corresponding to a change in the ri of the surrounding medium. Phase detection schemes have provided higher sensitivity and lower limits of detection as compared to other techniques [1]. The phase of the GMR signal varies abruptly around the resonance condition and this property is utilized in phase detection of GMR.

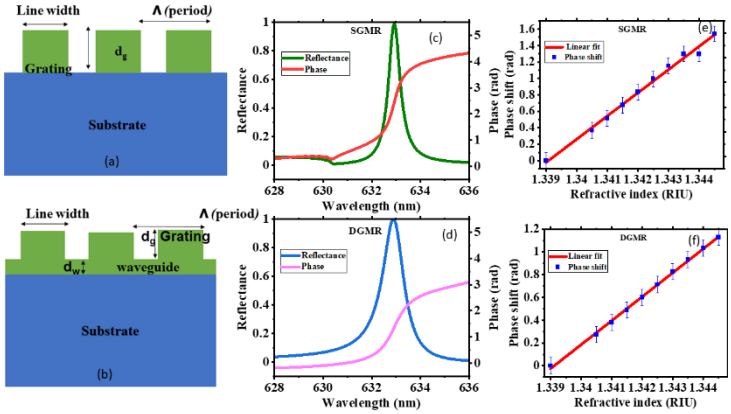

Apart from the double layer structure consisting of waveguide and grating layers (DGMR), single layer grating structure (SGMR) can also exhibit guided mode resonance phenomenon. Here we compare the phase sensing capability of SGMR and DGMR for TM polarization through simulations. The Ansys FDTD simulation tool [2] was employed for the study. Both SGMR and DGMR were designed to have the resonance at 632.8 nm. The refractive index of the cover medium was varied from 1.339 to 1.3445 in steps of 0.0005. From simulations, it is observed that SGMR shows better phase sensitivity as compared to DGMR.

References

1. Sahoo et. al., Sci Rep 7, (2017).

2. Ansys Lumerical FDTD, https://www.ansys.com/en-in/products/photonics/fdtd.

GNO116 Stability analysis of the PT-symmetric Lugiato-Lefever model

Priyanka Chaudhary[1], Akhilesh Kumar Mishra[1,2,]*

[1]Deptartment of Physics, IIT Roorkee, Roorkee 247667, India.
[2]Centre for Photonics and Quantum Communication Technology, IIT Roorkee, Roorkee 247667, India.
**Corresponding author: akhilesh.mishra@ph.iitr.ac.in*

We study cavity soliton (CS) formation and Kerr frequency comb generation in whispering gallery mode (WGM) resonator using Lugiato-Lefever model with parity-time (PT)-symmetric potential in the anomalous -dispersion regime.

In 1987, Lugiato and Lefever (LL) developed a model commonly known as Lugiato and Lefever equation (LLE) that has been extensively used to describe optical dissipative structures in the domain of cavity non-linear optics [1]. The system under investigation is depicted in fig.1 which consists of a cavity of radius r. The normalized complex slowly varying envelopes of the various eigenmodes can be obtained by using the modal expansion model [1, 2]. LLE model for the present system can be expressed as

$$\frac{\partial\psi}{\partial\tau} = -(1 + i\alpha)\psi + i|\psi|^2\psi + V(\phi)\psi - i\frac{\beta_2}{2}\frac{\partial^2\psi}{\partial\phi^2} + F, \qquad (1)$$

where $\psi(\Phi,\tau)$ is the complex envelope of the total intracavity field, $\phi\in[-\pi,\pi]$ is the azimuthal angle along the circumference, and τ is the dimensionless time, α is frequency detuning, β is the dispersion parameter, F is the dimensionless external pump field intensity, and parity-time (PT)-symmetric potential $V=A(\cos\phi+iV_0\sin\phi)$ with A=0.1, and V_0=-1 [2, 3].

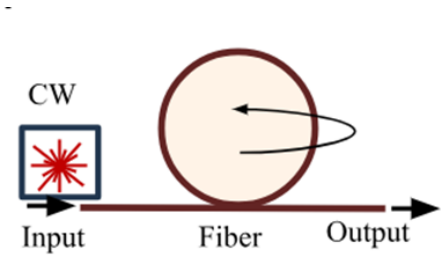

Fig. 1. Schematic of a CW laser pumped ring resonator. The coupling is achieved by using a tapered fiber.

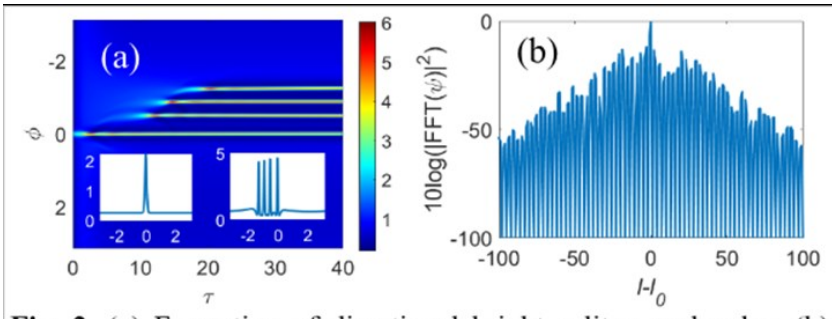

Fig. 2. (a) Formation of directional bright soliton molecules, (b) corresponding Kerr comb. Simulation parameters are , , and and the initial pulse: .

The bright cavity soliton in nonlinear optical cavities is a widely known phenomenon. In fig.2 (a), we observe the formation of a directionally tuneable cavity soliton molecule, initiated with an extremely narrow and small gaussian pulse. Here, term "soliton molecules" refers to multi-peaked solitons. The corresponding Kerr comb generation is shown in fig.2 (b). We may use these resonators in optoelectronic applications for data storage.

References

1. L. A. Lugiato, et al., *Physical review letters 58.21, 2209 (1987).*
2. C. Godey, et al., *Physical Review A 89.6, 063814 (2014).*
3. C. M. Bender, et al., *Physical review letters 80.24, 5243 (1998).*

GNO117 Abruptly Autofocusing Ring Airy Gaussian Vortex beam through PT symmetric Potential

Shakti Singh[1], and Akhilesh Kumar Mishra[2],
[1]Department of Physics & [2]Centre for Photonics and Quantum Communication Technology, Indian Institute of Technology Roorkee, Roorkee-247667, Uttarakhand, India
ssingh7@ph.iitr.ac.in, akhilesh.mishra@ph.iitr.ac.in

Introduction: The Ring Airy Gaussian vortex beams (RAGV), which are characterized by their remarkable abruptly autofocusing (AAF) nature [1], have revolutionized the domain of optical communications. Due to the field structure, these beams are non-diffracting in nature and possess self-healing properties. The study of optical beams in different types of potential has rapidly gained momentum due to its remarkable applications.

Theory and Results: The propagation of RAGV in PT symmetric potential is governed by the equation,

$$\nabla_{\perp}^{2}u + 2ik\frac{\partial u}{\partial z} + V(r)u = 0. \qquad (1)$$

We solve above equation assuming following solution-

$$u(r,\varphi,0) = A_0 A_i\left(\frac{R_0 - r}{bw}\right)exp\left(-\left(\frac{R_0 - r}{w}\right)^2\right)r^l e^{il\varphi}, \qquad (2)$$

where A_0 is constant amplitude of the field, A_i is the Airy function, R_0 is the radius of the primary ring, b is distribution function parameter, l is the topological charge of the beam [2]. V_r is the PT symmetric potential [3] whose mathematical expression is given by,

$$V(r) = cos\left(\frac{R_0 - r}{w}\right) + idsin\left(\frac{R_0 - r}{w}\right). \qquad (3)$$

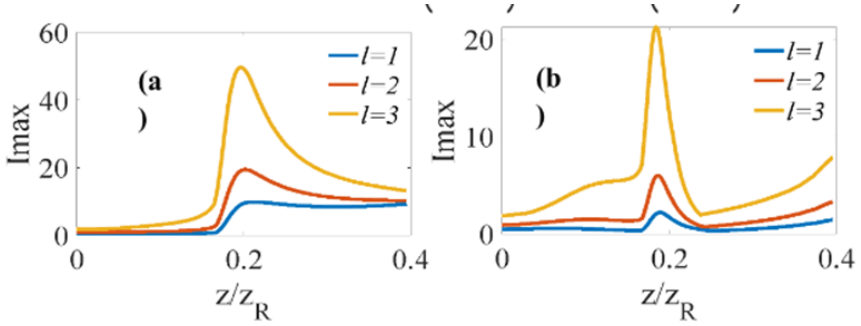

Figure 1. Maximum peak intensity evolution of RAGV beam in PT symmetric potential for b=0.12 with loss/gain coefficient (a) *d=-0.5* (b) *d=0.5*. Simulation parameters: *w=0.8mm* R_0*=1mm,* λ*=795nm* and *a=0.05*

Figure (1) shows that with larger topological charge *l maximum peak intensity* (I_{max}) gets larger. Also, I_{max} assumes far larger values for positive *d* as compared to that for negative *d* .

Conclusion: In summary we have found PT symmetric potential significantly affects the intensity profile of the RAGV beam during propagation.

References

1. D. G. Papazoglou et. al.," Opt. Lett. 36, 1842 (2011).
2. S. Singh et. al., "J. Opt. Soc. Am. B 40, 2287-2295 (2023).
3. C. M. Bender et. al., Phys Rev Lett 80, 5243–5246 (1998).

GNO145 Thermal Response of Nematicons in a Parabolic Potential

N M Sajitha[1], T P Suneera[2]*

[1]Department of Physics, Govt. College Madappally, Calicut University, Kerala, 673102, India

[2]Department of Physics, Govt. College Madappally, Calicut University, Kerala, 673102, India

**Corresponding author: sajitha.n.m@gmail.com*

The spatial optical solitary waves in nematic liquid crystals (NLCs) are referred to as nematicons. The nematicons are widely used in all-optical interconnects, readdressable configurations, all-optical steering, and routing devices [1].

The thermal response of nematicons in a parabolic potential has been studied numerically by employing the finite difference method. The model equations of the system are given by,

$$2i\frac{\partial X}{\partial z}+\frac{\partial^2 X}{\partial x^2}+\frac{\partial^2 X}{\partial y^2}+X\sin^2\xi+\frac{1}{2}Ye^{\frac{iz}{1+\gamma(\tau)}}\sin 2\xi+V(x,y)X=0,$$

$$2i\gamma(\tau)\frac{\partial Y}{\partial z}+\frac{\partial^2 Y}{\partial x^2}+\gamma(\tau)^2\frac{\partial^2 Y}{\partial y^2}-Y\sin^2\xi+\frac{1}{2}Xe^{\frac{-iz}{1+\gamma(\tau)}}\sin 2\xi-V(x,y)Y=0,$$

$$\nu(\tau)\nabla^2\xi+(|X|^2-|Y|^2)\sin 2\xi+2Re\left(XY^*e^{\frac{-iz}{1+\gamma(\tau)}}\right)\cos 2\xi=0,$$

where, $V(x,y)=V_0(x^2+y^2)$. The thermal response coefficient (τ) is the solution of the heat equation, $\mu_T\nabla^2\tau=-|X|^2-|Y|^2$.

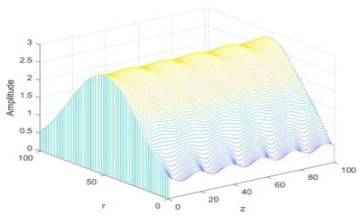

Fig. 1

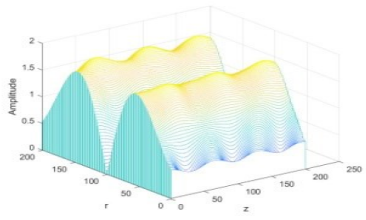

Fig. 2

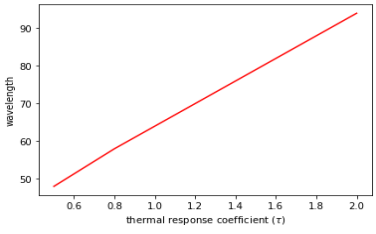

Fig. 3

Single-peak nematicons exist only in the absence of a thermal response coefficient and exhibit periodic oscillation as shown in Fig. 1. The double-peak nematicons are obtained in the presence of a thermal response coefficient as plotted in Fig. 2. As the thermal response coefficient increases, the wavelength of periodic oscillation increases linearly as depicted in Fig. 3. Higher harmonics of nematicons can be generated by varying the values of the thermal response coefficient in a parabolic potential.

References

1. Assanto, G., Peccianti, M.: Spatial solitons in nematic liquid crystals. IEEE Journal of Quantum Electronics 39(1), 13–21 (2003).

GNO245 Analysis of Raman Scattering on two-soliton Interaction among Highly Nonlinear Materials

*Abhisek Roy and Partha Roy Chaudhuri**
Department of Physics
Indian Institute of Technology Kharagpur
**roycp@phy.iitkgp.ac.in*

This paper explores two-soliton dynamics among highly nonlinear fibers, specifically, chalcogenide fiber. We focus on two temporally separated solitons in a single-mode fiber, revealing significant modification of Kerr-induced interaction by interpulse Raman scattering.

Our research has focused on the impact of interpulse Raman scattering on the nonlinear interaction between two temporally separated pulses. We conclude that in highly nonlinear materials, the solitons propagate shorter distances without any interaction. At the same input power, without Raman interaction, highly nonlinear materials show collision much earlier between the two soliton pulses, and when Raman effects are included, the soliton pulses separate near 40m, indicating an out-of-phase collision.

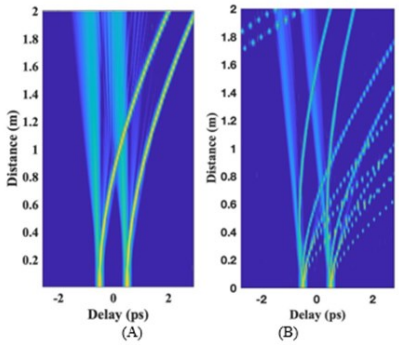

Fig. 1 Two-soliton interaction at peak power of 200W, (A) for silica fiber, and (B) for chalcogenide (As_2Se_3).

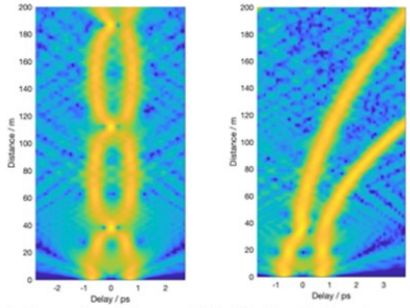

Fig. 2: Temporal evolution over 200m fiber length of two temporally separated pulses when Raman term is excluded (left) or included (right).

References

1. G. P. Agrawal, *Nonlinear Fiber Optics, 1989, Chap. 6.*
2. P. Balla, et al. *Effect of Raman scattering on soliton interactions in optical fibers. J. Opt. Soc., vol. 34, No. 6, pp. 1247-1254, 2017.*
3. K.Ogusu, K. Shinkawa*, "Optical nonlinearities in As2Se3 chalcogenide glasses doped with Cu and Ag for pulse durations on the order of nanoseconds" Opt. Exp., vol. 17, no. 10, 2009.*

GNO246 Employing Z-Scan Technique for the nonlinear concentration dependent study of Hemoglobin

Md. Haider Ansari[1], Shagufta Gull[1], Nitesh Kumar[2], Umakanta Tripathy[2], Salla Gangi Reddy[1].*

[1]Physics Department, SRM University -AP, Andhra Pradesh India - 522502
[2]Department of Physics, Indian Institute of Technology (Indian School of Mines) Dhanbad,826004, Jharkhand, India
**haideransari_md@srmap.edu.in*

The nonlinearity of hemoglobin is studied using Close and Open aperture Z-scan techniques at various concentrations and constant activation laser (CW) power. The thermal lensing effect is attributed to the nonlinearity in this case. According to this concentration-dependent study, we found that nonlinear refractive index and absorption coefficient increases with hemoglobin concentrations. Due to the effects of self-defocusing and reverse saturation absorption, the hemoglobin has a negative n_2 and a positive β. Excited-state absorption is also caused via the RSA effect.

The CA Z- Scan experiment revealed no asymmetry because the hemoglobin concentration was lower, resulting in moderate nonlinearity in the sample The study may also be used to estimate hemoglobin concentrations in human blood cell samples using both the OA and CA configurations.

From 0.5 μM to 150 μM of hemoglobin is prepared as suspensions in Pbs buffer. We began with a lower value of 0.5 μM because the hemoglobin concentration in human serum is less than 0.6 μM.

References

1. S. Bahae et.al., IEEE, J Quan Electronics 26, 4 (1990)
2. Koushki.et. al., J Mol. Liquid 325, 11516 (2021)

GNO247 Decoration of the Sb_2Se_3 nanowires with $CsPbBr_3$ nanocrystals and Study the Nonlinear Optical Response

*Naresh Chandra Maurya, and K. V. Adarsh**

Department of Physics, Indian Institute of Science Education and Research Bhopal, Bhopal 462066 India
**Corresponding author: adarsh@iiserb.ac.in*

The incorporation of lead halide perovskite nanocrystals with low dimensional materials shows an enormous tendency in optoelectronic devices as in solar cells and photocatalysts processes [1-4], while a comprehensive study of the nonlinear optical (NLO) properties is yet to be established in these co-operatives systems because a robust nonlinear response is of essential for optical limiting and switching applications [5]. In this study, we decorated the $CsPbBr_3$ nanocrystals on the Sb_2Se_3 nanowires and studied the nonlinear optical behavior of the decorated system $CsPbBr_3@Sb_2Se_3$ using the Z-scan technique. Our findings reveal a remarkably strong excited-state absorption (ESA) phenomenon in $CsPbBr_3@Sb_2Se_3$, starkly contrasting to the pristine materials ($CsPbBr_3$ nanocrystals and Sb_2Se_3 nanowires) with 532 nm excitation wavelength in the nanosecond regime. We attribute this observed ESA to the efficient charge transfer processes, which occur between the $CsPbBr_3$ nanocrystals and Sb_2Se_3 nanowires. Further, quenching in the photoluminescence (PL) intensity of $CsPbBr_3$ nanocrystals in the presence of Sb_2Se_3 nanowires corroborates our idea. Moreover, we also demonstrate our device's optical limiting and switching performance. Overall, our results provide a valuable degree of freedom to engineer nonlinear optical responses for hybrid system-based photonic devices.

References

1. S. Zhang *et al., Energy Environ. Sci.* ***15****, 244 (2022).*
2. X. Tang *et al., Sensors and Actuators B: Chemical* ***245****, 435 (2017).*
3. Y.-F. Xu *et al., J. Am. Chem. Soc.* ***139****, 5660 (2017).*
4. X. Liu *et al., Solar Energy Materials and Solar Cells* ***187****, 249 (2018).*
5. R. W. Boyd, *Nonlinear Optics, 3rd ed (Academic Press, Amsterdam ; Boston, 2008).*

GNO248 Exploring Ultra-broad Supercontinuum Generation Using Chalcogenide Fiber

Protik Roy[1], Partha Roy Chaudhuri[1]
Indian Institute of Technology Kharagpur, 721302, India
Email - roycp@phy.iitkgp.ac.in

To optimize and design the pulse propagation, we investigate a chalcogenide glass fiber with elliptical and circular core cross-section. We take $As_{40}S_{60}$ and $As_{42}S_{58}$ as core and cladding materials for standard step index fiber. By optimizing the fiber structure, we calculate the nonlinear coefficient (γ), and the group velocity dispersion (GVD, β_2), for the fundamental modes of the fibers.

Fig. 1 presents the numerical results related to SCG obtained by launching a hyperbolic secant pulse with a width of 200 fs, and a peak power of 1 kW at a wavelength of 3.15 µm into a 10 cm long circular core fiber. The result demonstrates the SCG of 2.1 µm wavelength band at a distance of 4.2 cm. In the case of the elliptical core fiber shown in Fig. 2., the input pulse experiences the SCG of 2.2 µm at a distance of 3.3 cm when the pulse is launched at 2.8 µm wavelength.

It is noteworthy that when utilizing an elliptical cross-section, the flat wavelength band further increases and this flatness is achieved with a shorter fiber.

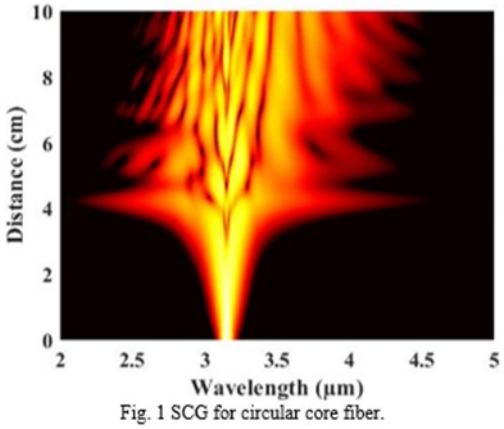

Fig. 1 SCG for circular core fiber.

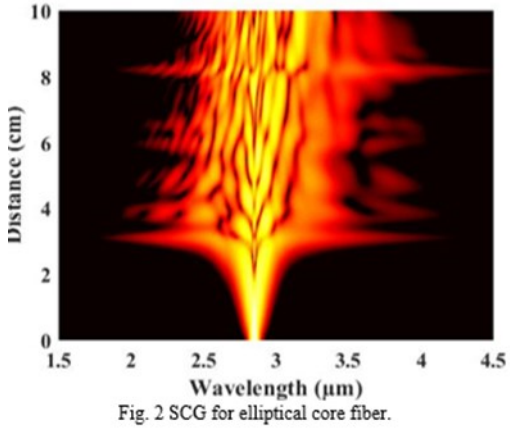

Fig. 2 SCG for elliptical core fiber.

References

1. G. P. Agrawal, Nonlinear Fiber Optics, 1989, Chap. 6.
2. A. Salem, R. Cherif, and M. Zghal, "Raman Response of a Highly Nonlinear As 2 Se 3 -based Chalcogenide Photonic Crystal Fiber," Progress in Electromagnetics Research Symposium (2011).

GNO251 Fiberized mid-infrared single-photon sources in Few-Mode Fibers

Shruti Jain, Deepak Jain
Optics and Photonics Centre, Indian Institute of Technology Delhi, New Delhi, India
shruti@physics.iitd.ac.in

The development of fiber technology in the mid-infrared (mid-IR) wavelength region has opened up numerous possibilities for the creation of all-fiberized mid-IR single photon sources. There are only a few demonstrations of mid-infrared single-photon sources and not even a single source based on fibers. The mid-infrared wavelengths offer fundamental vibrational absorption to several molecules and gaseous, making them attractive for spectroscopy and sensing applications. Specific mid-infrared wavelengths offer low atmospheric scattering and absorption, which makes them attractive for free space, long haul, and secured optical communication through satellites. In this work, we have optimized the fiber parameters (such as core diameter and refractive index difference between core and cladding) for Germania glass to achieve a zero dispersion wavelength (ZDW) at different wavelengths of available pump sources such as 2 µm (Tm, Ho-doped silica fiber laser), 2.75 to 3 µm (Er, Ho, Dy-doped ZBLAN fiber laser), and 3.5 µm (Er -doped ZBLAN fiber laser). The core diameter and NA have been tuned to achieve the first or second ZDW at desired wavelengths in 2 to 10 µm wavelength region. We have calculated the phase shift for small core diameters for pumping at 2.5 µm and achieved phase-matching for LP01 mode. Since coupling pump light into such fiber is difficult to attain, we calculated phase shift for large core diameters for pumping at 2.58 µm. Phase-matching condition is being fulfilled for a wide range of frequency for LP21x mode, While, LP21y , it occurs at a specific frequency 2.06 um (~145.5THz) as idler wave and 3.465 um (~86.5THz) as signal wave because of effective index profile of LP21x mode is more linear compared to the LP21y mode. The proposed fibers can prove a milestone in the development of fiberized mid-infrared single photon sources.

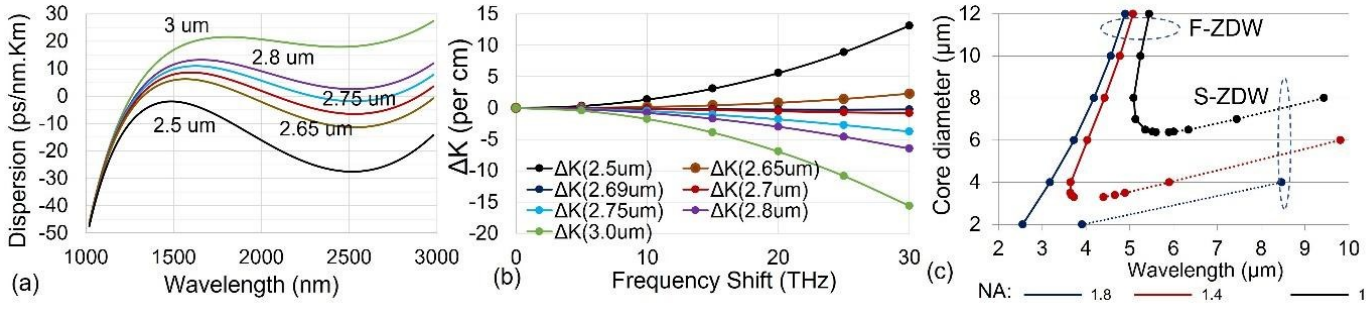

Fig.1. (a), (b) and (c) Calculated phaseshift and dispersion for different core diameters.

References

1. D. Jain *et al., "Scaling power, bandwidth, and efficiency of mid-infrared supercontinuum source based on a GeO2 doped silica fiber," 36(2), A86-A92, JOSA B (2019).*
2. J. W. Fleming *et al., "Dispersion in GeO2-SiO2 glasses," Applied Optics, 23(24), 4486, (1994).*
3. C-M. Lee *et al., "A fiber-integrated nanobeam single photon source emitting at telecom wavelengths," APL 114, 171101 (2019).*

GNO252 Novel large mode area bend compensated "ARC" fibers for high-power lasers

Soorej Thekkeyil[1], Anirban Dhar[2], Deepak Jain[1]*
[1]Optics and Photonics Centre, Indian Institute of Technology Delhi, New Delhi, India
[2]Fiber Optics & Photonics Division, CSIR-Central Glass & Ceramic Research Institute, Kolkata, India
**soorej@opc.iitd.ac.in*

A fiber laser is more efficient and effective in high-energy multi-kW industrial laser applications than other conventional laser technologies. However, undesirable effects such as non-linear phenomena (SRS, SPM, and SBS) and modal instability (MI) thresholds limit the power scaling. Here, we investigate a bend-compensated ARC-fiber design that can ensure single-mode operations by coiling fiber to increase the relative losses of higher-order modes (HOMs). Bend compensation techniques have been developed to use selectively suppress all HOMs by tailoring the refractive index of the optical fibers. This design uses a combination of a low-NA parabolic core with a negative slope-clad refractive index profile. We have optimized the bending diameters and mode area scaling of few-mode large mode area (LMA) graded index fiber for high-power fiber lasers. This design is particularly immune to bend-induced mode distortion and effective area shrinking. We perform numerical simulations using the full-vectorial finite element method (FEM) to analyse the double-clad fiber design with dimensions of 120/300/400 µm. Here, we achieved an effective area of 3000 µm^2 for the fundamental mode (FM) at 62 cm bend diameter, while offering losses of more than 56 dB/m for the HOMs and lower than 0.1 dB/m for the FM at 1060 nm wavelength, and the power overlap factor discrimination between FM and least lossy HOM is given as 52.14 %. The circular symmetry design ensures easy handling and use of fiber in any orientation of the bend. This fiber can be coiled to facilitate integration into a compact laser system, and it is adaptable to different wavelengths too. Here we have got an effective area that is as large as can be offered by rod-type fibers. These fiber designs will open the pathways to tackle limitations for achieving high average power and high peak power fiber lasers and amplifiers.

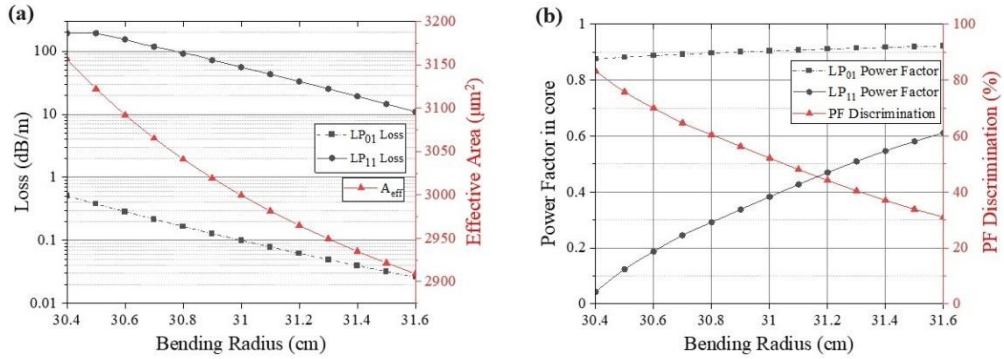

Fig. (a) calculated bending losses and effective area (b) power factor of FM & HOM in the core w.r.to bend radii for 0.025 NA fiber with 120 µm core thickness and alpha parameter, α = 1.8.

References

1. D. Jain *et al, "Extending single mode performance of all-solid large-mode-area single trench fiber," Optics Express, vol. 22, no. 25, p. 31078, Dec. 2014.*
2. J. M. Fini et al, "Bend compensated large-mode-area fibers: achieving robust single-modedness with transformation optics," *Optics Express, vol. 21, no. 16, p. 19173, Aug. 2013.*
3. D. Marcuse, "Influence of curvature on the losses of doubly clad fibers," *Applied Optics, vol. 21, no. 23, p. 4208, Dec. 1982.*
4. D. Jain *et al, "Demonstration of ultra-low NA rare-earth doped step index fiber for applications in high power fiber lasers," Optics Express, vol. 23, no. 6, p. 7407, Mar. 2015.*

Category 6

Green Photonics (GPH)

GPH253 Solid State Lighting using Multiple Phosphor Layers Exited by Blue Laser Beam: Experimental and Theoretical Study of Thermal Behaviour

*Aayushi Soni[1,2], Satish Kumar Dubey[1], Ravibabu Mulaveesala[1],Dalip Singh Mehta[1,2]**

[1] *Centre for Sensors, Instrumentation and Cyber Physical System Engineering, Indian Institute of Technology Delhi, New Delhi, India, 110016*
[2] *Green Photonics Laboratory, Department of Physics, Indian Institute of Technology Delhi, New Delhi, India, 110016*
*Corresponding author: *mehtads@physics.iitd.ac.in*

We report laser based solid state lighting for generating broadband light source for general illumination and visible light communication. We have used a combination of three phosphors and a single blue laser source for exiting these phosphors. We demonstrate two topologies layer-by-layer and side-by-side arrangement of these phosphors coated on glass slides by screen printing. One dimensional, Third Order, thermal model circuit is designed for these phosphors using average phosphorescent decay lifetime obtained experimentally using time resolved photo photoluminescence. Here, phosphors are place in order of their refractive index variation. We report that parallel or side by side topology shows least temperature as compared to that of all the junctions in layer-by-layer model. Experimental results of spectral distribution of red, yellow and green phosphor exited by blue light will be presented along with the result of lifetime measurement for all three phosphors will be also presented. Optical properties such as ,color rendering index (CRI), correlated color temperature (CCT) and CIE 1931 chromaticity coordinates and along with equivalent electronics thermal circuit will be also presented. Laser based solid state lighting has great future for general illumination with high brightness and high directionality, and visible light communication.

Acknowledgement: The authors are thankful to DST-SERB for Project Number CRG/2022/003490 for financial assistance. Also, thankful to IITD-Sonipat Campus for characterization facility of Time-Correlated Single Photon Counting and Steady-State Photoluminescence.

GPH254 Design and Development of Laser-Driven Multiple Phosphors Converted White Light Source in Concentric Ring Configuration with High Thermal Stability

*Dheeraj Kumar,[1]R.K. Varshney,[1] D. S. Mehta[1]**

[1]*Department of Physics, Indian Institute of Technology Delhi, New Delhi-110016, India*
Corresponding author: mehtads@physics.iitd.ac.in

Solid-state-lighting (SSL) is the current state-of-art technology for general-purpose illumination, high-tech displays application, and electronic devices [1]. In the era of SSL for artificial intelligence and robotic driving with high brightness white light emitting diode (LED) could not survive due to its efficiency droop

(ED) [2]. ED limits the generation of photons per unite area of LED by limiting input current densities. It's very much predetermined for an ultrahigh-brightness and high spatial resolution the most predicated solutions could be a laser diode which produces light like LED and operates much higher current and do not suffer from ED. In SSL the phosphor-converted laser diode (pc-LD) white light source, LD is focused onto the small area of phosphor for an ultra-high brightness illumination but the early thermal degradation and even in extreme cases phosphor resin burning appear. The most feasible approach for producing white light in pc-LD source is similar to pc-LED in which a blue LD is used to excite a down -conversion yellow phosphor ($Y_3Al_5O_{12}$: Ce) for generation of yellow photons. Further, the residual blue photons which are extracted from the phosphor layer due to scattering, combines with yellow photons to generate white light. But yellow phosphor possesses an optical spectrum that lack of deep red color parameter (R_9~100%) and color rendering index (CRI) <60.To improve the quality of white light we introduce a significant amount of red and green emitter and removal of thermal heating used a rotating wheel. In this paper, we used three-color commercially available phosphor $SrAlSiN_3$: Eu (627.0nm - Red), $Y_3Al_5O_{12}$: Ce (555.0nm - Yellow) and $SrBaSiO_3$: Eu (515.0nm - Green) combination for the experiment to design a sun like full spectrum (SFS) white light source with high thermal stability. We took a combination red and green with yellow in all possible configurations. High power blue LDs (λ=450.0nm $\Delta\lambda$=5.0nm P=1.5Watt) are aligned to illuminate rotating wheel attached with a 12V dc- motor, coated in novel concentric ring (width 5.0mm each) configuration pattern with green, yellow, and red phosphors. The rotating wheel system protects phosphor burning from direct exposer of high-power lasers as well as makes the illumination uniform. The proposed systems with inner ring of green middle one of yellow and outer most coated with red phosphor has CRI 87 and the color temperature is 5572K cool white light with color coordinates very close to proper white light (0.33, 0.33). This work can be internally involved in illumination systems such as artificial solar simulator and headlamp.

Acknowledgment: D.K., R.K.V., D.S.M. thanks to DST (project: DST-SERB/CRG/2022 /003490). D. Kumar, PMRF fellow acknowledges the financial support from MoE.

References

1. Weisbuch C. et al., *C. R. Physique, 19 (2008)*
2. [Dubey A.K. et al., *Laser Physics Letters, 17 (2020)*

GPH255 Efficiency enhancement analysis of nanostructured silicon-perovskite tandem thin film solar cells

Nitish Shrivastava[1], Jolly Xavier[1*]*

[1]SeNSE, Indian Institute of Technology Delhi, Hauz Khas New Delhi-110016
[*]Corresponding author: idz218415@iitd.ac.in, jxavier@sense.iitd.ac.in

Solar cell is one of the most promising sources for sustainable and clean energy. It has been observed that over 30% of sun light reflected back from top surface of the bared silicon solar cell [1]. Nanostructuring of the top surface is one of the best methods that can reduce the reflection losses in the solar cell [2]. In the present work, we study a silicon-perovskite heterostructure for tandem thin film solar cells where we incorporate a triangular lattice nanostructured pattern with parabolic morphology in order to enhance the optical absorption efficiency of solar cell.

Fig. 1 gives the numerically computed optical absorption for a spectral region of 400 nm to 1200 nm where the schematic of lattice structure of the nanostructured thin film has been shown in the inset of Fig. 1 (a-b). From the graphs, it is clear that the light absorption has been enhanced in nanostructured surface as compared to planar sample. The absorption in nano-structured thin film is enhanced by means of proper

geometrical latice structure and morphology on the surface. In the present Si-perovskite tandem solar cell scheme, the absorption is enhanced in visible region and as well as in the near infra-red region that will also enhance the over all efficiency of tandem solar cell. We further give over all rationale of the design and diverse near and far field optical analysis or the spectral region of study. We extend our study to the complete electrical characterization inorder to estimate the I-V characteristics as well as the short circuit current density of the heterostructure thin film, in order to investigate the over all performance of the studied thin film solar cell.

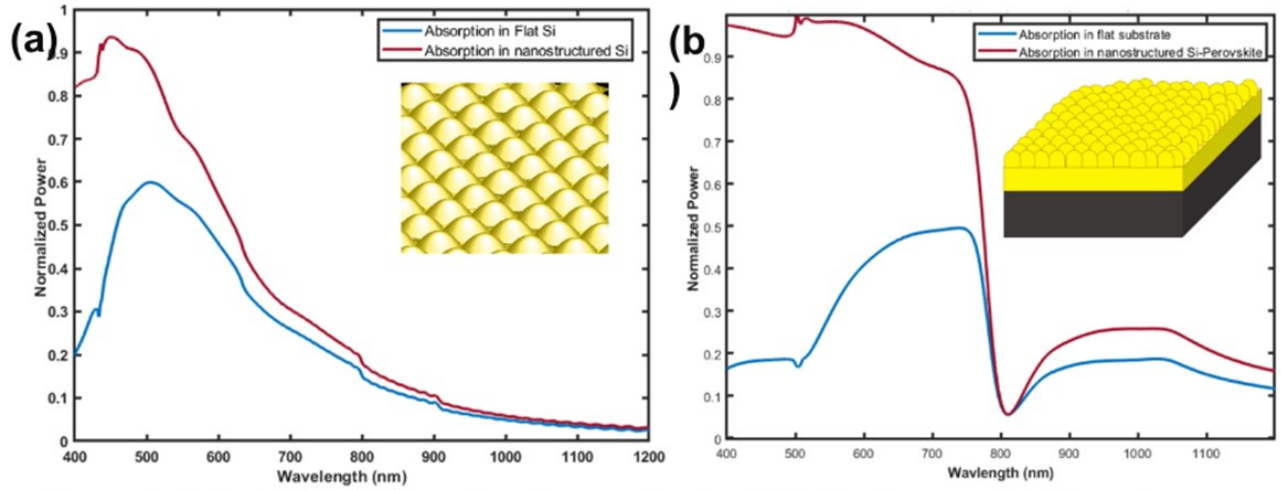

Figure 1: Optical absorption spectra of a nanostructured thin film in comparison to a planar sample. **(a)** Silicon thin film (~500 nm) **(b)** Tandem silicon-perovskite heterostructure (Silicon thickness: 500 nm and Perovskite thickness: 300nm.

References

1. Tooghi et. al., *Sci. Rep.* ***10****, 18699, (2020).*
2. P. Tockhorn, et. al., *Nature Nanotechnology* ***17****, 1214–1221 (2022).*

Category 7

Integrated Optic Circuits and Devices (IOC)

IOC282 Design of a Waveguide based Silicon Intensity Modulator

Anjali A R[1,], Basudev Lahiri[2], and Pranabendu Ganguly[1]*

[1]Advanced Technology Development Centre,
[2]Department of Electronics and Electrical Communication Engineering,
Indian Institute of Technology, Kharagpur,721302, India.
**anjaliraj504@gmail.com*

Silicon photonics is of current interest due to CMOS compatible fabrication process steps, and its transmittance property in telecom wavelengths. In this work, design of a rib waveguide-based silicon intensity modulator is considered. A large cross section silicon rib waveguide (LCRW) was designed using OptiFDTD software on a silicon-on-insulator (SOI) platform with device layer thickness of 5 µm. The dimensions of the waveguide were optimized such that it supports only the fundamental TE and TM modes. After the modal analysis, the rib width and height have been optimized as 6 µm and 2.25 µm. The computed effective indices of the waveguides were 3.44189 and 3.44174, for TE and TM modes, respectively. In order to utilize the designed LCRW as a phase modulator, the initial step is to provide suitable doping to the substrate to make use of free carrier plasma dispersion effect in silicon [1]. This helps in altering the effective refractive index of the propagating modes under the influence of an electrical bias (Drude-Lorentz model).The finalized doping depth, electrode separation and the doped regions are shown in Fig.1. The optimized doping configuration contains n and p type impurities uniformly distributed along a depth, d (0.5 µm to 0.75 µm).The device layer was considered to have slight p-doping, whereas, highly doped n region has a doping concentration of $10^{20}/cm^3$. In this configuration, the estimated change of effective index was ~ 0.028 for 5 Volt biasing (using Silvaco TCAD). Finally, this phase modulator was placed in one arm of a rib waveguide based Mach Zehnder Interferometer (MZI), where a phase change can be created with respect to the reference arm, by applying electrical signal. The intensity of light output of this MZI structure depends on this phase difference. Two 3dB splitter/coupler and four S-type bent waveguides [2], were utilized for complete design of intensity modulator.

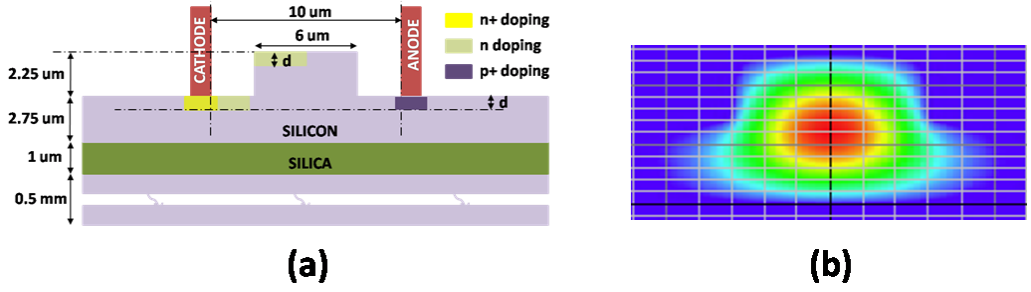

Fig.1: Designed phase modulator in SOI substrate (a), and the fundamental TE mode profile (b).

References

1. G. T. Reed et. al., *Integrated Photonics for Data Communication Applications, 69-121(2023).*
2. S. Samanta et. al., *J. Optics, 20, 095801, 2018.*

Category 8

Imaging and Super-resolution (ISR)

ISR283 Waveguide-assisted TIRF mode of illumination for various cellular Imaging

*Anuj Saxena[1], Azeem Ahmad [2], Vishesh Dubey [2], Hong Mao[2],Balpreet Singh Ahluwalia[2],Dalip Singh Mehta[1]**

[1]Indian Institute of Technology Delhi, Hauz-Khas, New Delhi 110016, India
[2]Department of Physics and Technology, UiT The Arctic University of Norway, Tromsø 9037, Norway
**Corresponding author: mehtads@physics.iitd.ac.in*

Fluorescence microscopy (FM) is a powerful tool to image transparent specimen like specific molecules/ proteins and sub-cellular structures. The purpose of fluorescence microscopy is to highlight only the items of interest against a black background by using labelling. Fluorescence imaging has become the mainstay of microscopy in the field of biology due to its inherent selectivity. Besides providing sub-cellular resolution, it allows for direct visualization of the inner workings of physiological processes (such as Ca-signaling, division). At present, several improved fluorescent proteins and probes are supporting this technique.

Herein, we report a compact design of waveguide based total internal reflection fluorescence (wTIRF) microscopic system. The proposed system uses a microscope glass slide (1mm thick) to guide the total internal reflection (TIR) mode of illumination and generates evanescent field over its surface. The microscope glass slide behaves as multimodal waveguide which has several advantages over chip-based waveguide TIRF at the cost of depth of resolution. wTIRF is single-shot imaging as no waveguide scanning is required and achieve automatic averaging intensity high contrast images with around 600nm axial resolution from the surface of the glass plate. For distinct validation of wTIRF, the comparison between wTIRF and epi-fluorescence microscopic images of polystyrene spheres (PS) of the same field of view is shown. To demonstrate the applicability of the developed system in the cell biology, the system was used to image various cell lines such as U2OS and Mouse embryonic fibroblast (MEF) cells.

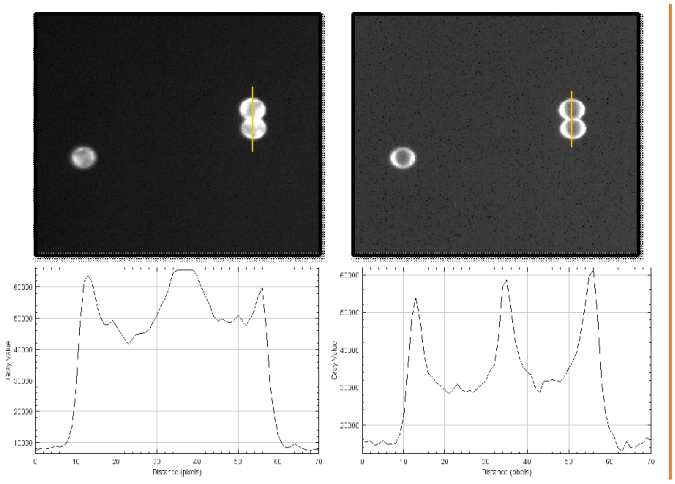

Fig.1 (a),(b) are Epi-fluorescence and wTIRF images of PS of size 7.3µm recorded with 20X/0.8NA. (c) and (d) are line plot across yellow line in image (a) and (b) respectively.

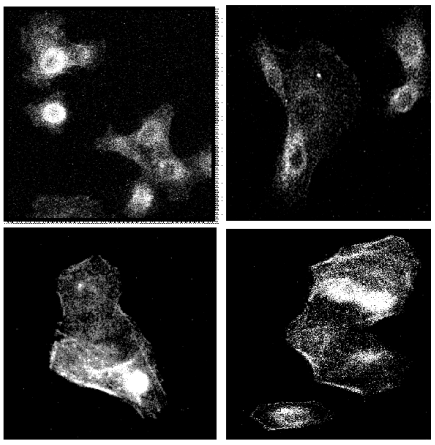

Fig. 2 (a,b) MEF and (c,d) U2OS cells stained with phalloidin alexa fluor 488nm, recorded by wTIRF.

References

1. Ramachandran, S., Cohen, D. A., Quist, A. P., & Lal, R. (2013). High performance, LED powered, waveguide based total internal reflection microscopy. *Scientific reports*, *3*(1), 2133

ISR284 High-resolution imaging with random illumination

Prateek Agrawal, Tanushree Karmakar, and Rakesh Kumar Singh*

Laboratory of Information Photonics and Optical Metrology, Department of Physics, Indian Institute of Technology (Banaras Hindu University), Varanasi, 221005, Uttar Pradesh, India
**Corresponding author: e-mail prateekagrawal.rs.phy21@itbhu.ac.in*

Structure illumination enhances the resolution with a large field of view (FOV) in the imaging system. Such illuminations mostly focus on the conventional system with circular symmetry for an imaging system. However, other apertures have also attracted attention for different reasons and their own advantages. For instance, an annular aperture in the imaging system increases its focal depth and narrower point spread function [1]. Such specially designed apertures may find applications in optical microscopy, and endoscopy. However, due to the nature of its dual cut-off, its full spectrum reconstruction is still a challenging task. Recently, random illumination has also been used for resolution enhancement through the iterative generation of the synthetic aperture from the reconstructed object waves under various random pattern illuminations and using a low-pass circular filter [2].

In this paper, we present a new method for resolution enhancement using random pattern illumination. Here, we use an annular aperture filter in the frequency space and demonstrate its advantages over the low-pass circular aperture filter. The annular aperture with a large obstruction ratio (ε) 0.9 is selected for the same. The simulation for the object and their spectra passing through the annular aperture of $\varepsilon = 0.9$ is shown in Figure 1(a) and 1(b) respectively compared with the reconstructed object and their spectra as shown in Figure 1(c) and Figure 1(d) respectively. In conclusion, we have proposed a new scheme for enhancing resolution in the imaging system.

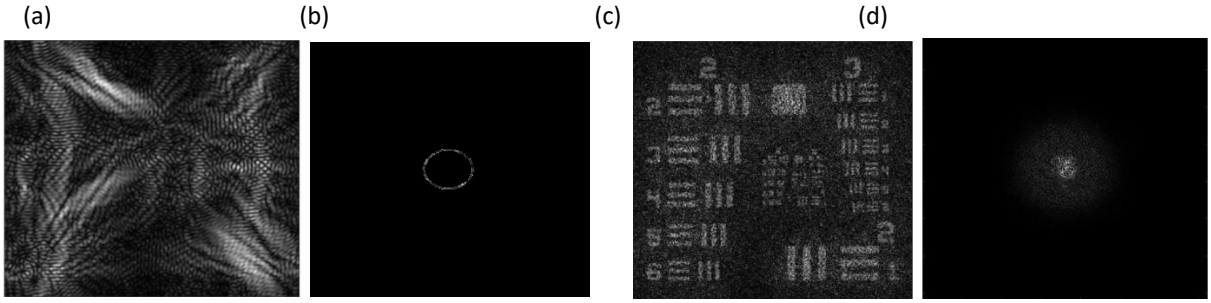

Figure 1: (a) and (c) is the image of the direct and reconstructed object respectively with (b) and (d) their respective Fourier spectra.

Acknowledgment: Support Science and Engineering Research Board (SERB) India CORE/2019/000026

References

1. Hildén, P. et. al., Optics Express 31(7), 11102-11115 (2023).
2. Zheng, J. et. al., Journal of Optics 17(8), 085301 (2015).

ISR285 Plenoptic Image Superresolution

Snehal Tonpe[1,], J. Sreekantha Reddy[2], Chayan Bhar[3], Amit Pratap[4], Jagannath Nayak[5]*

[1]Snehal Tonpe is with the Center for High Energy Systems and Sciences, Hyderabad, Telangana, India, 500069 and the Department of Electronics and Communication Engineering, National Institute of Technology, Warangal, Telangana, India, 506004
[2,4,5] J. Sreekantha Reddy, Amit Pratap, Jagannath Nayak are with the Center for High Energy Systems and Sciences, Hyderabad, Telangana, India, 500069.
[3]Chayan Bhar is with the Department of Electronics and Communication Engineering, National Institute of Technology, Warangal, Telangana, INDIA, 506004.
**Corresponding author: sv721067@student.nitw.ac.in*

Many applications like forensic, surveillance, medical, and satellite imaging require zooming the area of interest in an image. However, digital zooming is limited by the spatial resolution of an imaging system. The plenoptic camera is an innovative technology as it captures the radiance and provides both spatial and angular information. Plenoptic camera is different from conventional camera. It has array of micro lens placed between objective lens and image sensor. Each Micro Lens Array (MLA) forms a whole image. Our developed plenoptic camera has 28x28 MLA and an objective lens of 25mm. In other words, our plenoptic camera gives 784 low resolution images in single frame. Images were captured under lab-generated artificial turbulence at the receiver plane. We developed super-resolution algorithms to obtain turbulence-free high-resolution image. Our Super-resolution technique extracts sup-pixel information from multiple low-resolution images to get high-resolution images. We implemented noise adaptive parameters with the steepest gradient optimization to avoid overfitting and noise amplification. It was observed that the resolution of an image has increased without artifacts. The proposed algorithm is fast, easy to implement, and gives better results compared to other interpolation methods. We successfully obtained super-resolved image up to 8 times (8x) the original image with increased SNR (Signal to Noise Ratio) and better SSIM (Structural Similarity) index than other super-resolution methods.

References

1. Tom E Bishop, Sara Zanetti, and Paolo Favaro. Light field Superresolution. IEEE International Conference on Computational Photography (ICCP), pages 1–9, (2009).
2. Martin Alain and Aljosa Smolic. Light field super-resolution via lfbm5d sparse coding. IEEE international conference on image processing (ICIP), pages 2501–2505. (2018).
3. Y. Huang, W. Wang, L. Wang, Video super-resolution via bidirectional recurrent convolutional networks. IEEE Trans. Pattern. Anal. Mach. Intell. 40(4), 1015–1028 (2018).
4. Zhen Cheng, Zhiwei Xiong, Chang Chen, and Dong Liu. Light field super-resolution: A benchmark. In Proceedings of the IEEE Conference on Computer Vision and Pattern Recognition Workshops, (2019).
5. Plenoptic camera market, global opportunity Analysis and Industry Forecast,2020-2030, https://www.alliedmarketresearch.com/plenopticcamera market-A14947, pp- 193, (2021)

ISR286 Sampling the Light Source for single pixel detection

Tanushree Karmakar, Prateek Agrawal, and Rakesh Kumar Singh*

Laboratory of Information Photonics and Optical Metrology, Department of Physics, Indian Institute of Technology (Banaras Hindu University), Varanasi, 221005, Uttar Pradesh, India
**Corresponding author: tanushreekarmakar.rs.phy20@itbhu.ac.in*

Conventional camera like charged coupled detector (CCD) or complementary metal oxide semiconductor (CMOS) needs millions of pixels to capture or sample a complete information. To boost resolution of an image number of pixels in camera has been increasing over the years even up to over 100 megapixels. But what if one single pixel is used in the detection process and burden of sampling is shifted from camera to the light source? Target object is illuminated by a series of spatially resolved patterns called as structured light where single pixel detector (SPD) records the intensity value corresponding to each light pattern [1].

In this paper, we present our idea on experimental measurement of diffraction pattern in a non-interferometric approach and in an in-line geometry using a single pixel detection strategy. This is realized by using the structured light illumination and shifting the sampling process from the camera to the light source. Proof of principle is presented with estimation of the diffraction pattern at a distance z from an incoherent circular source. In order to experimentally test, we consider structured illumination with a cosine basis of an incoherent circular aperture and its diffraction pattern is evaluated. The sparse diffraction pattern at a distance z_i=3.6 mm from the focal plane is shown in Fig. 1(b) which is interpolated digitally and result is shown in Fig. 1(c). Fig. 1(a) represents the optical geometry for illumination with structured light and single pixel detection.

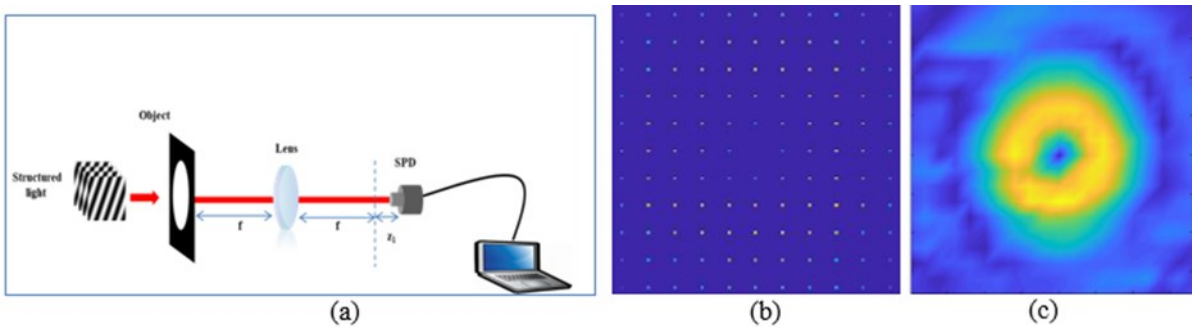

Figure 1. (a) Optical geometry of experimental set up; Experimental result: diffraction pattern of the circular aperture at distance z_i=3.6 mm from the focal plane (b) sparse distribution; (c) Interpolated distribution

In conclusion, we have presented a new method based on the structured light illumination along with initial results for two dimensional measurement of the diffraction pattern of an incoherent source from a single pixel detection.

Acknowledgment: Tanushree Karmakar would like to acknowledge support from DST-INSPIRE (IF190840) and Science and Engineering Research Board (SERB) India CORE/2019/000026.

References

1. Edgar, M.P. et al., Nature Photon 13, 13–20 (2019).
2. Mandal, A.C. et al., Sci Rep 12, 4564 (2022).

ISR287 Landscaping SAM and OAM with Tightly Focused Vector Lissajous Beam Embedded with Vortex Phase

*V. Ashwaanth[1], K.B. Rajesh[1]**

[1] Department of Physics, Chikkanna Govt. Arts College, Tiruppur 641602, TN, India
**Corresponding author: rajeskb@gmail.com*

Vector Lissajous beams (VLB) are a class of structured light beams formed by the superposition of two mutually orthogonal, coherent, and synchronized sinusoidal oscillations with slightly different frequencies and are characterized by their unique and intricate intensity patterns. VLB is often described as a generalized form of CVBs in the vector beams with two parity polarization order (p,q). Manipulation of these polarization index offers the advantage to engineer the imaginary parts of beam in longitudinal component and control the local distribution of Spin Angular Momentum (SAM) associate with circular polarization in the beam [1]. Recently, Svetlana N. Khonina et.al proposed a method for generation of VLBs using metalenses based on subwavelength grating (SG) and demonstrated tightly focused VLB with proper choice of (p,q) also assures the negative energy [2]. Wu et.al numerically investigated the chiral properties of VLBs and manipulation of chiral particle [3]. In this work, we numerically investigated the SAM and OAM of tightly focused VLB and demonstrated that upon selective choice of polarization parity (p,q) and the inclusion of vortex phase generate many novel land scape of SAM and OAM distribution suitable for several novel spinning and rotational manipulation of trapped micro and nano particles. As an example here we demostated the for the VLB with order (3,3) generated four intense spots with SAM inphase with the OAM vectors fig-(1-b)where as the inclusion of vortex phase generated different landscape of SAM and OAM in every quadrant fig(1-a).

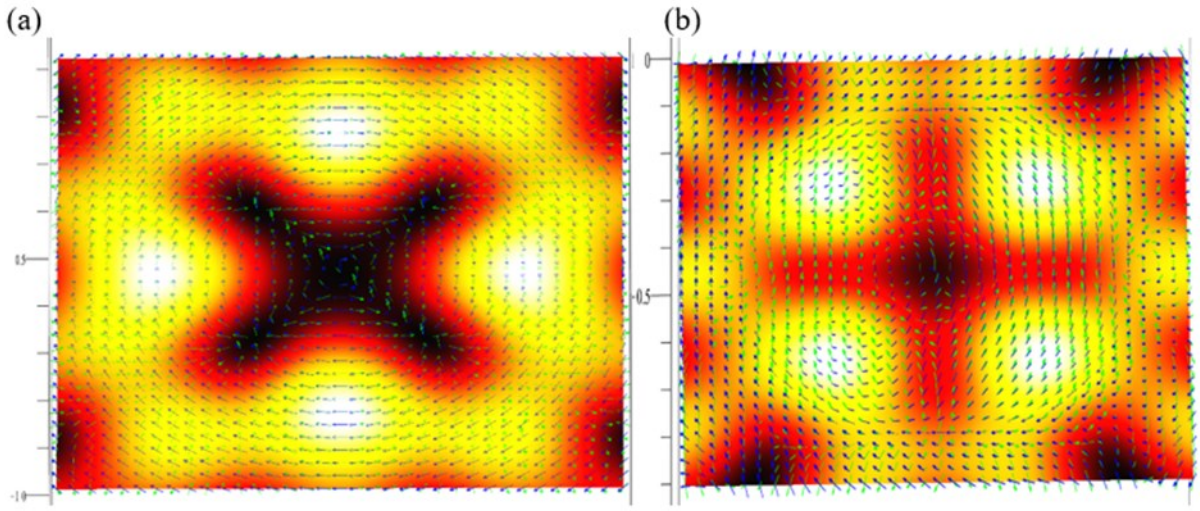

References

1. Sveltlana N. Khonina et. al., *Photonics. 2022, 9(2)121 (2022).*
2. Sveltlana N. Khonina et. al., *Opt. Express 29, 18634-18645 (2021).*
3. Hao Wu et. al., *Opt. Express 30, 3592-3600(2022).*

ISR288 Disordered to Defined: Deconvolution Techniques for Object Reconstruction from Scattered Light

*Yukti Pandey, Nandan S. Bisht**

Department of Physics, Soban Singh Jeena University, S.S.J. Campus Almora 263601
**Corresponding author: bisht.nandan@gmail.com*

Investigating the retrieval of obscured objects in a unique imaging setup, where a laser beam passes through a rotating diffuser, creating incoherent light [1]. This light illuminates the target object, causing image convolution with the Point Spread Function (PSF) of a static diffuser. Advanced techniques like Weiner [2], Lucy [3], and Blind Deconvolution [4] are applied to reconstruct these obscured objects. Our preliminary outcomes and rigorous analysis demonstrate the effectiveness of various deconvolution methods in restoring the original object from convoluted images. This research provides valuable insights into light propagation and object retrieval under challenging conditions. These initial findings set the stage for further exploration in optical imaging through diffusive media, offering potential for future discoveries and advancements in this evolving field.

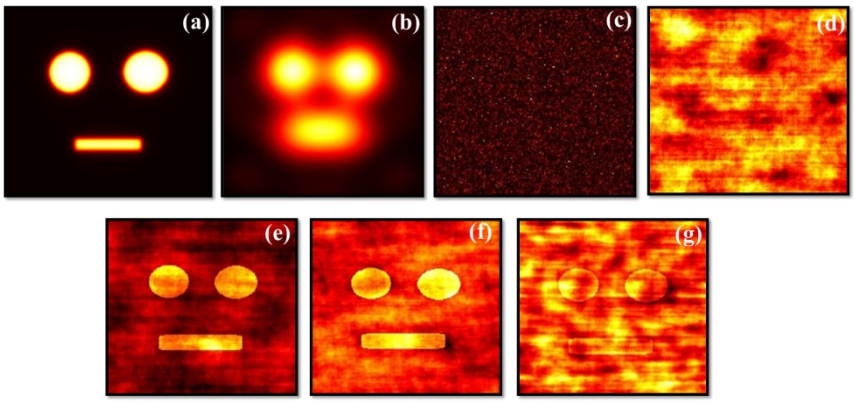

Figure 1: (a) Target object; (b) Image of the object illuminated by incoherent light; (c) PSF of the imaging system; (d) Scrambled image; (e) Reconstructed object using Lucy Richardson deconvolution; (f) Reconstructed object using Weiner deconvolution; (g) Reconstructed object using Blind deconvolution.

References

1. E. Edrei et. al., *Sci. Rep. 6, 33558 (2016).*
2. J. H. Letcher, *RSNA 74th scientific assembly and annual meeting, 21 (1988).*
3. A. Tsabary et. al., *J. Mod. Opt. 69,850-860 (2022).*
4. A. M. Bronstein et al. *2nd IEEE International Symposium on Biomedical Imaging: Nano to Macro (2004).*

Category 9

Lasers Applications & Beam Optics (LSB)

LSB128 Transverse mode filtering of a diode laser using a solid spacer three-mirror ring cavity at 1064nm

Shreyan Goswami[1], Ravi Kesharwani[2], Suresh Doravari[2], Manasadevi P Thirugnanasambandam[2]*

[1]SVNIT, Ichchhanath Surat- Dumas Road, Keval Chowk, Surat, Gujarat-395007
[2]IUCAA, PO Bag 4, Ganeshkhind, Pune-411007
**Corresponding author: goswamishreyan@gmail.com*

The pre-stabilized laser in LIGO detectors [1] have stringent requirements regarding frequency noise, power noise, and pointing stability. In this work, we design and implement a three-mirror rigid spacer ring cavity called Pre-mode cleaner (PMC) to provide spatial transverse mode filtering of the laser output. At the same time, it also reduces beam jitter or spurious beam deformations. We use a 3-mirror cavity for our PMC with mirrors separated by a solid steel SS304 spacer. It comprises of two flat mirrors, with reflectance of 0.98 and 0.99, and the end mirror is a highly reflective concave mirror with a radius of curvature of 1000m. The total cavity length is 344 mm. A Pound Drever Hall (PDH) lock [2,3] keeps the diode laser (Orion 1064nm) resonant inside the PMC by actuating on end mirror and hence controlling the cavity length. The experimental schematic is shown in Figure 1. We chose 17MHz as the EOM modulation frequency for PDH locking which will be done using a Moku:Lab [4]. The sideband harmonics and higher-order modes are separated by the choice of modulation frequency and length of the triangular cavity. We obtain a PDH error signal similar to that obtained based on frequency-domain simulations (Figure 1).

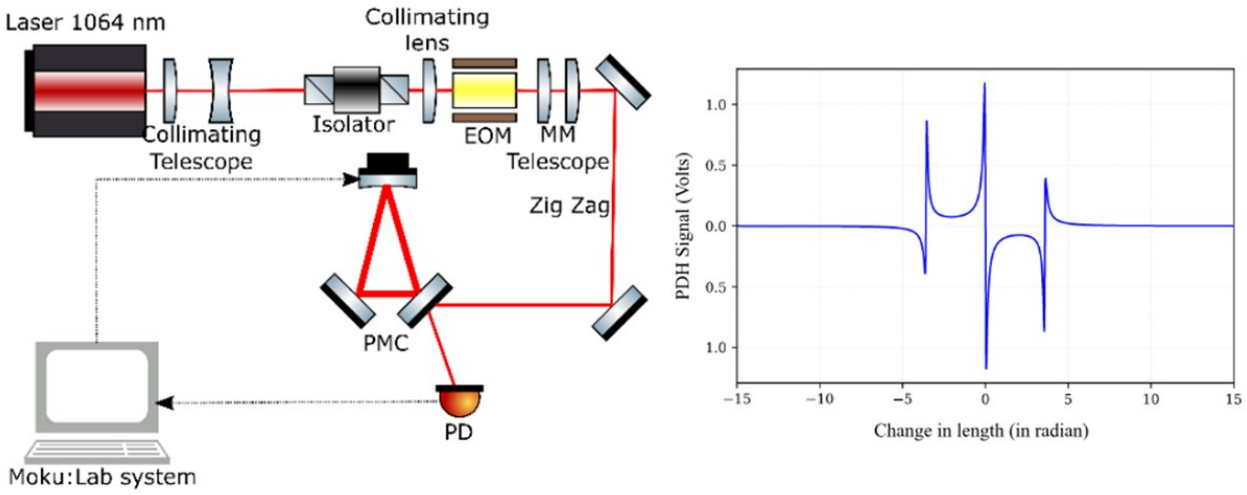

Figure 1. The experimental schematic of diode laser PDH locked to a PMC (left) and the simulated PDH error signal (right).

References

1. Jan Hendrik Põld, *Gottfried Wilhelm Leibniz Universität Hannover, Diss., 2014, 138 S.*
2. Eric D. Black, *American Journal of Physics 69, 79-87 (2001)*
3. R. W. P. Drever et.al., *Applied Physics B: Lasers and Optics, 31:97–105, 1983. 14*
4. https://www.liquidinstruments.com/products/hardware-platforms/mokulab/

LSB289 Tailoring spatial coherence by layered interface

Ankita Chowdhury[1], Vishal Prajapati[1], Rakesh Kumar Singh[1]*
[1]Laboratory of Information Photonics and Optical Metrology, Department of Physics,
Indian Institute of Technology (Banaras Hindu University), Varanasi 221005, India
**Corresponding author: ankitachowdhury.rs.phy21@itbhu.ac.in*

Spatial coherence property of light is a fundamental feature which characterizes the degree of correlation between two distinct points in space of an optical wave. Understanding and tailoring coherence has implications in a wide range of applications ranging from imaging to telecommunication [1].

This paper presents an investigation on tailoring the spatial coherence, defined in terms of degree of coherence (DOC) $\eta(r_1, r_2, w)$, by interaction of light with a layered interface. In order to estimate the $\eta(r_1, r_2, w)$ for a transverse wave in the vectorial domain, a 2×2 cross-spectral density matrix $\overleftrightarrow{W}(r_1, r_2, w)$ (CSD matrix) is used. Interaction of the stochastic vector light field with the layered media is realized by using the angular spectrum method, Fresnel coefficient and with appropriate co-ordinate transformation for light propagation in different media having refractive indices n_1 & n_2 ($n_1 \neq n_2$) as shown in figure-1(a). This procedure is implemented for both orthogonal polarization components of the light and then the CSD matrix is expressed as [2],

$$W^{\leftrightarrow}(r_1, r_2, \omega) = \langle E^*(r_1; \omega)\, E(r_2; \omega) \rangle \tag{1}$$

where r_1 & r_2 are two spatial points in the light.

$$\text{Degree of coherence is } \eta(r_1, r_2, \omega) = \frac{Tr\, W^{\leftrightarrow}(r_1, r_2; \omega)}{\sqrt{Tr\, W^{\leftrightarrow}(r_1, r_1; \omega)}\ \sqrt{Tr\, W^{\leftrightarrow}(r_2, r_2; \omega)}} \tag{2}$$

Here, incident beam is partially coherent Gaussian Schell Model beam and its interaction is considered with the interface between air(n_1=1) and a millimetre-thick media (n_2)

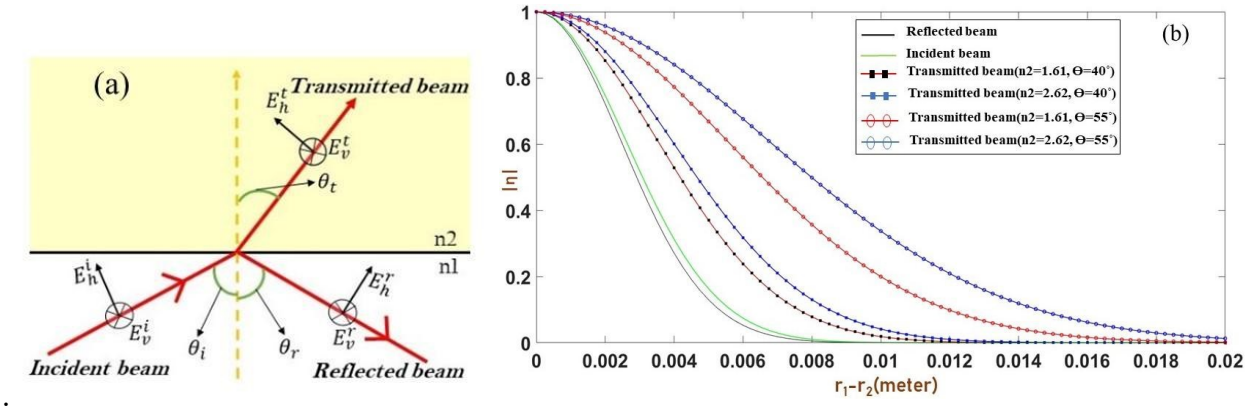

Fig:1(a) Represents a geometry of light beam at the interface, (b) plot of η vs. (r_1-r_2) at Θ = 40° & 55° for different material of n_2 = 1.61 & 2.62.

This result shows that by increasing n_2 longer coherence length can be achieved and increasing Θ affects more than n_2 to make the coherence length longer.

Acknowledgement: Financial support from Board of Research in Nuclear Sciences (BRNS Grant No. 58/14/04/2021-BRNS/37092) is acknowledged.

References

1. Abhinandan Bhattacharjee et. al., *JOSAA 40, 411-416 (2023).*
2. Lahiri, M., et al., *Physical Review A 86, (2012)*

LSB290 A Comparative Study of Extraordinary and Ordinary Modes in Self-Focusing of Elegant Hermite Cosh-Gaussian TEM_{04} Mode Laser Beam in an *Collisionless Magnetized Plasma*

B. D. Vhanmore [1], S. P. Rajmane [2], K. Y. Khandale[4], P. T. Takale[4], S. D. Patil[3], M. V. Takale[4]*

[1]Department of Physics, D Y Patil College of Engineering & Technology, Kolhapur, 416006 India
[2]Department of Nanoscience and Technology, Shivaji University, Kolhapur, 416 004 India
[3]Department of Physics, Devchand College Arjunnagar, Nipani 416 216 India
[4]Department of Physics, Shivaji University, Kolhapur, 416 004 India
**Email: bdvphysuk@gmail.com*

In this present study, we take advantage of the elegant hermite cosh-Gaussian laser beams ability to focus on themselves in collisionless magnetized plasma. The ponderomotive force is the primary cause of the nonlinearity in the dielectric constant that is being considered here. Using WKB and paraxial approximations in the context of a parabolic wave equation approach, differential equations for the beam width parameters in the two transverse dimensions of the beam have been developed. Fourth order Runge-Kutta is used to numerically solve these equations. On a graphic, the impact of decentred parameters in the beam's two transverse dimensions as well as polarization modes has been shown and described.

LSB291 Sub-diffraction spot formation with circularly polarized light

*Bhavesh Pant, Brijesh Kumar Mishra and Brijesh Kumar Singh**

Department of Physics, School of Physical Sciences, Central University of Rajasthan, Ajmer, Rajasthan - 305817, India
**Corresponding author: brijeshsingh@curaj.ac.in*

Abstract: We experimentally demonstrated a method to generate a sub-diffraction limit spot by focusing a left circularly polarized light using a specific optical element (OE). Instead of a high numerical aperture (NA) system with a small focal length, we applied this method for a system with a large focal length.

Introduction: The diffractive nature of light limits the focal spot size of a conventional imaging system to a diffraction limit of $0.5\lambda/NA$, *where* λ is the wavelength [1]. A sub-diffraction limited spot has various significant applications, such as in high-resolution Raman spectroscopy, optical tweezers, high-resolution imaging, stimulated emission depletion microscopy, and so on [2]. Researchers have used tight focusing conditions using a high NA lens to generate a sub-diffraction limited spot with circularly polarized light [3]. However, the limitation with a high NA is the short focal length and complex fabrication. Here, we experimentally demonstrate the formation of a sub-diffraction spot using a standard lens of large focal length *(f = 30 cm).*

Sub-diffraction spot formation: In this approach, the left circularly polarized beam, obtained from a linearly polarized Gaussian beam with the help of a quarter wave plate, is passed through an optical element (OE)

that is made up of two materials of different refractive index (RI) [Fig. 1]. This OE generates two regions of opposite phases in the beam's cross-section as the beam passes through the OE. For a proper ratio between the two regions of OE based on our numerical calculation, the sub-diffraction spot is obtained at the focal plane of the lens [Fig. 2(b)]. From calculations, the obtained spot size (46.8 µm) is about 1.14 times smaller than the diffraction-limited spot of 53.2 µm for our focusing system. Hence, this method is suitable for optical systems with large focal lengths. The spot size can be further reduced by precise control of the ratio between the two regions of the OE and using a high NA lens.

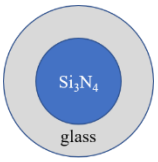

Fig. 1. Geometry of the OE

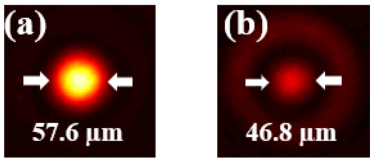

Fig. 2. Intensity distribution at focus (a) without OE, and (b) with OE

References

1. J. Lindberg, *J. Opt. 14, 083001 (2012).*
2. S. W. Hell, et al., *Opt. Lett. 19, 780–782(1994).*
3. G. Chen, et al., *Sci. Rep. 6, 29068 (2016).*

LSB292 Stability of dark solitons in optical system supported by cubic and quintic nonlinearities along with PT symmetric Scarff II complex potential

Jaseera C P[1,3], Thasneem A R[2], Aysha Muhsina K[1]*
[1] Department of Physics, Government Arts and Science College Kozhikode,University of Calicut,673018
[2] Department of Physics, Farook College, Kozhikode, University of Calicut,673632
[3]Department of Physics, Government Arts and Science College Nadapuram,University of Calicut,673506
**Corresponding author: jaseerachilappurath@gmail.com*

Introduction

Spatial solitons are self-trapped optical beams that propagate through a medium as a result of the balance between diffraction and nonlinear response of the medium. In this paper we study the stability of soliton in Parity-time (**PT**)-symmetric self-defocusing systems which support real eigenvalue spectra up to a threshold value of complex potential.

The Mathematical formulation

Beam propagation in nonlinear system governed by Nonlinear Schrodinger Equation (NLSE)

$$i\frac{\partial\psi}{\partial z} + d\frac{\partial^2\psi}{\partial x^2} - \beta|\psi|^2\psi - \beta_2|\psi|^4\psi + (v_r + iv_i)\psi = 0$$ Where

$$v_r + iv_i = v\,Sech^2(x) + i\varepsilon\,Sech(x)Tanh(x)$$

Where ψ is the amplitude of propagating beam, d is diffraction coefficient, β and β_2 are coefficients of Kerr and quintic nonlinearity respectively, υ_r and υ_i are coefficients of real and imaginary components of PT symmetric potential **[1]**. Considering a stationary solution and solve eigen value equation numerically for first four Eigen states by varying system constants.

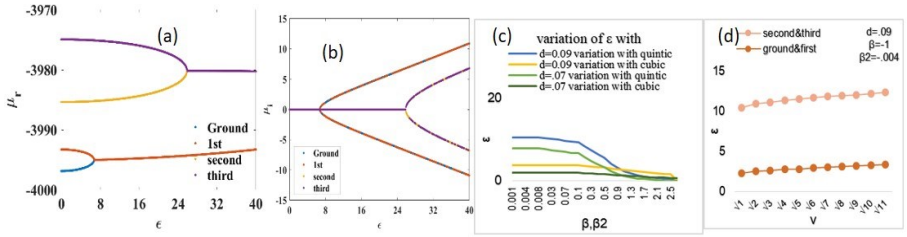

Fig: 1 (a) real part of Eigen value (b) imaginary part of Eigen value (c) variation of threshold ε with non-linearity (d) variation of threshold ε with real potential

Result and discussion

A soliton is said to be stable only if the imaginary part of the Eigen value μ is zero. The findings demonstrate that nonlinearity and the depth of the real potential well determine the threshold value of the coefficient of the imaginary component of the symmetric potential at which the spontaneous breaking of symmetry occurs.

References

1. Yan Z, Wen Z and Hang C 2015 Phy. Rev. E 92 022913

LSB293 Influence of critical beam radius on domains of order of skew-cosh-Gaussian laser beam for self-focusing / defocusing in collisionless plasma

K. Y. Khandale[1,2], A. T. Valkunde[3], R. T. Patil[2], A. R. Patil[2], S. S. Patil[4], P. T. Takale[4], S. D. Patil[4], M. V. Takale[1]**

[1]*Department of Physics, Shivaji University, Kolhapur, Maharashtra 416 004, India.*
[2]*Rajarshi Chhatrapati Shahu College, Kolhapur, Maharashtra 416 004, India*
[3]*Department of Physics, Government Polytechnic, Khamgaon, Buldhana 444 312, India*
[4]*Department of Physics, Devchand College, Arjunnagar, Kolhapur 591 237, India.*
**Corresponding author: atvalkunde@gmail.com , mvtphyunishivaji@gmail.com*

In the present theoretical investigation, the skewness parameter s and order of skewness n enhances the electric field amplitude of skew-cosh-Gaussian (skew-chG) laser beam which has led us to explore many interesting aspects of evolution of spot size of laser beam propagating in collisionless plasma. Here, Akhmanov's parabolic wave equation approach sets up the beam-width parameter equations for the skew-chG laser beam propagating in collisionless plasma under paraxial and WKB approximations. The nonlinearity in the dielectric constant of collisionless plasma is basically due to ponderomotive force. In the present article, an analytical treatment to reduce the complexity arising through dual dependence of n and s in the beam-width parameter equations has led us to explore the domain dependent impact of minimum critical beam radius on the evolution of beam-width parameter differential equation. The different domains in plots of beam-width parameter equations against critical beam radius for given values of skewness parameter, $s = 0.5$ and 1.0 implies the possibilities of focusing as well as defocusing of the laser beam which

are revealed in final plots of beam-width parameter against dimensionless distance of propagation. However, the high-resolution plots of beam-width parameter equations against critical beam radius for given values of skewness parameter, s = 0.5 and 1.0 throws light on intricacies in propagation dynamics of spot size. Results are shown graphically and discussed.

References

1. S.A. Akhmanov, A.P. Sukhorukov, Khokhlov R V, *Sov. Phy. Usp., 10, 609-636, (1968).*
2. M.S. Sodha, A.K. Ghatak, V.K. Tripathi, *Prog Opt., 13, 169-265, (1976).*
3. M.V. Takale, S.T. Navare, S.D. Patil, et al., *Opt. Commun., 282, 3157-3162, (2009).*
4. A.T. Valkunde, B.D. Vhanmore, et al., AIP Conf. Proc, *1953, 140088, (2018).*
5. T.U. Urunkar, S.D. Patil, et al., *Commun. Theor. Phys., 70, 220-224, (2018).*
6. K.Y. Khandale, P.T. Takale, et al., *Indian J. Pure Appl. Phys., 60, 967-972, (2022).*

LSB294 Theoretical and Experimental Study of Propagation of Optical Airy Beam through Random media

Kumari Jaishree[1,2], Dr. Brijesh Kumar Singh[2]*

[1] Center for High Energy Systems & Sciences, Hyderabad, India-500069
[2] Department of Physics, Central University of Rajasthan (CURAJ), Rajasthan, India - 305817
** Corresponding author: kumarijaishree1234@gmail.com*

We present the theoretical and experimental study of non – diffracting, non – spreading and self - accelerating Airy beam[1]. The propagation of 2D Airy beam was done in free space as well as through Random media. On propagating the beam through Random media, we have observed its self - healing property at certain diffraction lengths. While propagating the beam, the main focus was kept on the main front lobe of the beam which acquires the maximum intensity[2] of the beam. After a certain length, it was observed that the beam shows its profile as perturbation resilient which means it is healing itself on obstructing it and it was found out that the length upon which it regains its intensity and profile depends upon the amount of randomness or turbulence present in the phase of the Random media taken.

The theoretical study of the propagation of the Optical Airy beam was done in MATLAB in which the beam is propagated through a random phase screen of randomness 0.511 * 10^(-3) in which the self—healing property of the beam was observed then to verify the observed property experiments was done in LMR Lab (CURAJ), in which a simple diffuser was made, which allows the beam to propagate through it and at the same time, it create some obstruction in the profile of the Airy beam.

To represent the self – healing of the main lobe, a numerical parameter called ‘correlation coefficient’ is also found out, which represents the relation between the intensity of the main lobe on the propagation distance. And other interesting thing that we found out is that once the main lobe heals itself then internal power of the beam will rearrange itself as such that it tries to heal other secondary lobes also.

References

1. G.A. Siviloglou, J. Broky, A. Dogariu, and D.N. Christodoulides, *Observation of Airy Beams Phys. Rev. Lett. 99, 23(2007)*
2. B. K. Singh, R. Remez, Y. Tsur, and A. Arie, *Super – Airy beam: self – accelerating beam with intensified main lobe, Opt. Lett. 40, 4703 (2015).*

LSB295 Focussing Properties of Azimuthally Polarized Axisymmetric Bessel Modulated Vortex Gaussian Beam Through a Dielectric Interface

M.Lavanya[1], D.Thiruarul[2],M.Amal[1],K.B.Rajesh[2], Z.Jaroszweicz[3]

`1 Department of Physics, PSGR Krishanmmal College for Women, Coimbatore,641001.

2 Department of Physics, Chikkanna Government Arts College, Thiruppur ,641602.

3 National Institute of Telecommunications, Warsaw Poland ,02-677.

Corresponding author: rajeskb@gmail.com

The tight focusing properties of azimuthally polarized axisymmetric Bessel-modulated Gaussian beam with quadratic radial dependence (QBG beam) in high numerical aperture system through dielectric interface is analyzed numerically By vector diffraction theory. It is noted that increase in beam parameter increased the spot size and focal depth. It is also observed that for a single spot is observed in case of greater than 2 two spots with different intensity variations are observed. But in case of using complex values from μ, the spot size is very much confined and Focal depth increased considerably. We also observed that by using annular Obstruction with δ=0.5 and δ=0.75 a highly confined focal spot with FWHM of 0.378 λ having large focal depth around 31.42λ is obtained for complex valued μ.

LSB296 Self-focusing and defocusing of TEM$_{0p}$ mode Hermite Gaussian laser beams in collisional plasma with Impact of linear absorption

M. V. Takale[1], K. Y. Khandale[1,2], P. T. Takale[1], S. S. Patil[3], S. D. Patil[3]*

[1]Department of Physics, Shivaji University, Kolhapur, Maharashtra 416 004, India.
[2]Rajarshi Chhatrapati Shahu College, Kolhapur, Maharashtra 416 004, India
[3]Department of Physics, Devchand College, Arjunnagar, Kolhapur 591 237, India.
**Corresponding author: mvtphyunishivaji@gmail.com*

In the present theoretical investigation, the authors explored the impact of linear absorption on self-focusing and defocusing of the first five TEM*0p* mode Hermite-Gaussian laser beams in the collisional plasma. The nonlinearity in dielectric function taken into account herein is primarily because of the elastic electron–ion collisions. It seems that modes with even values of p exhibit self-focusing whereas modes with odd values of *p* exhibits defocusing behaviour of beam-width parameter variation with dimensionless distance of propagation. It has been found that absorption is crucial for the self-focusing of laser beams and that the self-focusing nature of the beam-width parameter decreases with propagation distance. The entire theoretical formulation is established using Akhmanov's parabolic wave equation approach under paraxial and WKB approximations. By using fourth order Runge –Kutta method the numerical computation is completed. Finally the behaviour of beam-width parameters with the dimensionless distance of propagation is presented graphically and discussed.

References

1. S.A. Akhmanov, A.P. Sukhorukov, Khokhlov R V, *Sov. Phy. Usp., 10, 609-636, (1968).*
2. M.S. Sodha, A.K. Ghatak, V.K. Tripathi, *Prog Opt., 13, 169-265, (1976).*
3. M.V. Takale, S.T. Navare, S.D. Patil, et al., *Opt. Commun., 282, 3157-3162, (2009).*

4. N. Kant, M.A. Wani, A. Kumar, *Opt. Commun., 285, 4483-4487, (2012).*
5. S.T. Navare, M.V. Takale, S.D. Patil, et al., *Opt. Lasers Eng., 50, 1316-1320, (2012).*
6. P. Sharma, *AIP Conf. Proc. 1670, 030029 (2015).*
7. A.T. Valkunde, S.D. Patil, M.V. Takale, et al., *Optik, 158, 1034–1039, (2018).*
8. K.Y. Khandale, P.T. Takale., S.S. Patil, et al., *J. Phys.: Conf. Ser., 2426 012005, (2023).*

LSB297 Spatiotemporal evolution of nanosecond laser produced Zn Plasma

Nikhil Varghese[1], Reji Philip[2], Smijesh N[1]*

[1]Ultrafast Optics Group, School of Pure and Applied Physics, Mahatma Gandhi University, PD Hills, Kottayam - 686 560, Kerala, India
[2]Ultrafast and nonlinear Optics Lab, Light and Matter Physics, Raman Research Institute, Bangalore - 560080
**Corresponding author: varghesenikhil@mgu.ac.in*

The emission characteristics of a nanosecond (ns) laser-produced plasma (LPP) strongly depend on laser parameters as well as the nature and pressure of the ambient gas [1, 2]. We investigated the spatio-temporal evolution of a ns Zinc LPP using optical emission spectroscopy (OES). The spatio-temporal variation of emissions from the plasma as a function of irradiation energy is investigated. Further, the evolution of plasma as a function of ambient pressure (P_b) and irradiation energy at a fixed integration time is also studied and reported. At initial timescales of plasma expansion and for all E_l's investigated, l_n maximizes closer to the target surface, whereas at later timescales, ln maximizes farther from the target. On the other hand, li appears at earlier timescales and decreases thereafter, signifying possible recombination. At lower E_l, the emission intensity of neutrals (l_n) is higher than that of ions (l_i), whereas at higher E_l, l_i dominates. Upon varying the pressure from 0.08 Torr to 200 Torr, while l_n and l_i increase monotonously for shorter distances, l_n and l_i increase, reach a maximum, and then decrease at larger distances. Details of this investigation and its discussion are presented.

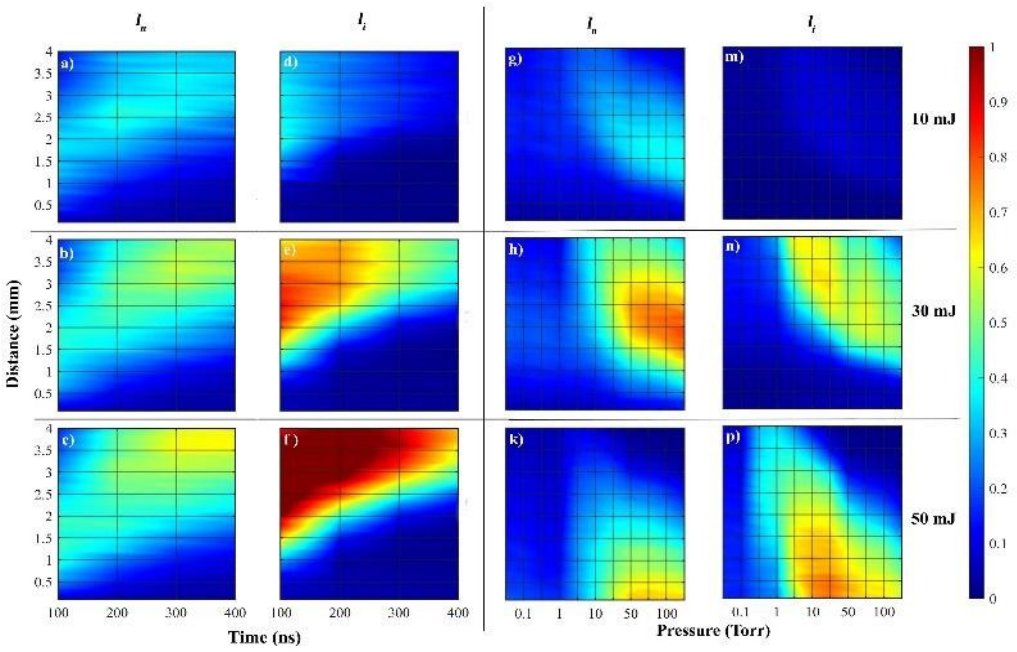

Figure 1: A 3 ×4 matrix of 2D plots, with each element in the first two columns representing the variation of l_n [a - c] and l_i [d- f] as a function of time (X-axis) and distance from the target on (Y-axis). The next two show the variation of the l_n [g - k] and l_i [m-p] as a function of pressure (X-axis) and distance (Y-axis)

References

1. SS Harilal, Beau O'Shay, Yezheng Tao, and Mark S Tillack. Ambient gas effects on the dynamics of laser produced tin plume expansion. *Journal of Applied Physics, 99(8):083303, 2006.*
2. N Smijesh, Kavya H Rao, and Reji Philip. Influence of pulse width on the laser ablation of zinc in nitrogen ambient. *Applied Physics A, 122:1–6, 2016*

LSB298 Design analysis of ground based laser system for satellite laser ranging and counter operation

Sakkiyudheen Vahid N A[1], Parvathy Rajesh Nair[1], Sourav Paul[2], S Veerabuthiran[2]** and Jagannath Nayak[2]*

[1]Department of Electronics, Cochin University of Science and Technology, Cochin, 682022
[2]CHESS, DRDO, Hyderabad, 500058
***Corresponding author: sveerabutriran.chess@gov.in*

**Corresponding author: zakkiyudheen@pg.cusat.ac.in*

Low earth orbit ISR (Intelligence, Surveillance, and Reconnaissance) satellites monitor military activities on ground with very high spatial resolution. These satellites employ high-quality electro-optical sensors like CCD and CMOS to take high resolution images of ground surface. These satellites can be dazzled or blinded by high energy lasers operating from ground surface. This paper discusses the design aspects laser systems that can track and take counter actions against ISR satellites. Primarily, a low energy pulse laser is used to range and track the satellite. Laser pulse is transmitted towards the low earth orbit satellite. The retroreflector fitted in the satellite reflects back to the receiver. Time of flight concept is used to measure the exact distance between the station and satellite. However, achieving millimeter accuracy in SLR poses challenges due to atmospheric disturbances, instrumental errors, and satellite motion. A detailed analysis has been carried out that covers radar link equations, atmospheric condition, background conditions, sub system parameters etc. A laser with few milli joule of energy is determined to be sufficient for tracking satellite that carries retroreflector. In the context of countering satellites, the paper explores the design of a high-power pulse laser system to potentially disrupt the electro-optical imaging sensors. The analysis includes theoretical studies to estimate the required power level under various conditions. The proposed system consists of a high-power laser source, transceiver optics, detectors, and other subsystems, capable of detecting and tracking satellites up to long ranges in slant range. When necessary, it can initiate countermeasures, firing high-energy pulses at overhead satellites to disrupt their optical sensors. The study suggests that a solid-state laser having specifications such as pulse energy few joules, pulse width few Nano seconds can saturate or damage imaging sensors under different atmospheric conditions in low Earth orbit. Detailed system configurations, encompassing laser transmitters, receiver detectors, event timers, and tracking systems, are provided, contributing to the development of ground-based satellite ranging systems. This technology aims to enhance space control and security in the context of evolving geopolitical dynamics.

References

1. Y. Butt, "Effects of chinese laser ranging on imaging satellites," Science and Global Security, vol. 17, no. 1, pp. 20–35, (2009).
2. J. J. Degnan, "Millimeter accuracy satellite laser ranging: a review," Contributions of space geodesy to geodynamics: technology, vol. 25, pp. 133–162, (1993).

LSB299

Effect of Spatial Chirp On Autofocusing Beams

*Sandeep Mishra[1, 2, *], S K Mishra[1], Akhilesh Kumar Mishra[2, 3]*

[1]Instruments Research & Development Establishment, Dehradun-248008, India
[2]Department of Physics, Indian Institute of Technology Roorkee, Roorkee-247667, Uttarakhand, India
[3]Centre for Photonics and Quantum Communication Technology, Indian Institute of Technology Roorkee, Roorkee- 247667, Uttarakhand, India
**sandeep_m@ph.iitr.ac.in*

Three-dimensional caustic surface of a rotational symmetric beam exhibits an autofocusing property. Beams emanating from a caustic surface $r(z) = b - a^n$ meet at a focal distance $f = \sqrt[n]{b/a}$ [1]. At input plane these beams are expressed as-

$$u(r) = \exp\left[-\frac{(r-ba)^n}{w_o^2}\right]\exp(i\psi_{r0}), \qquad (1)$$

where the phase function ψ_{r0} is defined as

$$\psi_{r0} = \frac{kn^2(an-a)^{1/n}(r-b)^{2-1/n}}{(n-1)(2n-1)}, \qquad (2)$$

here $k = 2\pi/\lambda$ is the wavenumber and λ is the wavelength. Different values of phase functions can be obtained by setting different even values for n. To study the effects of chirp, a factor $\exp\left[-ic\left(\frac{r}{w_0}\right)^2\right]$ is introduced in the expression (1) of the rotational symmetric beams, where c is the spatial chirp parameter [2]. We have numerically conducted propagational studies of such beams in free space as well as weak turbulence conditions.

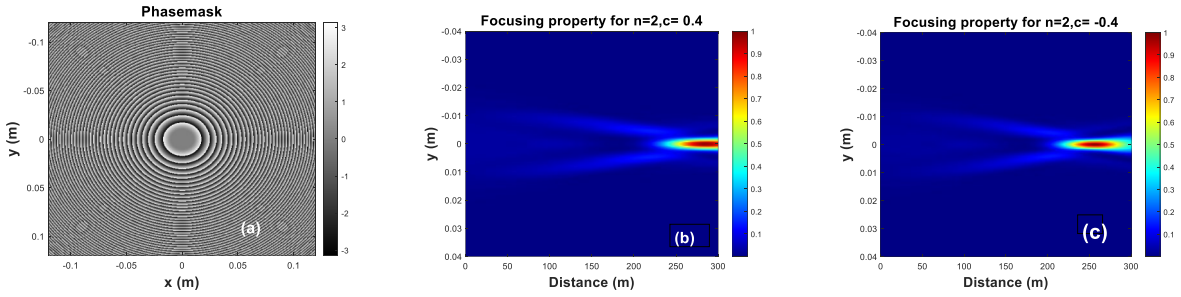

Figure 1. (a) Phase mask to generate autofocusing beams, propagation dynamics of the beam for (b) c=0.4 and (c) c=-0.4.

As depicted in fig. 1 (b) and (c), the spatial chirp modifies the focusing property of the beam in free space.

References

1. Xin Wang, et. al., "Design of autofocusing beams based on accelerating beams", Vol. 39, No. 1 / January 2022 / Journal of the Optical Society of America A.
2. Shakti Singh, et. al., "Ring Pearcey Vortex beam dynamics through atmospheric turbulence," Vol 40, Issue 9. Pp 2287 /2023/ Journal of the Optical Society of America B.

Category 10

Microwave and THz Photonics (MWT)

MWT319 Identification of Microplastics Contamination in soil using Terahertz Imaging Technique

M.Meenaakumari[1], E. Manikandan[1,2]

[1]School of Electronics Engineering, Vellore Institute of Technology, Chennai -600127
[2] Centre for innovation and product Development, Vellore Institute of Technology, Chennai -600127
**Corresponding author: manikandan.e@vit.ac.in*

In recent years, microplastics pollution has emerged as a significant contaminant in ecosystem, primarily due to its small size and long-lasting nature. Microplastics (MPs) are dispersed widely throughout ecosystems via natural processes like wind and water. Consequently, microplastics have infiltrated freshwater, soil, air, and the food chain. However, identifying microplastics within the complex matrix of soil has proven challenging. This paper presents a rapid, non-destructive method for the identifying of microplastics (PE) embedded in soil. The approach leverages emerging terahertz transmission spectroscopy imaging technology, coupled with a machine learning algorithm for analysis. The experiment involves a sample holder with two compartments: one filled with pre-treated soil (left) and the other containing a mixture of soil and microplastics at varying concentrations (1%, 2%,4% and 8%) (right).

Simultaneously, image processing is carried out on the physical sample across different frequency from 0.1THz to 0.7THz, employing a qualitative discrimination model based on Machine Learning algorithm. The images are segmented using binarization threshold and pixel properties are calculated. The terahertz transmission images of sample with different concentration of microplastic mixer are processed to visualize the presence of microplastics. This study demonstrates the potential terahertz imaging technology in detection of microplastics within soil, addressing a critical need for effective microplastic analysis in complex environmental matrices.

References

1. Hu, J., et.al., Study on the Identification and Detection of Walnut Quality Based on Terahertz Imaging. *Foods, 11(21), 3498(2022)*
2. Im, J., et.al., (2021). Detection of microplastic in salts using terahertz time-domain spectroscopy. *Sensors, 21(9), 3161 (2021)*
3. Cassar, Q.,et.al., Terahertz refractive index-based morphological dilation for breast carcinoma delineation. *Scientific reports, 11(1), 6457 (2021)*

MWT320 Repetition Rate Stabilization of Active Harmonic Mode Locked Fiber Laser based on Supermode Power Measurement

Siva Subramaniyam C N[1†], Joydip Dutta[1†], Sreeraj S J[1†], Balaji Srinivasan[1] and Deepa Venkitesh[1]*

[1]Dept. of Electrical Engineering, Indian Institute of Technology Madras, Chennai-36, India. [†]These authors contributed equally to this work
**Corresponding author: deepa@ee.iitm.ac.in*

Active harmonic mode-locked fiber lasers (AHML) are required in various applications such as microwave signal generation, optical clock distribution and photonic analog-digital converters [1]. However, the stability of the AHML is influenced by environmental distribution such as fluctuations in room temperature and vibrations causing variation in the cavity length resulting in issues such as increased timing jitter, pulse dropout, and frequency instability [2].This work focuses on novel control technique to stabilize the AHML from environmental disturbance based on power measurement of supermodes. Our experiments have shown that the integrated optical power of supermodes is higher in unstable conditions (approx. -10 dBm) than in stable conditions (< -32 dBm).

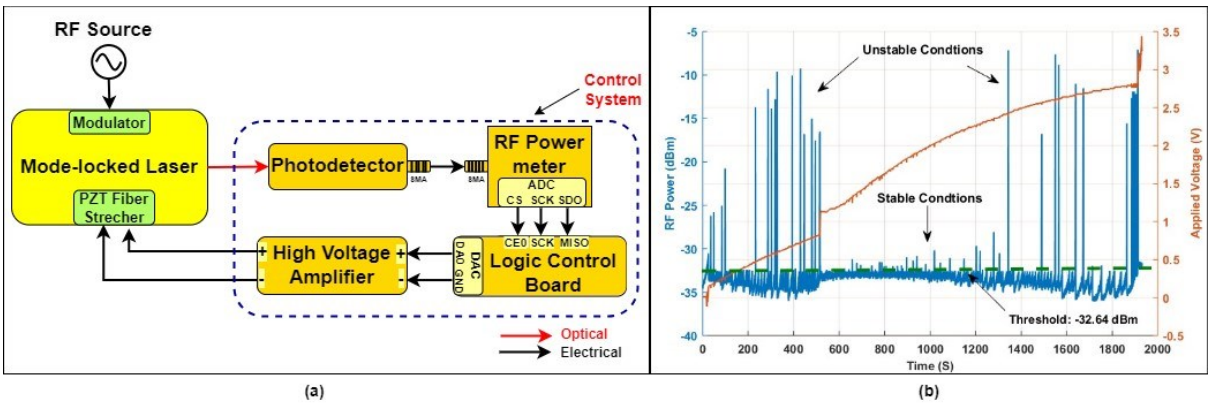

Figure (1): (a) Schematic diagram of our control system, (b) Control algorithm operation (RF power & Applied voltage) over time.

Fig 1 (a) shows the schematic diagram of our control system involving photodetector to convert the integrated optical power of the supermodes from AHML into an electrical signal which is measured using an RF power meter and sent to logic control board via ADC. The goal of the logic control board is to constantly monitor the RF power meter's output and ensure the integrated optical power of the supermodes remains minimized (< -32 dBm) to operate AHML in a stable regime by sending correction signal from the DAC to the PZT fiber stretcher via high voltage amplifier. Fig 1 (b) shows the voltage applied to the PZT fiber stretcher by the logic control board over ~1800 seconds while the control algorithm is operational. We are currently exploring the implementation of dynamic step correction to improve the efficiency of our control system.

References

1. G. C. Valley, *Opt. Exp.,15, 5, 1955–1982, (2007).*
2. *E. Yoshida et al., IEEE Photon. Technol. Lett., 11, 5, 548-550, May (1999).*

Category 11

Nano-photonics & Plasmonics (NPH)

NPH129 Selection of brightest gold nanotags for Surface-enhanced Raman spectroscopy

Megha Mehta[1], William Skinner[1], Sara Mosca[2], Benjamin Gardner[1], Francesca Palombo[1], Pavel Matousek[2], Nicholas Stone[1]*

[1]School of Physics and Astronomy, University of Exeter, Exeter EX4 4QL, UK

[2]Central Laser Facility, STFC Rutherford Appleton Laboratory, Oxford OX11 0QX, UK
**Nicholas Stone: n.stone@exeter.ac.uk*

The choice of Raman reporter is a significant aspect for improving the imaging sensitivity and multiplexing capabilities of SERS nanoparticles, particularly when attempting to read out Raman signals from NPs deeply buried in tissues[1-3]. In this study, we have investigated the combination of three AuNPs with a range of different Raman reporter molecules. Three resonant reporters, IR-125, IR-820, IR-797 and three non-resonant reporters (2-bi-(4-pyridyl) ethylene (BPE), biphenyl-4-thiol (BPT) and 4-mercaptobenzoic acid (MBA) bound to gold nanoparticles of different morphologies – nanospheres and nano-raspberries. We used commercially available AuNPs and in-house synthesised gold nano-raspberries (AuNRBs) using the green chemistry method[4] of reduction of gold ion by 2-[4-(2-hydroxyethyl)-1-piperazyl] ethane sulfonic acid (HEPES). The method carried out limits the need for extensive post-synthesis routines of biofunctionalization to improve sensitivity. The appropriate reporter concentration, and volume ratio of reporter to nanoparticle concentration parameters were analysed to provide a valuable assessment of the reporter molecule that gives maximum SERS enhancement for these AuNPs. We have used 785 nm laser excitation to find the brightest 'Raman reporter – gold nanoparticle' combination for further use in deep Raman multiplexed imaging. We have demonstrated that AuNRBs provide significant SERS enhancement with better sensitivity for Raman resonant reporters due to strong label binding affinity of dye to gold surface as compared to non-resonant dyes. It also explains inherently stronger signals generated by surface-enhanced resonance Raman scattering (SERRS), as opposed to surface-enhanced Raman scattering (SERS). These simple, scalable and tunable size AuNRBs are excellent candidates for predicting which Raman reporters could improve sensitivity and be used for deep Raman multiplexed imaging.

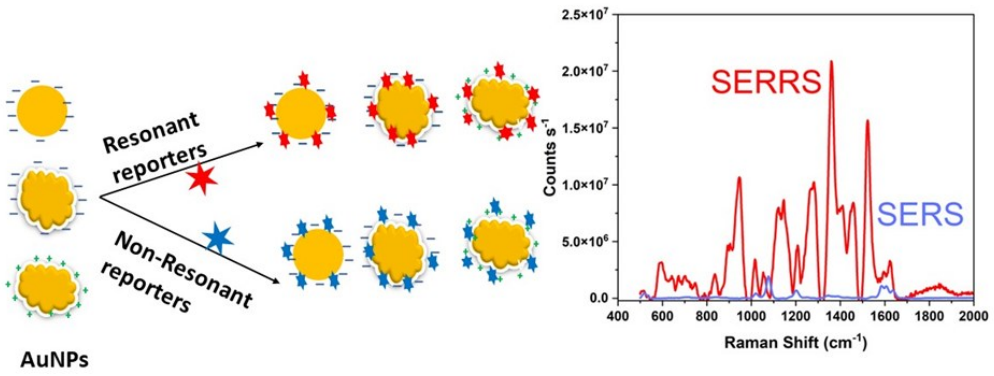

Figure 1. Schematic representation of different morphology gold nanoparticles after tagging with resonant and non-resonant reporter showing stronger SERRS enhancement than SERS.

References

1. P. Dey, A. Vaideanu, S. Mosca, M. Salimi, B. Gardner, F. Palombo, I. Uchegbu, J. Baumberg, A. Schatzlein, P. Matousek, Surface enhanced deep Raman detection of cancer tumour through 71 mm of heterogeneous tissue, Nanotheranostics 6(3) (2022) 337.
2. F. Nicolson, M.F. Kircher, N. Stone, P. Matousek, Spatially offset Raman spectroscopy for biomedical applications, Chemical Society Reviews 50(1) (2021) 556-568.
3. N. Stone, M. Kerssens, G.R. Lloyd, K. Faulds, D. Graham, P. Matousek, Surface enhanced spatially offset Raman spectroscopic (SESORS) imaging–the next dimension, Chemical Science 2(4) (2011) 776-780.
4. J. Johnston, E.N. Taylor, R.J. Gilbert, T.J. Webster, Improved molecular fingerprint analysis employing multi-branched gold nanoparticles in conjunction with surface-enhanced Raman scattering, International journal of nanomedicine 11 (2016) 45.

NPH130 Coupling NV centers to surface states in nanophotonic structures

*Faizan H. Lone[1], Sudha Maria S,[2] Nitesh Singh[1], Shivakiran Bhaktha B N[2], Rajesh V. Nair[1,]**

[1]Laboratory for Nanoscale Optics and Metamaterials (LaNOM), Department of Physics, Indian Institute of Technology Ropar, 140001, India
[2]Department of Physics, Indian Institute of Technology Kharagpur, West Bengal, 721302, India
**email: rvnair@iitrpr.ac.in*

The Tamm plasmon structures are recently proposed as a viable platform to modulate the emission dynamics of quantum emitters [1]. Nitrogen-vacancy (NV) centers in nanodiamond is proposed as a qubit due to its exceptional optical and spin properties. However, their emission is required to be modified to fully harness their use for quantum technologies. Here, the Tamm plasmon structure with coupled NV centers has been fabricated and the emission pattern has been measured. The reflectivity spectra (Fig. 1a) show the appearance of Tamm mode at 660 nm which overlap with NV center emission range. The NV center coupled with Tamm mode shows enhanced emission centered at 660nm while suppressing other modes in the emission as compared to emission from a reference sample (NVs in PVA film) as seen in Fig. 1b. Fig. 1c shows the decay measurements. The enhanced decay rate of the Tamm mode coupled with NV centers support the increase in the NV center emission as seen in Fig. 1c.

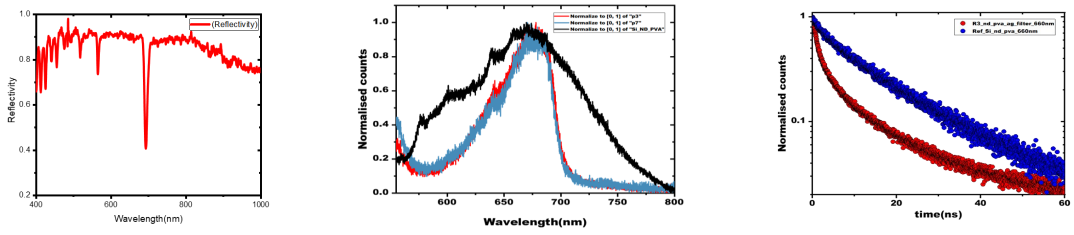

(a) (b) (c)

Fig. 1: (a) The measured reflectivity spectra from the Tamm structure, (b) The measured emission from the reference sample and nanodiamonds coupled to Tamm structure, (c) Comparison of decay curves

The emission spectra show the narrowing of NV emission at 660 nm and the lifetime has been reduced from 16 ns for the reference sample to 11 ns for the NV's coupled to Tamm structure. A comprehensive study on the wavelength depended lifetime of NV's has also been done. Our studies show the use of Tamm plasmon structures for

enhancing the emission from quantum emitters.

ACKNOWLEDGEMENTS
The authors acknowledge financial support from IIT Ropar, DST-ICPS, and DST-SERB.

References

1. T. Goto et. al., Phys. Rev. Lett., **101**, 113902 (2008).

NPH131 Novel method for the fabrication of titanium nitride thin films from sputtered metal films

*Liya Tony, I Packia Selvam, S.N. Potty**

Centre for Materials for Electronics Technology (C-MET)
Scientific Society, Ministry of Electronics & Information Technology, Government of India
Shoranur Road, Athani P.O, Thrissur 680 581
** Corresponding author – snpotty@cmet.gov.in*

Titanium nitride films possess distinctive structural, electrical, and optical characteristics, rendering them highly sought-after for a variety of technological applications. Typically, these materials are produced via physical vapor deposition (PVD) and chemical vapor deposition (CVD) techniques. This study focuses on the synthesis of titanium nitride thin films by the gas nitridation process of RF sputtered titanium metal films at a temperature of 600°C, utilizing ammonia gas as nitrogen source. At the given temperature, ammonia undergoes dissociation, resulting in the liberation of nascent nitrogen. Simultaneously, ammonia establishes a covalent bond with titanium metal film. In this study, we aim to analyse the optical and electrical properties of as-deposited metal films and the films obtained after nitridation. The films possess thicknesses within the range from 50 to 150nm. The structural investigation has been conducted using a combination of GI-XRD and Raman spectroscopy techniques. The electrical properties were analysed by using Hall measurement in the van der Pauw configuration. The optical properties were studied using the reflection and transmission spectra recorded in the visible range. The energy bandgap of the titanium nitride films were determined using the Tauc plot obtained from the transmittance spectra. The electrical and optical properties of the titanium nitride films with varying thickness were analysed in order to establish a correlation with plasmonic characteristics.

NPH132 Studies on the Magneto-Optical Faraday Rotation of surfactant assisted Fe_3O_4 nanoparticles

*Mubeena Rafi[1], Lakshmi B[2], Honey John[1,3], Pramod Gopinath[1,2]**

[1] Inter University Centre for Nanomaterials and Devices, Cochin University of Science and Technology, Cochin -682022, India
[2] International School of Photonics, Cochin University of Science and Technology, Cochin- 682022, India.
[3] Department of Polymer Science and Rubber Technology , Cochin University of Science and Technology, Cochin – 682022, India.
**Corresponding author: pramod@cusat.ac.in.*

Superparamagnetic magnetite (Fe_3O_4) nanoparticles were synthesized using chemical coprecipitation method with polyethylene glycol (PEG) as surfactant at room temperature. Structural, morphological, magnetic and optical properties of these nanoparticles were investigated using XRD, TEM, VSM and UV-Vis absorbance spectroscopy. Magneto-optical properties of magnetite nanoparticles (MNPs) were studied by

measuring the Faraday rotation, which is a measure of the material interaction with plane polarized light in presence of magnetic field. The Magneto-Optic Faraday Rotation (MOFR) studies were performed on stable dispersion of MNPs in ethylene glycol with a volume fraction of 1 x 10^{-3} for two laser sources of different wavelength (532 nm and 655 nm) upto a magnetic field of 2000 Oe. For both wavelengths, for the initial fields a gradual increase in rotation is observed and at higher fields the MOFR becomes saturated. Due to the saturation behaviour of MOFR and the superparamagnetic behaviour, the magneto-optical data are fitted using Langevin function. The magneto-optic response of Fe_3O_4 at 655 nm is more pronouncing compared to that at 532 nm. This is due to the intervalence charge transfer transition (IVCT) at 2.05 eV corresponding to two Fe sites differing only in oxidation state, namely $[Fe^{2+}]t_{2g} \longrightarrow [Fe^{3+}]_{eg}$. Controlling the optical properties by magnetic field as done in MOFR find wide applications in different fields.

References

1. Babukutty et.al., *Mater Res. Express 4, 035906 (2017).*
2. Narsetti et.al., J.Magn.Magn.Mater. 528, 167779 (2021).
3. Spivakov A et al. Nanomaterials 10, 1888 (2020).
4. Devi M et.al. Appl. Phys. A 106, 757(2012).
5. Lakshmi et.al. J. Mol. Liq. 123103(2023).

NPH133 Surface enhanced Raman scattering using periodic array of shape anisotropic nanostructures

Sathi Das[1], Jean-Claude Tinguely[2], Kanchan Saxena[3], Balpreet Singh Ahluwalia[2], Dalip Singh Metha[1#]*

[1]Bio-photonics and Green Photonics Laboratory, Indian Institute of Technology Delhi, Hauz-Khas, New Delhi-110016, India.
[2]Department of Physics and Technology, UiT The Arctic University of Norway, Tromsø, 9037, Norway.
[3]Amity Institute of Renewable and Alternative Energy, Amity University Uttar Pradesh, Sector 125 Noida, U.P., India
**Corresponding author: *dassat123@gmail.com, [#]mehtads@physics.iitd.ac.in*

Surface enhanced Raman spectroscopy (SERS) is a popular technique for real-time label-free detection of chemical and biochemical fields [1], [2]. An advanced SERS substrate includes 3D distribution of nanostructures, tuneable plasmonic enhancement, closely placed nanostructures for excitation of coupled plasmonic modes. The sensitivity of the substrate depends on nanostructure morphology, whereas the uniformity is dependent on the regular geometry of the nanostructure. Current literatures describe that the shape anisotropic nanostructures cause enhanced hotspots at sharp edges due to charge accumulation. Literatures with star shaped Ag and Au nanoparticles, shape anisotropic dendrites are demonstrated to create larger enhancement than the spherical shaped colloidal Ag NPs. However, the anisotropic NPs are unstable and agglomerate randomly, generating irreproducible hotspot orientation. Thus, solid substrates are preferable for long term durability.

We created template of PS beads on Si wafer, further utilised the PS template to induce anisotropy into the beads itself. The beads were heated with O_2 plasma to create etching and shrinking for various times. In this study, we examined the impact of shape anisotropy on the enhancement of SERS by creating a nanoscale template with a high degree of anisotropy. We investigated the effect of shape anisotropy on SERS enhancement upon development of a highly anisotropic nanosized template for SERS substrate. The created substrate was optimised using R6G as a probe molecule. Further a theoretical investigation using the finite difference time domain simulation was conducted to determine the amount of local electric field around the array of nanostructures. The comprehensive study provides valuable insights regarding the mechanism of

Raman enhancement in SERS.

References

1. B. Sharma, R. R. Frontiera, A. I. Henry, E. Ringe, and R. P. Van Duyne, "SERS: Materials, applications, and the future," *Materials Today, vol. 15, no. 1–2. 2012. doi: 10.1016/S1369-7021(12)70017-2.*
2. S. Das, K. Saxena, L. P. Goswami, J. Gayathri, and D. S. Mehta, "Mesoporous Ag–TiO2 based nanocage like structure as sensitive and recyclable low-cost SERS substrate for biosensing applications," *Opt Mater (Amst), vol. 125, 2022, doi: 10.1016/j.optmat.2022.111994.*

NPH134 Nonlinear Optical Study of Copper Indium Sulphide/Zinc Sulphide Core-Shell Quantum Dots

Syammohan V[1], Kailasnath M[1]*

[1]International School of Photonics, Cochin University of Science and Technology, Kochi, pin 682022, India

**syammohan1300190@cusat.ac.in*

Linear and nonlinear optical response of copper indium sulphide/zinc sulphide Quantum Dots (CIS/ZnS QDs) prepared by simple aqueous method is investigated. The morphological and optical characteristics of the sample were analysed using XRD, TEM, UV-Vis Absorption, and fluorescent spectroscopy. For the investigation of the sample's nonlinear response, the Z-Scan technique is employed along with Nd-YAG laser operating at a wavelength of 532 nm and pulse width of 6 ns as a laser source. The nonlinear optical property of the prepared sample was done with varying sample concentrations and LASER input power. It was observed that the sample showed Reverse Saturable Absorption (RSA) behaviour at all input powers and sample concentrations. However, as concentration increased, the sample showed enhanced RSA behaviour up to an optimum concentration, and from then, it started to decrease with increasing concentration. The CIS/ZnS QDs dispersed in water at this optimum sample concentration of 0.75 mg/mL is chosen for the intensity-dependent nonlinear study. The laser power varied from 30 µJ to 190 µJ and the sample continued to show RSA behaviour. The calculated nonlinear absorption coefficient at 100 µJ is 3.31×10^{-9} cm/W.

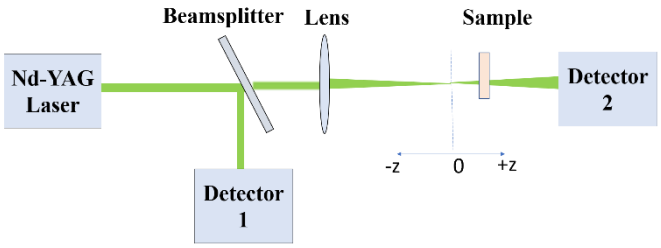

References

1. *TK Nideep et. al., Optik , 1101-1108 (2019).*
2. *M Ramya et. al., surfaces and interfaces, 26, 101345 (2021)*

NPH323 Real time detection of bacteria by plasmon-enhanced spectroscopy

Anjika Kumari[a], Sathi das [b], Meenakshi [b], Dalip Singh Mehta [*],

[a] Centre for Sensors, Instrumentation and Cyber-physical System Engineering, IIT Delhi.

[b] Department of Physics, IIT Delhi

[*]mehtads@physics.iitd.ac.in

Bacteria pose a major threat to ecosystem and connected life forms. A few diseases can be caused by bacteria. Development of efficient methods for detecting bacteria in sample is a significant interest for both environment and biologists. This can help in monitoring and addressing potential health and ecological concern. Plasmon enhanced spectroscopy (PES) is a powerful technique for detection of bacteria. The contaminants such as pathogens could be determined based on the shape of spectra and Nanoparticle which enhanced the spectrum signal.

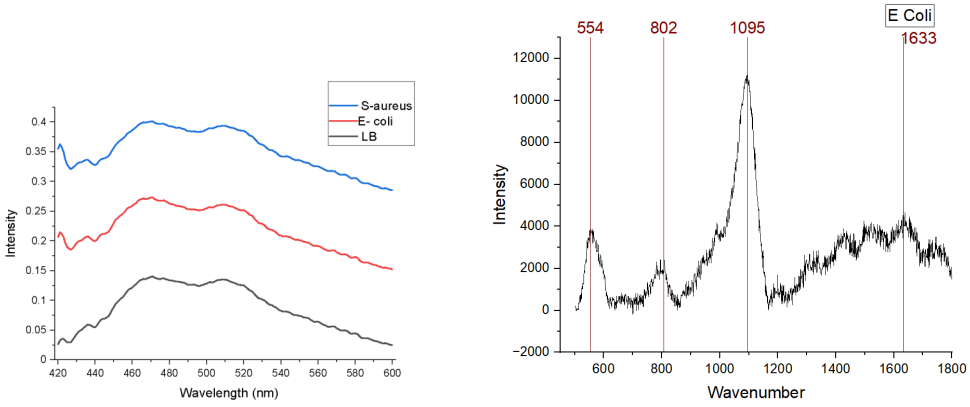

Fig1: The detection of bacteria with help of spectroscopy

References

1. Amini, K. and Kraatz, H.B., 2015. Recent developments in biosensor technologies for pathogen detection in water. JSM Environ. Sci. Ecol, 3(1), pp.1-9.
2. Tracy B, Gaida S, Papoutsakis E. 2010. Flow cytometry for bacteria: enabling metabolic engineering, synthetic biology and the elucidation of complex phenotypes. Curr. Opin. Biotechnol. 21:85–99.
3. Renggli, S., Keck, W., Jenal, U. and Ritz, D., 2013. Role of autofluorescence in flow cytometric analysis of Escherichia coli treated with bactericidal antibiotics. *Journal of bacteriology, 195(18), pp.4067-4073.*

NPH324 Tunable Transition Metal Dichalcogenide Based Metasurfaces in Anisotropic Medium

K. M. Anu[1], Jayasri Dontabhaktuni[1]*

[1]Department of Physics, Mahindra University, Hyderabad, India, 500043

**Corresponding author: jayasri.d@mahindrauniversity.edu.in*

Metasurfaces have emerged as powerful tool for manipulating electromagnetic waves at the nanoscale, enabling various applications in optics, telecommunications, and sensing [1,2]. In this study, we investigate

the design and potential applications of metasurfaces constructed using transition metal dichalcogenides (TMDCs) in anisotropic medium. TMDC's have received extensive attention in the past decade due to their extraordinary electronic, optical and thermal properties making them interesting for various optoelectronic applications, such as ultrafast modulation, light emission, photodetection and light harvesting as well as for fundamental investigations of strong light–matter interactions [3,4]. The anisotropic medium, in which these TMDC-based metasurfaces are embedded, introduces additional degrees of freedom for tailoring light -matter interactions. This anisotropy can be harnessed to achieve unprecedented control over wavefront shaping, polarization conversion, and dispersion engineering. We explore the fundamental physics underlying TMDC-based metasurfaces in anisotropic environments, providing insights into the design principles that govern their performance. Through theoretical modelling and validation, we demonstrate the tunability and versatility of TMDC-based metasurfaces in anisotropic medium. Furthermore, we discuss potential applications of these metasurfaces in the context of emerging technologies, including metasurface -enabled imaging systems, quantum optics, and on-chip photonic circuits. This research paves the way for the development of next-generation optical devices and systems with enhanced performance and functionality.

References

1. Genevet, P., et al. (2015). "Recent advances in planar optics: from plasmonic to dielectric metasurfaces." Optica, 2(5), 424-431.
2. Arbabi, A., et al. (2015). "Dielectric metasurfaces for complete control of phase and polarization with subwavelength spatial resolution and high transmission." Nature Nanotechnology, 10(11), 937-943.
3. Huang, Lujun, et al. "Enhanced light–matter interaction in two-dimensional transition metal dichalcogenides." *Reports on Progress in Physics 85.4 (2022): 046401.*
4. Zong, X., Li, L., Yu, K., & Liu, Y. (2022). Enhanced light–matter interactions in ultrathin transition-metal-dichalcogenide metasurfaces by magnetic and toroidal dipole bound states in the continuum. *Optics Express, 30(24), 43104-43117.*

NPH325 Dynamic emission tailoring using ultra-thin ENZ system

Arun Mambra, Ravi Pant and Joy Mitra*

School of Physics, IISER Thiruvananthapuram, Kerala 695551, India
**itsmearun18@iisertvm.ac.in*

Understanding the interactions between quantum emitters (QE) such as quantum dots or dye molecules, and resonant cavity has been a norm in cavity quantum electrodynamics (QED). This fundamental understanding can facilitate technologically advancements in the areas of lasing, cavity opto-mechanics, etc. While light-matter interaction is weak in general, it is significantly more interesting with the Epsilon Near Zero (ENZ) materials. In these materials the real part of dielectric permittivity goes to zero at the ENZ wavelength (λ_{ENZ}), consequently, for a low loss ENZ material the refractive index also becomes vanishingly small at λ_{ENZ}. This effect supports the excitations of non-propagative modes along with a pool of other non-intuitive properties within the ENZ media. [1] Tuning the material properties of ENZ media effectively controls the coupling between the non-radiative and radiative modes, within the media. This ability to tailor the emission spatially, spectrally, and temporally provides novel degrees of freedom in controlling emissions from embedded emitters within ENZ media and trapping fields within confined materials. The proposed geometry for emission tailoring is as shown in figure 1a, an ultra-thin layer of ENZ material on top of a thick SiO_2 slab with a point emitter encapsulated in an air bubble kept below it. The

ENZ layer is electrostatically gated to actively tune the plasma frequency, and hence the λ_{ENZ}. When the λ_{ENZ} of the thin-film matches the emission wavelength of the point emitter (1600 nm), far-field radiated power is quenched due to the non-radiative modes in the ENZ media (figure 1b). In order to actively control the coupling between non-radiative and radiative modes, the ENZ layer is electrostatically gated, which effectively tunes λ_{ENZ} and dynamically controls the quenching in far-field radiated power (figure 1c) with respect to gate voltage. Such spectral control of emission at nano-scale can develop newer understandings and facilitate technological developments for holography, sensing, and high-speed communication applications.

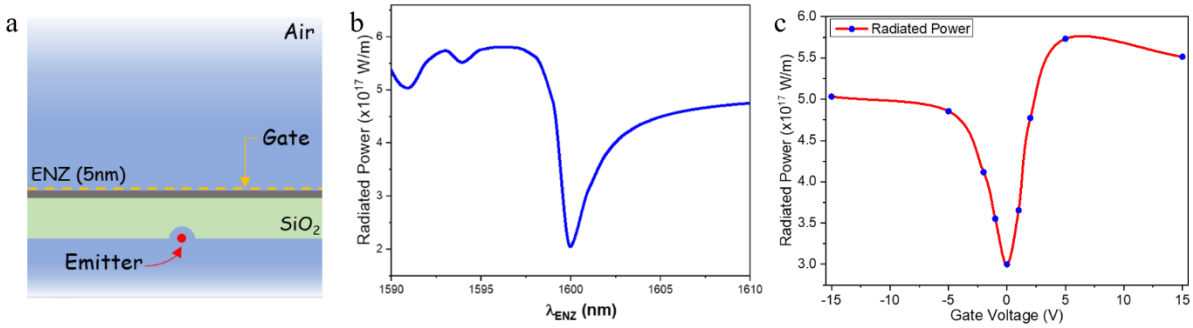

Figure 1: (a) Schematic of the Emission tailoring device with a 5 nm thick ENZ layer on top of a SiO_2 bulk with a point emitter placed beneath it. (b) Far-field radiated power versus λ_{ENZ} of the ENZ layer. (c) Dynamic tuning of radiated power using electrostatic gate applied over the ENZ layer for emission wavelength of 1600 nm.

References

1. Johns, Ben, et al. Journal of Applied Physics 127.4 (2020): 043102.

NPH326 Enhanced Detection of Rhodamine 6G Vibrational Bands through AuNPs Facilitated SERS

Ashish Omar[1], Neeraj Pant[2], Aditi Ghosh[1], Ekta[1]*

[1]Department of Materials Engineering, Indian Institute of Science, Bangalore-560012, India
[2]Instrumentation and Applied Physics, Indian Institute of Science, Bangalore-560012, India
**Corresponding author: ashishomar@iisc.ac.in*

Surface Enhanced Raman Spectroscopy (SERS) is revered for its ultra-sensitive detection capacities, often attributed to nanostructures providing 'hotspots'[1]. Our study prioritizes Rhodamine 6G, a marker molecule, and its interaction on a substrate constructed with gold nanoparticles (AuNPs) on a Silicon Nitride (SiN) base. The architecture results in nano-gaps, catalyzing an electromagnetic enhancement due to the AuNPs. Distinct vibrational bands of Rhodamine 6G within 1400-1600 cm^{-1} demonstrated notable amplification, spotlighting the molecule's unique resonance effects in the presence of AuNPs[2]. Our findings, indicating a discernable concentration-dependent enhancement at diminutive concentrations of Rhodamine 6G, underscore the potency of AuNPs in delivering ultra-sensitive detection. In parallel, traditional Raman measurements affirmed SERS' superior sensitivity. Our findings not only emphasize the efficacy of AuNPs in accentuating Rhodamine 6G's molecular signatures but also indicate potential applications in fields like pharmaceutical analytics and environmental sensing. We believe our methodology will be instrumental in advancing optical sensing innovations, optimizing detection limits, and pushing the frontier of non-destructive molecular assessments.

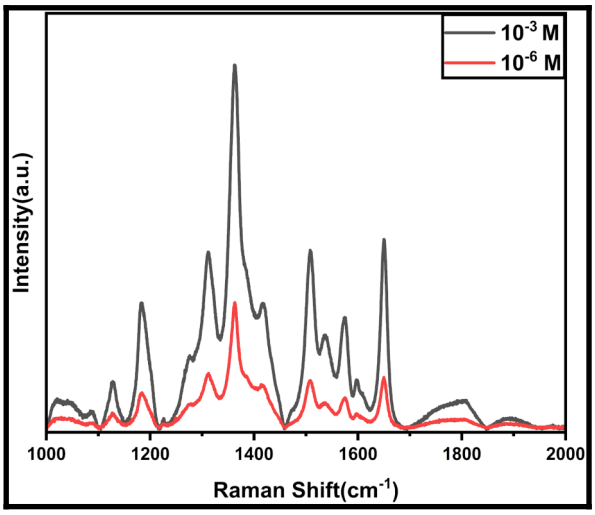

Figure 1: SERS spectra of R6G adsorbed on Au-coated SiN substrate with different concentrations: (a) 110^{-3} M (b) 1 10^{-6} M.

References

1. C. Wu et al., Colloids and Surfaces A: Physicochem. Eng. Aspects 506 (2016) 450–456
2. Masaki Ujihara et al., *Sensors 2017, 17(11), 2563*

NPH327 Optical and Optothermal forces on Colloids in Plasmofluidic Field

Chaudhary Eksha Rani[*1], *G V Pavan Kumar*[1]

[1]*Department of Physics, Indian Institute of Science Education and Research, Pune, 411008, India*
**Corresponding author: chaudhary.eksharani@students.iiserpune.ac.in*

Optical tweezers have emerged as a powerful tool to manipulate and study the physics of micro and nano sized particles ever since its first demonstration by Ashkin et al[1]. But, the inability of conventional optical tweezers to manipulate very small objects due to their diffraction limited laser spot and high laser power necessity, has led to a need to develop alternate trapping techniques like nano-optical tweezers which make use of surface plasmon resonances. Surface plasmons (SP) are resonant oscillations of the surface electrons with the incident EM field that propagate along the metal surface.

In this work, we study the trapping mechanism of plasmofluidic traps that couple plasmonic trapping with thermally-induced fluid flow[2]. Plasmonic trapping sites are generated by using optical excitation in total-internal reflection (TIR) based Kretschmann geometry to achieve large-scale nanoparticle assemblies with assistance from optothermal effects. By simulating the SP and consequent thermal fields using finite element method based COMSOL software, we study the interplay between the non-radiative effect of SP (intensity gradients) and the radiative effect of SP (temperature gradients). The temperature gradient creates a convective and slip fluid flow which drives nanoparticles afar to the heated excitation spots[3]. As the same flow tries to drive them away, the optical force due to SP holds them back at the excitation spot, forming a plasmofluidic trap. Since p-polarized light is most effective and s-polarized light is least effective in exciting SP, the intensity of surface plasmons can be controlled, thus enabling control over the consequent temperature distribution and optothermal effects. It is observed that when two SP excitation spots are in near vicinity, the SP fields can interfere to facilitate optical potential wells midway and lead to a line of temperature gradient and even temperature hotspots between the two excitations[4]. By using multiple parallel/ counter-propagating excitation beams with varying polarisations, various types of interference patterns and resultant temperature gradients can be generated which can give rise to interesting nanoparticle assemblies

under dynamic equilibrium. Through this study, we explore various parameters which enable precise manipulation of nanoparticles as well as lead to a better understanding of the plasmonic and optothermal fields at play[5].

References

1. A. Ashkin et al., *Opt. Lett. 11, 288-290 (1986)*
2. P. P. Patra et al., *Nat. Commun. 5, 4357 (2014)*
3. M. Fränzl, *Nat. Commun. 13, 656 (2022)*
4. P. P. Patra et al., *Faraday Discuss., 186, 95-106 (2016)*
5. D. Quinn et al., *Front. Nanotechnol. 5:1135408 (2023)*

NPH329 Fabrication of hole-particle pair hybrid plasmonic substrates for SERS based bio-sensing applications

*Jayakumar Pillanagrovi[1], and Dr. Shourya Dutta-Gupta[2]**

[1,2]Materials Science and Metallurgical Engineering, Indian Institute of Technology Hyderabad (IITH), Telangana, India, 502248

**Corresponding author: shourya@msme.iith.ac.in*

Plasmonic gold nanoparticles have been extensively used for diagnostic and therapeutic biomedical applications. The arrangement of the gold nanoparticles (AuNPs) on the substrates determines the sensitivity of the sensing substrates used for the diagnosis of different diseases. In this regard, hybrid substrates that are a combination of nanoparticles and nanoapertures (NPs-NAs) offer new avenues for realizing sensing platforms with improved performance. However, the fabrication of the hybrid substrate poses challenges from the processing methods, and requires expensive nanofabrication techniques. We present a simple low-cost approach for fabricating hybrid substrates using colloidal lithography (CL) in the combination of surface functionalization. CL allows fabricating substrates over large area at low-cost. Briefly, randomly spaced NAs with different sizes in 20 nm gold thin films made on functionalized substrates via CL. Subsequently, AuNPs are deposited into NAs using the electrostatic interaction between functionalized substrate and capping layer of AuNPs. Control on the number of particles is obtained by changing the NA size. It is even possible to deposit a single AuNP per aperture by a careful control of the aperture size and assembly parameters. The fabricated substrates can be integrated with microfluidic systems and offers a new avenue for real time bio-sensing of various biomolecules with an improved performance.

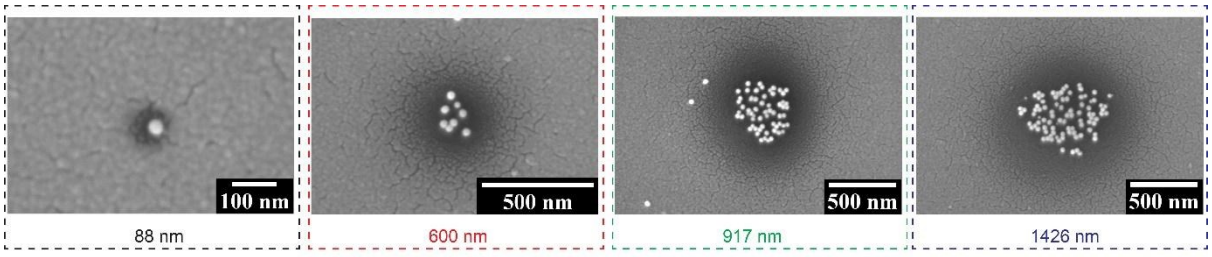

Figure 1: Hybrid plasmonic substrates. The AuNPs density controlled by tuning the NAs size by using different sizes of silica mask.

References

1. Hong Wei et. al., *Small, 4, 1296 (2008)*
2. Alexander Belushkin et. al., *ACS Nano, 12, 4453 (2018)*
3. Valentin Flauraud, et al, *Nature Nanotechnology, 12, 73 (2017)*
4. Aroonsri Ngamaroonchote et. al., *Langmuir, 37, 7392 (2021).*

NPH330 Chemically synthesized Silver nanorods for remote optical excitation of Single walled carbon nanotubes

*Lekshmi J, Vivek Kumar Shukla, Padmnabh Rai**
School of Physical Sciences, UM-DAE Centre for Excellence in Basic Sciences, University of Mumbai, Kalina, Santacruz (E), Mumbai-400098, India
Corresponding author: padmnabh.rai@cbs.ac.in

The interaction between the electromagnetic field and quantum emitters in the sub-wavelength regime has become a focal point in plasmonics. This field exhibits a broad spectrum of applications, including surface-enhanced Raman scattering (SERS), surface-enhanced fluorescence, solar cells, and optical sensing. Single-walled carbon nanotubes (SWCNTs) represent highly promising materials for exploring intense light-matter interactions. This study presents an approach to enhance Raman scattering from single-walled carbon nanotubes (SWCNT) by utilizing chemically synthesized silver nanorods (Ag-NRs). We synthesized Ag-NRs through a Polyol mediated chemical reduction method, yielding nanorods with an average diameter of 230 nm and a length of 5.70 µm. Silver nanorods with a length of 5.7 micrometers demonstrate several advantages in terms of surface plasmon propagation through the rod. Various techniques were employed to comprehensively characterize the synthesized Ag-NRs.
The surface-enhanced Raman spectroscopy (SERS) of SWCNT reveals a notable enhancement factor for characteristic Raman signals. The recorded amplification of the Raman signal using this design demonstrates a spectral count enhancement of approximately ~10^4 for the most prominent Raman mode. This approach offers a convenient and reliable method to monitoring surface-enhanced Raman scattering experiments for sensing of nanoscale volumes and the extended length plays a pivotal role in enhancing the propagation characteristics of surface plasmons, offering unique advantages for applications in remote optical excitation of quantum emitters.

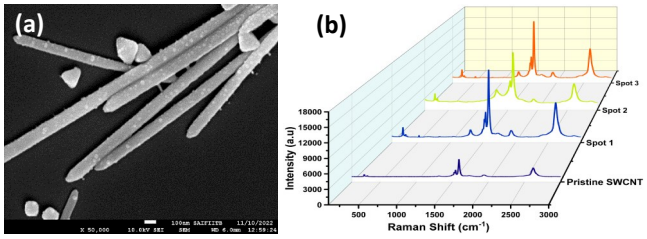

Fig. 1 (a) SEM images of the chemically synthesized Silver nanorods (Ag-NRs) **(b)** Raman spectra of single walled carbon nanotubes at different spots of the sample.

References

1. Padmnabh Rai et. al *Appl. Phys. Lett.* 111, 043104 (2017).
2. Tapas K. Das et. al *Plasmonics* 16, 1339 (2021).
3. Vimarsh Awasthi et. al *Surfaces and Interfaces* 28, 101556 (2022).

NPH331 Manipulating the spontaneous emission of quantum emitter embedded in SiC pillar lattice

Mohammed Ashahar Ahamad[1], Muhammed Anas Cu[1], Faraz. A. Inam[1]
[1]Aligarh Muslim University, Aligarh, Uttar Pradesh, India 202002
**corresponding Author: ashaharamu2020@gmail.com*

In the previous decade, the high refractive index dielectric materials have been widely implemented to enhance the emission rate of quantum emitter embedded in it. In our work, using COMSOL RF module, we have fabricated the Silicon Carbide (SiC) pillars-based lattice. These periodic array of SiC pillars is embedded with silicon-vacancy (SiV) single-color center which act as quantum emitter. The characteristic emission in SiV is around 856 nm[1]. Here, by using multipolar scattering resonances and local density of optical states (LDOS), we are manipulating the emission rate and have achieved an enhancement of more than seventeen times in the decay rate of the embedded SiV center in the SiC pillars lattice.

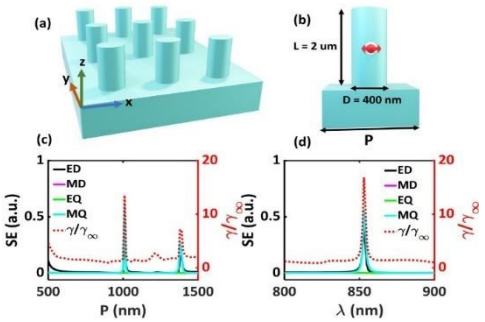

Fig 1.

In the figure 1(c), it is observed that only the electric dipole moment (ED) and magnetic quadrupole moment (MD) are well resonant with the structure for P: 1000 nm and their coherent superposition results in the maximum value of SE. Interestingly relative decay rate also peaks at P: 1000 nm which demonstrates that it is being well-tuned by the coherent superposition of Mie resonant modes induced in the SiC pillar lattice. Finally, we obtained SE and relative decay rate as a function of the wavelength of the optimized SiC lattice over the spectral ranges from 800 nm to 900 nm shown in attached fig1 (d). It is observed that both the electric dipole moment and magnetic quadrupole moment are well resonant around the 856 nm wavelength. Thus, their coherent superposition results in increasing the total electric field E at the source position and hence the local density of optical states (LDOS). This led to an enhancement of almost 17 times in the relative decay rate of the color center embedded in the SiC pillars.

References

1. Castelletto, S., & Boretti, A. (2020). Silicon carbide color centers for quantum applications. *Journal of Physics: Photonics, 2(2), 022001.*

NPH332 Creation of longitudinally polarized multiple spots by focusing phase modulated radially polarized beam with linear axicon

C.MohanaSundaram[1], K.Prabakaran[2], K.B.Rajesh[3], P.M.Anbarasan[1]*

[1]Department of Physics, Periyar University ,Salem, Tamilnadu, India
[2]Department of Physics, Mahendra Arts and Science College (Autonomous), Namakkal, Tamilnadu, India
[3]Department of Physics, Chikkanna Govt.Arts College ,Tiruppur, Tamilnadu, India
**Corresponding author: anbarasanpm@gmail.com*

We studied the tight focusing properties of an radially polarized Gaussian beam phase modulated with multi belt binary phase filter on the basis of the vector diffraction theory. We observed that focal segment with multiple focal spots structure separated with different axial distance can be generated by properly tuning the phase of the incident beam. This work is important for optical manipulation, optical data storage, micromachines and multiple optical trapping applications.

NPH333 Silicon nanoparticle-based near-infrared surface enhanced fluorescence without any "dielectric spacer"

*Pranabjyoti Patar, Prerna Joshi, and Venkata Ramanaiah Dantham**
Department of Physics, Indian Institute of Technology Patna, Bihta, Bihar, India - 801103,
**Corresponding author: dantham@iitp.ac.in*

Near-infrared (NIR) fluorescence spectroscopy is found useful for several biomedical applications such as immunotherapy, imaging, and diagnosis of cancer and various nephron-urological diseases [1]. It offers lower background compared to UV and visible fluorescence due to reduced scatter and lower auto-fluorescence of common assay substrates. However, the NIR fluorophores are not good emitters due to their lower intrinsic quantum yield than the UV and visible fluorophores. Therefore, there is a need to enhance the NIR fluorescence. A few researchers have successfully demonstrated the metal or plasmon-enhanced NIR fluorescence using suitable thin dielectric spacers between the fluorophore and metal nanoparticles [2].

High refractive index silicon (Si) nanoparticles recently attracted the researcher's attention due to their interesting optical properties [3] and many useful applications in cloaking and spectroscopy, nanoantennas, sensors, solar cells, and multi-functional metal surfaces. Unlike plasmonic nanoparticles, the Si nanoparticles support the geometrical (Mie) electric and magnetic multipolar modes upon optical illumination [4], allowing confinement of incident light's components into the sub-wavelength region. The local electric field intensity enhancement due to the excitation of multipolar modes can be used to enhance the NIR fluorescence. However, the Si nanoparticle-based NIR-SEF is not reported in the literature. Therefore, the present theoretical study emphasized on Si nanoparticle-based NIR surface-enhanced fluorescence (SEF).

Initially, the scattering spectra of single spherical-shaped Si nanoparticles of different sizes are plotted and characterized the observed modes using the multipolar decomposition. Later, the electric field intensity enhancement distribution inside and outside Si nanoparticles is plotted at the wavelengths of electric and magnetic type modes. Finally, the SEF enhancement (χ_{SEF}) is estimated by varying the excitation wavelength (λ_{ex}), fluorescence wavelength (λ_{em}), and separation (d) between the fluorophore and Si nanoparticle of different sizes. The χ_{SEF} is found to vary from 1 to 3 orders of magnitude when the λ_{em} falls in the NIR region. In contrast to the plasmonic or metal nanoparticle-based SEF, the maximum χ_{SEF} is observed when d = 0, indicating that the thin dielectric spacers between the fluorophores and Si nanoparticles are not required in Si nanoparticle-based SEF technique. This can be considered as a notable advantage over the conventional metal nanoparticle-based SEF, where dielectric spacers are mandatory. Finally, the average SEF enhancement $\langle\chi_{SEF}\rangle$ is also estimated.

References

1. Y. Ji et. al. *Adv. Drug Deliv. Rev. 167, 121-134 (2020).*
2. T. Mahata et. al., *Spectrochim. Acta A Mol. Biomol. Spectrosc. 283, 121739 (2022).*
3. C. Meier et. al. *Vol. 79, Springer, Heidelberg, pp.209 (2012).*
4. P. D. Terekhov et. al. *Phys. Rev. B, 96, 035443 (2017).*

NPH334 Whispering Gallery Mode Microring Resonator Sensor for Cancer and Diabetes Detection

Pranav George[1,2], A C Saritha[1], Ajith Ramachandran[2]*

[1]School of Pure and Applied Physics, Mahatma Gandhi University, Priyadarshini Hills, Kottayam, Kerala 686560, India
[2]Department of Physics, Christ College, Irinjalakuda, Kerala 680125, India
**Corresponding author: pranavgeorge.007@mgu.ac.in*

Whispering Gallery Mode (WGM) based sensing has emerged as a pivotal technique in contemporary optical sensing, primarily due to its rapid sensing capabilities and the exceptionally high quality factor it offers. A WGM-based optical sensor, operating at a wavelength of 1.55µm, is proposed for the detection of cancer cells in blood samples and diabetes markers in tear samples, and its performance is studied theoretically. The sensor comprises a microring with an approximate radius of around 10µm, intricately linked to a waveguide having a width of around 2µm. This miniaturized design facilitates its effortless integration into compact and portable devices. The sensitivity and quality factor of the proposed structure is studied with the help of finite element method. The proposed structure has shown a high sensitivity as well as a high quality factor of the range of 2000, indicating the possibility of utilizing it in sensing applications.

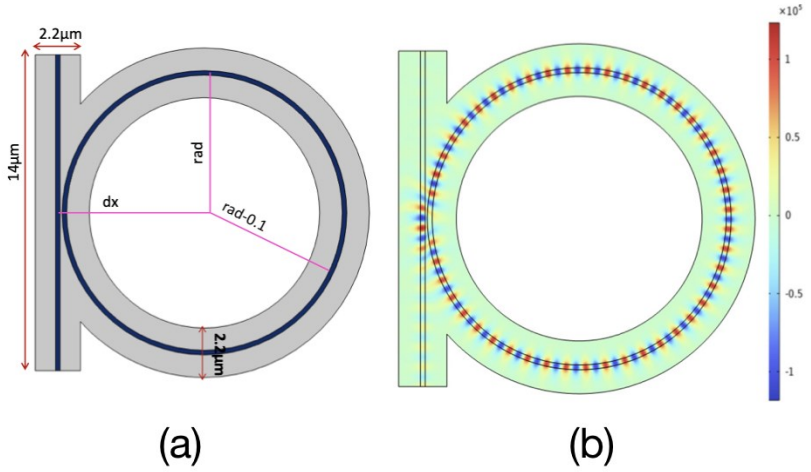

Figure 1: (a) The geometry of the WGM-based optical sensor. (b) The electric field pattern of the WGM at 1.55µm obtained with the help of finite element method.

References

1. Matsko AB et. al., *IEEE Journal of selected topics in quantum electronics 12, 3-14 (2006)*
2. Vollmer F et. al., *Nature methods 5(7), 591-6 (2008)*
3. Foreman MR et. al., *Advances in optics and photonics 7(2), 168-240 (2015)*
4. Yu D et. al., *Nature reviews methods primers 1, 83 (2021)*

NPH335 Numerical Study of Bismuth Ferrite and BP-Based Surface Plasmon Resonance Biosensor for virus SARS-CoV-2 Detection

Prateek Kumar Yadav[1], S. K. Srivastava[1,]*

[1]Department of Physics, Institute of Science, Banaras Hindu University, Varanasi, 221005, India.
[*]Corresponding author: S. K. Srivastava
Corresponding author's email: sanjay_itbhu@yahoo.com

The serious respiratory syndrome caused by coronavirus-2 (SARS-CoV-2) has been identified as a worldwide health issue in the coronavirus disease (COVID-19) pandemic. Therefore, this paper presents a numerical investigation of the Kretschmann configuration-based surface plasmon resonance (SPR) biosensor, a label-free, highly sensitive, low-cost device for detecting SARS-CoV-2. In the present paper, we propose an SPR-based biosensor for rapid detection of the SARS-CoV-2 virus using black phosphorous (BP) and bismuth ferrite ($BiFeO_3$). As a ligand layer, thiol-tethered ssDNA has been used. We investigated the characteristics of the various structures of the materials mentioned above in the proposed biosensor by depositing silver (Ag), $BiFeO_3$, and BP atop the BK-7 prism. Herein, three distinct structures (Structure I, II, and III) are presented and contrasted in order to identify SARS-CoV-2. In addition, the transfer matrix method

(TMM) has been used for all three structures. Compared to other structures for detecting SARS-CoV-2, structure III (BK-7 Prism-Ag-$BiFeO_3$-BP-ssDNA) exhibits high sensitivity (356.19°/RIU), detection accuracy (2.57), quality factor (122.40 RIU^{-1}), and limit of detection (1.40×10^{-5}). This work may lead to the developing of a significant biological sample-sensing device for the rapid and precise early detection of the SARS-CoV-2 virus.

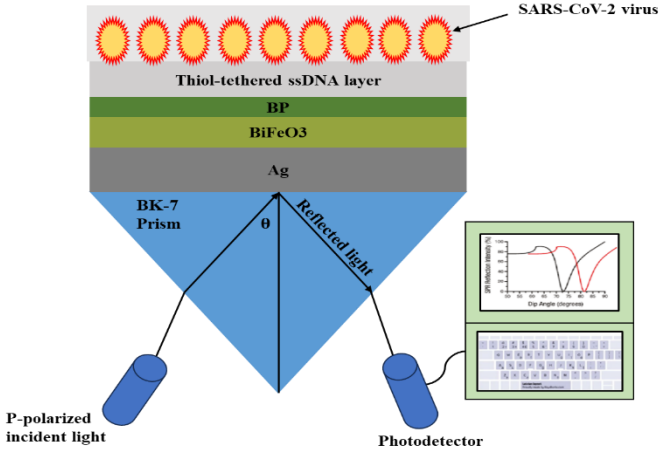

Fig. 1 Proposed configuration BK-7 prism-Ag-$BiFeO_3$-BP-ssDNA and PBS solution as sensing medium having optimized thickness

NPH336 Tailoring thermo-optical properties of curcumin dye with gold-silver bimetallic nanoparticles

Priya Mary, A Mujeeb

International School of Photonics, Cochin University of Science and Technology, Cochin, Kerala

*Email*johnpriyamary@gmail.com*

A laser-mediated approach was employed to synthesize gold-silver bimetallic nanoparticles aimed at tuning their localized surface plasmon resonance.The impact of these nanoparticles on the thermo-optical characteristics of curcumin dye was examined. The thermal diffusivity of curcumin was assessed in the presence of gold-silver bimetallic nanoparticles using the dual beam mode mismatched thermal lens method. Dual-beam thermal lens spectrometry was employed due to its high sensitivity. The thermal diffusivity measures the thermal transport between the particles. The structural and optical characterization of the bimetallic nanoparticles were carried out using the X-Ray Diffraction (XRD), Energy Dispersive X-Ray Spectroscopy (EDAX), UV–visible absorption spectroscopic technique and photoluminescence spectroscopic technique. The thermal diffusivity and fluorescence emission intensity of the samples were observed to decrease as the concentration of nanoparticles added to the dye solution is increased.

NPH339 Study of Embedded Metal Nano-disc Arrays and rings as Plasmonic back Reflector for High Performance Thin Film Amorphous Silicon Solar Cell

Sanket Kumar[1], Raj Kumar[2], Praveen C Pandey[1]*

[1] Department of Physics, Indian Institute of Technology (BHU), Varanasi, U.P 221005, India

[2] Department of Applied Sciences and Humanities, Indian Invertis University, Bareilly, U.P 243123, India

[*]Corresponding author, Email: - pcpandey.app@iitbhu.ac.in, Tel: - (+91)5427165473

In this work, a new arrangement of nanodisc arrays and rings is used to enhance the efficiency of thin-film a-Si solar cell with a thickness of 110 nm. The designed metal nano disc arrays plasmonic back reflector can improve the photocurrent and hence the efficiency. At first, a double layer SiO2/Si3N4 as the antireflection (AR) was analyzed. The study was carried out by a 3D finite difference time domain method and the optimized parameters were calculated to obtain higher efficiencies. We Analysed the results over a wide range of wavelengths(300-1200nm) using plane wave Source. We have also compared the results with different metal nano disc arrays with increasing height and metal nanorings. We found that Tungsten metal nanostructure gives good results in both types of structures (16.24 mA/cm^{2}For dual metal nanorings and 18.36 mA/cm^2 for metal nano disc arrays with 20nm thickness). As we increase the thickness of the nanostructure we found the optimized value of short circuit current density i.e. equal to 41.15 mA/cm^2 for dual nano rings and 44.17 mA/cm^2 for nano disc arrays for tungsten. We also observed the average absorbance in the Visible and near IR range(400-1000nm) is greater than 95% and plotted it. Finally, a relatively higher photocurrent and conversion efficiency of 44.17mA/cm2 and 35.12% were achieved for the optimized structure with nano disc arrays back reflector respectively.

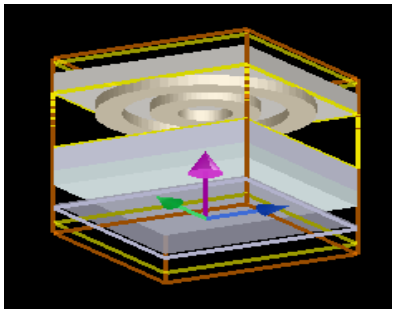

Fig.(1); It reprensts modelled structure of dual metal nano-rings without Silicon.

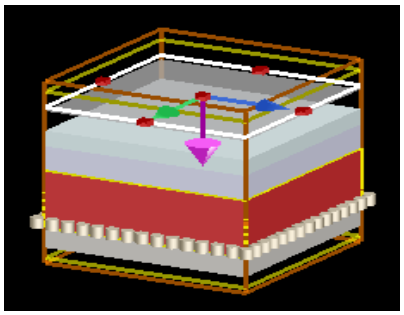

Fig.(2)It represents modelled structure of metal(W) nano-disc array with Silicon.

NPH340 Convergence angle affecting tightly focused aberrated beam

Sarita[1], Ankita Chowdhury[1], Rajan Jha[2], Rakesh K. Singh[1]*

[1]Laboratory of Information Photonics & Optical Metrology, Department of Physics, Indian Institute of Technology (Banaras Hindu University), Varanasi, 221005, India

[2]Nanophotonics and Plasmonics Laboratory, School of Basic Sciences, Indian Institute of Technology Bhubaneswar, Bhubaneswar, 751013, India

**Corresponding author: Sarita.rs.phy19@itbhu.ac.in*

An enhancement in near-field intensity is observed when a tightly focused beam having high convergence angle is scattered through a nanoparticle (NP). The average intensity enhancement is explained using Richard and Wolf's formalism followed by Mie theory and multipole expansion approach [1]. Variation in convergence angle affects the enhancement in near-field. The presence of spherical aberration is possible in a tightly focusing system, and this will influence the contribution of multipole order n . This paper presents results on effect of spherical aberration on near field intensity enhancement by varying convergence angle. Using Zernike polynomial, the expansion coefficient influenced by the aberration is expressed as,

$$A_n = (-i)^n E_0 kf \frac{2n+1}{2n^2(n+1)^2} \int_0^{\alpha} e^{ikW(\rho)} \sqrt{cos\theta} \left[\frac{P_n^1(cos\theta)}{sin\theta} + \frac{dP_n^1(cos\theta)}{d\theta} \right] sin\theta d\theta \quad . \qquad (1)$$

E_0 is the amplitude, k is the wave number, and f is the focal length of the lens. θ is the convergence angle, where $\theta_{max} = \alpha$. $W(\rho) = A_s\rho^4$ is the wave aberration, where A_s is the spherical aberration coefficient, and

$\rho = \sin\theta/\sin\alpha$ [2]. $P_n^1(\cos\theta)$ is associated Legendre polynomial. A silver NP of 50nm radius kept in a dielectric media glass is considered to excite from a spherically aberrated tightly focused linearly polarized beam. For A_s=1.0 , the average radial and tangential intensity enhancements are analyzed for a wide range of wavelength of incident beam. The effect on enhancement factor with change in convergence angle α is observed in Fig. 1.

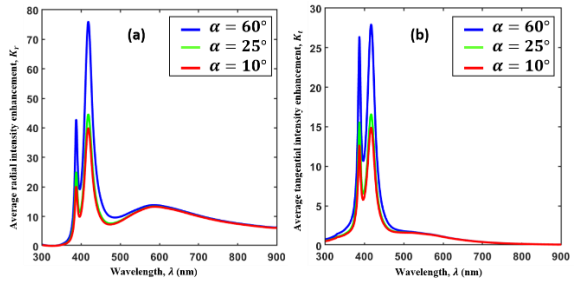

Fig. 1: Average (a) radial, and (b) tangential intensity enhancement observed for different convergence angle

Result shows that for the low convergence angle i.e. $\alpha = 10^0$, the enhancement factor is less, and the it increases with increase in convergence angle i.e. $\alpha = 25^0$, 60^0.

References

1. Mojarad et. al., *J. Opt. Soc. Am. B* 25, 651-658 (2008).
2. Malacara, Daniel, Optical shop testing. Vol. 59. *John Wiley & Sons* (2007).

NPH341 Surface Plasmon Resonance-Based Sensor for Detecting Impurity in Drinking Water

Mohd Uwais [1], Shakti Pada Mahato[1], Vipul Rastogi[1,2]*
[1]Department of Physics, Indian Institute of Technology Roorkee, INDIA 247667
[2]Center for Photonics and Quantum Communication Technology, Indian Institute of Technology Roorkee, Uttarakhand, INDIA 247667
**Corresponding author: muwais@ph.iitr.ac.in*

We present an SPR-based refractive index sensor for fluoride impurity in drinking water. The structure of the proposed sensor consists of a bimetallic layer of Al-Au between the glass prism and silicon layer, with the black phosphorous (BP) layer on top. The proposed sensor offers a maximum sensitivity of 358 deg./ RIU for fluoride detection in water.

Surface plasmon resonance (SPR) that occurs at the metal-dielectric interface due to the coupling of the incident TM polarised light with the charge oscillations on the metal surface is one of the most useful techniques in sensing [1]. The coupling leads to the SPR dip in the reflection curve. The refractive index variation near the metal-dielectric interface is easily probed by monitoring the position of the SPR dip. Structures consisting of a bimetallic layer, a dielectric layer, and 2D materials can result in high sensitivity of the SPR-based sensors [2]. There are several applications of SPR sensors, such as chemical sensing, gas sensing, and medical diagnostics. We propose an SPR sensor structure with Al-Au bimetallic layer, Si layer and

BP monolayer for impurity detection in drinking water.

Fig. 1(a) shows the schematic of the proposed sensor having the 30 nm Al layer, 10 nm Au layer, 5 nm silicon layer, and the monolayer of BP at the top. The refractive index of the water having fluoride impurity changes with fluoride concentration [3]. The numerical simulations on the proposed structure have been carried out by the transfer matrix method (TMM) at 633 nm wavelength [4]. Fig. 1(b) shows the SPR resonance curve for different fluoride concentrations and Fig. 1(c) shows the corresponding shift in the resonance angle. The sensitivity of the sensor is calculated from the slope of the resonance angle and refractive index plot. The proposed sensor shows a maximum sensitivity of 358 deg./RIU.

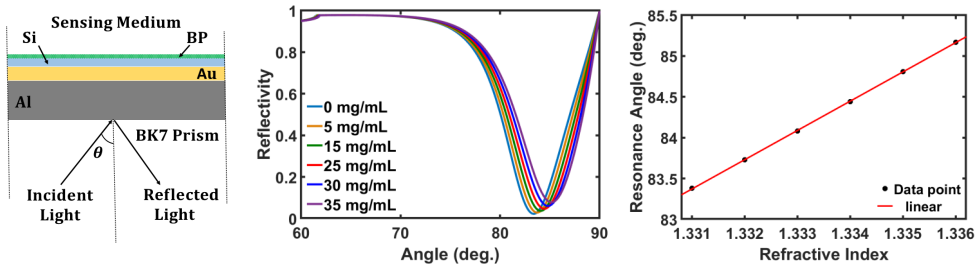

Fig. 1. (a) Schematic diagram of the proposed SPR-based sensor, (b) SPR response at different concentrations of fluoride, and (c) The variation of resonance angle with the refractive index of the fluoride-water solution.

References

1. S. A. Maier, Springer New York (2007).
2. M. Uwais et. al., *Phys. Scr., 98*(10), 105515 (2023).
3. Vikas et. al., J. *Opt.,* 51, 707-12 (2022).
4. B.D. Gupta et.al., *Sens. Actuators B: Chem.*, 107, 40–6 (2005).

NPH342 Dark-field microscopy studies of single silicon nanoparticles fabricated by electron beam evaporation technique

*S. Sahoo, A. M. Naik, R. Laha, and V. R. Dantham**
Department of Physics, Indian Institute of Technology Patna, Bihar – 801106, India
**Corresponding author: dantham@iitp.ac.in*

Abstract: Silicon nanoparticles (SiNPs) have attracted substantial attention and interest in the field of nanophotonics due to their exceptional optical properties and versatile array of applications. The SiNPs are commonly observed in the nanocluster films. These films can be deposited using plasma enhanced-chemical vapor deposition (PECVD) [1], Hot wire CVD, Microwave CVD, magnetron sputtering, laser ablation, and various physical vapor deposition (PVD) techniques. To optimize the performance of the SiNPs based photovoltaic devices [2] and nanosensors [3], one should know the optical properties of the SiNPs and these properties depend upon the various experimental conditions.

Therefore, herein, for the first time, we report the effect of thermal annealing, deposition parameters and polarization of light on the far-field optical properties of single silicon nanoparticles (SiNPs) studied using

a transmission-mode dark-field microscope. Initially, the SiNPs are fabricated using the electron beam evaporation technique using different deposition parameters and their morphology is studied using Atomic Force Microscope. Later, the scattering images and spectra of single SiNPs before and after thermal annealing process, are recorded using the dark field microscope. Finally, the polarization-dependent scattering images and spectra of single SiNPs are also recorded.

References

1. B. Rech et. al., *Sol. Energy Mater. Sol. Cells 66, 267-273 (2021).*
2. M. Sharma et. al., *Nanoscale Adv. 3, 3373-3383 (2021).*
3. C. M. Gonzalez et. al., *J. Mater. Chem. C 4, 4836- 4846 (2016).*

NPH343 Hot Electron Generation in Nano-spiked Plasmonic Cavity Array for sensing application

*Siddhartha Banerjee[1] *, Jolly Xavier[1] **

[1] SeNSE, Indian Institute of Technology Delhi, Hauz Khas, New Delhi - 110016

** Corresponding author: idz228535@iitd.ac.in , jxavier@sense.iitd.ac.in*

The generation of the localized surface plasmon resonance (LSPR) on the surface of plasmonic nanostructures has paved the way for advanced biosensing, surpassing the conventional detection limits. The electric field enhancement (electromagnetic hot spots) between two plasmonic nano structures at close quarters produces hot electrons with a change in the electron density of the material [1]. Techniques such as photo-injection are suitable to inject hot electrons from the metal crossing the Schottky barrier to the semiconductor leading to the development of photocurrent [2]. "Sea-Urchin" looking spiked nanoparticles serve a great interest in research of plasmonic materials as they can generate hot electrons at higher rate compared to other structures [3].

Here, by means of FEM analysis (Fig. 1), we investigate the electric field enhancement generated between the cavity of nano-star spike pairs and extend the study to an array of them. We further do a parametric study and identify the importance of using such an array to generate hot electrons whose applications are envisaged for light harvesting, enhanced photodetection, photo catalysis etc.

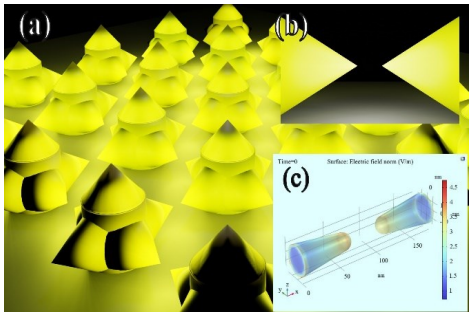

Figure 1: (a) Schematic of the periodic array of spiked nanoparticles (b)The tips at a chosen distance showing enhancement (c) Analysis of field enhancement in the nanospiked hotspot regions by varying the structural and morphological features.

References

1. Besteiro et. al.,The Journal of Physical Chemistry C 120.34 (2016): 19329-19339.
2. Govorov et. al., The Journal of Physical Chemistry C 117.32 (2013): 16616-16631.

3. Chang, Le, et al. ACS Energy Letters 4.10 (2019): 2552-2568.

NPH344 Investigation of two cascaded fibre optic surface plasmon resonance sensor

Sushil Kumar
Assistant Professor, Department of Physics, Sri Sankar College, Sasaram
(Constituent Unit of Veer Kunwar Singh University Ara) Bihar-821115
Corresponding author: skumarmaurya85@gmail.com

In modern age, the growth of sensors based on Surface Plasmon Resonance (SPR) has been established as a powerful sensing technology. The enhancement of sensor performance is an important issue for the development of SPR sensor. To measure simultaneously two kinds of chemical substance by using wavelength division multiplexing technology, we report a theoretical investigation for two cascaded surface plasmon resonance fiber optic sensors. Using the transfer matrix method, the transmitted spectrum of two cascaded SPR fiber optic sensor have been discussed and the calculation show that cascaded SPR fiber optic sensor should adopt different kinds and produce two resonance wavelengths with a greater difference.

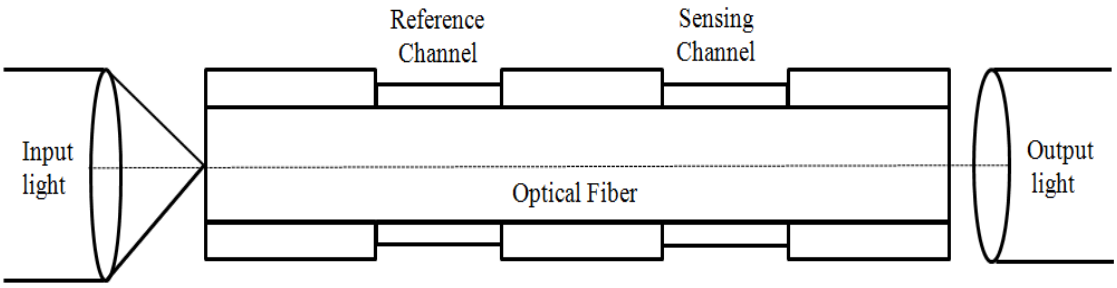

Fig: Schematic diagram of a dual channel waveguide coupled SPR sensor

NPH345 Optimization and Fabrication of Plasmonic Nanostructures using Electron Beam Lithography

*Yadav Rohit Umashankar, Parinda vasa**
Department of Physics, Indian Institute of Technology Bombay, 400076 Mumbai, India
*Email: parinda@iitb.ac.in**

Plasmonics mainly deals with the interaction of optical electromagnetic fields with metallic nanostructures [1]. It forms the basis of the research area of nanophotonics. The metallic nanostructures are of subwavelength dimensions and are capable of confining and significantly enhancing the electromagnetic fields in nano-meter-sized regions. These metallic resonances are generally of two types, one of which is of a propagating nature known as surface plasmons and the other is of the localized form called localized plasmons. The resonances observed in these metallic nanoantennas can be exploited for diverse photonic applications such as metamaterial engineering, single molecule detection, surface-enhanced Raman Scattering, surface-enhanced fluorescence, non-linear optics, and optical manipulation [2]. The difficulty lies in the fabrication of such nanometre-sized metallic nanoantennas. Several maskless lithography methods exist, such as direct laser writing, interference lithography, focussed ion beam lithography, electron beam lithography (EBL), etc. Among these, electron beam lithography is a very standard technique and belongs to the top-down nanofabrication method. This technique has been widely implemented for nanopatterning because the sys-

tem gives unique advantages of high resolution in feature size, high reliability in processing, and high flexibility in pattern replication. The resolution capability as good as 10nm by EBL has been reported [3]. However, the challenging part of the fabrication through EBL lies in the optimization of different parameters in consecutive processing steps. Here, we demonstrate the optimized steps and compare different metal deposition methods involved in the fabrication process. We also showcase different plasmonic nanostructures that have been fabricated and obtained with resolutions up to 60nm. Enhancing control over parameters at various stages enables the improvement of nanostructure features in terms of size, shape, and resolution.

References

1. Murray, W. A. & Barnes, W. L. Plasmonic materials. *Adv. Mater. 19, 3771–3782 (2007).*
2. Schuller, J. A. *et al. Plasmonics for extreme light concentration and manipulation. Nat. Mater. 9, 193–204 (2010).*
3. Vieu, C. *et al. Electron beam lithography: Resolution limits and applications. Appl. Surf. Sci. 164, 111–117 (2000).*

NPH346 Anisotropic nanostructures: a systematic exploration for SERS enhancement

Sathi Das[1], Jean-Claude Tinguely[2], Kanchan Saxena[3], Balpreet Singh Ahluwalia[2], Dalip Singh Metha[1]*

[1]Bio-photonics and Green Photonics Laboratory, Indian Institute of Technology Delhi, Hauz-Khas, New Delhi-110016, India.
[2]Department of Physics and Technology, UiT The Arctic University of Norway, Tromsø, 9037, Norway.
[3]Amity Institute of Renewable and Alternative Energy, Amity University Uttar Pradesh, Sector 125 Noida, U.P., India
**Corresponding author: dassat123@gmail.com*

Surface enhanced Raman spectroscopy (SERS) is a popular technique for real-time label-free detection of chemical and biochemical fields [1], [2]. An advanced SERS substrate includes 3D distribution of nanostructures, tuneable plasmonic enhancement, closely placed nanostructures for excitation of coupled plasmonic modes. The sensitivity of the substrate is dependent of nanostructure morphology, whereas the uniformity is dependent on the regular geometry of the nanostructure. Current literatures describe that the shape anisotropic nanostructures cause enhanced hotspots at sharp edges due to charge accumulation. Literatures with star shaped Ag and Au nanoparticles, shape anisotropic dendrites are demonstrated to create larger enhancement than the spherical shaped colloidal Ag NPs. However, the shape anisotropic NPs are prone to be unstable, show random agglomeration causing irreproducible and random orientation of hotspots. Thus, solid substrates are preferred for long durable and state SERS substrate. We created template of PS beads on Si wafer, further utilised the PS template to induce anisotropy into the beads itself. The beads were heated with O_2 plasma to create etching and shrinking for various times. We investigated the effect of shape anisotropy on SERS enhancement upon development of a highly anisotropic nanosized template for SERS substrate.

References

1. B. Sharma, R. R. Frontiera, A. I. Henry, E. Ringe, and R. P. Van Duyne, “SERS: Materials, applications, and the future,” *Materials Today, vol. 15, no. 1–2. 2012. doi: 10.1016/S1369-7021(12)70017-2.*

2. S. Das, K. Saxena, L. P. Goswami, J. Gayathri, and D. S. Mehta, "Mesoporous Ag–TiO2 based nanocage like structure as sensitive and recyclable low-cost SERS substrate for biosensing applications," *Opt Mater (Amst), vol. 125, 2022, doi: 10.1016/j.optmat.2022.111994.*

Category 12

Optical Data Storage & Display Devices (DSD)

DSD110 Optical Waveguide based Next Generation Head Up Display (HUD) for Avionics

Bhargab Das, Sudipta Sarkar Pal, Raj Kumar, Sanjit Debnath, and S. Anantha Ramakrishna*

CSIR-Central Scientific Instruments Organisation, Chandigarh 160030, India

**Corresponding author: bhargab.das@csio.res.in*

Head Up Display (HUD) is a critical cockpit display system for tactical aircraft as well as for commercial air transports which significantly enhances the aircraft pilot's situational awareness. HUD provides flight related crucial information to the pilot overlaid onto the real-world scene, so that the pilot can process both the information simultaneously without the need to look down and refocus onto the instrument panel. Conventional HUD systems are very bulky mainly due to the large clear aperture of the collimation/projection optics. The requirement of larger field of view (FOV) demands the usage of large aperture refractive lenses. Furthermore, the stringent requirement of parallax and binocular disparity requires an aberration controlled optical system which increases the number of optical elements in the collimation optics. In conjunction with the mechanical housing, the overall weight of the conventional HUD module is also significant. Recent advances in diffractive optical components (DOE) and holographic optical elements (HOE) have given birth to the next generation HUD systems. Optical waveguide concept coupled with DOE/HOE offers the prospects of realizing a HUD configuration with a smaller form factor compared to conventional HUD system. The use of planar structures significantly decreases the mechanical complexity simultaneously reducing the mass and volume. Taking advantage of the extensive knowledge and experience gained while developing the conventional HUD systems, CSIR-CSIO has taken the initiative towards the development of low-profile head up display for next generation indigenous fighter aircrafts.

Here, we present a planar optical waveguide-based head up display configuration mainly consisting of a collimation optical system and a set of surface relief gratings (SRG) as diffractive optical elements. The waveguide configuration consists of three linear SRGs of different sizes and geometry. All the three SRGs are on the same thick and transparent waveguide glass slab of suitable refractive index. Collimated light from the micro-display source is coupled inside the waveguide slab with the help of the input grating (IG), wherein the diffraction angle within the glass slab is higher than the critical angle for total internal reflection (TIR). The diffracted light from IG travels towards turn grating (TG) which expands the light in one direction as well as redirects the light distribution towards the third grating called the extraction grating (EG), wherein EG decouples the light from the waveguide slab. The dimensions of TG and EG depend on the desired pupil expansion in both the orthogonal directions in order to meet the targeted instantaneous field of view (*IFOV*) and total field of view (*TFOV*) requirements. The full-length article will include the various optical design aspects of waveguide-based HUD configuration.

Category 13

Optical Interferometry and Holography (HOL)

HOL118 Simultaneous Fabrication of Surface and Volume Grating Patterns via Denisyuk Holography

*Biplab Dhara[1], Sutirtha Banerjee[1], Susovan Giri[1], Sarbojit Mukherjee[2], Shivakiran Bhaktha B.N.[1]**
[1]Department of Physics, Indian Institute of Technology Kharagpur, Kharagpur 721302, India
[2]ATDC, Indian Institute of Technology Kharagpur, Kharagpur 721302, India
**kiranbhaktha@phy.iitkgp.ac.in*

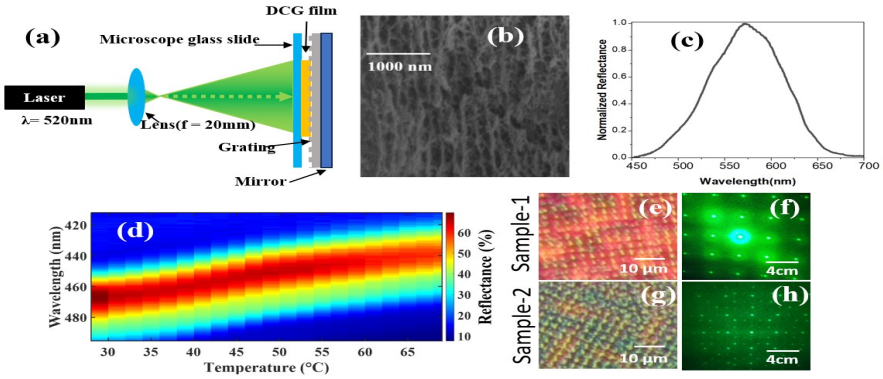

Figure 1: (a) Experimental set-up used for fabrication, (b) cross-sectional SEM image, (c) reflection spectrum, (d) temperature tunable reflection spectra of the DCG sample. (e) & (g) 20× microscope images, (f) & (h) laser diffraction patterns, for samples 1 & 2, respectively.

Optical gratings fabricated by a variety of methods, such as, ruling, holography, and interference lithography, play a fundamental role in various fields including spectroscopy, laser optics, and optical filters [1]. In this study, we present an approach to efficiently fabricate volume and surface gratings using a holographic technique[2]. This advancement holds the promise of driving progress in the development of diffraction gratings, tunable optical filters and cost-effective spectrometers [3]. The 2D gratings were fabricated by coating glass slides with a photosensitive dichromated gelatin (DCG) solution and exposing them within a Denisyuk-style setup utilizing a 2D grating as the object, as seen in Figure 1(a). Sample 1 received a 5-minute exposure, while sample 2 was initially exposed for 2.5 minutes and subsequently exposed for an additional 2.5 minutes after rotating it by 45º about the optical axis of the set-up. The cross-sectional scanning electron microscope image of one of the sample as seen in Fig. 1(b) shows the existence of Bragg structure across the volume of the sample. Figure 1(c) depicts the room temperature reflection spectrum of the sample, and Fig. 1(d) shows the same for the sample heated from 29 °C to 69 °C confirming the tunability of the reflection spectra. The developed surface holographic grating structures were also imaged using a 20× optical microscope as seen in Figs. 1(e) and 1(g) for samples 1 and 2, respectively. The size of the grating elements for samples 1 and 2 were measured to be 4.2 µm and 3.8 µm, respectively. These structures exhibited distinctive diffraction patterns under laser light illumination as shown in Figs. 1(f) and 1(h), respectively. The developed technique of multiple exposure to fabricate multiple grating structures in both volume and surface has wide application in combining multiple diffractive optical elements into one, increasing its compactness, portability and decreasing the cost of the optical elements [4]. The temperature-tunability enhances its capability in optical filter category. Further details will be presented in the conference, shedding light on the scope and potential of this approach.

References

1. Manfred Eich et al., J. Opt. Soc. Am. B 7, 1428-1436 (1990).
2. Rajib Ahmed et al., Nanoscale, 2017, 9, 266.
3. Min Huang et al., *Appl. Opt. 59, 8976-8986 (2020).*
4. Santonocito A et al., *Nanomaterials. 2023; 13(10):1633.*

HOL119 Enhancement of Fringe Density in Fresnel Biprism Based Digital Holography Microscopy

Deepak K. Jaduvanshi, Biswajit Pathak, C.S. Narayanamurthy*

Applied and Adaptive Optics Laboratory, Indian Institute of Space Science and Technology, Thiruvananthapuram, Kerala, 695547, India

**Corresponding author: deepak.21@res.iist.ac.in*

In this work, we enhance the interference fringe density in a Fresnel biprism based digital holography microscopy (FB-DHM) by generating two controllable +1 order beams using a multiplexed blazed grating, implemented with a liquid crystal spatial light modulator (SLM). Unlike the conventional FB-DHM design where the fringe density is fixed, here the angular separation between both the beams could be precisely controlled to adjust the fringe density in order to perform accurate and reliable single shot phase reconstruction by exploiting the programmable facility of the SLM.

Experimental Setup and Result: The schematic diagram of the experimental arrangement to enhance the interference fringe density, in a Fresnel biprism based DHM [1, 2] is shown in Fig. 1(a). Two beams were created using multiplexed blazed grating and the angular separation between both the beams was controlled programmably (the zoomed version near the FB region illustrates the variation in the angle) in order to adjust the fringe density such that a reliable and accurate phase reconstruction could be performed in a single shot, in the presence of fixed prism angle. Two different interference patterns, having different fringe density is shown in Fig. 1(b) along with the multiplexed blazed grating written onto the SLM.

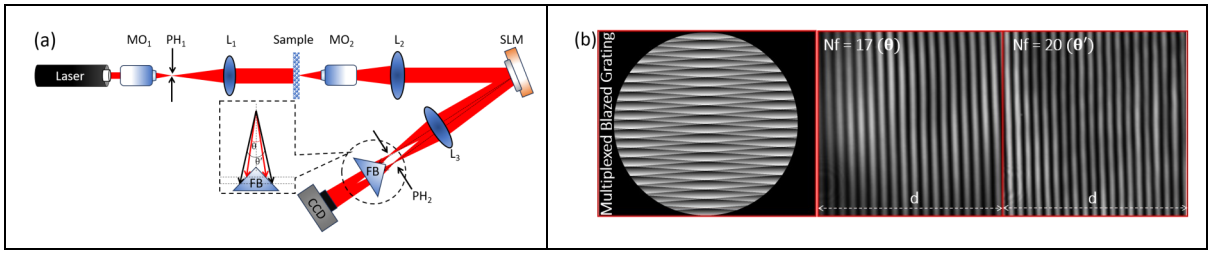

Figure 1(a) Shows schematic diagram of the Fresnel biprism based DHM with controllable beam separation to adjust fringe density, whereas Fig. 1(b) shows the experimentally obtained interference fringe pattern having different fringe density along with the multiplexed blazed grating written onto the SLM. MO: microscope objective; L: lenses; PH: pinhole; SLM: spatial light modulator; FB: Fresnel biprism; CCD: Charge coupled device.

References

1. Ebrahimi, Samira, et al., Appl. Phys. Lett. 112, 113701 (2018).
2. Doblas, Ana, et al., J. Opt. Soc. Am. 30, 140-148 (2013).

HOL120 Phase Modulation in Spatial Coherence by Modulating Intensity of Incoherent Source

Haneen V N, Dinesh N Naik*
Applied and Adaptive Optics Laboratory, Department of Physics, Indian Institute of Space Science and Technology, Thiruvananthapuram, Kerala, 695547.

**Corresponding author: haneenvn.22@res.iist.ac.in*

The van Cittert-Zernike theorem relates intensity distribution of an incoherent source with the spatial coherence of its propagated far-field. This concept has been used in techniques such as coherence holography, and studies have shown that spatial modulation of source intensity can synthesize/revive spatial coherence at specific shear values of the field [1]. Some earlier investigations have addressed the phase shifts occurring in the field when a grating is subjected to motion [2].

In this work, we examine phase modulation of the far-field spatial coherence using the dynamics of the intensity-modulated source. When a square wave amplitude grating of unequal duty cycle (PHYWE, 4 lines per mm) is illuminated with a quasi-monochromatic incoherent light, spatial coherence is revived at periodic intervals of shear values. A common path Sagnac radial shearing interferometer is used to visualize this spatial coherence as given in Figure 1(a).

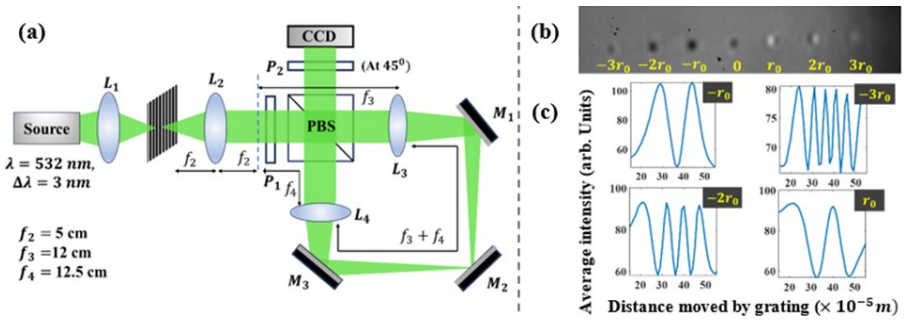

Figure 1:(a) Schematic of experimental setup (b) Recorded interferogram (c) Plot of average intensity variation in the interferogram with the movement of grating.

Figure 1(b) is one of the recorded interferograms that showing spatial coherence peaks at different shear values corresponding to the points r_0, $2r_0$, etc. The lateral motion of the grating with a step size of 0.01 mm induces a sinusoidal modulation in the intensity of those peaks, as in Figure 1(c). When the peak at the point $-r_0$ undergoes one sine cycle, the point r_0 undergoes a similar but out-of-phase variation, revealing conjugation in the accumulated phase. Similarly, the peak at $-2r_0$ exhibits a modulation that is twice that observed at $-r_0$, while the intensity at $r=0$ remains unchanged. This source-modulated phase shift technique has potential applications in optical interferometry schemes that employ incoherent light.

References

1. Naik, Dinesh N., et al, *Opt. Express,* 19658-69 (2012).
2. S. Wise et al., *Phys. Rev. Lett.* 95, 013901 (2005).

HOL121 Testing of freeform optics using Computer Generated Hologram

Mahendra Pratap Singh[1], Amit Agrawal[1], Kamal Kishor Pant[1], Lalit Mohan Pant[1]*

[1]Instruments Research and Development Establishment, Dehradun-248008
**Corresponding Author: mpsy79@gmail.com*

The efficiency of various optical systems can be enhanced by freeform optics. However, it is difficult to measure freeform optics due to lack of symmetry, complex shape and higher slopes. Most versatile technique to test freeform surface is based on computer generated hologram (CGH) because of its capability to test a large variety of surfaces [1]. We have designed a CGH for testing of freeform cubic surface required for wavefront coding LWIR Camera. The CGH is designed by computing the optical path difference (OPD) of rays originating normal to freeform surface to the CGH plane and is added to the OPD of the rays traced from reference surface to CGH. The desired order (+1 order) is separated from zero order as well as the next higher order by introducing tilt of 2 minutes. The resulting phase is re-sampled at CGH plane and encoded in the CGH. Minimum feature size on the CGH is 12 micron.

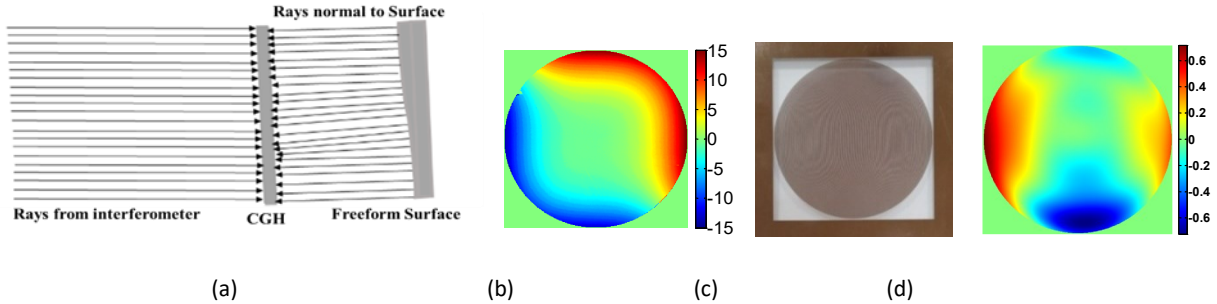

Figure 1(a) Test layout (b) Designed Cubic surface (c) Fabricated CGH (d) Measured error on surface

Diameter of the surface to be tested is 75 mm and surface form is given by:

$$Z=\alpha(x^3+y^3)\ ; \qquad |x|, |y|\leq 1$$

Where α is the strength of cubic phase. CGH was fabricated using maskless UV-photolithography technique and dry etching in form of an amplitude hologram. The transmitted wavefront error of substrate is less than 0.1 wave. The feature size and pattern height are measured by scanning white light interferometry. Freeform and CGH are put in the Fizeau interferometer (λ=0.6328μm)as shown in figure 1(a). Alignment of the CGH was done using fiducials on CGH and the test optics. Measured error on freeform surface is found to be 1.2 μm (figure 1(d)). We have designed and fabricated CGH and successfully tested a cubic freeform surface by minimising alignment errors during test.

References

1. Wyant J. C. et. al, "Using computer generated holograms to test aspheric wavefronts ", Appl . Opt . 11 (12) 2833 – 2839 (1972)

HOL122 Quantitative polarization microscopy for live cell imaging

Shivam Kumar Chaubey[1], Mohit Rathor[1], Rupen Tamang[2], Biplob Koch[2], Rakesh Kumar Singh[1]*
[1]Laboratory of Information Photonics and Optical Metrology, Department of Physics, Indian Institute of Technology (Banaras Hindu University), Varanasi 221005, India
[2]Department of Zoology, Banaras Hindu University, Varanasi 221005, India

**Corresponding author: shivamchaubey561@gmail.com*

Polarization measurement is desired in biology for different reasons [1]. Here, we demonstrate a label-free, non-invasive polarization digital holographic microscope (PDHM) for single-shot polarization imaging of cellular structures. The proposed technique is flexible to adjust carrier frequencies to meet the varying demands of different anisotropic samples [2]. The performance of the proposed technique is demonstrated by measuring the complex field of the live cancerous cell (U-87 MG). At the observation plane, a spatial frequency multiplexed interference pattern is produced by the interference between object and reference fields, which is represented as,

$$I(x,y) = I_0(x,y) + [c_x(x,y) + c_x^*(x,y)] + [c_y(x,y) + c_y^*(x,y)] \quad (1)$$

The spectrum of an interferogram, in general, contains four Fourier spectrums, and two of them are the conjugate of the remaining two peaks apart from the central DC term [2]. The experimental setup is shown in Fig. 1(a). Fig. 1(b) shows an experimentally recorded hologram of cancer cells (U-87 MG cells), and its Fourier transform is shown in Fig. 1(c). Fig. 1(d)-1(g) shows the retrieved amplitude distributions and corresponding wrapped phase distributions of the orthogonal X and Y components, and Fig. 1(h) and 1(i) represent the unwrapped phase distributions of orthogonal X and Y components of U-87 MG cell. The retrieved results show the well-resolved complex spatial structure of the cells, demonstrating the technique's applicability in numerous biological applications. This method can be utilized for cellular-level cancer discrimination by the polarization response.

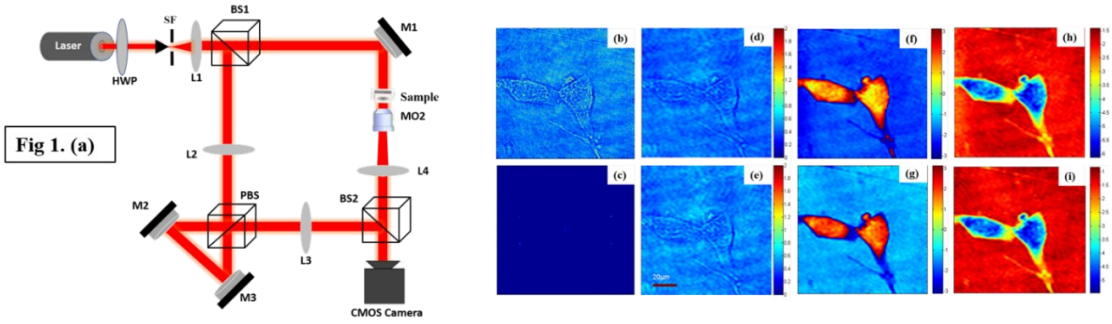

Figure 1. The PDHM experimental results for a single glioblastoma cell (U-87 MG): (a) experimental setup, (b) a recorded hologram, (c) corresponding Fourier spectrum, (d) and (e) represent amplitude distributions of the orthogonal polarization components, (f) and (g) are corresponding wrapped phase distributions, and (h) and (i) are unwrapped phase distributions (Scale bar=20 micron)

Shivam Kumar Chaubey acknowledges financial support from the Department of Biotechnology (DBT) - BT/PR35557/MED/32/707/2019.

References

1. Baoliang G. et. al., *ACS Photonics.* 8, 3440-3447 (2021).
2. Mohit, R. et. al., *ACS. Photonics.* (2023) https://doi.org/10.1021/acsphotonics.3c00963

HOL147 True definition of carrier-frequency for digital holograms of phase objects

Nishant Goyal[1], Kedar Khare[2]*
[1]Department of Physics, Indian Institute of Technology Delhi, New Delhi 110016 India
[2]Optics and Photonics Centre, Indian Institute of Technology Delhi, New Delhi 110016 India
**Corresponding author: phz218060@iitd.ac.in*

Digital Holography is an interferometric imaging modality that finds various applications in Optics and Photonics, such as bio-medical imaging, 3D imaging, quantitative phase imaging, etc. The demodulation of the off-axis digital holograms primarily requires an accurate estimation of carrier fringe frequency. Typically, an amplitude peak of the cross-term region in the Fourier domain of off-axis digital holograms is chosen to be the location for carrier frequency, and phase recovery methods such as the Fourier transform method (FTM) are then applied to recover the complex object wavefront. We point out that, in general, the peak location estimation is not the correct criterion to define the carrier frequency associated with holograms of phase objects. The amplitude peak is observed to shift unpredictably depending on the phase map of the object beam and with noise. Instead, the centroid of the power spectrum associated with the cross-term is the true definition of the carrier frequency required for the demodulation of digital holograms associated with phase objects. We study Mandel's viewpoint [1] on the carrier-envelope representation for digital holograms and show that the demodulation based on the centroid's location as carrier frequency provides a least-fluctuating (smoothest) envelope representation. The fluctuations are also quantified using the complexity parameter, which is observed to be lesser for the centroid-based recovery. The proposed definition is examined with simulated and experimentally recorded off-axis holograms and can help standardize off-axis digital holography instruments by removing the undesirable phase tilts (as shown in Figure 1) introduced due to incorrect carrier frequency estimate for phase objects.

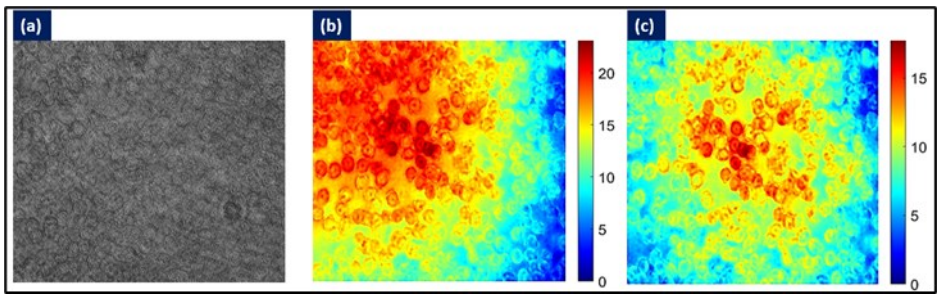

Fig. 1. (a) Off-axis digital hologram of densely populated RBCs. The unwrapped phase profiles are shown based on carrier frequencies estimated as (b) amplitude peak and (c) centroid criteria. The unnecessary tilt (and associated fluctuations) is observed to be removed in (c) compared to (b).

References

1. L. Mandel, "Complex representation of optical fields in coherence theory," *JOSA* ***57****, 613–617 (1967).*

HOL256 Practical considerations in imprinting of Holographic Optical Elements

Abhishek Tiwari, Rishabh and Shivani
Electro-Optics and Lasers, CoE, Bharat Electronics Ltd.
Jalahalli, Bangalore, India-560013
Email: abhishektiwari94@bel.co.in

With almost five decades of success in avionics sector, HUD device is now started coming in automotive applications. Various types and features of HUD exists in market spanning from bulk optics based refractive/reflective, freeform mirror based and finally latest in the sector is waveguide based. Waveguide based HUD not only saves lot of space and volume for the intended application but the incurred cost on the end application as well. Here, a basic 1-D concept proof has been done with the help of two Holographic Optical Element (HOE's) stacked together in one axis. These HOE's are imprinted with in house designed and developed imprinting technology. The transmission efficiency achieved from first and second HOE is 94% and 93.2% respectively. In this work, practical aspects of recording and calculation of transmissive and reflective HOE's has been presented. The HOE's have enormous applications ranging from automotive/ aircraft HUD, Head Worn/Helmet Displays, Medical applications, LIDARS, Scanning Instruments etc.

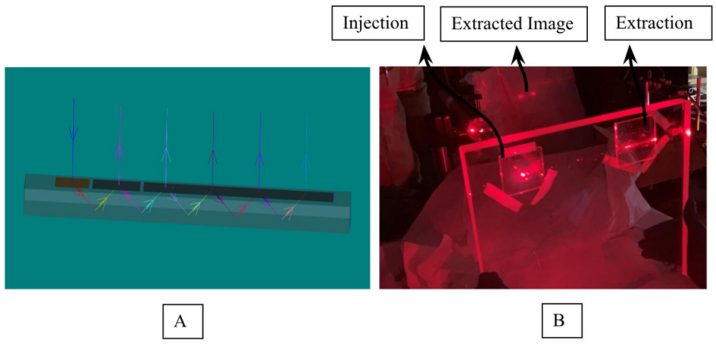

Figure 1: [A] Simulation of HOE on a rectangular waveguide in 1D. [B] Concept Proof of 1-D waveguide utilizing TIR phenomena and Kogelnik Coupled Wave Theory.

References

1. Ansys Zemax Optic Studio;
2. Wilmington et.al.,Waveguide Based Display, SID Int Symp Dis Tec, 44:278-280.

HOL257 Acceleration of layer-based CGH generation using GPU

Anuj Gupta, Bhargab Das and Raj Kumar*
CSIR-Central Scientific Instruments Organisation, Sector-30 C, Chandigarh - 160030
**Corresponding author: anujgupta@csio.res.in*

In the realm of computational holography, the generation of complex holographic patterns is an essential but computationally demanding task that eventually presents significant challenges for displaying object information effectively. The computational cost of CGH generation is directly influenced by the object size. Therefore, optimizing CGH generation algorithms for large matrix dimensions is crucial, particularly for practical applications. This work aims to increase the speed of CGH generation by changing the mode of calculation from sequential to parallel. We present a comparative study of two different modes of calculation, sequential on CPU and parallel on GPU, for CGH generation. We developed a code in Python programming language that generates the hologram using layer-based method. The method involves the layer-wise propagation of an object field from the object plane to the hologram plane. The code is run for the ob-

ject models at various matrix dimensions viz. 1024×1024 (1K), 2048×2048 (2K), 4096×4096 (4K) and 8192×8192 (8K) on CPU as well as GPU. The results in all the different simulation models are found to be completely consistent with each other.

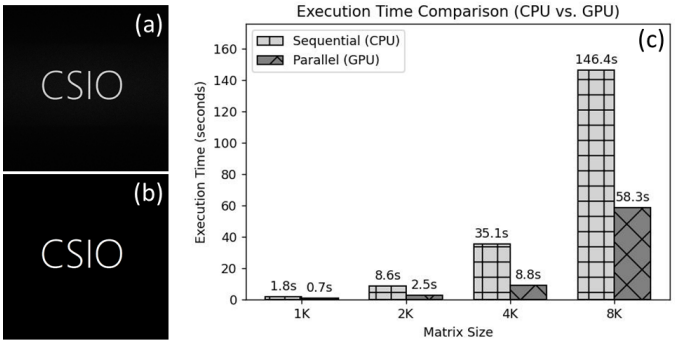

Fig. 1: (a) Original object of resolution 1024 × 1024, (b) Numerically reconstructed result (c) Execution times in CGH generation on CPU and GPU at various matrix dimensions

The system used for this work consists of a CPU with an Intel CoreTMi9-12900 processor, 16 cores, 24 threads, 32 GB RAM, and a GPU with T1000 Nvidia graphics card having 896 CUDA cores. The execution times for all the resolutions are observed and are shown in Fig 1(c) in the form of a bar chart. Our findings reveal that the speed increases by around 3 times when the code is run in parallel at GPU.

Acknowledgement

Authors acknowledge CSIR, India for providing financial support under project number MLP2014.

HOL258 Asymmetry in Central Wavelength Shift Curves due to Material Dispersion Introduced in a Spectral Interferometer

Athira T S[1], Dinesh N Naik[1]*

[1]Indian Institute of Space Science and Technology, Trivandrum, Kerala

**Corresponding author: athiratsoptics@gmail.com*

The introduction of dispersive material in an interferometer causes drastic change in the frequency of the output spectral fringe modulation resulting the shift of location of zero order fringes or stationary phase points[1]. Owing to this fact, various techniques in the spectral interferometry are developed to investigate the thickness as well as the refractive index of the dispersive material[2]. Central wavelength shift of the output spectral modulation, a tool widely used in weak measurements and spectral switches for amplifying physical quantities [3], exhibits a notable variation under dispersion. We present simulation results to discuss the effect of dispersion on central wavelength shift curves.

Suppose in a Michelson interferometer, a dispersive material of thickness t is inserted, the intensity of the output spectral fringes $I(\lambda)$ modulates according to the phase difference

$$\Delta\phi(\lambda) = \frac{2\pi}{\lambda}(\Delta d + (n(\lambda) - 1)t)$$

Where Δd , the air path delay and $n(\lambda)$ refractive index of material that depends on the wavelength by Sellmeier equation. The central wavelength shift is obtained by the formula $\delta\lambda = \frac{\Sigma\lambda I(\lambda)}{\Sigma I(\lambda)}$ is symmetrical when there is no dispersion as shown in the figure 1(a) and (b). The minimum central wavelength shift

occurs at zero path delay Δd =0 , corresponding to zero order fringe, for any width $\Delta\lambda$ of the input spectrum. Figure 1(c) and (d) show the centroidshift when a dispersive material of thickness *(t)* is introduced. The curve shows an asymmetry from zero dispersion case and the position of zero order fringe occurs at the stationary path delay. This holds the clue to use central wavelength shift as a tool to measure dispersion imparted in an optical system.

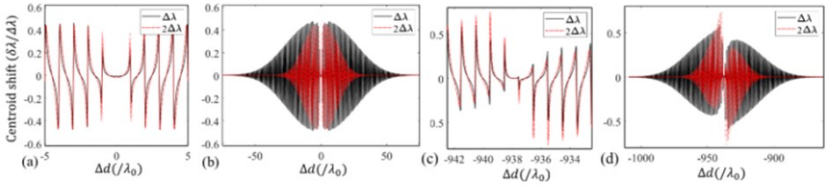

Figure 1 : The centroid shift per width of the Gaussian spectrum $(\boldsymbol{\delta\lambda/\Delta\lambda})$over the path delay (a)$\boldsymbol{\Delta d} = [-5\lambda_0, 5\lambda_0]$(b) $\boldsymbol{\Delta d} = [-75\lambda_0, 75\lambda_0]$ with zero dispersion $(\boldsymbol{c})\boldsymbol{\Delta d} = [-942.5\lambda_0, 932.5\lambda_0]$ $(\boldsymbol{d})\boldsymbol{\Delta d} = [-1012.5\lambda_0, -862.5\lambda_0]$ when a dispersive material of thickness $\boldsymbol{t = 1.1\ mm}$ is introduced for two different widths $\boldsymbol{\Delta d}$ of the input Gaussian spectrum, $\boldsymbol{\lambda_0}$ is central wavelength of the spectrum. .

References

1. C. Sáinzet. al., *Optics Communications* 110, 381-390 (1994)
2. Kumar, V. Nirmal, and D. Narayana Rao, *JOSA B* 12,9 (1995)
3. Yang Xuet. al., *Applied Physics Letters* 114,18 (2019)

HOL259 3D-imaging of subcellular components of eukaryotic cells using digital holographic microscopy

PriyankaThakkar[1], Arun Anand[2]*
[1] Department of Physics, Government Engineering College, Daman, U. T. of DNH & DD,Daman-396210.
[2] Department of Physics, Sardar Patel University, Vallabh Vidhyanagar-388120
**Corresponding author: vpriyankavora@gmail.com*

Eukaryotic cells such as plant cells contain subcellular components or organelles for conducting various functions in the cell. These include the nucleus, cell wall, stomata etc., which regulates cell's activities. These components can be quantified using quantitative phase contrast imaging techniques such as Mach-Zehnder Digital Holographic Microscopy (MZ-DHM). Digital Holographic Microscope eliminates the need of staining of transparent or semi-transparent plant cell. And three-dimensional optical thickness profiles of nucleus and cell wall can be obtained just by imaging the phase variation of light beam passing through the cells. This technique is useful in measurement of various parameters of the organelles in various conditions and thus may be helpful in the study of important activities like metabolism, growth, and differentiation of the cell.

HOL260

Sensing Wavefronts and Relative Phase of Superimposed Fields Combining the Intensity Distributions in Signal and Frequency domains

Pramod Panchal[1], Harikrishnan P[2] and Dinesh N Naik [2]
[1]India TMT Coordination Centre, Indian institute of Astrophysics,
2nd Block Koramangala Bangalore 560034
[2]Applied and Adaptive Optics Laboratory, Department of Physics,
Indian Institute of Space Science and Technology, Thiruvananthapuram, Kerala, 695547
**Corresponding author: pramod.panchal25@gmail.com*

Considering the optical field u_3 as a coherent superposition of two fields, u_1 and u_2 with intensity $I_j = |u_j|^2$ having different wavefronts, the intensity of the interference I_s in signal domain can provide the phase difference $(\emptyset)$ between them. However, the individual wavefronts cannot be obtained in this situation.

$$I_3 = I_1 + I_2 + 2\sqrt{I_1}\sqrt{I_2}\cos(\emptyset) \quad (1)$$

Whereas Shack-Hartmann Wavefront Sensor (SHWFS) can sense wavefront from the gradients from local Fourier transform; the phase differences between those wavefronts gets eluded during the sensing.

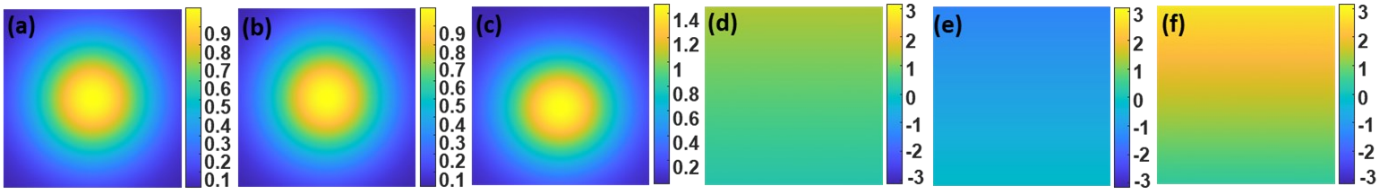

Figure 1: Amplitudes of (a) u_1, (b) u_2, (c) ; phase of (d) u_1, (e) u_2 and (f) relative phase between u_1 and u_2.

We explore the possibility of sensing the wavefronts and relative phase of superimposed fields combining their intensity distributions in signal and frequency domains. Optical fields u_1 and u_2 with Gaussian distributions (as shown in Fig1 (a)-(b)) having equal opposite tilt (as shown in Fig.1 (d)-(e)) and a relative constant phase of 0.5pi is considered. Fig. 1 (c) and (f) represents the amplitude of the superposed field and the relative phase. SHWFS is assumed to sense the wavefronts of u_1 and u_2 if sensed independently. If the wavefront difference is assumed to be small, allowing the focal spots corresponding u_1 and u_2 at each lenslet to be nearly overlapping when the wavefront of the superposed field is sensed, it is shown that the relative phase $\emptyset$ can be calculated using.

$$\emptyset = \cos^{-1}\left(\frac{(I_3-(I_1+I_2))}{2\sqrt{I_1}\sqrt{I_2}}\right) \quad (2)$$

Where, I_j are taken as the energies in the corresponding spots.

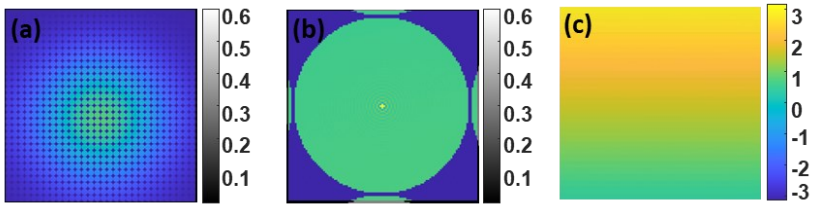

Figure 2: (a) Simulated spot diagram of superposed field, (b) enlarged portion of (a) and (c) relative phase obtained.

From the simulated spot diagrams shown in Fig. 2(a) (one of them enlarged and shown in Fig. 2(b)), the relative phase calculated using Eq. (2) is shown to match with the expected one shown in Fig. 1 (f). Further investigations and limitations need to be explored to improve the proposed scheme.

References

1. Sabrina Velghe, "Advanced wave-front sensing by quadri-wave lateral shearing Interferometry", Proc. of SPIE Vol. 6292, 62920E, (2006) · 0277-786.
2. Panchal Pramod et al, "Insensitivity of higher order topologically charged Laguerre–Gaussian beams to dynamic turbulence impact," *Optics Communications*, 495 (2021) 127023.

HOL261 Convergence Criteria for Recursive Formula used in Phase Measurement of Tilted Surface using Tunable Wavelength Interferometer

Harikrishnan P, Dinesh N Naik
Applied And Adaptive Optics Laboratory, Department of Physics,
Indian Institute of Space Science and Technology, Thiruvananthapuram, Kerala, 695547
**Corresponding author: harikrishnanp.21@res.iist.ac.in*

Single wavelength interferometers, due to inherent 2π phase ambiguities, fail to measure the surface profile where the height variations of the adjacent surface points sampled/imaged exceed one wavelength [1]. In such cases, multiple interferograms need to be recorded by using varying the wavelength of the laser source and phase maps using synthetic wavelength (ΔΛ) need to be generated for lifting the phase ambiguities and profile measurement [2]. The initial ΔΛ is taken as unambiguous in the sense that synthetic wavelength is larger than the height variation. A recursive algorithm is proposed in which the gradually reduced ΔΛs is used to increase the accuracy.

For obtaining the phase difference using recursive algorithm [2], the following formula is used.

$$(\Delta\emptyset)_n = \psi_n + 2\pi RND\left(\frac{1}{2\pi}\left(\frac{(\Delta\emptyset)_{n-1}\Lambda_{n-1}}{\Lambda_n} - (\Delta\emptyset)_n\right)\right)$$

Where ψ_n is the experimentally measured phase, $(\Delta\emptyset)_n$ is the improved phase by recursive calculation and RND = rounding the fractional value to the nearest integer.

In this work, we investigate the application of the recursive algorithm for obtaining the surface profile of a tilted surface. We explore the possibility of the convergence of the recursive algorithm even if the initial phase map from the synthetic wavelength is ambiguous due to the tilt of the object with respect to recording plane. A simulation is performed in which the mirror at one arm of a typical Michelson interferometer is tilted with respect to the camera plane. The interferograms are generated for a range of wavelengths starting from 895nm to 905nm with varying change of wavelengths. Figure 1(a) shows interferograms generated using a ΔΛ of 535microns. We take these initial wrapped phases itself as the starting guess of unambiguous phase. Now from the initial ΔΛthe successive ΔΛs are varied by tuning the laser wavelengths in Δλ as shown in the x axis of figure (d). From 1(b) and 1(c) it can be observed that the convergence area within the object surface is getting reduced, which means that finer the change in wavelength better the convergence (converges within 30 steps) even when the initial phase is not correct.

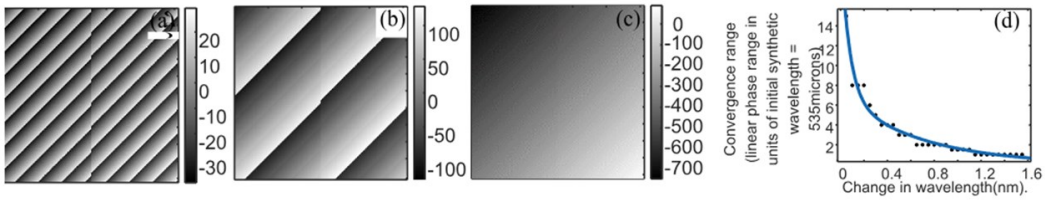

Figure 1: (a) Phase difference map when the change in wavelength is 1.5nm (b) Phase difference map when the change in wavelength is 0.4nm (c)Phase difference map when the change in laser wavelength is 0.05nm and (d) a plot of convergence range vs change in wavelength.

References

1. Kumar, U. Paul, et al. "Two-wavelength micro-interferometry for 3-D surface profiling." *Optics and Lasers in Engineering* 47.2 (2009): 223-229
2. Wada, Atsushi, Makoto Kato, and Yukihiro Ishii." Multiple wavelength digital holographic interferometry using tunable laser diodes." Applied optics 47.12 (2008): 2053-2060.

HOL262 Measurement of Ultralow Linear and Angular Velocity using Cyclic Interferometer

Laxman Mandal[*]*, Prakhar Maheshwari and A R Ganesan*
Applied Optics Laboratory, Department of Physics, Indian Institute of Technology Madras, Chennai 600036, Bharat.
**Corresponding author: laxman1995mandal@gmail.com*

Measurement of ultralow linear and angular velocity hold great potential for various applications in engineering, industry and research. XRD testing machines and tensile testing machines are good examples to name some. A novel method to accurately measure the linear and angular velocity of a rigid object in the ultralow-velocity domain is presented in this paper. Our approach utilizes a cyclic interferometer configuration that offers improved stability against environmental fluctuations.

Experimental procedure: To measure the linear velocity of an object, Avila et al. employed Michelson configuration with a measurement range of 1-10 mm/sec [1]. In this paper we present a cyclic interferometer-based setup with phase shifting method [2] which could measure linear velocity down to 1 μm/sec, as well as angular velocity of the order of 50 μrad/sec .

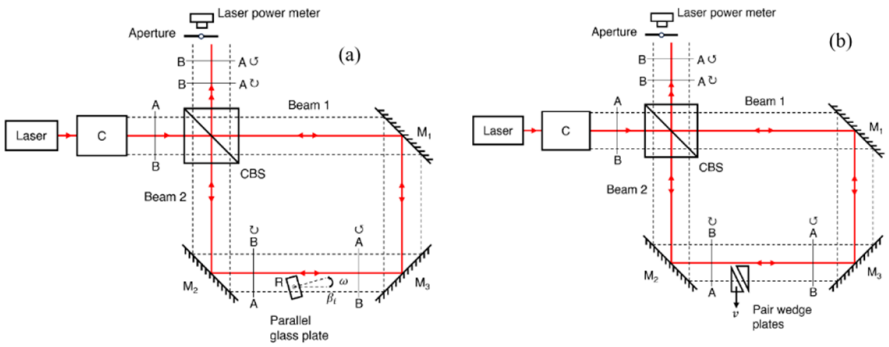

Fig.1 The schematic of the experimental setup for (a) Angular velocity (b) Linear velocity measurements.

In the cyclic setup shown in Fig. 1(a,b), a parallel glass plate(a) or a pair of wedge plates(b) is introduced across half of the beam and a power meter is used to record the intensity of the interference pattern with time. For measuring angular velocity, the parallel glass plate is rotated which introduces phase shifting and the intensity power at some point is recorded with time by a power meter. The angle of rotation of parallel glass plate ($\Delta\beta$) is calculated from the total phase shift at the point in a given duration T_a , and the angular velocity is deduced using the relation $\omega = \Delta\beta/T_a$. Similarly, one wedge plate is moved by $\Delta\gamma$ as shown in a time T_a to measure linear velocity as $= \Delta Y/T_a$. Measurement accuracies of 1 to 2% error has been achieved. Detailed theory and experimental results are presented.

References

1. M. A. R. Ávila, *et al*, Journal of Physics: Conference Series, 582 (1), 012041 (2015).
2. I. Shevkunov *et al*, Journal of Imaging, 8 (4), 87, (2022).

HOL263 Holographic microscope for inspection of surface defects

Mohit Rathor, Shivam Kumar Chaubey, Rakesh Kumar Singh*

Laboratory of Information Photonics and Optical Metrology, Department of Physics, Indian Institute of Technology (Banaras Hindu University), Varanasi, 221005, Uttar Pradesh, India

**Corresponding author: mohitrathor.rs.phy21@itbhu.ac.in*

Digital holographic microscope (DHM) is an important quantitative imaging technique with a wide range of applications based on Various experimental schemes for holography that have been proposed such as in-line, off-axis, and phase-shifting holography [1]. However, holographic image quality is severely disturbed by the coherent noise, particularly in the imaging of rough optical objects. Many methods have been developed to remove the speckle noise such as shifting and rotating objects [2], laterally shifting hologram aperture and computational de-noising but these techniques have some limitations.

Here, we propose a new low-coherence DHM for the quantitative imaging and numerical reconstruction of the objects using the polarization phase-shifting technique. This technique uses a low coherent source for interferometry in a highly stable experimental configuration based on the Fizeau geometry. Moreover, the proposed experimental system overcomes issues like speckle noise, alignment, and stability of the typical DHM system. The performance of this microscope is tested in imaging of metallic surface and initial results are presented here.

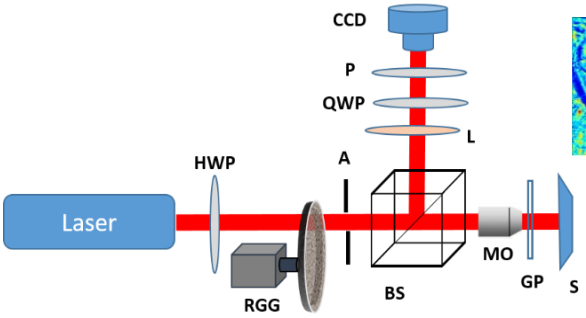

FIG.1: Experimental Setup: HWP: Half-wave plate; RGG: Rotating ground glass; A1: Aperture; BS- Beam splitter, MO- microscopic objective (10X); GP: Grid polarizer, L- Lens(f=100mm), QWP- Quarter wave plate, P- polarizer, CCD: camera

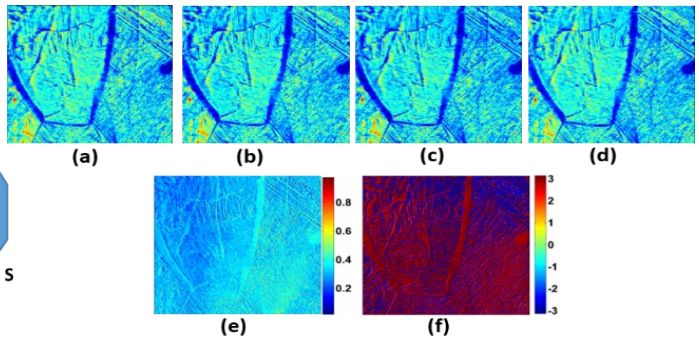

FIG.2: Experimental results (a),(b),(c)and (d) are recorded intensity holograms for different phase shift 0, π/2,π and 3π/2 respectively; (e) & (f) is the reconstruct amplitude and phase information corresponding to these holograms using four phase shifting approach for rough surface(welding sample).

In conclusion, we present a new design of the holographic microscope with low coherent source and demonstrated its application in detection of defects in the sample.

References

1. J.W. Goodman, (Viva books private limited, New Delhi,2008)
2. F. Pan, et al. Opt. Express 19, 3862-3869 (2011)

HOL264 Holographic Concentrators Recorded on Photopolymer Film for Photovoltaic Applications

*Rahul Mandal[1], Abhijit Ghosh[1]**

[1]Department of Physics, National Institute of Technology Durgapur, Durgapur 713209, West Bengal, India

**Corresponding author: aghosh.phy@nitdgp.ac.in*

In present work, photopolymer film preparation, recording of holographic concentrators and their characterization is presented. The composition of Photopolymer film is Acrylamide, N, N′ Methylene bisacrylamide, Triethanolamine, Azure II and Poly-vinyl alcohol [1, 2]. Photopolymer films of different film thickness were prepared, their achieved thickness were 46.90 µm and 79.04 µm as measured by 3D-Optical surface profilometer. Holographic concentrators were recorded on prepared photopolymer film (Fig. 1) by interfering converging spherical wavefront with mutually coherent planar wavefront [3] derived from He-Ne laser source (λ=632.8 nm).

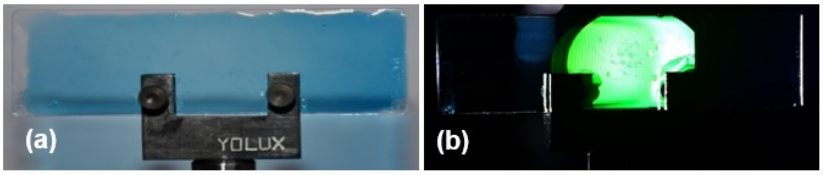

Figure 1. Photographs of **(a)** photopolymer film **(b)** recorded holographic concentrator.

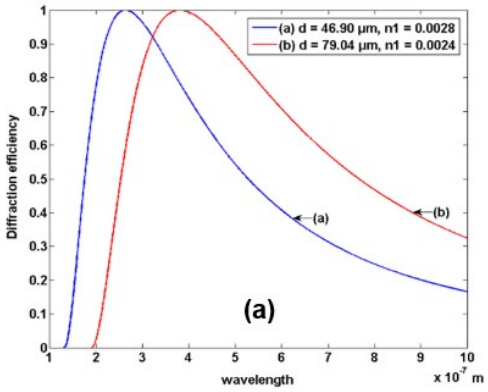

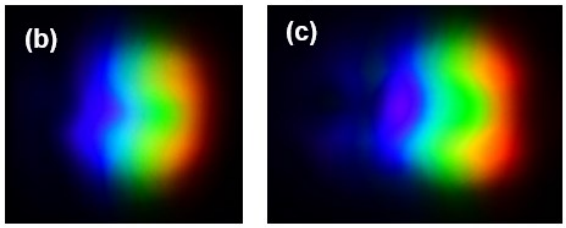

Figure 2. (a) Variation of diffraction efficiency with wavelength for different values of d and n_1 and at fixed Λ= 1.82 µm and n=1.49. Photographs of focussed spectra of white light diffracted by recorded concentrators on photopolymer film of thickness **(b)** 46.90 µm **(c)** 79.04 µm.

When typically recorded holographic concentrators were illuminated by a laser of wavelength 532 nm, measured diffraction efficiencies were 50% and 82.42% for film thickness 46.90 µm and 79.04 µm respectively. Wavelength selectivity curve of holographic concentrators for different achieved values of film thickness and depth of refractive index modulation have been plotted through simulation (Fig. 2a). Recorded holographic concentrators when played back by white light, focussed spectra were obtained, presented in Fig. 2(b–c). Dispersing and focussing property of concentrator is useful for solar cells of matched bandgap application [4].

References

1. H. Akbari et. al., *Appl. Opt.* 53 (7) 1343–1353 (2014).
2. J. Xu et. al., *Proc. of SPIE* 7851, (SPIE, December 2010), 254-261.
3. A. Ghosh et. al., *Measurement Science and Technology* 28(12), 125402 (2017).
4. A. Ghosh et. al., *Optik* 168, 625–649 (2018).

HOL265 Fabrication and Characterization of Diffuser Using Holographic Printer for Achieving Uniform Light Distribution

*Shelly Chaudhary, Bhargab Das, Raj Kumar**

CSIR- Central Scientific Instruments Organisation, Chandigarh, 160030, India

**Corresponding author e-mail address: raj.optics@csio.res.in*

In optical systems and displays, diffusers are crucial for controlling light distribution and minimizing hotspots, resulting in improved image quality. They come in various types, including ground glass, opal glass, roughened surfaces, and engineered surface holographic elements, offering solutions for different light control needs. Holographic diffusers outperform traditional diffusers in several parameters. They can be custom-designed for precise light scattering, offering tailored light distribution. With high diffusion efficiency, they are more efficient, while their thinner and lighter profile suits space-constrained applications.

Holographic diffusers also boast durability, providing uniform light distribution and flexibility. These features make them ideal for applications where precise light control is essential, such as optical systems, displays, and lighting.

In this paper, a holographic printer-based method for designing and optimizing holographic diffuser has been studied. It begins by exposing a photosensitive material to a laser-generated speckle pattern, sequentially recording sub-holographic diffusers. These sub-diffusers were optimized to form a tiled structure to create a final holographic diffuser with efficient light scattering properties, yielding a uniform light pattern. The research focuses on angular light scattering, real-time optimization of diffusion efficiency, and image quality analysis. The findings were then compared to those obtained with a ground glass diffuser as a reference point. Results show that the holographic diffuser achieved over 90% efficiency and precise control over light diffusion. Experimental data shows uniform light distribution, and image quality parameters were studied.

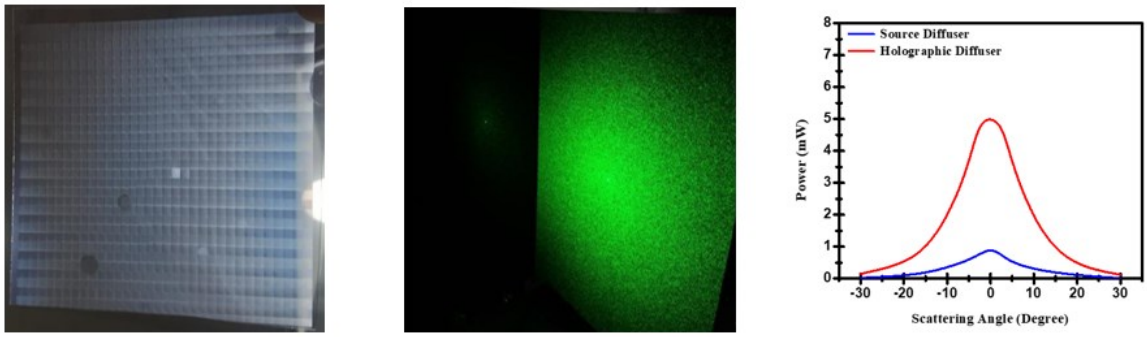

1 (a) 1 (b) 1 (c)

Fig.1(a): Recorded Holographic diffuser. Fig.1(b): Depicts the diffusing properties of the recorded holographic diffuser when illuminated by a laser beam. Fig.1(c): Graph depicting the relationship between the output power of scattered light and scattering angles, measured in micro-watts (mW) and degrees, respectively.

HOL266 Understanding the concept of Holographic Optical Elements as powered and non-powered diffractive element

Shivani, Rishabh, Abhishek Tiwari

Electro-optics and Lasers, CoE, Bharat Electronics Ltd.

Jalahalli, Bangalore, India-560094

Email: dahiyashivani21@gmail.com

In this contribution, we demonstrate the use of HOE as a powered and non- powered diffractive element. The HOE is first simulated in Zemax[1] in transmission mode using the appropriate construction beams and the recording material. The recording material used is BAYFOL HX 200[2] having better efficiency for visible range. The interference pattern imprinted onto the respective HOEs transform the properties of a wavefront in a similar way to the optical components. These properties of HOE along with their lightweight and economical replication process works as a good replacement for heavier and costlier optical components.

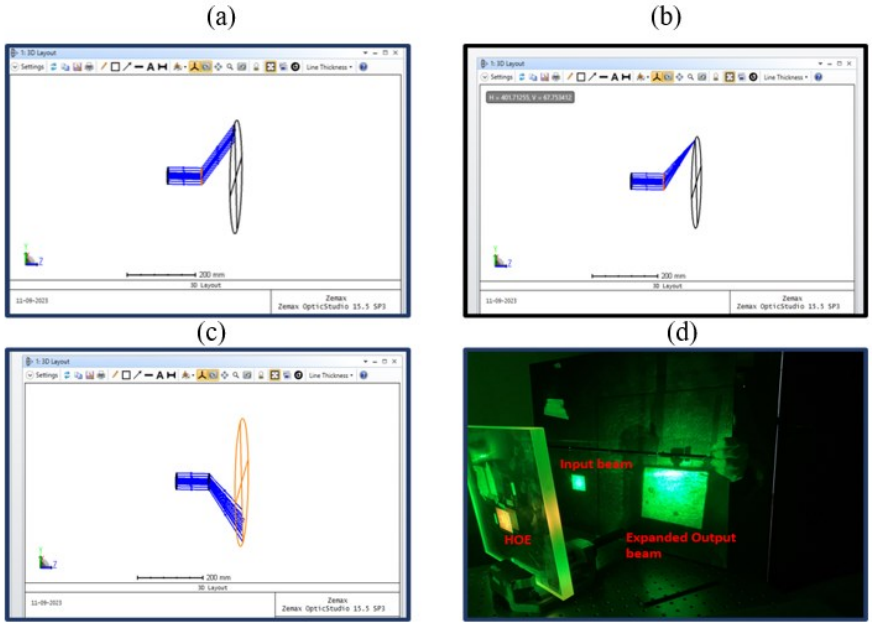

Figure 1: Demonstrates simulation of HOE as non-powered (in (a)) and powered (in (b)&(c)) diffractive element(d) experimental image showing a collimated beam being diverged after interacting with HOE.

References

1. Ansys Zemax Optic Studio;
2. Bruder FK, et.al., Polymers, 2017 Sep26;9(10):472.

HOL267 Measurement of Coherence-Polarization matrix by One-Shot Approach

Sourav Chandra[1], Rakesh Kumar Singh[1]*

[1]Laboratory of Information Photonics and Optical Metrology, Department of Physics, Indian Institute of Technology (Banaras Hindu University), Varanasi-221005, India
**Corresponding author: souravchandra.rs.phy19@itbhu.ac.in*

In the realm of spatially fluctuating light fields governed by Gaussian statistics, the utilization of intensity correlations through an intensity interferometer represents a robust and stable iHOLOGRnterferometric technique for complete 2×2 BCP matrix measurement, employing four distinct intensity measurements [1, 2]. In this paper, we present a new experimental technique and our initial results on detection of elements of the BCP matrix. This is realized by introducing a folded interferometric design and applying the correlations of only two Stokes parameters (SPs) namely S_0 and S_1.

Figure 1 shows a stochastic vector light source and its characterization by our double aperture common-path interferometer (DACPI) composed of two mirrors (M1 and M2) and one polarizing beam splitter (PBS). This design is used to capture the speckle interferogram of the orthogonal polarization components in one-shot. Two speckle interferograms of S_0 and S_1 are used to determine correlation of fluctuations of the SPs and subsequently certain combinations of these correlations are used to extract the BCP matrix elements as

$$C_{kl}(\Delta\mathbf{r}) = \langle \Delta S_k(\mathbf{r}) \Delta S_l(\mathbf{r}+\Delta\mathbf{r}) \rangle \qquad (k,l=0,1), \tag{1}$$

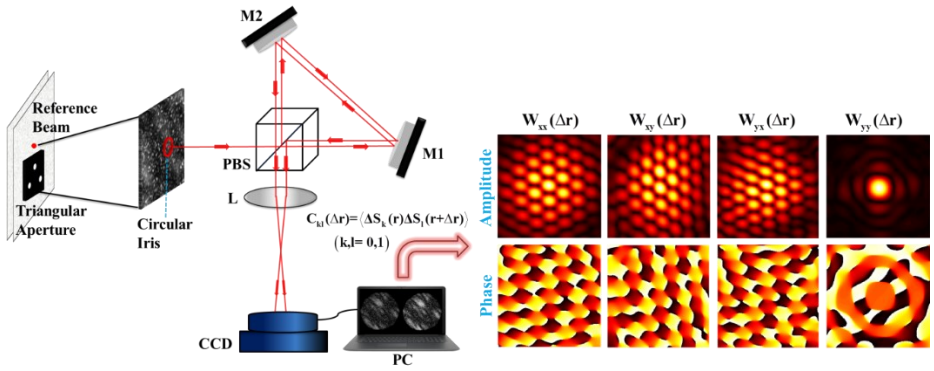

Figure 1: Schematic of one-shot measurement of 2×2 BCP matrix using DACPI. PBS: Polarizing Beam splitter; M1, M2: Mirrors, L: Lens; CCD: Charged-Coupled Device; PC: Personal Computer.

Sourav Chandra acknowledges the financial support from IIT (BHU), and support from Board of Research in Nuclear Sciences (BRNS—Grant no. 58/14/04/2021-BRNS/37092) is acknowledged.

References

1. R. V. Vinu et. al., *Appl. Opt.* 54, 6491-6497 (2015).
2. Z. Dong et. al., *Opt. Express* 28, 20634-20644 (2020).

HOL268 Holographic Imaging Through Turbid Media

Sree Renjini R S, Dinesh N Naik, C S Narayanamurthy*
Applied and Adaptive Optics Laboratory, Department of Physics, Indian Institute of Space Science and Technology, Thiruvananthapuram, Kerala, 695547
**Corresponding author: sreerenjini.22@res.iist.ac.in*

Conventional imaging in turbid conditions, like fog, is ineffective for producing high quality images. Holographic imaging is a promising and widely researching area. Studies show that, in comparison to conventional imaging, this method has a good imaging range and is immune to noise [1].

Here, we'll discuss imaging through turbid media using a single shot off-axis digital holographic approach (Fig 1). It uses a HeNe laser (λ=633nm) as the source and light reflected from the object is passed through a turbid media. By adjusting the amount of Dettol added to regular water, different densities of turbid medium are produced. A diode laser along with a power meter is used to quantify the density of turbid media in terms of attenuation lengths (AL). In order to record off-axis object holograms, we use a 4f imaging system along with an aperture in the Fourier plane that restricts the spectral spread, and by introducing a shifted point reference using an optical fibre in that plane. The reference beam is coupled to an optical fibre and the fibre tip is placed close to the aperture in the Fourier plane. Conventional images are also captured along with the holographic image by simply blocking the reference beam.

Holographic images are reconstructed using MATLAB (Fig 2). Fig 3 shows conventional and holographic reconstructed images at different attenuation lengths. By comparing both it is clear that holographic imaging technique has more imaging range than that of normal imaging.

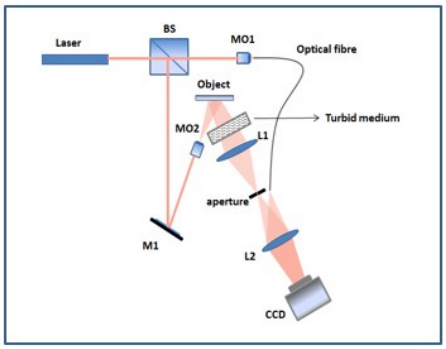

Fig 1: Schematic representation of experimental setup

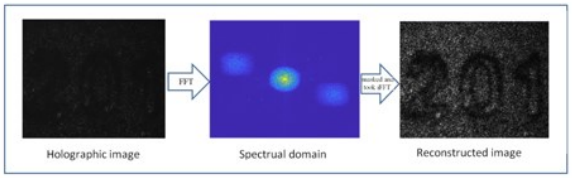

Fig 2: Process of reconstruction of experimentally obtained holographic image

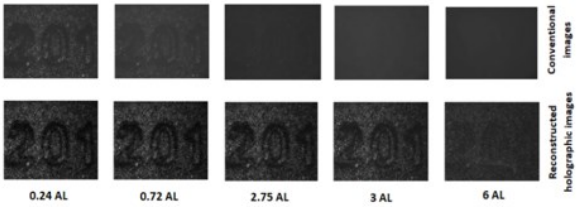

Fig 3: Experimentally measured conventional images and holographic reconstructions at five different attenuation lengths.

References

1. Alexander Gröger, et al. Appl. Opt. 62, D68-D76 (2023)

HOL269 A Deep Learning Approach For Volume Image Segmentation in Digital Holography

*Uma Mahesh R N[1], Arya Jayan[1,2], Anith Nelleri[1]**

[1]School of Electronics Engineering, [1,2]School of Advanced Sciences (Division of Physics), Vellore Institute of Technology (VIT), Chennai, Tamilnadu, India – 600127.

**Corresponding author: anith.nelleri@vit.ac.in*

A Deep learning-based three-dimensional (3-D) object hologram reconstruction and multi-depth volume image segmentation for digital holographic data is demonstrated. The 3-D image volume named “VIT” is constructed at various depth planes. The digital holograms of the 3-D image volume are formed using the four-step phase-shifting digital holographic (PSDH) technique. We utilize a deep learning methodology to reconstruct and segment the detected 3-D information by appropriately compiling a comprehensive dataset from the recorded digital holograms. The design of deep learning U-Network results in the reconstruction of multi-depth 3-D object volume information and the segmentation of the intensity image planes at various depths. Fig. 1 shows the creation of the 3-D object volume namely "VIT," where information is distributed across multiple depth planes, along with the schematic of the geometry for the hologram recording from the four-step phase shifted plane reference waves.

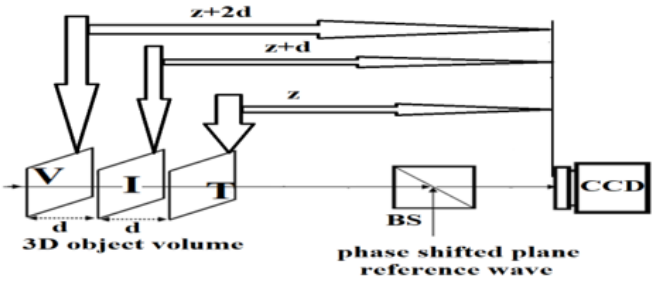

Fig.1: Schematic of the digital hologram recording geometry using 3-D object volume "VIT" with information distributed in various depth planes and separating distances z=10 cm and d=2 cm.

Fig. 2: Reconstructed intensity images using deep learning U-network at different depth planes (a) without image segmentation and (b) with image segmentation

Fig. 2 shows the results from a numerical experiment and serves as validation for the proposed concept.

References

1. Yi, F., Moon, I. and Javidi, B., 2017., *Biomedical optics express*, *8*(10), pp.4466-4479.
2. Nguyen, T., Bui, V., Lam, V., Raub, C.B., Chang, L.C. and Nehmetallah, G., 2017., *Optics express*, *25* (13), pp.15043-15057.
3. Pitkäaho, T., Manninen, A. and Naughton, T.J., 2019, May., In *Digital Holography and Three-Dimensional Imaging* (pp. Th3A-1). Optica Publishing Group.

HOL270 Characterization of occluded phase samples using lens less Fourier transform digital holographic interferometry

Subhash Utadiya,[1] Vismay Trivedi,[2] Atul Srivastava,[3] Humberto Cabrera,[4] Gyanendra Sheoran,[2] Arun Anand[5]*

[1]Applied Physics Department, Faculty of Technology and Engineering, The Maharaja Sayajirao University of Baroda, Vadodara 390001, India

[2]Department of Applied Sciences, National Institute of Technology Delhi, India

[3]Department of Mechanical Engineering, IIT Bombay, Mumbai, 400076, India

[4]MLAB, STI Unit, The Abdus Salam International Centre for Theoretical Physics, Strada Costiera 11, 34151 Trieste, Italy

[5]Optics Laboratory, Department of Physics, Sardar Patel University, Vallabh Vidyanagar, Anand 388120, India

**Corresponding author: subhashutadiya@gmail.com*

Lens less Fourier transform (LLFT) digital holography provides an easy way to compare object wavefronts at two different time instances. Since the phase reconstructions in lens less LLFT digital holography requires only one Fourier transform of the recorded digital hologram, it may be used for real time sample fea-

ture extraction. We present a technique using LLFT digital holography for the characterization of the transparent and occluded semitransparent objects by thermal loading. The LLFT digital holographic technique developed for quantification uses a collimated beam from a low power laser source to illuminate the phase object occluded by a ground glass diffuser [1, 2]. A point source located at the plane of the diffuser acts as the reference wavefront. The superposition of the probe and the refence wavefronts leads to generation of LLFT holograms, which can be numerically reconstructed by computing its Fourier transform. To identify defects as well as to characterize the occluded sample, it is thermally loaded, and sequence of holograms are recorded, while it is being loaded. Thermal loading of phase sample generates spatiotemporal change in its refractive index distribution due to heat diffusion. LLFT digital holography maps this refractive index change in terms of phase change of the probe beam passing through the object. The refractive index change depends upon the thickness and thermo-optic coefficient of the sample, and hence can be used to identify inhomogeneities in eth sample as well as to characterize it [1, 2]. We will present the results of investigation of occludes phase objects using LLFT digital holography and thermal loading [1, 2]

References

1. V. Trivedi, M. Joglekar, S. Mahajan, N. Patel, V. Chhaniwal, B. Javidi, and A. Anand, Opt. Laser Technol. 111, 439-446 (2019).
2. S. Utadiya, V. Trivedi, G. Sheoran, A. Srivastava, D. Claus, H. Cabrera, and A. Anand, Opt. Lasers Engg. 160, 107227 (2023).

HOL271 Exploring the Digital Micromirror Device for Optical Wavefront Shaping

*Abhishek R[1], Dennis T[2], Vaishnav Raj K[1, 4], Gadha T[1], Pranav K K[3], Jerin T[5], Govind G B[5], Pradeep A. V[3], Jijo P U[4], Sajeev D[5,]**

[1]*aiRender Technology Pvt Ltd, Bangalore-560066, Karnataka*

[2]*Amal Jyothi College of Engineering, Kanjirappally- 686518, Kottayam, Kerala*

[3]*Department of Physics, CUSAT, Kochi-682022, Kerala*

[4]*Government College Kasaragod, Vidyanagar-671123, Kasaragod, Kerala*

[5]*Government College Kariavattom, Kariavattom-695581, Kerala*

**Corresponding author: sajeevphy@gmail.com*

The interaction of light with a spatial light modulator is the fundamental tool for both wavefront shaping and diffraction experiments [1]. The Digital Micromirror Device (DMD), comprising an array of tiny micrometer-sized mirrors, is found to be an efficient spatial light modulator [2]. The main advantage of DMDs lies in their high-speed switching capability, the large angular separation between the incident and diffracted beams, their smaller pitch, and their blazed grating behaviour [3]. The digital micromirror device associated with commercial digital light projectors is explored for various diffraction and wavefront shaping experiments [4]. Here we describe diffraction experiments with repurposed digital light projectors (Infocus made) with a digital micromirror (Texas instruments 0.55" XGA 450). We estimate various diffraction parameters associated with fundamental diffraction experiments and discuss the anomalies based on the DMD structure. Since DMDs are potential candidates for applications demanding wavefront shaping in the field of 3D holographic reconstructions and imaging applications, understanding the fundamental characteristics of the DMD based on diffraction experiments plays a significant role in laying the founda-

tion for exploring such applications.

References

1. Yu-Xuan Ren1 et. al., Ann. Phys. 527, 7–8,(2015).
2. Brice Douet et. al., Emergent Scientist 5, 4 (2021).
3. Dana Dudley, et. al., SPIE. 4985, 29-35 (2003).
4. Sergei Panarin et. al., Am. J. Phys. 02-09 (2020).

Category 14

Optical Instrumentation, Fabrication and Metrology (IFM)

IFM123 Experimental Study of Interaction Effects of Process Parameters during Chemical Mechanical Polishing of Fused Silica Optical Glass

Aparajita Parashar [1,2,], Raj Kumar Pal[1,2], Vinod Karar[1,3]*

[1] *Academy of Scientific and Innovative Research (AcSIR), Ghaziabad, 201002, India*
[2] *CSIR-Central Scientific Instruments organisation (CSIR-CSIO), Sector-30, Chandigarh, 160030, India*

[3] *CSIR- Central Road Research Institute (CSIR-CRRI), New Delhi, 110025, India*

[*] *Corresponding author: aparajita.csio21j@acsir.res.in*

Chemical mechanical polishing (CMP) of fused silica optical glass is a tedious job, due to its brittle nature. Fused silica optical glass is used in astronomy, aeronautics and as a waveguide mirrors in laser applications. During CMP of fused silica optical glass several factor play dominating role [1]. In this study Taguchi's L16 array is used for design of experiment. This study is performed to understand the interaction effect of mechanical and chemical parameters [2] i.e., abrasive size (μm), abrasive concentration (wt.%) , and polishing time (minutes) on the material removal rate (MRR) and surface roughness (Ra) of the fused silica optical glass. It is observed that abrasive size plays dominating role for the MRR and polishing time is an influencing parameter for achieving a better surface roughness. The best value of surface roughness recorded using Taylor Hobson profilometer is 8 nm for a given set of parameters.

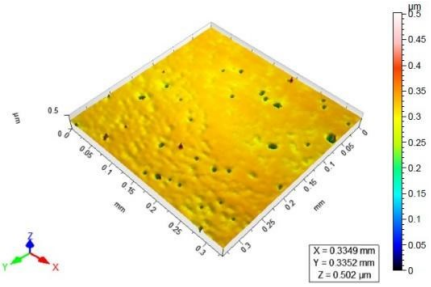

Figure 1:CCI result of best Ra

Figure 1: Polished workpiece

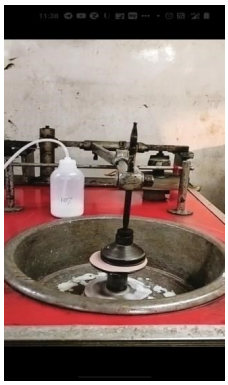

Figure 3:Experimental setup

References

1. T. I. Suratwala et. al., *Toward Deterministic Material Removal and Surface Figure during Fused Silica Pad Polishing, Journal of American Ceramic Society (2010).*

2. R.K. Pal et. al., *Material removal characteristics of full aperture optical polishing process, An International Journal of Machining Science and Technology, (2017).*

IFM124 Object detection in foggy and hazy conditions

*Jyoti B. Mohapatra[1], Akash Pal[2], Jyothish M.[3], Naveen K. Nishchal[4]**

[1,2,4]Department of Physics, Indian Institute of technology Patna, Bihta, Patna-801106, India
[2]ISRO Inertial Systems Unit, Thiruvananthapuram-695 013, India
**Corresponding author: nkn@iitp.ac.in*

In this modern era, optical pattern recognition is fetching considerable attention due its faster processing speed and optimal accuracy [1-3]. Among all the available techniques, fringe-adjusted joint transform correlator (FJTC) is one of the most used architectures for its advantages like non requirement of complex filter fabrication and precise alignments of the optical components. FJTC uses Fourier plane subtraction method and gives two auto-correlation peaks for a match by mitigating the undesired dc term from the correlation plane. Power spectra subtraction method also suppresses noise from the correlation output [1]. Object detection in noisy environments stands as a big challenge in pattern recognition. In real world applications, the input scene might be corrupted under different weather conditions like fog, snow, haze, and sunglare etc. which severely affect the detection process. Hence, the accuracy of the optical correlator is challenged. In this study, we propose a novel approach of enhancing the correlation capability especially scenarios under hazy and foggy conditions. An input scene is pre-processed and then put into the correlation process using FJTC. In pre-processing step dark channel prior (DCP) method is used to effectively de-haze the input images thereby enhancing the correlation peak intensity [2].

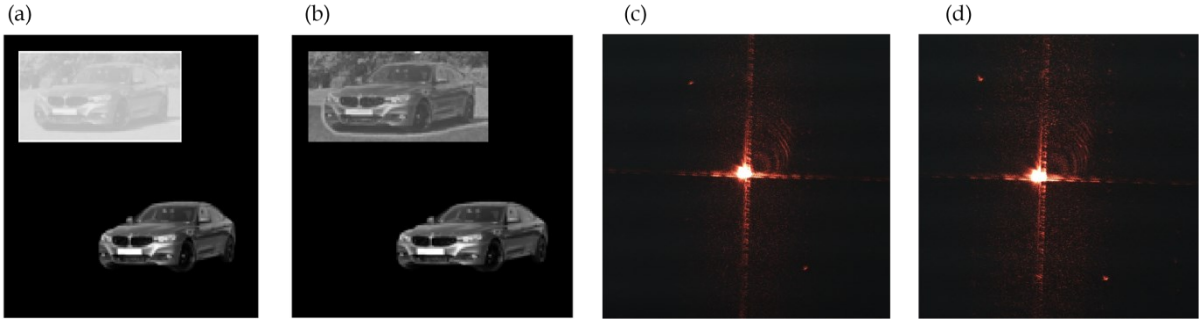

Figure1(a) joint image of car with fog density 0.5, (b) joint image of car with de-hazed input scene, (c) correlation output for joint images shown in (a), and (d) correlation output for joint images shown in (b).

The experimental results shown in the Figure 1 confirm the efficacy of the proposed method. This research will open a way for image correlation in adverse weather conditions useful in surveillance, security, and industrial quality control applications.

References

1. A. Bhagatji, N. K. Nishchal, A. K. Gupta, and B. P. Tyagi, Opt. Laser Technol. 40, 99-112 (2008).
2. K. He, J. Sun, and X. Tang., IEEE Trans.Patt. Anal. Mach. Intell. 32, 2341-2353 (2011).
3. R. Kumar, A. Shikder, N. K. Nishchal, and A. AlFalou, IEEE Photon. Technol. Lett. 35 (2023) (in press).

IFM125

Coherent population trapping in Rb vapour cells filled with Ar+N_2 buffer gas for application in atomic clock

Rajaiah K.[1], Manjula R.[2], Tiwari P.[2], Kappen M. J.[2], Biswas S.[2], Raha B.[2], Praveen K. C.[2], Nirmala S.[1], Venkatappa Rao T.[3], Pradhan S.[4], Umesh S. B.[2], Sriram K. V.[2], Upadhya P. C.[2]*

[1]*U R Rao Satellite Centre, ISRO, Bangalore-560017, India*
[2]*Laboratory for Electro-Optics Systems, ISRO, Bangalore-560058, India*
[3]*Department of Physics, NITW, Warangal-506004, India*
[4]*Bhabha Atomic Research Centre Facility, Visakhapatnam -531011, India*
**Corresponding author: krajaiah@ursc.gov.in*

Coherent Population Trapping (CPT) is a quantum interference phenomenon in three-level energy systems (Λ-system) under optical pumping. Quantum interference is commonly achieved by exciting the ground states of a Λ-system with two coherent fields generated by modulating drive current of a laser source with Radio Frequency (RF) that corresponds to ground state hyperfine splitting[1]. CPT in alkali atoms enables the development of miniaturized atomic clocks and frequency stability of these clocks depends on quality figure (q) and frequency shift of CPT resonance[1,2]. These characteristics primarily depend on critical parameters such as buffer gas pressure, laser excitation intensity and RF power.

In this study, we investigate the variation of 'q' with laser intensity at different buffer gas pressure values in Rb vapour cells. Our study shows that CPT resonance exhibits enhanced '*q*' at lower laser intensities (5-10 W/m^2) at which the estimated short-term stability is <2.0E-12 per sec (Fig. 1a). The light shift which affects the long-term stability of atomic clock, decreases at lower buffer gas pressure (Fig. 1b). These results help in selecting suitable system configuration as well as optimum operating parameters of atomic vapour cell in order to achieve superior frequency stability of CPT based atomic clock.

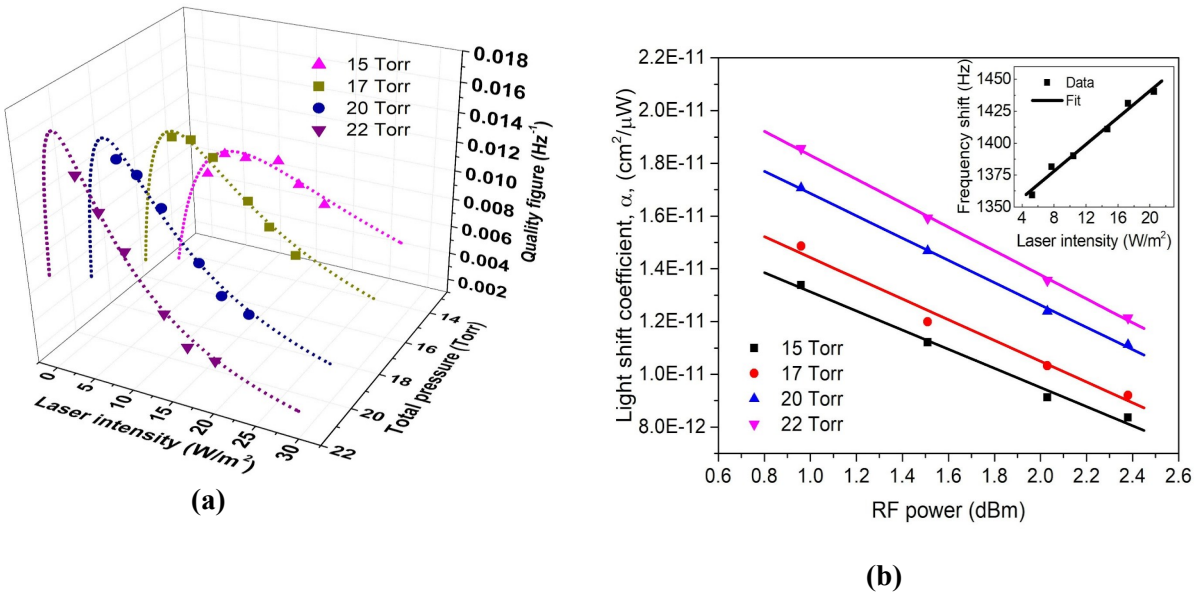

Fig. 1: (a) The change in *'q'* with laser intensity and buffer gas pressure. Dotted lines are theoretical fit to the experimental data points[1]. (b) Light shift coefficient as function of RF power. Solid lines are the linear fit.

References

1. Rajaiah et. al., *IJPAP, 60, 489-496 (2022).*
2. Vanier J, *Appl. Phys. B: Lasers and Optics, 81, 421 (2005).*

IFM126 Optical metrology using holo-shear lens

Lalit Mohan Pant [1], Mahendra Pratap Singh[1], Dali Ramu Burada[2], Chandra Shakher[3]*
[1] Instruments Research and Development Establishment, Dehradun, India,248008
[2] Department of Physics, Central University of Jharkhand, Ranchi, India, 835205
[3] Indian Institute of technology, (SeNSE), New Delhi, India, 110016

**Corresponding author: pant.lalitmohan@gmail.com*

A holo-shear lens is an optical component that produces lateral shear fringes either in single or orthogonal directions depending on the recording geometry of the holo-shear lens. In the present study, a holo-shear lens is developed to produce shear fringes in orthogonal directions and is utilised to establish the method for the measurement of spherical wavefronts. The measurements are validated with interferometry. The scheme is extended for the measurement of cylindrical wavefront.

The low cost solution for the profile metrology is the slope measurement techniques viz., the Foucault or knife-edge test, the Ronchi test, the Hartmann test, and the Shack-Hartmann test. These methods are very useful for the metrology of asymmetrical optical surfaces for which otherwise the interferometry requires auxiliary optics or computer generated hologram (CGH) which are test wavefront specific so very expensive. The shearing interferometry is very useful to extract the slope information of the wavefront. The common path nature of the shearing interferometer makes measurement less sensitive and useful for metrology applications. If a double frequency grating is written holographically, it is known as a holo-shear lens (HSL) and in a convergent beam, it produces the lateral shear fringe pattern [1,2]. A holo-shear lens is utilised to get the slope data to develop a metrology method for profile measurement. The experimental scheme is shown in Figure.1 (a).

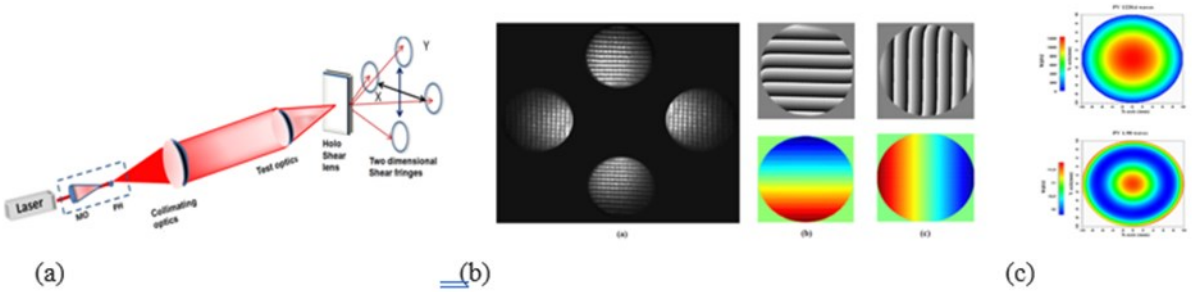

Figure1. (a) proposed scheme (b) The orthogonal shear fringes (c) The reconstructed profile and residual error

The method is developed for the spherical wavefronts for which various wavefront of different F# are taken. Figure 1(b) shows the shear fringes obtained from a spherical wavefront and Figure1(c) shows the reconstructed and residual error in the profile. The scheme is validated with the measurement of Fizeau interferometer and the results of the proposed method are comparable. The measurement is extended for the cylindrical profile. The scheme can be useful tool for freeform wavefront measurement.

References

1. Joenathan, C., et.al., *Optics communications 52.3 (1984): 153-156.*
2. Shakher, Chandra, et.al., *Applied optics 25.15 (1986): 2477-2479.*

IFM272

Depth resolved vibration line profiles with picometers sensitivity using a fully automated self-calibrated modified J_0 technique

Denny Melkay M George[1], Hari Nandakumar[1] and Shailesh Srivastava[1]*

[1]*Department of Physics, Sri Sathya Sai Institute of Higher Learning, Prasanti Nilayam, Sri Sathya Sai District, Andhra Pradesh – 515134*
**Corresponding author: dennymmgeorge@sssihl.edu.in*

We demonstrate the use of a custom-built line-field spectral domain optical coherence tomography (OCT) device for vibrometry. By using a linear fit to the zeroth order Bessel function near its first null, we achieve a self-calibrated reference that lends itself to automation. With an alternate-frame phase reversal of the sinusoidal driving waveform on the piezo mirror in the reference arm, the signal to noise ratio doubles, and also provides visualization of the phase of vibration of membranes, or inner reflecting layers. Low-cost automation of the image acquisition and signal processing is achieved using an Arduino microcontroller along with OpenCV based software on a PC. We demonstrate a sensitivity of 200 pm while also visualizing the vibration line profile of a latex membrane. Two CMOS cameras help in providing a conventional view of the region being imaged, and for acquiring the OCT data for vibrometry respectively. Our SD-OCT device operating at 850 nm provides a depth resolution of 18 µm and a lateral resolution of *18 µm X 50 µm,* along with a depth range of 3 mm. A sinusoidal sound signal from a speaker is used for excitation of the vibrating object. This is to our knowledge the first demonstration of using a very low-cost CMOS imaging camera-based SD-OCT for visualizing phase resolved vibration mode profiles.

Our technique has the potential to find application in depth resolved non-contact microelastography for detection of cancerous tissues.

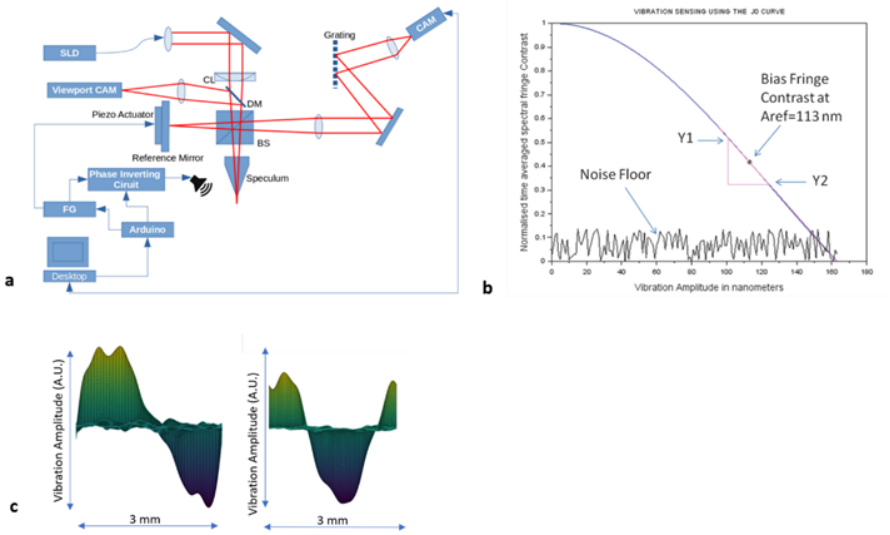

Figure a. Schematic of the setup used b. The curve of $J_0(2kA)$ vs amplitude of vibration A c. vibrational profiles of latex membrane showing linear cross-section of higher order vibrational mode containing nodes, positive and negative phases

References

1. D. Huang et. al., *Science*. 254(5035), 1178-81 (1991).
2. J. F. de Boer et. al., *Biomed. Opt. Express.* 8(7), 3248-80 (2017).
3. H. Nandakumar et. al., *OLEN.* 1275, 1005992 (2020).

IFM273 Background oriented schlieren imaging using smartphone

*Diganta Rabha[1], Vimod Kumar[1], and Manish Kumar[1]**

[1]Centre for Sensors, Instrumentation and Cyber-Physical System Engineering (SeNSE), Indian Institute of Technology Delhi, Hauz Khas, New Delhi-110016, India
**Corresponding author: kmanish@iitd.ac.in*

Background oriented schlieren (BOS) imaging is a useful technique for flow visualization. It allows for a large field of view imaging which is out of the reach of traditional mirror-based schlieren imaging. BOS implementation relies on high-end cameras, optics and computational software. While some authors have reported the use of mobile phones for capturing BOS raw images, they rely on external computational resources for the processing and visualization of the results. Here, we report a smartphone BOS system which not only captures images using a smartphone but also does all the processing on the smartphone We call our all-in-one smartphone schlieren as *pocket schlieren* to highlight its portability. The capability of smartphones in terms of hardware and processing power is well-known to all. In pocket schlieren, this enormous computational power and the superior quality optics embedded with the complementary metal oxide semiconductor (CMOS) image sensor have been exploited for schlieren imaging in real-time. To measure and reconstruct the density gradient image, the experimental setup is shown in figure 1(a), which requires a smartphone, a background pattern (which costs only Rs. 1) and the specimen under investigation. Our pocket schlieren application used for BOS visualization implements the optical flow algorithm to find the displacements (δy) in the image plane and finally the schlieren image. Thermal plumes and heat convection of soldering iron have been investigated using the proposed smartphone BOS system. From the quality of the obtained results, we are certain that pocket schlieren will prove to be useful for various scientific experiments as well as teaching and learning tools for general smartphone users.

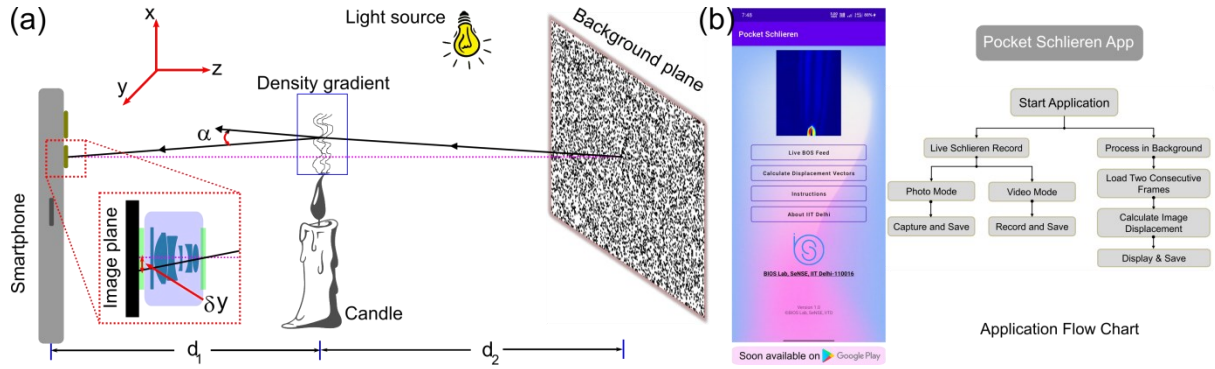

Fig. 1: Smartphone based BOS imaging. (a) Experimental setup, and (b) User interface and flow chart of the Pocket Schlieren Android application.

References

1. GS Settles et. al., *Optics and Lasers in Engineering 104, 9-21 (2018).*
2. A Martínez-González et. al., *Applied Optics 51, 3519-3525 (2012).*

IFM274 Total Leukocyte counting in diluted whole blood samples using fluorescence imaging

Bhargab Das[1,], Swati Bansal[1], Deepti R. Bathula[2], and Prateek Bhatia[3]*

[1]Micro and Nano Optics Center (μ-NOC), CSIR-CSIO, Chandigarh 160030, INDIA
[2]Department of Computer Science and Engineering, IIT Ropar, Ropar 140001, INDIA
[3]Department of Pediatrics, Advanced Pediatrics Center, PGIMER, Chandigarh 160012, INDIA
**Corresponding author: bhargab.das@csio.res.in*

Total leukocyte (i.e. white blood cell) count is the most basic requirements/tests for diagnosis, monitoring and treatment of several disease conditions in the human body. Leukocytes are one of the main defense mechanisms of our body against a wide spectrum of viral, bacterial, fungal etc. infections as well inflammations and allergies. The state-of-the-art blood cell counters are not optimal to meet the emerging needs of portable instruments for point-of-care sites such as physician offices, emergency rooms and other near patient settings. Therefore, an increasing amount of attention has been drawn towards the development of portable, easy-to-use blood cell count technologies. We demonstrate fluorescent labelling and imaging of white blood cells (leukocytes) in diluted whole blood samples (Figure 1). This technique involves very simple sample preparation together with inexpensive fluorescence imaging that makes it suitable for point-of-care device in situations that do not have access to central hematology laboratories. We have performed total leukocyte counting for 36 samples and the results show very good correlation with standard techniques.

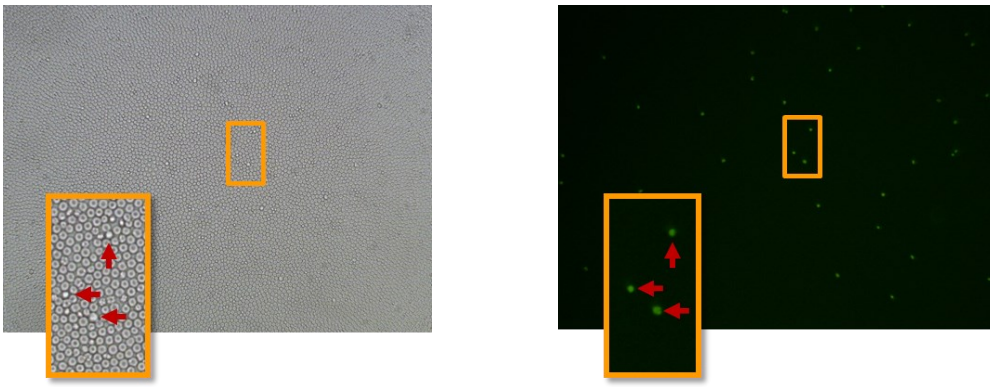

Figure 1: Brightfield (a) and fluorescent (b) image of the same sample slide captured using an eyepiece camera with 10X MO.

Acknowledgment:
The authors like to acknowledge DST, New Delhi, India for financial support through Bio-medical Instrumentation Hub at PGIMER, Chandigarh, India.

IFM275 Towards Realization of a Cold Atom Gravimeter for Field Applications

Hriday Dath, Radhika V. N, Pramod S S, Sasikumar K K, Rekha A R, Sasikumar S

ISRO Inertial Systems Unit, Thiruvananthapuram 695013, India.
E-mail: hridaysunildath@gmail.com

Interferometry using ultra cold ensemble of atoms harnessing the wave property of matter has garnered a lot of interest in recent years for developing very accurate quantum sensors [1-3]. It has been demonstrated

by numerous research groups worldwide for a wide range of applications exhibiting undeniable potential in inertial sensing, metrology, time keeping, studies on fundamental constants etc[4-5]. Our work attempts towards realization of a transportable gravimeter for field applications. We discuss the implementation of Magneto Optical Trap (MOT) of ^{87}Rb atoms in an optimized vacuum chamber, compact beam generation module and generation of atom cloud. The setup is presently realized in laboratory and we demonstrated coherent manipulation of ultra cold ^{87}Rb atoms with Raman laser pulses.

A compact ultra-high vacuum chamber was designed and realized in Titanium with viewports along the chamber surface for admitting laser beams. Chamber view ports were designed to have exact orthogonal alignment in the 6 cooling beam axis and laser beam collimator mounts are attached to body of chamber ensuring self alignment of MOT beams. Rb metal dispenser (SAES^{TM}) is placed in ultra-high vacuum using an electrical feed through in a view port. Magnetic Coils configured in Anti Helmholtz configuration were designed to produce a non uniform magnetic field of 12 G/cm and mounted to the chamber using recessed flanges to reduce heating. The optical circuit for beam generation was realized with half inch optics with optimized footprint in a board of area 60 cm x 40 cm. Raman beams are used for stimulated transfer of atom populations between two internal states that are energetically separated via a virtual state. Unlike the conventional Raman beam setup involving two separate frequency locked laser sources, here the beams are generated from a single seed laser source by using an Electro optic Modulator as per schematic in Fig 2. Raman beams are far detuned by 1.8 GHz (Δ) from the excited level and beams are frequency separated by 6.835 GHz (ω_{12}) corresponding to the ground state frequency separation of ^{87}Rb. Ultra cold atomic ensemble was accomplished at 15 μK, and successfully obtained sustained Rabi oscillations with frequency closely matching to the theoretical value. Further pursuing momentum transfer between the atomic states, which is an important attribute of two photon transitions for atom interferometry.

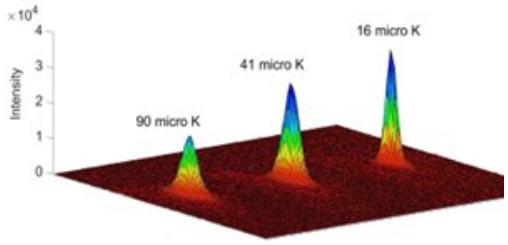

Fig 1: Intensity profile of atom clouds

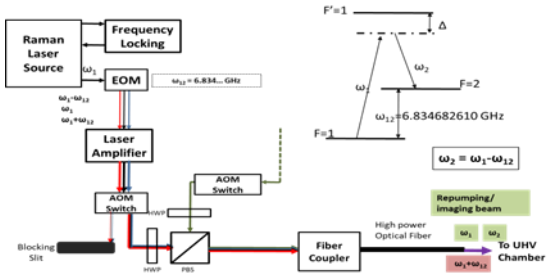

Fig 2: Schematic of Raman beam generation setup

References

1. X. Wu et al., Science advances, 5, 20 (2019)
2. V. M´enoret et al., Scientific reports, 8, 1-11 (2018)
3. K. Bongs et al., Nature Reviews Physics, 1, 731-739 (2019)
4. P. Asenbaum, M. A. Kasevich et al., Physical Review Letters, 125, 191101 (2020)
5. R. Geiger, A. Landragin, S. Merlet, and F. Pereira Dos Santos AVS Quantum Science, 2, 024702 (2020)

IFM276

Spectral Characterization of Linear Variable Filter (LFV) for Imaging Spectrometer

Kanchan Chandra[*], *Abhijeet Chakraborty* , *Dr. Sudhir Khare*
Instrument Research and Development Establishment, Dehradun
kanchan_irde@rediffmail.com

Abstract: Linear variable filters (LVF), also known as continuously variable filters, or gradient filters, are special types of filters, where the filters' spectral response changes continuously (or quasi-linearly), in a defined manner, along one dimension. LVFs are commonly used in various scientific, industrial, and research applications, such as spectroscopy, fluorescence analysis, and hyperspectral imaging. The key characteristic of an LVF is its ability to transmit or reflect light of different wavelengths at varying positions along the length of the device. We have developed a test setup for characterization of Linear Variable Filter (LVF) and spectral characterized the Linear variable filter. Before the performing the spectral characterize, we calibrate the test setup using a reference sample. Different parameter like spectral transmittance along the dimension, linearity of spectral position etc.

Introduction: Linear Variable Filter is widely used in Hyperspectral imaging for remote sensing. Spectral quality of the hyper spectral imaging sensor depends on the LVF, so spectral characterization is important and recommended to characterize the LVF before use it in the optical instrument[1].

Description of test setup: The test setup for the spectral characterization of LVF is comprises a Spectro-Radiometer with spectral resolution of 0.3 nm. There are two lens module of F number not greater than F# 3. The test setup is kept at the front of a broad brand collimator with a slit target and illuminated with a broad brand source (0.3 – 1 µm).

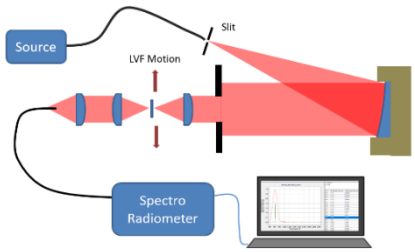

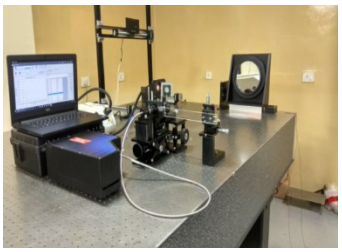

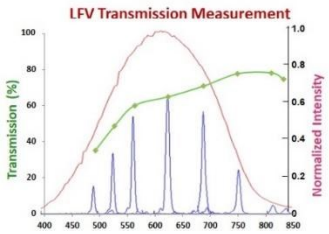

Figure 1: Layout of the Test Setup Figure 2: image of the developed Test Setup Figure 3: Measurement Result

The first lens module collects the radiation and incident on a very small spot at the LVF. The transmitted radiation then collected by the send lens module and coupled with a fiber optics cable which is connected with a spectro-radiometer. The LFV is mounted at the focal plane of the two lens module (common focal plane) with a 3 axis micro meter stage. The micrometer stage axis along the optical axis is used for the placement of the LVF at the common focal plane of the two lens module while other two axes are used for the spectral position change and keystone effect of the LFV. Calibration of the test setup: The calibration of the test setup is carried out using a 2 mm thick parallel glass plate (NBK7). The spectral transmission of the reference parallel glass plate is measured with a Fourier Transform Spectrometer (FTIR) which is calibrated with international standard.

Result: The spectral transmission of the LVF has been measured by using the developed test setup and the result is shown in the figure 3. The spectral transmission is increasing with the wavelength of the radiation.

Acknowledgement: The authors are grateful to Dr. Ajay Kumar, Director IRDE, for his encouragement and permission to publish this work.

References

1.Measurement and alignment of linear variable filters.Rob Sczupak, Markus Fredell , Tim Upton, Tom Rahmlow, Sheetal Chanda, Gregg Jarvis, SarahLocknar, Florin Grosu, Terry Finnell and Robert Johnson Omega Optical, 21 Omega Dr, Brattleboro, VT 05301.

IFM278 Silcon Beam-splitter for Multiwavelength bands

Rouchin Mahendra[1,2], Satyavir[1], BB Nautiyal[1], J R Meena[1], L M Pant[1], Ramesh Chandra[2]*

[1]Instruments Research & Development Establishment, Dehradun 248008, India
[2]Indian Institute of Technology Roorkee, Roorkee 247667, India
**rmahendra.irde@gov.in*

Multiwavelength bands electro-optical/infrared payloads are being developed for a variety of defence and commercial system applications. Many applications depend on its ability to detect and recognize low-contrast and distant targets in a complex environment. The development of such systems necessitates the use of specialized optical filters capable of separating different wavelength bands. In this work a silicon-based plate beam splitter for 45-degree angle of incidence has been developed to separate the bands from visible to mid-wave infrared (MWIR). This silicon beam-splitter separates MWIR from visible and near infrared (VNIR) and short wave infrared (SWIR).
In this paper, we have designed and developed this silicon beam-splitter for the payload that range from visible to mid-wave infrared. TFCalc 3.5.9 [1] thin-film software was used to design a dichroic[2]coating using variable metric method. Reflection and transmission spectra are shown in Figure 1.

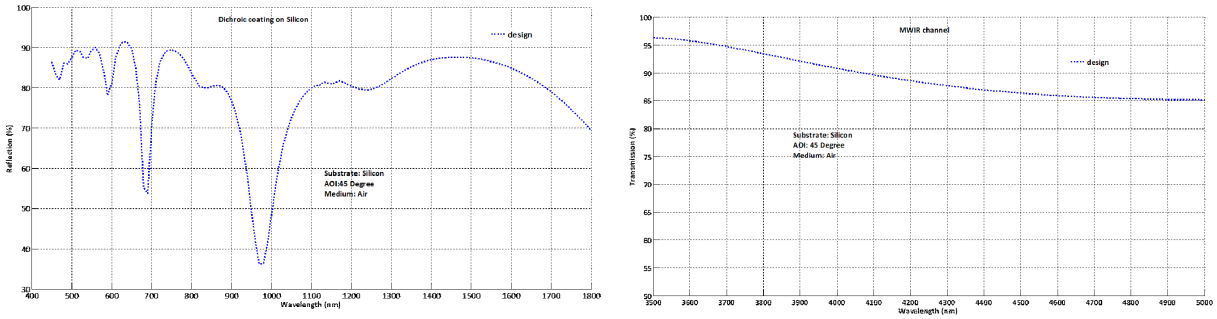

Figure 1: Reflection & Transmission curve for BS1: VNIR, SWIR & MWIR wavelength region

The thin-film was deposited on a silicon substrate with a diameter of 25 mm and a thickness of 3 mm using an ion-assisted electron beam evaporation coating system (M/S Tecport Optics Inc., Model: Symphony 9). An average reflection of ~75% in visible and ~83% in SWIR region was measured using double beam spectrometer 1050 (Make: M/s Perkin Elmer). An average transmission ~85% in the MWIR region was measured using FTIR frontier spectrometer (Make: M/s Perkin Elmer).

References

1. http://www.sspectra.com/index.html, “TfCalc: Software Spectra, Inc.”
2. H. A. Macleod, “A New Approach to the Design of Metal-dielectric Thin-film Optical Coatings,” *http://dx.doi.org/10.1080/713819742, vol. 25, no. 2, pp. 93–106, 2010, doi: 10.1080/713819742.*

IFM279

Spectroscopic Detection of Potassium and Phosphorous in Soil Samples

S. K. Pal*, P. K. Dey, P. Ganguly and S.K. Das Mandal

Advanced Technology Development Centre
Indian Institute of Technology, Kharagpur, 721302, India.
*skpal902@kgpian.iitkgp.ac.in**

Detection of phosphorous (P) and potassium (K) in soil is necessary to determine its absolute content, which directly effects the crop health and growth [1, 2]. In this work an optical setup has been used to determine the absorption wavelengths of these two macronutrients in different soil solutions. A quartz tungsten halogen lamp (wavelength range: 200-2500 nm, Model No. 66187, Oriel Instruments, USA) of 1000 watt maximum power was used for this experiment as a white light source. Light was passed through the cuvette containing soil sample and transmitted light was coupled to an OSA (Model No. MS9740A, Anritsu, USA). This OSA can operate within the wavelength range from 600 – 1750 nm. Initially, white light spectrum without soil sample was recorded, which was used as a calibration data. Then only P and K spectrum of different soil samples were extracted. Figure-1 shows typical experimentally obtained absorption dips for known K and P components in different soil solutions. It can be

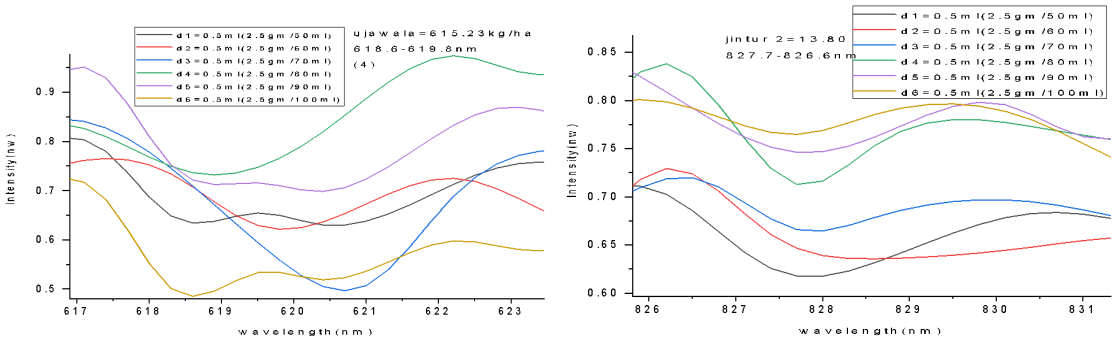

(a) (b)

Fig. 1: Transmission spectrum of (a) K and (b) P for a number of soil solutions.

noted from Fig.1, that K-absorption occurs within the wavelength range from 618.6 to 619.8 nm, whereas for P it is within 826.6-827.7 nm. We have also observed a linear relation between the K content in the soil and the absorption dip-wavelength for it. One may also correlate the absorbed light intensity with the amounts of P and K present in the soil samples, which will finally yield an in-situ optical sensor for detection of the amount of these macronutrients in soil. Detail experimental results for a number of soil samples (36 for K and 18 for P) will be discussed during the presentation of the paper.

References

1. P. Manikandan, et.al., Soil nutrients monitoring and analyzing system using Internet of Things. 2nd International Conference on Advance Computing and Innovative Technologies in Engineering (ICACITE), Greater Noida, India, pp. 301-305 (2022).
2. M. Masrie, et al., Integrated optical sensor for NPK Nutrient of Soil detection, IEEE 5th International Conference on Smart Instrumentation, Measurement and Application (ICSIMA), Songkhla, Thailand, pp. 1-4 (2018).

IFM280 Low Force Sensor using Digital Speckle Correlation

Surya Kumar Gautam[1], Vikas[1], Rajesh Kumar[1]*

[1]National Physical Laboratory, (CSIR-NPL)
New Delhi, Delhi 110012, India
**Corresponding author: suryagautam89@gmail.com*

We have undertaken the design and development of a force sensor specifically engineered for non-destructive measurement of forces within a low range, in contrast to traditional strain gauge-based force sensors [1]. The schematic representation of our force sensor is shown in Figure 1(a). This force sensor comprises a force-sensing element, a laser, and a CCD camera. The force-sensing element incorporates two beams; the lower beam is responsible for stabilizing and supporting the element, while the upper beam is tasked with force detection. Illumination of the upper beam is achieved through laser light, causing the field scattered by this beam to generate a speckle pattern at a distant plane. To capture this pattern, a CCD camera is positioned at the far plane, recording a reference speckle pattern (I_1). Subsequently, we apply a known force (F) using a standard weight under a constant gravitational acceleration. As a result, the upper beam undergoes a downward bending, leading to a slight shift in the speckle pattern. This shifted speckle pattern (I_2), is then recorded and subjected to comparison with the I_1 through the digital speckle correlation technique (DSC). By evaluating the disparities between these patterns, we compute slopes and present them in Figure 1(b) with respect to consecutive weights. In order to process the acquired data, we employ the DSC technique, as depicted in Figure 1(c).

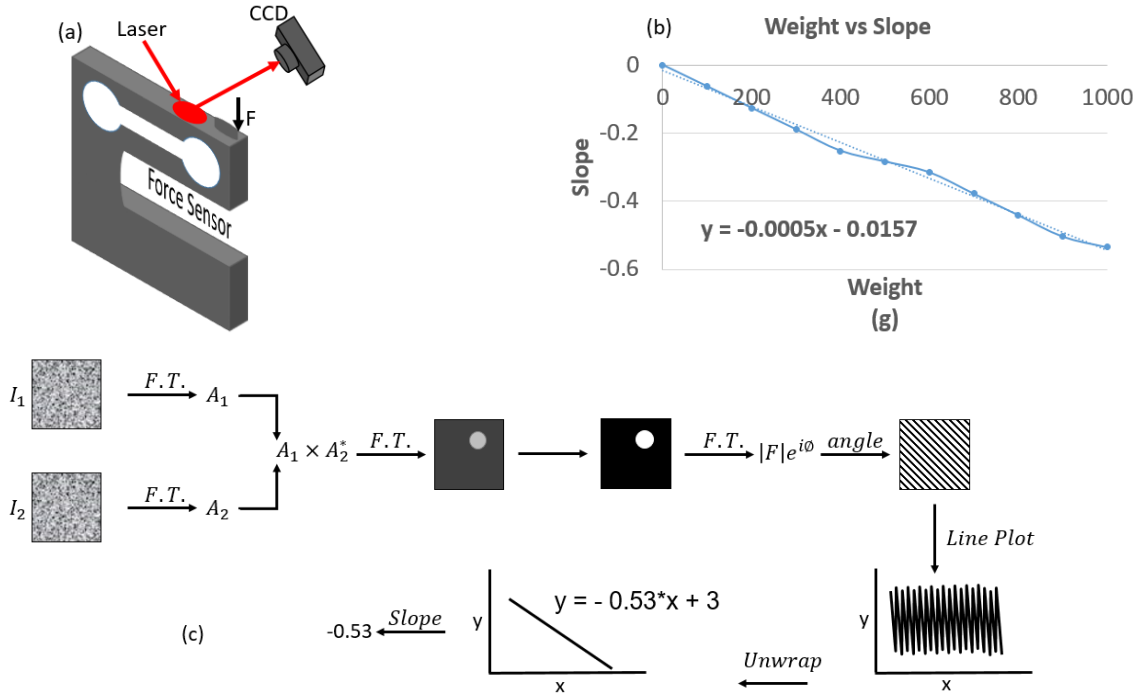

Figure 1

References

1. Liu M et. al., *Micromachines 10, 20 (2018).*

IFM281

Design and manufacturing of blazed grating based waveguide for near eye displays

Naresh Kumar[1], Rahul Rohila[1] Vinod Mishra[1, 2], Harry Garg, [1,2]*

[1]AcSIR-Academy of Scientific and Innovative Research, Ghaziabad, Uttar Pradesh, India
[2]CSIR-Central Scientific Instruments Organisation, Chandigarh, India
**Corresponding author: vnd.mshr@csio.res.in*

Near-eye displays find diverse applications in fields such as augmented reality, virtual reality, military training, medical surgery, and more. They immerse users in interactive digital experiences, enhance visualization in complex tasks, and offer real-time information overlay, making them indispensable tools for a wide range of industries and applications. Waveguide is one of the most component for near eye displays. Further, the design and manufacturing of blazed gratings are most crucial steps for development of efficient waveguides. The grating's functionality lies in its ability to efficiently couple and manipulate light, enabling immersive and high-resolution visual experiences. These precisely designed diffraction gratings redirect the incoming light with high accuracy. The optimized blazed profile of the gratings ensure the high diffraction efficiency and ensuring minimal light loss. Figure 1 shows the schematic of waveguide along with different design parameters

The fabrication of blazed gratings begins with a precision machining by diamond turning process, which imparts intricate grating structures onto a master stamp. Subsequently, a nanoimprinting process is employed to replicate these blazed grating structures with nanoscale precision across a waveguide's surface. The design and fabrication of blazed gratings through diamond turning and nanoimprinting open up new paths for compact, high-resolution, and immersive optical systems, paving the way for the next generation of wearable technology.

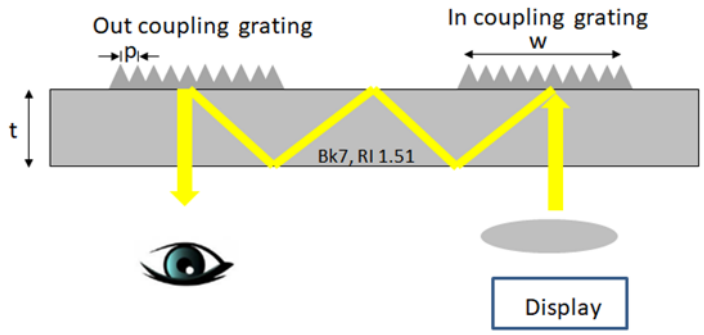

λ is design wavelength, p is grating periodicity, t is waveguide thickness, w is grating width (w)

Figure1: Schematic of waveguide for near eye display

Category 15

Optical Materials (MAT)

MAT277 Fabrication Study of Indigenously developed Broad band Chalcogenide Glass

#Neeraj Pandey[1], Raghvendra Singh[1], M. P. Singh[1], Amit Agrawal, K. K. Pant[1], D K Mishra[1], L M Pant[1], Rana Das Gupta[2], K. Annapurna[2], Ajay Kumar[1]

[1]Instruments Research & Development Establishment, Dehradun, 248008, India
[2]Central Glass and Ceramic Research Institute, Kolkata, 700032, India

#e-mail: neerajpandey.irde@gov.in

Infrared transmitting glasses are used for thermal imaging camera to enhance the night vision capability of an observer. chalcogenided glasses are suitable choice to cover the broader infrared band of electromagnetic spectrum. Under a collaborative project between DRDO and CGCRI Kolkata, an arsenic free chalcogenide glass has been developed having spectral transmission from 1 µm to 14 µm. The present work reports the study on the fabrication of optical component in indigenously developed chalcogenide glass and their characterization results. Imaging cameras working in short wave infrared (1µm-2µm), medium wave infrared (3µm-5µm) and long wave infrared (8µm-12µm) provide more information as compared to visible band. Optical glasses are useful in visible and short wave infrared. Silicon and germanium are used in medium wave infrared and long wave infrared. However due to their crystalline nature, fabrication is difficult and costly. Chalcogenide glasses provide a solution for infrared band, as they are easy to produce in bulk quantity and moulding process can be applied due to their low softening temperature. The constituents of developed chalcogenide glass are Ge, Sb and Se and having broadband transmission from 1µm to 1µm, so that it cover SWIR, MWIR and LWIR band of EM spectrum. The refractive index is 2.63 at 4µm wavelength. One flat sample of chalcogenide glass was polished using pitch polishing, while another flat sample is also fabricated using single point diamond turning machine. Fig: 1(a) and 1(b) display the samples and transmission measurement, while Fig: 1(c) and 1(d) display the results for surface profile and roughness measurement.

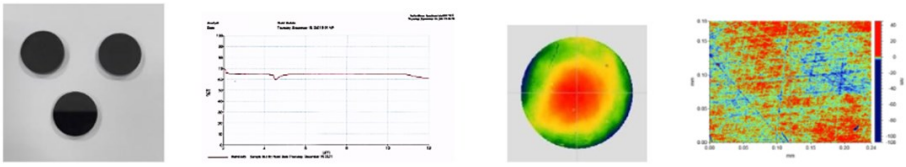

(a) (b) (c) (d)

Fig 1: (a) Chalcogenide glass samples (b) Transmission measurement (c) Surface form error 210 nm peak to valley (d) Surface roughness Ra 1.13 nm

References

1. D. F. Horne, Optical Production Technology, 2nd ed., Adam Hilger, Bristol (1983)
2. Robert E. Parks, *Optical Engineering, 33(3), 685-692 (1994).*
3. Amitava Ghosh et al, *Journal of Optics, 48, 266-271 (2019).*

MAT300 Enhanced UV emission: The substrate effect

*Amegha Sahni[1], Annie Sujatha[1]**

[1]Department of Physics and Nanotechnology, SRM Institute of Science and Technology, Kattankulathur, Tamilnadu -603203

**Corresponding author: anniesur@srmist.edu.in*

Despite ZnO being recognized as a robust UV emitter at room temperature, several reports include visible emissions (deep level emission/DLE), which have the potential to degrade the UV emission (UVE). Here, UVE of ZnO thin film has been studied with low cost and reliable deposition technique of sol-gel spin coating. This analysis compares ZnO thin films on two substrates with differing crystalline and conducting natures: micro glass slides (amorphous and non-conducting) and FTO substrates (crystalline and conducting), considering the fact that the substrate is plausible to affect the growth mechanism, which in turn can influence the crystalline as well as every other attribute of the material [1]. From figure 1, it is clear that the photoluminescence (PL) peak at UV region, 3.11 eV (398 nm) is intense for ZnO/FTO along with a diminished DLE. The reverse is the case with ZnO/glass, due to the native defects especially zinc vacancies, which are more likely to occur in n-type ZnO and play a significant role in generating visible green emission at approximately 500 nm [2]. The change of substrate did not affect the morphological and structural traits, but minimized the native defects to a greater extend owing to the increased crystallinity and decreased strain when grown on a crystalline and conducting substrate. The study underscores the significance of a substrate together with the possibilities for enhancing the optical properties of a material.

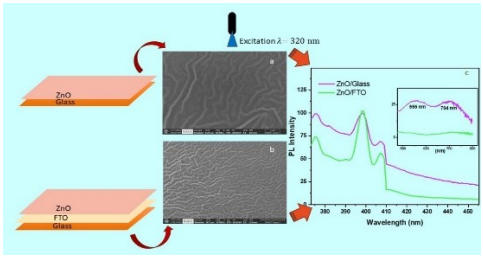

Figure 1; a and b are the HRSEM images of ZnO thin films coated on glass and FTO respectively. C depicts the photoluminescence spectra of both the specimens and the inset shows the visible emission.

References

1. E. Hasani et. al., *Journal of Electronic Materials*. 48, 4283-4292 (2019).
2. Janotti et al., *Reports on progress in physics*, 72, 126-501 (2009).

MAT-301 Photoluminescence properties of Eu:YVO_4 by co-doping monovalent (Li, Na, K) through economical Combustion method for various applications

*Anuradha[1], Arpita Dwivedi[1], Satyam Upadhyay[1], Amritanshu Pandey[2], Sanjay K. Srivastava[1]**

[1]Department of Physics, BHU, Varanasi-221005, India

[2]Department of Electronics Engineering IIT(BHU), Varanasi-221005, India

**Corresponding author: sanjay_itbhu@yahoo.com*

Lanthanide (Ln)-doped inorganic luminescent materials have been studied for applications in optoelectronics and biomedical applications including drug delivery, optical and magnetic imaging. Further, the inorganic nanoparticles have several advantages such as high photostability, narrow emission bandwidths, ab-

sence of blinking and long luminescence lifetime of the Ln^{3+} ions, which is highly desirable for sensitivity and bioimaging. The organic host provides a steady microenvironment for the Ln^{3+} emitters; low cytotoxicity as the host matrix traps the Ln^{3+} and tunability of the Ln^{3+} emission by designing the morphology and composition of the host material. The Ln^{3+}doped luminescent nanomaterials must be improvised to yield better emission efficiency, longer lifetime, and excellent photostability. So, choosing the material and devising a method to enhance luminescence outcome is paramount. In this context, yttrium orthovanadate (YVO_4) is an inorganic mixed metal oxide of great significance as it is a self-activated host.

Trivalent europium (Eu^{3+}) ions are excellent activators for red light generation in the YVO_4[1] matrix since there is strong VO_4^{3-}-Eu^{3+} energy transfer via exchange interaction which is favored by the overlapping of wavefunctions. There are also reports on methods to enhance the luminescence emission such as codoping with certain metal (mono-, di-, or tri-valent) ions in appropriate stoichiometry, tuning of synthetic parameters, and morphological variations.

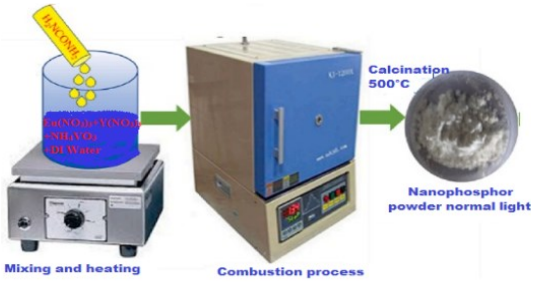

Fig.1. Synthesis of Eu:YVO_4 nanophosphor powder

Monovalent like Li^+, Na^+, and K^+-doped Eu:YVO_4 luminescent nano phosphors have been synthesized by cost-effective combustion technique. Various characterizations XRD, UV, PL, and FTIR were carried out to confirm successful formation of structures. Therefore, the nano phosphor is suitable for LEDs and other optoelectronic applications. The findings point towards the prospective future application of nano phosphor materials for anti-counterfeiting purposes as security ink and visualization of latent fingerprints for forensic purposes.

References

1. Dwivedi, A., et al., *Synthesis and enhanced photoluminescence properties of red emitting divalent ion (Ca2+) doped Eu: Y2O3 nanophosphors for optoelectronic applications.* Journal of Rare Earths, 2022. **40**(8): p. 1187-1198.

MAT302 Hydrothermal Synthesis of Colloidal VS_2 Quantum Dots for the Sensing of Ferric ion Turn-Off Fluorescence

Anushka Yadav[1], Pinky Sagar[2], Rajneesh Kumar[1,], S. K. Srivastava[1,]**

[1]*Department of Physics, Institute of Science, Banaras Hindu University, Varanasi, U.P., 221005*

[2]*Department of Physics, Mahila Mahavidyalaya, Banaras Hindu University, Varanasi, U.P., 221005*

**Corresponding Authors Email: rajneeshipr@gmail.com (Rajneesh Kumar) and sanjay_itbhu@yahoo.com (S. K. Srivastava)*

Quantum dots (QDs) are a prospective alternative to traditional organic fluorophores because they have exceptional physical and chemical characteristics, such as tunable photoluminescence, tremendous photostability, a significant Stokes shift, and an outstanding quantum yield[1]. TMD (Transition Metal Dichalcogenide) QDs, represented as MX_2 (M = Mo, W, and V..., X = S or Se), have a wide range of applications

because of their distinct physical, chemical, and electrical characteristics, such as high surface-to-volume ratios (due to small size), optoelectronic behavior, indirect bandgaps, stability, and quantum confinement effects[2].

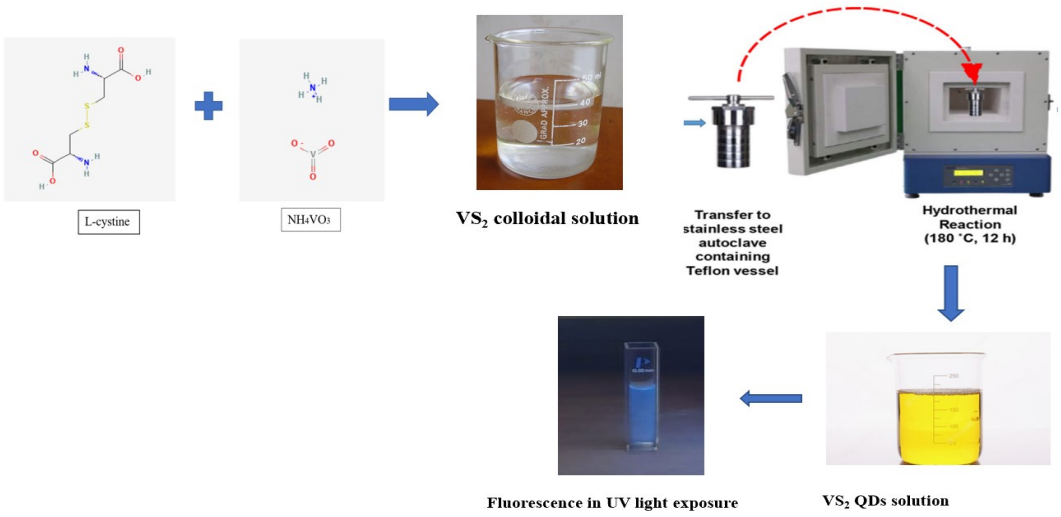

Fig. 1. Schematic illustration for synthesis procedure of VS2 QDs

In this work, hydrothermal synthesis, which is considered as an economical and eco-friendly approach that avoids complex procedures, difficult synthesis conditions, and uncontrollable product outcomes, has been adopted to synthesize VS_2 QDs. Further, the as-synthesized QDs have been employed as a fluorescent probe for the detection of Fe^{3+} ions. Interestingly, it is observed that the fluorescence of VS_2 QDs significantly quenched in the presence of Fe^{3+} ions. Also, the linear range of the sensor is found to be in the range of 25 nM to 1 µM. To validate the sensing experiments, PL (Photoluminescence) and TRPL (Time Resolved Photoluminescence) studies have been conducted, which depict that the quenching phenomena are both static and dynamic in nature.

References

1. Du, C., et al., *Water-soluble VS2 quantum dots with unusual fluorescence for biosensing.* Sensors an Actuators B: Chemical, 2018. 255: p. 926-934.
2. Kumar, R., et al., *Highly sensitive amoxicillin immunosensor based on aqueous vanadium disulphide quantum dots.* Journal of Electroanalytical Chemistry, 2021. 892: p. 115266.

MAT303 A Eu^{3+}doped functional nanophosphor as fluorescent biosensor for highly sensitive detection of dsDNA

Arpita Dwivedi[1], S. K. Srivastava[1]**

[1] Department of Physics, Institute of Science, Banaras Hindu University, Varanasi-221005, India

**Corresponding author: joinarpit@gmail.com, sanjay_itbhu@yahoo.com*

The revealing aspect of qualitative and quantitative presence of biological markers alongside other analytes, including DNA, proteins, and carbohydrates, can indicate disease states and physiological progressions. Sensitive and accurate detection of these at low levels has the unique advantage of potentially being used for identifying the earliest sign of cancer, TB, HIV, malaria, and other disorders [1,2, 3]. Lanthanide-doped core-shell nanomaterials have illustrated budding potential as luminescent materials, but their biological applications have still been very limited due to their aqueous solubility and biocompatibility. Hence, in present work we have reported a simple method for the synthesis of chitosan functionalized lanthanoid based core shell (Ca-Eu:Y_2O_3@SiO_2) phosphor. The chitosan functionalized Ca-Eu:Y_2O_3@SiO_2

phosphor contains hydroxyl, and amino groups which coordinate with the dsDNA and causes fluorescence enhancement and act as "turn on" sensor Fig. 1(a). The ratio of fluorescence intensity enhancement of phosphor is proportional to the concentration of dsDNA. The range 0.1–90 nM, with the limit of detection at ~16.1 pM under optimal experimental conditions Fig. 1(b). The enhancement in fluorescence response of functionalized core-shell phosphor with dsDNA is due to the antenna effect. Additionally, response of probe has been studied for the real samples.

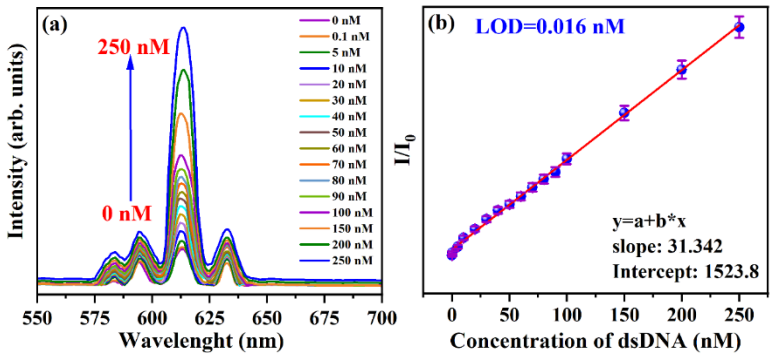

Fig. 7(a) Photoluminescence spectra of CEY@SiO_2-chitosan functionalized core-shell phosphors in the presence of different concentrations of dsDNA (b) curve is the characteristic peak emission intensity at different concentrations.

References

1. Godavarthi, S., et al, J. Photochem. Photobiol., B, 172, 36-41 (2017).
2. T. Arslan, et al , Anal. Biochem., 591, 113540, (2020).
3. B.T. Murti, et al, J. Photochem. Photobiol., B, 188 (2018) 159-176.

MAT304 Upconversion and Photoacoustic spectroscopic study of Er^{3+}/Yb^{3+} doped YVO_4 prepared via combustion synthesis method

*K V Cinumon[1], Kaushal Kumar[1]**

[1]Optical Materials and Bio-imaging Research Laboratory, Department of Physics

Indian Institute of Technology (ISM) Dhanbad, Jharkhand, India - 826004

**kkumar@iitism.ac.in*

Photoacoustic spectroscopy was developed as a result of Graham Bell's discovery of the photoacoustic phenomenon in 1880. In 1975 Allan Rosencwaig and Allen Gersho proposed the theoretical explanation of the photoacoustic effect in solids. This unique technique is very effective for studying the non-radiative transitions in samples while they interact with light.

In this study ytterbium (Yb^{3+}) and erbium (Er^{3+}), co-activated yttrium orthovanadate (YVO_4: Er^{3+}/Yb^{3+}) powder phosphors were synthesized by solution combustion method and were annealed at 800^0C for 2 hours. The X-ray powder diffraction (XRD) patterns confirmed that the zircon-type tetragonal structure of YVO_4 having space group $I4_1/amd$ was crystallized. The Debye-Scherrer equation is used to calculate the crystalline size (D) of the particles and the average size was found to be around 114.25 nm. The scanning electron microscopy (SEM) image showed particles of different shapes having their sizes in the micrometre range. Upconversion (UC) emission and constant wavelength mode photoacoustic (PA) spectroscopic study (by varying the chopping frequency) of the samples was done using a laser having a wavelength of

980nm. The thermal transition frequencies of the samples are also calculated from the Ln(f) – Ln(PAS) plot.

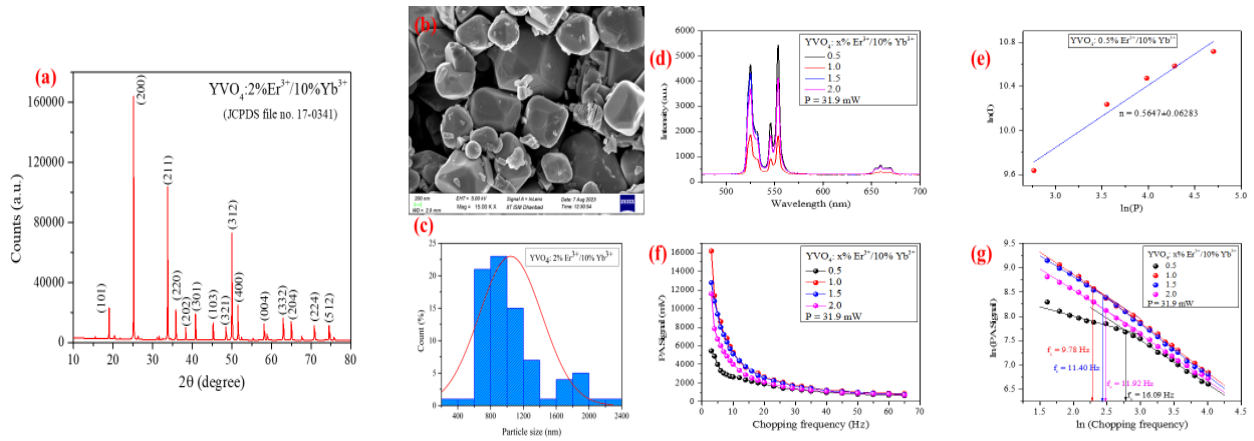

References

1. Bell, A.G., *Journal of the Society of Telegraph Engineers*. 9(34), 404–426 (1880)
2. Rosencwaig et al., *Journal of Applied Physics*. 47(1), 64–69 (1976)
3. G. Lohmueller et al., *Acta Crystallogr., Sect. B: Struct. Crystallogr. Cryst. Chem*. 29, 141–142 (1973)

MAT305 *In-situ* One-pot Novel Synthesis of $MoTe_2$@C Nano-Dots for Sensitive and Selective Detection of Hydrogen Peroxide Molecules via Turn-off Fluorescence Mechanism

Dr. Pinky Sagar[1], Prof. S. K. Srivastava[1]*

[1]1Department of Physics, Institute of Science, Banaras Hindu University, Varanasi-221005

**Corresponding author: sanjay_itbhu@yahoo.com*

Transition metal dichalcogenides (TMDs) have garnered significant attention due to their remarkable characteristics for optical, biological, chemical, and medicinal applications. We present a novel in-situ one-pot hydrothermal synthesis method for creating molybdenum ditelluride@carbon nano-dots ($MoTe_2$@C NDs) and explore their biosensing potential. Characterization using XPS, Raman, and TEM confirms $MoTe_2$@C NDs' structure. Photophysical properties reveal cyan fluorescence upon UV light exposure (λ = 365 nm) with a PL peak at ~431 nm (excitation wavelength ~350 nm). The synthesized sample effectively senses hydrogen peroxide (H_2O_2), displaying linear PL intensity decrease (R^2 = 0.9986) with H_2O_2 concentration and a detection limit of 14.22 nM. The PL quenching mechanism is explained using a three-level kinetic model involving charge-separated trap states ($1[D^+\cdots A^-] \leftrightarrow 3[D^+\cdots A^-]$). This innovative study holds promise for $MoTe_2$@C NDs' use as an H_2O_2 sensor in diverse applications.

MAT306

Enhanced Nonlinear Optical properties of ZnS with carbon encapsulated core-shell nanostructures.

Athulya K.S[1] *, JatinderbirSingh* [2] *Chandrasekharan K*[*]

Laser and Nonlinear Optics laboratory, Department of Physics, National Institute of Technology, Calicut-673601

[*]*E-mail address: csk@nitc.ac.in*

Due to the emergence of powerful lasers, there is a growing demand for enhanced protection of sensors and eyes against intense laser beams. Scientists are consistently exploring materials that can transmit low-intensity light while effectively absorbing high-intensity light, a category referred to as optical limiters [1].

Carbon wrapped nanoparticles are known for their exceptional nonlinear optical properties and ultrafast response[2]. In this study, we investigated the enhanced absorptive nonlinearity and optical limiting behaviour of Zinc Sulfide (ZnS) nanoparticles with graphite shell/core structure. The ZnS@C core-shell nanostructures were prepared by nanosecond Pulsed Laser Ablation in Liquid (PLAL) technique. A distinct absorption peak at 288 nm confirms the presence of a graphite layer around the ZnS nanoparticles and shoulder peaks in the broad UV absorption spectra between 309–345 nm can be attributed to the combination of the band of ZnS nanoparticle and π–π* transition of C=C bands of graphite .

The non-linear optical properties of core-shell nanostructure is investigated with the open aperture Z-scan . Nonlinear absorption coefficient for the core-shell structure is enhanced by three times as compared to pristine ZnS nanoparticles. The sample exhibits excellent optical limiting threshold value, make it suitable for use in optical power limiting and laser precautionary measures."

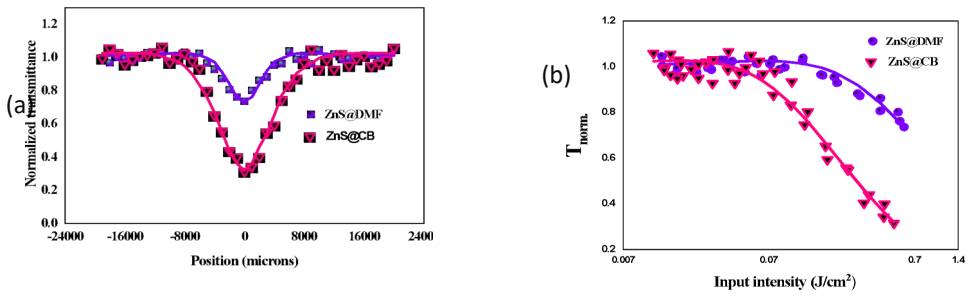

Fig: Open aperture Z-scan signature(a) and Optical limiting behavior (b) of ZnS@C core-shell structure (pink) and pristine ZnS nanoparticles (violet) at 0.138 GW/cm^2

References

1. Rashidian et.al., Rev. Adv. Mater. Sci. 40, 110-126, 2015
2. Shiju E et.al., Nano Ex.1 030026, 2020

MAT307 Synthesis, Structural, Optical and Photoluminescence properties of Samarium doped $Zn_3(VO_4)_2$

*Jaya Choudhary[1], Dr. Upendra Kumar Kagola[1]**

[1]Department of Physics, School of Applied Sciences, REVA University, Bangalore, Karnataka -560064

**Corresponding author: upendra80@gmail.com*

Among many phosphors, metal vanadate's are known as rare earth free luminescence materials and so applicable to optoelectronic devices[1]. $Zn_3(VO_4)_2$ is abbreviated as ZVO has potential applications in catalysis, low temperature magnetic devices, and batteries[2,3]. The broad emission profile of ZVO ranges from 400-900 nm. Considering the efficient energy transfer from VO_4^{3-} group to Sm^{3+} ions, it was selected as the dopant. In this work, the Sm^{3+}-doped $Zn_3(VO_4)_2$ microparticles were synthesized by a facile sol–gel technique and their phase structure, morphology and PL properties were investigated with different concentration of Sm^{3+} i.e., ZVO:Sm^{3+}(0%, 1%, 2%, 3%, 4%, 5%).

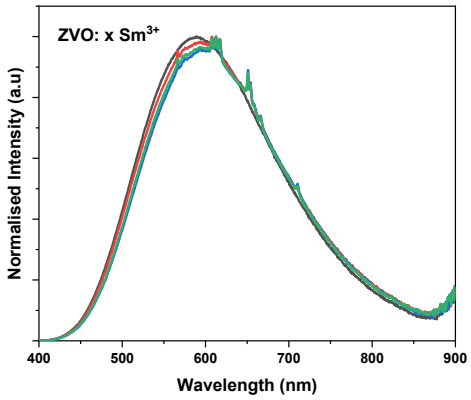

Figure: Photoluminescence spectra of ZVO: xSm^{3+} (x= 0, 2,3,4 mol%) under UV excitation.

References

1. Chauhan et. al., *Optic*. 238 (2021): 166682.
2. Bhuiyan et. al., *Cogent Phys*. 3 (2016): 1265778.
3. Zhu et. al., *Phys.Chem*.C 116 (2012): 2297-2302

MAT308 Cellulose acetate based photopolymer film for holographic application

*Komal Sharma[1,2], Girish C Mohanta[1,2] Bhargab Das[1,2] , Raj Kumar[1,2]**

[1]CSIR-Central Scientific Instruments Organisation, Chandigarh 160030, India

[2]Academy of Science and Innovate Research, Ghaziabad 201002, India

** E-mail address of corresponding author: raj.optics@csio.res.in*

Optical biosensing offer advantages of higher selectivity, sensitivity and cost effectiveness [1]. Recently, holographic biosensors using photopolymer film are under extensive research due to ease of preparation of photopolymer films ,cost-effective manner, and absence of wet chemical processing [2]. In the field of biosensing, the photopolymer film needs to be water stable so that it can interact with analyte. For the prepara-

tion of these films several essential components are required, including a binder, photoinitiator, monomer, cross-linker, and dye, which collectively contribute to achieving good efficiency and higher sensitivity. Furthermore, the solvent used in photopolymer films also plays a crucial role.

In the present study, cellulose acetate has been employed as a binder in a mixture of acetone and ethyl acetate for making water stable photopolymer film. Triethanolamine and erythrosine B were taken as photoinitiator and dye, respectively. Notably, the prepared film dries within 5 minutes, and recordings were made using a solid-state laser emitting at a wavelength of 532nm.Transmission geometry with 25^{o} angle between the beams is used for holographic record. The result show a diffraction efficiency of 50% in real-time measurements, as illustrated in Figure 1. Acrylamide serves as a monomer, and further efforts are being made to test capability of this film as a biosensor.

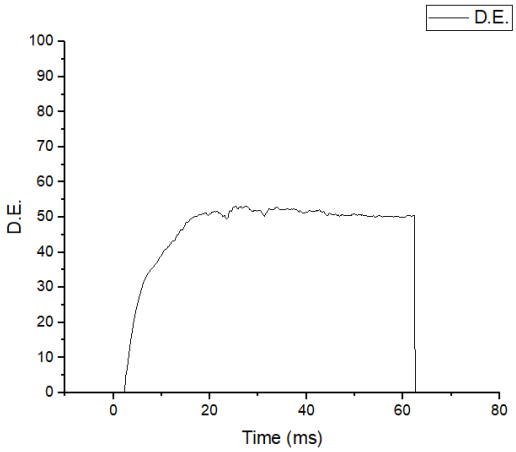

Figure 1 Diffraction efficiency for cellulose acetate based photopolymer film

References

1. P. Singh, Life Sci., Elsevier, 2017.
2. J.R. Lawrence et al., Optik (Stuttg). 112 (2001) 449–463.

MAT309 Carboxyalkyl chain length dependent Aggregation Enhanced Two Photon Absorption in Carbazole-Barbituric acid Donor-π-Acceptor system

*Lakshmi R[1], Meema Rasheed[2], Parvathy O C[2], Narayanapillai Manoj[2,3], Pramod Gopinath[1,3]**

[1]*International School of Photonics, Cochin University of Science and Technology, Kochi-682022, Kerala, India*

[2]*Department of Applied Chemistry, Cochin University of Science and Technology, Kochi-682022, Kerala, India*

[3]*Inter University Centre for Nanomaterials and Devices, Cochin University of Science and Technology, Kochi-682022, Kerala, India*

**Corresponding author: pramod@cusat.ac.in*

Aggregation Induced Emission (AIE) luminogens exhibit no emission in dilute solution and are induced to emit when aggregated at high concentration with restriction of intramolecular motions as the principle

mechanism. The AIE effect can be enhanced by specific structural modifications such as boosting the hydrophobic interactions and hydrogen bonding interactions.

In this work, we have investigated the role of hydrogen bonding interaction by varying the carboxyalkyl chain length of Carbazole-Barbituric acid D-π-A AIE system. We synthesized Butyl, Ethylhexayl, Heptyl, Octyl, Nonyl, Dodecyl Carbazole-Barbituiric acid (CBA) derivatives, studied their photophysical properties upon aggregation by UV-Vis spectroscopy, Steady state and Time-resolved fluorescence spectroscopy. The aggregate size and morphology was determined using DLS measurements and TEM images respectively. We utilized Open- Aperture Z-Scan technique with an Nd:YAG laser (1064nm) in order to measure the change in non-linear absorption co-efficient at different stages of aggregation and different carboxyalkyl chain lengths. Furthermore the knowledge about their energy levels was gained by using DFT in Gaussian 09 program package.

At the onset of absorption spectra we observed a red shifted tailing upon aggregation and extend of tailing toward 532nm is prominent in lower alkyl chain length molecule. We observed an aggregation enhanced two photon absorption and alkyl chain length dependent non-linearity. Butyl CBA with lowest alkyl chain length exhibits maximum TPA coefficient at NIR region and increase in alkyl chain length significantly decrease the TPA coefficient. The extend of absorption tailing upon aggregation opens up the possibility of such molecules as a potential non-linear material in aggregated/solid state. This inference is supported by the theoretical HOMO-LUMO bandgap calculations. Optical limiting threshold of all molecules were also determined.

References

1. Zhang, Hanjun, et al., *J. Mol. Liq.* 302, 112550 (2020).

MAT310 Influence of Plasmonic Effects of Group IB (Ag and Au) Metals in Tuning the Nonlinear Absorption Mechanism of rGO-MoS_2 Hybrid

*M. Abith and T.C. Sabari Girisun**

Nanophotonics Laboratory, Department of Physics, Bharathidasan University, Tiruchirappalli 620024, India

**sabarigirisun@bdu.ac.in*

In the recent era, variety of novel functional materials are being developed for the progress of laser-based applications. Among them complex frameworks made of organic-inorganic layered hybrids have gained a wide interest due to its structural tunability and enhanced nonlinear optical behaviour. Especially in the class of two-dimensional materials, graphene and its derivatives have gained wide recognition owing to perceptible flexibility and increased active surface region. Similarly, molybdenum disulfide (MoS_2) has proven time after time to be a potential candidate for ample applications like photocatalytic activity, electronic and logic devices, therapeutic actions, sensors and optical devices due to bandgap tunability and higher photo-response. Further, integrating Group IB metal nanoparticle like Ag and Au with organic-inorganic frameworks can enhance the physical and chemical properties ascribed to strong light absorption due to enhanced surface plasmon resonance effect at the excitation regime. Based on these facts, a series of Ag-rGO-MoS_2 and Au-rGO-MoS_2 complex systems with varying concentration of Ag and Au (2.5wt%, 5wt%, 7.5wt% and 10wt%) were prepared by facile hydrothermal technique. XRD confirmed the formation of hybrids made of mixed phase 1T-2H MoS_2, reduced graphene oxide and Ag/Au metals. Morphological studies showcased the formation of Ag as nanowires and Au as nanospheres upon MoS_2 microspheres em-

bedded within rGO layers. Under 532 nm Nd:YAG laser excitation, Z-scan experiment revealed all the samples depict reverse saturable absorption (RSA) ascribed to two photon absorption (2PA). However, different electronic transitions are found to be the pertaining reason for two photon absorption process like excited state (Au-rGO-MoS_2) and genuine (Ag-rGO-MoS_2) two photon absorption. Influence of Group IB metals in tuning the nonlinear absorption were analysed through theoretical estimation of absorption cross-section. These hybrids were dispersed in PMMA matrix and fabricated as a free-standing film (as shown in figure 1) and the optical limiting properties were studied. The potentiality of Ag and Au decorated MoS_2-rGO hybrid in the use of optical limiters for laser-based experiments will be discussed.

Figure 1. Free standing film of Ag-rGO-MoS_2 optical limiter

References

1. M. Abith et.al, *J. Mol. Liq.* 341, 117337 (2021).
2. M. Sheik-Bahae et.al, *IEEE J. Quant. Electron.* 26, 760–769 (1990).

MAT312 Structural, morphological and optical properties of fluorine and aluminium co-doped ZnO thin films

Nidhi Singh, Navina Wadhwani, R. K. Shukla and Anchal Srivastava

Department of Physics, University of Lucknow, Lucknow

**Correspondimg author: asrivastava.lu@gmail.com*

Solar cells have attracted extensive attention due to the increasing energy demands. ZnO semiconductor is a promising material for different applications such as gas sensors, liquid crystal displays, thin film transistor and solar cells.

In this study, we have co-doped 1at% fluorine and 1at% aluminum in ZnO thin films deposited on glass substrate to improve its properties such as conductivity, mobility, transmittance along with the decrease in resistivity for solar cell application. The structural and morphological properties of film have been studied by X-Ray diffractometer and FESEM. The optical properties such as absorbance, transmittance, reflectance, refractive index and extinction coefficient have been studied by UV-Vis spectrophotometer. The electrical measurements have been performed for conductivity, mobility and resistivity measurement. The photoconductivity measurement have been also done.

MAT313

Electrochemical Sensor for antibiotic Chloramphenicol Drug on MWCNT/GO Modified GCE by Voltametric techniques

*Priyanka[1], Amritanshu Pandey[2], Sanjay Kumar Srivastava[1]**

[1]*Department of Physics, Banaras Hindu University (BHU), Varanasi-221005, India*

[2]*Department of Electronics Engineering IIT(BHU), Varanasi-221005, India*

**Corresponding author: sanjay_itbhu@yahoo.com*

Antibiotics are used to treat and prevent bacterial illnesses in humans, plants, and animals, as well as being useful additions to boost livestock and poultry growth. Antibiotics are chemical substances that can kill or hinder the growth of bacteria, archaea, viruses, protozoa, microalgae, and fungi. Chloramphenicol (CAP) is a broad-spectrum antibacterial medication that is used to treat a variety of diseases in both human and animal medicine, including conjunctivitis, cholera, typhoid fever, plague, and skin infections. The electrochemical method, on the other hand, has the advantages of quick analysis, low-cost equipment, and simple operation. As a result, many electrochemical sensors for CAP detection have been created using diverse electrode materials. Nanoscales materials for electrochemical detection of CAP are of great interest in antibiotic residue diagnostics study in food products, which has been linked to a number of negative effects. In this work two carbon nanomaterials were used i.e., Multiwalled Carbon Nanotube (MWCNT) and graphene oxide (GO) for detection of CAP in which detection by electrochemical sensing. Furthermore, GO was prepared by using Modified Hummer's method which provides good platform the selective detection of CAP. The synthesized GO was characterized by sophisticated instruments such as transmission electron microscope (TEM), Raman analysis, XRD, scanning electron microscope (SEM), XPS and electrochemical characterization to examine the structural and morphological information of the GO/MWCNT. The electrochemical sensing of CAP is performed by the cyclic voltammetry (CV) and linear pulse voltammetry (LSV) method. The proposed electrochemical sensing platform for chloramphenicol detection has high selectivity, wide linear response for the range (15-600 µM) with low limit of detection. Furthermore, we performed the CAP detection in real samples with eye drop which give satisfactory result. The sensor demonstrated high selectivity, stability, reproducibility, and a gratifying recovery result.

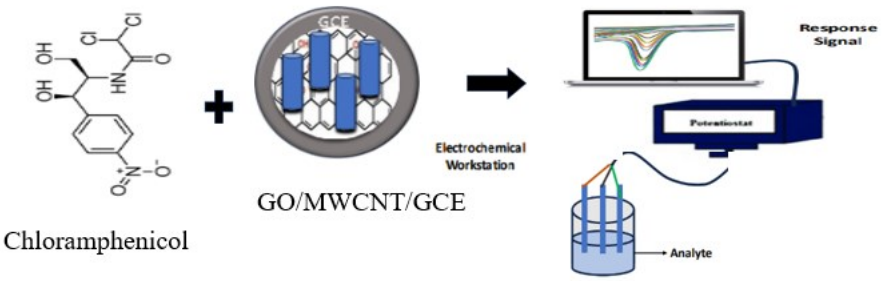

Figure 1. Represent the sketch of electrochemical detection of antibiotic Chloramphenicol Drug by using GO/MWCNT modified GCE.

References

1. N,Sebastian et.al., J. Inorg. Chem. Front., 6, 82-93(2019).

MAT314 Exploring the Impact of Zinc Doping on the Structural, Linear, and Nonlinear Optical Characteristics of NiO Films for Optoelectronic Applications

Ramseena Thundiyil[1,], P. Poornesh[1]*

[1] Department of Physics, Manipal Institute of Technology, Manipal Academy of Higher Education, Manipal 576104, India

**Corresponding author: ramseena.thundiyil@learner.manipal.edu or ramseenaanees18@gmail.com*

In this study, we have investigated the influence of Zinc (Zn) doping on the characteristics of NiO films prepared through the spray pyrolysis method. The Zn-doped NiO films were prepared at varying concentrations, specifically at 1, 5, and 10 wt%. The X-ray diffraction revealed that Zn doping led to a reduction in the crystallite size compared to pure NiO, with a slight increase as Zn concentration rose, indicating the incorporation of Zn into the NiO matrix. Further examination of vibrational modes and morphology was conducted through Raman spectroscopy and Atomic Force Microscopy (AFM), respectively. The investigation of optical energy bandgap via Tauc's plots indicated minimal fluctuations in bandgap with varying Zn concentrations. Nonlinear optical properties were assessed using a z-scan setup with a continuous-wave laser at 632 nm. In the z-scan configuration with an open aperture, all films demonstrated Reverse Saturable Absorption (RSA), also found that nonlinear absorption coefficient increased with higher Zn concentrations. Additionally, the third-order nonlinear optical susceptibility exhibited an enhancement with the introduction of Zn doping. In summary, our results suggest that Zn-doped NiO thin films have significant potential for applications in the realm of optoelectronic applications.

MAT315 Synthesis and Optical Properties Study of Undoped and Carbon doped ZnO Quantum Dots

*Sharda Pandey[1], R. K. Shukla[1] and Anchal Srivastava[1]**

[1]Department of Physics, University of Lucknow, Lucknow-226007, Uttar Pradesh, India.

**Corresponding author: asrivastava.lu@gmail.com*

In this study, undoped and 2 wt%, 4 wt%, 6 wt% and 8 wt% of carbon doped ZnO quantum dots (QDs) are prepared using sol-gel method. 3-Aminopropyltriethoxysilane (APTES) is used as surface modifier for the further modification in the surface morphology of the undoped and carbon doped ZnO QDs. The structural analysis of all the prepared samples were analyzed using X-ray diifraction (XRD) technique. The optical parameters, refractive index (n), extinction coefficient (k), dielectric constant (ε) and conductivity have been calculated using absorption and transmission spectra recorded by UV- Visible spectrophotometer. The fluorescence spectra of prepared samples has been analysed using photoluminescence spectrophotometer for different pH values 5-12 and different ZnO QDs of undoped and carbon doped sample concentrations ranges between (0.25% - 6%).

References

1. Ozgur, U. et al. A comprehensive review of ZnO materials and devices. J. Appl. Phys. https: // doi.org/10.1063/1.19926 66 (2005).
2. Fu, Y. S. et al. Stable aqueous dispersion of ZnO quantum dots with strong blue emission via simple solution route. J. Am. Chem. Soc. **129**, 16029–16033. https://doi.org/10.1021/ja075 604i (2007).

MAT317 Investigations and Advancements in Clad Layers of Sintered Silicon Carbide Mirrors for Space Optical Applications

Tayaramma D.P.V Jalluri, C.V. Ramana Reddy, Veena John, A.R. Srinivas, R.Venkateswaran, K.V.Sriram*

Laboratory for Electro-Optical Systems (LEOS-ISRO), Peenya Industrial Estate, Bengaluru

*Pin code:5600058. *e-mail Id: pushpavalli@leos.gov.in/pushapvalli4@gmail.com*

To achieve the stringent demands of high resolution and light assembly efficiency, primary mirrors with large apertures are being employed for space telescope payload optics. Silicon carbide (SiC) has recently supplanted zerodur, ule glasses, and be materials, due to its inherent superior qualities such as thermal stability and radiation resistance. Telescope optics should meet stringent specifications 12 nm Root Mean Square (RMS) and surface micro-roughness less than 2nm RMS over 1.2 m diameter. The sintered silicon carbide can't be used for optical applications as produced, since sintered SiC is porous in nature with micro -structural defects of grain boundaries and discontinuities. This limitation can be mitigated by an appropriate surface modification processes, viz., depositing a thick or thin film of coating on the sintered SiC substrate[1]. In the present research work, the attempts are made to coat SiO_2, Si, SiC on sintered silicon carbide substrate using PVD technique, thermal spray method and CVD techniques respectively. Subsequently, these clad layers have been polished and achieved optical requirements in terms of PTV, RMS and micro-roughness (Fig). The final properties/features of the three SiO_2, Si, SiC coatings on sintered silicon carbide mirrors are given in the Table1. Non-destructive testing such as dye-penetrant tests, x-ray radiography, micro-Raman analysis, Microstructural cauterization XRD, EDAX, Micro-Raman, Mechanical characterization nano-indentation has been carried out in different states of mirror fabrication. These mirrors have been qualified for space use by conducting space-worthy tests like thermo-vacuum cycling, thermal storage, humidity, thermal shock cycling on SiC mirrors/samples.

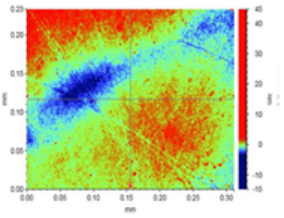

Fig:Surface micro-roughness 2D profiles for polished SiC coatings on SSiC

Table 1: Comparison table for the properties/features of the three SiO_2, Si, SiC coatings on sintered silicon carbide mirrors

Parameter		Sio_2 Coating	SiC Coating	Si Coating
Micro-Roughness (Nm)	R_a	9.11	6.4	9.1
	R_q	12.8	8.3	12.0
Surface Finish (Nm)	Pv	74.8	108.5	86.75
	Rms	9.8	11.4	9.46
Nano-Hardness (Gpa)		5	36.5	11.8
Young's Modulus (Gpa)		60	494.8	146.2
Fabrication Time (Weeks)		2	5	1
Clad Preparation Time		1 week	1 Month	2 Days
Yield Rate		50 %	30%	70 %

References

1. T.D.P.V. Jalluri, S. Somashekar, A. Dey, R. Venkateswaran, S. Elumalai, B.Rudraswamy, K. V. Sriram, Characterization of thermal sprayed Si on sintered SiC for space optical applications, Surface Engineering 37, (2021), 558.

MAT318 Electrical and photoconductivity properties of green synthesized ZnO nanoparticles and nanocomposites

*Vishnu Kumar Dwivedi, Nidhi Singh, Navina Wadhwani, R K Shukla and Anchal Srivastava**

Department of Physics, University of Lucknow, Lucknow, Uttar Pradesh, India-226007

**Corresponding author: asrivastava.lu@gmail.com*

The photoconductivity is a phenomenon in which the electrical conductivity of a material increases upon exposure to light. The study of photoconductivity is performed in this article for the three samples zinc oxide (ZnO) nanoparticles (NPs), boron nitride (BN) NPs and ZnO/BN nanocomposite. All the three samples used here were prepared by green synthesis method using fruit peel extract. These three samples were characterized using X-Ray diffraction, field emission scanning electron microscopy, UV-Visible spectroscopy and Fourier transform infrared spectroscopy. The range of particle size calculated by X-Ray diffraction data for ZnO NPs, BN NPs and ZnO/BN nanocomposite is found in the range of 12-42nm, 3-41nm and 7-38nm respectively. The current–voltage characteristics in dark and under ultra violet (UV) illumination irradiated by an UV bulb of 300W in the wavelength range 365nm was performed for an applied voltage of 0 -30V for all the three samples. The variations of dark current (I_{dc}) and the photocurrent (I_{pc}) with applied voltage were studied for power-law relationship for all the three samples. The study of photoconductivity was performed using UV light at a bias voltage of 5V to obtain the photo response for all the three samples.

Category 16

Optical System Design (DES)

DES106 Design of Spine Based Conformal Optics In MWIR Band Using Fixed Correctors

Sandeep Mishra, Ranabir Mandal, P K Sharma

sandeepmishra.irde@gov.in

Instruments Research & Development Establishment, Dehradun-248008, India

Conformal optics refers to use of optical dome/windows that deviate from conventional form to best satisfy the contour and shape needs of system platforms. Most of the aero platforms usually employ some sort of electro-optic (EO) systems for threat perception and its mitigation. Thermal imagers, laser and IR seekers, surveillance cameras, laser range finder are examples of such EO systems. For aircraft application these EO systems are positioned in belly or chin mounted configuration while in other applications EO systems are usually placed at the head section of the platform. Optical domes/ windows are often used to protect these electro-optical systems from deteriorating effects of atmosphere. Conventional windows for airborne pay-loads are often discontinuous with the aircraft or platform skin. These windows in form of a protruding structure increase aerodynamic drag, which consumes more fuel and thus reduces the amount of available mission time and restricts the aerodynamic performance of platform. Conformal optical systems utilizing optical windows which conform smoothly to the external shape of the platform to improve aerodynamics can be used to greatly enhance the weapon or platform efficiency.

Monolithic contoured conformal domes/windows in form of unconventional shapes such as conics, ogive, polynomial etc. can be used to reduce air drag. Use of these highly contoured windows is limited due to complexity associated with fabrication and testing methods and these windows tend to limit performance of EO systems at oblique angles as these tend to introduce optical aberrations. Correction of their aberrations with varying field of regard (FOR) poses a complexity in optical design point of view. Out of many possible approaches of aberration compensation, fixed correctors approach can be implemented easily.

In this paper optical design of an optical system with a monolithic contoured window in transparent ceramic material Magnesium Aluminate Spinel ($MgAl_2O_4$) is considered. The aberrations arising with varying field of regard (FOR) were analyzed and fixed correctors were used to mitigate the aberration. The optical performance of the system was maintained using fixed correctors. Spinel was considered as material of choice for conformal window as it has excellent transmission in visible to MWIR band, excellent mechanical properties suitable to high speed application. Another advantage of spinel is that it can be can be slip casted into a desired shape which can be further processed to realize highly contoured domes.

References

1. James P. Mills, “Conformal Optics: Theory and Practice”, Proc. SPIE Vol. 4442,10 Dec 2001, doi:10.1117/12.449962
2. Blake G. Crowther, Dean B. McKenney, James P. Mills, "Aberrations of Optical Domes," Proc. SPIE 3482, 21 September 1998; doi: 10.1117/12.32202
3. Patrick A. Trotta, "Precision conformal optics technology program," Proc. SPIE 4375, 7 September 2001; doi: 10.1117/12.439165

DES107

Compact dual FOV discrete zoom catadioptric SWIR Imaging System

Shivangi Dubey, Ravinder Reddy M

Centre of excellence, Product Development and Innovation Centre, Bharat Electronics Limited 560013

**Corresponding author: shivangidubey@bel.co.in*

Advanced Electro-optical surveillance system incorporates multiple sensors along with the complexity of the designing. In this article an approach for designing in small form factor is elaborately discussed. Designed SWIR HD optical system operates at f/11 for NFOV and f/5 for WFOV with 80mm aperture size. Various discrete Zoom design architecture is explored which comprises mirror arrangement for compact designing which induces alignment issue along with performance degradation [1]. Catadioptric architecture for the same configuration provides total track length of 250 mm and total track length of 200mm is achieved by incorporating catadioptric and prism reflecting surface architecture with spot < 15um for WFOV and spot < 14um for NFOV.

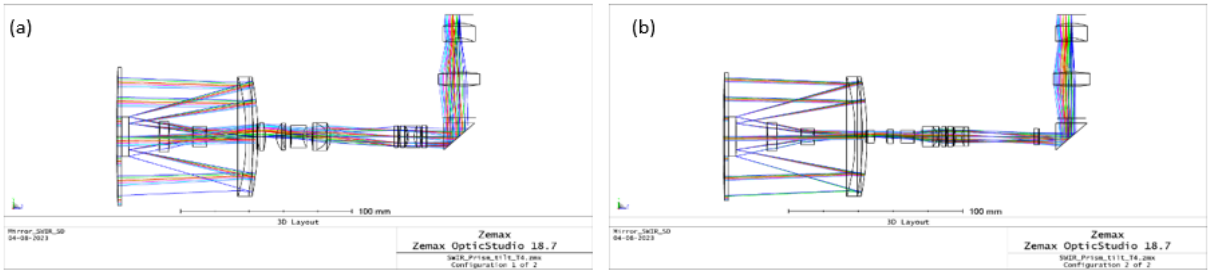

Fig1. Optical Layout of the Catadioptric Dual FOV SWIR Imaging system (a) NFOV with effective focal length 900 mm (b) WFOV with effective focal length 400 mm.

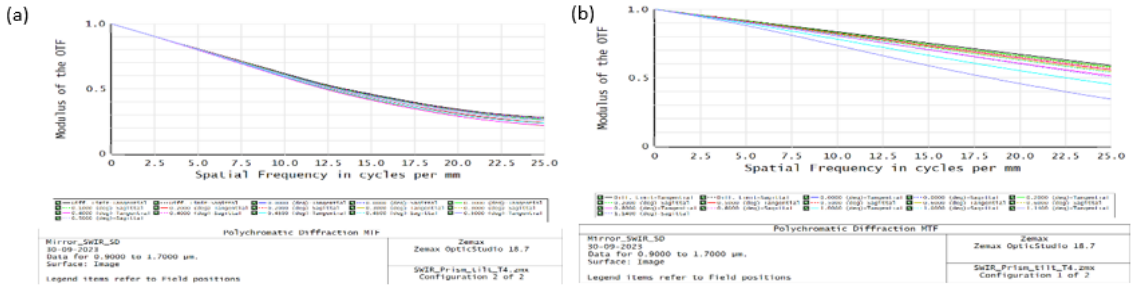

Fig2.FFT MTF is shown for the Catadioptric dual FOV optical design (a) On axis MTF > 0.4 at 25 cy/mm for WFOV. (b) On axis MTF > 0.2 at 25 cy/mm for NFOV.

References:

1. Manish Uniyal,P. K. Sharma;" Optical design of a compact high-definition dual-field zoom lens in 0.9–1.7- micron SWIR spectral band" 10.1007/s12596-020-00598- 3(2020)
2. Jose M. Infante, Marta C., Wang Lin, Juan Carlos, Pablo Benitez, Guillermo Biot, Hammed, Andres F.; "Design of a Compact objective for SWIR applications"; Proc.SPIE 8167, Optical design and engineering IV, 81670K (2011)

DES207 3D field-of-view of remote focusing microscopy system

*Dinesh Saini[1], Manish Kumar[1,2]**

[1]Optics and Photonics Centre, Indian Institute of Technology Delhi, Hauz Khas, New Delhi-110016, India
[2]Centre for Sensors, Instrumentation and Cyber Physical System Engineering, Indian Institute of Technology Delhi, Hauz Khas, New Delhi -110016, India
**Corresponding author: kmanish@iitd.ac.in*

Remote focusing is a useful technique to enable 3D scan of a sample without a need to move either the sample or the sample facing microscope objective. However, the proper understanding of the remote focusing phenomena is still not well understood. In this paper, we have carried out a raytracing-based analysis of a remote focusing system using a pair of 4x microscope objectives. We use Ansys Zemax OpticStudio for our analysis. In remote focusing, a 3D object space is imaged onto a 3D intermediatory image space. This is achieved by using a pair of microscope objectives with tube lenses arranged back-to-back. A third microscope objective is used to physically scan along this intermediate 3D image plane [1, 2]. This avoids disturbing the sample. In our work, we show that a low-magnification microscope objectives system supports remote focusing without the need for a tube lens. This realization makes it better than a prior implementation [3]. Figure 1 shows the simulated system. We observed the behavior of on-axis and off-axis field points kept in object space. We used the Strehl ratio parameter to determine the lateral and axial extent of the remote focusing system (Figure 2). The Strehl ratio of >= 0.8 is required for good imaging. For the 4x objective (TL4X-SAP – Thorlabs; fov-5.5mm, working distance–17.0mm), it was observed that the lateral field of view (fov) reduced from 5.12 mm to 0.50 mm at the axial extent of ±7.0 mm from the focal plane in the object space. Maximum axial extent is achieved when the objectives are arranged in a 4F configuration. Thus, a full 3D field of view of a remote focusing system can be determined.

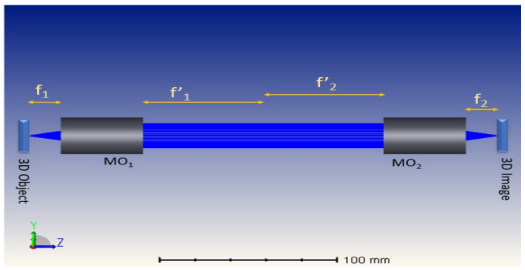

Figure 1: Schematic of remote focusing setup

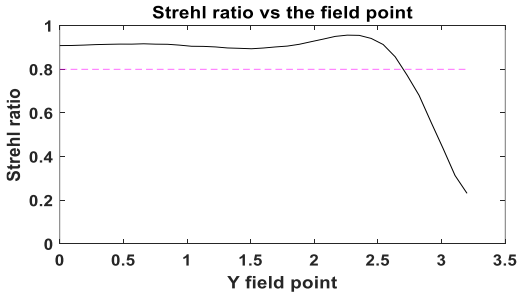

Figure 2: Plot of Strehl ratio vs the lateral field

References:

1. E. J. Botcherby, et al., *Optics Communications, vol. 281, pp. 880−887* (2008).
2. Manish Kumar, et al., *Optics Express* 26, 13027-13041 (2018).
3. Maximilian Hoffmann, et al., *Optica* 6, 1166-1170 (2019)

DES208 Design of an off-axis three mirror multispectral Imager in VNIR and SWIR region with ultra -wide field of view using free-form surfaces

Gokul G. Nair[1], Dr. Madhavi Sachin Thakre[1], Amitvikram Kurulkar[1]*

[1]HyperSpectral Optics Division, Optical Systems Group, Sensor Development Area, Space Applications Centre, Indian Space Research Organisation , Ahmedabad, Gujarat, India - 380015

**Corresponding author: gokul@sac.isro.gov.in*

Multi Spectral Electro-Optical Payloads in VSWIR region has numerous applications in Vegetation, Land Coverage, coastal and inland monitoring, soil-water pollution, cryosphere monitoring, and information on the atmosphere and clouds. A multispectral Imager with bands in VNIR and SWIR which provides wide swath and medium resolution is highly preferrable for these applications. Lens based optical systems create the requirement of single lens assembly for each band due to the selection of lens material which requires high performance in multiple bands for this High FOV. This will result in a heavier payload with critical band to band registration requirements. Considering the Mirror based design, Unobscured reflective optical systems are preferred. Three mirror anastigmatic optical designs can provide aberration-free system irrespective of the wavelength. However, aberrations increase with the increase in the system FOV, so a wide FOV system is difficult to design.

In this paper, a design approach which is effective in designing high FOV optical systems catering to multiple bands is proposed. While designing from the conventional TMA system, the FOV is increased gradually and optimised by changing the surface properties from spherical to asphere. But this ultra -wide FOV creates the requirement of insertion of free-form surfaces which will give more freedom to the optimisation of system performance. Due to the non-availability of a common detector in both VNIR and SWIR region, the beam has been split using a dichroic beam splitter creating two paths, one for VNIR and one for SWIR. Finally, an off-axis three mirror anastigmatic imaging system with a focal length of 200 mm, an F-number of 3 and an ultrawide FOV of 68° x 4° is designed using 2 freeform and an aspheric mirror. The system has been optimised and achieved the Optical performance in terms of MTF, Distortion and Field curvature. This demonstrates that the single TMA assembly with freeform surfaces can provide the optimal solution to medium resolution, ultrawide FOV multispectral payloads in VNIR and SWIR region.

References

1. Joseph, G. (2015). Building earth observation cameras. CRC press.
2. J. P. Rolland, M. A. Davies, T. J. Suleski, C. Evans, A. Bauer, J. C. Lambropoulos, and K. Falaggis, “Freeform optics for imaging,” Optica 8(2), 161 (2021).
3. K. Thompson, “Description of the third-order optical aberrations of near-circular pupil optical systems without symmetry,” J. Opt. Soc. Am. A 22(7), 1389 (2005).

DES209 Design of a reflective type free-form combiner based augmented reality Head-up Display

Rahul Rohilla[1,2], Harry Garg[1,2], Vinod mishra[1,2], Vipan Kumar [1,2]*

[1]Academy of scientific and innovation research (Acsir) , Ghaziabad 201002 , India

[2]CSIR-Central scientific instrument organization, sector30c, Chandigarh-160030, India

**corresponding author: rahul.csio19J@acsir.res.in*

Optical design of head up display for fighter aircraft is always a challenging task due to limited space of

cockpit. A refractive type petzval projection design is used in fighter aircraft. In such design there are need of two combiner to get the total field of view. These combiner are partially coated glass plate with see-trough properties. Improper alignment of these two combiner generate the ghost image is one of the key problems in this kind of system. So the purposed work of this paper is to design a single combiner based head-up display system. It can reduce the weight, size of head up display as per requirement of next generation of fighter aircraft. A reflective type optical system is design with of partially coated free-form combiner for high brightness OLED source pixel size is 12 um, resolution 1280 x 1024, wavelength 543 nm.

In head up display system image source projects image on partial coated combiner, this combiner superimposed the projected image on see through real view. A classical refractive type head up-display is a binocular type petzval projection system. It has a 6 to 8 lens optical design having F-no 1 to 1.5. [1]. A reflective type system is designed for larger field of view it has a two sub modules, ie relay optics and partially coated see through combiner. Relay optics projected the magnified image of OLED source in air, this intermediate image is redirected by the partially coated combiner at design eye point [2].

References

1. T. Chand, S. K. Debnath, S. K. Rayagond, and V. Karar, "Design of refractive head-up display system using rotational symmetric aspheric optics," *Optik (Stuttg)*, vol. 131, pp. 515–519, Feb. 2017, doi: 10.1016/j.ijleo.2016.11.048.
2. H. Peng *et al.*, "Design and fabrication of a holographic head-up display with asymmetric field of view," *Appl Opt*, vol. 53, no. 29, p. H177, 2014, doi: 10.1364/ao.53.00h177.

DES210 Optics Design of Long Range Dual FOV LWIR Imaging System Based on Cooled Detector

Rakesh Nangia, Ranabir Mandal, P K Sharma*

Instruments Research & Development Establishment, Raipur Road, Dehradun 248008, India

**Rakesh Nangia: rakeshnangia.irde@gov.in*

A thermal imaging system images infrared energy emitted from a body with temperature and is extensively used in areas such as surveillance, reconnaissance and fire control in military applications [1]. Dual field-of-view optical systems are commonly used in infrared imaging systems. The wide field-of-view (WFOV) is used for observing a large scene area and searching for possible targets of interest. The narrow field-of-view (NFOV) is then used for seeing a magnified view of the same and for final target recognition and identification [2].

Here a long range dual field of view (DFOV) thermal imaging system operating in long wavelength infrared (LWIR) band is proposed. The parameters of the system are f/number 2.7, effective focal length (EFL) 520mm/130mm and 7.7-9.3 µm spectral region. The detector is based on 640X512 staring focal plane array (FPA) having active sensor are of 9.6mmX7.68mm and cold shield distance of 19.4mm. To gain optimum image quality and compactness, both aspheric and diffractive surfaces were used in the design.

The schematic layout and modulation transfer function (MTF) curves of the system are shown in figure 1 & 2 respectively. The designed optics is implemented in a folded configuration so that the system can be fitted in a given space envelope.

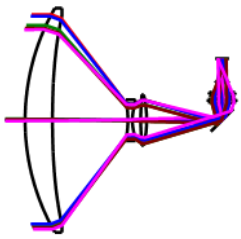

Fig. 1a NFOV

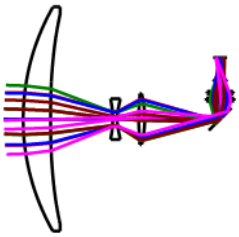

Fig. 1b NFOV

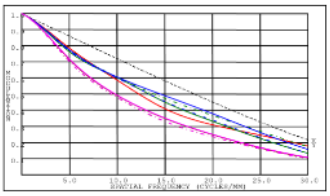

Fig. 2a MTF (NFOV)

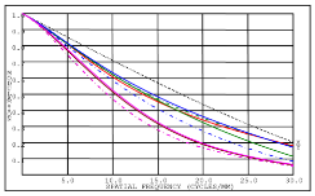

Fig. 2b MTF (WFOV)

References

1. Seok Min Hong, Hyun Sook Kim, Wee Kyung Yu, Guk Hwan Lee, Eon Suk Yoon, Yong Chan Park, Se Chol Choi, Joo Hyoung Lee, "Advanced thermal imaging system for tank sights," Proc. SPIE 5783, Infrared Technology and Applications XXXI, (31 May 2005)
2. Tao Xiong, Chang-cheng Yang, "Long wavelength infrared dual field-of-view optical system," Proc. SPIE 6722, 3rd International Symposium on Advanced Optical Manufacturing and Testing Technologies: Advanced Optical Manufacturing Technologies, (14 November 2007)

DES211 Optical Design Scheme for Multiband Optical System

Ram Prakash Nautiyal[1], Kiran Sharma[2], Ranabir Mandal[1], P. K. Sharma[1]*

[1]Instruments Research and Development Establishment, Raipur Road, Dehradun, Uttarakhand, India, Pin 248008

[2]Graphic Era Deemed To Be University, Clemen Town, Dehradun, Uttarakhand, India,

Pin 248002

Ram Prakash Nautiyal : ramprakashnautiyal@gmail.com*

Optical systems are being used for the surveillance and reconnaissance since long time in military as well as in civil operations. There are various types of optical systems like day camera, night vision devices and laser range finders (LRF) etc., which compliments each other to do complete surveillance. Hence we require many optical systems to collect the various types of information. Packaging of these cameras in a single unit requires large space. In addition, these types of systems suffer alignment issues and assembly of these instruments becomes critical. These types of systems also have large weight and volume.

To overcome from these types of problems, single channel optical design scheme has been proposed for multiband optical systems. This design scheme combines various optical systems into a single channel optical system at the design stage. Single channel design scheme utilises modular design approach. The first optics module will be common for all after that the optical path will be splitted in to desired directions with the help of bending or splitting optical components. After that other optical modules will be designed as per the requirements. Due to this proposed scheme the overall weight and size of the system get reduced and system becomes light weight and compact. The problem of alignment during assembly gets also removed due to the single optical output channel.

Here, optical design of single channel optics for laser range finder and laser designator (LD) has been discussed. The Ray diagram of the proposed scheme has been given in following figure-1.

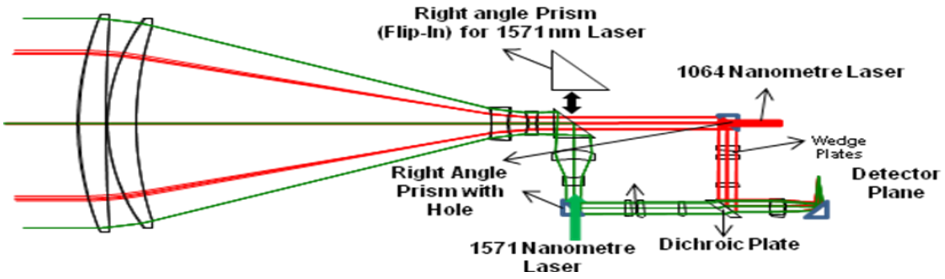

Figure-1 Ray diagram

References

1. D. P. Juyal et. al., IEEE Conference on Lasers and Electro-Optics, vol 1, 146–147 (2001)
2. R. P. Nautiyal et. al., ICOL-2019, Springer Proceedings in Physics 258, 415-418 (2021).

DES212 Optics Design of Common Aperture Dual-Band Imaging System

Vishal Bhushan[1*], *Manish Uniyal*[1]
[1]*Instruments Research & Development Establishment, Raipur Road, Dehradun-248008*

[*]*vishal.irde@gov.in*

Dual band imaging enables simultaneous acquisition of images from a common scene in two separate spectral bands (e.g., visible combined with an infrared band or short-wave infrared combined with mid-wave infrared). It provides a higher degree of discrimination with high signal to noise ration, especially for fast frame rate applications. In practice, this often requires that the images be acquired along two separate channels, or optical paths, one for each spectral band. Common aperture design approach provides an added advantage by reducing the overall weight and parallax problem.

This paper presents optics design of dual band (SWIR/MWIR) optics with a front common optics in Catadioptric configuration. The layout of the complete optics has been shown in figure 1. The two spectral channels have been separated by a dichroic beam splitter used after the front Catadioptric optics. The separated spectral channels are then imaged onto the Focal Plane Array of the respective detectors. The optics has been optimized and analyzed using CodeV® optical design software. Stray light analysis has been carried out using FRED software and two baffles have been provided to reduce the stray light. The designed baffles are shown in figure

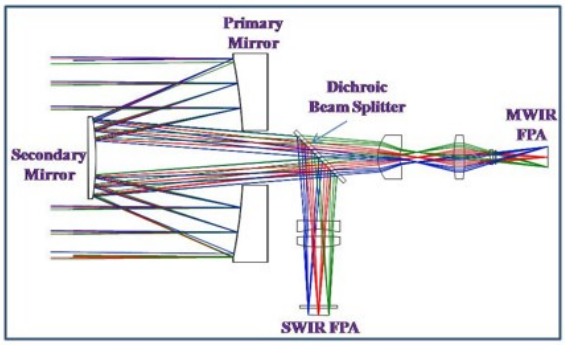

Figure 1. Optical Layout

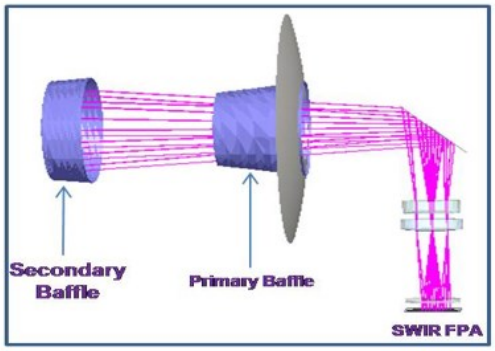

Figure 2. Baffle Layout

Authors are thankful to the project team from Vision Instrumentation Design Centre of IRDE for their help and valuable inputs. Authors are also grateful to Group Director, Optical Design Division and Director IRDE for their guidance, inspiration and encouragement.

References

1. Miguel P. Snyder, Jay N. Vizgaitis , " Optical design study for 1-5µm spectral band", Proc. SPIE7298 (2009) 729810.
2. CodeV® is a product of Optical Research Associates/ Synopsis, Pasadena, CA.
3. FRED is a product of Photon Engineering, Tucson, AZ.
4. W. Smith, Modern Optical Engineering, the Design of Optical Systems, McGraw Hill, New York (1966).

Category 17

Optical Sources and Illumination Engineering (SIE)

SIE399 Abruptly autofocusing circular Airy derivative beams in free space and disorder media

*Anita Kumari[1], Vasu Dev[1], Vishwa Pal[1]**

[1]Department of Physics, Indian Institute of Technology Ropar, Rupnagar, Punjab 140001, India

** vishwa.pal@iitrpr.ac.in*

Optical beams possessing abrupt autofocusing and self-healing properties are highly desirable in various applications, such as in biomedical treatment, high-resolution imaging, optical material processing, etc. In these applications, the beam requires to propagate through various components as well as disorder media, and encounters various undesirable effects such as beam dispersion, fluctuations in intensity, beam obstruction and coherence loss, therefore, the propagation properties of may get modified [1]. We have generated a special type of Circular Airy derivate beam (CADB), and investigated its propagation in free space as well as in disorder media to characterize the abrupt autofocusing and self-healing properties. The abrupt autofocusing is quantified by calculating the k-value (ratio of maximum intensities observed at $z > 0$ and $z = 0$ planes) [2]. The strength of turbulent media is characterized by Strehl ratio (SR), and overlap integral (C) is used to quantify the self-healing as well as distortions caused by the disorder media. The results for propagation of CADB in free space (SR=1) and strong disorder media (SR=0.3) are shown in Fig.1. As evident, the CADB exhibits autofocusing both in free space as well in disorder media (Figs. 1(a) and 1(b)). However, the abruptness in the autofocusing (k-value) decreases significantly with an increase in the strength of disorder (Fig.1 (c)). The autofocusing distance is found to be increased with an increase in the strength of disorder. Figure 1(d) shows the variation in C as a function of z for different values of SR, indicating that the overlap becomes minimum at the autofocusing distance. This suggests that the disorder media causes the spatial distortions as well as beam wandering, and at the autofocusing distance a slight change in intensity distribution results a significant change in the value of overlap integral. A detailed numerical and experimental study on self-healing of CADB is also performed, and found that the CADBs possess good self-healing abilities.

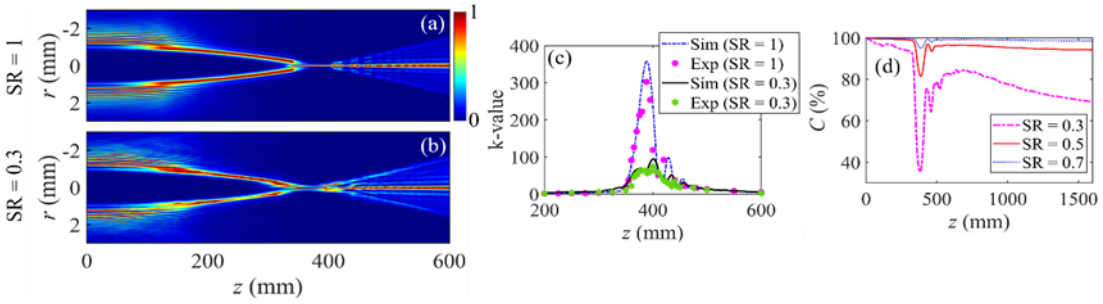

Fig. 1. Intensity distribution of CADB as a function of propagation distance (a) in free space (SR = 1), and (b) in strong disorder media (SR = 0.3). For the propagation of CADB in free space and disorder media of different strength, the variation in (c) k-value, and (d) overlap integral (C).

References

1. MA Cox et. al., *IEEE Journal of Selected Topics in Quantum Electro*. 27, 1-21 (2020).
2. A Kumari et. al., *Optics & Laser Tech.* 168, 109837 (2023).

SIE400

Innovative Daylighting Solutions: Assessing the Fresnel Lens for Optimal Interior Lighting Sustainability

Kiranjot Kaur[1,2], Harry Garg[1,2], Virendra Kumar[3]*

[1]Academy of Scientific and Innovative Research (AcSIR-CSIO), Ghaziabad, Chandigarh, India, 201002

[2]Mechanical Design & Fabrication Laboratory (MDF), CSIR- Central Scientific Instruments Organisation, Sector -30 C, Chandigarh, India, 160030

[3]Department of Physics, Hindu College, University of Delhi, University Enclave, Delhi – 110007, India

**Corresponding author: kiranjot.csio20a@acsir.res.in*

The work focuses on sustainable and energy-efficient daylighting design solutions for tubular daylighting systems using Fresnel lenses. The proposed design offers a sustainable approach to enhance natural lighting in buildings, reducing dependence on artificial lighting and subsequently decreasing energy consumption and greenhouse gas emissions. Implementing such system not only improves the visual quality and comfort of indoor spaces but also aligns with global efforts to create more sustainable environmental and endorses health management. Daylighting, efficaciously utilizes natural light within buildings fulfilling illumination needs, increased visual comfort and prevent Vitamin D deficiency.

This study focuses on the design and characterization of a passive tubular daylighting system that employs a Fresnel lens as a solar concentrator for daylighting systems. The research aims to develop an efficient daylighting system by optimizing aspects such as light transmission and optical efficiency for photometric range of 380 nm – 720 nm. This research paper conducts a comparative analysis of daylighting systems for flat plate, dome-shaped, and Fresnel lens configurations to determine the most effective approach for optimal interior lighting.

The study delves into each design's capacity to harness and distribute sunlight efficiently within indoor spaces. Simulation and optimization using TracePro 7.3.4 software assess the system's performance through ray trace diagrams and irradiance maps at different intervals. Comparative analysis is conducted for flat plate, dome-shaped, and Fresnel lens collectors. The results affirm the Fresnel lens's showed outperformed with 165 lux in morning, 810 lux in afternoon and 151.5 lux in evening. The developed system will be compact in size and has potential of daylight collection with desired efficiency replacing artificial lighting.

References

1. Kumar et. al., *Renew. Energy* 202, 1198-1214 (2023).
2. Garg et. al., *Lighting Research & Technology*, 554-570 (2023).
3. Onubogu et. al., *Int. Journal of Photoenergy*, 1-29 (2021).
4. Gupta et. at., *Appl. Opt*. 59, 5358 (2020).
5. Li et. al., *Renew. Energy* 20, 389–404 (2000).

SIE401

An L_2-Norm Based Quadratic Cost Function for Advancing the Wavefront Shaping Through Scattering Media

*Amit Kumar, Ayush Sharma S K Biswas**
Bio-NanoPhotonics Laboratory, Department of Physics Sciences,
Indian Institute of Science Education and Research (IISER) Mohali
Knowledge City, Sector 81, SAS Nagar, Punjab, India 140306,
**Corresponding author: skbiswas@iisermohali.ac.in*

The cost function in feedback-based wavefront shaping is one of the sensitive optimization function. There has been a trade-off between intensity enhancement and the gradient contrast differentiation between the structured light patterns in wavefront shaping. We have developed an L_2-norm based quadratic cost function (L2QN) in Genetic algorithm for advancing the intensity enhancement and the gradient contrast differentiation of two stages contrast assisted structured light. Both the simulations (fig.1a) and experiments (fig.1b) have been performed, and it has been found that the proposed (L2QN), significantly differentiating the contrast and structural uniformity for focusing light through scattering media. The potential applications of the method demonstrated in this study can be extended into holographic displays, structured light illumination microscopy, photo-lithography, photothermal treatments, dosimetry, laser materials processing, and energy control inside and outside an incubation system.

In standard iterative method based wavefront shaping[1-4], few popular cost functions have been reported, such as target intensity (η=Eta), peak-to-background ratio (PBR)[2-9], Pearson's correlation coefficient (PCC)[7,8] and standard deviation[4].The intensity and PBR cost functions are suitable for focus-spot formation. However, focusing the light into desired patterns at the specific region of interest is significantly challenging than focusing on spots.

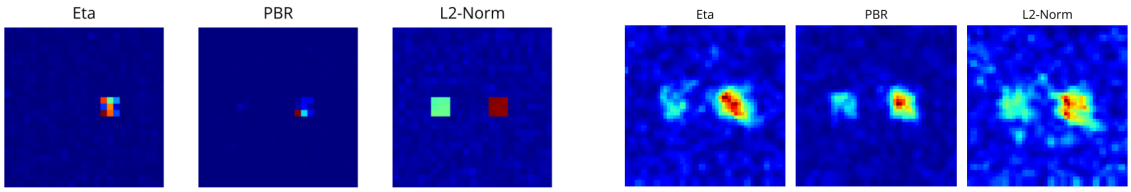

Fig 1: Two level contrast and intensity recovery, (a) simulation results, (b) experimental results

References

1. P. Sebbah, Waves and Imaging through Complex Media (Springer Dordrecht, 2001)
2. O. S. Ojambati, "Optical energy on demand," Nat. Phys. 18, 227–228 (2022)
3. A. P. Mosk, A. Lagendijk, G. Lerosey, and M. Fink, "Controlling waves in space and time for imaging and focusing in complex media," Nat. Photon. 6, 283–292 (2012)
4. D. B. Conkey, A. N. Brown, A. M. Caravaca-Aguirre, and R. Piestun, "Genetic algorithm optimization for focusing through turbid media in noisy environments," Opt. Express 20, 4840–4849 (2012).
5. B. R. Anderson, P. Price, R. Gunawidjaja, and H. Eilers, "Microgenetic optimization algorithm for optimal wavefront shaping," Appl. Opt. 54, 1485–1491 (2015).
6. D. Wu, J. Luo, Z. Li, and Y. Shen, "A thorough study on genetic algorithms in feedback-based wavefront shaping," J.Innov. Opt. Health Sci. 12, 1942004 (2019).
7. B. Zhang, Z. Zhang, Q. Feng, Z. Liu, C. Lin, and Y. Ding, "Focusing light through strongly scattering media using genetic algorithm with SBR discriminant," J. Opt. 20, 025601 (2017).

8. X. Zhang and P. Kner, "Binary wavefront optimization using a genetic algorithm," J. Opt. 16, 125704 (2014).
9. L. Wan, Z. Chen, H. Huang, and J. Pu, "Focusing light into desired patterns through turbid media by feedback-based wavefront shaping," Appl. Phys. B 122, 204 (2016).

SIE402 Wavelength Switchable & Tunable Noise like pulse laser using intracavity loss tuning

Santosh C R[1,], Gowrishankar R[1], Shailesh Srivastava[1]*
[1]Department of Physics, Sri Sathya Sai Institute of Higher Learning, Prasanthi Nilayam Campus, Puttaparthi, Andhra Pradesh, India 515134
**Corresponding author: santoshcr@sssihl.edu.in*

We report, for the first time, wavelength switchable and tunable noise like pulse (NLP) laser from an erbium doped fiber laser modelocked using the nonlinear polarization rotation technique. In contrast to tunable lasers that employ different types of spectral filters[1], the tuning mechanism in our work is a simple manipulation of intracavity loss using an inline attenuator. When the cavity loss is low, the EDF is saturated and hence the gain around 1560 nm is larger. Increase in the intracavity loss shifts the peak of the EDF's gain to 1530 nm.[2]

Self-starting, stable modelocked NLPs are generated at a pump power of around 100 mW. The repetition rate of the cavity is 1.3 MHz (Fig. 1(a)) with an average output power of around 13 mW. Fine tuning of the intracavity loss, through an inline attenuator leads to continuous tunability of the central wavelength of the laser output across the C-band (1535 nm to 1565 nm) as shown in figure 1(c). In addition, switching the intracavity loss between two different pre-set values leads to a wavelength switchable laser output. The characteristic double scale autocorrelation trace along with a smooth and broad optical spectrum indicates the generation of noise-like pulses from the cavity (Fig 1(b) and (c)).

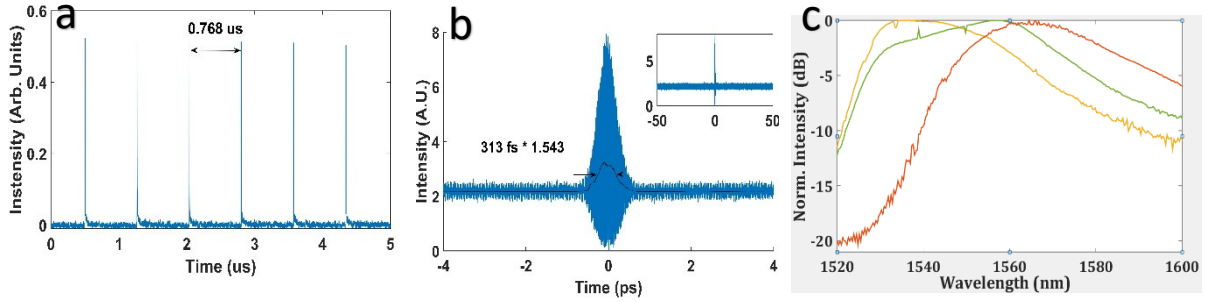

Figure 1: Wavelength Tunable NLPs: a) Oscilloscope traces of NLPs with pulse spacing of 768 ns; b) Autocorrelation trace, Inset: Double scale trace with 100 ps pedestal; c) Tunable optical spectrum of NLPs

On account of the adaptable output spectrum and the simplicity of the tuning mechanism, we believe, these lasers could be useful for a variety of applications including spectroscopy, sensing, and optical coherence tomography.

References

1. Santosh. C R, R. Gowrishankar, and S. Srivastava, "Versatile wavelength tunable noise-like pulse generation from an erbium doped fiber laser using an intra-cavity Michelson interferometer," *Laser Phys.*, vol. 33, no. 9, p. 095104, Sep. 2023.
2. P. M. Becker, A. A. Olsson, and J. R. Simpson, *Erbium-Doped Fiber Amplifiers*. Elsevier, 1999.

SIE403

Bidirectional modelocked tunable dual noise like pulse emission from a single laser cavity

Santosh C R, Gowrishankar R, Shailesh Srivastava*

Department of Physics, Sri Sathya Sai Institute of Higher Learning, Prasanthi Nilayam Campus, Puttaparthi, Andhra Pradesh, India 515134

**Corresponding author: santoshcr@sssihl.edu.in*

We report, for the first time, bidirectional modelocked wavelength tunable dual noise like pulse (NLP) emission from an erbium doped fiber laser modelocked using the nonlinear polarization rotation technique. A directional multiplexing within the cavity allows for independent modelocking in the clockwise and counter-clockwise directions. The presence of interferometric spectral filters[1] in the CW and CCW directional allows for independent tunability of the central wavelengths of the two modelocked pulse trains. In addition, manipulation of the spectral filters allows switchable single, dual and multi wavelength emission. Self-starting, stable modelocked NLPs in the CW and CCW directions were generated at a pump power of around 300 mW. The repetition rates of the CW and CCW NLPs were 1.274 MHz and 1.276 MHz respectively(Fig. 1(a)). Fine tuning of the spectral filters leads to continuous tunability of the central wavelength of the laser output across the C-band (1530 nm to 1565 nm). In addition, coarse tuning the filters leads to a switchable single, dual and multi-wavelength outputs. The characteristic double scale autocorrelation trace along with a smooth and broad optical spectrum indicates the generation of noise-like pulses from the cavity (Fig 1(b) and (c)).

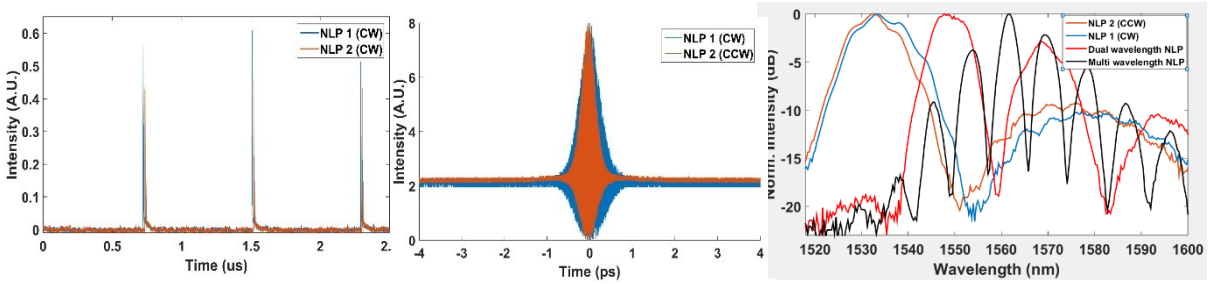

Figure 1: Dual NLPs: a) Oscilloscope traces of NLPs; b) Autocorrelation trace; c) Tunable optical spectrum of NLPs

A single laser source with versatile dual pulse emission, such as this, will prove to be a versatile source in many applications like sensing and transient time resolved spectroscopic studies.

References

1. Santosh. C R, R. Gowrishankar, and S. Srivastava, “Versatile wavelength tunable noise-like pulse generation from an erbium doped fiber laser using an intra-cavity Michelson interferometer,” *Laser Phys.*, vol. 33, no. 9, p. 095104, Sep. 2023.

Category 18

Optoelectronic Devices (OED)

OED347 Implementation of Frequency encoded Pauli Y gate based Quantum mechanical phase shift oscillator in photonic band gap crystal

Ayan Dey[1], Sourangshu Mukhopadhyay[1]*

[1]Department of Physics, The University of Burdwan, Golapbag, Burdwan-713104, West Bengal, India

[*]Corresponding author: ayandeybwn@gmail.com

Abstract: Pauli Y gate is an important fundamental gate in the family of quantum logic. The gate matrix of this 1-qubit gate is

$$\begin{pmatrix} 0 & -i \\ i & 0 \end{pmatrix}$$

Where the gate operation is

$$\begin{pmatrix} 0 & -i \\ i & 0 \end{pmatrix} \begin{pmatrix} I_1 \\ I_2 \end{pmatrix} = \begin{pmatrix} -iI_2 \\ iI_1 \end{pmatrix}.$$

There are found several works where Pauli Y gate are implemented by the quantum property of light [1, 2]. In this paper, we propose a new concept of using the mechanism of Pauli Y gate to develop a quantum oscillator in photonic band gap structure-based crystal where the output states of the system will oscillate along with its phase. The truth table of the oscillator is depicted in Table-1.

Table-1: Truth table of the Pauli Y gate-based oscillator

Condition	Input		Oscillatory output	
	A	B	C	D
The initial inputs are given to both A and B	$I_1(\upsilon_1)$	$I_2(\upsilon_2)$	$-i\ I_2(\upsilon_2)$	$i\ I_1(\upsilon_1)$
The inputs are withdrawn	$-I_1(\upsilon_1)$	$I_2(\upsilon_2)$	$-i\ I_2(\upsilon_2)$	$-i\ I_1(\upsilon_1)$
	……..	…….	$-i\ I_2(\upsilon_2)$	$i\ I_1(\upsilon_1)$
	……..	……..	$-i\ I_2(\upsilon_2)$	$-i\ I_1(\upsilon_1)$
	…….	……..	Continued……	

The detailed circuit diagram and the all-optical operation using photonic band gap crystals are demonstrated in the paper.

References

1. Baishali Sarkar et. al., *J Opt.* 46, 143–148 (2017).
2. Paromita De et. al., *Opt. Laser Technol.* 152, 108141 (2022).

OED350 Enhanced photovoltaic performance of *insitu* grown rGO/TiO_2 hybrid-based dye sensitized solar cells

Lakshmi Srinivasan[1], Narayanapillai Manoj[1,2], Pramod Gopinath[1,3]*
[1]Inter University Centre for Nanomaterials & Devices
[2]Department of Applied Chemistry
[3]International School of Photonics
Cochin University of Science & Technology, Kerala, India,682022.
Corresponding author email: pramod@cusat.ac.in

A mesoporous nanostructure of anatase TiO_2-rGO hybrids were synthesized using hydrothermally modified solgel method. The TiO_2 nanocrystals grow in situ in the hybrid preparation while the graphene oxide sheets are simultaneously reduced to graphene layers. Graphene sheets are grown solely on ellipsoidal TiO_2 nanocrystals, exposing high energy {001} and {010/100} facets. The hybrid was created with Cetyltrimethylammonium bromide (CTAB) as the capping agent and has a minimal graphene content than as-grown TiO_2. By using transmission electron microscopy (TEM), X-ray diffraction (XRD), X-ray photoelectron spectroscopy (XPS), and Fourier transforms infrared spectroscopy (FTIR), the nanostructure of the obtained nanohybrids were characterized. The rGO/TiO_2 composite photoelectrode-based dye-sensitized solar cell (DSSC) has a high energy conversion efficiency of 7.8% compared to a DSSC based on pure TiO_2 photoelectrode efficiency of 5.9%, and this improvement is accompanied by an increase in both short-circuit photocurrent density and open-circuit voltage. The critical component causing the enhanced photogenerated electron transfer ability and decreased charge recombination is the incorporation of two-dimensional graphene nanosheets in the TiO_2 electrodes.

References

1. Padmanabhan. N.T et al Catalysis Today 348,63-71(2020).
2. Zhu.M et al Journal of Power Sources, *262*, 349-355(2014).

OED351 Photoluminescence spectra and site selective excitations of Eu^{3+}:Y^{3+}-$SrTiO_3$ for visualizations of latent fingerprints and red LEDs.

*Satyam Upadhyay [a], Arpita Dwivedi [a], Monika Srivastava [b], S. K. Srivastava [a *]*
[a] Department of Physics, Institute of Science, Banaras Hindu University, Varanasi, 221005, India.
[b] School of Materials Science and Technology, Indian Institute of Technology (Banaras Hindu University), Varanasi, India
[*]Corresponding author: S. K. Srivastava
ORCID ID: 0000-0001-6535-0712
Corresponding author's email: sanjay_itbhu@yahoo.com

Abstract: We have synthesized europium and yttrium doped strontium titanate (Eu^{3+}:Y^{3+}-$SrTiO_3$) for visualizations of latent fingerprints and red LEDs with varying concentration of Eu and Y has been depicted in the figure 1. Strontium titanate (STO) is an ABO_3 type of phosphor material that is mainly used in the field of latent fingerprint visualization, LED fabrication, solar cells, and hydrogen production. The STO can be improved using most promising trivalent rare earth elements (REE). Especially red–luminescence of Eu^{3+}–doped perovskites under UV radiation had widely investigated. $SrTiO_3$ is a well-known perovskite-

type incipient ferroelectric with a large dielectric constant. The doping of REE with perovskite materials opens a new era for researchers and improves the fluorescent properties of these phosphor materials. The as -synthesized nanophosphors are analyse using various characterization techniques such as UV-vis, PL spectra, powder XRD, transmission electron microscopy techniques. Powder XRD pattern reveals the approximate crystallite size and consistent with TEM. The europium concentration is optimized using photoluminescence measurement and the intensity is maximum at 3 mol % Eu. The Eu^{+3} doped Y^{3+}-$SrTiO_3$ (3 mol % Eu) phosphor have CIE coordinates as x = 0.656, y = 0.344 and a CCT value is 2435 K with 95 % color purity, respectively, which make this nanophosphor best suitable for LFP detection, security ink, LEDs, and several optoelectronic applications. In the future, we have performed the detection of latent fingerprint and also the lifetime decay analysis for red LEDs applications [1].

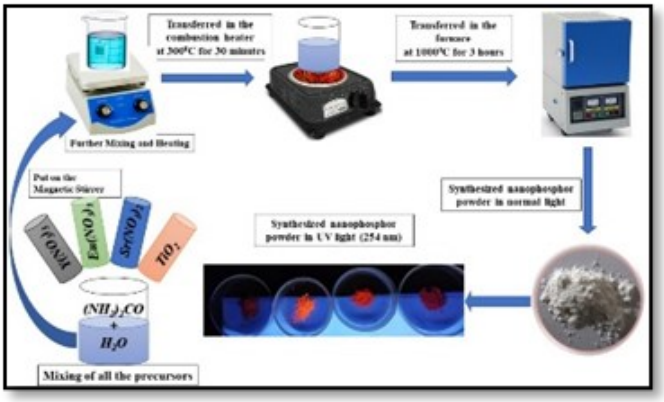

Figure 1: Schematic representation of synthesized nanophosphors

References

1. Yeshodamma, S., et al., *Monovalent ions co-doped SrTiO3:Pr3+ nanostructures for the visualization of latent fingerprints and can be red component for solid state devices.* Journal of Luminescence, 2019. **208**: p. 371-387.

OED352 Optical And Electrical Characterisation of NiO/ZnO Heterojunction Using Pulse Laser Deposition Technique

Siddhartha Panwar[1] Anirban Mitra[1]

[1]Department of Physics, Indian Institute of Technology Roorkee-247667, Uttarakhand, India

siddhartha_p@ph.iitr.ac.in

INTRODUCTION-

ZnO is a n- type of semiconductor with a large bandgap of 3.3 eV. Due to its large band gap, ZnO has been a very dominant material for photodetectors, photo-sensing, etc. On the other hand, NiO is a p-type semiconductor that also has a large bandgap of order 3.8 eV. These materials are UV-active materials due to their large bandgap.

EXPERIMENTAL SECTION-

An Nd-Yag laser with an energy density of 140mJ/pulse and a wavelength of 355nm was employed for this deposition. In this process, we use 30K laser shots for NiO film deposition and 9K laser shots for ZnO film deposition. The distance between the substrate and the target is 4.5 cm. The temperature of the substrate is set to 400°C throughout the procedure. We anneal at 400° C after the deposition of each layer.

The oxygen pressure during the whole deposition process is 30 mTorr.

RESULTS-

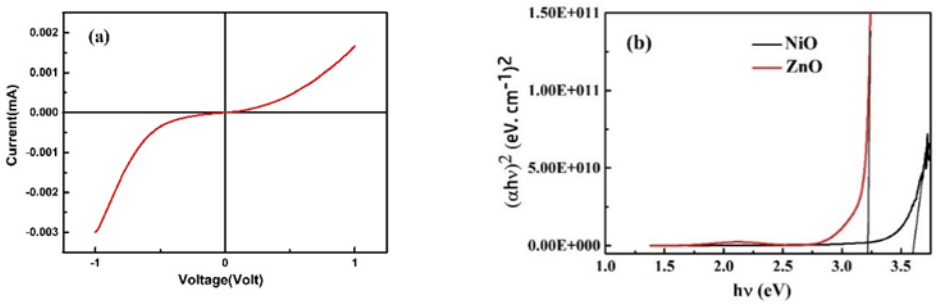

FIGURE 1. (a) I-V characteristics of NiO/ZnO heterojunction (b) Plot of $(\alpha hv)^2$vs. hv

The I-V characteristic was measured in dark condition. Figure1 (a), NiO/ZnO heterojunction device shows rectifying current flow. The plot of $(\alpha hv)^2$ versus hv is presented in Fig. 1 (b), the optical bandgaps of NiO and ZnO films were estimated to be 3.58 eV and 3.22 eV respectively.

CONCLUSION-

In summary, we deposited NiO and ZnO films upon a glass substrate using the pulse laser deposition technique. NiO and ZnO films have transmittances in the visible region of around 80%–90% and 40%, respectively. NiO and ZnO films have thicknesses of 550 nm and 308 nm, respectively.

OED353 Optical phase shift keying scheme using Kerr switch

Suranjan Lakshan[1], Sourangshu Mukhopadhyay[1]*

[1]Department of Physics, The University of Burdwan, Golapbag, Burdwan-713104, West Bengal, India

**Corresponding author: laxmansur21@gmail.com*

Abstract: Optical Kerr material is found highly potential in all-optical switching. Several researchers are seen in last few decades, where these Kerr material are used in communication and computation of optical data [1-2]. Again Phase Shift Keying (PSK) is established as a very potential digital modulation scheme, which is used in transportation of digital data in long distance communication [3]. In this paper, the authors propose a new concept of developing optical PSK signal using light as both carrier wave and message signal. In the figure 1 the block diagram of the scheme is given.

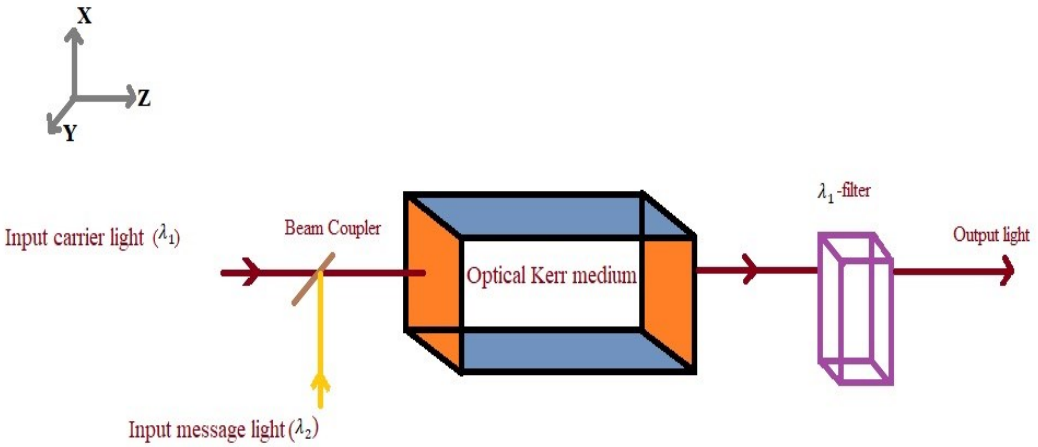

Fig.1: The block diagram of optical PSK system

The whole scheme is all-optical/ photonic and hence it is superfast in nature.

References

1. Agnijita Chatterjee et. al., *J Opt*. 46, 415–419 (2017).
2. Shuvra Dey et. al., *Optoelectron Lett.* 15, 317–320 (2019).
3. Baishali Sarkar et.al., *J Opt.* (2023).

OED354 Polymer dispersed liquid crystal film for tunable surface plasmon resonance

*Vaibhav Sharma[1], and Aloka Sinha[2]**

[1,2] Department of Physics, Indian Institute of Technology Delhi, New Delhi, India-110016

aloka.sinha@physics.iitd.ac.in

Abstract: Surface plasmon resonance (SPR) is an exciting phenomenon that is widely used in biosensing applications. SPR applications are typically static, and the geometry of the setup dictates the coupling conditions [1]. Liquid crystals (LCs) are exciting materials for SPR because they exhibit unique electro-optic properties. The electrically controlled orientation of LC molecules affects their RI and optical response of SPR [2]. Controlling the coupling condition is one of the key benefits of using LC in SPR-based applications. However, the major problems of using commercial LCs in the SPR are their durability, response time, and interaction with the external environment. Hence to overcome these problems, we propose a polymer-dispersed liquid crystal (PDLC) film in the SPR phenomena to tune the coupling condition using an external electric field. PDLC is an interesting material in which the LC droplets are dispersed within a polymer matrix, which helps to protect the LC layer from physical damage and environmental factors and enhances the overall durability of the SPR. In addition, the PDLC offers several advantages, such as no leakage of material, higher response time, and they are not influenced by any gravitational force and mechanical shock. Here, we describe a numerical and experimental observation of the displacement of SPR by using PDLC as a dielectric layer. The Kretschmann configuration setup is used to study the SPR response, and an external voltage is applied to the PDLC layer to shift the resonance angle. (See Fig. 1). The experimental finding shows that by adjusting the applied voltage, the RI of the PDLC can be modified. This change in RI at the metal-dielectric interface shifts the SPR angle (See Fig. 2). This can provide flexibility in various experimental designs. The voltage-induced shifts in plasmon resonance can be utilized for optical modulation, enabling the development of new types of modulators and switches in integrated photonic circuits.

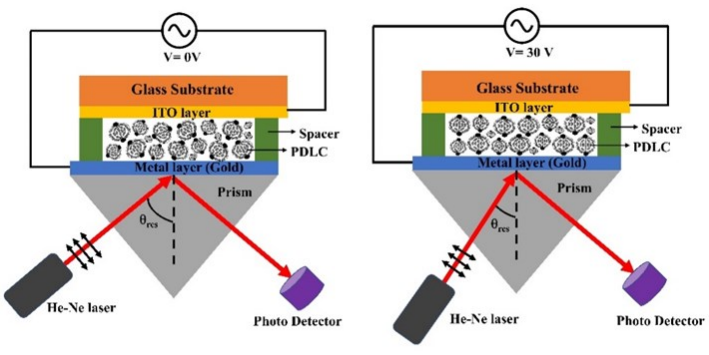

Fig. 1. Kretschmann configuration of tunable SPR using PDLC layer.

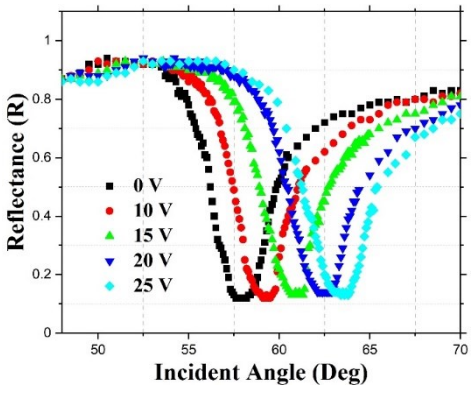

Fig. 2. Experimental observation of displacement of SPR with the applied voltage.

References

1. V. Yesudasu, et.al., *Heliyon,* 7 (3), (2021).
2. A. Vahedi, et.al., *Plasmonics*, 15, 61–71, (2020).

OED135 High Sensitive, Self Powered and Flexible UV Photodetector Realized with Eco-Friendly Zn-Al:LDH Ns/NiO/Spiro-MeOTAD Heterojunction

*Alphi Maria Thomas[1], Soon-Gil Yoon[1]**
[1]Chungnam National University, Daejeon, 34134, Republic of Korea
**Corresponding author: sgyoon@cnu.ac.kr*

The development of efficient and high sensitive UV photodetectors (PD) is a hot topic of research in the recent times. The advancement of semiconductor-based optoelectronics has enabled to design and fabricate various UV PDs that efficiently detect UV radiation, however, currently there is a great deal of research on novel functional materials to achieve more winning properties like lower power consumption, flexibility, portability etc. Layered double hydroxides (LDH), an emerging class of anionic clay with lamellar structure, have attained considerable attention in the field of material science due to their unique thermal, optical and dielectric properties. LDH nanostructures have been widely utilized for many applications, including energy, healthcare, catalysis and optics.

Herein, we report an efficient, self-powered and flexible UV PD based on Zn-Al:LDH nanosheets (Ns), in which a heterojunction is formed with n-type Zn-Al:LDH Ns, p-type NiO thin film and Spiro-MeOTAD polymer on flexible PET/ITO substrates. Eco-friendly and vertically oriented LDH Ns are formed by dipping FTS sputtered-10% Al doped ZnO (AZO) thin film in DI water for 12 hours. A high sensitive photoresponse, which is in the order of 10^2 to 10^3, is obtained without an external bias, when the devices are illuminated with UV light. At 0.6 mW/cm^2 UV intensity, the responsivity and detectivity of the devices are found to be 4.4 mA/W and 3.2 × 10^{11} Jones, respectively. Moreover, the device shows a very stable performance up to 1000 bending cycles at a bending strain of 4%, confirming the excellent flexibility of the devices.

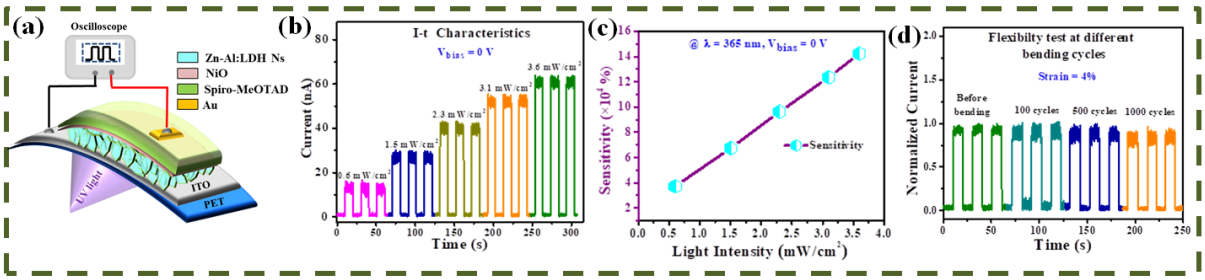

Figure 1: (a) The device structure (b) I-t characteristics at different UV intensities (c) Sensitivity (d) Flexibility test with different bending cycle

References

1. Alphi Maria Thomas et. al., *ACS Appl. Mater. Interfaces*, 13, 51, 61434 (2021).

OED136 Single wavelength Optical beam steering using carrier injected Tunable Grating Antennas

Krishnanunni R A [1], Sooraj Ravindran [1]
[1] Dept. of Avionics, Indian Institute of Space Science & Technology, Valiamala P.O, Thiruvananthapuram, 695547.

Optical Phased Arrays (OPAs) offer a cost-effective and high-speed technique for steering optical beams, which operate similar to phased array antennas in radar systems. In a typical OPA, 2-D beam steering is achieved by combining the phased array principle along with wavelength tuning. These OPAs have various applications, including LiDAR and free-space optical communication, where compactness, cost-efficiency, and energy efficiency are essential [1]. For these applications, the ability to change the steering angle of an OPA using a single wavelength is important as it eliminates the need for a high-power tunable laser[2].

In this work, we propose a unique method of beam steering in an OPA using single wavelength. Continuous beam steering of up to 3^0 was achieved by employing a tunable grating antenna. The grating teeth of the antenna is made in the form of a p-i-n modulator as shown in Fig. 1. The p & n doped regions are formed on both sides of the grating teeth. Applying a forward bias injects charge carriers into the intrinsic region (grating teeth), altering the effective refractive index of the grating, thus changing the direction of the out-coupled beam. To verify the steering capability of tunable grating antenna, we couple an optical fiber to the device and measure the coupling efficiency between the fiber and the device. The position of the fiber is precisely adjusted for peak coupling efficiency with the grating antenna. When a forward bias voltage is applied, effective refractive index of the grating changes. The index change influences the direction of the beam emitted from the grating antenna, as demonstrated by variation in coupling efficiency as shown in Fig. 2. The ability to vary the coupling efficiency in accordance to the applied bias confirms the beam steering ability of the grating antenna using single wavelength.

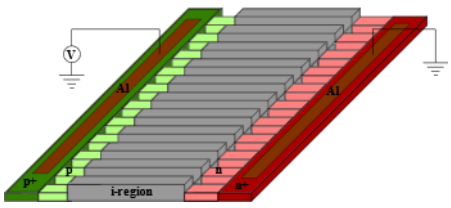

Fig.1 Schematic design of tunable grating antenna

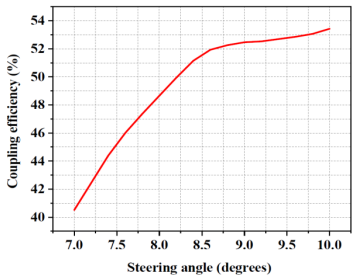

Fig. 2 Coupling efficiency vs steering angle.

References

1. Martijn J.R. Heck., Nano photonics. 2017 Jan 6;6(1):93-107.
2. Tyler NA et. al., Optics express. 2019 Feb 18;27(4):5851-8.

OED137 Integrated LED-Pumped Semiconductor Optical Amplifier

*V. Nithin and M. R. Shenoy**
Physics Department, IIT Delhi, New Delhi - 110016
**Corresponding author: mrshenoy@physics.iitd.ac.in*

Optical pumping of semiconductor optical amplifiers (SOAs) and semiconductor lasers is important to realize all-optical communication and function devices. [1,2] Typically, a pump laser, at a suitable wavelength, is used to generate carriers in the active medium, which then gives rise to signal amplification/lasing process. Alternatively, LEDs could be used as optical pump [3]; in addition to having the advantage of low-cost, LED's can be integrated into the device structure of the semiconductor laser/amplifier. In this paper we propose the design of an LED-pumped SOA wherein the LED is integrated in the structure of the SOA. Figure 1 shows a schematic of the LED-pumped SOA. Light generated by the LED is transversely coupled into the semiconductor active medium. The unabsorbed pump is reflected back into the active medium using the integrated Bragg reflector. The steady-state simulation was carried out using modified Connelley's model[2]. Figure 2 shows the variation of signal gain with LED pump power for two different LEDs of wavelengths of 1310 nm and 1350 nm with 50 nm FWHM. The LED spectrum is assumed to be gaussian in shape (see inset figure). Note that the gain is higher at $\lambda_c = 1310$ nm; also, it was observed that there is very little change in gain upon increasing $\Delta\lambda$ to 100 nm. Detailed results and discussion will be presented.

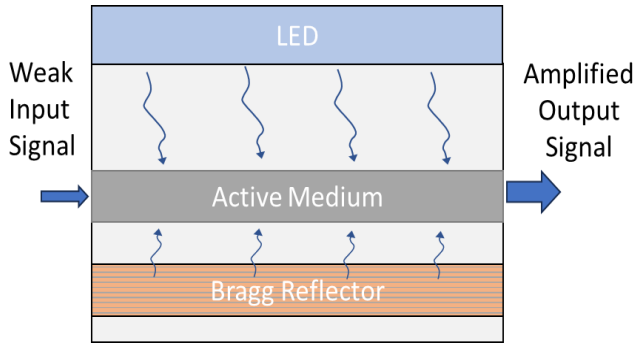

Fig.1: Schematic of LED-pumped SOA

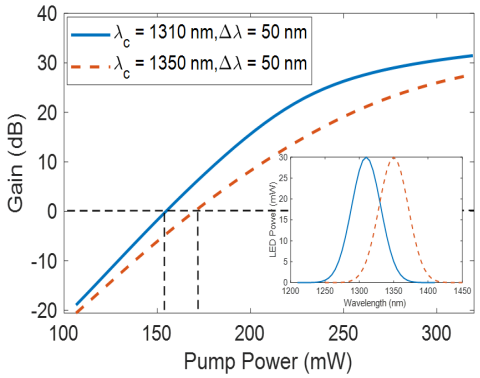

Fig.2: Variation of signal gain with LED Power; inset figure shows LED spectrum.

References

1. McCann *et al.*, *J Appl Phys* **97**, 053103 (2005).
2. Nithin V, M. Shenoy, and Y. Kumar, *IEEE Photonics J* **13**, 1 (2021).
3. Huang *et al.*, *Opt Express* **24**, 12043 (2016).

OED148 Fabrication and characterisations of 2D-MoS_2 thin films for optoelectronic and photonic device applications

Geeta[1], Eric Kumi Burimah[1], Animesh Jha[3]*
[11] School of Chemical and Process Engineering, University of Leeds, United Kingdom, LS2 9JT
**Corresponding author: g.sharma@leeds.ac.uk*

Molybdenum disulphide (MoS_2) and is a transition metal-dichalcogenides (TMD) material has layered structure. Recently it has drawn significant attention for exploring optoelectronic and photonic properties at sub-nanometre scale. The TMDs possess direct bandgap which is quite attractive for device engineering

and applications in photovoltaic, energy storage, and bandgap engineered light-sources. We have synthesized 2H MoS_2 using hydrothermal synthesis at 240 ºC for 24 h. The as synthesized powder was used for the fabrication of MoS_2 thin films using femto-second pulsed laser deposition (fs-PLD). The deposited films are stoichiometrically congruent with that of synthesized material. The materials were characterised using XRD, UV-vis absorption spectroscopy and Raman spectroscopy. Figure 1 below shows the Raman spectra of MoS_2 films grown at different temperatures (400 ºC and 600 ºC). Shift in the Raman bands are seen for the films deposited at different temperatures. The structural and optical properties of deposited films were analysed and compared. Such a comparative analysis may offer materials fabrication platform in future for engineering optoelectronic and photonic devices on silica glass and silicon platforms.

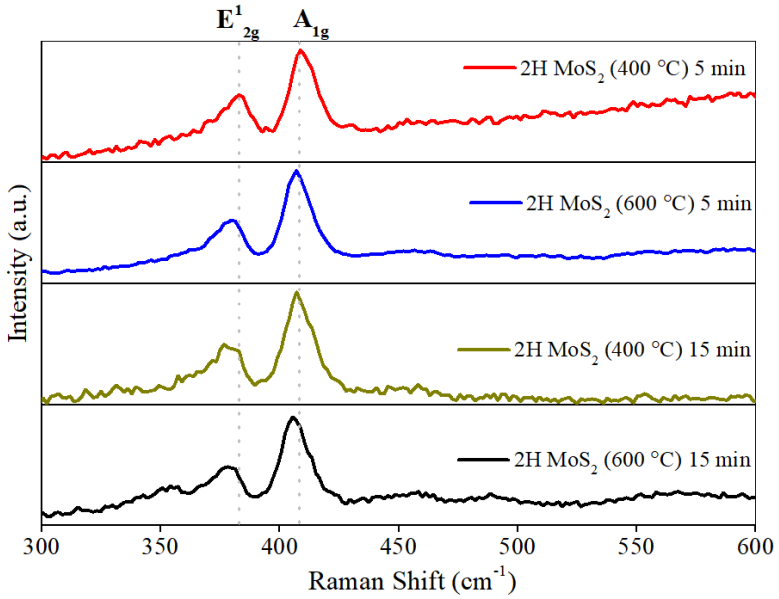

Figure 1: Comparison of Raman spectra of MoS_2 films grown at different temperature

Category 19

Photonic Crystals & Metamaterials (PHC)

PHC140 Design and Optimization of Graphene based Wiregrid Terahertz Polarizer

Anjali, R.K.Varshney, and Sunil Kumar

Department of Physics, Indian Institute of Technology Delhi, Hauz Khas, New Delhi, 110016, India

**Corresponding author: Anjali@physics.iitd.ac.in*

For the analysis of terahertz (THz) electromagnetic wave propagation, the polarisation must be characterised and controlled. In this context, the research and development of suitable polarizer devices are necessary [1-4]. Here, we describe a graphene -based THz polarizer that has been optimised for high polarization extinction ratio (ER), low insertion loss. The design and optimised outcomes of the graphene-based THz polarizer for the normal incidence are shown in Fig. (1). Numerical simulations have been performed using CST software based on finite difference time domain (FDTD) method.

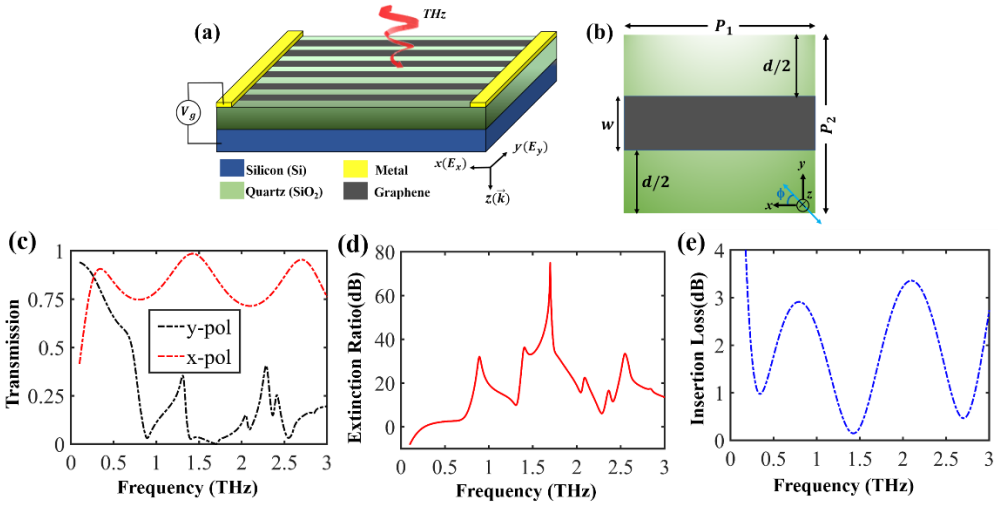

Fig. 1 (a) 3D schematic of the proposed structure (b) Unit cell of the proposed device (c) Amplitude transmission spectra for x and y polarized THz field (d) Extinction ratio and (e) insertion loss, corresponding to transmission spectra (as shown in part (c)), for E_F=50 meV and τ = 4 ps, P_1 =40 µm, P_2=45 µm, d =20 µm, , and w=25 µm respectively.

In the metastructure, graphene ribbons/strips are layered on top of a quartz-silicon substrate with a thickness of 100 µm. After cautious tuning, we were able to achieve a high value of ER of up to 75 dB (Fig.1(d)) with a very low insertion loss (Fig. 1(e)) at the targeted frequency of 1.7 THz. Furthermore, an average value of ER ~15 dB in the wide frequency range of 0.9 to 2.5 THz is also demonstrated.

References

1. L. Ju et.al., " Nat. Nanotechnol. 6, 630–634 (2011).
2. F. D'Apuzzo et.al., Nat. Commun. 8, 14885 (2017).
3. D. Sarker et.al., Opt. Express 29, 42713 (2021).
4. Anjali et.al., J. Opt. Soc. Am. B, 40(7), 1688-1695(2023).

PHC141 Hybrid Dark Resonant States for Thin Film Sensing

Sukhvinder Kaur[1,], Ravendra K. Varshney[1] and Dibakar Roy Chowdhury[2]*

[1]Department of Physics, Indian Institute of Technology Delhi, Hauz Khas, New Delhi, 110016, India

[2]Department of Physics, Ecole Centrale School of Engineering - Mahindra University, Jeedimetla, Hyderabad, Telangana, 500043, India

**phz198496@iitd.ac.in*

Metamaterials are artificial structures appropriately designed to manipulate electromagnetic waves. They exhibit two types of resonance response, namely bright and dark modes, on interaction with incoming electromagnetic radiation. Bright modes are excited via direct interaction with incident radiation, while dark modes are excited indirectly, often leading to lower radiative losses [1]. Due to indirect excitation, the coupling of dark modes is a challenging task as it reduces the intensity of the resonance. Minimal radiative losses in dark modes make them well-suited for sensing as they show large shifts in resonance frequency even for small perturbations [2]. In the present study, the coupling of dark resonating states is achieved by strategically placing two asymmetric split ring resonators (SRRs) in a mirror configuration [3]. By monitoring the interaction between these coupled dark resonances and the surrounding environment, we can detect even subtle variations in the thickness, making this approach valuable for a range of applications, including chemical analysis, environmental monitoring, and biomedical diagnostics.

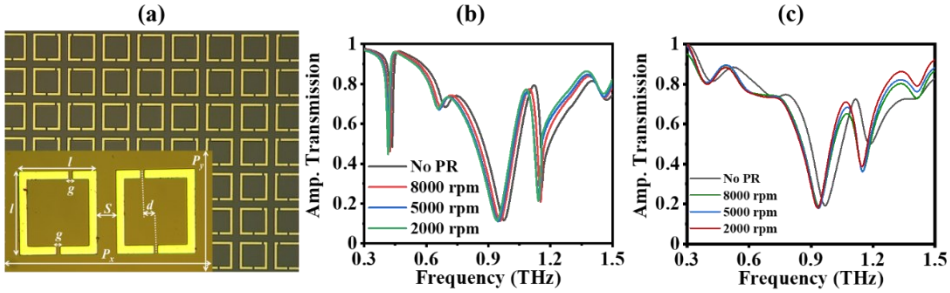

Fig. 1: Optical microscopic image of the proposed structure (Inset: unit cell of the fabricated structure with P_x= 150 µm, P_y=75 µm, l_r =60 µm, w_r=7 µm, g= 3 µm, d= 20 µm (b) Simulated and (c) Experimental transmission spectra depicting the shift in resonance frequency for different thicknesses of analyte layer.

Figure 1(a) shows the optical microscopic image of the proposed structure containing two asymmetric mirror resonators. The simulated and experimental transmission spectra for varying thicknesses of the analyte are shown in Figures 1(b) and 1(c), respectively. The simulation spectra show a shift in resonance frequency of hybrid dark modes by 20GHz and 42GHZ for an analyte of thickness 6 µm. In summary, the hybrid dark resonant structures can be utilized for thin-film sensing.

References:

1. Singh, R., et al., *Physical Review B*, 79(8), p.085111 (2009).
2. Zhao, W., et al., Plasmonics, 10, pp.469-474 (2015).
3. Kaur, S., et al., Journal of Applied Physics, 130(24) (2021).

PHC367 An Ultrathin Metamaterial Absorber with Ring-Disc Resonators using SiC Material

*Anil Kumar[1], Amritanshu Pandey[2], and S. K. Srivastava[1]**

[1] *Affiliated with Department of Physics, Banaras Hindu University, Varanasi, Lanka-221005 (INDIA)*

[2] *Affiliated with Department of electronic engineering, Indian Institute of Technology, BHU, Varanasi (India)-22100*

**corresponding author: sanjay_itbhu@yahoo.com*

In this work, a metamaterial absorber (MMA) is designed using ring-disc resonators structure. The simulation results indicate that the proposed metamaterial absorber can achieve up to 98 % absorptivity at wavelength 5.5 μm. The MMA structure is optimized to achieve nearly perfect absorption in terms of thickness of dielectric layer, radius of disc, width of rind etc. Present silicon carbide (SiC) and gold (Au) based MMA shows almost similar behavior for the transverse electric (TE) and transverse magnetic (TM) polarized incident light. It also shows the incidence angle independent absorption for the range 0-45 deg. The present MMA design shows highly polarization and angle independent behavior due to the symmetry in the structure. The mechanism behind the present MMA absorber is also explained in terms of impedance matching conditions.

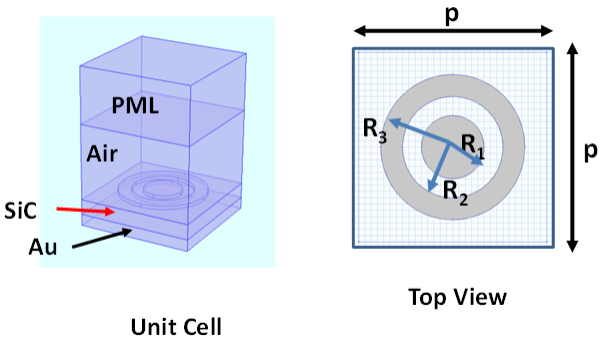

Fig: Schematic design of the proposed metamaterial (a) unit cell and (b) top view of unit cell

References:

1. V. Velselago et. al. Soviet Physics Uspekhi 10 (4) 509-514 (1968)
2. D.R. Smith et. al. Science 305(5685) 788-792 (2004).
3. C.M. Watts et. al. Nature photonics 8(8) 605-609 (2014).
4. N.I. Landy et. al. Physical review letters 100 (20) 207402 (2008).
5. D. Smith et. al. Physical review E 71(3) 036617 (2005).

PHC368 Robust microwave transport in topological ring resonator

Geetanjali Jena[1,], Gopal Kulkarni[2], Ravendra K. Varshney-[1], Dibakar Roy Chowdhury[2]*

[1]*Department of Physics, Indian Institute of Technology Delhi, Hauz Khas, New Delhi 110016, India*

[2]*Department of Physics, Mahindra University, Jeedimetla, Telangana 500043, India*

**Corresponding author: phz228023@physics.iitd.ac.in*

Over the past few years, topological photonic crystal (TPC) has seen phenomenal growth due to its various

intriguing properties, including backscattering immune wave transport, robust wave propagation, and uni-directional transmission [1-4]. This work studies a metallic rod-based TPC exhibiting robust energy transport in the microwave frequency regime.

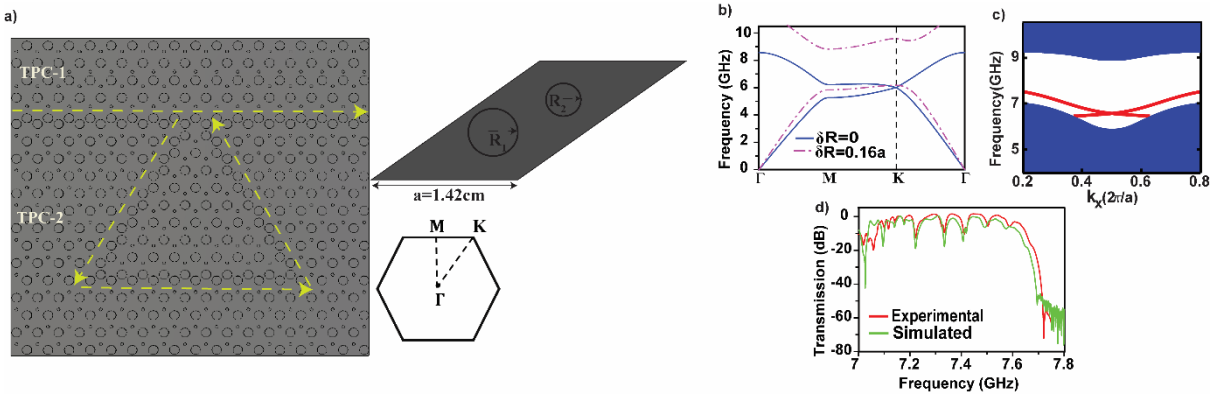

Figure 1: a) proposed TPC with the left panel showing the rhomboid unit cell of the TPC consisting of two Al rods of radius R_1= 0.23 a and R_2= 0.07 a and first Brillouin zone of TPC; the yellow dotted line indicates the direction of energy propagation b) bulk band topology for δR=0 and δR=0.16 a c) projected band diagram of the TPC with blue shaded region indicating the bulk photonic bands and red solid lines showing the excited edge states d) simulated (green) and experimental (red) transmission spectra of the TPC

The schematic of the proposed structure is illustrated in Fig. 1(a), which consists of a ring-shaped resonator being coupled to a straight topological waveguide. As shown in Fig. 1(b), the degeneracy at the K (K') point of the unperturbed TPC (δR=0) can be lifted by introducing a geometrical perturbation in the rod diameters (δR=0.16 a), which leads to opening up a topological band gap of ~ 2.56 GHz .The coupling of TPC-1 and TPC-2 through the zigzag domain boundary leads to the excitation of topological edge states, as evident from the red solid lines of Fig. 1(c). The robust microwave propagation of the proposed structure is shown in Fig. 1(d), which indicates a high transmission of ~0 dB in the investigated frequency regime. This study provides a promising platform for realizing various potential microwave devices, including slow light waveguides, lossless devices, and efficient sensors.

References

1. Zheng Wang et. al., *Nature* 461, 772-775 (2009).
2. Yuting Yang et. al., *Physical review letters* 120, 217401 (2018).
3. Min Wu et. al., *Optics Express* 30, 6275-6283 (2022).
4. Sambhu Jana et. al., *Optics communication* 529, 129111 (2023).

PHC369 Frequency Selective Surface for Third Harmonic Generation Using Split Ring Resonator at THz Frequencies

*Mitali Sahu[1] and Partha Roy Chaudhuri[1]**

[1]Department of Physics, Indian Institute of Technology, Kharagpur, India, 721302

**Corresponding author: roycp@phy.iitkgp.ac.in*

We report here new designs of frequency selective surface (FSS) metamaterials (MM) composed of patterned split-ring resonators (SRR) to obtain third harmonic generation (THG) at THz frequencies. The efficient THG is obtained by aligning the fundamental (ω) and third harmonic (3ω) frequencies with the resonances of our proposed metasurface structure, leading to energy confinement in both steps of excitation at

$\omega\ (3.7\ \mathrm{THz})$ and radiation at $3\omega\ (11.1\ \mathrm{THz})$, with an input intensity of $0.4\mathrm{MW/cm^2}$. SRRs are used in the proposed structure because of their high sensitivities to electromagnetic waves.

Summary: The proposed THz FSS device is made from symmetric SRRs of MM, which are periodic structures with a band pass frequency response. One-unit cell geometry of the nonlinear FSS is shown in Fig. 1. A split ring slot is patterned on a geometrically thin copper layer that sits on a thin nonlinear dielectric layer substrate with the design parameters. Being driven by the strong magnetic dipole resonance at the pump wavelength and a high-quality mode at the harmonic wavelength, the efficient TH radiation is generated predominantly along the vertical directions under the normally incident plane-wave excitation. The field enhancement yielded by the proposed FSS is shown in Fig. 2. Figure 3 shows the plot of mode field distributions corresponding to the fundamental and third harmonic one. These results are new as regards third harmonic in THz using our engineered MM structure.

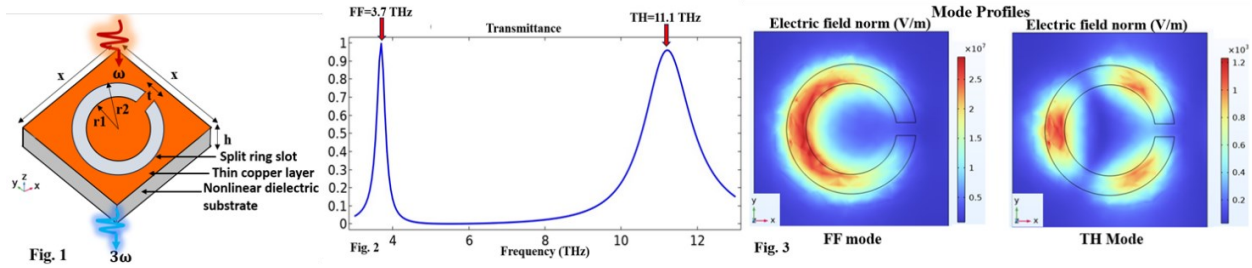

Fig. 1. Schematic illustration of the unit cell of proposed nonlinear FSS surface**. Fig. 2** Computed transmittance plot of FF mode and TH mode as a function of incident frequency. **Fig. 3** Field enhancement of FF and TH mode.

References:

1. B Jin et. al., J. Opt. 19, 094005 (11pp) (2017).
2. A Theodosi et. al., Opt. Express.30, 460-472 (2022).

PHC370 Asymmetric Reflections in Defective Photonic Crystals with Atomic Doping

Nancy Ghangas, Shubhrangshu Dasgupta*

Department of Physics, Indian Institute of Technology Ropar, Rupnagar, Punjab (140001).

**nancy.19phz0006@iitrpr.ac.in*

Parity-Time (PT) symmetric systems in periodic structures represent a captivating realm of research within the field of optics. These structures possess a distinctive symmetry, where the Hamiltonian remains invariant under a combined operation of parity(P) and time-reversal(T). Remarkably, PT symmetric periodic structures exhibit exceptional optical properties, including coherent perfect absorption[1], unidirectional invisibility[2] and unidirectional lasing[3]. In periodic structures, this symmetry manifests as a periodic modulation of refractive index or gain/loss distribution, contributing to a non-Hermitian Hamiltonian and unidirectional reflection with special type of singularities[4,5]. A comprehensive review of unidirectional reflectionless light propagation in photonic devices at exceptional points has been provided in both PT-, non-PT, and PT anti-symmetric optical systems[6,7]. It has also been shown numerically in a simple two-layer non-PT symmetric slab by tuning the imaginary part of the refractive indices and thicknesses of the slabs[8]. In our work, we have demonstrated the non-reciprocal reflection in defective photonic crystals when the defect layer is doped with three-level atoms [see Fig. 1]. The photonic crystal with defect layer acts as a two-mode cavity. Once this layer is doped with atoms, the defect frequencies are red shifted in the

transmission spectrum. The spectral properties of defect modes can be controlled with the control field Rabi frequency, G. We observe, using scattering matrix formalism, that the crystal behaves as non-PT symmetric one by violating symmetry relations of the corresponding matrix. The transmission in the crystal is reciprocal but there is an interplay in reflection and absorption for two modes lying in the photonic bandgap of the crystal as shown in Fig. 2 for one of the modes.

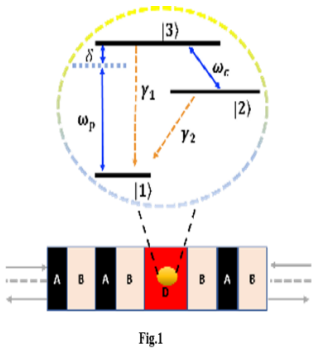

Fig.1

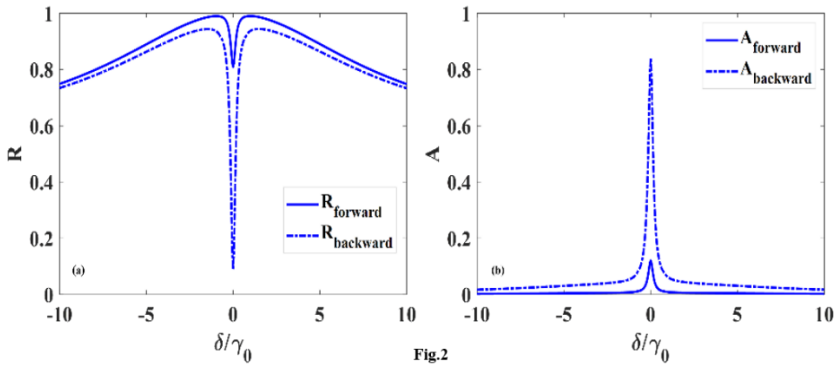

Fig.2

Fig.1. A schematic diagram of lambda type three level system, in the configuration $B(AB)^N D(BA)^N B$. The refractive indices $n_A = 2.22$, $n_B = 1.41$, $n_D = 1.05$, N=5. The susceptibility of the defect layer $\varepsilon(\omega) = n_D^2 + \chi$, where χ is for atoms. We have also chosen $n_i d_i = \frac{\lambda}{4}, (i \in A, B)$, *where* d_i is the width of the i-th layer and $\lambda = 632.8nm$ near the middle of the bandgap and $n_D d_D = \frac{\lambda}{4}$. The atom (decay rate γ_{12}, n is the number density) is driven by field with Rabi frequency G and detuning, $\delta = \omega - \omega_0$.

References

1. W. Xiong et al., Phys. Rev. A 101, 063822 (2020).
2. Z. Lin et al., Phys. Rev. Lett. 106, 213901 (2011).
3. H. Ramezani et al., Phys. Rev. Lett. 112, 043904 (2014).
4. Jin-Hui Wu, M. Artoni, and G. C. La Rocca, Phys. Rev. Lett. 113, 123004 (2014).
5. H. Ramezani et al., Phys. Rev. Lett. 113, 263905 (2014).
6. Yin Huang et al., Nanophotonics 6, 977 (2017).
7. You-Lin Chaung et al., Opt. Exp. 379, 769 (2020).
8. Yun Shen, Xiao Hua Deng, and Lin Chen, Opt. Exp. 22, 019440 (2014).

PHC371 Electromagnetic response of liquid crystal based tunable all-dielectric quasiperiodic metasurfaces

Pratiksha Sakhare[1] and Jayasri Dontabhaktuni[1]*

[1]Department of Physics, Ecole Centrale School of Engineering, Mahindra University, Hyderabad, India - 500043.

**Corresponding author: jayasri.d@mahindrauniversity.edu.in*

The control of light-matter interaction in metasurfaces offers an unprecedented potential for manipulation and tuning of light. All-dielectric metasurfaces have been gathering lot of interest in the recent years due to their intense localization of fields, excitation of magnetic modes as well as giving rise to novel resonant modes such as anapoles, quasi-BIC states, etc. [1, 2]. Liquid Crystals have attracted great attention due to the optical anisotropy and flexible control through optical, thermal, magnetic and electrical fields [3]. In the current work we present a detailed numerical investigation of Tellurium (Te) based 2-D Penrose-quasiperiodic metasurfaces in the air with five-fold symmetry. We calculate scattering response, near-field and far-field radiation profiles of Tellurium (Te) based quasiperiodic metasurfaces as a function of liquid crystal orientations in infrared frequency range. Our results from these calculations show higher rotational symmetries of the response and give rise to multi-functional metasurfaces as a function of the liquid crystal orientations.

References

1. P Sakhare et. al., *Scientific Reports*, *13* (1), 6780 (2023).
2. K Koshelev et.al., *Science Bulletin*, *64*(12), 836-842 (2019).
3. A Santonocito et. al., *Nanomaterials, 13* (10), 1633 (2023).

PHC372 All-optical 2 x 2 switch based on nonlinear photonic crystal ring resonator

Priyanka Kumari Gupta[1], Punya Prasanna Paltani[2,3], Shrivishal Tripathi[1,3]*

[1]Department of Physics, IIIT Naya Raipur, Chhattisgarh 4936611 (priyanka@iiitnr.edu.in)

[2]Department of Physics, IIIT Naya Raipur, Chhattisgarh 4936611 (punya@iiitnr.edu.in)

[3]Department of ECE, IIIT Naya Raipur, Chhattisgarh 4936611 (shrivishal@iiitnr.edu.in)

**Corresponding author: Priyanka Kumari Gupta (priyanka@iiitnr.edu.in)*

This paper proposes a novel 2 x 2 all-optical switch using a two-dimensional square lattice of 31 x 35 dielectric rods in an air medium. The dielectric rods are made up of a direct bandgap material, gallium arsenide (GaAs), having a high refractive index value of 3.4 and Kerr (nonlinear) coefficient of 3.1 x 10^{-16} m^2/W. The basic 2 x 2 state of the photonic crystal-based optical switch (bar and cross states) is implemented using the nonlinear Kerr effect. The photonic bandgap diagram is calculated using the plane wave expansion method, shown in Figure 1, and the suggested structure is shown in Figure 2. The finite-difference time-domain method is used to find the operational power intensity value for the cross and bar states and the performance parameters of an optical switch, such as the extinction ratio, insertion loss, and cross-talk values. The resonance/operating wavelength is at 1558 nm, and the power intensity values are 110 W/μm^2 and 200 W/μm^2, respectively, for the cross-state and bar states. The cross-state and bar-state extinction ratio values are 3.36 dB and 15.60 dB. Similarly, the insertion loss values are 2.43 dB and 0.985 dB, and cross-talk values are -5.80 dB and -16.59 dB for the cross-state and bar state, respectively. Hence, an all-

optical 2 x 2 switch using gallium arsenide dielectric rods is proposed, which is highly suitable nowadays for switching purposes.

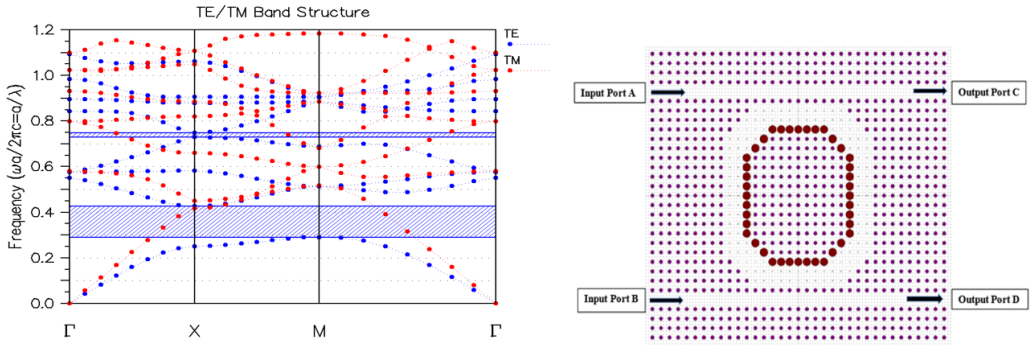

Fig. 1. PBG range of GaAs glass rods: 0.292 <a/λ < 0.426 and 0.730 <a/λ < 0.748 (TE Polarization)

References

1. M. Ghadrdan et al., *Opt. Quantum Electron*.,48(5),1–9 (2016).
2. M. Djavid et al., *Photonic Netw. Commun*., 35(1), 90–96 (2018).
3. P. K. Gupta et al., *Fib. Inte.* 41(5-6),143-153 (2022).

PHC373 Realizing an Optical Micro-Cavity in a $CuCo_2O_4$-W-$CuCo_2O_4$ Thin Film Stack for Spectrally Selective Solar Absorbers

*Silpa S[1], Srinivas G[2], Arup Biswas[3], Harish C. Barshilia[2], Vinayak B. Kamble[1]**

[1]*School of Physics, Indian Institute of Science Education and Research Thiruvananthapuram 695551 India.*

[2]*Surface Engineering Division, CSIR-National Aerospace Laboratories, Bangalore 560017, India.*

[3]*Spectroscopy Division, Bhabha Atomic Research Center, Mumbai 400 085, India*

**Corresponding author: kbvinayak@iisertvm.ac.in*

The ability to tap the potential of non-renewable sources is severely limited by the availability of suitable and efficient materials. The choice of materials in that case considers not only the performance indices such as efficiencies but also the earth's abundance (cost), environment friendliness, stability, ease of fabrication, scalability, reproducibility, etc. For efficient conversion of solar energy to thermal energy, specially designed spectrally selective materials are highly recommended. On these benchmarks, oxide thin films made by sputter deposition methods surpass most other classes of materials, which involve complex designs of energy harvesters or chemically or thermally unstable materials. Here, we design a dielectric-metal -dielectric multilayer stack with an optical micro-cavity of a 12 nm tungsten layer formed between two dielectric layers of transition metal oxide $CuCo_2O_4$ (CCO). This has led to enhanced solar absorption[1] (α= 0.9) and low thermal emittance (ε<0.2). The cavity-induced enhanced absorption has been demonstrated through experiments as well as multiphysics simulations. The material characterizations revealed that the underlying spinel crystal structure and the nano-sized grain-like morphology of CCO layers caused enhanced visible absorption. The simulation results satisfactorily reproduce the experimental reflectance and demonstrate maximum power dissipation in the metallic layer in visible as well as NIR regions.

References

1. Silpa, S. *et al.* (2023) 'Realizing an Optical Micro-Cavity in a $CuCo_2O_4$-W-$CuCo_2O_4$ Thin Film Stack for Spectrally Selective Solar Absorbers,' Adv. Optical Mater. 2023, 2300567.

PHC374 Terahertz Transmission studies on plasmonic hole arrays of different geometries

Vaishnavi Sajeev[1], Koijam Monika Devi[1] and Dibakar Roy Chowdhury[1]

[1]Department of Physics, Mahindra University, Hyderabad, 500043, India

vaishnavi20pphy009@mahindrauniversity.edu.in

The phenomenon of light passing through small apertures, known as extraordinary transmission (EOT), has been the subject of extensive research and has garnered significant interest in the scientific community [1] [2]. In this work, we perform a comparative analysis of circular and square hole arrays operating within the Terahertz (THz) frequency range, employing numerical simulations using CST Microwave Studio. Fig. 1 depicts the THz transmission through the circular and square hole arrays. Noble metals like Al, Au, and Ag on a Si substrate are employed for constructing the metal-based hole arrays. Our results indicate that despite variations in the metal type, the THz transmission spectra (fig. 2), and the position of resonance peaks exhibit remarkable consistency, primarily attributed to the high conductivity of these metals (~10^7 S/m). Both Rayleigh's and Wood's anomalies are also observed in the transmission spectra. Also, we have studied the transmission characteristics by changing the periodicity while keeping the hole radius and total thickness constant as shown in Fig. 3. Notably, our study unveils significant disparities in resonant quality (Q) factors and resonance characteristics between circular and square hole arrays and also on changing the periodicities as well. We attribute these distinctions to the influence of corner effects in square resonators, leading to increased resistance and consequent reductions in resonance Q factors. We believe our findings can be helpful in realizing ultra-sensitive sensors along with a narrow band pass filter for the terahertz regime.

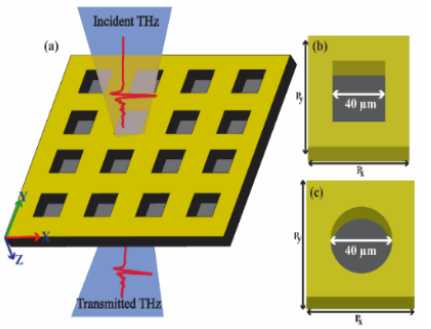

Fig. 1. (a) Artistic view of THz pulse passing through the hole arrays, (b) Unit cell of Square, and (c) Circular hole array perforated with a metal sheet on a Si substrate

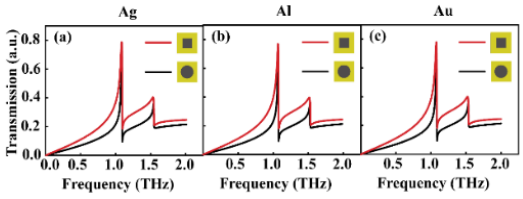

Fig. 2. Transmission peaks of circular (black curve) and square (red curve) hole arrays for different metals

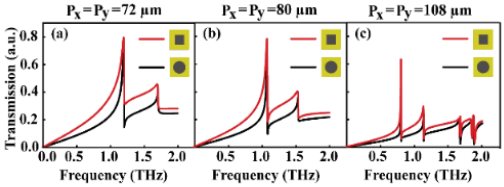

Fig. 3. Transmission peaks of circular (black curve) and square (red curve) hole arrays by varying the periodicity

References:

1. R. S. Anwar et. al., Digit. Commun. Networks **4**, 244 (2018).
2. T. W. Ebbesen et. al., Nature **391**, 667 (1998).

PHC375 Ultra-compact Dielectric Metalens in Mid-Infrared region

*Vishakha Sharma[1], Yogita Kalra[2,3] Ravindar Kumar Sinha[1,3]**

[1] *TIFAC-Center of Relevance and Excellence in Fiber Optics and Optical Communication, Department of Applied Physics, Delhi Technological University, Delhi, India*

[2] *Gautam Buddha University, Greater Noida, Gautam Budh Nagar, UP-201312, India*

Dielectric metalens have demonstrated excellent proficiency in effective light field manipulation and have been suggested for a number of devices with specialized functions. The higher aspect ratio of the unit cell nevertheless has drawbacks, making it much fragile and prone to breakage. In this study, we introduce a model concept to reduce the length of the nanopillar in the mid IR region. Proposed dielectric metalens is made up of hollow cylindrical nanopillar composed of amorphous silicon and the substrate of silica material. The electromagnetic analysis shows that the optimized height of our design is way smaller compared to the solid cylindrical meta-atom[1]. Also, the obtained results show that the designed metalens have high focusing efficiency upto 80% with polarization independent characteristics.

References

1. Z. Yao, W. Chen, Y. Chen, Double-layer metalens with a reduced meta-atom aspect ratio, Opt. Lett. 46 (2021) 1510. https://doi.org/10.1364/ol.422339.

Category 20

Photonic Networks, Switching Interconnects & Access (NET)

NET321 Quantum networks: A trapped ion cavity qed-based approach

Chilukoti Ashok[1,], Abhijit Kundu[1], Sumit Achar[1], and Arijit Sharma[1,2,*]*

[1]Department of Physics, Indian Institute of Technology Tirupati, Yerpedu-517619, A. P., India

[2]Center for Atomic, Molecular, and Optical Sciences and Technologies, Indian Institute of Technology Tirupati, Yerpedu-517619, A. P., India

**Corresponding author: cashok@iittp.ac.in, arijit@iittp.ac.in*

Quantum networks and the quantum internet are the epitome of secure communication [1]. They are pivotal for achieving unprecedented security through entanglement, no-cloning theorem and quantum key distribution (QKD) schemes. Cavity qed (quantum electrodynamics)-based trapped ion platforms are promising candidates for distributed quantum information processing and quantum networks. Compared to other systems, they offer a versatile opportunity to serve as deterministic single-photon sources with long coherence times due to the cooled, trapped ion, high interaction probability with single-mode fields, scalability, and high-fidelity quantum gates.

In our group at IIT Tirupati, our focus lies on the development of an on-demand, deterministic, narrowband, single photon generation scheme based on a trapped calcium ion ($^{40}Ca^{+}$) coupled to the single mode field of a high finesse cavity. This system offers the potential to effectively serve as a quantum node within an extended and scalable quantum network [2] using an interesting combination of "flying" and "stationary" qubits. Towards this objective, we are currently optimizing the design of the cavity qed-based ion trap platform through numerical simulations [see Fig.1] that assess various aspects such as the probability of photon emission, the temporal characteristics of generated photons, and the fidelity of photon production, all of which are critical for evaluating whether the proposed quantum node is well-suited for quantum networking applications. In this poster presentation, we will share the technical design of the experimental system, and also discuss the ongoing progress and outcomes of our numerical simulations.

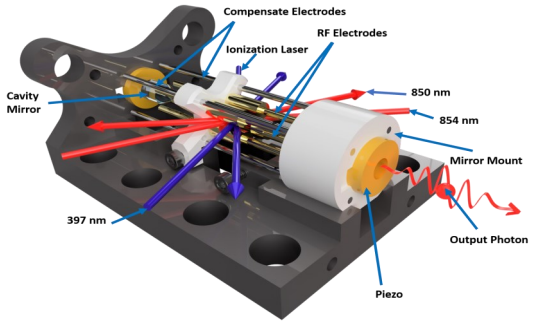

Fig. 1. Schematic of experimental setup

Arijit Sharma expresses gratitude for financial support from CAMOST and IIT Tirupati. Chilukoti Ashok acknowledges financial support from the I-Hub Quantum Technology Foundation, IISER Pune, via the Chanakya Postdoctoral Fellowship. Sumit Achar is thankful for financial support from CSIR (Government

of India) in the form of a Junior Research Fellowship (JRF).

References

1. H. J. Kimble, *Nature* 453, 1023-1030 (2008).
2. T. Walkar, *PhD Thesis* (University of Sussex, 2020).

NET322 An all optical quantum phase shift gate using Kerr Material

Minakshi Mandal Suranjan Lakshan, Mir Nadim Sarfaraj, Ayan Dey and Sourangshu Mukhopadhyay*
Department of Physics, The University of Burdwan, West Bengal, India, 713104
email: minakshi.bcc@gmail.com

Light can be used very successfully for implementation of quantum logic gates. The optical properties of light are used here to encode the qubits of the quantum gates.

Several quantum optical logic gates have been implemented using light as carrier signal. These gates are Pauli X, Y, Z gates, Hadamard gate, Square root of Controlled Z gate, Universal SWAP gate, phase shift gate, Toffoli gate, Fredkin gate etc [1-3]. To implement these gates different types of optical switches are used. The switches are Pockels cell based electro-optic modulators, semiconductor optical amplifier, photonic band gap crystal, etc.

Here in this paper we propose a completely new scheme of implementing optical phase shift gate in quantum domain. This phase shift gate uses optical Kerr material based switches. The schematic block diagram of quantum optical phase shift gate is shown in Fig. 1. Here the inputs I_1 and I_2 are given with the wavelength λ_1 and the phase controlling light I_3 is given with the wavelength λ_2. At output O_2 a $\lambda_1$pass filter is used.

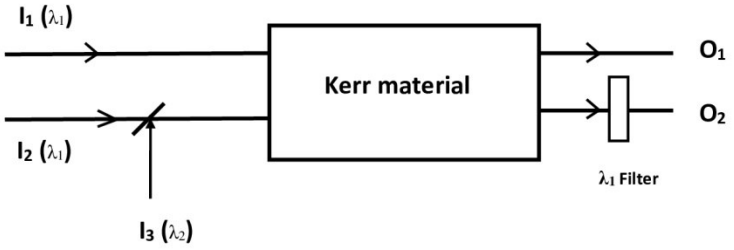

Fig. 1: Block diagram of phase shift gate

No electronic biasing signal is required here. For this reason this type of gate functions with a very high speed greater than THz limit. The power consumption is also found very low. Again as there is no electronic switching, so parallelism of light is highly exploited.

References

1. M. Mandal et. al. *Springer Proceedings in Physics*, 258, 687-690 (2021)
2. M. Mandal et. al. *Journal of Optics*, 52(1), 145-153 (2023).
3. M. Mandal et. al. *IET Optoelectronics*. 15, 52-60 (2021).

Category 21

Quantum Information (QI)

QI376 Activation of hidden nonlocality using local filtering operations based on CGLMP inequality

Asmita Kumari
S. N. Bose National Centre for Basic Sciences, Block JD, Sector III, Salt Lake, Kolkata 700106, India
Corresponding author: asmita.physics@gmail.com

Entanglement is necessary but not sufficient to demonstrate nonlocality as there exist local entangled states which do not violate any Bell inequality. In recent years, the activation of nonlocality (known as hidden nonlocality) by using local filtering operations has gained considerable interest. In the original proposal of Popescu [1] the hidden nonlocality was demonstrated for the Werner class of states in $d \geq 5$. In this paper, we demonstrate the hidden nonlocality for a class of mixed entangled states (convex mixture of a pure state and color noise) in an arbitrary d-dimensional system using suitable local filtering operations. For our demonstration, we consider the quantum violation of Collins-Linden-Gisin-Masser-Popescu (CGLMP) inequality which has hitherto not been considered for this purpose. We show that when the pure state in the aforementioned mixed entangled state is a maximally entangled state, the range of the mixing parameter for revealing hidden nonlocality increases with increasing the dimension of the system. Importantly, we find that for $d \geq 8$, hidden non-locality can be revealed for the whole range of mixing parameter. Further, by considering another pure state, the maximally CGLMP-violating state, we demonstrate the activation of nonlocality by using the same local filtering operation.

References

1. S. Popescu, Phys. Rev. Lett. 74, 2619 (1995).

QI377 Preliminary Investigations Of Quantum Maps On Photonic Qubits

*Bibia Alif[1], B Swathy Krishna[1] Sajeev D[1,]**
Government College Kariavattom, University of Kerala, Thiruvananthapuram, Kerala 695581
**Sajeev D: sajeevphy@gmail.com*

Quantum bits, which are generally known as qubits, experience decoherence - the loss of coherence when interacting with the environment [1], which poses a significant challenge to quantum computing and cryptography applications. Understanding the mechanism of decoherence is crucial for error mitigation and deeper analysis of quantum processes. Quantum map is a method used to understand, characterize, and reconstruct the quantum process. The primary aim of quantum maps is to obtain a process matrix, also known as a χ matrix, that fully characterizes the quantum process [2][3]. In this paper, we focus on numerically reconstructing the χ matrix for a quantum process involving the interaction of an optical qubit with a birefringent communication channel environment [4].

Our approach specifically examines the decoherence effects on an optical polarization qubit within a birefringent channel environment. By numerically reconstructing the output density matrix, we calculated the corresponding χ matrix for various input states. Subsequently, we analysed the changes in the elements of

the χ matrix as the number of passes through the channel sections varies. Figure 1 shows the plot of the χ matrix for the decoherence of a birefringent channel along the Z-axis on the Bloch sphere. The paper concludes by highlighting the potential of further research on the process matrix to gain deeper insights into the mechanisms of decoherence. By enhancing our understanding of decoherence, we can effectively mitigate its effects, ultimately leading to improved quantum communication capabilities.

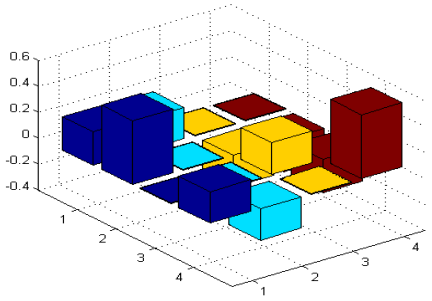

Figure 1. Plot of χ matrix with decoherence along Z direction.

References

1. AJ Berglund. Quantum coherence and control in one-and two-photon optical systems (2000). arXiv preprint quant-ph/0010001.
2. Isaac L Chuang and Michael A Nielsen. Prescription for experimental determination of the dynamics of a quantum black box. Journal of Modern Optics, 44(11-12):2455–2467, 1997.
3. Sajeev Damodarakurup, Marco Lucamarini, Giovanni Di Giuseppe, David Vitali, and Paolo Tombesi. Experimental inhibition of decoherence on flying qubits via “bang-bang” control. Physical review letters, 103(4):040502, 2009.
4. Z Wu, S Li, W Zheng, X Peng, and M Feng. Experimental demonstration of simplified quantum process tomography. The Journal of Chemical Physics, 138(2), 2013.

QI378 Anisotropy-assisted thermodynamic advantage of a local-spin thermal machine

Chayan Purkait[1], Suman Chand[2], Asoka Biswas[1]*

[1]Department of Physics, Indian Institute of Technology Ropar, Rupnagar, Punjab 140001, India

[2]Dipartimento di Fisica, Università degli studi di Genova, 16146 Genova, Italy

**Corresponding author: 2018phz0001@iitrpr.ac.in*

We study quantum Otto thermal machines with a two-spin working system coupled by anisotropic interaction represented by a parameter γ . Depending on the choice of different parameters, the quantum Otto cycle can function as different thermal machines, including a heat engine, refrigerator, accelerator and heater. We aim to investigate how anisotropy plays a fundamental role in the performance of the quantum Otto engine (QOE) operating in different time scales. We find that while the engine’s efficiency increases with the increase in anisotropy for the quasistatic operation, quantum internal friction and incomplete thermalization degrade the performance in a finite-time cycle causing a decrease in work and efficiency in finite-time operation, representing irreversibility. We show that the irreversibility in engine operation increases with γ . We also discuss the effects of incomplete thermalization on engine performance. Further, we study the QOE with one of the spins ('local' spin) as the working system. We show that local work extraction is

more robust than the global one, and the efficiency of such an engine can surpass the standard quantum Otto limit, along with maximum power, thanks to the anisotropy. This can be attributed to quantum interference effects. Specifically, in finite-time operation, the efficiency oscillates with respect to the time of the unitary processes of the global system. Therefore, a local spin OQE can outperform the same QOE operating in a long time limit, and this outperformance in efficiency is directly associated with maximum power generation. We demonstrate that the enhanced performance of a measurement-based QOE originates from the same interference effects, as in a local-spin QOE for their finite-time operation.

References

1. Chayan Purkait, Suman Chand and Asoka Biswas, "Anisotropy-assisted thermodynamic advantage of a local-spin thermal machine", arXiv:2309.04757.
2. Vinjanampathy, Sai, and Janet Anders, "Quantum thermodynamics", *Contemporary Physics* 57.4 (2016): 545-579.

QI379 Quantum Synchronization between two spins group coupled via a spin-chain

Jatin Ghildiyal, Manju, Shubhrangshu Dasgupta, Asoka Biswas*
Department of Physics, Indian Institute of Technology Ropar, Punjab 140001, India
**Corresponding author: jatin.20phz0017@iitrpr.ac.in*

Synchronization is a universal phenomenon, which was first observed by Huygens in a classical clock pendulum [1] and later explored in a large variety of classical systems. However, in the realm of quantum mechanics, exploration of synchronization is relatively new. Recently, researchers have studied synchronization among spins which have no classical analogy. A spin chain represents a versatile model for a broad range of materials where spins are arranged in a one-dimensional lattice with an interaction strength that diminishes with increasing distance. This concept extends to the intriguing notion of a spin bus, enabling long-range interactions for solid-state quantum computing [2]. In this work, we focus on quantum synchronization (QS) and entanglement between two spin-chains, each modelled as a pseudo-bosonic system (thanks to the Holstein-Primakoff transformation) indirectly coupled by another such chain (with odd number of spins). At low temperatures, this intermediary chain, playing the role of a spin-bus, can be considered as a single spin in its ground state doublet. Treating the synchronizing spin-chains as a bosonic system enables us to employ Mari's measure [3] to study the QS. This makes our approach to the QS of spins fundamentally different from those usually used, based on quasi-probability distributions [4].

Both the entanglement and the QS are manifestations of quantum correlations. Interestingly, both, the QS measure [3] and the entanglement criterion [5] find their roots in the Heisenberg uncertainty principle, particularly in the context of EPR-like variables [6,7]. Therefore, the spin chains can exhibit the both for a certain parameter regime. We have found that it is indeed so, and these chains exhibit limit cycle trajectories, as well, as a precondition of the QS. The boson-number dependent nonlinear interaction between the chains lead to the QS and prepare the chains in non-Gaussian states, which warrants to employ the entanglement criteria based on higher-order moments [8].

References

1. C. Huygens, *Oeuvres completes,* vol. 7. M. Nijhoff, (1897).

2. M. Friesen et al., *Phys. Rev. Lett.* 98, 230503 (2007).
3. A. Mari et al., *Phys. Rev. Lett.* 111, 103605 (2013).
4. T. Lee and H. Sadeghpour, *Phys. Rev. Lett.* 111, 234101 (2013).
5. S. Mancini et al., *Phys. Rev. Lett*. 88, 120401 (2002).
6. D. Garg et al., *Phys. Lett. A* 457, 128557 (2023).
7. Manju et al., *Phys. Lett. A* 482, 129039 (2023).
8. E. Shchukin and W. Vogel, *Phys. Rev. Lett.* 95, 230502 (2005).

QI380 Experimental realization of two qubit teleportation and four bit dense coding

Sayuj.p[1], Ben T Paul[1], N.C. Randeep[1]*
1 Department of Physics, Government Arts and Science College, Meenchanda, Calicut, Kerala 673018, India
**Corresponding author: sayujpchemanchery@gmail.com*

Quantum teleportation and dense coding are quantum tasks in which an unknown quantum state sends from one location to another in first one and classical bits sends between two locations in the later. We introduce a quantum circuit for creating generalized Bell states [1] as shown in Figure 1. We develop appropriate quantum circuit for realizing two qubits teleportation and four bits dense coding. We experimentally demonstrate these circuits in IBM quantum computer and calculate fidelity of teleportation and efficiency of dense coding.

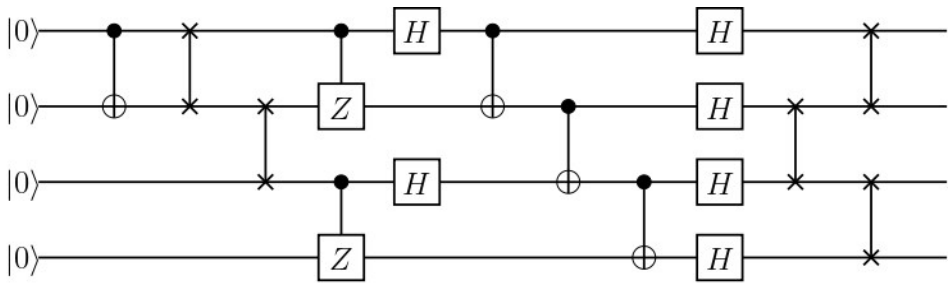

Figure 1: Quantum circuit for creating Generalized Bell States

References

1. G. Rigolin, Phys. Rev. A 71, 032303 (2005).

Category 22

Quantum Optical Technologies (QOT)

QOT381 Controllable Phonon Blockade in a Mechanical Resonator coupled with superconducting qubits driven by Squeezed light

Anjan Samanta[1,2], Paresh Chandra Jana[2]

[1]Dept. of Physics, Sabang Sajanikanta Mahavidyalaya, Lutunia, Paschim Medinipur, 721166, India

[2]Dept. of Physics, Vidyasagar University, Paschim Medinipur, 721102, India

Corresponding to: anjan.samanta744@gmail.com

We have analyzed the phonon statistics in a Nanomechanical resonator, which is coupled with Superconducting qubits and driven by squeezed light. The quantum nature of a mechanical resonator can be achieved by the phonon blockade mechanism. The non-linearity must be very large as compared to the optical mode line width to suppress the unwanted transitions. We observe the strong phonon antibuncing effect i.e., unconventional phonon blockade mechanism which relies on close to Gaussian states under weak driven squeezed light. By numerical solution of second-order correlation functions, we analyze the sub-Poissonian phonon statistics. We can control phonon blockade effects by controlling the amplitude and phase of driven squeezed light. Due to the high nonlinearity of the system and interaction strength between superconducting qubits and cavities, the phonon blockade effect is controlled. The present mechanism has much more attractive applications in optical communication and sensitive measurements such as the detection of gravitational waves or noise-free amplifications and use for development of quantum computers, and generates second harmonics.

Results & Discussion:- In this paper, we shall analyze the numerical simulation of the Phonon Blockade mechanism [Fig-1, Fig-2] for an optomechanical system described by the Hamiltonian. Effective phonon interaction induced by the qubit and phonon antibunching effect was observed for weak coupling regime and controlled detuning between the mechanical resonator and the Qubit. Phonon blockade can be tunable under strong and weak-driven squeezed light. Phonon blockade can be enhanced by controlling different system parameters and the strength and phase of the squeezed light. To reduce the negative impact by the environment, we have to use low temperature and high frequency of mechanical frequency (we use 5 GHz). So optimal phonon blockade appears near zero detuning and agrees with the analytical result.

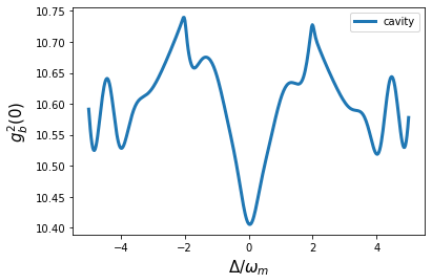

Fig-1

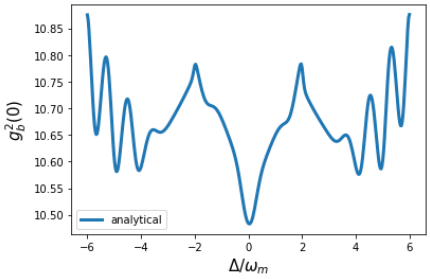

Fig-2

References

1. H. Q. Shi, X. T. Zhou, X. W. Xu, N. H. Liu, Scientific Reports, 8:2212 (2018)

QOT382 Free Space Deterministic Secure Quantum Communication with Two-Mode Squeezed States

*Chirang Patel, Bhargav Cheekati, Ashok Kumar**
Department of Physics, Indian Institute of Space Science and Technology (IIST)
Thiruvananthapuram, Kerala 695547, India
**Corresponding author: ashokkumar@iist.ac.in*

Abstract: Quantum communication is a secure way to transmit information using the unique properties of quantum states. This research uses the squeezing phase of two-mode squeezed states (TMSS) to transmit information securely. The squeezing phase of a TMSS can only be revealed by performing a joint measurement on both modes. This makes TMSS ideal for quantum communication, as it allows two parties, Alice and Bob, to send secure messages that cannot be eavesdropped without their knowledge. Our study aims to practically implement this protocol by modelling real-world factors like losses, excess noise, and atmospheric effects.

Methodology and Results: In deterministic secure quantum communication with TMSS protocol, Alice generates Two-Mode Squeezed States, sends one mode to Bob via a quantum channel, and keeps the second one with her [1]. Alice then encodes a message in the squeezing phase of her mode via a local oscillator in a homodyne measurement. Bob also performs homodyne detection on his mode and combines the results with Alice's homodyne detection results, which allows Bob to retrieve the squeezing phase that contains the message.

The mode sent to Bob is only affected by the atmosphere during transmission. To study the practicality of the protocol, we use a beam splitter (BS) model to mimic losses and introduce excess noise through the empty port of the BS. We model the excess noise by considering one mode of the TMSS, which is in a thermal state. The results of our analysis are shown in Fig. 1. We have considered different amount of squeezing, given by s-parameter, as 0.25, 0.5, 1 and 1.5 (inset in Fig. 1, SNL: Shot Noise Limit). As expected, squeezing reduces with increase of loss and excess noise (Fig. 1 (a, b)). Fig. 1(c) represents the squeezing presents after travelling through atmosphere, here we have considered atmospheric attenuation which quantifies the overall signal loss due to absorption and scattering as it travels through the atmosphere [2].

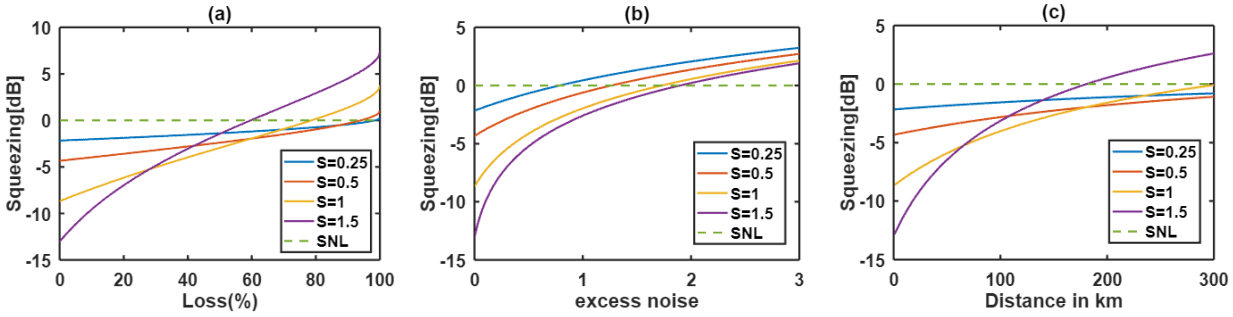

Fig.1 (a) Squeezing vs losses, (b) squeezing vs excess noise, (c) squeezing vs propagation distance in atmosphere.

References

1. Alberto M. Marino et. al., *Phys. Rev. A 74, 022315* (2006).
2. Tasio Gonzalez-Raya et. al., *arXiv:2303.17224* (2023).

QOT383 Optomechanical Entanglement via pump modulation in hybrid system embedded with doble quantum dots

Madhav K. Singh[1], Pradip K. Jha[2] and Aranya B. Bhattacherjee[3]*
[1]Department of Physics, Swami Sahjanand College, Jehanabad (Magadh University Bodh Gaya) Bihar 804408, India
[2]Department of Physics, DDU College, Dwarka, (University of Delhi), New Delhi, 110078. India
[3]Department of Physics, Birla Institute of Technology and Science,Pilani, Hyderabad Campus, Hyderabad - 500078, India
**madhavkrsingh89@gmail.com*

We consider a hybrid optomechanical system incorporating dual quantum dots. A driving force in the form of an amplitude-modulated laser applied, and the resonance frequency of the two quantum dots is also subjected to modulation. We examined the entanglement characteristics in the present system. By harnessing these modulation techniques exert precise control over the entanglement over the entanglement among the system's various degrees of freedom. Exploring the conditions for the emergence of entanglement between macroscopic object is crucial for understanding its fundamental nature and potential applications in quantum technologies. The novel approach holds significant promise for the realization of efficient quantum memories suitable for continuous variable quantum information processing.

References

1. A. Mari et. al., *Phys. Rev. Lett.* 103, 213603 (2009).
2. Rong-Xin Chen et. al., *Phys. Rev. A* 89, 023843 (2014).
3. Alessandro Farace et. al., *Phys. Rev. A* 86, 013820 (2012).
4. F. Galve et. al., *Phys. Rev. Lett.* 105, 180501 (2010).
5. G. Passetti et. al., *Phys. Rev. Lett.* 131, 023601 (2023).

QOT384 Continuous variable entanglement using optomechanics

*Greeshma Gopinath and Sankar Davuluri**
Department of Physics, BITS Pilani, Hyderabad Campus, Hyderabad 500078, India.
**Corresponding author: sankar@hyderabad.bits-pilani.ac.in*

We present a new method to entangle propagating optical fields using two spatially separated coherent states that are fed into the optomechanical cavity. Optomechanics and quantum back-action nullifying meter (QBNM) [1] technique are used to create entanglement.

The optomechanical system depicted in Figure 1(a) consists of rigidly fixed end mirrors, denoted as m_1 and m_2, each having a decay rate ζ. The perfectly reflective optomechanical mirror (OMM) in the middle divides the cavity into two sub-cavities ensuring that the field in sub-cavity-1 (SC1) is not mixed with the field in sub-cavity-2 (SC2) and vice-versa. The SC1 and SC2 are driven by coherent input fields, with annihilation operators $\hat{b}$ and $\hat{d}$ respectively. The annihilation operators for the output fields from SC1 and

SC2 are $\hat{B}$ and $\hat{D}$, respectively. The quantum mechanical radiation pressure force on the OMM can be used to create correlations between the two output fields such that they are entangled.

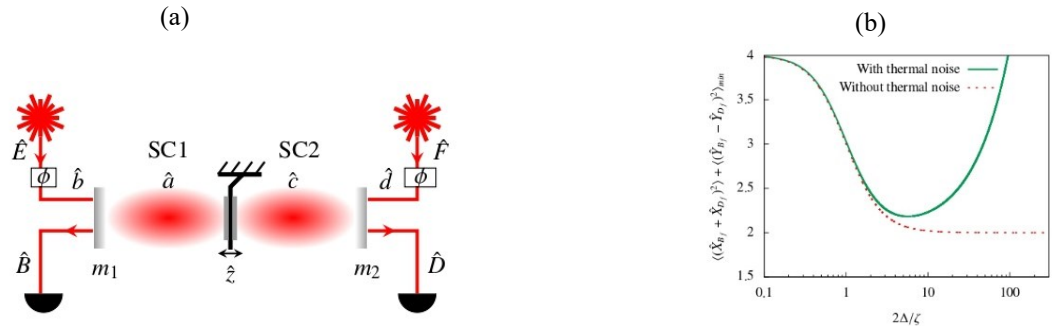

Figure 1: (a) Optomechanical cavity with perfectly reflective mechanical mirror in the middle. The mirrors m_1 and m_2 are rigidly fixed, while the center optomechanical mirror can oscillate. (b) Entanglement as a function of ratio) of detuning and cavity decay at room temperature.

Entanglement is verified using Duan criterion [3] $\left\langle \left(\hat{X}_{B_f} + \hat{X}_{D_f}\right)^2 \right\rangle + \left\langle \left(\hat{Y}_{B_f} - \hat{Y}_{D_f}\right)^2 \right\rangle < 4$ and $[\hat{X}_{B_f}, \hat{Y}_{B_f}] = [\hat{X}_{D_f}, \hat{Y}_{D_f}] = 2i$, where $\hat{X}_{B_f}$ ($\hat{X}_{D_f}$) and $\hat{Y}_{B_f}$ ($\hat{Y}_{D_f}$) are the fluctuations in amplitude and phase quadratures of $\hat{B}(\hat{D})$. This sufficient criterion for proving entanglement also ensures the system's stability within the region where this criterion is satisfied. Dependence of entanglement on detuning is shown in Figure 1(b). It can be seen that, while large detuning results in the lowest value for Duan criterion, it simultaneously raises the Duan criterion value in the presence of thermal noise. Entanglement generated using this method is robust against room temperature thermal noise for parameters taken from experimental work Ref [4].

References

1. S.Davuluri et al., JOSA B 39.12, 3121-3127 (2022).
2. M. Aspelmeyer et al., Rev. Mod. Phys. 86, 1391 (2014).
3. L.-M. Duan et al., Phys. Rev. Lett. 84, 2722 (2000).
4. M. Rossi et al., Nature 563, 53 (2018).

QOT385 Possibility of all-optical-switching in PT-symmetric coupled micro-cavities

Kousik Mukherjee[1], Paresh Chandra Jana[1]
[1]Department of Physics, Vidyasagar University, Midnapore, 721102, India
**Corresponding author: kousikmukherjee89@gmail.com*

We theoretically analyzed the optical bistability in parity-time-symmetric coupled micro-cavities, where two cavities are coupled by photon tunnelling; one of the cavities contains Kerr-nonlinear medium. Using Heisenberg-Langevin equations of motion, we have obtained steady state mean cavity photon number for different photon tunnelling strength, nonlinear strength and gain-to-loss ratio. A high degree of coherent influence and tunability via Kerr-nonlinearity and photon tunnelling strength over the bistable behaviour is discussed. The impact of the exceptional point on the characteristics of bistability is also reported. The

model system exhibits switching behaviour and tunable zero intensity window. Our result may be useful to design efficient all-optical switch and optical sensor.

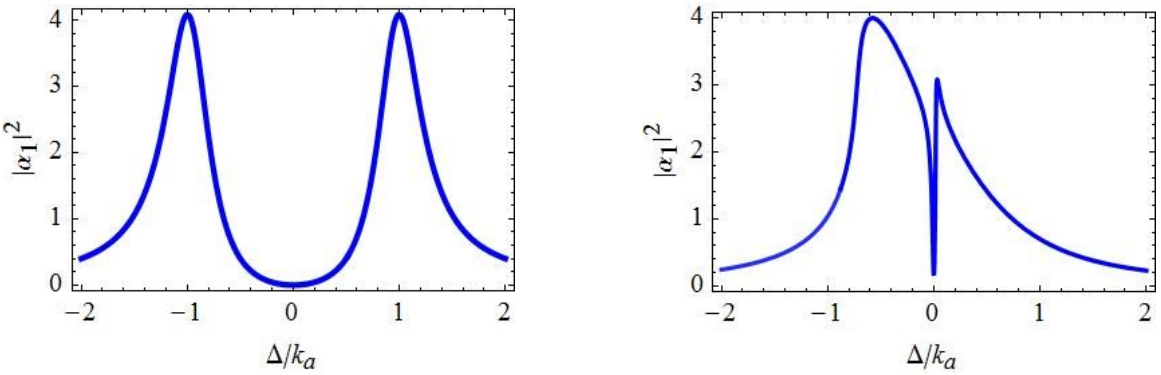

(b)

Figure 1: Plot of mean cavity photon number as a function of normalised detuning for (a) $k_b/k_a = 0.01$, $J/k_a = 1$ (b) $k_b/k_a = 0.01$, $J/k_a = 0.1$, $U/k_a = 0.1$. Other parameter is $\Omega_d/k_a = 1$.

References

1. O. Kyriienko et. al., *Phys. Rev. Lett.* 112, 076402 (2014)
2. K. J. Vahala, *Nature (London)* 424, 839 (2003)
3. K. Mukherjee and P. C. Jana, *Physica E* 117, 113780 (2019)

QOT386 Multi-photon Lasing in the Incoherently Pumped Two Quantum Dots-Photonic Crystal Cavity System

Lavakumar Addepalli[1] and P K Pathak[1]
[1]School of Physical Sciences, Indian Institute of technology Mandi, Kamand, Himachal Pradesh, 175005, India
Authors e-mail address: (d20034@students.iitmandi.ac.in, ppathak@iitmandi.ac.in)

Summary

We show the emission into the cavity mode in the incoherently pumped two quantum dots (QDs) - single mode photonic crystal (PhC) cavity is due to single and multi-photon transitions. We study the effect of exciton-phonon interactions present in the system non-perturbatively by making polaron transformation [1].

We consider two separate QDs coupled to single mode PhC cavity. The Hamiltonian for the system in rotating wave approximation (RWA) of cavity mode frequency is given by,

$$\hat{H} = \hbar\Delta_1\sigma_1^+\sigma_1^- + \hbar\Delta_2\sigma_2^+\sigma_2^- + \hbar(g_1\sigma_1^+a + g_2\sigma_2^+a + H.C.) + \widehat{H_{ph}}. \qquad (1)$$

Here, the detuning $\Delta_i = \omega_i - \omega_c$ and ω_i, ω_c are the transition frequency between ground state, $|g_i\rangle$ and excitonic state, $|e_i\rangle$ for the i^{th} QD, cavity mode frequency respectively. The lowering and raising operators

for QDs are given by $\sigma_i^+ = |e_i\rangle\langle g_i|$, $\sigma_i^- = |g_i\rangle\langle e_i|$, g_i is the exciton-cavity mode coupling constant and a is the cavity field annihilation operator. The last term in (1) represents the exciton and longitudinal acoustic (LA) phonon interaction,

$$\widehat{H_{ph}} = \hbar\Sigma_k \omega_k b_k^\dagger b_k + \hbar\Sigma_i \lambda_i^k \sigma_i^+ \sigma_i^- \left(b_k + b_k^\dagger\right) \quad (1)$$

Here, $b_k(b_k^\dagger)$ is the annihilation(creation) operator of k^{th} phonon bath mode of frequency, ω_k and λ_i^k is the coupling strength of exciton $|e_i\rangle$ to the k^{th} mode of phonon bath. We perform polaron transformation, $\widehat{H'} = e^S H e^{-S}$, where $S = \Sigma_i \sigma_i^+ \sigma_i^- \Sigma_k \lambda_i^k \left(b_k^\dagger - b_k\right)$ and make Born-Markov approximation to derive the master equation [2,3]. The incoherent processes present in the system are written in Lindblad super-operator form, $L[\hat{O}]\rho = \widehat{O^\dagger}\hat{O}\rho - 2\hat{O}\rho\widehat{O^\dagger} + \rho\widehat{O^\dagger}\hat{O}$. The master equation for the incoherently pumped system is given below,

$$\dot{\rho_s} = -\frac{i}{\hbar}[H_s, \rho_s] - L_{ph}\rho_s - \frac{\kappa}{2}L[a]\rho_s - \Sigma_{i=1,2}\left(\frac{\gamma_i}{2}L[\sigma_i^-] + \frac{\gamma_i'}{2}L[\sigma_i^+\sigma_i^-] + \frac{\eta_i}{2}L[\sigma_i^+]\right)\rho_s \quad (2)$$

The above master gives complete information about the dynamics and steady state properties of the system. To obtain the steady-state QDs populations, cavity mode statistics, equation (2) is numerically integrated using quantum optics toolbox [4]. By obtaining cavity mode rate equation upon tracing out QD states, we show net multi-photon emission into cavity at optimal parameters of QDs detuning and incoherent pumping rate.

References

1. Xu, D., & Cao, J., *Frontiers of Physics*, *11*(4), 1-17(2016).
2. Roy, C., & Hughes, S., *Physical Review X*, *1*(2), 021009 (2011).
3. Verma, J. K., Singh, H., & Pathak, P. K., *Physical Review B*, *98*(12), 125305 (2018).
4. Tan, S. M. J. Opt. B: Quantum Semiclass. Opt, 1, 161 (1999).

QOT387 An uncertainty relation based study of quantum correlations in optomechanical systems

Manju, Asoka Biswas, Shubhrangshu Dasgupta*

Department of physics, Indian Institute of Technology Ropar, Punjab 140001, India

**Corresponding author: 2018phz0009@iitrpr.ac.in*

Spontaneous synchronization is one of the most attractive phenomena, which was first observed by Huygens in a classical clock pendulum system [1]. Two nonlinearly coupled harmonic oscillators are said to be classically synchronized, when their respective generalized positions and generalized linear momenta become equal, at long times. In quantum systems, however, such synchronization is inherently not possible due to Heisenberg's uncertainty principle. Since, it is not possible to attain the above conditions. In such case, Mari et. al., [2] proposed a figure of merit to measure the degree of quantum synchronization. Synchronization phenomenon and quantum correlations have been studied for a long by two different communities, and recently their relation started to be explored [2-6]. This aspect of synchronization is drawing much more attention. The common ingredient for the emergence of these features can be attributed to the mutual interaction between subsystems. Quantum correlation between the interacting systems can also manifest itself as entanglement. To verify entanglement in the system, we use the separability criterion proposed by Mancini et. al [5]. From the proposed measure of both, we observed that both these properties are defined in terms of second order moments of a set of conjugate quadratures. Also, the upper limit for synchronization measure and the entanglement marker is set by the same uncertainty relation. Therefore, it is

natural to expect certain relation between them. With this objective, we proposed two different schemes to achieve the same between two indirectly coupled mechanical oscillators [6,7]. It is shown that in the presence of amplitude modulation, both the oscillators can be quantum synchronized and entangled simultaneously. By employing uncertainty-based synchronization measure and entanglement criterion, we probed the generalized relation between two independent phenomenon.

References

1. C. Huygens, Oeuvres completes, vol. 7. M. Nijhoff, (1897).
2. A. Mari et. al., Phys. Rev. Lett., 111, 103605 (2013).
3. C.-G. Liao et. al., Phys. Rev. A 99, 033818 (2019).
4. V. Ameri et. al., Phys. Rev. A 91, 012301 (2015).
5. S. Mancini et. al., Phys. Rev. Lett. 88, 120401 (2002).
6. D. Garg et. al., Physics Letters A 457, 128557, (2023).
7. Manju et. al., Physics Letters A 482, 129039, (2023).

QOT388 High Fidelity Room Temperature Single photon emission from colloidal quantum dots

*Manojkumar V, Geetha K. Varier, E. S. Kannan, Radhika Vathsan and P. Nandakumar**
Department of Physics, BITS Pilani K. K. Birla Goa campus, Goa 403 726
**Corresponding author: nandan@goa.bits-pilani.ac.in*

Single-photon sources are essential to quantum technologies such as quantum cryptography, quantum computation, and quantum metrology. Semiconductor quantum dots are one of the widely studied single photon sources. In this work, we demonstrate the room-temperature single-photon emission from individual CdSe quantum dots synthesized via a chemical route and demonstrate the use of an in-house-built scanning confocal microscope for single-photon emitter excitation and readout.

Monodisperse CdSe nanoparticles are synthesized via the chemical route by adding olive oil solution containing selenium in cadmium oleate at 300^0C and heating for 15 minutes. The CdSe quantum dots are characterized using optical absorption spectroscopy and fluorescence spectroscopy. The colloidal quantum dots are spin-coated on a glass coverslip, and the size and monodispersity are characterized by scanning electron microscopy. Images of well-separated quantum dots are acquired using the confocal microscope. The fidelity of single-photon emission is studied using a Hanbury-Brown and Twiss setup attached to the confocal microscope. Our studies show that single photon sources can be synthesized and characterized in a cost-effective manner using components normally present in a standard optics laboratory.

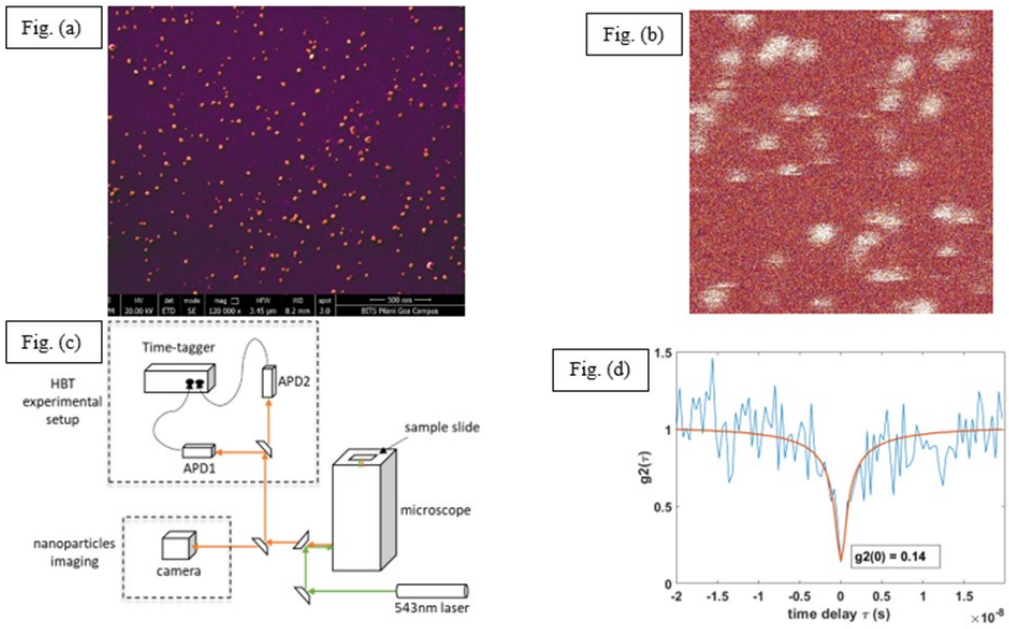

Figures (a) SEM image of the monodisperse quantum dots. (b) The confocal image of CdSe quantum dots. (c) The experimental setup for imaging and the detection of single photon sources. (d) Measured second-order correlation function $g2(\boldsymbol{\tau})$ as a function of time delay for a single CdSe quantum dot.

QOT389 Design of an Oscillator circuit using tristate quantum optical phase shift gate

Mir Nadim Sarfaraj and Sourangshu Mukhopadhyay*
Department of Physics, The University of Burdwan, Golapbag, Burdwan, West Bengal, India, 713104
**Email: mirnadim222@gmail.com*

Quantum logic gates are the backbones of quantum computing system. Various all-optical quantum gates are developed by using different encoding techniques [1-3]. These logic gates can be used to design various optical systems like oscillators, flipflops, latches, memories, etc. Tristate phase shift gate is an important logic gate which is designed by using joint encoding of frequency and phase of optical signal [4]. In this communication, authors developed an all-optical oscillator circuit by utilizing the tristate phase shift quantum gate. The proposed oscillator is capable of oscillating any arbitrary pairs of phase-value. Electro-optic modulators of suitable biasing voltages can be used to obtain the desired amount of phase shift. All-optical implementation of the tristate oscillator circuit is capable of processing higher number of signals with excellent operational speed than that of a conventional Boolean system. Authors also explained a method of designing such oscillator circuit on photonic crystal-based layout. In this case, the desired phase shifts can be obtained by controlling the optical path length through the waveguide. The photonic crystal-based optical oscillator can process optical signals with minimal loss and much improved bit rate in the order of THz. The truth table for tristate quantum optical phase shift oscillator is shown in Table – 1.

	Inputs			Outputs			Phase differences		
	I_1	I_2	I_3	O_1	O_2	O_3	θ_1	θ_2	θ_3
When the external signals are present	f_1	f_2	f_3	$-f_1 e^{i\varphi}$	f_2	f_3	$\pi+\varphi$	0	0
After the external signals are removed	$-f_1$	f_2	f_3	$f_1 e^{i\varphi}$	f_2	f_3	φ	0	0
	f_1	f_2	f_3	$-f_1 e^{i\varphi}$	f_2	f_3	$\pi+\varphi$	0	0
	$-f_1$	f_2	f_3	$f_1 e^{i\varphi}$	f_2	f_3	φ	0	0
	f_1	f_2	f_3	$-f_1 e^{i\varphi}$	f_2	f_3	$\pi+\varphi$	0	0
	This will continue.								

Table - 1: Truth table for tristate quantum optical phase shift oscillator.

References

1. S. Dey et al, 'Approach of implementing phase encoded quantum square root of NOT gate', Electron. Lett., 2017, 53, (20), pp. 1375– 1377.
2. S. Dey et al, 'All-optical high frequency clock pulse generator using the feedback mechanism in Toffoli gate with Kerr material', J. Nonlinear Opt. Phys. Mater., 2016, 25, (1), p. 1650012 (11 pp)
3. M.N. Sarfaraj et al, All-optical scheme for implementation of tri-state Pauli-X, Y and Z quantum gates using phase encoding, Optoelectronics Letters, 17 (2021) 746–750.
4. M.N. Sarfaraj et al, Photonic crystal-based tristate phase shift quantum gates using joint encoding of frequency and phase, Journal of Optics, 2023 (accepted for publication).

QOT391 Phonon-assisted interaction between two modes of a field mediated by two quantum dots

P K Pathak

Indian Institute of Technology Mandi, Mandi 175 001, Himachal Pradesh, India

**Corresponding author: ppathak@iitmandi.ac.in*

Using a polaron master equation approach, we investigate the unusual cooperative two-photon resonance between two-modes of a field inside a semiconductor cavity containing two quantum dots. The cooperative two-mode two-photon resonance occurs when two off-resonant quantum dots, initially prepared in exciton states, emit one photon in each cavity mode and de-excite simultaneously. Using such two-photon two-mode interaction we propose to generate an entangled state of two qutrits (tripartite unit of quantum information). The bases for the qutrits are formed by the states of the cavity modes containing 0, 1 and 2 photons. We also discuss the effect of exciton-phonon coupling on the entanglement and the probability of generating two-qutrit state.

References

1. J. K. Verma, Harmanpreet Singh, P. K. Pathak, and S. Hughes, Phys. Rev. A102, 063701 (2020).

QOT392

Simultaneously effect of hydrostatic pressure and impurity on entropy and heat capacity of double quantum wire

Priyanka[1] and Rinku Sharma[1,]*
[1]Department of Applied Physics, Delhi Technological University, Delhi-110042, India
**Email-rinkusharma@dtu.ac.in*

The impact of hydrostatic pressure and impurity on the entropy and heat capacity in an InAs double quantum wire has been investigated. A 2D electron gas is confined in a parabolic lateral potential and subjected to a crossed electromagnetic field. Initially, eigen-energies are obtained using the diagonalization method, then entropy and heat capacity are calculated numerically for different values of hydrostatic pressure and impurity. The entropy versus temperature for various values of pressure and impurity is found to show a structure with a minimum at low temperatures (as shown in fig. 1). Moreover, heat capacity variation with the temperature for various values of pressure and impurity shows the peak at low temperature and decreases at high temperature (shown in fig. 2). As entropy increases with an increase in temperature in the presence of an external magnetic field. Energy level splitting due to Rashba spin-orbit coupling seems to play a role in the results obtained.

Expression for entropy and heat capacity are given by:

Mean Energy, $$U = -\frac{\partial \ln Q}{\partial \beta}$$

Heat Capacity, $$C_v = \frac{\partial U}{\partial T} = k_B \beta^2 \frac{\partial^2 \ln Q}{\partial \beta^2}$$

Result

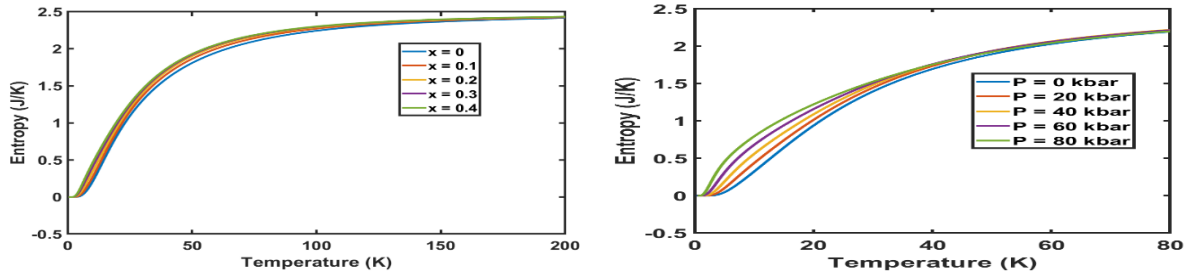

(a) (b)

Figure 1 (a-b): Entropy variation with the temperature for different value of hydrostatic pressure and impurity, respectively.

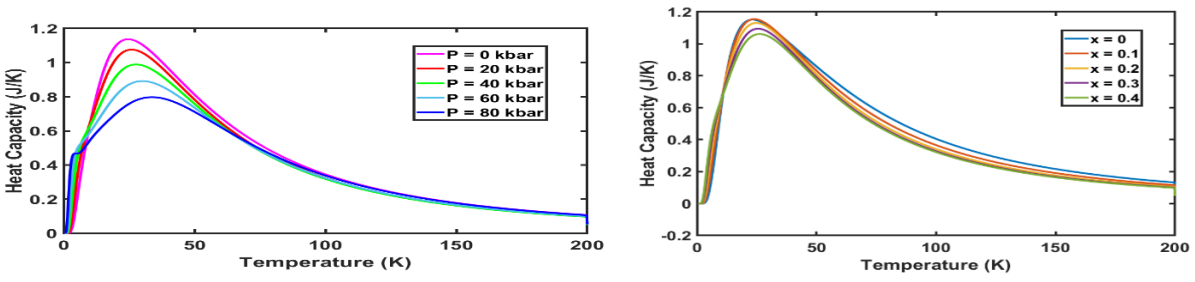

(a) (b)

Figure 2 (a-b): Heat capacity variation with the temperature for different value of hydrostatic pressure and impurity, respectively.

QOT393

Progress towards an all-optical trapped ion-based portable atomic clock

Rishabh Pal[1,], Vikrant Yadav[1], and Arijit Sharma[1,2,*]*

[1]Department of Physics, Indian Institute of Technology Tirupati, Yerpedu-517619, A.P., India

[2]Center for Atomic, Molecular, and Optical Sciences and Technologies, Indian Institute of Technology Tirupati, Yerpedu-517619, A. P., India

**Corresponding author: ph22d502@iittp.ac.in, arijit@iittp.ac.in*

Portable atomic clocks have revolutionized applications in GPS (Global Positioning System) and navigation systems, civil and strategic communication [1,2], power grids and radar synchronization, etc. Optical clocks have the potential to surpass their microwave counterparts in performance due to higher Q factor ($\nu_0/\Delta\nu$, where ν_0 is the central frequency and $\Delta\nu$ is the linewidth of the transition) which ensures higher stability. This enables higher stability for all-optical atomic clocks. In addition, using an optical clock-based synchronization increases the rate of key transmission in QKD schemes [3].

In our group at IIT Tirupati, we aim to develop an all-optical trapped ion-based portable atomic clock using a trapped ion $^{40}Ca^{+}$ (calcium) ion. In $^{40}Ca^{+}$ ion the clock transition at 729 nm, which is between 3 $^{2}D_{5/2}$ and 5 $^{2}S_{1/2}$ levels (Fig. 1) with a natural linewidth of 130 mHz. One of the major advantages of using $^{40}Ca^{+}$ ion is that all the relevant transitions are accessible with the commercially available laser diodes. To drive the clock transition in a coherent manner, the clock laser at 729 nm needs to have e a sub-Hz linewidth which can be achieved using PDH (Pound-Drever-Hall) technique [4] laser frequency stabilization over a narrow cavity resonance. In this poster, we are going to present simulations on cavity design and mounting points which involve active vibration isolation, thermal isolation, and acoustic isolation. We shall also present our ongoing simulations using SIMION for efficient trapping of a single ion to determine ion trap parameters and identify the trajectory and the power spectrum of ion motion. Finally, we shall discuss the design and operating parameters of an imaging device for the diffraction limited imaging of a single trapped ion.

Arijit Sharma expresses gratitude for financial support from CAMOST and IIT Tirupati. Rishabh Pal acknowledges financial support from IIT Tirupati. Vikrant Yadav is thankful for financial support from CSIR (Government of India) in the form of a Junior Research Fellowship (JRF).

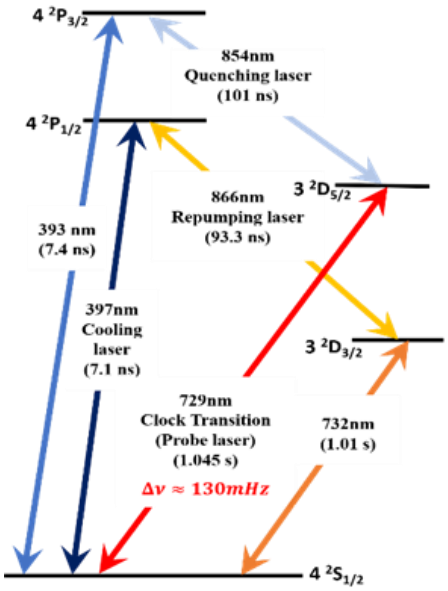

Fig. 1: Energy level diagram of calcium ($^{40}Ca^{+}$) ion

References

1. Marlow et al., *IEEE Transactions on Ultrasonics, Ferroelectrics, and Frequency Control* 68, 2007-2022 (2021).
2. N. Poli et. al., *La Rivista del Nuovo Cimento* 36, 555-624 (2013).
3. J.C. Bienfang et al., *Optics Express* 12, 2011-2016 (2004)
4. R. W. Fox, et. al., *Experimental Methods in The Physical Sciences* 40, 1-46 (2003).

QOT394 Spectral Purity Optimization of SPDC Generated Photon Pairs for Quantum Photonic Applications

Siddhant Vernekar[1], Jolly Xavier[1]**

[1] SeNSE, Indian Institute of Technology Delhi, New Delhi, India - 110016

**Corresponding author: idz20228534@iitd.ac.in , jxavier@sense.iitd.ac.in*

Spontaneous parametric down-conversion (SPDC), a reliable nonclassical photon generation process, is essential to quantum information science and technology [1]. Band pass filters have historically been used to achieve spectral purity, an essential quality needed for effective photon-pair creation, resulting in lower count rates. To reduce the requirement for such filtering, this study investigates how to improve SPDC spectral purity using pulsed pump lasers (bandwidth optimization) and refractive as well as structural features of periodically poled crystals through temperature and poling period optimization. Fig. 1 gives the computed results of the joint spectral intensity of the signal and idler photon pairs generated through SPDC in a Type II phase matched periodically poled potassium titanyl phosphate (PPKTP) nonlinear crystal. We also analyse both degenerate and non-degenerate SPDC generated photon pairs in this study. Due to its highly desirable potential to create entangled photon pairs, the former finds particular use in precision metrology using entanglement-based Quantum Key Distribution protocols. Non-degenerate SPDC, on the other hand, is favoured in single-photon metrology and hailed in single-photon QKD protocols because it can predictably herald individual photons at wavelengths compatible with cheaper detectors. Furthermore, in periodically poled nonlinear crystals such as PPKTP or PPLN, the phase-matching process critically depends on careful temperature adjustments, highlighting the significance of managing external conditions to maximize SPDC efficiency [2]. In conclusion, this work comprehensively analyses methods for maximizing the SPDC process's potential, emphasizing quantum purity's crucial contribution to the development of quantum information science and metrology.

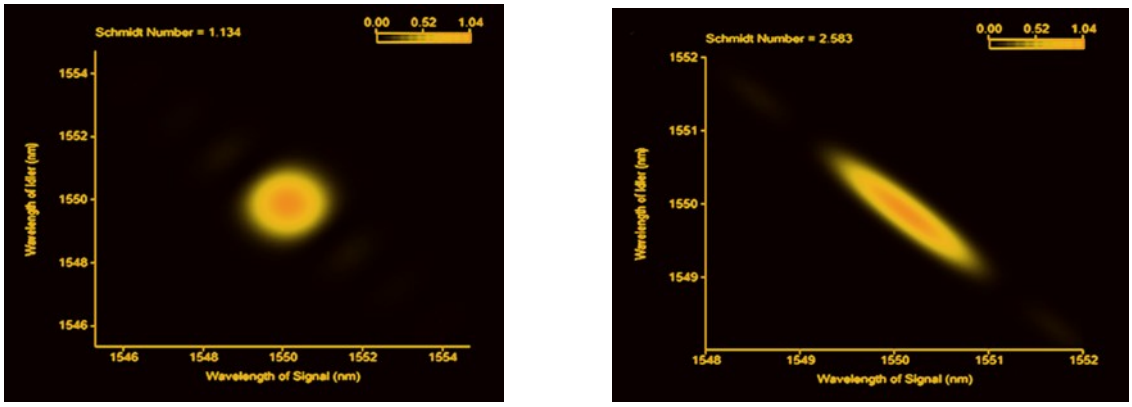

Fig. 1: Joint spectral intensity analysis of Type II, PPKTP crystal with crystal length 25mm, and poling period=46.5µm at temperature 25 °C respectively for Pump beam bandwidth of 0.5nm (a) and Pump beam bandwidth of 0.1 nm (b)

References

1. D. Browne et al, *Progress in Quantum Electronics*, **54**, 2–18 (2017).
2. K. Zielnicki et al., *Journal of Modern Optics*, **65**, 1141-1160, (2018).

QOT395 The Wigner Approach to High-NOON States by Blending Quantum and Classical Light

Simanshu Kumar[1], Nandan S Bisht[2]*

[1]Department of Physics, Kumaun University Nainital, S.S.J. Campus, Almora, 263601, Uttarakhand, India.

[2]Department of Physics, Soban Singh Jeena University, S.S.J. Campus, Almora, 263601, Uttarakhand, India.

**Corresponding author: bisht.nandan@gmail.com*

Recently, high-NOON states have emerged as a promising resource for quantum technologies, such as precision measurements and sensing. However, preparing and characterizing these states experimentally is a challenging task. Here, we present a comprehensive theoretical approach that describes the preparation of high-NOON states by blending quantum correlated light and classical light [1], using the Wigner representation [2]. We provide the analytical representation of the high NOON states which has been experimentally demonstrated [1]. This study emphasises the realization of states that facilitate the comprehension approach. In this scheme, the NOON states are prepared with highly entangled states of multiparticles, which have been widely studied especially in quantum information science and quantum metrology [3]. In NOON states, N identical particles are prepared in a superposition of all particles being in one state (e.g., all in the "0" state) and all particles being in another state (e.g., all in the "N" state) [4]. Recent research is focused on the application of the NOON state for enhanced sensitivity in various measurements, such as phase estimation and frequency measurement [5]. The Wigner approach offers a more general framework for understanding the behaviour of high-NOON states and can be used to design novel experimental schemes for their preparation and characterization.

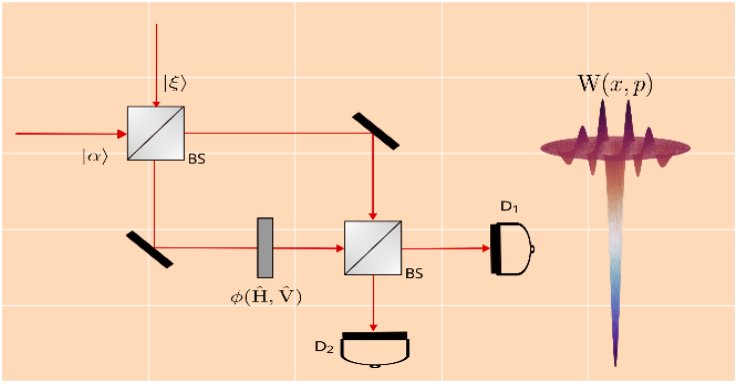

Figure illustrates the interference of classical coherent light α and SPDC light ξ in a Mach-Zehnder interferometer, leading to the resulting Wigner representation W (x, p).

References

1. I. Afek, O. Ambar, and Y. Silberberg, Science 328, 879 (2010).
2. E. P. Wigner, Phys. Rev. 40, 749 (1932).
3. J. P. Dowling, Contemp. Phys. 49, 125 (2008); V. Giovannetti, S. Lloyd, and L. Maccone, Phys.

Rev. Lett. 96, 010401 (2006).

4. A. P. Lund, T. C. Ralph, and H. L. Haselgrove, Phys. Rev. Lett. 100, 030503 (2008).
5. M. Mitchell, J. Lundeen, and A. Steinberg, Nature (London) 429, 161 (2004).

QOT396 Continuous variable quantum node using optics

*Sreeshna Subhash, and Sankar Davuluri**

Department of Physics, BITS Pilani, Hyderabad Campus, Hyderabad, 500078, India

**sankar@hyderabad.bits-pilani.ac.in*

Quantum communication [1] over long distances requires quantum nodes with strong capabilities for storing and exchanging quantum states [2] without significant decoherence. We endeavor to create such a quantum node by using a four level atomic system in double lambda configuration. The four atomic levels |j>, where j=a,b,c,d, has energies $\hbar\omega_j$, with $\hbar$ is the reduced Planck constant and ω_j, as frequency. Two strong classical fields with Rabi frequencies Ω_1, and Ω_2, drive |b> - |d> and |c> - |d> transitions, respectively, as shown in Fig.1. The transitions |b> - |a> and |c> - |a> are coupled by two weak quantum fields which are represented by destruction operators $\hat{a}_1$ and $\hat{a}_2$, respectively, as shown in Fig. 1.

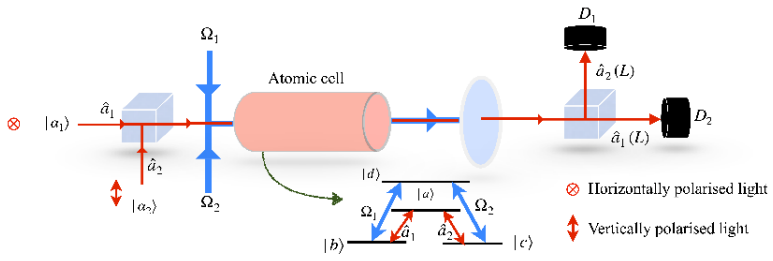

Fig. 1 The input quantum states $|\alpha_1\rangle$ and $|\alpha_2\rangle$ can be sent either to detector D_1 or D_2 by controlling Ω_1/Ω_2. The $|\alpha_1\rangle$ and $|\alpha_2\rangle$ are the eigenstates of $\hat{a}_1$ and $\hat{a}_2$, respectively.

By varying Ω_1/Ω_2 value, we achieved controlled quantum state swap between the output fields $\hat{a}_1(L)$ and $\hat{a}_2(L)$. The Doppler broadening effect study showed that this quantum node can achieve near-perfect quantum state swap up to a temperature of 30 K. Additionally, the efficiency of quantum state swap and the controlled preparation of superposition of initial states at room temperature are studied.

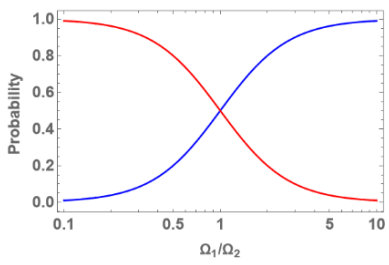

Fig 2 The red and blue lines represent the probability of finding the state $|\alpha_1\rangle$ and $|\alpha_2\rangle$, respectively, at detector D_1.

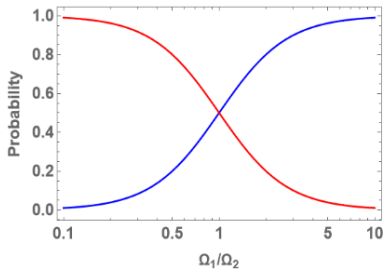

Fig 3 The red and blue lines represent the probability of finding the states $|\alpha_2\rangle$ and $|\alpha_1\rangle$, respectively, at detector D_2.

References

1. Sangouard, Nicolas, et al. *Reviews of Modern Physics* 83.1 (2011): 33.
2. Su, Xiaolong, et al *Physical Review Letters* 117.24 (2016): 240503.

QOT397 Optical bistability/multistability in a hybrid optomechanical system assisted by Kerr-nonlinearity and amplitude modulated drive field

*Surabhi Yadav[*1], Vijay Bhatt[2], Aranya B Bhattacherjee[1], Pradip K. Jha[3]*

[1]Department of Physics, Birla Institute of Technology and Science, Pilani, Hyderabad Campus, Telangana 500078, India

[2]Department of Physics and Astrophysics, University of Delhi, New Delhi 110009, India

[3]Department of Physics, DDU College, University of Delhi, New Delhi 110078, India

**Corresponding author: p20190049@hyderabad.bits-pilani.ac.in*

Cavity quantum optomechanics studies quantum phenomena involving the interaction of optical and mechanical modes within a cavity. Such a system typically consists of one fixed mirror and another movable mirror. The radiation pressure force exerted by photons circulating inside the optomechanical cavity alters the mean position of the mechanical. The circulating photons mediate coupling between the optical mode and mechanical degrees of freedom. Optical bistability is a nonlinear phenomenon characterized by mean photon number and has been studied in various optomechanical systems [1] and under the effect of various types of interactions [2]. Optical bistability has potential applications in optical switches [3], all-optical devices, and logic gates [4].

This work theoretically investigates the optomechanical interaction between an optical field and a mechanical mode mediated by a Kerr nonlinear medium inside an optical cavity and simultaneously driven by an external amplitude-modulated pump field and a probe field. We show that switching between bistability and multistability is influenced by the rocking parameter and Kerr nonlinearity and is essential in tuning the system's bistable to multistable behavior.

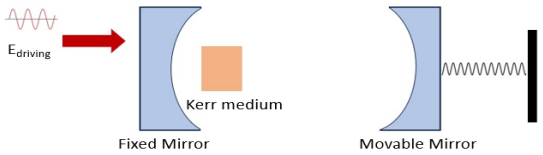

Figure 1: The schematic of the proposed hybrid optomechanical system with a Kerr nonlinear medium inside the optical cavity. The optomechanical cavity is driven by an amplitude-modulated light field.

$$H = \hbar\Delta_a a^\dagger a + \frac{\hbar\omega_m}{2}(p^2 + x^2) + \hbar\eta {a^\dagger}^2 a^2 - \hbar g x a^\dagger a + \iota\hbar[E_0 + \epsilon_c cos(\Omega t)](a^\dagger - a)$$

References

1. C. Jiang et. al., *Phys. Rev. A* 88, 055801 (2013).
2. C. Wang C et. al., *Appl. Opt*. 54 4623–8 (2015).
3. Z. Wang et. al., *Optics Communications* 282, 1574-1578 (2009).

4. P. Wen et. al., *Optics communications 219*, 383-387 (2003).

QOT398 Creation of Room Temperature Single Photon Emitters in Hexagonal Boron Nitride

Debdip Guchait[1], Swetha K[1], Pragya Joshi[2], Nitesh Singh[1], Biswanath Chakraborty[2], Rajesh V. Nair[1,]*
[1]Laboratory for Nanoscale Optics and Metamaterials (LaNOM), Department of Physics, Indian Institute of Technology Ropar, 140001, India
[2] Department of Physics, Indian Institute of Technology Jammu, Jagti, 181221, India
**email: rvnair@iitrpr.ac.in*

Solid state single photon emitters are emerging as the building blocks of quantum photonic applications, computation, and information processing due to its robustness and scalability. Hexagonal boron nitride (h-BN) is a prime candidate which can host bright, stable and deterministic single photon emitters and optically addressable spins deep within its wide bandgap [1]. Here, we discuss the creation and detection of single photon emitters in h-BN flakes at room temperature. The h-BN flakes are mechanically exfoliated using standard scotch tape method on to a silicon substrate. They are subsequently irradiated with electron beam to create optically active defects. The flakes are imaged using a home-built confocal microscopy setup to identify the emitters. After locating the emitters, its emission properties are studied by measuring the photoluminescence (PL) spectra. Fig. 1a shows the confocal image with a region marked P1 from which the PL spectra is measured as given in Fig. 1b.

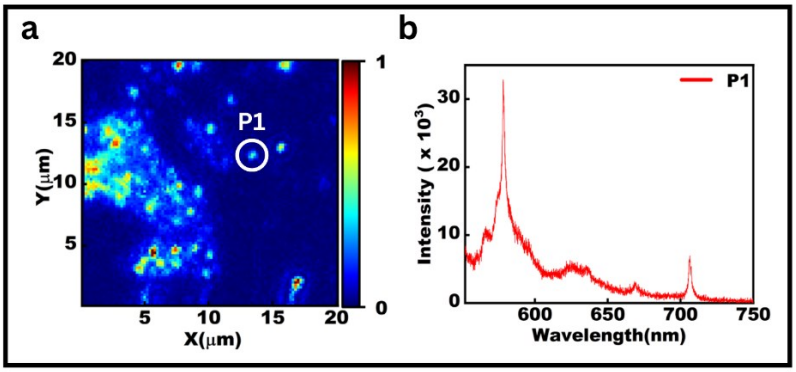

Fig. 1: (a) The confocal map of the sample with single photon emission point (P1), and (b) shows the measured emission from the P1 point.

The PL spectra show sharp emission peaks at 578 nm and 706 nm, which are known as the zero phonon line emissions. The emission peak at 578 is accompanied with phonon induced sideband emissions. Nevertheless, the emission peak exhibit very high Debye-Wall factor with more coherent emission at 578 nm. The second order autocorrelation measurements confirm the single photon emission from P1 point with stable emission counts. A comprehensive study on the multispectral defects is conducted to find out their emission dynamics. Such stable and narrow coherent emission is required for quantum technology applications.

References

1. Aharonovich et. al., *Nano Lett*. 22, 9227-9235 (2022).

QOT434 Quantum-Enhanced Nonlinear Sagnac Interferometer

*Priyanka M. and, Ashok Kumar**

Department of Physics, Indian Institute of Space Science and Technology, Thiruvananthapuram, Kerala, 695547.

**Corresponding author: ashokkumar@iist.ac.in*

Abstract: Optical gyroscopes are well known for their efficiency to measure the angular velocity. However, the shot noise limit of the lasers limits the precision with which the angular velocity is measured. Quantum resources promise to beat the shot noise limit and allow us to reach the ultimate precision limits. We have theoretically analyzed a Nonlinear Sagnac Interferometer (NSI), which uses entangled photons produced in a four-wave mixing process to obtain quantum-enhanced sensitivity. We found that the angular velocity sensitivity of a hybrid nonlinear-linear gyroscope can be improved significantly over the conventional Sagnac interferometer.

Methodology: An optical gyroscope works on the principle of the Sagnac effect. With classical sources such as laser, the sensitivity of the phase measurement is limited by the shot noise limit. This sensitivity could be improved by replacing the beam splitter of a traditional Sagnac interferometer with a nonlinear optical component [1]. We designed an NSI using SU(1,1) geometry, in which a four-wave mixer replaces the beam splitter. Since the fields generated in a four-wave mixing process are quantum entangled, such interferometers possess certain unique properties [2]. As a result, they can have quantum-enhanced precision in phase sensing. However, merely replacing a beam splitter with a four-wave mixer does not make the NSI achieve desirable sensitivity. This is because the phases gained by each of the arms of the Sagnac interferometer appear as phase-sum in the output intensity expression of the NSI. Since these phases are equal and opposite in the case of a gyroscope, the phase sum will erase the essential phase information. In order to rectify this issue, we included a linear loop within this gyroscope so that the phase terms appear as phase differences in the intensity expression. Using this design, we calculated the angular velocity sensitivity and showed that it beats the shot noise limit.

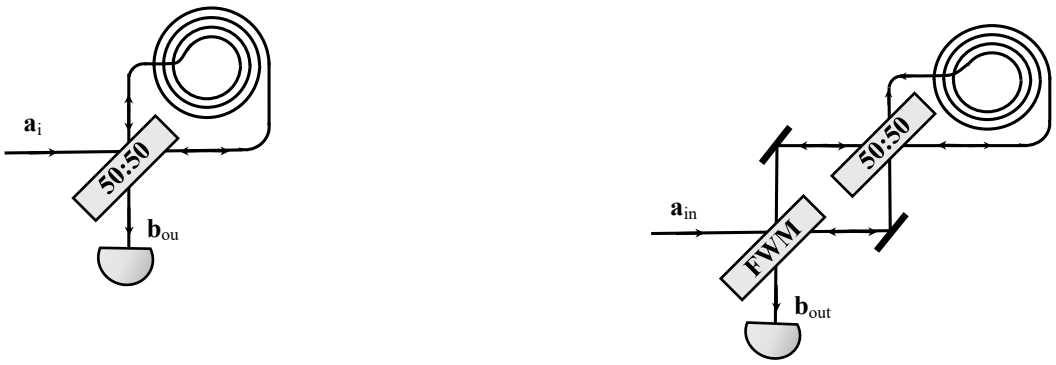

Fig. 1. (a) Traditional Sagnac interferometer with a 50:50beam splitter and fiber loop. (b) A hybrid nonlinear-linear Sagnac interferometer.

References

1. Wen Zhao et. al., *Appl. Phys. Lett.* 122, 064003 (2023).
2. Z. Y. Ou et. al., *APL Photonics 5*, 080902 (2020).

QOT142

Experimental Generation of Bright Two-Mode Squeezed Light and Probing its Spatial Quantum Correlation Dynamics

*Jerin A Thachil, Chirang Patel, Ashok Kumar**
Department of Physics
Indian Institute of Space Science and Technology
Thiruvananthapuram-695547
**Corresponding author: ashokkumar@iist.ac.in*

Squeezed states of light have gained a lot of attention given that they exhibit noise levels below the standard quantum limit (SQL), the minimum noise limit in classical physics. This property makes it an important resource in numerous applications like quantum-enhanced sensing and quantum imaging, quantum communication, and quantum information processing.

In this work, we generate bright two-mode squeezed states of light using a non-degenerate four-wave mixing process in a double-lambda configuration in hot ^{85}Rb vapor. We use a strong (≈ 600 mW) pump beam near the D1 line of Rb (795 nm), having a waist of 550 μm at the center of the cell. A weak probe (≈ 100 μW) beam which is shifted ≈ 3 GHz to the red of the pump, is obtained from a small portion of the pump using an acousto-optic modulator. The orthogonally polarized pump and probe beams are then made to intersect at an angle of 0.4° at the center of the Rb vapor cell, which is held at a temperature of 125°C. In this process, two photons from a single pump beam are converted into a pair of photons- probe and conjugate. Fig. 1(a) shows the images of entangled twin beams. The generated twin beams exhibit strong quantum correlations between their photons. The double-lambda configuration overcomes the limitations usually associated with atomic vapor systems, such as fluorescence, atomic fluctuations, and other nonlinear processes.

In the present experiment, we measured a quantum noise reduction in the intensity difference of 4 dB, corresponding to a 60% noise reduction from the SQL. Fig. 1(b) shows the squeezing measured with respect to SQL at a noise analysis frequency of 500KHz.

We also investigate the distribution of spatial correlations between the entangled twin beams generated using a structured pump and seed probe profile and study their dynamics.

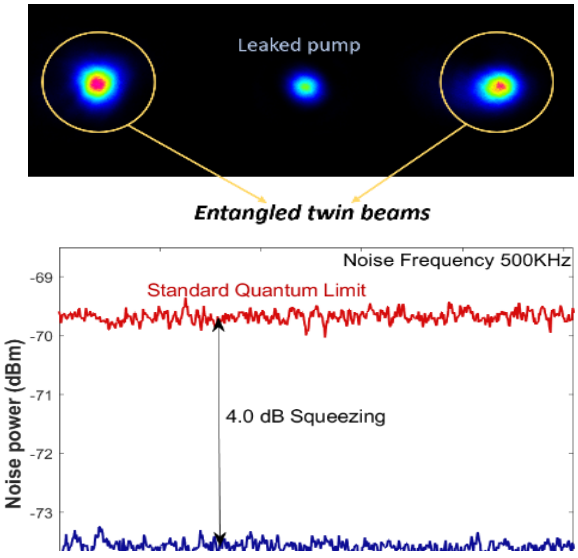

Fig.1 (a) Images of generated twin beams, and (b) noise reduction vs time at noise analysis frequency of 500KHz.

References

1. C.F.McCormick, A.M.Marino, V.Boyer, and P.D.Lett, *Phys.Rev.A* 78,043816 (2008)
2. R. C. Pooser et.al , *Opt. Express* 17, 16722-16730 (2009)
3. G. Nirala et al., *Sci. Adv*.9, eadf9161(2023)

QOT143 Quantum advantage in optical ranging

*Sankar Davuluri**

Department of Physics, BITS Pilani, Hyderabad Campus, Hyderabad, 500078, India

**sankar@hyderabad.bits-pilani.ac.in*

Quantum optics has evolved into an indispensable tool to enable future quantum technologies. One of the basic application of optics is to measure the distance of an object of interest. For very small distance measurements, optical interferometry [1,2] is one of the advanced technologies today. For eg: LIGO (Laser interferometer gravitational wave observatory) uses a giant Michelson interferometer to measure small displacements in suspended test masses to detect gravitational waves. On the other hand, Lidar (Laser imaging detection and ranging) is most useful for measuring laser distances. We explore the quantum advantage in both interferometers and lidar by introducing entangled laser [3] fields. Using entangled light, we propose a novel optomechanical interferometer design which has better sensitivity than a squeezed light interferometer [4]. Similarly, using entanglement in conjunction with quantum cross-correlated homodyne measurement, we describe a novel quantum lidar design which not only outperforms the classical lidar but also can negate the stealth properties of the target. The quantum lidar design can also be applied for imaging low-reflective objects immersed in noisy environment.

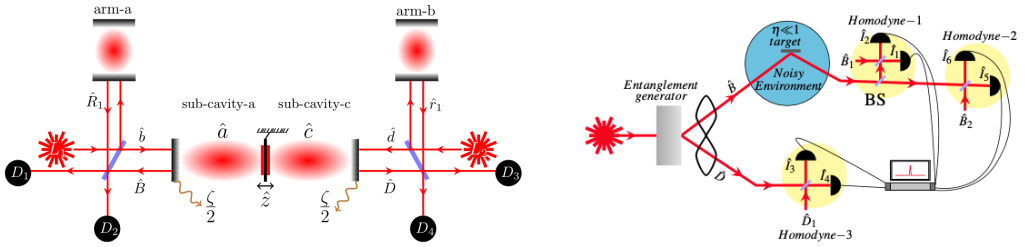

References

1. Sankar Davuluri, *Opt. Lett*. 46, 904-907 (2021)
2. Sreeshna Subhash, Sanket Das, Tarak Nath Dey, Yong Li, and Sankar Davuluri, *Opt. Express 31*, 177-191 (2023)
3. Gopinath, Greeshma, Yong Li, and Sankar Davuluri. *arXiv preprint arXiv:2307.10956* (2023)
4. Sreeshna Subhash, Sanket Das, Tarak Nath Dey, Yong Li, and Sankar Davuluri, *Opt. Express 31*, 177-191 (2023)

QOT146 Hybrid Quantum Engineering with photon-magnon coupling at room temperature for next generation quantum information devices.

*Kuldeep Kumar Shrivastava, Biswanath Bhoi, Rajeev Singh**
Nano-Magnetism and Quantum Technology Laboratory, Department of Physics, Indian Institute of Technology (Banaras Hindu University), Varanasi, 221005, Uttar Pradesh, Bharat.
** rajeevs.phy@iitbhu.ac.in*

Photon-magnon coupled (PMC) hybrid systems hold great promise for applications in quantum processing technologies. Specially, controlling the interactions, including various types of anti-crossings, between photon (P) and magnon (M) modes is crucial for the development of information processing devices with desired tunability and scalability. Multimode PM coupling with switching features from level repulsion (LR) to level attractions (LA) is theoretically proposed and demonstrated through numerical simulations for two different hybrid systems i.e., two photon-one magnon mode (2-1 PM) and three photon-one magnon modes (3-1 PM). Although, individual photon modes display dissipative couplings with the magnon mode, when designed as 2-1 PMC system, one photon undergoes a transition to coherent coupling, while the other maintains its dissipative coupling with magnon. On the other hand, in the case of a 3-1 PMC system, their combination results in a shift to coherent coupling for one photon, a transition from dissipative to coherent coupling for the second photon while the third photon retains its dissipative coupling with magnon mode. The numerically calculated LR and LA due to coherent and dissipative coupling in these two PMC systems are presented in Fig. (c-e). Characteristic features of these multi-mode interactions (Fig. g-h) are analysed with the help of our own developed quantum mechanical model just by controlling some parameters at room temperature.

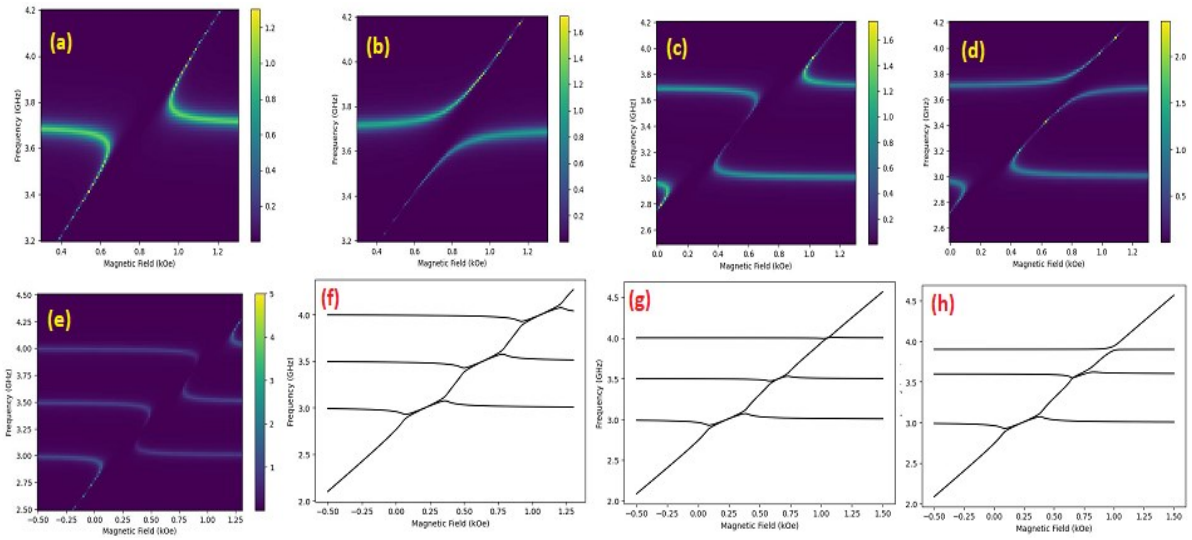

Figure: (a/ b) LA/ LR for 1 magnon and 1photon mode, (c) 1 magnon and 2 photon modes showing LA for individual systems, (d) hybrid of (c) after parameter tuning shows LA+LR (e) 1 magnon 3 photon modes LA for individual systems, (f-h) eigen value curve for (e) after parameter tuning showing transition from LA to LR.

References

1. Tiwari T, Roy D & Singh R (2020). Interplay of coherence and interaction in light propagation through waveguide QED lattice- arXiv preprint arXiv:2010.14935.
2. Bhoi B, Kim B, Jeon H-C & Kim S-K (2022). Coupling induced transparency and absorption in a

magnon-multiphoton hybrid system *J. Appl. Phys.* 132, 243901.

3. Scully M O and Zubairy M S, Quantum Optics (Cambridge University Press, 1997).
4. Harder M, Yao B M, Gui Y S & Hu C-M (2021). Coherent and dissipative cavity magnonics *J. Appl. Phys.* 129, 201101.

Category 23

Singular Optics & Laser Speckles (SIN)

SIN144 Identifying topological charge of discrete optical vortices

*Vasu Dev, and Vishwa Pal**

Dept. of Physics, Indian Institute of Technology Ropar, Rupnagar, Punjab India 140001
**Corresponding author: vishwa.pal@iitrpr.ac.in*

Optical vortices (OVs) have widespread applications in optical communications, tweezing, high-resolution imaging and microscopy, etc [1]. The phase of OVs is represented by $\exp(il\phi)$, leading to an orbital angular momentum of $l\hbar$ per photon, where l is called the topological charge (TC). Examples like Laguerre-Gaussian beams and Bessel beams are considered as continuous OVs due to their continuous intensity and phase distributions over the contour. However, these OVs are limited in high-power applications because they originate from a single laser source. Therefore, an alternative approach using phase-locking of lasers/coherent beam combining is proposed. This involves arranging a finite number of lasers (N) in a 1D ring array, where the intensity at the centre is zero, and the phase circulates from one laser to the next, either clockwise or counterclockwise direction. Such beams are known as discrete optical vortices (DOVs) [2]. Most of the applications of OVs are linked to the TC, hence its precise measurement is crucial. Additionally, discrete systems exhibit distinct behaviour from continuous systems, therefore, methods for determining TC in continuous OVs may not be applicable to DOVs. Hence, we present a novel interference-based approach to accurately determine the magnitude and sign of unknown TC of DOV. The interference pattern of a DOV is obtained when one selected reference laser interferes with itself and with all the lasers in the DOV (Figs. 1(a)-1(c)). Different phase distributions of l=0 and $l\neq0$ result in shifted fringes in the interference pattern. Therefore, on averaging the interference pattern of l=0 with unknown $l\neq0$, a variation in fringe visibility (V) as a function of laser index (j) is observed, and the number of dips in the fringe visibility curve is found to be proportional to the magnitude of TC of unknown DOV, as shown in Figs. 1(d)-1(g). To determine the sign of TC, we average its interference pattern with that of l=1, where a positive TC reduces the number of dips by 1, and a negative TC increases it by 1. Moreover, we also found that the presence of phase disorder does not influence an accurate determination of TC, and the method works well over a broad range of TCs of DOV for different system sizes N [2].

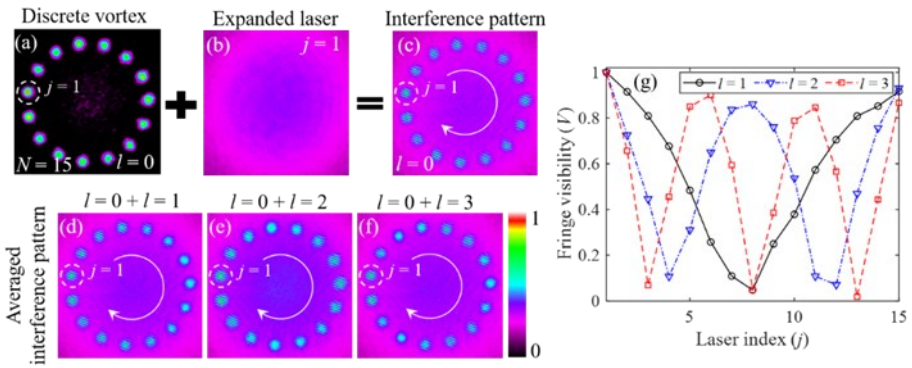

Figure 1 Experimental results for determining TC of DOV of system size N = 15 and l=1-3

References

1. Halina Rubinsztein-Dunlop et. al., *J. Opt*. 19, 013001 (2017).
2. V. Dev, and Vishwa Pal, *Phys. Rev. Applied* 20, 034071 (2023).

SIN404 Role of Quasi-monochromaticity in Spin-Orbit Interaction of Light

*Harish Kumar and Nirmal K. Viswanathan**

School of Physics, University of Hyderabad, Gachibowli, Hyderabad 500046

**Corresponding author: nirmalsp@uohyd.ac.in*

Spin-orbit interaction (SOI) of light is revolutionising the understanding of light and light-matter interaction, providing a deeper understanding, enriching the fundamental and applied aspects [1]. In optical systems maintaining symmetry the SOI leads to spin-to-orbital (SO) angular momentum (AM) and orbital-to-spin (OS) AM conversions, conserving the total AM. On the other hand, symmetry breaking leads to the appearance of the spin-Hall (SH), orbital-Hall (OH) effects of light [2]. Almost all fundamental optical processes including the reflection, refraction, interference, diffraction, and scattering involving inhomogeneous and anisotropic interactions have been shown to provide a deeper understanding of the SOI of light. Most of these processes involve investigation of the SOI effects in the real and momentum space of monochromatic source of light.

Here we present results due to SOI arising due to quasi-monochromaticity of light interacting with a generic elliptically birefringent anisotropic medium. Polarization filtering the output beam in a state orthogonal to the input beam (Fig. 1 (a)) leads us to the observation of periodically arranged phase singularity and phase saddle as a function of crystal rotation angle and wavelength (Fig. 1 (b)). In addition, the interaction leads to anomalous phase delay (Fig. 1 (c)) and group delay characteristics around the phase singularity, leading to phase flip and enhanced group delay as one comes close to and crosses the singularity. Weak measurement method in the polarization-frequency domain is used to quantify the phase and group delay characteristics arising due to the interaction. Details of the results and the emergence of SOI due to the interaction will be detailed in the presentation.

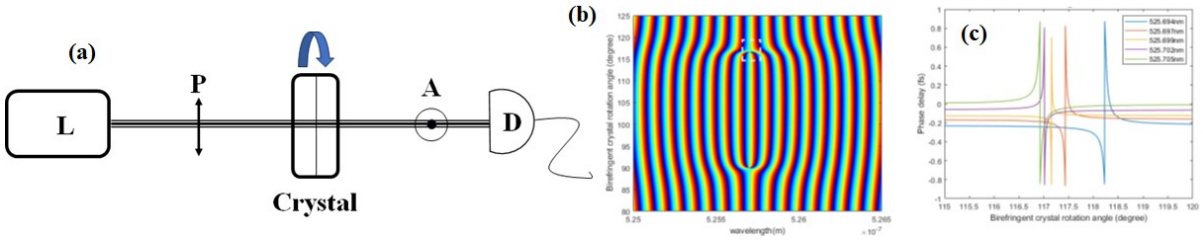

Fig. 1. (a) Schematic of the setup, (b) Phase map and (c) phase delay plot.

References

1. K.Y. Bliokh et. al., Nat. Photon., 9, 796-808 (2015).
2. M. Kim et. al., Laser Photonics Rev., 2200046 (2022).

SIN405

Vortices in correlation function

Akanksha Gautam[1], Rakesh Kumar Singh[1]*

[1]Laboratory of Information Photonics and Optical Metrology, Department of Physics, Indian Institute of Technology (Banaras Hindu University), Varanasi 221005, India

**Corresponding author: akankshagautam1007@gmail.com*

Singular optics traditionally centers on the examination of fully coherent, monochromatic optical fields. These fields exhibit regions of zero amplitude and undefined phase characteristics, commonly referred to as optical vortices [1]. For a while now, singular optics has expanded into correlation functions, introducing 'coherence vortices' for phase singularities of complex coherence functions. Experiments were performed to verify the presence of these singularities as ringlike dislocations in the complex coherence function [2] and in the phase structure [3]. Here, we present a new method for the creation of vortices in the complex coherence function of the partially coherent beam using the polarization basis of the light.

In the space-frequency domain, the spatial coherence properties of the field at any cross-sectional plane z, at a pair of transverse points $\boldsymbol{r}_1$ and $\boldsymbol{r}_2$ are defined by the complex spatial coherence function, expressed as $W(\boldsymbol{r}_1, \boldsymbol{r}_2) = \langle E_x^*(\boldsymbol{r}_1, \omega) E_y(\boldsymbol{r}_2, \omega) \rangle$, where $E_p(\boldsymbol{r}, \omega)\ (p \equiv (x, y))$ is a realization of the orthogonal field components at a point r and w is the frequency of the source. The asterisk and angular bracket denote the complex conjugate and ensemble average, respectively. Fig. 1 shows simulation results of the generation of vortices in the two-point correlation function of the orthogonal polarization components with topological charges 2 and 3. Such singularities and helical phase structures can be inserted in the correlation of the orthogonal polarization components using a suitable phase mask in one of the orthogonal basis of the light.

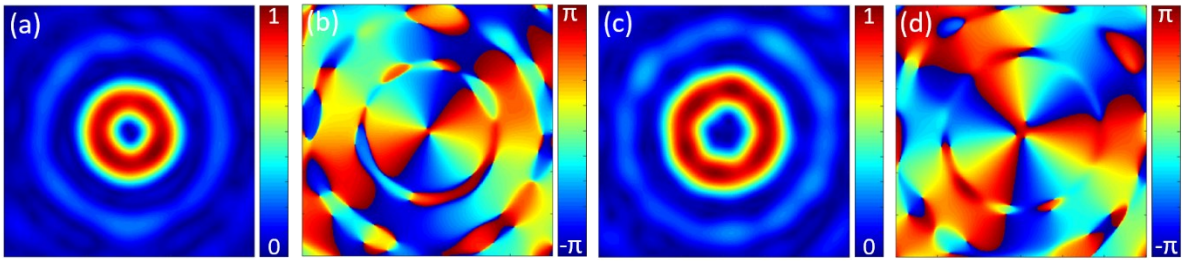

Fig. 1 Amplitude and phase distribution of the complex spatial coherence function (a) and (b) for topological charge *l=2* and (c) and (d) for topological charge *l=3*, respectively.

Akanksha Gautam would like to acknowledge DST-INSPIRE (Grant No. – IF180930) and IIT (BHU).

References

1. M. S. Soskin et.al., *Prog. Opt.* 42, 219-276 (2001).
2. D. M. Palacios et. al., *Phys. Rev. Lett.* 92, 143905 (2004).
3. W. Wang et. al., *Phys. Rev. Lett.* 96, 073902 (2006).

SIN406

Detection of vortex beam with high topological charge

Amit Yadav[1], Tushar Sarkar[1], Takamasa Suzuki [2], Rakesh Kumar Singh[1]*

[1]Labotray of Information Photonics and Optical Metrology, Department of Physics, Indian Institute of Technology (BHU), Varanasi Uttar Pradesh, India 221007.

[2]Electrical and Electronic Engineering, Niigata University, Niigata, Japan.

**amityadav.rs.phy20@itbhu.ac.in*

Light beams possessing orbital angular momentum (OAM) referred to as vortex beams (VBs). These beams exhibit a helical wavefront, which can be described by an exponential factor represented as exp ($il\varphi$), carries a well-defined OAM of $\pm l\hbar$ per photon, where l is the topological charge (TC) and φ indicates azimuthal angle [1]. The beam possessing OAM holds great potential for practical applications such as microparticle manipulation, free-space optical communication, etc. Detection of topological charge of the vortex beam is desired in various applications and several interferometric and non-interferometric techniques have been developed [2]. However, experimental detection of vortex beam with high TC is yet a challenging problem.

In this work, we present a new experimental method for the detection of topological charge of the vortex with large TC and its phase structure. This is realized by using the superimposition of the orthogonal basis of the beam, one with vortex and other without it. The topological charge of the vortices is determined by counting the number of petals.

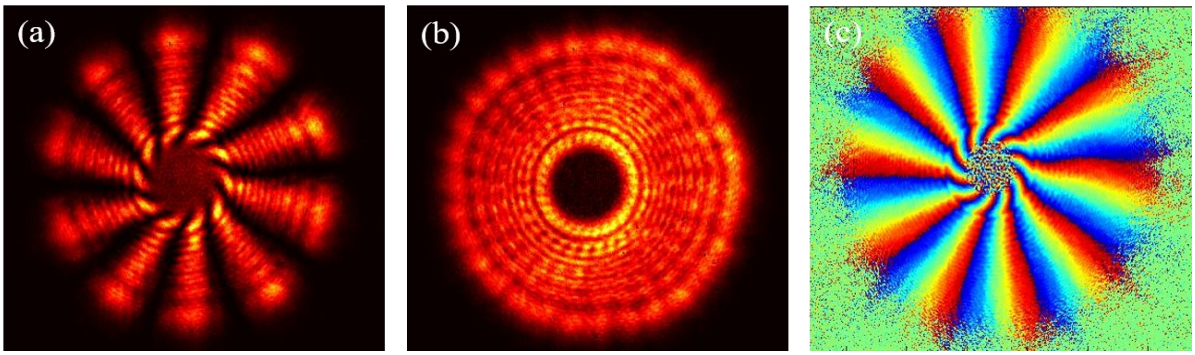

Fig. 1. Experimental results: (a) petals representing TC (b) intensity pattern of the vortex and (c) its phase with TC *l*=10.

In conclusion, we have presented experimental tests on the detection of the topological charge of the vortex beam.

Acknowledgment: Amit Yadav acknowledges the University Grant Commission, India for financial support as Senior Research Fellowship.

References

1. Barnett, and M. J. Padgett, Orbital Angular Momentum (CRC, Boca Raton, FL, 2016).
2. Alison M. Yao and Miles J. Padgett, "Orbital angular momentum: origins, behavior, and applications," Adv. Opt. Photon. 3, 161-204 (2011)

SIN407

Polarization based spatial-filtering using spin-orbit beams

Anuj Maurya[1], Sarvesh Bansal[1], B. S. Bhargava Ram[2], and P. Senthilkumaran[1,3]*
[1] Department of Physics, Indian Institute of Technology Delhi, Hauz Khas, New Delhi-110016
[2]Laboratory for Electro-Optics Systems (LEOS-ISRO), I cross, I Stage, Peenya Industrial Estate, Bengaluru-560058
[3]Optics and Photonic Centre, Indian Institute of Technology Delhi, Hauz Khas, New Delhi-110016
**E-mail: bansalsarvesh.s@gmail.com*

Structured optical fields containing singularity are being studied in the past few years, and a tremendous increase in research activities involving phase singularities and polarization singularities have been observed [1]. The polarization singularities are also known as spin-orbit beam. We introduced for the first time, a novel method to perform isotropic as well as anisotropic edge detection using these beams.

In image processing, edge enhancement is one of the most significant tools for analysis, and pattern recognition. Edge enhancement can be achieved using various digital gradient algorithms [2]. An optical Fourier processing system can also be implemented to achieve edge enhancement using different filters such as amplitude and phase filters [3]. The requirement of various types of edge detections leads to development of isotropic and anisotropic edge enhancement. Directional edge detection (anisotropic) can be achieved by 1D Hilbert transform filters and isotropic edge detection by radial Hilbert transform [4,5]. The 1D Hilbert transform and radial Hilbert transform can be obtained using Heaviside step phase filter and spiral phase filter, respectively. Apart from amplitude and phase filters, the polarization of the beam can also be used to filter the high frequencies. Isotropic and anisotropic edge enhancement can also be performed using inhomogeneous structured polarizations, viz. spin-orbit beams.

We have used lemon-star polarization dipole to demonstrate the polarization based spatial filtering. The linear polarization states present in lemon star dipole are used to extract different types of edges present in object. Polarizer is used to select the linear polarizations state from the polarization distribution. As a result, a vortex core is employed in the system, whose position depends upon the orientation of polarizer, performing different types of edge enhancement. This polarization based spatial-filtering may find potential application in birefringent samples such as biological cells, photo-elastic materials and so on.

References

1. P. Senthilkumaran, *IOP Publishing*, 2053-2563, 2018)
2. M. K. Prasanna et. al., *International Journal of Advanced Computer Research* 4, 532 (2014).
3. R. Bracewell et. al., *American Journal of Physics 34*, 712–712 (1966).
4. J. A. Ferrari et. al., *Optics Communications 283*, 2803–2806 (2010).
5. C.-S. Guo, et. al., *Optics letters 31*, 1394–1396 (2006).

SIN408 Diversity in Speckle of Polarization Structured Light on Propagation through Turbulence

Basant Kumar[1,3], Priyanka Lochab[2], Devinder P. Ghai[3], Jagannath Nayak[1], P.Senthilkumaran[3] & Kedar B. Khare[3]*

[1] Center for High Energy Systems & Sciences, Hyderabad, India-500069

[2] Department of Applied Sciences and Humanities, Indira Gandhi Delhi Technical University for Women, Delhi, India-110006

[3] Department of Physics, Indian Institute of Technology, Delhi, India-110016

** Corresponding author: bkumar.chess@gov.in*

We discuss the diversity and the resultant classifiability that exists among speckle patterns, which are generated when different configurations of polarization structured light fields as well as scalar fields, propagate through turbulence. Speckle patterns generated theoretically for C-point, V-point and scalar fields, indicated visually perceivable differences among themselves [1]. Specifically, for V-point field, the speckle pattern showed an intertwined noodle like pattern. This kind of speckle pattern was not reported earlier to the best of our knowledge. Presence of wool like soft appearing speckle pattern for C-point beam was also observed. The theoretical results were then verified experimentally. The experimental results showed stark resemblance to the theoretically generated speckle patterns.

Intensity statistics analysis of the three speckle groups did not reveal any significant classification among them, despite significant visually divergent morphology. The speckle patterns were analysed using the Gray Level Co-occurance Matrix (GLCM) features [2], which is a texture classification methodology, employing the analysis of spatial and directional co-occurance of repeatable pixel values thereby allowing the analysis of textures and patterns. A total of 23 GLCM parameters were evaluated for all the three groups of speckles. The GLCM statistical data was then used to construct a classification basis by employing the Principal Component Analysis (PCA) methodology.

The deployed methodology classified the speckle patterns accurately, thereby indicating that the speckle patterns are not completely random, indeed diverse among themselves and are accurately classifiable. The classifiability is also an indication that the speckle patterns preserve some characteristics of the original optical field, along with the strength of random turbulence, which led to its creation.

References

1. Basant Kumar, Priyanka Lochab, Esha Baidya Kayal, Devinder P. Ghai, P. Senthilkumaran, & Kedar Khare (2022) Speckle in polarization structured light, Journal of Modern Optics, 69:1, 47-54, DOI: 10.1080/09500340.2021.1996646
2. Clausi DA. An analysis of co-occurrence texture statistics as a function of grey level quantization. Can J Remote Sens. 2002;28:45–62.

SIN409 Study of Classical Non-Separability of a Vector-vortex beam Reflected from a Prism

Bibek Kumar Patra[*], Maruthi M. Brudavanam

Department of Physics, Indian Institute of Technology Kharagpur, Kharagpur, West Bengal 721302, India

[*]Email:bibek.patra18@iitkgp.ac.in

Brewster differential microscopy based upon simple reflection from glass interface is a powerful technique

to perform edge enhanced imaging [1]. Here we propose a Brewster experimental technique to modulate the degree of non-separability [2,3] by reflecting a classical non-separable beam CNSB [2,3,4] from a prism (N-BK7). The degree of non-separability of the beam can be estimated by measuring the degree of polarization (DOP), and linear entropy (S_L) [3,4]. The DOP can be calculated from Stokes polarimetry.

Experimentally we have generated a CNSB by using a horizontally polarized Gaussian beam coming from a He-Ne laser of wavelength 632 nm. This beam is collimated using two lenses and the polarization state is varied using a half-waveplate (HWP). Then the linearly polarized beam from HWP is made to incident on a spatial light modulator (SLM) which converts only the horizontally polarized beam to a vortex beam of order 2 and the vertically polarized beam remains unaffected. This forms a CNSB whose non-separability can be modulated by changing the fast axis of the input HWP. This CNSB is made to fall on a prism refractive surface and the prism is rotated from 20^o – 80^o for each input HWP angle varied from 10^o-35^o and the Stokes parameters are measured in each case. Then DOP is calculated using Stokes parameters and S_L is estimated in each case. It is found that the plot of S_L with respect to HWP angle is shifting for different reflected angles from the prism as shown in Fig. 1. The reason behind this shift is due to change in reflection coefficient for H and V polarized light with respect to prism rotation angle (**θ**). The detailed experimental results and analysis will be presented during the conference.

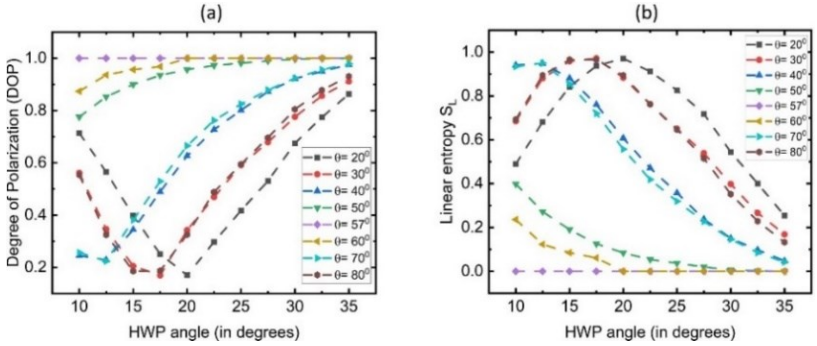

Fig. 1: Variation of (a) DOP and (b) S_L with respect to HWP for a different prism rotation angle (**θ**).

References

1. R. Wang et. Al., *Appl. Phys. Lett*. 121, 231103 (2022)
2. C. Samlan et. al., *arXiv*. 1506.07112 (2015).
3. C. Perumangatt et. al., *Opt. Commun*. 355, 301 (2015)
4. F. Toppel et. al., *New J. Phys*. 16, 073019 (2014)

SIN410 Transverse Spin Variations due to High-NA Focusing

Cyriac Raju,[1,2] and Nirmal K. Viswanathan[2,]*

[1]Department of Physics, Indian Institute of Science Education and Research Tirupati, Tirupati, Andhra Pradesh, India – 517507.

[2]School of Physics, University of Hyderabad, Hyderabad, Telangana, India – 500046.

**Corresponding author: nirmalsp@uohyd.ac.in*

Spin-orbit interaction (SOI) of light is an emerging idea to understand the characteristics of light under different physical conditions and upon its interaction with materials.[1] A propagating beam of light carries spin angular momentum (SAM) and orbital angular momentum (OAM), respectively associated with its polarization and phase structure. These AM aspects of a light beam, upon interacting with each other during propagation or upon interacting with material leads to the SOI and related effects. The interplay

between the polarization and trajectory of a light beam, due to the SOI, can lead to the transverse variation of spin (and vice versa), which is known as the spin Hall effect (SHE) of light.[2] The SOIs are thus inherent in many basic optical processes including reflection, refraction, propagation, focusing, and imaging and have attracted wide attention in recent years, playing an important role in almost all emerging areas of optical physics.

In this work, we simulated the focusing of an optical beam-field using Python programming to (re) understand the emerging characteristics of the beam in the SOI context. We focused a linearly / circularly polarized Gaussian beam using a high-numerical aperture (NA) lens and analysed the emerging beam-field characteristics in the focal region of the lens. Notable observations include emergence of spin component in the focal region, and transverse-longitudinal spin variations in the focal region. The new features are quantified via Stokes parameter calculations, and we could notice complex and asymmetric spin separation behaviour, showing opposite spins in the four quadrants of the transverse plane and along the propagation direction. These complicated and non-trivial observations suggest very involved and intricate behaviour of optical fields in the focal region in 3D. This additional degree of freedom along the direction of propagation could be highly valuable in various areas like near-field optics, optical patterning, and optical manipulation.

References

1. K.Y. Bliokh et. al., Nat. Photon., 9, 796 (2015).
2. Weixing Shu et. al., Phys. Rev. A 101, 023819 (2020).

SIN411 Optical image encryption using Hermite-Gaussian Beam Speckles

Harsh Vardhan[1], Ravi Kumar[1], Salla GangiReddy[1]*
[1]Department of Physics, SRM University - AP, Andhra Pradesh - 522502, India
**Corresponding author: harshvardhan_r@srmap.edu.in*

Most optical cryptosystems use the spatial distribution of amplitude, phase, and polarisation of light to encrypt a two-dimensional image or piece of information. In this study, we propose a new asymmetric cryptosystem using the Hermite-Gaussian beam speckles (HGBS) as security keys. In conventional optical cryptosystems, mostly random phase masks are used as security keys, which are found to be vulnerable to various attacks such as KPA, CPA, COA, etc [1, 2]. The HGBS are generated optically in the current study by scattering of a HG beam of different transverse modes $HG_{m,n}$ where (m and n are the horizontal and vertical modes) through GGP. The mode parameter serves as additional keys in the proposed cryptosystem. The original image is first phase encoded and modulated with an HGBS phase mask to obtain the complex image which is Fresnel propagated with distance z_1. Afterwards, the phase truncation operation is performed, and the phase part is reserved as private key and amplitude part is further processed. The discrete wavelet transform is used to process the amplitude part to obtain the encrypted image. The proposed technique is robust against potential attacks such as noise, occlusion attacks, and known plaintext attacks (KPA). The sensitivity of all the security keys along with the HGBS speckles is also tested by calculating correlation coefficient (CC) and mean squared error (MSE). The validity and feasibility of the proposed method are confirmed by the numerical simulations.

References

1. B. Javidi et. al., *J Opt.* 18, 083001 (2016).
2. W. Chen et. al., *Adv. Opt. Photon.* 6, 120 (2014)

SIN412 Fractional topological charge measurement of optical vortex beam using joint transform correlator

*Allarakha Shikder, Jyoti B. Mohapatra, and Naveen K. Nishchal**

Department of Physics, Indian Institute of Technology Patna, Bihta, Patna 801 106, India

**nkn@iitp.ac.in*

Optical vortex beams with fractional topological charges (TC) have gained interest among the researchers' community for their unique intensity and phase distributions. All potential applications of fractional vortex beam require accurate measurement of orbital angular momentum associated with fractional TC [1]. In this study, we propose a novel technique to measure the fractional TC of a vortex beam using a joint transform correlator (JTC). The JTC is a suitable technique that provides a real-time match between two patterns [2]. The proposed technique offers fast fractional TC measurement since it does not require a complicated architecture. The vortex beam contains a spiral phase front expressed by $exp(il\varphi)$, where l denotes TC and φ is the azimuthal angle. Vortex beams with integer TC create fork-shaped interference pattern of equal number of dark petals after interfering with a tilted Gaussian beam, as *shown in Figure 1(a) for TC = 5* [3,4]. Figure 1(b) shows the interference pattern corresponding to fractional TC, $l = 5.5$, where the symmetry of those integer number of petals is broken and there will be a continuous change in intensity as the fractional TC changes due to the creation of a new petal. This change of intensity variation in the interference pattern for TC value 5 to 6 has been shown in Fig. 1(c) in steps of 0.2. These results are segments of 30 × 100 pixels of the pattern, as shown in red box in Fig. 1(a). The fractional TC can be determined by comparing the correlation peak heights of the interference pattern segments between fractional and integer TCs. The plot of correlation peak height of interference pattern segments of different fractional TCs with integer TC is illustrated in Fig. 1(d). The red and green lines correspond to the correlation with TC values 6 and 5, respectively.

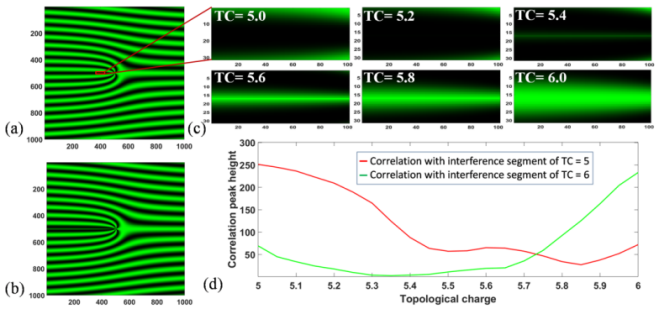

Fig. 1 Interference pattern of a tilted Gaussian beam with a vortex beam of TC = (a) 5 & (b) 5.5, (c) Segment of interference patterns corresponding to different TC values, (d) Plot of correlation peak height respect to TCs.

The authors acknowledge the funding from the SERB, Govt. of India, grant No. CRG/2021/001763. Mr. A. Shikder acknowledges the Prime Minister Research Fellowship, Govt. of India, ID-2701807.

References

1. Zhang et al., Nanophotonics 11, 241-273 (2022).
2. Nishchal et al., Opt. Eng. 45(2), 026401 (2006).

3. Ma et al., J. Opt. Soc. Am. A 38, 115-123 (2021).
4. Shikder et al., Appl. Opt. 62, D58-D67 (2023).

SIN413 Application of Fujii algorithm in laser speckle imaging for the determination of intermittent dynamics of drying dispersions of white paint

Keerthana S H, P Radhakrishnan, A Mujeeb*[1,2]
[1]*International School of Photonics, Cochin University of Science and Technology, Kochi 682022, Kerala, India*
[2]*Kerala University of Digital Sciences, Innovation and Technology, Thiruvananthapuram 695317, Kerala, India*
Email: keerthanashankar@cusat.ac.in*

Dynamic laser speckle imaging is an efficient optical method used widely to explore the dynamics of turbid media of biological, medical or industrial importance. It is a non-destructive method which is also cost-effective in nature. The temporal as well as spatial resolution of the imaging techniques are also very high. Image processing algorithms such as Time History of Speckle Patterns (THSP) and Co-Occurrence Matrices (COM) are widely employed to extract information from the speckle images captured via this technique. These algorithms provide the activity map but do not provide the numerical results. Also, these algorithms can extract only the information regarding certain regions of the images rather than providing the complete information of the images. Hence in this paper, we employed a powerful statistical method, Fujii algorithm, for determining the intermittent dynamics of drying dispersion of white paint. The complete information of the speckle image sequence can be obtained through the Fujii algorithm. The work also discusses some numerical results associated with Fujii algorithm for the first time. Quantitative method of Inertia Moment is also utilized to confirm the results.

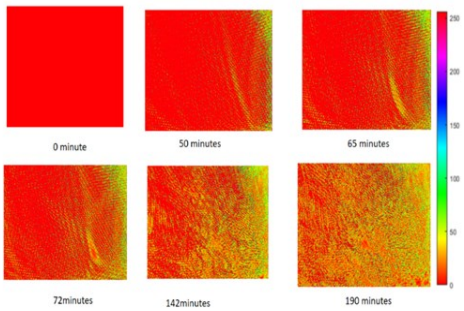

Fig 1. Fujii activity images of intermittent stages

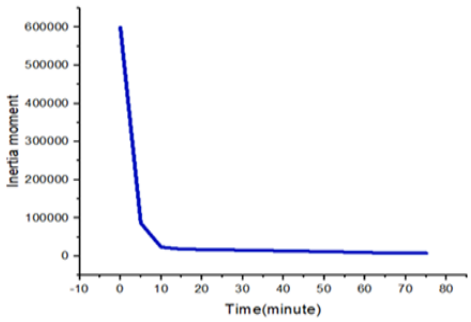

Fig 2. Variation of Inertia Moment with time

References

1. Hitoshi, et al., "Blood flow observed by time-varying laser speckle." *Optics letters* 10.3 (1985): 104-106.
2. Cariñe, J., R. Guzmán, and F. A. Torres-Ruiz. "Algorithm for dynamic speckle pattern processing." *Optics and Lasers in Engineering* 82 (2016): 56-61.

SIN414 Interpretations of Stokes polarimetry in the spin-1 context: a tensor description of light

Maitreyi Jayaseelan[1,*]
[1]*School of Physics, University of Hyderabad, Gachibowli, Hyderabad-500046*
**Corresponding author: maitreyi.jayaseelan@colorado.edu*

We explore polarisation beyond the familiar pseudo-spin-1/2 context. We analyse Stokes polarimetry, and transformations produced by common optical elements, in the context of a spin-1 system where higher-order tensor components play a role. We discuss the different internal and external degrees of freedom, and their coupling, in an optical lemon field in this context.

For a complex paraxial field $\boldsymbol{E} = (E_+, E_-)$, the coherence matrix $\Phi_2(\boldsymbol{E}) = \langle \boldsymbol{E}^\dagger \boldsymbol{E} \rangle$ can be resolved into components proportional to the identity $\mathbb{I}_2$ and the Pauli spin operators, with the Stokes parameters as the coefficients of expansion [1]. The state of polarisation is thus completely described by scalar and vector (rank-1) quantities. Beyond the pseudo-spin-1/2 description however, higher spin moments must be considered: spin-1 systems are described by both spin and nematic operators which are quadratic forms of the spin operators [2]. We examine polarisation in the spin-1 context, demonstrating the rank-1 and rank-2 tensor character of circular and linear polarisation, respectively, with a simple experimental measurement of the Stokes parameters with a rotating quarter wave plate (Fig. 1) [3]. We discuss descriptions of familiar optical elements such as quarter and half wave plates in this expanded operator basis, and identify forms of coupling between spin tensor moments, and orbital angular momentum in the Stokes polarimetry of an optical lemon field.

*We thank Prof. Nirmal K. Viswanathan, University of Hyderabad, for helpful discussions.

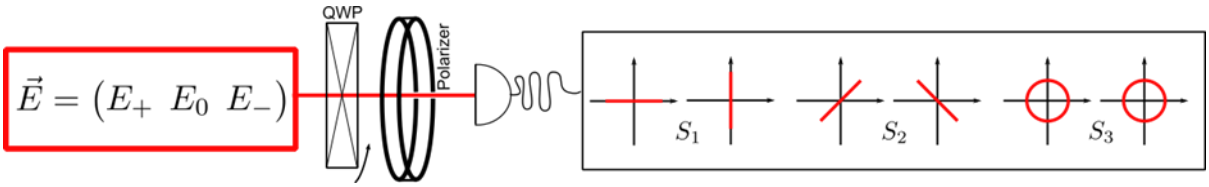

Fig.1: Stokes polarimetry with a rotating quarter wave plate.

References

1. U Fano, Phys. Rev. **93**, 121 (1954)
2. M R Dennis, J. Opt. A: Pure Appl. Opt. **6,** S26 (2004)
3. B Schaefer, E Collett, R Smyth, D Barrett, B Fraher, Am. J. Phys. **75**, 163–168 (2007)

SIN415 Coherence Vortices: A complete mathematical and experimental analysis

Md. Haider Ansari[1], Vinny Cris M[1], Preeti Gangwani [*2,3], Salla Gangi Reddy[1], Shashi Prabhakar[3], J. Banerji[3], and R. P. Singh[3]*
[1]*Physics Department, SRM University -AP, Andhra Pradesh India - 522502*
[2]*Sardar Vallabhbhai National Institute of Technology, Surat, India, -395007*
[3]*Quantum Science and Technology Laboratory, Physical Research Laboratory, Ahmedabad, India 380009*
**haideransari_md@srmap.edu.in*

The azimuthal index or topological charge of the accessible optical vortices is denoted by m and they have an orbital angular momentum of m ħ per photon. In a coherent system with a clearly defined phase, the vortices have been examined. However, a fascinating area of research in singular optics has emerged for imperfectly coherent systems, where the phase is not clearly defined. A partially coherent beam, or "coherence vortex," can also exhibit optical vortices in the correlation function. Additionally, a well-known indicator of an optical vortex is a ring-shaped intensity distribution. With coherent beams, this shape can be seen clearly, but not with partially coherent beams. Furthermore, when a coherence vortex is present, the ring shape can be seen by performing an intensity correlation between beams that are only partially coherent. In this investigation, a partially coherent beam was employed with a coherence function. In an effort to produce higher order coherence vortices, we explore the analytical and experimental studies on coherence vortices, which can be realized through intensity correlation functions. The following four conclusions are drawn from our studies:

1. One can generate a very high order vortex of charge $\pm(|l_2| + |l_1|)$ by cross correlating two scattered vortex fields whose topological charges are $|l_2|, |l_1|$ but with opposite signs.

2. When $|l_2| = |l_1| = |l|$ our results are finding the cross correlation between a scattered vortex Sand its anti -vortex and we will be able to produce a vortex of order ±2 $|l|$.

3. If one plots the radius of the dark core as a function of z for a few values of z and uses the formula Δr =2z $(\sqrt{|l_2| + |l_1|})/\omega_0 k$ then one can immediately find the value of topological charge from the slope. This may be another way of measuring the topological charge of a higher order vortex.

4. When $|l_1|$ and $|l_2|$ have the same sign, then also the cross correlation is a vortex, of order $\pm(|l_2| - |l_1|)$.

References

1. G Gbur.et.al., Optics COMMN. 222, 117-125 (2003).
2. Cleberson. R. et.al., Optics Lett. 40, 2747-2750 (2015).

SIN416 Analysing Weighted Composite Vortex Beams

*P M Pooja, Nikhil Vangety and Sourabh Roy**
Dept. of Physics, National Institute of Technology Warangal, India.
**sroy@nitw.ac.in*

A Vortex beam is structured light with helical phase and a singularity at its center, described by $exp(il\varphi)$, where *l* is the topological charge and φ is the azimuthal angle. In this work, we have collinearly combined two consecutive topological charges l_1=*2* and l_2=*1*, with weighted amplitude as given in eqn. (1),

$$E(r,\phi,z) = \sin\theta\big(E_1(r,\phi,z)\big) + \cos\theta\big(E_2(r,\phi,z)\big) \quad (1)$$

Here, θ is the weight. At θ= 0^0, we have a pure l_2 beam. As θ increases to 22.5^0, 45^0, 67.5^0, the on-axis vortex beam becomes off axis, a novel beam of interest with crescent shaped intensity pattern (Fig 1) [1].

At $\theta=90^0$ it is purely l_1 The average OAM depends on the weighted superposition of two topological charges. It is close to TC when phase singularity is close to centre and decreases as θ increases. This manipulation of average OAM has application in particle manipulation, optical communication, etc [2]. Further, composite vortex beam rotates during propagation. Here, we use rotation matrix $\begin{bmatrix} cos\alpha & -sin\alpha \\ sin\alpha & cos\alpha \end{bmatrix}$ to rotate the vortex beam at z = 0 by various angles, which is an added degree of freedom for applications. Notably, the phase also rotates with intensity (Fig 2). We plot the intensitycorrelation between$l_1=2$, $l_2=1$, with l_2 as the reference beam. At 78.75, the intensity pattern is very sensitive, the correlation coefficient slowly starts to increase (Fig 3).

Fig. 1 Left to right: θ = 0°, 22.5°, 45°, 67.5°,90°

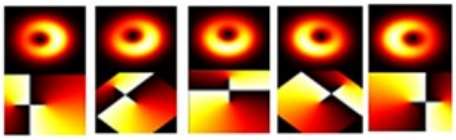

Fig. 2 θ = 15° and rotation at angles from left to right $\alpha = 0, -\pi/4, -\pi/2, -3\pi/4, -\pi$ at z = 0

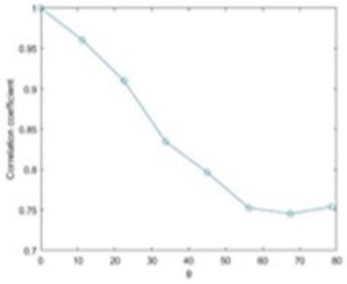

Fig. 3 Intensity correlation

References

1. V Sokolenko et al "Determination of the refractive index profile and surface topography of optically smooth objects using interference of optical vortices", 2021 J. Phys.: Conf. Ser. 2103 012166.
2. Guo, M.; Le, W.; Wang, C.; Rui, G.; Zhu, Z.; He, J.; Gu, B. "Generation, Topological Charge, and Orbital Angular Momentum of Off-Axis Double Vortex Beams", Photonics 10, 368 (2023).

SIN417 Complete Quantification of Weak Anisotropy of Crystals

*Upasana Baishya and Nirmal K. Viswanathan**

School of Physics, University of Hyderabad, Hyderabad, Telangana, India – 500046.

**Corresponding author: nirmalsp@uohyd.ac.in*

Crystal anisotropy is one of the oldest and most widely investigated optical property of materials and is going through a renaissance of sorts in the context of singular optics [1]. With the use of ultra-thin films for applications and devices and more recently with the emergence of 2D materials with exotic topological characteristics the need to investigate and understand the fundamental dielectric, magnetic and magneto-electric anisotropies of such materials is becoming essential. The ultra- / atomically- thin nature of these materials and their weak anisotropy necessitates the need to develop high-sensitivity measurement methods.

Crystal birefringence is due to the two orthogonal polarized eigen modes propagating at two different speeds along the eigen directions. The resulting phase delay and group delay are polarization dependent, leading to a change in the state of polarization of the output beam as a function of the light beam and material characteristics. Even propagating along the eigen direction of the crystal, small anisotropy variations can lead to spatially varying phase delay between orthogonal elliptically polarized modes, changing the state of polarization across the output beam. To understand the whole picture, we need to study the elliptical birefringence (due to coupled linear-circular birefringence) which introduces additional

complexity to the material characteristics.

We present an experimental method wherein extreme cross-polarization of a beam of polarized light propagating through crystals (like calcite or quartz) is carried out using weak measurement method to extract the coupled material properties. The possibility to separate and investigate orders of magnitude lower contribution of one of the birefringence with respect to the other provides valuable information into the crystal, its quality, and the underlying fundamental aspects [2]. Intrinsically based on the appearance of optical singularities due to light-matter interaction, investigating the crystal behaviour around the singularities offers high-sensitivity advantage to unravel hidden characteristics of the crystals.

References

1. M. V. Berry and M. R. Dennis, Proc. R. Soc. Lond. A 459, 1261–1292 (2003)
2. K.Y. Bliokh et al., Optica 3, 1039-1047 (2016).

SIN418 Generation of optical vortex beams with large depth-of-focus

*Vasu Dev[1], Rajesh Menon[2], Vishwa Pal[1,]**

[1]Dept. of Physics, Indian Institute of Technology Ropar, Rupnagar, Punjab 140001 India.

[2]Dept. of Electrical & Computer Engineering, The University of Utah, Utah 84112, USA.

**Corresponding author: vishwa.pal@iitrpr.ac.in*

Optical vortices (OVs) have attracted recent advances due to their potential applications in fundamental sciences and applied fields. Owing to their twisted wavefront, OVs carry an additional degree of freedom called orbital angular momentum of $l\hbar$ per photon, where l is the topological charge (TC). For various applications such as microscopy, imaging, drilling, and guiding the microparticles, tightly focused OVs with large depth-of-focus (DOF) are required [1]. DOF of an optical field with respect to a lens is defined as the axial distance for which the optical field remains focused. The DOF is inherently limited for a conventional focusing lens, posing a fundamental challenge for researchers seeking to expand this range. Therefore, methods such as computational enhancement, wavefront coding, axicons, multiple discrete foci lenses, metalenses, and optimized apodizers are proposed to extend the DOF. In most cases, the increase in DOF is small, while these methods are plagued by several drawbacks, including reduced resolution, degraded image quality, noise amplification, polarization sensitivity, and an increase in side lobes [1]. We propose an efficient method to increase the DOF of OVs by several orders of magnitude by using a flat multilevel diffractive lens (MDL) [1]. The MDL consists of multiple rings of different heights, where the height of each ring corresponds to a particular phase value, hence, MDL is polarization insensitive. The ring heights are selected from a gradient-descent-directed binary search algorithm [2]. When an OV of suitable beam size is incident on the MDL, after propagating a certain distance (working distance) it gets focused, and remains focused up to a significant propagation distance (large DOF) (Figs. 1(a) and 1(c)). We have found that with MDL, the DOF of OVs increases with TC (Figs. 1(a) and 1(c)), whereas, without MDL, OVs of the same initial size diverge significantly (Fig. 1(b) and 1(d)). Figures 1(e)-1(f) also indicate that the beam size remains nearly the same when OVs pass through the MDL.

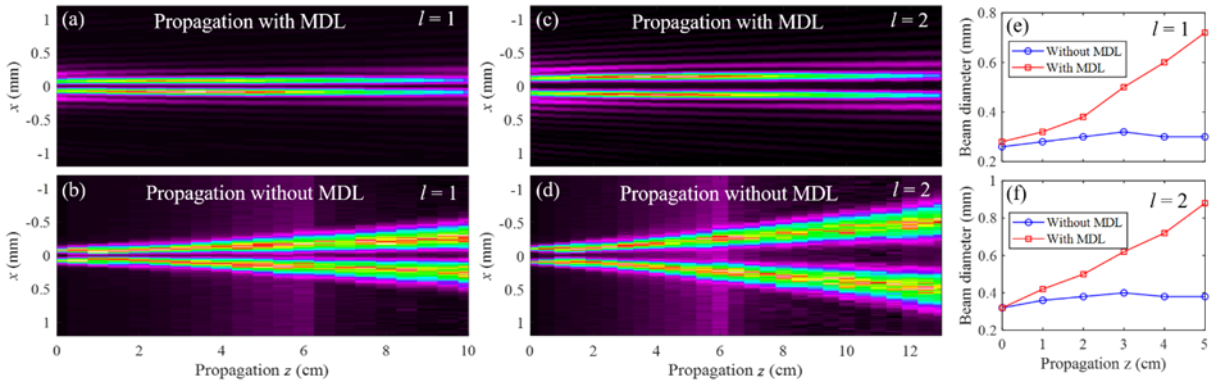

Figure 1 Experimental results for propagation of Ovs with and without MDL for l = 1-2.

References

1. Sourangsu Banerji et. al., *Optica* **7**, 214-217 (2020).
2. Sourangsu Banerji et. al., *Sci. Rep.* **9**, 5801 (2019).

Category 24

Theory, Modelling & Simulation (THM)

THM419 Identifying optimal practices in VQE through quantum computation of ground state energies of H_2 and LiH

Abhijit Hazra[1†], Alok Sharan[1]*
[1]Department of Physics, Pondicherry University, R.V. Nagar, Kalapet, Puducherry, India, PIN-605014.
Corresponding authors: [*]alok.phy@pondiuni.edu.in, [†]abhijitamazing@pondiuni.ac.in

Quantum computation of ground and exited state energies of small molecular Hamiltonians are feasible using Variational Quantum Eigensolver (VQE); which can be implemented in Noisy Intermediate-Scale Quantum (NISQ) devices [1-4]. In order to extend VQE to bigger molecules and periodic systems we require to find best practices within the VQE pipeline. In this work we focus to find out the best classical and fermion to qubit encoder under different circumstances. Usage of such optimizer can converge energy calculation with small number of iterations and time; hence reducing the resource usage as well as paving the way for computing energies for more complex and strongly correlated systems. A suitable choice of fermion to qubit encoder for a given Hamiltonian can lead to reduced circuit depth and reduced Pauli terms in the decomposed Hamiltonian thereby reducing the calculation time. We begin with computing ground state energies of H_2 (at 100 different bond lengths) and LiH (at 50 different bond lengths) using VQE implemented via noise free quantum simulator and IBM's quantum backends. All these energies are also calculated numerically to be used as a reference for comparing quantum computed energies. We have used Unitary Coupled-Cluster Single and Double excitations (UCCSD) variational form as ansatz for both H_2 and LiH molecule at all bond lengths [5]. Three separate fermions to qubit encoders (Jordan-Wigner, Parity and Bravyi-Kitaev) has been used to map the ansatz and Hamiltonians for H_2 and LiH at each bond lengths. We have chosen seven different classical optimizers (Gradient Descent, Powell, SLSQP, CG, SPSA, COBYLA and TNC) for our study at tolerance levels of 10^{-5}, 10^{-6} and 10^{-7} Hartree. In order to determine the best optimizers under different scenarios we benchmark on the basis of average optimization time and optimization steps taken by classical optimizers taken over all bond lengths for each molecule. Calculation has been done in all combination of three different fermion to qubit encoders and seven different classical optimizers each at 3 different tolerance level. The conclusions obtained for noise free simulators can be practiced in future in fault tolerant quantum computers and conclusions obtained via real quantum backends may be practiced in present NISQ devices to solve complex problems with optimal resource usage.

References

1. Alberto Peruzzo et.al., *Nat Commun* 5, 4213 (2014).
2. Yunseong Nam et. al., *npj Quantum Inf* 6, 33 (2020).
3. Oscar Higgott et. al., *Quantum* 3, 156 (2019).
4. Ken M. Nakanishi et. al., *Phys. Rev. Research* 1, 033062 (2019).
5. Jonathan Romer et. al., *Quantum Sci. Technol.*, 4, 014008 (2019)

THM420 Modelling and Analysis of FM-FBG Sensors

Ajay Kumar[1], Anurag Sharma[1,2]*
[1]Department of Physics, Indian Institute of Technology Delhi, New Delhi,110016
[2]Optics & Photonics Centre. Indian Institute of Technology Delhi, New Delhi,110016
**Corresponding author: ajaykumargainpura@gmail.com*

Fiber Bragg gratings (FBGs) have been extensively used for sensing parameters like refractive index, temperature, and strain; however, in practical environments two or more parameters affect the sensor. Hence, it is important to design sensors which can simultaneously measure two or more parameters. In this respect, few mode FBGs have been developed (see, e.g., [1]). Modelling of such sensors involves computing of reflections for the higher order modes (HOMs) requiring a method for bi-directional propagation of LP_{lm} modes. We have recently developed an efficient method for this propagation which effectively reduces the $3D$ propagation to $2D$ thereby reduces the computational effort by order of magnitude [2].

In this paper, we discuss the modelling of a two mode FBG by etching its core diameter from 19.5 μm to 14.1 μm [1]. The simultaneous measurement of temperature and refractive index including cross sensitivity between a temperature and refractive index is investigated by measuring the reflection spectra of LP_{01} and LP_{11} modes. Due to higher fraction of power in the surrounding medium, the wavelength shift is more for the LP_{11} mode than that for the LP_{01} mode due to refractive index change while the temperature change produces almost same shift [1,3]. The wavelength shift due index variation and temperature variation is shown in Fig.1 and Fig. 2, respectively. More results and features will be presented at the conference.

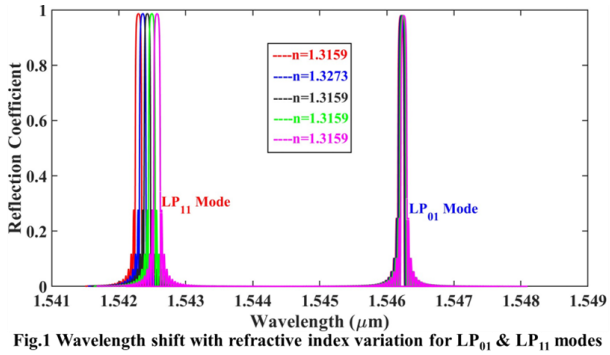

Fig.1 Wavelength shift with refractive index variation for LP_{01} & LP_{11} modes

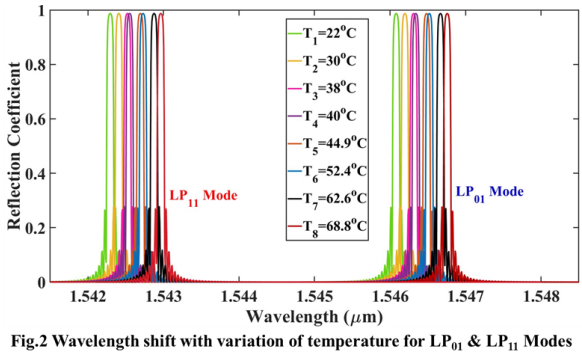

Fig.2 Wavelength shift with variation of temperature for LP_{01} & LP_{11} Modes

The work was supported by a fellowship from CSIR to Ajay Kumar.

References

1. Hang Zhou Yang et. al., *Sens. Actuator A Phys*. 228, 62-68 (2015).
2. Ajay Kumar et. al., *Frontiers in Optics + Laser Science (2022),* Paper ID: JTu5B.60.
3. A. N. Chryssis et. al., IEEE Photon. Technol. Lett., 18(1), 178-180 (2005).

THM421 Average transmittance of Sine hyperbolic Gaussian vortex beam (ShGvB) in vertical anisotropic oceanic turbulence

*Athira T Das[1], Rajesh R[2] Pramod Gopinath[1,3]**
[1]*International School of Photonics Cochin University of Science and Technology, Kochi, 682022, India*
[2]*Naval Physical Oceanographic Laboratory, Kochi, 682021, India*
[3]*Inter University Centre for Nanomaterials and Devices, Cochin University of Science and Technology, Kochi, 682022, Kerala, India*
**Corresponding author: pramod@cusat.ac.in*

Vortex beams carry orbital angular momentum (OAM) with spiral phase, and can be used to encode data into the laser for communication purposes, which will be useful for enhanced information-carrying capacity with better security. Due to these properties, propagation properties of various vortex beams have been studied, which mainly aim to find the conditions for better optical wireless communication performance in underwater turbulence. The performance of the beam can be improved by increasing the average transmittance of the beam in underwater turbulence. Average transmittance is defined as the ratio of the average received intensity to the intensity at the receiver plane with no turbulence [1]. While considering oceanic propagation, many studies have been done on horizontal propagation. However, the vertical propagation study is at an infant stage, which makes it difficult because of the significant turbulence caused by the gradients in salinity and temperature.

In this study, the impact of anisotropic underwater turbulence on the average optical transmittance of Sine hyperbolic Gaussian vortex beam (ShGvB) along the vertical direction of propagation is considered [2]. The influence of the displacement parameter of the beam and beam waist radius are studied by using the anisotropic spatial power spectrum which considers the influence of the ocean depth, salinity and temperature [3]. The results are compared with that of the Sinh Gaussian beam (ShGB). The average transmittance of ShGvB in underwater turbulence is found to be higher than the ShGB.

References

1. Keskin, Aysan, and Yahya Baykal, *Waves in Random and Complex Media* 31.6, 2385-2396 (2021).
2. Zhang, Yalin, Xiaoxin Zhou, and Xiuhua Yuan, *Optics Communications*, 440, 100-105 (2019).
3. Lin, Zhiru, et al, *Optics Express,* 30.21, 38804-38820 (2022).

THM422 Manipulation of Subluminal Light Propagation in Graphene Nanostructures

Rohit Mukherjee[1], Avishek Gupta[1], Manoj Mishra[2], Nitu Borgohain[3], Nitya Garg[1]*
[1]*Department of Physics, Sarala Birla University, Ranchi, India-835103*
[2]*Department of Physics, Mody University of Science and Technology, Sikar, India-332311*
[3]*Department of Physics, University of Science and Technology, Meghalaya, India-793101*
**Corresponding author: rohitmukherjee670@gmail.com*

This article presents the investigation of the subluminal to superluminal light propagation within quantized four-level graphene nanostructures. By using density matrix formalism [1, 2], and Liovillie's equation, properties of electromagnetically induced transparency (EIT) and enhancement of the group index (n_g) of the probe pulse in four-level graphene nanostructures is analyzed. It has been observed that group index

can be precisely manipulated by suitable choice of Rabi frequency of the control fields and detuning's. Furthermore, group velocity of the probe pulse from superluminal to subluminal and vice versa can be tuned by suitable choice of control field and magnetic field. The results of the present investigation will be useful for new applications such as graphene-based nano-electronic devices, all-optical switching, and quantum computing.

References

1. M. Abbas, F. Badshah, H. Ali, A. Munir, Ziauddin, and P. Zhang, *Phys. Scr.* 98, 075929 (2023).
2. F. Xu, J. Zhu, S. Fan, and Y. Qi, *Mod. Phys. Lett. B* 20, 1950226 (2019).

THM423 Random discrete inhomogeneity in two-dimensional coherent spectroscopy simulations

*Bhaskar De[1], Rohan Singh[1]**
[1]Department of Physics, Indian Institute of Science Education and Research (IISER) Bhopal, Bhopal, Madhya Pradesh, India, PIN-462066
**rohan@iiserb.ac.in*

The optical properties of semiconductor nanostructures are dominated by the quasi-particle exciton, a bound electron-hole pair. Studying exciton physics is of enormous interest in the domain of quantum information, quantum optics and photonics, for its characteristics similar to an isolated coherently superposed two level system. Two dimensional coherent spectroscopy (2DCS) is an efficient technique to study the coherent dynamics of systems using ultra-short pulses [1]. The 2DCS simulation has been used to extract the homogeneous and inhomogeneous linewidth simultaneously [2]. The continuous Gaussian-type inhomogeneity has been seen in large ensemble of quantum dots and TMDC monolayers. But in few quantum dots [3] and in presence of localized emitters [4] earlier mentioned process is not applicable as those system does not have a proper Gaussian distribution of oscillators.

Here we report a computational method to simulate 2D spectra with arbitrary inhomogeneity by convolving a two-dimensional distribution function. Randomizing the oscillator strength in the distribution enable us to generate the 2D spectra with discrete inhomogeneity. We also prescribe a procedure to extract information about the discrete inhomogeneity from 2D spectra. This method will be applicable to understand the resonant line shapes of few quantum dots [5], localized emitters in TMD monolayers etc where we find discrete and continuous inhomogeneity together.

References

1. D. M. Jonas, *Annu. Rev. Phys. Chem*. 54, 425 (2003).
2. M. E. Siemens, et al., *Opt. Express* 18, 17699 (2010).
3. J. Kasprzak et al., *Nat. Photonics* 5, 57 (2011).
4. Y. -M. He et al., *Nat. Nanotechnol.* 10, 497 (2015).
5. E. W. Martin et al., *Phys. Rev. B* 97, 081301(R) (2018).

THM424 Estimation of Optical Turbulence for High Energy Laser Propagation

G Nageswara Rao, Amit Pratap, A Sreekar and Jagannath Nayak*
Centre for High Energy Systems and Sciences, Vignyanakancha PO, Hyderabad-500069
**Corresponding author: nageswararao.chess@gov.in*

Optical turbulence of atmosphere dictates the performance of Laser beam in many applications like free space laser communication, ground to satellite communication, High energy Laser systems (HEL), etc. Various parameters of atmosphere like temperature, pressure, relative humidity, wind speed and direction, solar flux etc. collectively define the optical turbulence parameter.

Depending upon the strength of the turbulence, the HEL will undergo various effects. For instance, under low turbulence conditions, the beam wandering effect is predominant resulting in larger effective spot diameter and reduced power density and signal at receiver plane. However, under moderate turbulence conditions, wavefront of the laser will also be degraded and beam will be broadened. In deep turbulence conditions, apart from the phase distortions, the intensity fluctuations will also be present.

In many of practical applications, it is not possible to install setup for measurement of optical turbulence and therefore estimation of this parameter using models is important for performance evaluation of laser systems without using additional instrumentation.

For this purpose, 40 years of IMDAA 3-Hourly Pressure Level Dataset [1] has been utilized for estimating optical turbulence strength from 1978 to 2018 using meteorological parameters based on Frederickson and Davidson model [2] up to boundary layer. The details of this database was documented in the reference [1]. However, this data is very huge and will be difficult to utilize in real-time applications. Therefore, most probable optical turbulence parameter was estimated based on Perot analysis (based on histogram and arranging in the descending order). This will represent the optical turbulence at a given location and time. This most probable parameter is estimated in various regimes namely yearly, seasonal, monthly, daily and hourly.

The results for most probable optical turbulence were validated against Scintillometer measurements at Hyderabad continuously during January to April 2023. It was found that trend of optical turbulence has been produced well by the estimated most probable methodology. Moreover, the night time high turbulence which is a peculiar feature during winter season at Hyderabad as seen in scintillometer measurements was also captured in the estimated values. In order to quantify the validation, error analysis was carried out in terms of HEL range. This HEL range was calculated in terms of delivered power density cut off at target using both estimated and measured optical turbulence. More than 80% occurrence of values falls between -20 to 20% error in HEL range and thus provides real time range estimation of HEL system.

References

1. S. Indira Rani, *et al., J. of Clim.,* https://doi.org/10.1175/JCLI-D-20-0412.1 (2021).
2. Frederickson, *et al., J. of Appl. Met.,* 39. 1770-1783 (2000).

THM425 High Performance Terahertz Hollow Core Antiresonant Fiber with Sector Cladding tubes

Maharaja Balaji[1*], *Sathiyan Samikannu*[1]
[1]*Department of Electronics and Communication Engineering, SRM Institute of Science and Technology, Kattankulathur, Chennai-603203, Tamilnadu, India*
**Corresponding author: mb6383@srmist.edu.in*

This paper presents a novel four-sector cladding tube hollow core antiresonant fiber designed for terahertz communication application at the operating frequency of 0.5 - 2.8 THz. The Zeonex is selected as the background material for the proposed model. Numerical analysis is performed using COMSOL multiphysics software to investigate the fiber's performance with various cladding tube thicknesses. This model expresses the low confinement loss of 4.46×10^{-4} dBcm^{-1}, minimal effective material loss of 4.76×10^{-4} dBcm^{-1}, and wide low-loss transmission bandwidth of 0.9 THz. Furthermore, it also provides a high power fraction of 99.9% and a broad flat zero dispersion profile.

Proposed design

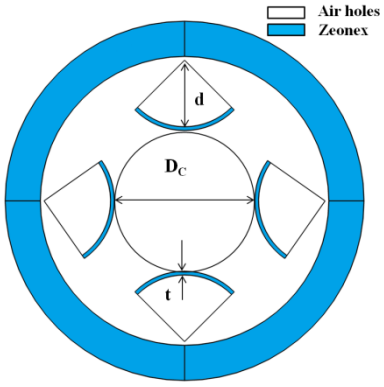

Fig. 1. Proposed fiber model

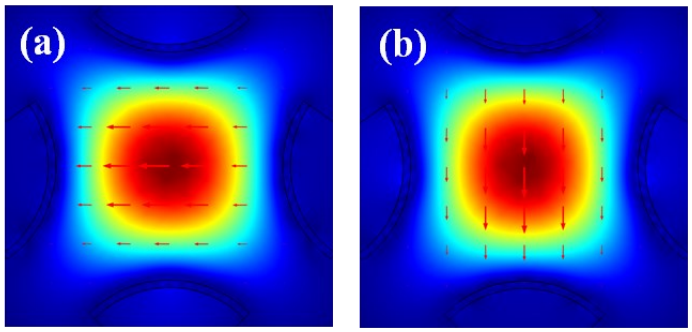

Fig. 2 Field distribution (a) X-polarization (b) Y-polarization

Fig. 1 depicts the proposed model schematic. The dimensions of the fiber are the core diameter D_c= 3 mm, sector tube radius d = 1.5 mm, and cladding tube thickness t= 0.10 mm. Fig. 2 represents the fundamental mode's field distribution and X and Y polarization.

References

1. Ziwei Yuan et al. "Study on the high birefringence and low confinement loss terahertz fiber based on the combination of double negative curvature and nested claddings." J. Phys. D: Appl. Phys. 55, no. 11 (2021):115106.
2. Zixuan Du et al. "Highly birefringent hollow-core antiresonant terahertz fiber with a thin strutmicro-structure." Opt. Express 30, no. 3 (2022): 3783-3792.

THM426 Effects of cavity-mediated processes on the polarization entanglement of photon pairs emitted from quantum dots

Parvendra Kumar
Optics and Photonics Centre, Indian Institute of Technology Delhi, Hauz Khas, New Delhi, 110016
Corresponding author: parvendra@opc.iitd.ac.in

One of the best sources of entangled photon pairs on demand is semiconductor quantum dots [1-3]. The fine structural splitting of exciton states, however, typically sets a limit on the degree of entanglement. This work theoretically investigates the generation of polarization-entangled photon pairs under two-photon excitation and cavity-assisted two-photon emission, both in the weak and strong cavity coupling regimes. We show and clarify three different ways in which the degree of entanglement is reduced by cavity coupling in conjunction with an excitation pulse. First, cavity coupling introduces an uneven ac-Stark shift of the horizontally and vertically polarized exciton states in strong coupling regime, which result in additional splitting of exciton states. Second, it causes undesirable two-photon states to form by inducing cross-coupling between the exciton states even in the weak coupling domain. The reduction of entanglement is further aided by higher excited states of the cavity modes. As a result, in the context under consideration, cavity coupling, which is typically necessary for the effective collection of emitted photons, weakens entanglement in both the weak and strong coupling regimes.

References

1. Y. Chen, M. Zopf, R. Keil, F. Ding & O. G. Schmidt, Nat. Comm. 9, 2994 (2018).
2. H. Jayakumar, A. Predojević, T. Kauten, T. Huber, G. S. Solomon & G. Weihs, Nat. Comm. 5, 4251 (2014).
3. N. Akopian, N. H. Lindner, E. Poem, Y. Berlatzky, J. Avron, D. Gershoni, B. D. Gerardot, and P. M. Petroff, Phys. Rev. Lett. 96, 130501 (2006).

THM427 Non-Paraxial Beam Propagation Method for Silicon Photonics

Pratiksha Choudhary[1], Anurag Sharma[1,2]

[1]Department of Physics, Indian Institute of Technology Delhi, New Delhi, 110016, India

[2]Optics & Photonics Centre, Indian Institute of Technology Delhi, New Delhi, 110016, India
[1]phz188425@iitd.ac.in; [2]asharma@iitd.ac.in

Silicon photonics is based on waveguiding structures which have high index contrast. Therefore, a full vectorial treatment for wave propagation is necessary. Further, the usual paraxial approximation employed for evolutionary wave propagation methods is not valid as it also assumes low index contrast (see, for example, [1]). Thus, we require a non-paraxial full vectorial method for wave propagation. There have been attempts, with varying degrees of success, to move beyond the paraxial iterative approach employing Pade's approximants [2]. For full vectorial propagation, finite difference time domain (FDTD) methods are generally used, although they are computationally intensive, especially for 3-D structures. We had previously developed a wide-angle, non-paraxial scalar propagation method [3]. The method is based on symmetrized splitting of the non-paraxial propagation operator. The same idea has now been incorporated in the full vectorial wave equation. Our method can be used for propagating a certain incident wave, such

as a mode, through a specific structure. In this work, we have discussed our method and its applications to, e.g., propagation through a tapered structure.

We consider the propagation of the fundamental mode of a rectangular silicon waveguide as a numerical example.The waveguide has a width of 500nm, and a height of 220nm, with refractive indices of core and cladding, respectively, are n_{core}=3.45(silicon) and n_{clad}=1.45 (glass) and a wavelength of 1550nm. The width tapers down to 300nm over 20 micron length. Some results are given in the figures and more examples will be presented at the conference.

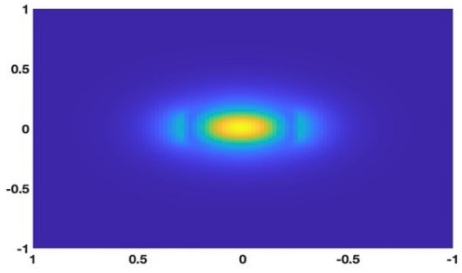

Fig.1 Intensity profile of fundamental mode for rectangular waveguide.

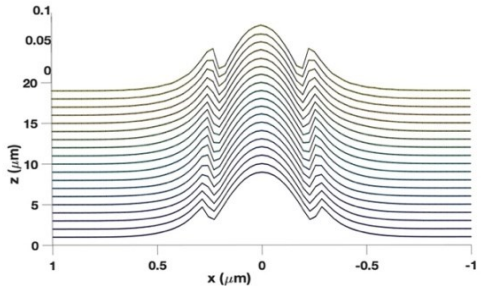

Fig.2 Propagation of mode through a taper structure.

Work partially supported by UGC fellowship to P. Choudhary.

References

1. W.P. Huang and C.L. Xu, IEEE J. Quantum Electron., Vol. 29, pp. 2639-2649 (1993).
2. D. Yevick, Jun Yu, W. Bardyszewski, M. Glasner, Vol. 7, pp. 658-660 (1995).
3. D. Bhattacharya and A. Sharma, Opt Quantum Electron., Vol. 39, pp. 865-876 (2007).

THM428 Resonant structure for improved directionality and extraction of single photons

Sagar Chowdhury[1], Rituraj[2], Srini Krishnamurthy[1,3], Vidya Praveen Bhallamudi[1]*
1. Dept. of Physics, Quantum Center in Diamond and Emerging Materials (QuCenDiEM), Indian Institute of Technology, Madras, India,
2. Indian Institute of Technology, Kanpur, India,
3. Sivananthan Laboratories, Bolingbrook, IL, USA
**Corresponding author: Praveen.bhallamudi@iitm.ac.in*

Wide band gap dielectrics like diamond, SiC and hBN are promising for room temperature quantum devices due to the presence of colour centers or defects that can also be spin active. These defects are addressable either individually or collectively. They are used as an on-demand single photon source (SPS) for quantum communications and in spin-based quantum sensing applications. However, a few factors limit the efficiency of these defect-based quantum devices. The large refractive index (~ 2.2 at emission wavelength) results in smaller escape angle of emission and, thus, poorer light collection efficiency. The emission at a chosen frequency is further limited by phonon-assisted broadening of photoluminescence. Our work aims to address both these challenges. We have developed a design algorithm that exploits Mie-resonance [1] and Kerker conditions [2], and designed a metasurface using use Finite-Difference Time

-Domain and Rigorous coupled-wave analysis methods for enhanced forward emission at ZPL (637 nm) from diamond nitrogen-vacancy (NV) centers. Accordingly we predict ~ 90% far-field photon collection efficiency and with an angular spread of 20^0 in the forward direction. The metasurface design is fairly fabrication tolerant. For example, the location of defect/emitter centre can vary by ~50 nm within the medium and still achieve ~60% efficiency. The structural parameters such as height, diameter, and periodicity of the meta-elements can be varied to shift the resonance to 737 nm ZPL corresponding to silicon-vacancy (SiV) center of diamond or to that of defect enters in other materials SiC and hBN. Our dielectric metasurface design approach provides a pathway for the development of efficient SPS for quantum applications.

References

1. Zhao, Qian, et al. "Mie resonance-based dielectric metamaterials." *Materials today* 12.12 (2009): 60 -69.
2. Van de Groep, J., and A. Polman. "Designing dielectric resonators on substrates: Combining magnetic and electric resonances." *Optics express* 21.22 (2013): 26285-26302.

THM429 Numerical Demonstration of Fading Memory in Sparse Event Excited in Frantic Photonic Structure

Sujal Gupta[1,], Jolly Xavier[1,2,]**

[1]Optics and Photonics Centre, IIT Delhi, Hauz Khas, New Delhi-110016, India
[2]SeNSE, IIT Delhi, Hauz Khas, New Delhi-110016, India
**Corresponding author: opz228317@opc.iid.ac.in, jxavier@sense.iitd.ac.in*

The intricate dance of chaos and probability, intertwined with structural geometry, unlocks scientific possibilities, offering novel insights into manipulating energy and generating sparse events. These seldom natural phenomena, including hurricanes and tsunamis, are associated with unpredictable energy dynamics and control driven by complex probabilistic mechanisms. Here we study the numerical estimations demonstrating the frantic photonic structure's (FPS) ability to generate and harness chaotic high-amplitude seldom waves with specific measurements such as spatial localization and ultrashort durations to enhance energy storage.

Specifically, when one contemplates a cumulative process involving the summation of all possible whimsical waves in FPS, the subwavelength confinement of localized rare seldom wave $\Psi(r,t) \propto J_0(k|r|)\frac{\sin(\frac{\partial\omega}{2}t)}{t}$ appears from the Bessel wave J_0, ensuring a prominent energy focal point with minimal side lobes (Fig. 1b). FPS is estimated to store more than three times the energy of their classical counterparts, primarily due to the equipartition of energy among their degrees of freedom. This remarkable FPS model paves the way for applications in energy storage technologies, carrying significant and far-reaching potential across a broad spectrum of fields such as telecommunications, materials science, optical computing, and imaging. It promises enhanced efficiency and compactness in these domains.

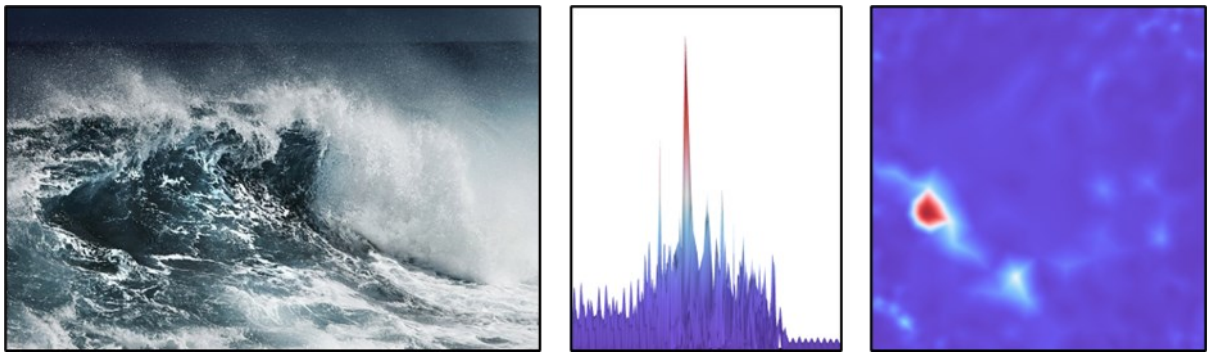

Fig.1 (a) Sparse event in Nature. (b) Numerical inception of seldom wave in FPS. (c) Top view of energy density time average of seldom wave.

References

1. Meade, Robert D. et. al., *Princeton Uni. Press* (2008).
2. Liu, Changxu, et al., *Nat. Phys.* 11, 358-363 (2015).

THM430 Frequency Splitting in Dissimilar Coupled Disks

*S V Varun[1], K Shadak Alee[1]**

[1] Department of Physics and Nanotechnology, SRM Institute of Science and Technology, Kattankulathur, Tamil Nadu-603203

**Corresponding author: shadakk@srmist.edu.in*

Optical microresonators with closed concave boundaries have the ability to trap light strongly inside. Once the trapped light inside the structure is interfered at a specific frequency, it can be retained inside the resonator with minimum loss [1]. But there is an extension of light waves happening to the surrounding medium in the form of an evanescent field [2]. Any disturbances on the evanescent field cause changes in the spectral features of the resonant mode either in the form of mode broadening [3], mode shifting or mode spitting [4]. These changes in the resonant mode are monitored, analysed, and used as a sensing signal. In this study, we used a coupled microcavity system that consists of disks with different refractive indices. Finite difference time domain simulations were employed to measure spectral features of this system. We chose disks with refractive indices 1.49 and 1.59. The radius of the first disk was taken as 1.6μm and the radius of second disk was adjusted to 1.621μm to match the individual resonant frequencies at 580 nm (Fig.1a). When a coupled disks is formed frequency splitting has been observed as shown in Fig. 1b.

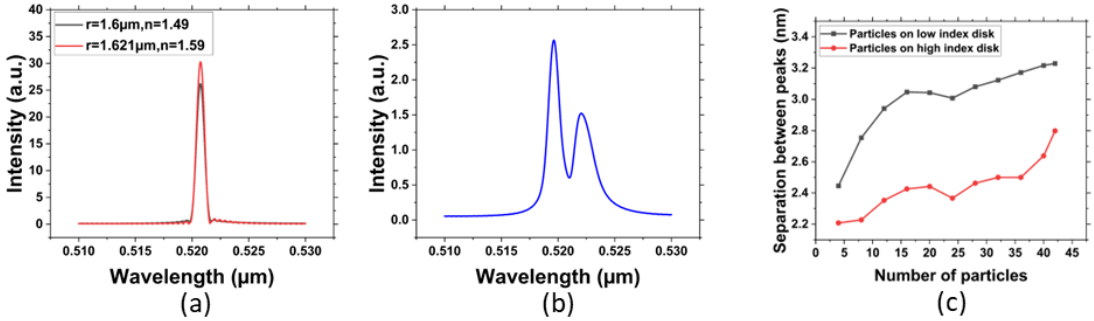

Fig.1 (a) Resonant spectrum of each disk. (b) Frequency splitting of coupled disks. (c) Plot of separation between peaks against number of particles placed on low index and high index disks separately.

Next, we performed calculations to determine the spectral separation of whispering gallery modes (WGM) in this unique coupled system. We systematically attached nanoparticles with a diameter of 40nm and refractive index of 1.45 at the bright spots of the WGM pattern on each individual disk. As shown in Fig.1c, it is clear that there is a difference in spectral separation when nanoparticles are placed on disks with high and low refractive indices respectively. Furthermore, we observed that the spectral separation increases as more nanoparticles are added. This characteristic demonstrates the potential of this structure as a refractive index sensor.

References

1. He et. al., *New J. Phys.* 15, (2013).
2. F. Khozeymeh et. al., *Sens. Actuators B Chem.* 281, 998 (2019).
3. S. Mehrabani et. al., *Appl. Phys. Lett.* 102, (2013).
4. Y. Zhi et. al., *Advanced Materials* 29, (2017).

Category 25

Ultrafast Optics (UFO)

UFO431 Realization and parametric analysis of All-PM All-Normal Yb-doped ultrafast fiber laser

*Akshay Raj R, Munukutla Sri Sai Satish, Shyamal Mondal**

Dept. of Applied Physics, Defence Institute of Advanced Technology, Pune – 411025, Maharashtra, India

**email: shyamal.kgec@gmail.com*

Fiber lasers have been a robust alternative to solid state lasers since its inception. Yb-doped fiber based lasers existed from 2010 [1], but it had free space elements which reduced the advantages offered by an all-fiber configuration, which came as late as 2014 [2]. In this work, a Yb-doped fiber laser in an all-normal dispersion regime has been developed by using all-PM fiber components. The resonator was pumped by a 976 nm butterfly laser diode followed by WDM (Lightel-976/1060), gain fiber (Liekki-PM-Yb-6/125), output coupler (Lightel-90/10), Semiconductor Saturable Absorber Mirror (SESAM, BATOP), Chirped Fiber Bragg Gratings (CFBG, Technica). The length of the PM-Yb-doped fiber has kept as 1.5 m. The laser was realized in a linear cavity and the stability of such an oscillator is governed by the parameters of Chirped Fiber Bragg Grating (CFBG) and the modelocker used in it. The modelocker used in this study was a SESAM and observed the output pulses with varying configuration of the same. SESAMs having rise-times of 3, 9, 35, 500 ps, respectively, were used in the setup and compared the results with CFBG having respective bandwidth of 5, 10, 15, 20 nm, centered at 1060 nm wavelength. With the available SESAMs, it is observed that with increase in rise time of the same, the pulses tend to reduce the threshold of multi-pulsing barrier. In conclusion, a stable modelocked Yb-doped fiber laser was developed and did a parametric study with different configurations of SESAM and CFBG. The optimum results were obtained for CFBG having 5 nm bandwidth and SESAM with 35 ps rise time. However, the optical spectrum and the pulse width for the same is yet to be measured.

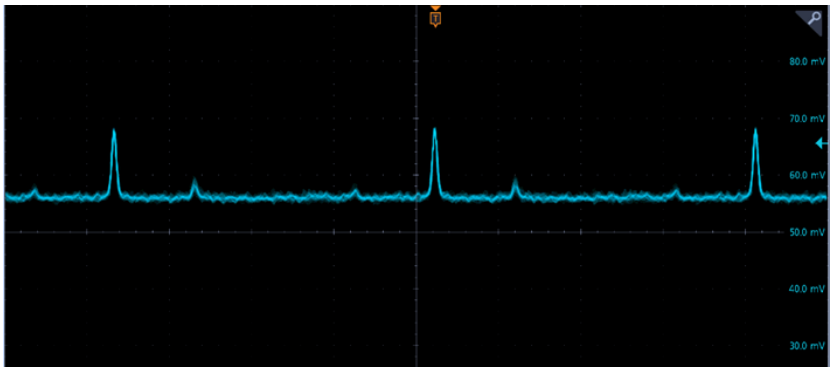

Fig.1: Modelocked output from Yb-doped All-PM Fiber laser

References

1. Zhang et al., "High-energy subpicosecond pulse generation from a mode-locked Yb-doped large-mode-area photonic crystal fiber laser with fiber facet output." IEEE Photonics Technology Letters 22, no. 5 (2010): 350-352.
2. Zhang, Lei, Jiaqi Zhou, Zhaokun Wang, Xijia Gu, and Yan Feng. "SESAM mode-locked, environ-

mentally stable, and compact dissipative soliton fiber laser." IEEE Photonics Technology Letters 26, no. 13 (2014): 1314-1316.

UFO432 Wavelength Dependent Optical Limiting and Saturable Absorption in Silver Nanocrystals.

Amit Kumar Pradhan[1], Chitra Dolai[1], Suman Kumar[2], Amiya Priyam[2], Prasanta Kumar Datta[1]*

[1]Department of Physics, Indian Institute of Technology Kharagpur, Kharagpur-721302, India

[2]Department of Chemistry, School of Physical and Chemical Sciences, Central University of South Bihar, Gaya-824236, India

Anisotropic Silver nanocrystal (NC) was synthesized by using both a mild stabilizer and mild a reductant, sodium citrate and hydrazine hydrate [1]. The sample have Plasmon peak at 550nm, confirmed by UV-VIS Absorption spectroscopy (the sample is named as Ag-550). Transmission electron microscopy (TEM) confirms the pentagonal nanoplate structure of Ag-550. In previous works optical nonlinear (NL) properties of Ag-550 were studied CW regime, which revealed that Ag-550 only shows reverse saturable absorption (RSA) [2]. In this research work we characterized the NL optical properties of Ag-550 by Z-scan technique in femtosecond regime using both resonant and off-resonant pump wavelength. The phenomenon of reverse saturable absorption was shown to be prevalent in off-resonant excitation, while in resonant excitation, optical transparency was observed to be dominant. The outcomes, i.e., optical transparency and SA−RSA switching, will open ways for a variety of diverse applications such as optical switching, limiting, and bio-imaging.

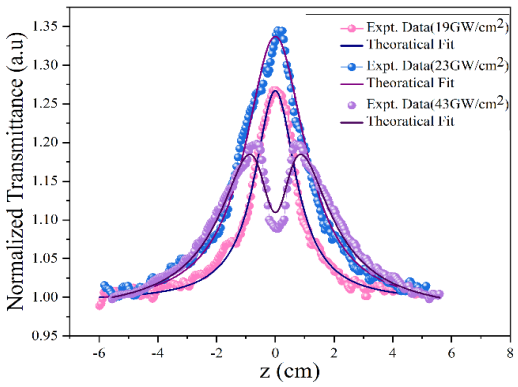

Table 1. Extracted nonlinear absorption parameters

Input Intensity(GW/cm^2)	I_{sat}(GW/cm^2)	β_{eff}(cm/GW)
19	78	0.205
23	78	0.4
43	29	0.49

References

1. Satarupa Pattanayak, et al. Dalton Trans., 2014, 43,11826
2. Bhavesh K. Dadhich, et al. Photochem. Photobiol. Sci., 2017, 16, 1556–1562

UFO433

Utilizing transient absorption spectroscopy in exploring the ultrafast dynamics in perovskite solar cells

Anusha Puliparambil Thilakan[1], Jia-Xing Li[2], Tzu-Pei Chen[4], Shao-Sian Li[5], Chun-Wei Chen[4], Minoru Osada[6], Kazuhito Tsukagoshi[6], Takayoshi Sasaki[6], Atsushi Yabushita[2], Kaung-Hsiung Wu[2], and Chih-Wei Luo[2,3]

[1]Department of Physics, School of Advanced Sciences, Vellore Institute of Technology, Vellore, India,[2]Department of Electrophysics and [3]Center for Emergent Functional Matter Science, National Yang Ming Chiao Tung University, Hsinchu 30010, Taiwan,[4]Department of Materials Science and Engineering, National Taiwan University, Taipei 10617, Taiwan, [5]Graduate Institute of Biomedical Optomechatronics, Taipei Medical University, Taipei 110, Taiwan,[6]The International Center for Materials Nanoarchitectonics (WPI-MANA), National Institute for Materials Science, Tsukuba 305-0044, Japan

** Correspondance email: anusha.pt@vit.ac.in*

We present fundamental mechanisms which governs the stability of perovskite solar cells by transient absorption spectroscopy (TAS). Femtosecond pump probe experiments were performed on UV irradiated perovskite solar cells with TiO_2 as electron transport layer (ETL). The enhanced stability was observed with 2D TiO_2. The ultrafast carrier dynamics, such as electron diffusion, electron injection, hole transfer and the electron-hole recombination, which are involved in the UV-induced degradation of TiO_2-based perovskite solar cells have been unveiled by time-resolved pump probe spectroscopy. The vital role of electron-hole recombination was identified for the UV-induced degradation of perovskite/compact-TiO2 heterojunction solar cells. The presence of oxygen vacancy states in compact TiO2 can act as e-h recombination centers in the perovskite solar cell. The report summarises the potential use of TAS to propose 2D TiO_2 as a promising candidate for ETL in perovskite solar cell devices.

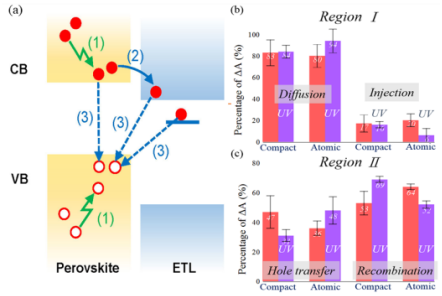

Fig.1(a) Photo-carrier dynamics at ETL/perovskite heterojunction. (b) Averaged amplitudes in percentage from the ΔA from transient absorption kinetics

References

1. Anusha Puliparambil Thilakan, e.t al, *ACS Applied materials and Interfaces*, 11, 21473-21480 (2019).
2. Anusha Puliparambil Thilakan, et.al,. *SOLAR* RRL,7, 2300314, (2023).

Category 26

Any other topics related to Optics and Photonics (OTH)

OTH138 Concentration Dependent Thermo-Optic Properties of $CePO_4$ nanorods

Anita Mary Peter[1], Kailasnath M[1]*

[1]International School of Photonics, Cochin University of Science and Technology, Kochi, India

**anitamary@cusat.ac.in*

The thermal and optical properties of Cerium Phosphate($CePO_4$) Nanorods prepared by a simple hydrothermal method is explored in this study. The morphological and optical characteristics were analysed using XRD, TEM, UV-Visible Absorption and Photoluminescence Spectroscopy. The thermal diffusivity of $CePO_4$ Nanorods dispersed in Ethylene Glycol(EG) at different concentration is measured. A mode-mismatched dual beam thermal technique which is a highly sensitive photothermal method, is employed to measure the thermal of $CePO_4$ -EG nanofluids. The results show that the thermal diffusivity of the nanofluid depends on the concentration of $CePO_4$ nanorods. It was observed that the thermal diffusivity of the EG base fluid decreases with the addition of $CePO_4$ nanorods upto an optimum concentration after which it begins to increase. At a concentration of 5mg of $CePO_4$ nanorods dispersed in 10ml of EG, the thermal diffusivity values almost match the thermal diffusivity of Ethylene Glycol. As the concentration of $CePO_4$ nanorods is increased to 1mg/ml, the thermal diffusivity value is enhanced to 9.92x 10^{-08}. Hence $CePO_4$ nanorods can be used to tune the thermal diffusivity of the base fluid.

.

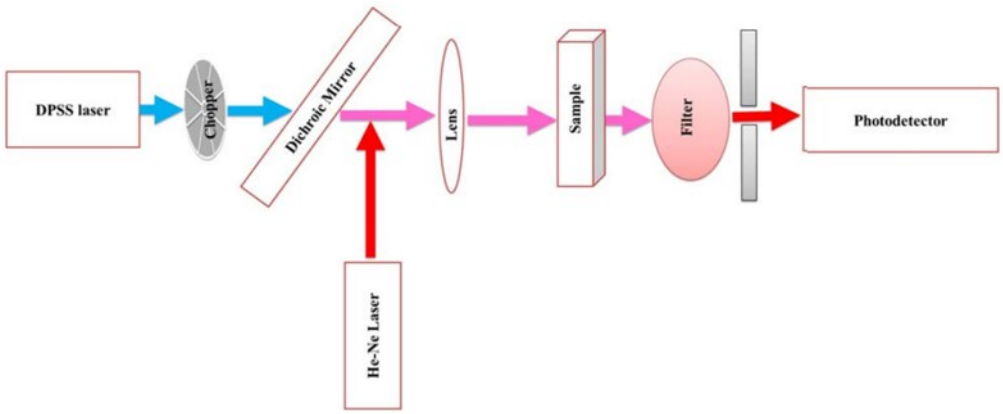

Figure 1. Schematic of Dual Beam Thermal Lens Experimental Setup

References

1. Ramya M et. al., *Mater. Res. Express* 6 126208 (2019).
2. Vijesh et. al., *Int. J. Therm. Sci*. 126, 137-142 (2018)

OTH355

Design and development of dielectric mirror for MWIR region

A S Upadhyaya, Suman Awasthi, L M Pant*
Instrument Research & Development Establishment
Raipur Road
DehraDun 248008
**asu.irde@gov.in*

Mid-Wave Infrared (MWIR) thermal cameras are mainly used in 3.6 – 4.9 µm region. Optical design of such an infrared imager is carried out based on many input parameters like range, size of system etc. In optical design of a system a mirror is used for folding of beam and make a compact system. A super miniaturize system is designed using six times folding by mirrors. Aluminium and gold mirrors are widely used in infrared imagers. These mirrors provide a wide band and good reflection in the desired MWIR band. The metal mirrors require careful handling during integration of the system to avoid any surface damage, which impact on image formation of the system. In the present work, mirror is designed and deposited using dielectric materials. Entire band of 3.6-4.9 µm is covered for reflection, using a dielectric coating. To design the coating, silicon is selected as high index material and silicon di oxide is selected as low index material. Quarter wave thickness of alternate materials used to form only 7-layer stacks. Then the design is tuned for 45-degree angle of incidence with average polarization. Electron beam gun evaporation system is used to deposit the mirror. Deposition parameters like rate, temperature, partial pressure for both the materials are derived. Initially 3-layer coating is deposited to check the compatibility of materials with each other. After few trials a 7-layer coating is deposited on BK 7 glass. Reflection of the coated substrate is measured using FTIR at 45-degree angle of incidence. With the 7-layer coting 98% reflection is achieved in 3.6 – 4.9 µm waveband as shown in figure 1. This coating is also subjected to environmental test as per MIL-C-48497 and passes the parameters of stability.

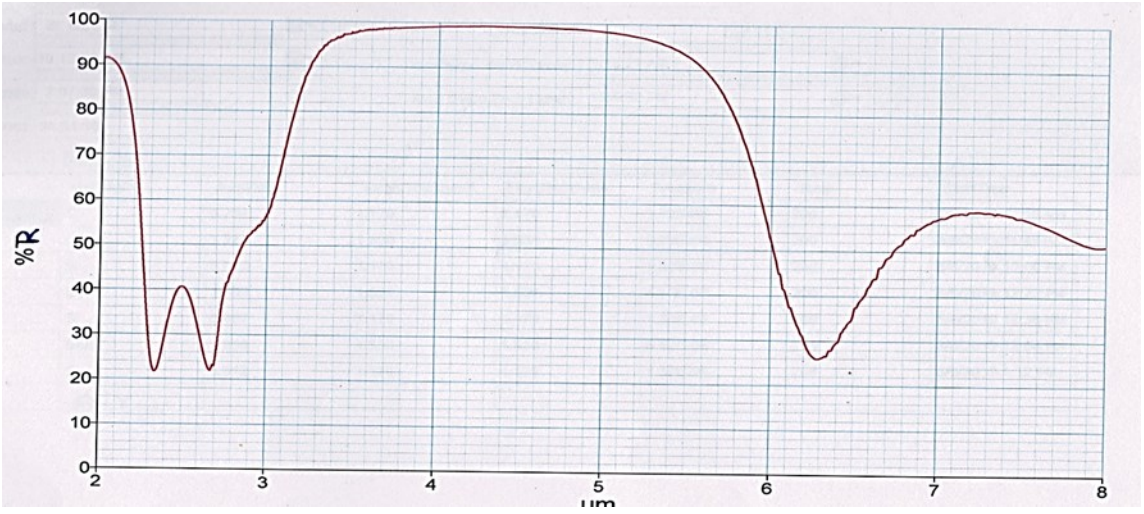

Figure 1. Reflection vs wavelength of mirror

References

1. Hong-xing He et al, Proc. of SPIE Vol 11338, 1133804-1(2019).
2. Rik ter Horsta et al, Proc. of SPIE Vol. 7018 701808-9 (2008).

OTH356 High efficiency anti-reflection coating for dispersive silicon solar cells

Anil Kumar, A S Upadhyaya, Suman Awasthi & L M Pant*
Instruments Research & Development Establishment (IRDE), Raipur Road Dehradun-248008
**anil.irde@gov.in*

Silicon is the basic material used for mass production of solar cell devices. Solar cell converts light energy directly into electrical energy through photo-voltaic effect. It is rapidly growing and increasingly important renewable alternative to conventional fossil fuel electricity generation. Among all photovoltaic materials, silicon is most basic and abundant material in micro and nano-electronics and photovoltaic industry. In this work, we have developed a high efficiency anti-reflection coating for crystalline silicon solar cells. Broad-band multilayer anti-reflection coating using oxides and fluoride materials have been designed and developed on p-type c-silicon substrate. A comprehensive study of designing this coating is based on optical interference transfer–matrix theory for minimizing overall reflectance. Overall physical thickness of the coating is measured with stylus profiler technique and found to be as per the designed thickness of coating. The coating has passed environmental test as per MIL-C-48497. Ta_2O_5 and SiO_2 are most preferred dielectrics for visible, NIR and SWIR regions AR applications due to negligible absorption, high internal transmission and non-dispersive optical properties. These materials are stable coating materials when applied to substrates like glass and silicon. The developed coating has been characterized using Perkin Elmer spectrophotometer with universal reflectance accessory and the reflection characteristics are shown in Fig. 1. The average reflection value achieved is as low as ~5% in 400-1100nm spectral region. The low value of reflectance suggests that multilayer design proposed in this study can be employed for standard ARC solution.

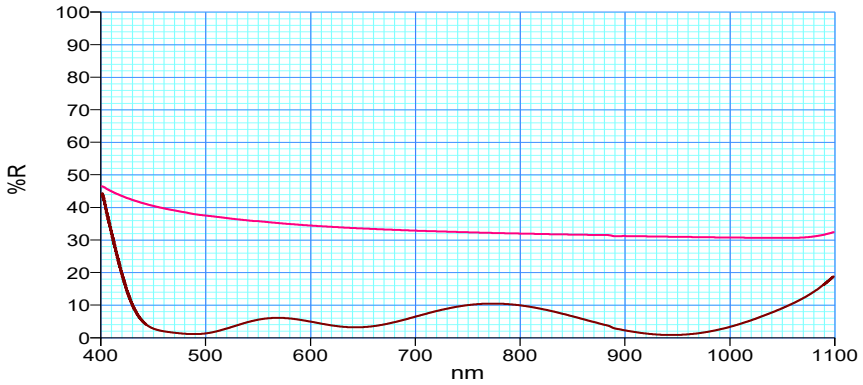

Figure.1 Spectral reflectance curve of uncoated and anti-reflection coated silicon

References

1. Andreani LC, et. al., Adv. Phys., Vol. 4, No. 1 (2019)
2. Ronald R. Willey, Practical Design of Optical Thin Films, Fourth edition, Willey Optical, Consultants.

OTH357 Chromium doped Al_2O_3 nanophosphors for Potential Deep Red LED Applications

Chinnu Susan John[1], V. Biju[2]*

[1,2]Department of Physics, University of Kerala, Kariavattom, Thiruvananthapuram-695581, Kerala, India

**Corresponding author: bijunano@gmail.com*

In this work, we report the incorporation of chromium ions (Cr^{3+}) in the Al_2O_3 lattice and detailed analysis of the photoluminescence spectra. Nanostructured Cr: Al_2O_3 with different dopant concentrations (0 to 1.5 mol%) are prepared by an energy efficient solution combustion method. X-ray Diffraction (XRD) confirms the formation of hexagonal α-Al_2O_3 of space group R-3c (167). The average crystallite sizes of the samples fall in the range of 30-40 nm. The incorporation of Cr^{3+} ions in the Al_2O_3 host lattice is indicated by the slight changes in lattice parameters on doping.

The presence of two main absorption bands centred around 396 nm and 558 nm are confirmed from the Ultraviolet-Visible Diffuse Reflectance Spectra (UV-Vis DRS) which corresponds to two spin allowed transitions of Cr^{3+} ions [1]. The slight change in the onset of these optical absorption bands with increase in the concentrations of Cr^{3+} ions is analyzed from the Kubelka- Munk plot.

Photoluminescence (PL) spectra shows the formation of an intense narrow emission band centred at 694 nm due to spin forbidden transition $^2E \rightarrow {}^4A_2$ of Cr^{3+} ions [1]. The excitation spectra show two broad bands centred around 397 nm and 533 nm. From the PL spectra of samples containing different concentrations of Cr^{3+} ions, optimum concentration is found to be 0.5 mol%. Photoluminescence quantum yield of this sample is found to be 7.22 %. Temperature dependent variation of the PL spectra in the range of 300 K to 500 K is done. The thermal quenching temperature is found to be at 373 K with an activation energy of 0.42 eV. This value is higher than that previously reported for Cr doped Al_2O_3 samples synthesized through co-precipitation method indicating better thermal stability of the present samples [2]. Good quantum yield and high thermal activation energy indicate the potential of this sample to be employed as a deep red phosphor for LED applications.

References

1. Lewis, Prinston Melroy, et. al., *Current Applied Physics* 32, 71-77 (2021).
2. Van Quang, Nguyen, et al., *Dalton Transactions* 50.36, 12570-12582 (2021).

OTH358 A Proposal to Differentiate Drug-induced Toxic Changes in Fluorescence Cellular Nuclei Images Using Deep Learning Approach

Dikshitha CM[*], Satyavratan G, and Ramakrishnan S

[-] Centre of Excellence for Medical Device Regulations and Standards

Department of Applied Mechanics and Biomedical Engineering,

Indian Institute of Technology Madras, Chennai - 600036, Tamil Nadu, India

**Corresponding author: am21s025@smail.iitm.ac.in*

Cytotoxicity is the resultant of toxic actions of various drugs on living cells. Evaluation of cytotoxicity helps in determining potential toxic chemicals for pharmaceutical safety. Drug-induced toxicity causes structural alterations such as nuclear shrinkage, loss of cell membranes, and cellular leakage. Methods to determine cytotoxicity include imaging-based assay techniques. Fluorescence imaging provides a detailed investigation of the cellular structures and captures the biomarkers of cytotoxicity such as morphology and texture changes without disrupting their native state. Recent literature utilized fluorescence cell nuclei images for toxicity evaluation in drug screening by employing deep learning techniques. In this study, a deep learning-based multi-class classification of cell nuclei images for cytotoxicity analysis is performed using a customized Convolutional neural network (CNN) and pre-trained Alexnet. For this, fluorescence microscopic cell nuclei images of HLI cardiac mouse cells with DAPI staining are obtained from a public dataset. 84 Drug-untreated and 252 drug-treated cell nuclei images of cyclophosphamide at each concentration namely, 1.25, 5, and 10 µM are considered. The results of Alexnet show higher performance metrics as compared to CNN for all the epochs and learning rates. The maximum difference in accuracy between deep networks is found to be 20.59%. This work appears to be clinically useful for the drug development processes.

OTH359 Asymmetric Color Image Cryptosystem based on Chaotic Henon Iris Masks (CHIM) with Various Domains

R.Girija[1], H.Singh[2], G. Abirami[3]*

[1]Centre for Health Innovations and Department of CSE,

SET, MRIIRS, Faridabad, Haryana- 121004

[2]The NorthCap University, Gurugram, Haryana- 122017.

[3]Computing Technologies, SRMIST, Chennai, Tamilnadu-603203

**Corresponding Author: girija.srikanth09@gmail.com*

Traditional random phase masks have a dynamic role in double random phase encoding. Since symmetric cryptosystems are susceptible to numerous attacks, asymmetric cryptosystems have been proposed; in these cryptosystems, chaotic henon map iris masks (CHIM) are built in lieu of conventional phase masks. There are different transform domains where the encryption and decryption processes are carried out. The asymmetric cryptosystem, IRIS, and chaotic henon map are the foundations of the proposed system's security. An iris image is shared by the source and destination. Therefore, it is appropriate that the organization and broadcaster share the secret keys in the suggested system. Furthermore, Iris keys have a strong correlation with both the origin and the destination. Various transforms such as Fresnel, Fractional Fourier and Gyrator transforms are considered for this asymmetric cryptosystem. Numerical simulations and analyses, including noise, occlusion, correlation coefficient, and sensitivity analyses, have been carried out to verify the resilience of the suggested asymmetric cryptosystem.

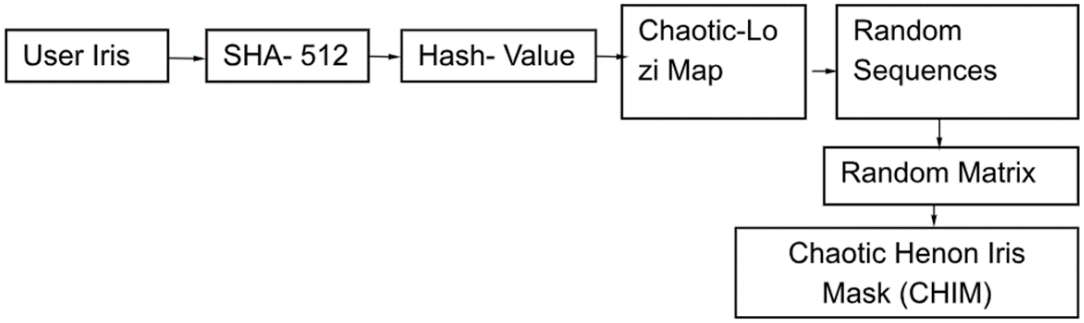

Figure 1: Construction of Chaotic Henon Iris Masks (CHIM)

References

1. Wang, Y., Zhao, Q., Xu, W., Li, F., Yan, J., Liu, S., & Su, Y. (2023). Optical encoding and hiding scheme for a double image based on chaotic fingerprint phase masks and phase-shifting digital holography. *Applied Optics*, *62*(29), 7577-7587.

OTH360 Effect of annealing conditions on structural and luminescence properties of calcium magnesium silicate phosphors

Harshad C[1], Navya Sara Kuriyan[2], M.Sabeena[2]*

[1]Department of Physics, Farook College, Calicut, Kerala, 673632

[2, 2]Department of Physics, Cochin University of Science and Technology, Cochin, Kerala, 682022*

**Corresponding author: sabeena@cusat.ac.in*

Nowadays, Eu^{3+} doped calcium magnesium silicate (CMS:Eu^{3+}) phosphor gains attention due to its wide range of applications in solid state display devices such as white light emitting diodes (w-LED) and biological applications. The present article focuses on the modification of morphology and crystal structure of CMS:Eu^{3+} phosphor prepared at three different stoichiometricratios via solid state reaction methods at two different annealing temperatures and times. The morphology and crystal structure of the host lattice are also analyzed to identify the nature of the host lattice and the effect of Eu^{3+} dopant addition into the host lattice sites. The annealing temperature and duration of annealing of both undoped and Eu^{3+} doped samples were varied from 800°C for 5 hours to 1000°C for 8 hours. The chosen stoichiometric ratio were 2:1:2, 3:1:2 and 1:1:1 for the optimization of akermanite($Ca_2MgSi_2O_7$), merwinite ($Ca_3MgSi_2O_8$) and monticellite ($CaMgSiO_4$) phases of CMS and CMS:Eu^{3+} separately.The crystal structure, morphology and photoluminescence emission were analyzed by X-ray diffraction (XRD) analysis, Field Emission Scanning Electron Microscopy (FESEM) and Photoluminescence (PL) spectroscopy.

XRD analysis of CMS and CMS:Eu^{3+} confirms the formation of a combination of akermanite,merwinite and monticellite phases at an annealing temperature of 800˚C for 5 hours at three different stoichiometricratios. Annealing at 800˚C for 5 hours resulted in the agglomerated morphology for the samples with ratio 3:1:2 and 1:1:1 whereas, particle formation in 2:1:2 irrespective of Eu doping. The photoluminescence emission spectrum is either absent or feeble at these annealing conditions with transitions $^5D_0 \rightarrow {}^7F_J$ (J=1,2,4), $^5D_1 \rightarrow {}^7F_J$(J=4,6).As the annealing temperature increases to 1000˚C for 8 hours, CMS and CMS:Eu^{3+} with a ratio of 3:1:2 optimize to merwinite phase with a defined particle morphology whereas 2:1:2 and 1:1:1, a combined phases of akermanite, merwinite and monticellite with major peaks corresponding to akermanite and monticellite respectively is formed. Also, the improvement in the particle morphology irrespective of Eu doping is noticed. The photoluminescence emission in the red region is enhanced with these annealing conditions with the similar transitions corresponding to annealing temperature of 800˚C for 5 hours.

OTH361 Synthesis And Photoluminescence Analysis Of Terbium Doped Barium Tungstate Nanophosphor.

Mariya Sunny[1], Dinu Alexander[1,2]

Nanoscience Research Centre (NSRC), Department of Physics, Nirmala College, Muvattupuzha, 686661, Kerala, India

Department of Physics, Nirmala College, Muvattupuzha,686661, Kerala, India

**Corresponding author: dinu@nirmalacollege.ac.in*

Terbium doped Barium Tungstate ($Ba_{(1-x)}WO_4$:xTb^{3+}(x=0, 0.01, 0.03, 0.05, 0.07, 0.09)) nanophosphors were synthesized by the facile co-precipitation method. The structural and morphological investigations of the samples were done by the X-ray powder diffraction (XRD) and Field Emission Scanning Electron Microscopy analysis (FESEM). For the detailed spectroscopic investigation, Photo-luminescence (PL) analysis was also done. From PL analysis, the excitation and emission spectra of Tb doped nanophosphors were recorded. The emission intensity for the host excitation was observed to be increasing up to 5% Tb doped sample and then was decreasing due to the concentration quenching. It was observed that by performing colorimetric analysis on the recorded emission spectrum, for 5% Tb doped sample the colour co-ordinate obtained under (275 nm) host excitation was in the green region (0.27,0.60). Further the photocatalytic property of pure and terbium doped Barium Tungstate nanophosphor was also investigated.

OTH362 Femtosecond laser ablated binary phase grating in fused silica for beam-splitting applications

Prajal Chettri[1], Sidhant Dewan[2], and Shailesh Srivastava[3]*
[1, 2, 3] FEMTO FabULLAS, CRIF, Department of Physics, Sri Sathya Sai Institute of Higher Learning, Prasanthi Nilayam, Andhra Pradesh 515134, India
**Corresponding author: prajalchettri@sssihl.edu.in*

Advancements in femtosecond laser micromachining (FLM) have given rise to a novel technology enabling the fabrication of dispersive optical elements like diffraction gratings. Binary phase gratings (BPGs) in particular are a special type of gratings where the phase between two unit cells is modulated as π radians. As a result, the efficiency of all the even-order diffracted signals will fall to zero. Using this phenomenon, BPGs can therefore be used as efficient beam splitters for various applications [1], [2]. While photolithography can also produce such elements [3], direct laser writing offers distinct advantages in terms of process flexibility and simplicity [4]. It eliminates the requirement for various patterned masks or chemical etching. In this work, the feasibility of fabricating binary phase grating in fused silica using femtosecond laser ablation was explored. The fabricated gratings are characterized using SEM imaging (Figure 1(a)). The basic features of the fabricated gratings were found to confirm known theoretical results. A parametric study on the 1st–order diffracted power with respect to 0th–order diffracted power as a function of duty cycle was performed (Figure 1(b) and 1(c)). The maximum ratios for single-scan and multi-scan ablation were found to be 65% and 83.4% respectively for a duty cycle of 0.5. Due to the inherent characteristics of the fabrication process, these gratings can also serve as surface microstructured surface-enhanced Raman scattering (SERS) substrates, offering potential use in lab-on-a-chip applications.

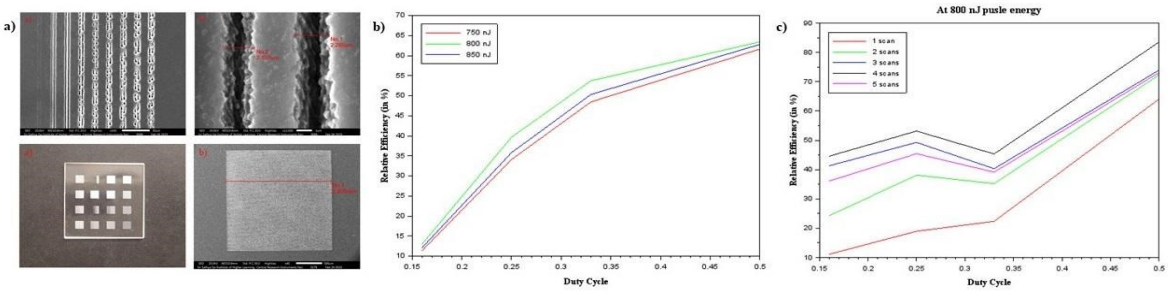

Figure 1: a) SEM images of the fabricated BPGs, b) and c) Parametric studies on the ratio of 1st-order diffracted power with respect to 0th-order diffracted power as a function of duty cycle for different pulse energies in single-scan ablation and number of scans in multi-scan ablation respectively.

References

1. Killat, U *et al.*, *Fiber & Integrated Optics* 4.2 (1982): 159-167.

2. Wang, Bo *et al*., *Applied Optics* 47.22 (2008): 4004-4008.
3. Tseng, Shuo-Yen, *et al*., *Optics Express* 14.19 (2006): 8737-8744.
4. Karosas, Jonas *et al.*, *Procedia CIRP* 111 (2022): 613-616

OTH363 Exploring Suitable Solvents for Drop-on-demand or Continuous Inkjet Printing Using Laser-induced Shockwaves

Rakshith Kamath,[1] Kailash C. Jena[1,2,]*
[1]Department of Physics, Indian Institute of Technology Ropar, Rupnagar, Punjab-140001, India
[2]Department of Biomedical Engineering, Indian Institute of Technology Ropar, Rupnagar, Punjab-140001, India
**Corresponding author: kcjena@iitrpr.ac.in*

Our research focused on finding suitable solvents for Drop-on-demand or Continuous Inkjet printing from Newtonian fluids. We used laser-induced shockwaves to create microdroplets and microjets and analysed their behaviour using dimensionless parameters such as Ohnesorge, Weber, and Reynolds numbers. Our study focused on droplets with Ohnesorge numbers ranging from 0.01 to 0.239 and we conducted experimental studies using laser pulse energies of 100 µJ, 200 µJ, and 400 µJ, which were above the threshold energies required to create laser-induced shockwaves. The microdroplets we created had Weber numbers ranging from 5 to 3100 and Reynolds numbers ranging from 16 to 4800. By analysing these dimensionless parameters, we constructed phase diagrams to better understand the printability of the droplets. We found that microdroplets with higher Ohnesorge numbers ranging from 0.0929 to 0.239 can be utilized as solvents for inks in Inkjet printing, especially at lower laser pulse energies of 100 µJ and 200 µJ.

References

1. Tagawa et. al., *Phys. Rev. X* 2, 031002 (2012).
2. Delrot et. al., *Phys. Rev. Applied* 6, 024003 (2016).
3. Derby et. al., *Annu. Rev. Mater. Res.* 40, 395-414 (2010).

OTH364 Design and Development of Ta_2O_5/MgF_2 multilayer anti-reflection coating for visible optics

Rashmi Negi

Thin-Film Division, Instruments Research & Development Establishment

Raipur Road, Dehradun - 248 008, INDIA

E-mail: rashminegi.irde@gov.in

Reflection loss that occurs at the glass-air interface, limits the performance of many optical devices such as eyeglass, camera lenses, or any optical systems. Antireflection (AR) coating on the glass components reduces the reflection loss and improves efficiency of such devices. In this paper, a broadband (bandwidth~280nm) AR coating in the visible region has been designed and developed using Ta_2O_5/MgF_2 multilayer stack. The thicknesses of individual thin layers are numerically optimized to get maximum transmission in visible region.

The deposition of multilayer coating was carried out inside coating plant fitted with diffusion and rotary pumps. The evaporation was carried out in high vacuum (2-3 x 10^{-5} mbar) using electron beam gun and thermal evaporation and in-situ layer thicknesses was measured by crystal monitor. The transmission characteristic of coated substrate was tested using double beam spectrophotometer (Supplied by M/S Perkin Elmer) and the measured transmission spectrum of the 4-layer AR coating was compared with that of simulated spectrum.

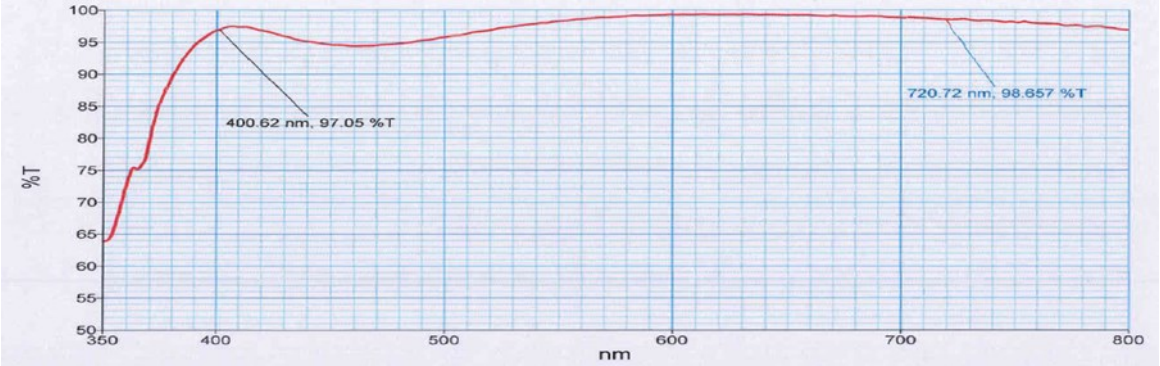

Experimental Spectral Transmission characteristics of AR coated BK7 sample

And it was seen that the dual side AR coating on BK7 glass increases the average transmission by 7% as compared to that of bare glass substrate in the wavelength region of 480 nm - 760 nm.

References

1. H.A. Macleod, "Thin-film optical filters", Fourth ed., New York, CRC press, 2010.
2. J. A. Dobrowolski and B. T. Sullivan, "Universal antireflection coatings for substrates for the visible spectral region," Appl. Opt. 35, 4993-4997 (1996).

OTH365 PT symmetric optical structure with linearly graded refractive index

Siddivinayaka T S[1], Abdul Jaleel[1], K Shadak Alee[1]*
[1]Department of Physics and Nanotechnology, SRM Institute of Science and Technology, Kattankulatur, Chennai-603203
**Corresponding author: shadakk@srmist.edu.in*

The concept of parity time (PT) symmetry was originally introduced by Bender and Boettcher in their study of non-Hermitian Hamiltonians, which exhibit both complex and real eigenvalues depending on a critical parameter that determines the degree of non-hermiticity [1]. In optics, structures with PT-symmetry can be realized using balanced optical gain and loss components. These structures offer unique optical properties such as laser-absorber modes, single mode lasing, and unidirectional reflection [2,3]. So far, these investigations have been limited to media with constant refractive index profile. But structures with graded index profile have not been investigated to the best of our knowledge. However, graded index materials have shown promising applications in photonic crystals for integrated optical systems including focusing lenses, beam splitters, couplers, [4] etc. Here, our work focuses on the PT symmetric structures which have graded refractive index profile. Structures with graded index offer high Q resonant modes and wide bandgap. Under PT-symmetric condition, these systems realize laser-absorber modes for a small gain/loss

contrast as compared to large gain/loss contrast in the structure with homogenous and isotropic refractive index. In addition, the left and right reflection coefficients of a particular resonant mode drop to zero at two distinct values of gain/loss contrast. This finding highlights the structure's capability to switch its unidirectional invisibility from loss port to gain port, a behavior not observed in homogeneous and isotropic media where it is limited to the gain port when operating above the PT threshold point. Moreover, this graded index structure allows for precise tuning of laser-absorber modes by adjusting either the length of the dielectric medium or modifying the graded index profile. As a result, it enables the realization of single-mode operation instead of multiple modes seen in homogenous and isotropic media. More results of our work will be provided at the time of conference.

References

1. C. M. Bender, et al, "$\mathcal{PT}$-symmetric quantum mechanics." *Journal of Mathematical Physics* 40, no. 5 (1999): 2201-2229
2. A. A. Zyablovsky, et al, "PT-symmetry in optics." *Physics-Uspekhi* 57, no. 11 (2014): 1063.
3. L. Feng, et al, "Non-Hermitian photonics based on parity–time symmetry." *Nature Photonics* 11, no. 12 (2017): 752-762.
4. Q. Zhu, L. Jin, et al, "Graded index photonic crystals: a review." *Annalen der Physik* 527, no. 3-4 (2015): 205-218.

OTH366 Patch Based Analysis of Cell Painted Fluorescence Microscopy Images using Gradient and Intensity Features

Sreelekshmi P S[1], Rohini P[2] and Ramakrishnan S[1]*
[1] Centre of Excellence for Medical Device Regulations and Standards
Department of Applied Mechanics and Biomedical Engineering,
Indian Institute of Technology Madras, Chennai - 600036, Tamil Nadu, India
[2] Department of Electronics and Communication Engineering,
Indian Institute of Information Technology Design and Manufacturing,
Kancheepuram, Chennai-600127, Tamil Nadu, India,
**Corresponding author: lekshmishyam2009@gmail.com*

Fluorescence microscopy-based cell painting technique captures high content morphological information of cell organelles. Automated quantitative analysis of these cell painted images can provide deeper insights to the critical mechanisms in the cell structure. The difference in the size, shape, and spatial distribution of cell components motivates for multiscale feature extraction and analysis of these cell painted images. This is important for understanding the organelle specific changes in the cell structure due to internal or external interactions. In this study, patch based multiscale analysis of cell painted organelles is performed using gradient magnitude and mean intensity features. For this, cell painted images of nuclei, endoplasmic reticulum (ER), and cytoplasm from a public database is obtained. Gradient magnitude and mean intensity features from the image patches of sizes 3,5,7 and 9 are extracted and are statistically analysed. The obtained results show significant variations in the mean and standard deviation among considered organelles for all patch sizes. The mean intensity feature provides highest mean percentage deviation of 0.71 and 0.66 for nuclei vs ER and ER vs cytoplasm at patch size 9. Gradient magnitude produces maximum mean percentage deviation of 0.51 for nuclei vs cytoplasm at patch size 5. Thus, the discriminative ability of gradient magnitude and mean intensity features for characterizing the multiscale distribution of cell painted organelles has been explored. The obtained results suggest the employability of these features for classifying the morphological changes in the sub cellular organelles.

Theses

Computational Modeling of Optogenetic Control of Neuronal Signaling

Himanshu Bansal
Department of Physics and Computer Science, Dayalbagh Educational Institute, Agra 282005, India

To understand the human brain, the most complex system in the known universe, is one of the greatest scientific challenges [1]. Although tremendous progress has been made, much remains to be understood, that include its architecture, causal relationship between structures and functions, neural connectome, neural coding and signal processing, and various neurological disorders [2]. A better understanding of how the brain works is important to not only know the biological basis of consciousness, but to also develop the brain-computer interfaces and smarter artificial intelligence [3]. It is therefore essential to develop neuroimaging tools with high spatiotemporal resolution and techniques to study and control neurons that are non-invasive, have high precision and high efficiency, are fast and cost-effective. Early neuromodulation techniques including direct brain stimulation and ultrasound neuromodulation involves injection of direct electric current via electrodes and ultrasound waves to produce heat or mechanical force to change membrane properties, respectively. However, these techniques do not provide cell-type specificity, which limits their potential to understand causal relationships between different neurons and behavioral activities [4].

Neurophotonics is an emerging multidisciplinary area of research that deals with the development of tools for optical imaging and control of neurons in the brain. In neurophotonics, optogenetics has revolutionized neuroscience by allowing control and monitoring of neuronal activity in cultured cell, tissue, and living animals with unprecedented spatiotemporal resolution [5-7]. Optogenetics does not involve direct invasiveness to targeted cell as required in electrical stimulation. Therefore, it has proven its potential for a wide range of applications in and beyond neuroscience, significantly improved the way many neuroscience studies were performed earlier, and contributed to our understanding of the mechanism and biology underlying several neurological diseases [7-9]. For optogenetic control, the natural light-sensitive proteins found in microbial species are genetically inserted into the desired neural populations. These genetically modified neurons can be precise turn-on or -off with light.

A major challenge in optogenetics is to achieve low-power, high-frequency, and high-fidelity control of neuronal signaling [7, 10-12]. Although each component in optogenetics continues to evolve rapidly to meet these challenges, there is a tremendous scope for optimizing ongoing experiments for better efficiency. There are more than hundred types of light-sensitive proteins, having different spectral- and light-sensitivity, kinetics, ion-selectivity, ion-transportation mechanisms and protein stability [12]. On the other hand, there are more than thousand types of neurons in our brain, having different morphology, size, ion-channel composition and spiking patterns. Experimental testing of each opsin and its combinations with different neurons in healthy as well as pathological conditions is a very challenging task. The problem further persists when optimized photostimulation and physiological conditions are needed to get the desired control [7, 11, 12]. Although newly discovered opsins have the potential to meet the challenges, a detailed experimental study is needed to optimize their response. Thus, computational modeling has tremendous scope in this area.

Computational optogenetics can help in virtual testing of new opsins in a variety of cells with realistic physiological properties. Theoretical simulations can virtually assess the limitations and suitability of different opsins for specific applications. They also assist in correctly interpreting complex experimental results. Despite having urgent need of such theoretical models, a very few opsins were modelled [13]. Since the introduction of Channelrhodopsin-2 (ChR2), there are a large number of opsins have been discovered exhibiting complex photocycle kinetics [13, 14]. As the newly discovered opsins have potential to overcome challenges and have wide scope of applications, the theoretical models for newly discovered important opsins were urgently needed as their potential applications. Therefore, the objective of this thesis

was to formulate accurate computational models for optogenetic control of neurons expressed with newly discovered opsins.

The thesis presents new accurate computational models of optogenetic control of neurons expressed with light-sensitive proteins. The mathematical models of the light-sensitive proteins used in optogenetics are based on the photocycle of each protein [15, 16]. In general, all the channelrhodopsins utilize retinal as their light-sensing counterparts. On illumination with light, the retinal molecule undergoes photoisomerization within ~ fs and triggers the opsin photocycle. The photocycle of each opsin have different intermediate states and kinetics [15, 16]. Based on the reported photocycle kinetics and photocurrent response of individual opsins, computational models of a large number of opsins have been formulated for the first time. These theoretical models were integrated with biophysical models of different neurons to design, (i) low-power and ultrafast optogenetic excitation with different channelrhodopsins namely, ChR2, ChR2(H134R), ChETA [17], Chronos, Chrimson, CsChrimson, ChrimsonR [18], vf-Chrimson [19], ReaChR [20], bReaChES [21], and ChRmine [22], (ii) temporally precise inhibition with single-spike resolution using light-driven chloride pumps, namely NpHR [6], eNpHR3.0 [23] and Jaws [24], and light-driven chloride channel, namely GtACR1 [25], and (iii) low-power high-fidelity high-frequency bidirectional control with experimentally reported opsin pairs, namely ChR2-NpHR, ChR2(H134R)-eNpHR3.0, and Chrimson-GtACR2 [26], and new prospective opsin pairs, namely, Chronos-Jaws, CheRiff-Jaws, Chronos-eNpHR3.0, and vf-Chrimson-GtACR2. The accuracy of the formulated theoretical models has been validated by comparing the simulated results with the reported experimental results, which are in excellent agreement [16-26]. Further, a detailed theoretical study of optogenetic control over a wide range of optical and physiological conditions have been presented to get better understanding and new insights. Optimization of photostimulation and physiological conditions has also been carried out for low-power, high-fidelity and high-frequency control of neurons. The minimum irradiance threshold and high-frequency limits of different opsin pairs for bidirectional optogenetic control have been determined. Further, new opsin pairs have also been designed for low-power and high-frequency control (Table 1) [27-29].

Table 1. Minimum irradiance threshold and high-frequency limit of high-fidelity optogenetic control of neocortical interneurons with different reported and proposed opsin pairs [27-29].

Opsin Pair	Minimum Irradiance Threshold for Sustained Control		High-frequency Limit
	For excitation	For suppression	
ChR2-NpHR	I_{470} = 5 mW/mm^2	I_{593} = 21 mW/mm^2	100 Hz
ChR2(HR)-eNpHR3.0	I_{470} = 0.75 mW/mm^2	I_{593} = 1.8 mW/mm^2	60 Hz
Chrimson-GtACR2	I_{470} = 0.75 mW/mm^2	I_{593} = 1.8 mW/mm^2	10 Hz
Vf-Chrimson-GtACR2	I_{593} = 0.6 mW/mm^2	I_{470} = 0.04 mW/mm^2	20 Hz
CheRiff-Jaws	I_{470} = 0.014 mW/mm^2	I_{593} = 0.8 mW/mm^2	100 Hz
Chronos-Jaws	I_{470} = 0.02 mW/mm^2	I_{593} = 0.8 mW/mm^2	180 Hz
Chronos-eNpHR3.0	I_{470} = 0.02 mW/mm^2	I_{593} = 1.8 mW/mm^2	250 Hz

Blindness due to retinal degenerative diseases is a major challenge and cannot be accurately cured using existing methods. Recently in 2021, the first human trial of optogenetic-based restoration of partial vision in a blind patient has been reported in Nature Medicine [9]. In the thesis, a detailed theoretical study of the photoresponse of retinal ganglion neurons expressed with reported and prospective opsins has shown that ChRmine allows reliable excitation of these neurons at two orders of magnitude lower light intensities

than ChrimsonR opsin used in the reported human trial. Under continuous illumination, ChRmine-expressing RGNs begin to respond at very low irradiances ~10^{-4} mW mm^{-2} , and evoke firing upto ~280 Hz, highest among other opsin-expressing RGNs, at 10^{-2} mW mm^{-2} (Figure 1) [30]. The first spike latency in ChRmine-expressing RGNs is shorter by an order of magnitude, along with stable latency of subsequent spikes compared to other opsins. The present study highlights the importance of ChRmine as a potential opsin for optogenetic retinal prostheses.

Spike failure due to photocurrent desensitization is a fundamental challenge in optogenetics. In this thesis, a novel method of co-expressing bistable opsins with fast channelrhodopsins has been proposed to overcome the challenge on which a patent has also been filed. Using the proposed method, the spiking fidelity in these neurons can be sustained even at lower irradiances of subsequent pulses (77% of initial pulse intensity in ChETA-ChR2(C128A)-expressing neurons) or by illuminating red-shifted light pulses at appropriate time intervals (Figure 2) [31]. High-fidelity spiking up to 60 Hz can be evoked in ChETA-ChR2 (C128S), ChETA-SSFO and ChETA-SOUL-expressing neurons, which cannot be attained with only SFOs. The proposed method provides a means for low-power, high-frequency, high-fidelity sustained firing in neurons, necessary to study various long-term neural functions and neurodegenerative disorders, and enhance the utility of optogenetics for biomedical applications [32].

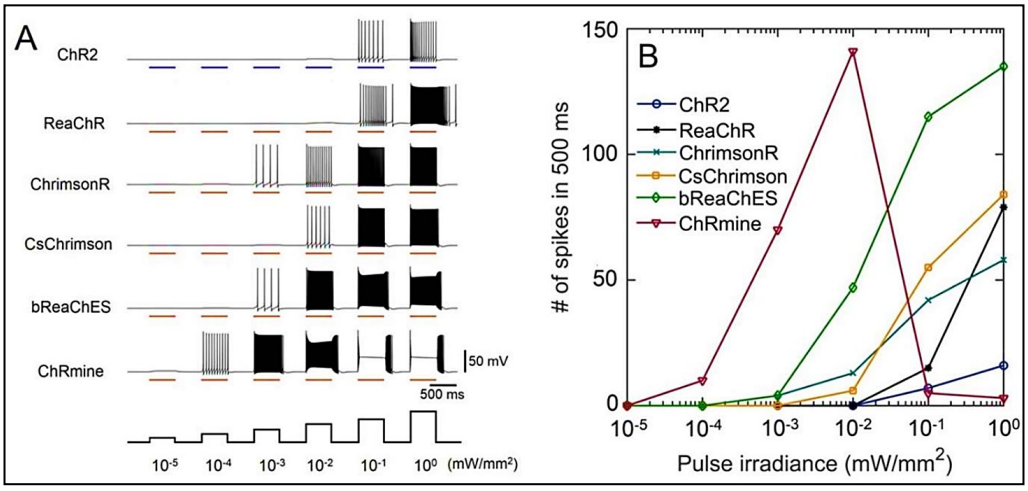

Figure 1. Low-power optogenetic excitation of retinal ganglion neurons in the retina. (A) Variation of membrane potential with time on illuminating with 500 ms light pulses of increasing irradiances. (B) Corresponding variation of average firing rate with pulse irradiance [31].

The fundamental process of information processing and memory formation in the brain is associated with complex neuron firing patterns, which can occur spontaneously or be triggered by sensory inputs. However, the light pulses used in optogenetics have been primarily restricted to square waveforms. A detailed theoretical analysis of the temporal shaping of light pulses in optogenetic excitation of hippocampal neurons and neocortical fast-spiking interneurons expressed with ultrafast (Chronos), fast (ChR2), and slow (ChRmine) channelrhodopsins were also presented. Optogenetic excitation has been studied with light pulses of different temporal shapes that include square, forward-/backward ramps, triangular, left-/right triangular, Gaussian, left-/right-Gaussian, positive-sinusoidal, and left-/right-positive sinusoidal [33]. Different light shapes result in significantly different photocurrent amplitudes and kinetics, spike-timing, and spontaneous firing rate. The results demonstrate that non-square waveforms generate more naturalistic spiking patterns compared to traditional square pulses. These findings provide valuable insights for the development of new optogenetic strategies to better simulate and manipulate neural activity patterns in the brain, with the potential to improve our understanding of cognitive processes and the treatment of neurological disorders.

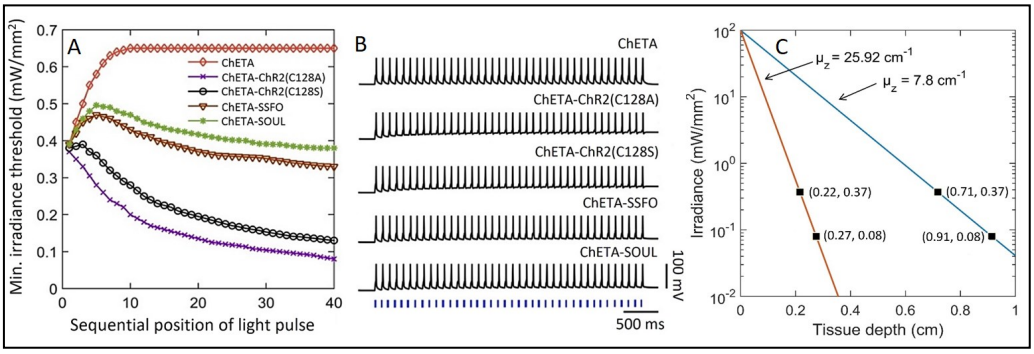

Figure 2. Low-power and deeper noninvasive excitation with novel combination of ChR2(C128A) and ChETA. (A) Variation of minimum irradiance threshold to evoke spikes at 10 Hz using pulses of 10 ms, and (B) Corresponding spiking patterns for different ChETA-SFO combinations. (C) Excitable depth different brain tissues [32].

Cardiac optogenetics has proven its potential to overcome limitations associated with electrical stimulation of the heart. However, excitation of heart cells in deeper regions is challenging due to scattering and absorption of light [34]. A detailed computational study of optogenetic control of electrical activity in opsin-expressing human ventricular cardiomyocytes shows that optical excitation of deeply situated heart cells is possible upto ~7.46 mm and 10.2 mm from the surface with ChRmine at wavelength 585 nm and 650 nm, respectively (Figure 3) [34, 35].

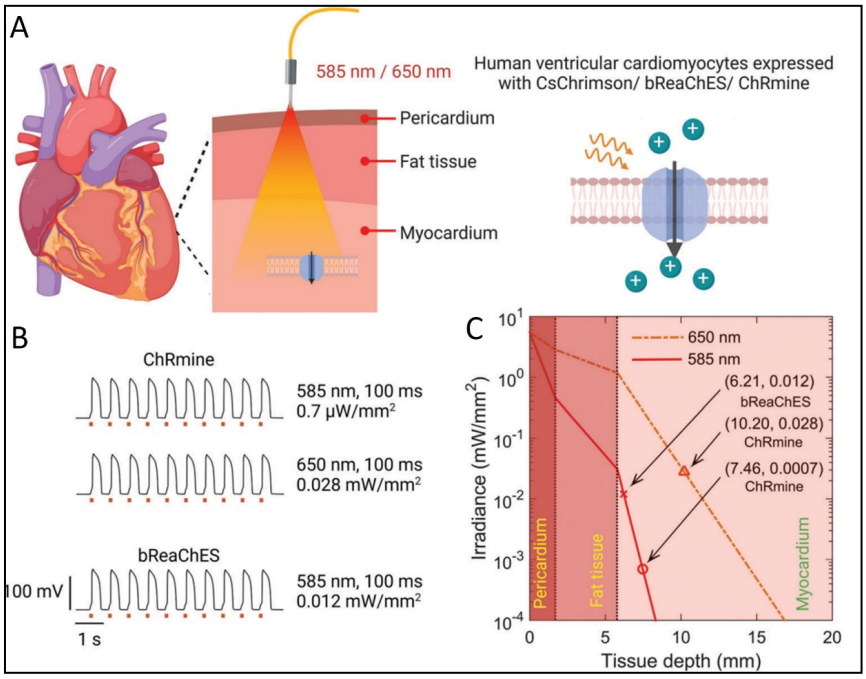

Figure 3. Noninvasive deep optogenetic excitation of cardiac cells in human heart. (A) Schematic of optogenetic excitation of human heart expressed with channelrhodopsin. Tissue surface is illuminated with safe (5 mW/mm^2) light intensity. (B) Light-evoked spikes in human ventricular cardiomyocytes expressed with ChRmine and bReaChES on illuminating with indicated pulse widths, irradiances, and wavelengths. (C) Corresponding excitable tissue depths [35].

Insights from the theoretical work presented in the thesis have encouraged experimentalists to conduct new experiments with proposed opsins in the thesis [36]. A recent study published in Nature has used ChRmine for efficient control of the heart, as predicted from our theoretical work [37]. Furthermore, a study published in Nature Electronics has reported that the theoretically predicted irradiance thresholds and kinetics with ChR2 and ChRmine are consistent with their experimental results [38].

The study is an important contribution in the highly challenging emerging area of neurophotonics and is useful for designing optogenetic circuits for different biomedical applications that include cure for neurological diseases, probing temporal spike coding and designing advanced brain-computer interfaces.

Acknowledgement: Department of Science and Technology, India for INSPIRE Fellowship for 2017-2022.

References

1. S. Krohn, N. V. Schwanenflug, L. Waschke et al., Sci. Adv. **9**(5), eabq3851 (2023).
2. S. Panzeri, M. Moroni, H. Safaai et al., Nat. Rev. Neurosci. **23**(9), 551-567 (2022).
3. X. Tang, H. Shen, S. Zhao et al., Nat. Electron. **6**, 109-118 (2023).
4. E. Urai, B. Doiron, A. M. Leifer et al., Nat. Neurosci. **25**(1), 11-19 (2022).
5. E. S. Boyden, F. Zhang, E. Bamberg et al., Nat. Neurosci. **8**(9), 1263-1268 (2005).
6. F. Zhang, L. P. Wang, M. Brauner, Nature **446**(7136), 633-639 (2007).
7. V. Emiliani, E. Entcheva, R. Hedrich et al., Nat. Rev. Methods Primers **2**, 55 (2022).
8. E. Entecheva and M. W. Kay, Nat. Rev. Cardiol. **18**(5), 349–367 (2021).
9. J. A. Sahel, E. Boulanger-Scemama, C. Pagot et al., Nat. Med. **27**(7), 1223-1229 (2021).
10. G. Faini, D. Tanese, C. Molinier et al., Nat. Commun. **14**(1), 1888 (2023).
11. S. F. Owen, M. H. Liu & A. C. Kreitzer Nat. Neurosci. **22**(7), 1061-1065 (2019).
12. Bansal, S. Shikha & Y. Zhang, Nat. Biomed. Eng. **7**(4), 349-369 (2023).
13. J. C. Williams, J. Xu, Z. Lu et al., PLoS Comput. Biol. **9**(9), e1003220 (2013).
14. P. M. Boyle, J. C. Williams, C. M. Ambrosi et al., Nat. Commun. **4**(1), 2370 (2013).
15. C. Engelhard, I. Chizhov, F. Siebert et al., Chem. Rev. **118**(21), 10629-10645 (2018).
16. F. Schneider, C. Grimm & P. Hegemann, Ann. Rev. Biophys. **44**, pp.167-186 (2015).
17. L. A. Gunaydin, O. Yizhar, A. Berndt et al., Nat. Neurosci. **13**(3), pp.387-392 (2010)
18. N. C. Klapoetke, Y. Murata, S. S. Kim et al., Nat. Methods **11**(3), 338-346 (2014).
19. T. Mager, D. L. de la Morena, V. Senn et al., Nat. Commun. **9**(1), 1750 (2018).
20. J. Y. Lin, P. M. Knutsen, A. Muller et al., Nat. Neurosci., **16**(10), 1499-1508 (2013).
21. C. K. Kim, S. J. Yang, N. Pichamoorthy et al., Nat. Methods **13**(4), 325-328 (2016).
22. J. H. Marshel, Y. S. Kim, T. A. Machadoet et al., Science **365**(6453), eaaw5202 (2019).
23. V. Gradinaru, F. Zhang, C. Ramakrishnan et al., Cell **141**(1), 154-165 (2010).
24. S. Chuong, M. L. Miri, V. Busskamp et al. Nat. Neurosci. **17**(8), 1123-1129 (2014).
25. E. G. Govorunova, O. A. Sineshchekov, R. Janz et al., Science **349**(6248), 647-650 (2015).
26. J. Vierock, S. Rodriguez-Rozada, A. Dieter et al., Nat. Commun. **12**(1), p.4527 (2021).
27. N. Gupta, H. Bansal, and S. Roy, Neurophoton. **6**(2), 025002-025002 (2019).
28. H. Bansal, N. Gupta, and S. Roy, Neuroscience **449**, 165-188 (2020).
29. H. Bansal, N. Gupta, and S. Roy, Biomed. Phys. Eng. Exp. **6**(4), 045011 (2020).
30. H. Bansal, N. Gupta, and S. Roy, J. Neural Eng. **18**(4), 0460b8 (2021).
31. H. Bansal, G. Pyari, and S. Roy, J. Neural Eng. **19**(2), 026032 (2022).
32. H. Bansal, G. Pyari, and S. Roy, Indian Patent, Application No. 202211077093, Filed on Dec 30, 2022.
33. H. Bansal, G. Pyari, and S. Roy, Photonics **10**(5), 571 (2023).
34. G. Pyari, H. Bansal, and S. Roy, J. Physiol. **600**(21), 4653-4676 (2022).
35. G. Pyari, H. Bansal, and S. Roy, Pflügers Arch. Eur. J. Physiol. (2023). DOI: 10.1007/s00424-023-02831-x
36. B. Hsueh, R. Chen, Y. Jo et al., Nature **615**, 292–299 (2023).
37. L. K. Too, W. Shen, D. A. Protti et al., Sci. Rep. **12**, 19312 (2022).
38. J. Taal, I. Uguz, S. Hillebrandt et al., Nat. Electron. **6**, 669–679 (2023).

Common-path Optical Coherence Tomography with Quasi-Bessel beam from Negative Axicon Optical Fiber Tip Probe

Kaushal Vairagi
Academy of Scientific & Innovative Research, Ghaziabad, India
CSIR- Central Scientific Instruments Organisation, Chandigarh, India

Introduction

Optical coherence tomography (OCT) is a low-coherence interferometry based non-invasive optical imaging technique analogous to ultrasound imaging. It provides micron order resolution with few millimetres imaging depth in biological tissue. OCT has demonstrated great potentials in many clinical applications, such as ophthalmology, dermatology, endoscopy, dentistry, angiography etc.

The technique initially reported by D. Huang et al. [1] in the year of 1991 as time domain OCT has experienced significant progress in terms of resolution and speed through technological development and application demands till the date. But, there is a trade-off between Lateral resolution and depth of focus (DOF) that need to be removed for high resolution in-depth imaging. This trade-off is due to the application of diffracting Gaussian beam where, smaller beam waist also reduces the Rayleigh range. The use of non-diffracting beam such as Bessel's beam has proven its capability in removing this trade-off in free space OCT but for endoscopic applications there is a need for all-fiber extended DOF probes. Recent studies show such probe for Bessel beam generation using conical frustum tip [2], multi-micro axicon [3], a No core fiber positive axicon [4], and also based on other approaches like, simple phase mask consisting of graded-index (GRIN) fiber [5], high-efficient fiber-based filter [6], coaxially focused multimode (CAFM) beam [7], etc.

In search of another alternative for DOF extension we have developed a novel Reflective Axicon as proposed by McLeod [8] in 1954, for Quasi-Bessel beam generation on the tip of a optical fiber and explored its capability in OCT imaging using common-path configuration. The research work aims to develop a common-path OCT system using an optical fiber with negative axicon tip generating Bessel beam to probe the sample.

Methodology Used

The present work is carried out in following steps:

Development of negative axicon optical fiber tip for bessel beam generation

The Negative axicon optical fiber tip is fabricated inside the tip of a highly Ge doped optical fiber with core diameter~3μm.The high concentration of Ge makes the etching rate of the core material in HF solution higher compared to silica cladding. The optical fiber is superficially dipped into 48% HF solution which etches inside the optical fiber to form a capillary in the fiber tip. The developed negative axicon has been named as "Deep Seated Negative Axicon (DSNA)" due to the fact that the apex of negative axicon is situated deep inside the fiber tip end. From now onwards the negative axicon will be called as DSNA in rest of the article.

Characterization of DSNA and output beam parameters

To characterize the DSNA we have done Far field beam profiling and Near field beam profiling using home made setups and beam parameters such as Depth of focus, spot size, intensity profile etc are obtained.

Development of CPOCT imaging system.

Experimental setup:

We have used a Superlum M-S-840-B-I-15 SLD Broadband light source centered at 840 nm and having a ~45nm FWHM bandwidth, an 840±50 nm broadband circulator for delivering and collecting light to and from the sample through DSNA, and delivering the interference signal to a home-built linear-in-wavenumber spectrometer. The core air interface of the DSNA tip with a measured reflectivity of 0.13% generates the reference signal for interference. The sample needs to be placed on a 3-axis Nanomax-300 translational stage platform for scanning while the DSNA probe is held in a fiber clamp on a micro-stage facing the sample at a distance of about 100µm. Figure 1 shows the experimental arrangement of the described system.

On the software side, a LabVIEW program has been written to control and synchronize the scanning and data acquisition. Data logging and real time processing for the image construction has also been implemented in the LabVIEW program utilizing parallel processing. A zig-zag 2D scan algorithm has also been implemented for 3D imaging.

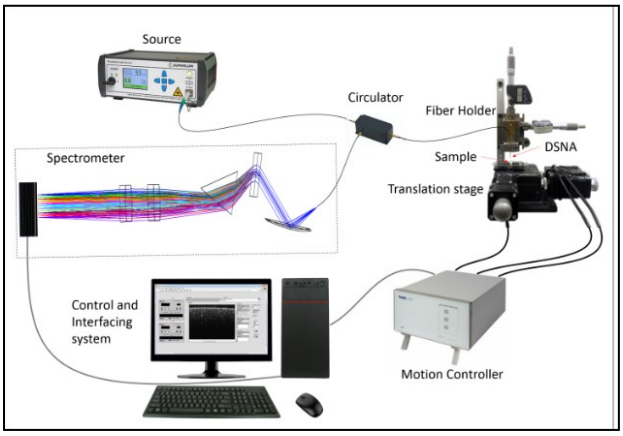

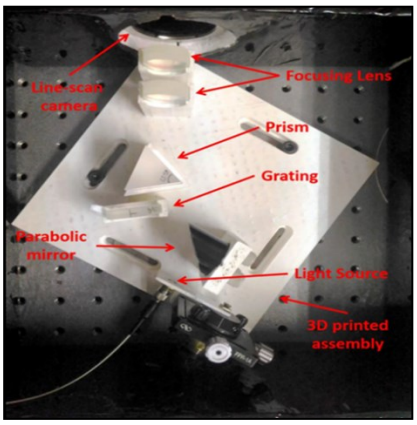

Figure 1. (left) Experimental arrangement for Common-path OCT, inset shows microscopic image of a silver coated DSNA. Figure 2. (right) Linear-in-wavenumber spectrometer assembly

Optimization of negative axicon optical fiber tip for the application in CPOCT imaging.

The DSNA has been optimized in terms of length, energy efficiency and working distance for providing best imaging performance with the current experimental arrangement in CPOCT imaging.

Results and their interpretation

Fabrication results and DSNA geometry

The optical microscopic images show that the DSNA has two parts. The first part, named as primary axicon apexed at the core and adiabatically stretches into the first cladding. The second part, named as secondary axicon, is a frustrum cone located entirely in the second cladding region. There is a discontinuity in the slope at the junction of the primary and secondary axicons due to the difference in doping concentration of 1st and 2nd cladding resulting in different etching rate. There are 4 major geometrical parameters of the DSNA, apex angle of primary axicon (θ), apex angle of secondary axicon (φ), opening diameter of secondary axicon (O) and total length of the DSNA (L)) as represented in Figure 4. θ and φ are constants for a given Refractive index profile of fiber subject to the concentration of etching acid i.e. 48% HF, and does not vary with etching time. For a 40min etched sample θ and φ are measured to be 45° and ~8.5° respectively. Variation in the etching time results in variation in DSNA length (L), the experimental results are plotted in Figure 4. The opening diameter varies accordingly with the length.

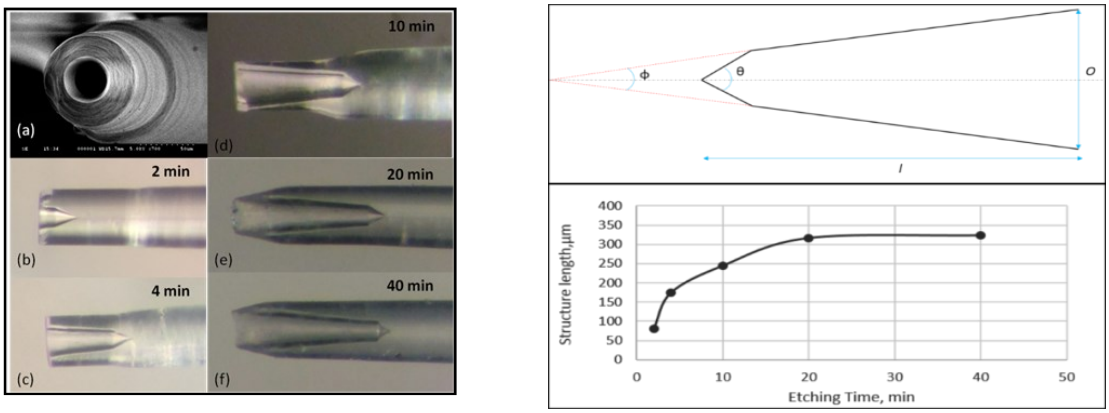

Figure 3(left)(a) FESEM image of negative axicon from top (b-f) microscopic images of negative axicon tip with different etching time. Figure 4(right) Schematic of axicon geometry(above), Variation of axicon length with etching time(below)

Far field beam profiling

After fabrication of DSNA tip, other end of the fiber is butt coupled to 632nm He-Ne laser and the beam profile is observed on a paper screen. A 13MP digital photography camera is used to capture the screen images. The distance of screen from the tip is varied from 5mm to 25mm with 1mm step size. The images are then processed in MATLAB for generating line scan. The results are summarised in the Figure 5. below.

Near-field beam profiling

To find out the quality of Quasi-Bessel beam generated by DSNA, we have experimentally investigated the beam parameters using a homemade near field beam profiler consisting of a fiber clamp mounted on a 5-axis manual translation stage for alignment and translation of the beam, a 40x microscopic objective to magnify the beam and a Pixelink microscopic camera to record the profile. The experiment is done using a 850nm SLD source having 45nm FWHM bandwidth and the results are summarised in Figure 6. A FWHM DOF of 345μm and a spot size variation of 5-20μm for 0-1200μm propagation distance is obtained for a 40min etched DSNA sample.

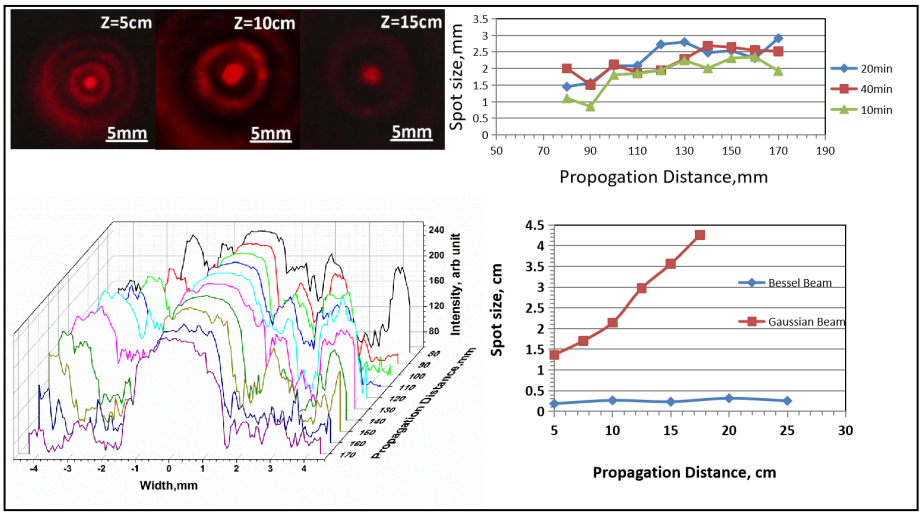

Figure 5. (a) shows the transverse beam profile recorded at mentioned distances. (b) We also compared the central spot size of the beam generated from negative tip fabricated with different etching time and found similar behaviour with propagation distance. (c) represents a 3D plot of line scan of transverse beam profile recorded by varying distance from 80mm to 170mm from the tip. (d) we observe that the spot-size for central spot of the BB, ~2 mm, is quasi-invariant whereas the spot size of the Gaussian like beam, ~1.5 cm, increases 3 times over a shorter distance.

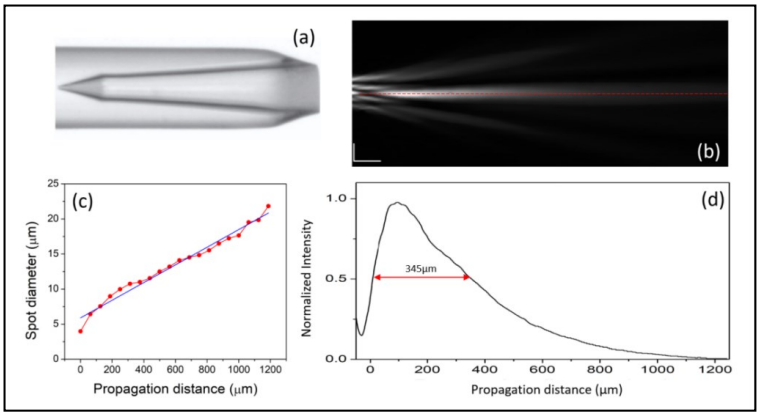

Figure 6 (a) Microscopic image of DSNA, (b) Experimentally obtained longitudinal beam profile of the beam coming out of the DSNA, (c) central spot size variation with propagation distance. (d) Normalized Intensity distribution of the central spot along the direction of propagation, FWHM shows the DOF to be 345 μm

DSNA optimization: Fabrication time and axicon length

The reference signal in this CPOCT configuration is generated from optical fiber core material-air interface along the Axicon length(AL) of DSNA. It adds a fixed path length difference of "2 x AL" other than the working distance resulting in a loss of sensitivity. In order to minimize the path length difference AL must be reduced in the current conventional common-path configuration without sacrificing quality of BB. We have chosen etching time as a control parameter for preparing samples of different lengths while keeping HF acid concentration and ambient temp constant. Samples are fabricated for 4, 5, 6, 7, 8, 10, 20, 30 and 40min etching time and 3D beam profile is obtained for each sample using the near field beam profiler. However only 4, 7, and 40min sample profiles are shown here. Figure 7A(a-II, b-II, c-II) shows the longitudinal cross-section obtained from the 3D profile for corresponding adjacent DSNA. The red line indicates the end-face of DSNA and a linescan from the center along the propagation direction provides the longitudinal intensity profile, Figure 78B(c) for the respective samples. The FWHM DOF obtained from the intensity profiles is 251μm, 413μm and 342μm for 4min, 7min and 40min sample respectively.

Figure 7B (a) shows experimentally obtained intensity distribution inside the air cavity for a 40min etched sample. The focus of microscopic objective is translated inside the cavity with 10μm step size, images are captured at every step and then stacked together to get the complete 3D profile in Fiji. The longitudinal cross-section obtained from the 3D profile provides intensity distribution inside the axicon which is a result of multimodal interference as the air cavity is acting like a multimode waveguide in which light propagation is guided by refection instead of Total Internal Reflection (TIR). This explains the principal of evolution of BB from DSNA.

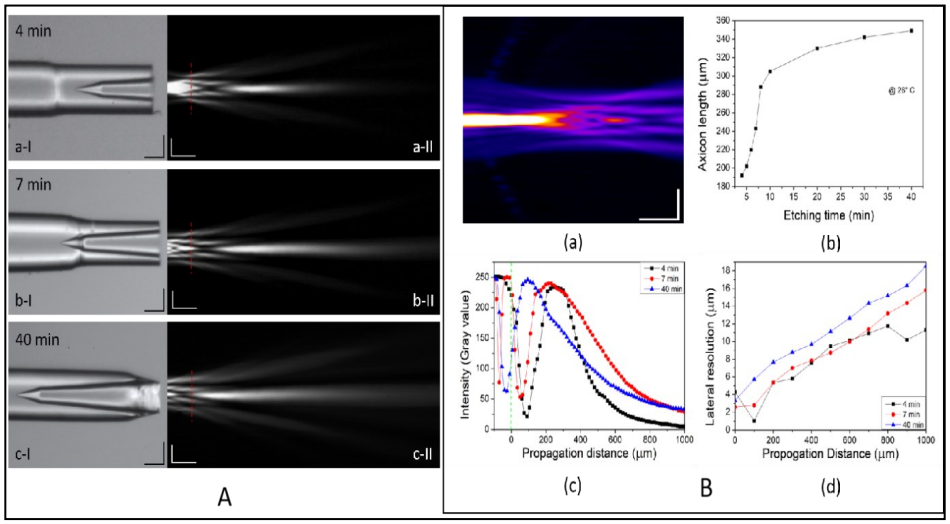

Figure 7 A (a-I, b-I, c-I) are the microscopic images of DSNA fabricated at 4 min, 7 min, 40 min of etching time respectively. The scale bar represents 50μm. (a-II, b-II, c-II) shows the experimentally obtained longitudinal beam profile for the corresponding DSNA (in the left), the red line indicates the end-face of DSNA, the vertical scale bar represents 20μm while the horizontal one represents 100μm.

(B) (a) Experimentally obtained intensity distribution inside the DSNA cavity showing the evolution of beam (from left to right) as a result of multimodal interference. Vertical scale bar represents 20μm while horizontal represents 50μm (b) variation in axicon length with etching time. (c) a comparison of intensity profiles of the beam from the center along the direction of propagation for 4min(black), 7min(red), 40min(blue) etched samples. A shift of the intensity profile towards the end face (green dashed line) is observed with the increase in etching time. (d) a comparison of spot size i.e., FWHM of central spot of the beam for 4min, 7min, 40min etched sample, a positive zero shift is observed between 7min and 40min etched sample.

Figure 7B (c) shows a comparison of these intensity profiles which indicates that the central spot starts forming closer to the end-face as the length of DSNA increases. This results in a positive zero shift in lateral resolution with the increasing length as shown in Figure 7B (d), and also lessen the working distance. Considering these facts, we have chosen 7min etched sample having 243μm AL, ~100μm working distance, a central spot divergence angle of just 0.013°and 413μm FWHM DOF to be ideal for imaging in the current configuration.

Silver coated DSNA for Loss reduction and Energy efficiency

The DSNA exhibit significant loss of optical power due to optics leaking through the cladding which is unable to contribute in the formation of the Bessel beam. The power loss is due to the fact that the modes in the air cavity are guided by reflection and not TIR. Figure 8(a) shows the transverse beam profile from DSNA recorded on a paper screen, inset shows the Bessel beam at the center of the figure as a bright white spot due to camera saturation, the loss can be visualized clearly from the figure. To reduce the losses, we have coated the DSNA with silver nano-particles using the silver mirror reaction with Tollens' reagent and 0.5M Glucose solution. A considerable gain is observed in the BB power as shown in Figure 8 (b). After fabricating DSNA on the fiber tip, it is dipped in 0.5ml Tollens' reagent filled in a vile and 0.1ml of 0.5M Glucose solution is added further to start the reaction. It takes around a minute to complete the reaction, after which the fiber is taken out carefully and washed with running DI water to get rid of any sticked precipitates. The quantitative analysis as shown in Figure 8 (d), indicates that the power loss has been reduced from ~67% in uncoated DSNA to less than 15% in coated DSNA and the conversion efficiency has been increased to nearly 85%.

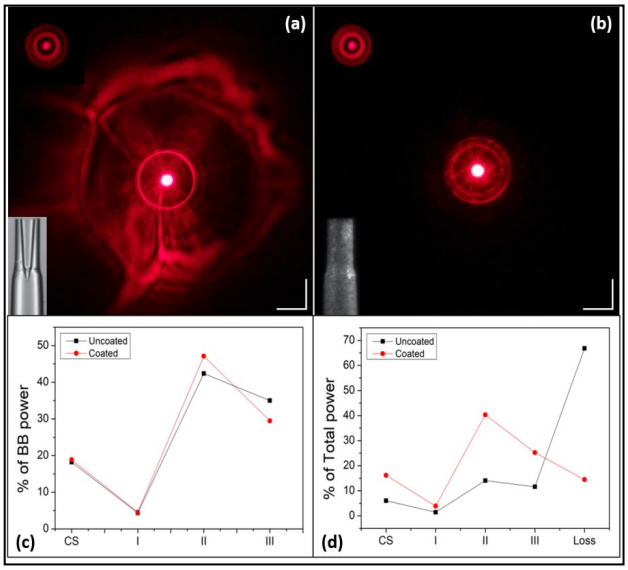

Figure 8 (a) Transverse intensity distribution from 7 min etched DSNA sample, (inset on the upper left shows the Bessel beam visible as a bright spot in the center of the figure due to camera saturation, inset on the bottom left shows the microscopic image of sample), the two rings other than the bright spot come from the leakage. (b) The transverse intensity distribution from silver coated DSNA, (inset on the upper left shows the Bessel beam visible as a bright spot in the center of the figure due to camera saturation, inset on the bottom left shows the microscopic image of coated DSNA), the reduced leakage can be visualized clearly. The scale bar shows 10mm (c) the graph shows power distribution among the central spot and rings wrt. the BB power, (d) the graph shows power distribution among the central spot(CS), rings(I,II,III) and leaked power wrt the total output power.

We have measured the power distribution among the BB rings to find out the energy efficiency of the beam. The quantitative results are shown in Figure 8 (c). The DSNA generated BB contains ~20% power in the central spot and falls in the low Fresnel number. regime with Fresnel number. N~5 and hence can be considered as highly energy-efficient BB [9]. High energy efficiency leads to low SNR penalty as compared to Gaussian beam and provides high contrast images [10].

The measurements are done using a 660nm fiber coupled bench-top laser source and PM100USB power meter with S121C sensor head from Thorlabs. The power meter is translated away from the DSNA tip in order to remove the rings from the sensing area one by one leaving only central spot at the end. The collective power is recorded at every step and then individual power in the rings is calculated.

System performance:

The Lateral resolution obtained from the DSNA generated Bessel beam ranges from 2µm to 15µm for 0 to 1000µm axial distance as shown in Figure 7B(d). We have compared DSNA with cleaved HI780 fiber tip (N.A -0.14) by scanning Group 6 and 7 of the 1951 USAF resolution target to experimentally determine the lateral resolution with 1µm step size in fast as well as the slow axis. The OCT en-face images are shown in Figure 9. The lateral resolution obtained in case of DSNA is 4.38, 4.92 and 6.20µm for 300, 600 and 900µm distance respectively, whereas in case of cleaved tip it is 6.20, 7.81 for 300 and 600µm respectively. The cleaved tip has not been able to resolve any element of 6th and 7th group for 900µm. The lateral resolution is increased considerably from the theoretical value due to high density scanning [11].

To obtain the axial resolution, depth dependent sensitivity and SNR, a broadband silver mirror was employed as the sample which was placed in front of the probe. The axial resolution of the system is obtained from the FWHM of the linear point spread function (PSF). The average axial resolution is found to be ~7.3µm. The depth dependent sensitivity is expressed in terms of measured SNR, which is given by $SNR(dB) = 20\log(I_{samp}/\sigma_{bg})$ where, I_{samp} is the background-subtracted image intensity from the mirror in the sample arm, and σ_{bg} is the standard deviation of the image background intensity [12]. The sensitivity is obtained by adding the an additional ~19 dB loss which was inserted by loosening the connector at the source end to avoid spectrometer saturation[4]. The cleaved tip sensitivity is also obtained in similar way by

adding an additional loss of ~35 dB. A peak sensitivity loss of ~17dB is faced by the DSNA based QBB CPOCT system as compared to the Gaussian beam.

Imaging Results

To assess the imaging performance, we have used standard sample of fresh onion flesh, and scotch tape. The images are shown in Figure 10. Considering a RI of 1.35, ~520µm depth is obtained in the onion flesh and onion rings are distinctly visible, the depth in onion also depends on its quality and can vary from sample to sample. In scotch tape with a measured single layer thickness 60µm, imaging depth of ~780µm is obtained with DSNA whereas, 360µm is obtained with cleaved fiber tip.

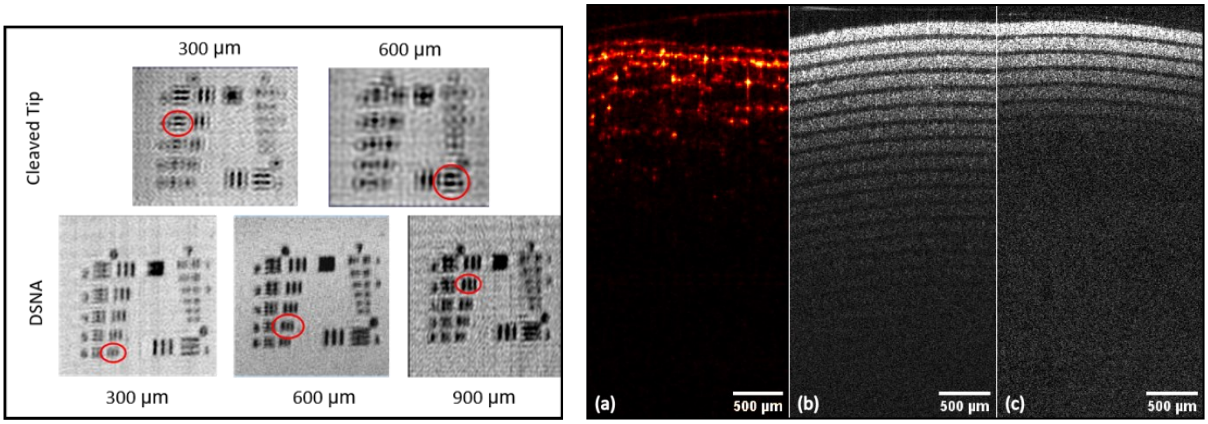

Figure 9. (left) Experimental determination of lateral resolution with varying distance from the probe using a USAF-1951 resolution target 6th and 7th Group. The red circle highlights the resolved element in the group. Figure 10. (right) OCT images of (a) Onion, (b) scotch tape (DSNA), (c) scotch tape(Cleaved tip)

The images show visibly good contrast and focusing in depth due to energy-efficiency and large DOF of the BB. The developed system is also capable of 2D scanning

Conclusion

To conclude, we have developed a novel reflective axicon on the tip of a optical fiber which generates an energy-efficient Bessel beam having nearly 20% power in the central spot. The conversion efficiency has been improved from ~33% to ~85% by reducing the leakage with silver coating. An extended DOF of 413µm which is nearly 15 times as compared to the standard SMF axicon probe is obtained from the DSNA. By compromising a sensitivity loss of 17dB as compared to the gaussian beam A lateral resolution of 6.2µm up to a depth of 0.9mm is achieved with high density scanning which along with the extended DOF of 413µm minimizes the trade-off in OCT imaging. The probe provides high contrast images and can be upgraded to a side viewing endoscopic probe by using a microprism reflector, and is capable of provide excellent imaging with a long range CPOCT system.

References

1. Huang D, Swanson EA, Lin CP, et al. Optical Coherence Tomography HHS Public Access. Science (80 -). 1991;254(5035):1178-1181. doi:10.1002/jcp.24872.The
2. Kim JH, Han JH, Jeong J. Common-path optical coherence tomography using a conical-frustum-tip fiber probe. IEEE J Sel Top Quantum Electron. 2014;20(2). doi:10.1109/JSTQE.2013.2277817
3. Weber N, Spether D, Seifert A, Zappe H. Highly compact imaging using Bessel beams generated by ultraminiaturized multi-micro-axicon systems. J Opt Soc Am A. 2012;29(5):808. doi:10.1364/josaa.29.000808
4. Wang W, Wang G, Ma J, Cheng L, Guan B-O. Miniature all-fiber axicon probe with extended Bessel focus for optical coherence tomography. Opt Express. 2019;27(2):358. doi:10.1364/oe.27.000358
5. Lorenser D, Yang X, Sampson DD. Ultrathin fiber probes with extended depth of focus for optical co-

herence tomography. Opt Lett. 2012;37(10):1616. doi:10.1364/OL.37.001616
6. Qiu J, Shen Y, Shangguan Z, et al. All-fiber probe for optical coherence tomography with an extended depth of focus by a high-efficient fiber-based filter. Opt Commun. 2018;413(December 2017):276-282. doi:10.1016/j.optcom.2017.12.048
7. Yin B, Hyun C, Gardecki JA, Tearney GJ. Extended depth of focus for coherence-based cellular imaging. Optica. 2017;4(8):959. doi:10.1364/OPTICA.4.000959
8. McLeod JH. The Axicon: A New Type of Optical Element. J Opt Soc Am. 1954;44(8):592. doi:10.1364/JOSA.44.000592
9. Lorenser D, Christian Singe C, Curatolo A, Sampson DD. Energy-efficient low-Fresnel-number Bessel beams and their application in optical coherence tomography. Opt Lett. 2014;39(3):548. doi:10.1364/ol.39.000548
10. Curatolo A, Munro PRT, Lorenser D, et al. Quantifying the influence of Bessel beams on image quality in optical coherence tomography. Sci Rep. 2016;6:1-12. doi:10.1038/srep23483
11. Shen K, Lu H, Baig S, Wang MR. Improving lateral resolution and image quality of optical coherence tomography by the multi-frame superresolution technique for 3D tissue imaging. Biomed Opt Express. 2017;8(11):4887. doi:10.1364/boe.8.004887
12. Agrawal A, Pfefer TJ, Woolliams PD, Tomlins PH, Nehmetallah G. Methods to assess sensitivity of optical coherence tomography systems. Biomed Opt Express. 2017;8(2):902-917.

Generation, Modulation and Detection of Phase Structured Laser Beams for Sensing Application

Pritam P Shetty

Indian Institute of Information Technology, Design and Manufacturing, Kancheepuram, Tamil Nadu

Abstract

Electromagnetic radiation carries energy and momentum. The momentum may involve linear and angular part. Light from laser can carry angular momentum of two types called spin angular momentum associated to polarization and orbital angular momentum associated to spatial distribution. Circularly polarized beam carries spin angular momentum (SAM) and Laguerre-Gaussian (LG) beam carries orbital angular momentum (OAM). In this work, various viable methods for LG beam generation is proposed and demonstrated. The tunability of thermal lens in nanofluid by electrical or optical means allowed for dynamic lenses for beam shaping. Further a new type of common path interferometer called Thermo-optic refraction interferometer (TORI) is proposed. LG beam propagation through milk as medium is studied as a function of its phase structure deterioration. The deterioration in phase structure is quantified and used to measure fat content in milk.

Objectives

The objectives of the research work are as follows:

a. To design and develop an economical method for generating Laguerre-Gaussian (LG) beams with variable topological charges.
b. To understand the properties of Laguerre Gaussian beams and their interaction with different media as a function of their topological charge.
c. To develop a sensing modality using LG beam as illuminating source.

Existing Gaps Which Were Bridged

The research gaps that were bridged in the work:

a. The accessibility to affordable phase and diffractive elements is limited owing to the fabrication complexity and associated materials.
b. Low cost and tunable solution for Hermite Gaussian like beam generation other than spatial light modulator and digital micromirror device.
c. Optically induced thermal lenses in nanofluids can be a potential method for dynamic lens system. The control and tunability of these thermal lenses are not studied well. Further, the electrical modality for thermal lens generation is not well explored for beam shaping.
d. Astigmatic Optical mode converters are useful for beam mode conversion with high efficiency. But the lenses used in such mode converters are static. A dynamically tunable lens by means of optical and electrical modality can allow switchable mode conversion.
e. A new type of common path interferometry is proposed which is not limited by its usage due to small sample and reference beam separation.

Most Important Contributions

Generation of the Laguerre Gaussian beam using simple optical elements

PET sheets are most commonly found plastic sheets used as overhead projector sheets. These sheets are affordable and available in various thickness. The refractive index of PET transparent sheets is 1.5651. This is also flexible for different azimuthal angles which is important for generating OAM beams. PET sheets allow clean shear cuts with fine edges which is important to have a clean beam profile after transmission. Further, the absorption is minimum in the visible spectrum (450nm to 700nm) which will cause less impact on propagation losses of the beam. PET sheets are cut in square from using scissors and mounted over 3D printed holders as shown in Figure. The screw can be used for adjusting the spiral phase to achieve tunable topological charge of LG beams. The angles were changed upto 10°.

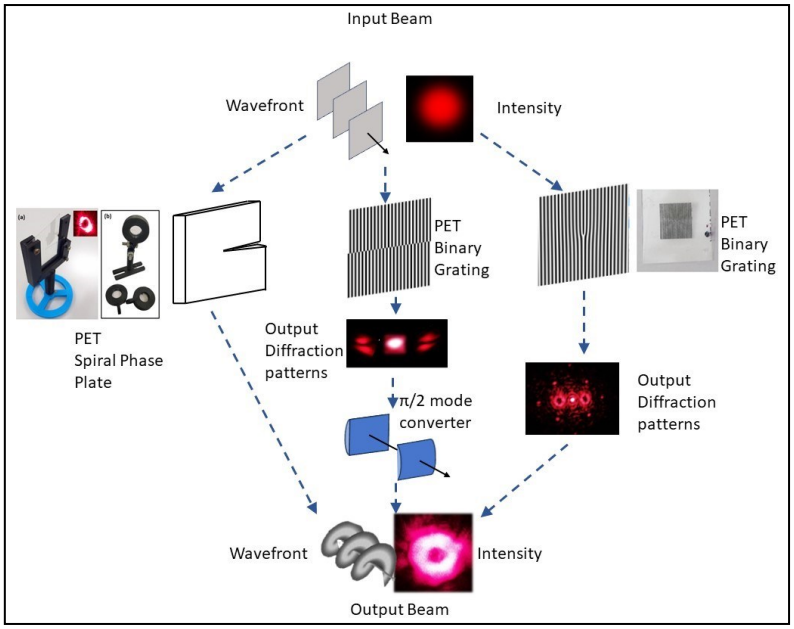

Figure 1: Methods to generate Laguerre Gaussian beam.

Binary amplitude gratings are diffractive optical elements with regions of high and low intensity transmission. The diffraction and the output beam pattern in these gratings can be controlled using the parameters such as pitch, relative fringe shifts, duty cycle of the grating material of grating substrate. This gives better control to generate low topological charges of orbital angular momentum of beams, that include Hermite Gaussian and Laguerre gaussian beams.

A phenomenon to generate Hermite Gaussian structured beams

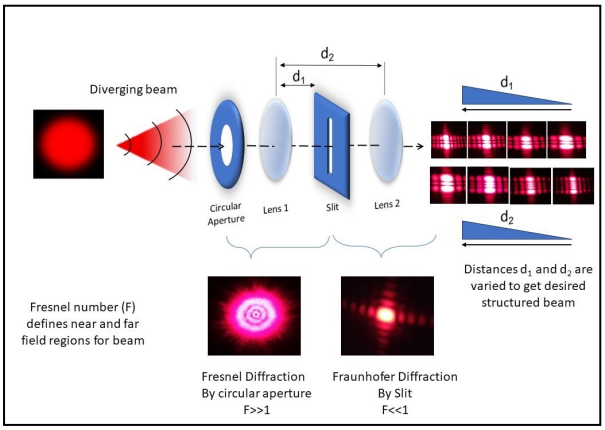

Figure 2: Synergic Fresnel and Fraunhofer diffraction

Diffraction, arising from the wave-like nature of light, manifested at edges. The well-known diffraction phenomena, namely Fresnel and Fraunhofer, have diverse individual applications. However, the combined effects of these two phenomena have not been thoroughly studied and understood, despite their importance in comprehending compound optical instruments. This research investigates and demonstrates the synergistic patterns resulting from the combination of Fresnel and Fraunhofer diffractions. The observed combined diffraction patterns exhibit characteristics similar to Hermite-Gaussian Beam intensity distributions, as validated through both simulations and experimental results. This work contributes to a deeper understanding of complex diffraction in optical instruments and offers a pathway for robust fabrication of micro gratings[1].

Imaging and measurement of thermal lens region within nanofluid

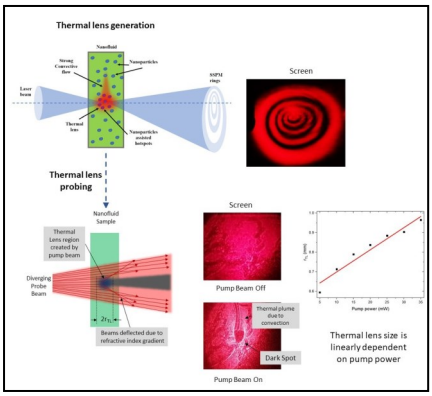

Figure 3: Thermal lens generation in nanofluid and its probing

The remarkable nonlinear optical response exhibited by two-dimensional (2D) nanomaterials such as Molybdenum disulfide (MoS2) has garnered significant attention. In this study, we investigate the formation of thermal lenses in dispersions of MoS2 nanoflakes using a pump-probe configuration with mode mismatch. By observing the intensity patterns of the pump and probe beams, we gain visual insights into the temporal evolution of photothermal lens formation. The influence of MoS2 nanoflake concentration on the thermo-optic properties of the dispersions is explored using thermal lens spectroscopy. Additionally, a novel technique based on thermo-optic refraction is proposed for measuring the size of the thermal lens region. It is observed that the size of the thermal lens region increases with higher pump power. Leveraging the observed thermal lens modulation, we successfully demonstrate a "normally on" all-optical switch that exhibits exceptional modulation of the output beam signal by the pump beam[2].

Near vicinity thermal lens optics with respect to Laguerre Gaussian beams

This study highlights the importance of temporally switchable optical mode conversion in optical communication and computing applications. We have successfully developed an optically switchable mode converter based on thermo-optic refraction. To achieve this, we utilized MoS2 nanofluid as medium, where a

thermal microlens is formed by focusing a laser beam (referred to as the pump beam). Above the focal point of the pump beam within the nanofluid, a convective thermal plume is generated, which acts as an astigmatic thermal lens. Through experimentation, it was observed that the thermal lens causes the conversion of Laguerre-Gaussian (LG) beams into Hermite-Gaussian (HG) beams, and vice versa, when they pass through it.

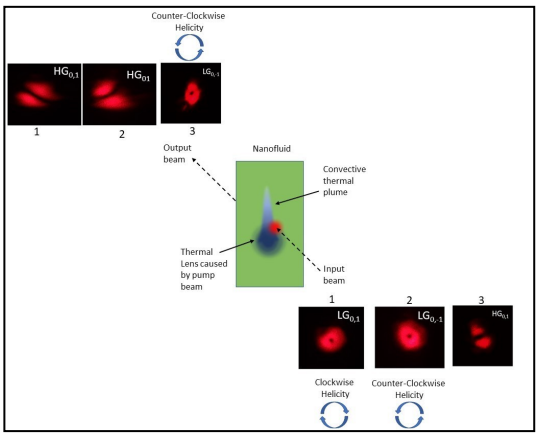

Figure 4: Mode conversion after transmission through thermal lens

Consequently, this mode converter enables the easy determination of the topological charge of the LG beam. A theoretical explanation for this mode transformation by considering the different optical paths experienced by the Fourier components of the LG beam as it propagates through the convective plume is provided[3].

An electrically controllable mode converter for topological charge measurement

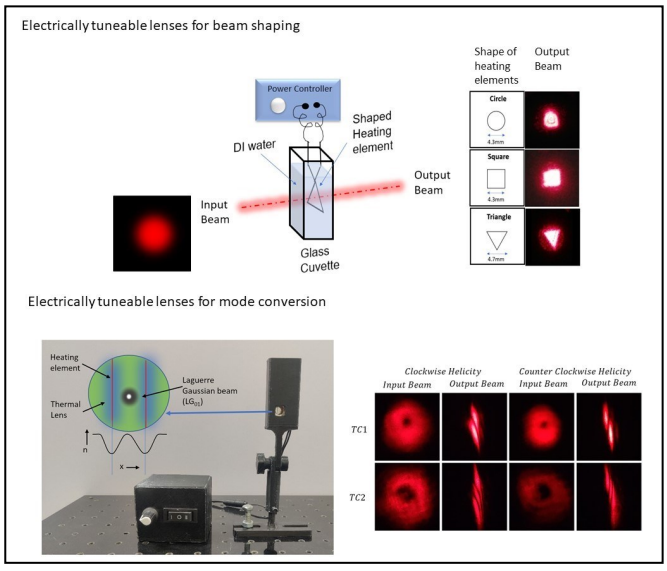

Figure 5: Electrically generated thermal lenses for beam structuring and mode conversion.

Heating elements with distinctive shapes immersed in a fluid have the ability to generate thermal lenses in their vicinity. The strength of these thermal lenses is directly proportional to the current passing through the heating elements. By bending the elements into common shapes such as squares, circles, and triangles, structured beams can be generated. Moreover, when multiple heating elements are arranged in a parallel configuration, a cylindrical lens-like profile is formed within the liquid medium. This profile can be effectively utilized for mode conversion purposes.

A new common path interferometric method called Thermo-optic refraction interferometry and application to milk fat detection.

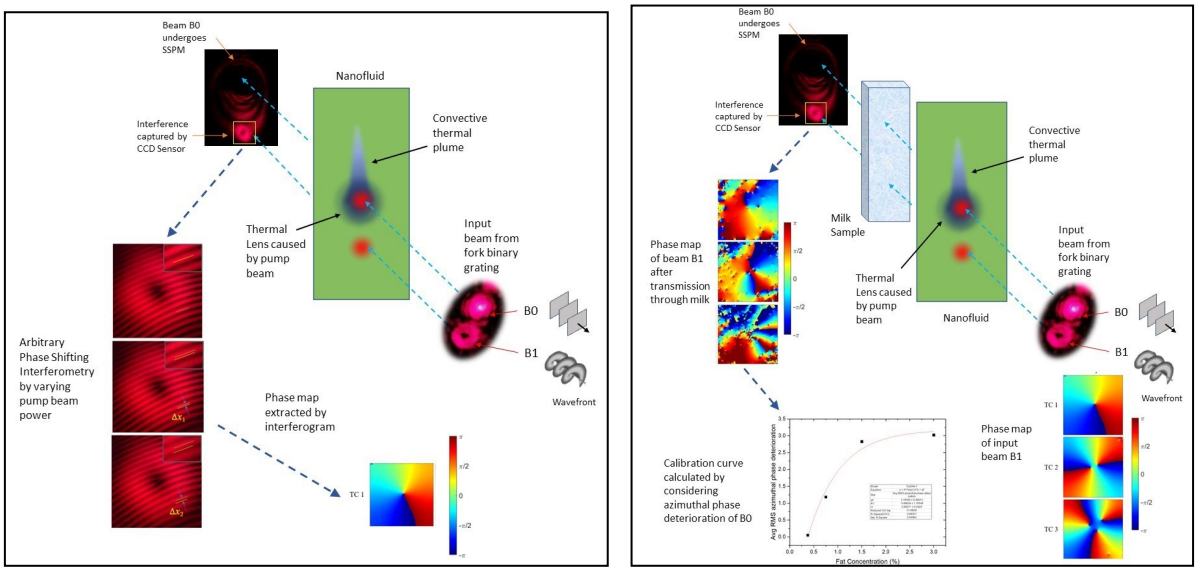

Figure 6: Thermo-optic refraction interferometer (left panel). Milk Fat estimation using Thermo optic refraction interferometer (right panel)

Common path interferometers (CPI) are highly valuable for their compactness and ability to resist vibrations. However, a common challenge in CPI arises from the small separation between the reference and sample beams. This limitation makes it difficult to send a reference beam through a sample, hindering the ability to study the interaction of beams with materials based on their phase structure. This research introduces a promising solution that opens up new possibilities for interferometry. The study proposes and demonstrates a novel approach utilizing thermo-optic refraction to enable both beams to pass through the sample and investigate the phase degradation resulting from their relative interaction within the material medium.

Termed thermo-optic refraction interferometry (TORI), this technique leverages the phenomenon of thermal lensing to superpose a higher order vortex beam with a nonvortex beam. By optically pumping the non -vortex beam, controlled expansion is induced. The interaction between the expanding non-vortex beam and the vortex beam within the sample generates an output interferogram. Analyzing the phase deterioration exhibited in the output interferogram provides insights into the medium-induced phase changes.

To illustrate the effectiveness of TORI, the experiments were conducted using milk samples and measured the root mean square (RMS) azimuthal phase deterioration of the OAM beam. The results showcase the potential of this technique to study phase variations driven by the medium. By overcoming the limitations of traditional CPI setups, this innovative approach broadens the capabilities of interferometric analysis[4].

References

1. P.P. Shetty et. al., Opt. Laser Technol. 130(April), 106340 (2020).
2. P.P. Shetty et. al., Opt. Mater. (Amst). 112, 110777 (2021).
3. P.P. Shetty et. al., J. Quant. Spectrosc. Radiat. Transf. 274, 107867 (2021).
4. P.P. Shetty et. al., J. Opt. 25(8), 085601 (2023).

Generation and Characterization of Spatially Controlled Structured Light with Exotic Propagation Properties

Vasu Dev

Department of Physics, Indian Institute of Technology Ropar, Rupnagar, Punjab 140001, India.

Light possesses various spatial and temporal degrees of freedom, such as amplitude, phase, polarization, time, and frequency. Controlling these aspects for generating light with complex field distributions possessing exotic propagation properties, has renewed its interest in numerous applications both in fundamental science as well in applied fields[1]. Due to this there has been growing interest in synthesizing such complex light field distributions, also called as structured light. Typically, the output from a laser consists of a Gaussian distribution, which exhibits physical limitations for various applications. However, with continuous advancements, it has become possible to control the distribution of light in different degrees of freedom[2]. In this thesis, our aim has been to develop simple, cost-effective, and efficient outer-cavity and intracavity methods for the generation and characterization of novel spatially structured light with customised intensity and phase distributions as well as possessing exotic propagation properties. In addition to these, our emphasis has also been to improve the quality, resolution, resilience against perturbations, and spectral range of spatially controlled structured light.

Chapter 1 is an introduction to the thesis, where we begin with the role of structured light in the modern world by mentioning its applications in fundamental and applied fields where conventional Gaussian beams pose physical limitations. We have discussed various types of spatially structured light along with their propagation properties, obtained by tailoring light in its various spatial degrees of freedom[1,2,3]. Further, we have discussed the generation of spatially structured light based on various outer-cavity and intracavity methods[3]. We have also described the analytical and numerical methods for modelling the laser cavities as well as the propagation and quantification of spatially structured light. We have also provided a brief overview of spatial light modulators including the mechanism for modulating light in the amplitude and phase degrees of freedom.

In **Chapter 2**, we have presented an outer-cavity method for tailoring the light in amplitude degree of freedom to generate high-quality uniform-intensity beams with customized shapes, using diffractive optical elements (DOEs). The phase of DOEs is obtained by an iterative method (modified Gerchberg-Saxton algorithm) that involves spatial Fourier filtering (Fig. 1)[4]. The obtained DOEs consist of a simple design (smooth phase distribution), which makes them easier to fabricate. An input laser beam with Gaussian intensity distribution illuminates the DOE, and after propagating a certain distance (working distance) transforms into the desired uniform-intensity output beams with customized shapes such as square, annular, rectangular, hollow square, and plus spatial shapes. The quality of the output beams is quantified by calculating root mean square error (RMSE) with respect to the ideal beams. We have performed a detailed robustness analysis on the quality of shaped output beams against various types of imperfections in an input beam, such as misalignment with respect to DOE, presence of speckle noise, asymmetry, presence of higher order transverse modes, and mismatch of beam sizes. We have found that the shaped output beams with reasonably good quality are obtained over a broad range of imperfections. However, in the case of speckle noise, the quality of shaped output beams can be further improved by an additional external spatial Fourier filter of suitable transmission function. Furthermore, to investigate spectral properties of method, we have designed a DOE for a particular wavelength and illuminated it with an input beam over a broad range of wavelengths. We have found that the quality of shaped output beams remains excellent over a broad spectral range. However, the working distance decreases with an increase in the wavelength[4].

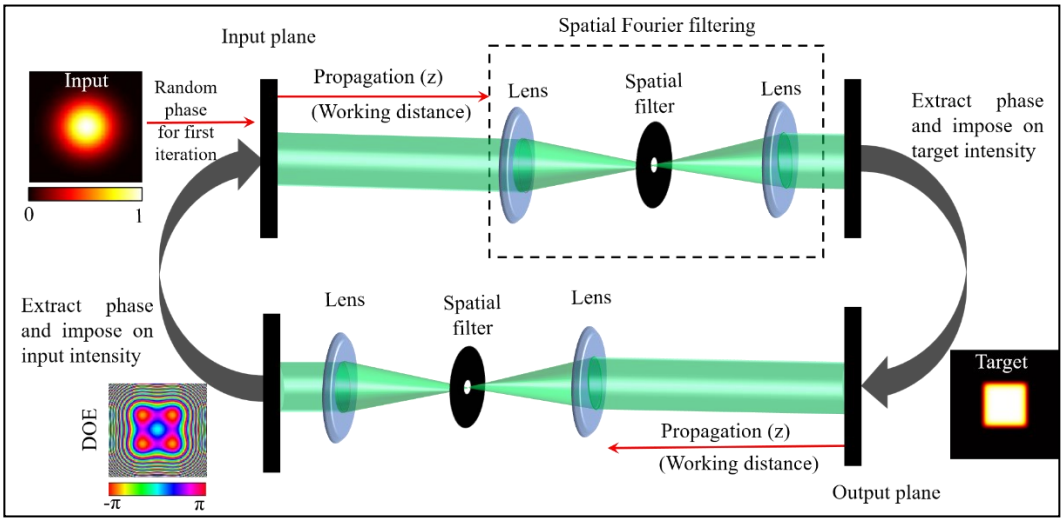

Figure 1. Modified Gerchberg-Saxton algorithm to obtain phase distribution of DOE.

In **Chapter 3**, we have presented tailoring of light in the amplitude and phase degrees of freedom for generating special type of structured light (called aberration laser beams (ALBs)) containing multiple bright lobes and possessing unique propagation features, such as autofocusing and self-healing in both free space as well as in turbulent media[5]. The ALBs are generated, based on an outer-cavity method, using a DOE whose phase distribution consists of radial and periodic angular dependence. We have presented a detailed mathematical formulation for describing the propagation of ALBs in turbulent media by solving Huygen-Fresnel integral using stationary phase method. We have found that the presence of turbulence leads to distortions in the spatial intensity distribution of ALBs, as well as causes beam wandering. The effect of turbulence on the propagation of ALBs is quantified by calculating overlap integral with respect to ALB in free space. The ALBs possess good autofocusing properties both in free space as well as in turbulent media, where on-axis peak intensity becomes maximum with tight focusing. In particular, the autofocusing properties of ALBs remain invariant, irrespective of turbulence strength. The autofocusing distance can be controlled from any small to large values, by controlling the ALB parameters. Further, we have also investigated the spectral dependence of autofocusing of ALBs in a turbulent medium and found that autofocusing distance does not depend on the turbulence, however, it decreases with an increase in wavelength. Furthermore, we have performed a detailed investigation of self-healing of ALBs both in free space as well as in turbulent media of different turbulence strengths. We have found that, both in free space and turbulent media, the truncated ALB self-heals by redistributing the intensity within the beam. The ALBs self-heal reasonably well even or a large amount of truncation (~ 60%). The maximum self-healing always occurs at autofocusing distance, which remains invariant irrespective of the amount of truncation and strength of turbulence. A good agreement between theory, simulations, and experimental results is obtained[5].

In **Chapter 4**, we have presented the generation of asymmetric aberration laser beams (aALBs) with controlled intensity distribution, based on an outer-cavity method employing a DOE with phase asymmetry[6]. We have introduced the phase asymmetry in DOE by shifting coordinates in a complex plane, which provides additional control over spatial intensity distribution of beam. We have derived the mathematical formulations for general aALBs as well as the special cases of it. We have shown that in an ideal ALB containing equal intensity bright lobes (Fig. 2(a)), by introducing asymmetry most of the intensity can be transferred to any one of the single lobe, and generates a high-energy density (Figs. 2(b)-2(d)). Further, we have explored the mechanism of asymmetric control of intensity in aALBs, and found that the asymmetry parameters control the position of indeterminate phase point of the trigonometric phase term in aALB, which creates a controlled asymmetric intensity distribution in the near-field plane. As a result of propagation, it provides a controlled transfer of intensity within aALB. In general, for a given parameter m of aALB, the precise spatial location of high-energy density lobe can be controlled by the precise variation in the asymmetry parameters (w, β), and we have determined empirical relations for them. We have found that for the specific values of β and m, the intensity in the high-energy-density lobe can be enhanced by

several times the intensity in other lobes (Figs. 2(b)-2(d)). Where amount of intensity in a particular lobe is calculated by the method of diffraction efficiency which is the ratio of intensity in a lobe to the total intensity of the beam. Further, we have investigated the propagation of aALBs, and found that similar to ALBs, the aALBs possess good autofocusing properties, which are not affected by the asymmetry. The autofocusing distance in aALBs can be varied from small to large values by changing the beam parameters. We have found a good agreement between the experimental results and numerical simulations[6].

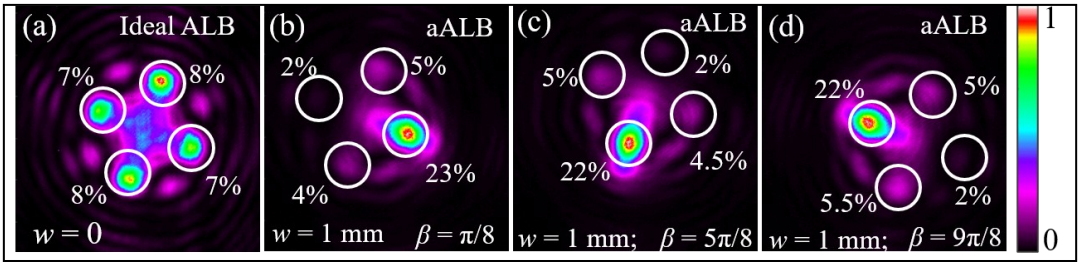

Figure 2 Experimental results. Intensity distributions of (a) ideal ALB and (b)-(c) asymmetric ALBs for different values of β. White circles mark the location of each lobe along with its diffraction efficiency.

In **Chapter 5**, we have presented the generation of high-energy densities by suppression of higher-order sidelobes in the far-field of phase-locked lasers. We have generated an array of lasers in various 1D and 2D array geometries in a degenerate cavity and phase-locked them in the in-phase [out-of-phase] configuration with the far-field coupling using Gaussian apodizer [binary circular aperture][7]. Owing to the non-uniform amplitude and definite geometry, the far-field of phase-locked lasers consists of higher-order sidelobes. These sidelobes contain a significant amount of energy, which limits the use of an output beam for high-power applications. Our method relies on modifying the combined field (near-field and far-field) distribution of phase-locked lasers to obtain uniform amplitude and phase distributions in a near-field plane, which enables the formation of a high-power density lobe (zeroth-order) in the far-field. We have demonstrated our method for phase-locked lasers in various array geometries, such as square, triangular, Kagome, random, and 1D ring. The results are quantified by calculating the diffraction efficiency of the zeroth-order lobe. It is found that for long-range in-phase locked laser arrays, the diffraction efficiency of the zeroth-order lobe can be improved by several factors ($\sim 3-4$). The improved diffraction efficiencies are found to be in a range of $90\% - 95\%$ (for 2D arrays) and $\sim 75\%$ (for 1D ring array). Further, we have analyzed the robustness of our method against various factors, such as the range of phase-locking, system size, and presence of topological defects in a 1D ring array. We have also investigated our method for out-of-phase locked lasers in a square array, where the zeroth-order has no intensity. We have obtained a high-energy-density zeroth-order lobe with a high diffraction efficiency of 81%[7].

In **Chapter 6**, we have presented a novel and efficient intra-cavity method for the generation of high-power discrete optical vortices with precisely controlled topological charges (l) by phase-locking one-dimensional (1D) ring array of lasers in a degenerate cavity that involves spatial Fourier filtering[8]. Owing to the special geometry of a degenerate cavity, it enables an efficient formation of a 1D ring array of lasers, where each laser consists of a nearly fundamental Gaussian distribution, and is independent from each other. Initially, the lasers consist of random phase distribution and are equally probable. To force them into a desired phase -locked state of optical vortex configuration, we employ a special Fourier filter (amplitude mask) at the Fourier plane inside the cavity (Fig. 3(a)). The spatial Fourier filtering mechanism helps to eliminate the undesired phase distributions by introducing additional losses to them, thereby, enabling the lasers to find a correct phase distribution in the form of a desired discrete optical vortex (Fig. 3). We have performed a detailed investigation on the propagation, such as divergence and self-healing, of discrete optical vortices, and compared them with the conventional continuous optical vortices. We have found that for a given system size (number of lasers) and fixed distance between the neighboring lasers, the size of a discrete optical vortex and its divergence does not depend on the topological charge, which is found to be different than the conventional continuous optical vortices (Laguerre-Gaussian/Bessel-Gaussian beams). Further, we have performed a detailed investigation of self-healing by partially truncating a discrete optical vortex in the

waist plane (z = 0) and propagated plane (z > 0). To quantify the self-healing, we have calculated an overlap integral to analyze the similarities between the self-healed and ideal discrete optical vortices. The results show that partially truncated discrete optical vortex can self-heal reasonably well. Moreover, we have found that the self-healing distance increases with the value of topological charge of discrete optical vortex. The self-healing distance is also found to be dependent on the amount of blocking, particularly, it increases with an increase in the amount of blocking. We have obtained a good agreement between the analytical and numerical results[8].

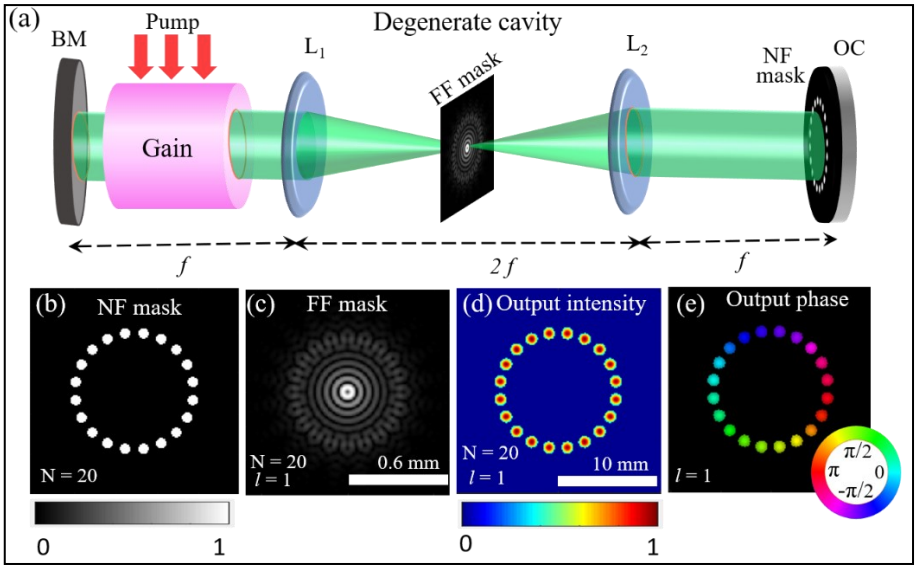

Figure 3 (a) Schematic of the degenerate cavity. Transmission functions of (b) near-field mask and (c) far-field mask. (d)-(e) Intensity and phase distributions of generated discrete vortex with N = 20 and l = 1.

In **Chapter 7**, we present a novel and efficient method for accurate determination of magnitude and sign of topological charge (l) of an unknown discrete optical vortex, which is formed by an array of lasers in a 1D ring geometry[9]. We have presented a simple analytical formulation of working principle of our method. It relies on measuring the interference pattern of a discrete optical vortex, which is obtained by interfering a single selected laser with itself and with all the other lasers in a 1D ring array, using a Mach-Zhender interferometer (Figs. 4(a)-4(c)). The interference pattern is quantified by analyzing the fringe visibility at each laser in a 1D ring array. The discrete laser arrays with l = 0 and l ≠ 0 have different phase distributions, thus produce interference patterns with shifted interference fringes. The averaging of these phase-shifted interference patterns gives rise to a variation in the fringe visibility as a function of laser number in the discrete optical vortex, thus enabling the identification of l (Figs.4(c)-4(f)). The magnitude of l of a discrete optical vortex is found to be proportional to the number of dips observed in the fringe visibility curve (Fig. 4(g)). Further, for an accurate determination of sign of an unknown discrete optical vortex (l ≠ 0), we have averaged the interference pattern of it with the interference pattern of known l = +1. The number of dips in the fringe visibility curve increases by one for a positive value of l and increases by one for a negative value of l. We have also investigated the robustness of our method against the presence of phase disorder that may occur due to the presence of aberrations in a system. It is found that the phase disorder does not affect an accurate measurement of the topological charge of an unknown discrete optical vortex. We have demonstrated our method for discrete optical vortices with topological charges from small to large values and accurately determined their magnitude and sign. We have provided a theoretical description along with numerical and experimental results, and found an excellent agreement between them, indicating that our method is accurate and highly efficient[9].

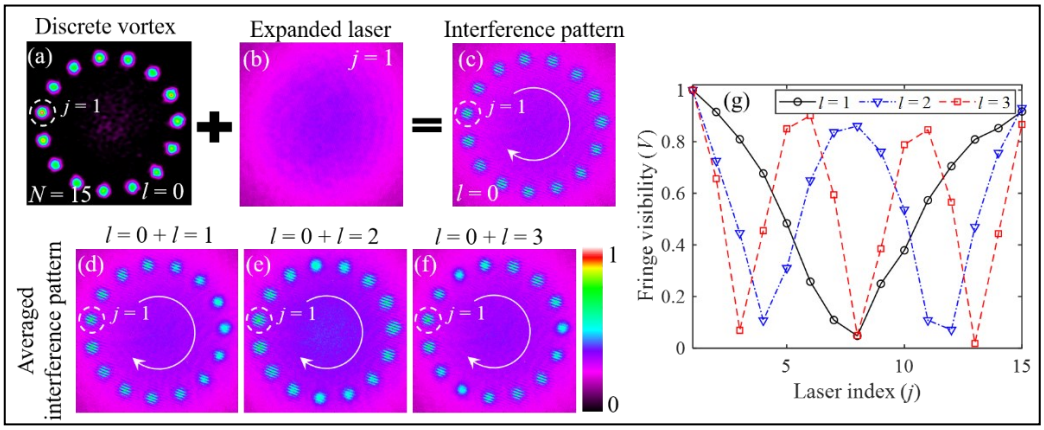

Figure 4 Experimental results for determining TC of DOV of system size N = 15 and l=1-3.

At the end, the conclusive chapter (**Chapter 8**) contains a summary of the results discussed in the aforementioned main chapters of the thesis. We also consider some future directions that might aid in gaining a deeper understanding of structured light and its propagation properties.

References

1. F. M. Dickey and S. C. Holswade, Laser Beam Shaping – Theory and Techniques (Marcel Dekker, 2000).
2. A. Forbes, M de Oliveira, M.R. Dennis, Nat. Photon. 15, 253 (2021).
3. A. Forbes, Laser Photonics Rev. 13, 1900140 (2019).
4. Vasu Dev, Andra N. K. Reddy, and Vishwa Pal, Opt. Commun. 475, 126226 (2020).
5. Vasu Dev, et al., Phys. Rev. Appl. 16, 014061(2021).
6. Sachleen Singh, Vasu Dev, and Vishwa Pal, J. Opt. 24 125601, (2022).
7. Vasu Dev, Andra N. K. Reddy, and Vishwa Pal, J. Opt. Soc. Am. B 39, 2254 (2022).
8. Vasu Dev, and Vishwa Pal, J. Opt. Soc. Am. B 38, 3683 (2021).
9. Vasu Dev and Vishwa Pal, Phys. Rev. Appl. 20, 034071 (2023).

A study of optical properties of Europium (Eu) based rare earth nanomaterial and their applications

Arpita Dwivedi

Department of Physics, Institute of Science, Banaras Hindu University, Varanasi-221005

Introduction :

Luminescence is the emission of electromagnetic radiation (photon) usually in the visible range, which involved the radiative transition between energy levels of the atoms, molecules and materials. Luminescent materials called phosphors, are defined as solids that can absorb, and convert certain types of energy into radiation of light [1-3].

In the last few years, rare earth (RE) doped luminescent material are widely explored by researcher due to its attractive optical features. The rare earth doped nanophosphors materials have good thermal stability, excellent chemical properties fast response, environmental safety, sustaining and sharp emission bands as well as luminescence efficiency with color purity. These properties in rare earths are arising due to its par-

tially filled 4f electrons which make it superior over the other nanophosphor materials. Hence, rare earth doped nanophosphor materials are extensively used is numerous applications. The f-f transitions in rare earth being forbidden by La-Porte parity, show poor absorptions and low quantum yields, when lanthanides are doped in a host matrix, perturbations caused by the host in the vicinity of the dopant induce mixing of the odd parity f-orbitals of the lanthanide with even parity d or p orbitals of host. The mixing relaxes the selection rules and enhances absorption and emission spectra observed [3-5]. The direct excitation of lanthanoids is very inefficient it can be enhanced by attachment of light harvesting chromophore which improve the absorption of light, and transfer energy to lanthanoids through 'antenna effect'. The complex of europium ion (Eu^{3+}) with crystalline host matrices or glass, also exhibit this photoluminescence property. Further, to enhance the optical properties of rare earth the impurity elements elements/ions have used extensively. These impurity materials are generally rare earth or transition metal ions, alkali metal ions and alkali earth metal ions, there are terms as "activators". Activators modify the local crystal field to enhance the emission intensity significantly. Among the various rare-earth ions, Europium (Eu^{3+}) ion has been significant an activator, and shows intense red emission in a narrow band at 613 nm due to electric dipole transition ($^5D_0 \rightarrow {}^7F_2$) excited with UV light. Furthermore, the well-regulated method for the preparation of RE-doped nanoparticles is more important. As the properties of nanomaterials depend on their novel shape and size. Due to their extremely small size, these materials have relatively large specific surface area. At small sizes, significant fraction of dopant ions is present near the surface regions, and behave differently from their bulk's materials. Smaller size of nanostructured luminescent materials enabling penetration of low energy electrons have made them attractive nanocrystalline materials and play an outstanding role in display devices, optical telecommunications, solid state laser, biosensor, etc. applications [5-12].

In this thesis, different types of Eu^{3+} doped fluorescent nanomaterials have been synthesized to explore it optical properties and its applicability in LEDs, display devices, solid state laser, biosensor, and as sensing probe. The detailed outcome of the optical properties and synthesised nanophosphor with applications are further described chapter wise. The present thesis is organized into seven working chapters as follows:

Chapter 1: The literature review, origin and its importance of lanthanides and Eu-doped materials has been given in this chapter. In this chapter, history and the basic information about luminescence, the rare-earth element and the development in the field of luminescent materials are provided. This chapter also provides the fundamental knowledge of spectroscopic terms and few important definitions, which are necessary to understand the rest of the discussions. The optical properties of the rare earth doped materials energy transfer mechanism have been discussed in brief. Since nanomaterials are used in a variety of applications (such as displays, optoelectronic devices, biosensor, organic light emitting diodes etc.), therefore a brief discussion about their use is also presented. Finally, the aim and outline of the thesis is presented.

Chapter 2: This chapter explains briefly about various experimental techniques and synthesis methods which are used throughout the study to produce our results. The characterization techniques like X-ray diffraction (XRD), scanning electron microscopy (SEM), transmission electron microscopy (TEM) and high resolution-TEM (HR-TEM) have been used for morphology and microstructural details. Raman spectroscopy (for structural properties) and Energy Dispersive X-ray Spectroscopy (EDS) have been used for elemental analysis. Apart from this, other characterization technique like UV-Vis, Fourier Transform Infra-Red spectroscopy (FTIR) and Photoluminescence (PL), and Lifetime measurement have been used for optical analysis of synthesized materials.

Chapter 3: In this chapter, synthesis and characterization of $Eu:Y_2O_3$ nanophosphor (EYN) and EYN dispersed polyvinyl alcohol (PVA) fluorescent film (EYF), with subsequent studies of sensing behavior for the detection of arsenic ions (As^{3+}) in real water samples has been discussed. Fluorescence intensities of EYF have been found to decrease quickly with As^{3+} ion contents due to the reduction in the population of Eu^{3+} ions in the $^5D_0$ level due to formation of direct or indirect coordinate bonds with Eu^{3+}. The limit of detection obtains as 57.5 ng/L (0.057 ppb) with 0-100 µg/L linear range respectively. Moreover, sensing probe has been examined with different river water samples. Furthermore, the EYF sensing probe shows a visible color change with the contaminated water under UV-Vis light which useful for the onsite detection

of arsenic concentration. Hence, EYF endows a promising pathway for a portable, low-cost sensing device for the detection of arsenic ions in real water samples.

Chapter 4: In this chapter, we have synthesised $Y_2O_3:Eu^{3+}$, xCa^{2+} (X = 0, 1, 3, 5, 7, 9, 11% of Ca^{2+}) nanophosphor through a facile solution combustion method. The emission intensity of $Y_2O_3:Eu^{3+}$, xCa^{2+} (5 mole %) has been increased 8-fold as compared to $Eu:Y_2O_3$. Doping with Ca^{2+} ions enhance the emission intensity of $Eu:Y_2O_3$ nanophosphors due to an increase in energy transfer in $Ca^{2+}\rightarrow Eu^{3+}$ through asymmetry in the crystal field, and by introduction of radiative defect centers through oxygen vacancies in the yttria matrix. Nanophosphor also reveals high thermal stability, and quantum yield as estimating activation energy 0.25 eV, and 81%, respectively. CIE, CCT, and color purity values (>98 %) show an improved red-emitting nanophosphor in the warm region of light, makes this material superior for various other optoelectronics devices.

Chapter 4 (b): In second part of the fourth chapter, the $Y_2O_3:Eu^{3+}$, xCa^{2+} (5 mole %) nanophosphor, is used as a sensitive and selective probe for the detection of Fe^{3+} ions. Under ideal conditions (pH 4-10), the turnoff-fluorescence-based proposed probe exhibits a low limit of detection (63.2 nM) with a linear range of 10-90 M and is unaffected by the interference of various other metal/biological reactive species. As a result, the proposed sensing probe, which demonstrated significant results with real water samples, iron tablets, and human blood serum, can be utilized in the medical, pharmaceutical, and industrial sectors for the measurement and analysis of iron concentration in wastewater.

Chapter 5: In the present chapter, we have discussed variation of photoluminescence emission intensity, energy transfer and multicolor tunability properties in a series of Eu^{3+} ions doped $Ca_{0.05}Y_{1.93-x}O_3:0.02Ho^{3+}$ (CYO:Ho^{3+},xEu^{3+}) nanophosphors. By adjusting the doping ratio of Ho^{3+}/Eu^{3+}, the as-synthesized nanophosphor accomplishes multicolour tunability from green-yellow to red. The energy transfer from $Ho^{3+}\rightarrow Eu^{3+}$ has been confirmed through electric dipole-dipole interaction with critical distance 15.146 Å. Moreover, nanophosphor have high thermal stability with an activation energy ~ 0.21 eV, and the quantum efficiency of 83.6%. CIE coordinate illustrates that the singly doped Ho^{3+}, and Eu^{3+} lie in the green and red region, respectively, while the as-synthesized CYO:Ho^{3+},xEu^{3+}shows tunability from green to red. Hence, the CYO:Ho^{3+},xEu^{3+} nanophosphor may be a near-UV excited multicolour colour-tunable pertinent candidate with potential prospects for multicolour- display and near-ultraviolet lighting applications.

Chapter 6 (a): In this chapter, we have synthesized divalent (Ca^{2+}) doped $Eu:Y_2O_3@SiO_2$ core-shell nanomaterial first time as fluorescent labelling agent for advance forensic and solid-state lighting applications. It has been found that PL emission intensity depend on the coating layers of SiO_2, and optimal fluorescence intensity has been obtained for the 10 vol % of SiO_2 (TEOS) coating and enhancement of intensity is ~36 % than uncoated sample. For optimised sample CIE coordinates has been found as (x= 0.425 , y = 0.569) and CCT value is ~ 2115 K ,color purity, and CRI 80%, and 98% respectively, which make this phosphor is suitable for various optoelectronic application. The optimised phosphor further tested for the visualization of latent finger print and as security ink. The findings establish that synthesise core shell phosphor can be effetely used for security ink, LPF for forensic applications.

Chapter 6 (b): In this chapter , we have synthesis of water-stable chitosan functionalized Lanthanoid based core shell (Ca-$Eu:Y_2O_3@SiO_2$) phosphor. Chitosan finalization makes them biocompatible and water stability, and also provides functional groups such as hydroxyl, and amino groups which coordinate with the biomolecules. Further, the functionalised core-shell phosphor used for the detection of DNA. It has been observed that fluorescence emission intensity enhances linearly with the addition of DNA. It might be due to energy from DNA to functionalised core-shell phosphor. Furthermore, the experimental result specifies that Ca-$Eu:Y_2O_3@SiO_2$-chitosan sensor exhibit good analytical performance with limit of detection 16.1 pM. These results indicate that functionalised core-shell phosphors are simple, low cost, portable and capable for rapid detection of DNA and suitable for the biological applications.

Chapter 7: Summary, Conclusions and future prospects: This chapter summarizes the overall results, focusing the important findings of the thesis and we have also discussed some future prospects. We have studied the effect of Eu^{3+}, and other RE ions doping in Y_2O_3. In brief in this thesis co-doping with divalent (Ca^{2+})

ion, formation of film with PVA, core shell structure, and multicolor tunable nanophosphor has been synthesised. Detailed characterization of prepared samples has given, and sample optimised for their applicability in different fields such as for metal ion sensor, sensing of biomolecule, and for solid state lighting application has been given. In the end this chapter include summery of the entire thesis and future work.

References:

1.S. Gai, et. al., Chem. Rev., 114, 2343-2389, (2014).

2.K. Murthy, et. al., Trans Tech Publ, 1-34, (2014).

3.D. Singh, et. al., Optical Materials, 317-352, (2016).

4.P. Reineck, et. al.,, Advanced Optical Materials, 5, 1600446, (2017).

5.L.-N. Jin, et. al., CrystEngComm, 16, 3816-3828, (2014).

6.J. Shen, et. al., 5687-5697, (2008).

7.A. Escudero, et. al., Top. Curr. Chem., 374, 1-15, (2016).

8.T.K. Christopoulos, et. al., Analytical chemistry, 64. 342-346, (1992).

9.S. Wani, et. al., 19, 241-247, (2017).

10.H. Zou, et. al., Frontiers of Materials Science, 12, 327-34, (2018).

11.C. Li, J. Lin, et. al., Journal of Materials Chemistry, 20, 6831-6847, (2010).

12.H. Huang, et. al.,, Analyst, 144, 6789-6811, (2019).

Optical, magnetic and magneto-optical characteristics of $CoFe_2O_4$ and Ni based magnetoplasmonic nanostructures

Lakshmi B.

International School of Photonics,

Cochin University of Science and Technology, Cochin-682022.

Magnetoplasmonics is an exciting field of research where magnetism and plasmonics, and the mutually influencing effects of the two are explored in nanostructures. Magnetoplasmonic systems, in general, consist of magnetic and plasmonic components, giving the properties and functionalities of both kinds, to the nanostructure. There are prominently two important research pathways in this field; namely the one that deals with modifying/enhancing the magnetic and magneto-optic properties of the system through the presence and surface plasmon resonance (SPR) of plasmonic component, and the second one being the modulation of the wave vector of propagating plasmons through an externally applied magnetic field. The field of biomedicine, is yet another promising platform where magnetoplasmonics has been used for various therapeutic and diagnostic applications. It is expected that combining magnetic nanoparticles (NP) with plasmonic components can decrease cytotoxic effects of the system as well as enable magnetic field induced controllability in various aspects of biomedicine, such as targeted drug delivery and magnetic hyperthermia.

The thesis focuses on exploring the possibilities for observing and tuning two extremely interesting magnetoplasmonic effects, namely, modifying and enhancing, the magnetic and magneto-optic properties, respectively, of magnetoplasmonic nanostructures through plasmonics, which give them interesting properties

that could have significant technological impacts. Magnetoplasmonic systems are synthesized using cobalt ferrite, $CoFe_2O_4$ (CoF) and nickel (Ni) as the magnetic components while gold (Au) is chosen as the plasmonic part of the systems. CoF is a ferrimagnetic dielectric material with widespread applications. Ni is a magnetic metal that shows lower oxidation tendency as compared with similar metals like Fe and Co and hence has a better stability. Even though Ag shows better plasmonic responses as compared with Au, since the magnetoplasmonic systems are considered to have important biomedical applications, Au is chosen as the plasmonic part owing to its lesser cytotoxicity than Ag. The synthesis, structural, optical, compositional, surface and magnetic characterizations of CoF, Au, CoF-Au, Ni and Ni-Au nanosystems form the prominent part of the thesis work, with special emphasis given to the Magneto-optic Faraday Rotation (MFR) studies on these systems. Ni and Ni-Au samples are also examined for their biomedical cytotoxicity effects.

In the initial part of the thesis work, the optical band gaps present in CoF NP powder synthesized chemically were measured using a detailed procedure involving the collection of optical information from the sample using Diffuse Reflectance Spectroscopy (DRS) technique, followed by extracting the absorption coefficients using the Schuster-Kubelka-Munk differential equation method. The band gap measurement was done from the Tauc curves generated thereon using a piecewise linear fitting algorithm[1], where the entire Tauc spectrum was carefully examined, without leaving any region especially those towards the lower energy side. The algorithm that worked through the processes of linear fitting, segmentation and merging, identified a set of potential linear fitted regions of the spectrum that could possibly represent the absorption onset and the corresponding base line segment. On finer evaluation of all these segments the regions satisfying a set of critical criteria have been identified as the actual absorption onset and the base line segment corresponding to it. The band gaps calculated as the intersection of these two line segments yielded the direct and indirect band gap values as 1.5 ± 0.01 eV and 0.79 ± 0.01 eV[2]. The direct band gap estimation procedure for CoF nanopowder has been shown in Fig. 1. The band gap value obtained for the NP powder, which was smaller than that reported for the material in previous reports, was further validated using the data obtained through magnetization and XPS analysis. The magnetic moment per formula unit for CoF obtained from magnetization data was 4.03 μ_B, which being larger than that for a completely inverse spinel structure, indicated that the CoF NP synthesized in this work could be having a partially inverse spinel structure. From the peak fitting of the core level narrow scans of the Co $2p_{3/2}$ and Fe $2p_{3/2}$ levels obtained through XPS, the degree of inversion was calculated to be 0.52, which confirmed that the CoF NP indeed existed in partially inverse spinel structure that reportedly has much smaller band gap values than structures with completely inverse spinel structure.

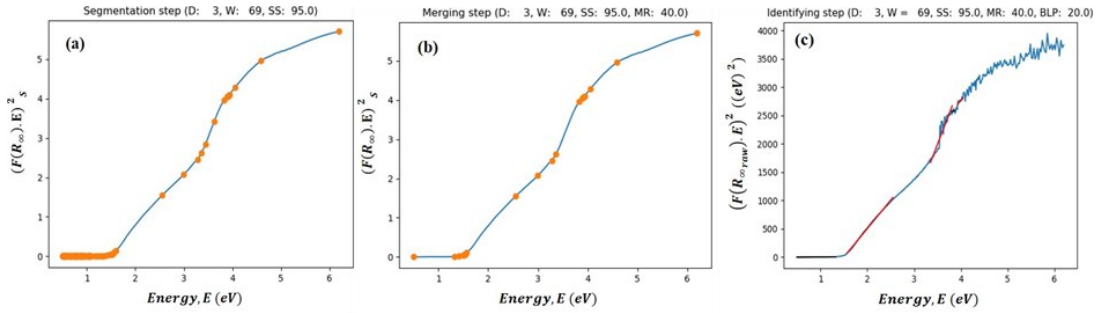

Fig. 1. Different steps performed to identify the appropriate absorption onset-base line segment (T_{ABS}-T_B) pair corresponding to direct band gap absorption. (a) Segmenting the curve at different nodal points based on the R^2 values of linear fits to the spectrum (b) Merging of various bisected segments based on the forward angle inclinations and (c) The identified base line segments T_B (black lines), and the linear segments T_{ABS} representing different possibilities for absorption onset (red lines). The values of the parameters namely, degree of the polynomial (D), window size (W), segmentation sensitivity (SS), merge relaxation (MR) and base line proportion (BLP) used for different steps have also been mentioned along the top of the curves.

The detailed optical characterization on CoF NP was followed by the MFR measurements on colloidal dispersions of CoF NP in PVA-water medium (sample labelled as CoF-P). MFR measurements were carried

out using a custom-made measurement system, the schematic of which are shown in Fig. 2.

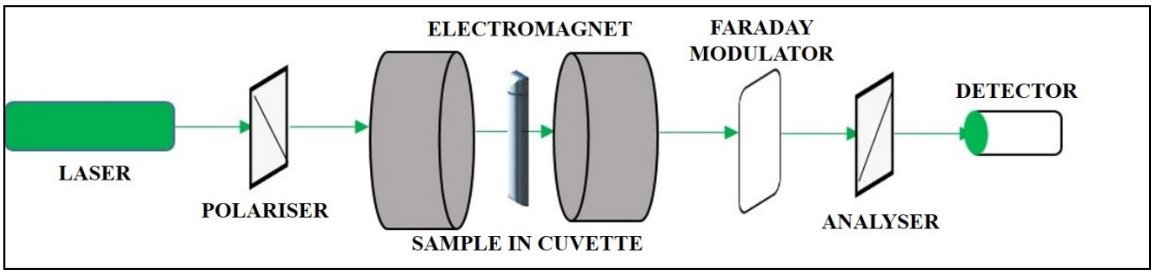

Fig. 2. Schematic diagram of the custom made magneto-optic measurement system.

Two additional synthesis procedures for CoF NP with slightly different parameters were carried out in an attempt to control the size range of the NP[3]. It was found that 2wt% PVA-water medium offered necessary stability to the dispersions in the presence and absence of magnetic field. The MFR responses were initially measured for two different volume fractions (0.6×10^{-3} (C1) and 0.9×10^{-3} (C2)) of CoF-P samples at 532 nm, following which the data was appropriately fit using Langevin-type function[4]. The MFR responses for C1 and C2 volume fractions of the CoF-P samples have been shown in Fig. 3 (a). From the fits, two important parameters were derived, namely the saturated MFR value (B_s) and the field necessary to bring in saturation in chain length and thus in MFR values (represented by the parameter A). For the sample C2, B_s was seen to be larger than the sample C1, as expected. An interesting observation was that the parameter A was larger for C2 than C1 indicating that the magnetic field necessary to bring saturation in MFR values was smaller for the sample with higher concentration. This was considered justifiable because the chain formation initiates and grows at rather smaller applied fields for samples containing larger number of magnetic NP. MFR studies were also performed on magnetoplasmonic colloidal mixtures of CoF and Au NP prepared by performing ultra-sonication procedure on selected concentrations of CoF-P and Au-P nanocolloids. An interesting enhancement for MFR values was observed for certain typical mixtures with respect to the MFR values of pure CoF-P samples. The MFR enhancement patterns obtained for the volume fraction of 1.2×10^{-3} (labelled as C3) are shown in Fig. 3 (b).

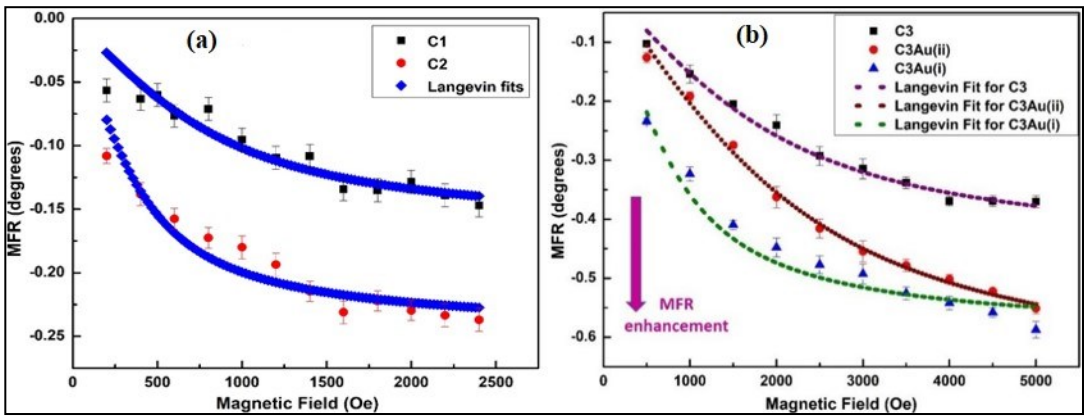

Fig. 3 (a). MFR of C1 and C2 samples of CoF NP at 532 nm wavelength. (b) MFR patterns of C3, C3Au(i) and C3Au(ii) samples; Langevin fits to the curves have also been shown.

The observed effect was explained on the basis of a novel proximity effect of surface plasmon resonance (SPR) of Au NP[5]. The experimentally observed MFR patterns validated the proposed pathway of MFR enhancement. It was observed that the concentrations of both the participating entities were extremely significant to see the subtle effect of MFR enhancement. Enhanced MFR was obtained in two typical concentrations since there were adequate concentrations of both the participating entities such that necessary MFR as well as enhancement in it could both be obtained. The conclusions drawn from experimental observations were further validated through the parameters obtained from Langevin fits to the MFR patterns. This is the

first time report of such a magnetoplasmonic phenomenon in colloidal mixture samples where MFR enhancement is produced due to proximity effect of SPR.

In addition to CoF and CoF-Au systems, the work was further extended to synthesizing and characterizing Ni-Au magnetoplasmonic bimetallic system and compare its structural, magnetic, optical and magneto-optical properties with pure Ni NP. A facile, less time consuming, relatively inexpensive and unconstrained chemical synthesis routine was developed for synthesizing Ni-Au NP, by avoiding high temperature refluxing procedures, inert gas atmospheres and templates[6]. The synthesis routine was accurately reproducible and scalable. Through detailed structural, compositional, surface and optical characterizations, the Ni-Au NP were seen to be possessing a unique intertwined crystal structure where the Ni and Au atomic planes were blended at different locations within the entire NP. The schematic of such a Ni-Au NP is shown in Fig. 4.

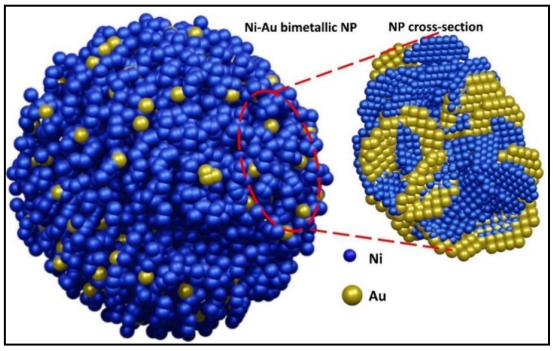

Fig. 4. Schematic representation of Ni-Au NP along with the cross-sectional view showing intertwined Ni and Au planes.

A striking difference was noticed in the dispersibility between Ni and Ni-Au NP in acetone medium. While Ni NP formed urchin-like clusters of large sizes in the dispersed state, Ni-Au NP were seen as individual NP of much smaller sizes, with absolutely no clustering effect. This pointed out the difference in the basic forces of interaction between the two types of systems and indicated the reduction in magnetic moment of Ni-Au NP, due to the inclusion of non-magnetic Au component. In order to validate the above mentioned observation, detailed magnetic characterizations were performed on Ni and Ni-Au NP through which drastic reduction in saturation and remanent magnetizations, and coercivity were noted between Ni and Ni-Au NP, though the individual Ni and Ni-Au NP were spanning similar size ranges. With the ZFC and FC magnetization curves far from coinciding at room temperature, Ni NP showed a much higher inversion temperature. However, the Ni-Au NP were close to being completely superparamagnetic with an almost coinciding ZFC-FC curve at room temperature. The mode blocking temperature calculated by fitting the difference between ZFC and FC magnetization for Ni-Au NP lognormally[7], came out to be 47 K, showing that even at such a low temperature, a considerable majority of Ni-Au NP were already superparamagnetic. This indicated the extent by which magnetic properties could be tuned using the inclusion of non-magnetic components such as Au. The transformation from the completely ferromagnetic behaviour of Ni NP to the more desirable SPM behaviour of Ni-Au NP at room temperature has applications in cases where an SPM behaviour along with the presence of plasmonic properties for nanostructures are necessary, such as in the field of biomedicine. The magnetization curves for Ni and Ni-Au NP have been shown in Fig. 5.

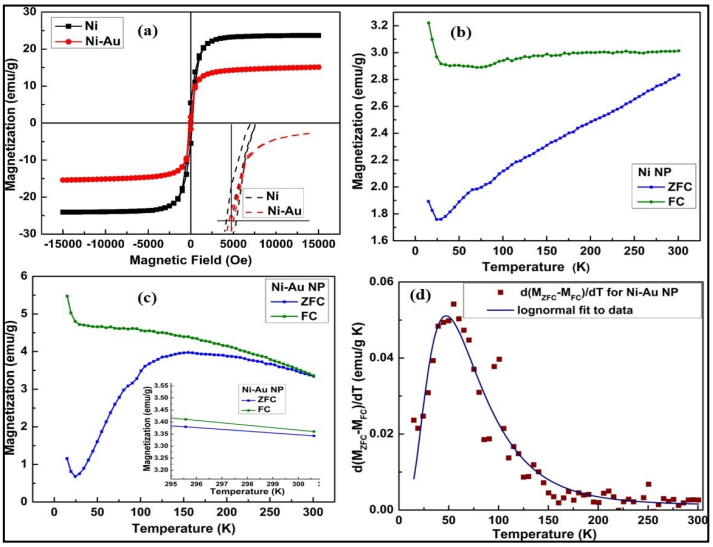

Fig. 5. Magnetization studies on Ni and Ni-Au samples. (a) M-H at room temperature for Ni and Ni-Au samples; inset shows an enlarged view of the curves at low fields representing the drastic difference in behaviour, M-T measurements in ZFC-FC mode from 15 to 300 K for (b) Ni and (c) Ni-Au NP; inset of (c) shows the enlarged view of the behaviour near room temperature and (d) $d(M_{ZFC} - M_{FC})/dT$ curve for Ni-Au NP along with the lognormal fit to the data.

Since both magnetic and plasmonic responses were obtained from Ni-Au NP, MFR measurements were performed on their colloidal dispersions in ethylene glycol medium in a wavelength dependent manner. Ni-Au NP exhibited enhanced specific MFR values over the entire wavelength range, which corresponded well with their absorbance spectra. A plasmonic peak due to the absorption by Au was seen in the MFR pattern of Ni-Au sample at no magnetic field, while this peak was seen to be suppressed yielding more or less uniform MFR values in the entire wavelength range for applied fields of 200 and 400 Oe. Plausible causes could be that an applied magnetic field supresses the pure optical component to MFR pattern that comes from Au, while relatively promoting the pure magneto-optical component that comes from magnetic Ni, the net effect due to both these making the MFR enhancement more uniform.

Since one of the potential areas of application of magnetoplasmonic systems is that of biomedicine[8], the cytotoxicity effects of Ni and Ni-Au NP were studied on macrophage cell line RAW 264.7 for the durations of 24 and 48 hours. The results of cell viability for Ni and Ni-Au NP has been shown in Fig. 6. It could be seen that the cell viability percentage was generally larger for Ni-Au NP than the corresponding concentration of Ni NP. Given the smaller overall percentage of Au atoms in Ni-Au NP, this observation was considered welcoming. A reduced cytotoxicity effect, combined together with promising plasmonic and superparamagnetic properties make Ni-Au NP excellent candidates for biomedical applications while their interesting MFR behaviour could be put to use in applications including magnetic field sensing and data storage.

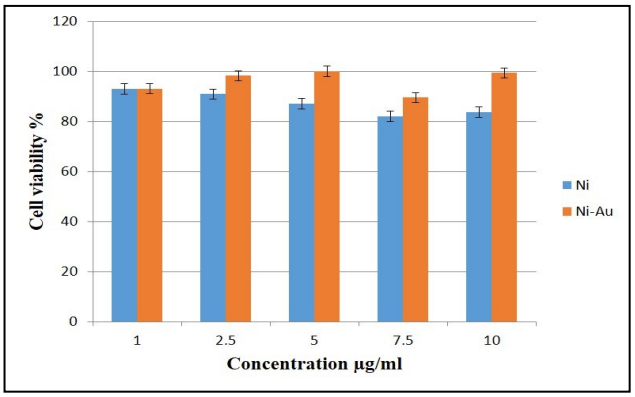

Fig. 6. Cytotoxicity effects of Ni and Ni-Au NP for the duration of 24 hours.

References

1. (a) A. Escobedo-Morales, I. I. Ruiz-Lopez, M.deL. Ruiz-Peralta, L. Tepech-Carrillo, M. Sanchez-Cantu, J. E. Moreno-Orea, Automated method for the determination of the band gap energy of pure and mixed powder samples using diffuse reflectance spectroscopy, Heliyon 5 e01505 (2019). https://doi.org/10.1016/j.heliyon.2019.e01505
(b) A. Escobedo-Morales, I.I. Ruiz-Lopez, GapExtractor v1.0, 2018. https://data.mendeley.com/datasets/j9ypzmdx5n/draft?a=bfc2457b-5b5c-427e-9120-5c9c455f5057.
2. B. Lakshmi, Babitto Joe Thomas, Pramod Gopinath, Accurate band gap determination of chemically synthesized cobalt ferrite nanoparticles using diffuse reflectance spectroscopy, Adv. Powder Technol. 32 3706 (2021). doi: https://doi.org/10.1016/j.apt.2021.08.028
3. K. Maaz, A. Mumtaz, S.K. Hasanain, A. Ceylan, Synthesis and magnetic properties of cobalt ferrite ($CoFe_2O_4$) nanoparticles prepared by wet chemical route, J. Magn. Magn. Mater. 308 289 (2007). https://doi.org/10.1016/j.jmmm.2006.06.003
4. B. Lakshmi, Pramod Gopinath, Investigating the Langevin behaviour of Faraday rotation in soft ferrimagnetic $CoFe_2O_4$ nanoparticles dispersed in PVA-water medium, J. Phys.: Conf. Ser. 2357 012001 (2022). doi: 10.1088/1742-6596/2357/1/012001
5. B. Lakshmi, Pramod Gopinath, Faraday rotation enhancement due to proximity effect of surface plasmon resonance in magnetoplasmonic colloidal mixtures, J. Mol. Liq. 390 123103 (2023). https://doi.org/10.1016/j.molliq.2023.123103
6. B. Lakshmi, Pramod Gopinath, Ni–Au magnetoplasmonic nanoparticles with a unique intertwined crystal structure showing excellent reduction and tunability of the superparamagnetic blocking temperature, Nano-Struct. Nano-Objects 34 100950 (2023). doi: https://doi.org/10.1016/j.nanoso.2023.100950
7. J.S. Micha, B. Dieny, J.R. Régnard, J.F. Jacquot, J. Sort, Estimation of the Co nanoparticles size by magnetic measurements in Co/SiO_2 discontinuous multilayers, J. Magn. Magn. Mater. 272–276 E967 (2004). https://doi.org/10.1016/j.jmmm.2003.12.268
8. L.L. Hou, Y. Wan, J.Y. Li, J.R. Zhang, K. Cui, S.J. Li, Electrochemical synthesis of NiAu bimetallic nanostrips and their application for hydrazine detection, Int. J. Electrochem. Sci. 14 5075 (2019). https://doi.org/10.20964/2019.06.55

An uncertainty relation based study of quantum correlations

Manju

Department of Physics, Indian Institute of Physics Ropar, Rupnagar, Punjab 140001, India

The urge to explore the quantum correlations has motivated physicists for many years. Study of quantum correlations is important for advancing our understanding of quantum mechanics, developing new quantum technologies, exploring the foundations of physics, and enabling practical applications that leverage the unique properties of quantum systems. It plays a pivotal role in the ongoing development and realization of quantum information science and technologies. It has practical implications for various real-world applications. For example, quantum cryptography relies on the security offered by quantum correlations[1], ensuring secure communication and data transmission. Quantum sensors utilizing quantum correlations[2] can offer enhanced sensitivity for precise measurements, impacting fields such as healthcare[3], environmental monitoring[4].

In the quantum realm, the study of synchronization is relatively recent and has gained significant attention due to its potential implications for various fields, such as quantum information processing and communication[5,6]. The phenomenon of spontaneous synchronization has been widely investigated in classical systems[7] since it was first observed by Huygens in the 17th century[7]. A nice and detailed discussion of generic nature of synchronization can be found in[8]. Quantum models such as Josephson junctions[9], van der Pol os-

cillators[10,11], Kerr-anharmonic oscillators[12] and spin systems[13] have demonstrated synchronization as well. It is envisaged that the quantum synchronization is a manifestation of certain correlations which are of purely quantum origin. There are some recent studies that explore the relation between the quantum synchronization and different measures of quantum correlations[13-16].

In first and second part of thesis, we will explore the phenomenon of quantum synchronization and its connection with entanglement. Exploring these connections sheds light on the underlying mechanisms and implications of quantum synchronization. This thesis exclusively deals with this issue and attempts to develop a generic understanding of their inherent relation. Optomechanical systems[17], which involve coupling mechanical oscillators to electromagnetic fields inside an optical cavity, provide a suitable platform for studying synchronization and its connections with entanglement. In the third part of thesis, we will propose the uncertainty based entanglement criterion for bipartite mixed states. The thesis is structured into five chapters.

Chapter 1: Introduction

Quantum synchronization: Two coupled harmonic oscillators, described by the displacements $q_j(t)$ from their respective equilibrium positions and the linear momenta $p_j(t)\ (i \in 1,2)$, are said to be synchronized, if they maintain $q_-(t) = \{q_1(t) - q_2(t)\}/\sqrt{2} \to 0$ and $p_-(t) = \{p_1(t) - p_2(t)\}/\sqrt{2} \to 0$, at long times. This corresponds to complete classical synchronization. In quantum systems, however, such synchronization is inherently not possible due to Heisenberg's uncertainty principle. As the position and momentum quadrature cannot be measured simultaneously at any time t, it is not possible to attain $q_-(t), p_-(t) \to 0$. In such case, the following quantification of synchronization has been proposed in terms of quantum fluctuations[14]:

$$S_c(t) = \langle q_-^2(t) + p_-^2(t)\rangle^{-1} \tag{1}$$

in terms of the synchronization errors $q_-(t)$ and $p_-(t)$, where $\langle\cdots\rangle$ denotes the expectation (or mean) values of the corresponding operators. Expanding these operators around their mean values, $q_-(t) = \langle q_-(t)\rangle + \delta q_-(t)$, $p_-(t) = \langle p_-(t)\rangle + \delta p_-(t)$, and using the limit of zero mean of these quadrature differences, a modified form of the measure of quantum synchronization can be obtained as

$$S_q(t) = \frac{1}{\langle \delta q_-(t)^2 + \delta p_-(t)^2\rangle} \leq 1$$

The uncertainty principle sets the value of S_q between 0 and 1 and the complete quantum synchronization refers to the upper limit of the above inequality, i.e., $S_q = 1$.

Entanglement: On the other hand, quantum correlation between the interacting systems can also manifest itself as entanglement. Entanglement[18] is one of the most well-known and extensively studied forms of quantum correlation. It lies at the heart of many intriguing and counter-intuitive phenomena in quantum physics and plays a crucial role in various areas. For a coupled bosonic system (like that of two harmonic oscillators), the joint variables q_- and p_- (which have been used to quantify synchronization in [14]) satisfy the following uncertainty relation: $\langle(\delta q_-(t))^2\rangle + \langle(\delta p_-(t))^2\rangle \geq 1$. If the state of this coupled system is separable, the following inequality is also satisfied, as shown by Duan and his coworkers[19] (DC):

$$\langle(\delta q_-)^2\rangle + \langle(\delta p_+)^2\rangle \geq 1 \tag{2}$$

where the transformation $p_- \rightarrow p_+$ is made using partial transposition, using Peres's prescription[20]. This means that violation of this inequality (2) refers to inseparability. It is known that the violation of the DC criterion is sufficient to detect entanglement for continuous-variable states. Using standard algebraic identity, the following criterion for separability can be derived from the DC criterion:

$$E_D = \langle(\delta q_-)^2\rangle\langle(\delta p_+)^2\rangle \geq \frac{1}{4} \tag{3}$$

violation of which indicates entanglement. This is the same criterion as derived by Mancini et al. for mesoscopic oscillators in optomechanical setup[21]. As was shown in[22], the relation (3) is stronger than the DC criterion.

In the literature, it is often said that two coupled quantum system may not exhibit synchronization and entanglement simultaneously. Both are two independent properties. However, from the proposed measure of both, it can be observed that these properties are understood in terms of the second order moments of a set of conjugate quadratures. Also, it can be observed that the same uncertainty relation has been used to set the upper limit for quantum synchronization measure and lower limit of entanglement criterion, so we expected that there may exist specific conditions for simultaneous existence of both. The main goal of this thesis is to investigate analytically and numerically the relationship between the quantum synchronization and the entanglement and to study an uncertainty-based entanglement criterion for bipartite mixed states. We aim to detect entanglement of various generalized bipartite mixed state using the proposed entanglement criterion.

Chapter 2: Quantum synchronization and entanglement of indirectly coupled mechanical oscillators in cavity optomechanics: A numerical study

In this chapter, we presented a systematic study on the interplay between quantum synchronization and entanglement between two indirectly coupled mechanical oscillators in a double cavity optomechanical system. Each mechanical oscillator is suspended inside a cavity and is coupled with the cavity mode via linear and quadratic dependence on its displacement from the equilibrium position. In the rotating frame of laser frequencies, the total Hamiltonian H takes the following form:

$$H = \sum_{j=1,2}\left[\Delta_{cj}a_j^\dagger a_j + \frac{\omega_{mj}}{2}\left(q_j^2 + p_j^2\right) - g_1^j a_j^\dagger a_j q_j + g_2^j a_j^\dagger a_j q_j^2 + \iota E(1+\eta_D\cos(\Omega_D t))\left(a_j^\dagger - a_j\right)\right] - J\left(a_1^\dagger a_2 + a_2^\dagger a_1\right)$$

Here, $\Delta_{cj} = \omega_{cj} - \omega_{lj}$ is the detuning of the jth cavity mode from the respective driving field, $a_j\left(a_j^\dagger\right)$ is the annihilation (creation) operator for the jth cavity mode, $q_j\left(p_j\right)$ refer to the dimensionless position (momentum) operators for the jth mechanical oscillator, g_1^j and g_2^j are the linear and the quadratic coupling constant between cavity and mechanical resonator. The term J is the coupling constant of cavity modes through an optical fiber. The driving fields with intensity E are modulated with frequency Ω_D and amplitude η_D.

Based on these realizations, we have shown that when both the mechanical oscillators are linearly coupled to the cavity mode, the oscillators are synchronized without entanglement. Also, the level of quantum synchronization is poor. But when we consider quadratic coupling as well in our simulation, quantum synchronization increases beyond what was achieved without it. Moreover, entanglement between the oscillators starts appearing with non-zero quadratic coupling. To be more clear, we showed that appropriate choice of parameters in the presence of both type of coupling leads to the greatly enhanced quantum synchronization and entanglement between the indirectly coupled oscillators. At the end, we explored the effect of system parameters on quantum synchronization and entanglement. Following these findings, in Chapter 3 of this thesis, we did a similar analysis in a more generic optomechanical system. This analysis is expected to pro-

vide some insight into correlated behavior of synchronization and entanglement.

Chapter 3: Entanglement boosts quantum synchronization between two oscillators in an optomechanical setup

In this chapter, we considered a more generic optomechanical system in which one of oscillator makes the cavity while the other is kept suspended inside the cavity. Both the oscillators are coupled to the same cavity mode via linear and quadratic dependence on their displacement from their respective equilibrium positions. An indirect always on coupling between the two is also mediated via the same cavity mode. In the rotating frame of laser frequencies, the total Hamiltonian H takes the following form:

$$H = \Delta a^{\dagger}a + \sum_{j=1,2}\left[\frac{\omega_{mj}}{2}\left(q_j^2 + p_j^2\right) + \left(-g_1^j q_j + g_2^j q_j^2\right)a^{\dagger}a\right] - g_3 q_1 q_2 a^{\dagger}a + \iota E[1 + \eta_D \cos(\Omega_D t)](a^{\dagger} - a)$$

Here, $\Delta = \omega_c - \omega_l$ denotes the cavity mode detuning; ω_{mj} is the frequency of jth mechanical oscillator; $a^{\dagger}(a)$ is the creation (annihilation) operator of cavity mode, satisfying the commutation relation $[a, a^{\dagger}] = 1$; $q_j(p_j)$ is the dimensionless position (momentum) operator of jth mechanical oscillator , satisfying the commutation relation $[q_j, p_{j'}] = \iota\delta_{jj'}$; the driving field is modulated with a frequency Ω_D and amplitude η_D .

With this realization, we first demonstrated classical synchronization between the oscillator via limit cycle trajectories, which is a precondition for quantum synchronization. Further, we showed that when the cavity is strongly amplitude-modulated, the two coupled oscillators are nearly complete quantum synchronized and entangled simultaneously. Moreover, both the synchronization and entanglement exhibit a tongue, which is a quantum analogue of classic Arnold tongue like behavior. The entanglement gets always associated with the synchronization, though reverse is not true. This behavior exists for a large range of system parameters. We provided an analytic condition for the simultaneous existence of entanglement and quantum synchronization to support our numerical findings. Our results open up a newer perspective to interpret the quantum synchronization and entanglement on the same footing.

Chapter 4: Strong entanglement criteria for mixed states, based on uncertainty relations

In this chapter, we proposed a strong entanglement criterion for bipartite mixed states, which correctly identifies the correct domain of relevant parameters for entanglement. Our criterion uses Peres-Horodecki partial transposition applied on a suitable uncertainty relation. The variances in this uncertainty relation do not involve any classical mixing uncertainty, and is therefore purely of quantum mechanical nature. We showed by explicit analysis that our criterion successfully detects entanglement not only in pure states, but also in several generalized mixed states including Werner state, and we found that it correctly reveals the lower bound of mixing probability of the Bell state in the Werner state. Thus, it turns out to be stronger than any other known criterion. We further showed that our criterion reduces to the Schrondinger-Robertson partial transpose (SRPT) inequality for the pure state.

Chapter 5: Conclusions

In conclusion, we have explored the interconnection between quantum synchronization and entanglement between two mechanical oscillators in two different optomechanical models. For both the optomechanical scenarios we have considered, we found that in the presence of cavity-oscillator coupling, varying linearly and quadratically with their displacements from their respective equilibrium positions, the mechanical oscillators are nearly complete quantum synchronized and entangled simultaneously. More precisely, in the presence of amplitude modulation with the same frequency as that of the oscillators, quantum synchronization measure and entanglement criterion are simultaneously satisfied in steady state. We further found that synchronization is more robust than the entanglement against thermal excitation, while they change in the

similar way for a large range of values of the frequency differences of the two oscillators. In the third scenario, we proposed a strong entanglement criterion for bipartite mixed states. Using this criterion, we detected entanglement in pure as well as in several generalized mixed states. We found that the proposed criterion correctly reveals the parameter domain (as identified by the PPT criterion) for identifying the entanglement of considered state. Moreover, the proposed criterion reduces to the SRPT inequality.

References

1. G. Adesso et. al., Journal of Physics A: Mathematical and Theoretical 49, 473001 (2016).
2. Q. Zhuang et. al., Phys. Rev. A 97, 032329 (2018).
3. N. Aslam et. al., Nature Reviews Physics 5, 157–169 (2023).
4. S. E. Crawford et. al., Advanced Quantum Technologies 4, 2100049 (2021).
5. K. Makino et. al., Science Advances 2, 1501772, (2016).
6. Q. Xie et. al., Mathematical and Computer Modelling 35, 145–163, (2002).
7. C. Huygens, Oeuvres completes, vol. 7. M. Nijhoff, 1897.
8. A. Pikovsky, M. Rosenblum, and J. Kurths, "Synchronization: a universal concept in nonlinear science," 2002.
9. K. Wiesenfeld et. al., Phys. Rev. Lett., 76, 404 (1996).
10. T. E. Lee et. al., Phys. Rev. Lett. 111, 234101 (2013).
11. S. Walter et. al., Annalen der Physik 527, 131–138, (2015).
12. N. Lorch et. al., Phys. Rev. Lett. 117, 073601 (2016).
13. A. Roulet et. al., Phys. Rev. Lett. 121, 063601 (2018).
14. A. Mari et. al., Phys. Rev. Lett. 111, 103605, (2013).
15. V. Ameri et. al., Phys. Rev. A 91, 012301 (2015).
16. G. Manzano et. al., Scientific Reports 3, 1439, (2013).
17. M. Aspelmeyer et. al., Reviews of Modern Physics 86, 1391 (2014).
18. R. Horodecki et. al., Reviews of Modern Physics 81, 865 (2009).
19. L.-M. Duan et. al., Phys. Rev. Lett. 84, 2722 (2000).
20. A. Peres et. al., Phys. Rev. Lett. 77, 1413 (1996).
21. S. Mancini et. al., Phys. Rev. Lett. 88, 120401 (2002).
22. G. S. Agarwal et. al., New Journal of Physics 7, 211 (2005).

Multimodal Optical Imaging and Spectroscopic Techniques for Cancer Screening and Diagnosis

Pramila Thapa

Bio and Green Photonics Lab, Indian Institute of Technology Delhi, New Delhi

Abstract

Conventional cancer screening and diagnostic techniques are costly, time-consuming, and available only in big city hospitals[1]. Equipping these techniques in villages, local clinics, or small hospitals could significantly lower healthcare costs and patient travel time, making early cancer diagnosis and treatment accessible to masses[2]. To accomplish this task, fast and dependable screening methods, such as multi-modal optical imaging and spectroscopic devices, are required[3]. These techniques are non-contact, non-invasive/ minimally invasive methods and have great potential for real-time and accurate diagnosis of cancer[4]. Since these devices work in a visible and near-visible range of electromagnetic spectra, it is also known as optical biopsy.

Given the above discussion, there is a strong requirement for the development of non-contact, non-invasive, quick, and accurate systems that can offer quantitative information for cancer progression in in-vivo mode to reduce cancer mortality and morbidity. The optical techniques employing AF and FL across diverse modalities, including imaging, spectroscopy, and micro-spectro-endoscopy, have the capability to investigate the in-vivo progression of cancer, especially when employed in a multi-modal approach in a non-contact and non-invasiveness manner.

The present thesis aims to develop non-contact, non-invasive/minimally invasive, fast, and accurate systems for cancer screening and diagnosis using optical techniques in a multi-modal approach. Combining these multimodal optical techniques assisted with machine learning, the proposed thesis is entitled **"Multimodal Optical Imaging and Spectroscopic Techniques for Cancer Screening and Diagnosis,"** which focuses on early-stage cancer screening, cancer detection, cancer margin assessment with intraoperative use of the developed multimodal optical systems in different cancers. AF and FL are optical methods used in imaging, spectroscopy, and micro-spectro-endoscopic modalities.

The thesis provides eight chapters. The first chapter is the introduction. In the second chapter, we have developed FL-based imaging and spectroscopic device breast cancer diagnosis with margin assessment during the intraoperative procedure. In the third chapter, after validating the devices, early-stage breast cancer has been classified. In the fourth chapter, we have developed new optical devices adding AF for oral cancer screening and diagnosis. In the fifth chapter, the micro-spectro-endoscope is developed for probing cellular structures during cancer progression. After the development of all-optical devices, the study of fluorescence with an exogenous dye in the cancerous area has been done in chapter six. Chapter seven deals with the integration of AF in a micro-spectro-endoscope probing a new disease autoimmune disease, protein uria, and has proven its potentiality in probing new diseases as well. At last, chapter eight deals with the conclusion and future scope. Overall, the thesis overview of field-portable, multi-spectral, and multi-modal devices using auto-fluorescence imaging, fluorescence imaging and spectroscopy, and micro-endoscopy-based point-of-care tools. These advancements have the potential to revolutionize the screening, real-time diagnosis, treatment, and prevention of oral and breast cancer, enabling faster and more effective healthcare interventions. Further, the convergence of technologies, along with AI and machine learning software, can be used to analyze data.

Fluorescence imaging and spectroscopy for breast cancer classification and tumor margin detection

In this chapter, we have developed FL-based smartphone imaging and spectroscopic point-of-care multi-modal devices for detecting invasive ductal carcinoma in tumor margins during tumor removal. These multi-modal devices are portable, cost-effective, non-invasive, and user-friendly. Molecular level sensitivity of the FL process shows different behavior in normal, cancerous, and marginal tissues. FL-based methods are

highly specific and sensitive and have potential in breast cancer detection. Simultaneous FL imaging and spectroscopy during intra-operative procedures of breast cancer have great advantages in the detection of tumor margins as well as in the classification of tumors to healthy tissues. Intra-operative real-time confirmation of breast cancer tumor margin is the aim of surgeons. Therefore, there is an urgent need for such techniques and devices that fulfill the surgeon's priorities. We observed significant spectral changes, such as red-shift, full-width half maximum (FWHM), and increased intensity as we approached the tumor center from normal tissue. High contrast in FL images and spectra are also recorded for cancer tissues compared to healthy tissues. Preliminary results for the initial trial of the devices are reported in this chapter. A total of 44 spectra from 11 invasive ductal carcinoma patients (11 spectra for invasive ductal carcinoma and the rest are normal and negative margins) are used. Principle component analysis is used to classify invasive ductal carcinoma with an accuracy of 93 %, sensitivity of 75%, and specificity of 92.8%. We obtained an average 6.17 ± 1.66 nm red shift for IDC concerning normal tissue. The red shift and maximum FL intensity indicate $p<0.01$. These results described here are supported by histopathological examination of the same sample. In the present manuscript, simultaneous FL-based imaging and spectroscopy are accomplished for the classification of IDC tissues and breast cancer margin detection.

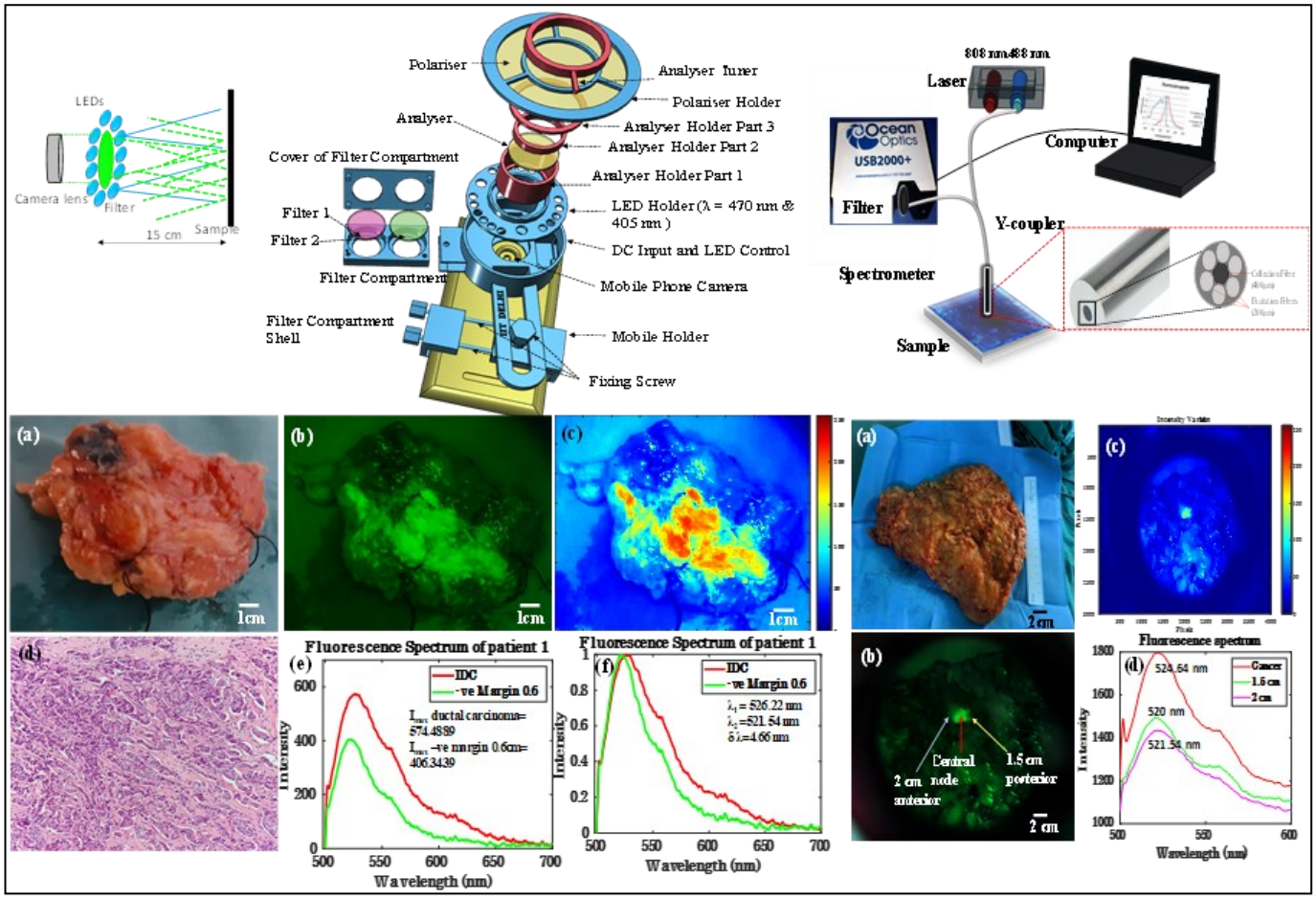

Figure 1. Experimental Setup of developed FL-based imaging and spectroscopic system with the Fl images and spectra of resected breast tissues. FL spectra are of cancerous tissue and normal tissue with margins.

Optical imaging and spectroscopy for early-stage breast cancer detection

In this chapter, we have used a previously developed system for early-stage breast cancer detection during intraoperative procedures. Breast cancer is the most common cancer among women worldwide and can be treated if diagnosed at an early stage. FL techniques have a considerable impact on tumor detection as FL is highly sensitive to the biochemical and biophysical structure of the tissues, providing novel techniques for early and noninvasive diagnosis of cancer. Due to the high sensitivity of FL, it can be used in early-stage

breast cancer detection. Fluorescence-guided surgery (FGS) using an exogenous agent in breast cancer is a well-known method that locates tumors and margins during intra-operative procedures. FL-spectroscopy and FL-imaging have shown the potentiality in FGS of breast cancer independently. Combining these two modalities in a single system improves the success rate of FGS, which can give tumor-free tissues. The chapter aims to analyze and classify early-stage breast cancer, locally advanced breast cancer (invasive ductal carcinoma), and normal tissue. The SVM-based classifier is used to classify these three cases. The positive predictive value for IDC, fibroadenoma, and normal breast tissues is 78.6 %, 87.5 %, and 100 %, respectively. The true positive rate for IDC, fibroadenoma, and normal breast tissues is 91.7 %, 87.5 %, and 50 %, respectively.

Multimodal and multispectral optical devices for oral cancer screening and diagnosis

This chapter elucidates the use of AF and FL techniques for in-vivo mode oral cancer screening. The survival rate of oral squamous cell carcinoma (OSCC) patients is low, but it can be improved using highly sensitive, specific, and accurate techniques. AF and FL techniques are very sensitive and helpful in cancer screening; being directly linked with the molecular levels of human tissue, they can be used as a quantitative tool for cancer detection. In this chapter, we report the development of multi-modal AF and FL imaging and spectroscopic (MAF-IS) smartphone-based systems for fast and real-time oral cancer screening. MAF-IS system is indigenously developed and offers the advantages of being a low-cost, handy, non-contact, non-invasive, and easily operable device that can be employed in hospitals, including low-resource settings. Here, we discuss the results of 43 individuals with 28 OSCC and 15 oral potentially malignant disorders (OPMDs), i.e., epithelial dysplasia and oral submucous fibrosis, using the developed devices. We observed a red shift in FL emission spectra in-vivo. We found red-shift of 7.72±6nm, 3 ±4.36nm, and 1.33±0.47nm in the case of OSCC, epithelial dysplasia, and oral submucous fibrosis, respectively, compared to normal. The results were compared with histopathology and found to be consistent. Further, the MAF-IS system provides results in real-time with higher accuracy and sensitivity compared to devices using a single modality. Our system can achieve an accuracy of 97% with sensitivity and specificity of 100% and 94.7 %, respectively, even with a smaller number of patients (28 patients of OSCC). The proposed MAF-IS device has great potential for fast cancer screening and oral cancer diagnosis in the future.

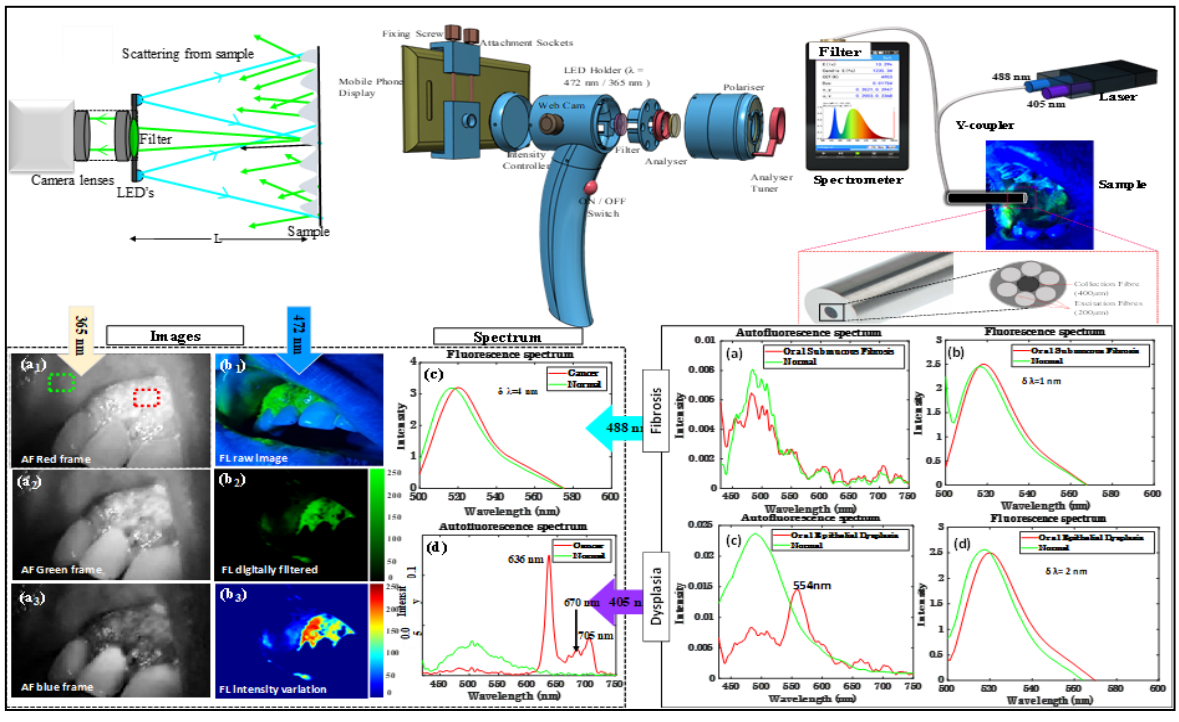

Figure2. Experimental setup of developed FL and AF-based imaging and spectroscopic device with AF and FL images and spectra of cancerous and normal patients.

Development of Micro-spectro-endoscope for oral cancer screening and diagnosis

This chapter describes the development of a multi-modal micro-spectro-endoscopic system with oblique illumination that combines two different techniques, FL micro-endoscopy and spectroscopy, simultaneously. The system can be utilized to obtain diverse information from the same location of the biological sample. The micro-endoscope allows one to view microscopic images, giving morphology and microstructures of the tissues deep within the body. We have only dealt with qualitative image information of malignant/ cancerous tissues in earlier chapters and have not looked at the microstructures of the tissues. During cancer progression, there is a change in the morphology of the cancer tissues. The malignant cells have a big, uneven nucleus size and shape, conspicuous nucleoli, and sparse and highly pigmented or pale cytoplasm. Thus, there is a need to define such changes in cancer patients during cancer progression to diagnose in the early stages. In the present chapter, we have developed a micro-spectro-endoscopic system using graded-index (GRIN) rod-lens, which makes it highly compact, and oblique incidence decouples illumination geometry with collection geometry, preventing CCD cameras from saturation and reducing the number of optical elements, thereby making the system further miniaturized and field-portable. Further, it also overcomes the disadvantages of undesired reflections from different optical elements. The experimental results of simultaneous imaging and spectroscopy of the biological samples are presented along with their quantitative spectroscopic parameters: peak wavelength shift, the area under the curve, and full-width half maximum (FWHM). The system's spatial resolution, spectral resolution, and field view are 4.38 μm, 0.5m, a $2.071X1.548\ mm^2$ respectively. The developed micro-spectro-endoscope can show the microstructures and give molecular information about the sample in a single shot. The proposed device is robust, field portable, and highly efficient and can be used for the fast screening of oral and skin cancer patients.

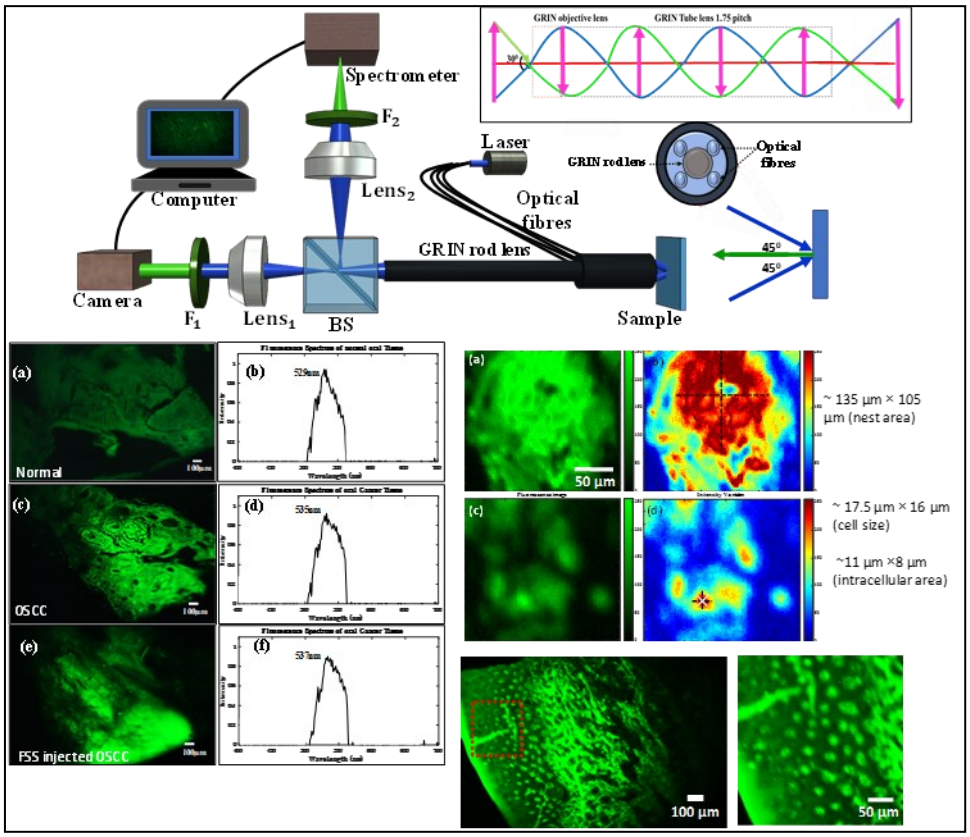

Figure 3. Experimental setup for micro-spectro-endoscope with the FL images and spectra of cancerous and normal tissues.

Study on concentration and pH-based Fluorescence Imaging and spectroscopy of fluorescein dye-tagged oral cancer tissues

Intravenous use of the FSS has been done extensively in cancer research owing to its high sensitivity. The spectral changes in FL spectra of cancerous tissues compared to normal one varies, as seen in previous chapters. However, these changes mainly depend on the used exogenous agent's concentrations/molarity, solvent nature, pH, etc. We have used FSS as an exogenous agent for FL imaging and spectroscopy of the cancerous tissues. This chapter studies FSS in oral cancer tissues with topical application with varying concentrations/molarity and pH values and statistical and spectroscopic analysis in ex-vivo and in-vivo OSCC patients. Oral cancer screening with exogenous agents is highly demanding due to high sensitivity, as the early diagnosis plays a vital role in achieving favorable outcomes for oral squamous cell carcinomas (OSCC) by facilitating prompt detection and comprehensive surgical removal. Optical techniques utilizing the local application of FSS or FGS offer potential for early OSCC detection. The use of fluorescein dye in oral cancer is significantly less, and there is a need to inspect the local application of fluorescein dye in oral cancer patients. Concentration-based investigations of the dye with OSCC patients are essential to ensure accurate FGS and screening with fluorescein labeling and to mitigate possible adverse effects. Additionally, analyzing the dye distribution within OSCC tissues can provide insights into their heterogeneity, a critical indicator of malignancy. We presented a concentration and pH-based study of FSS for local application in oral cancer screening. FL imaging and spectroscopy are performed for five different concentrations: 1:25, 1:50, 1:75, 1:100, and 1:125 (18.66 ± 0.06, 9.51± 0.02, 6.38 ± 0.01, 4.80 ± 0.004, and 3.85 ± 0.002 millimolar) in ex-vivo mode for OSCC tissues. The relationship between these five concentrations and statistical parameters is analyzed ex vivo. Through statistical analysis of the images and FL spectra, we have concluded that an optimal amount of dye is essential for the local application and extracting important parameters such as entropy, indicating tissue heterogeneity. Thus, two concentrations, 1:75 and 1:100 (6.38 ± 0.01, 4.80 ± 0.004 millimolar), are the most suitable for local application-based oral cancer screening.

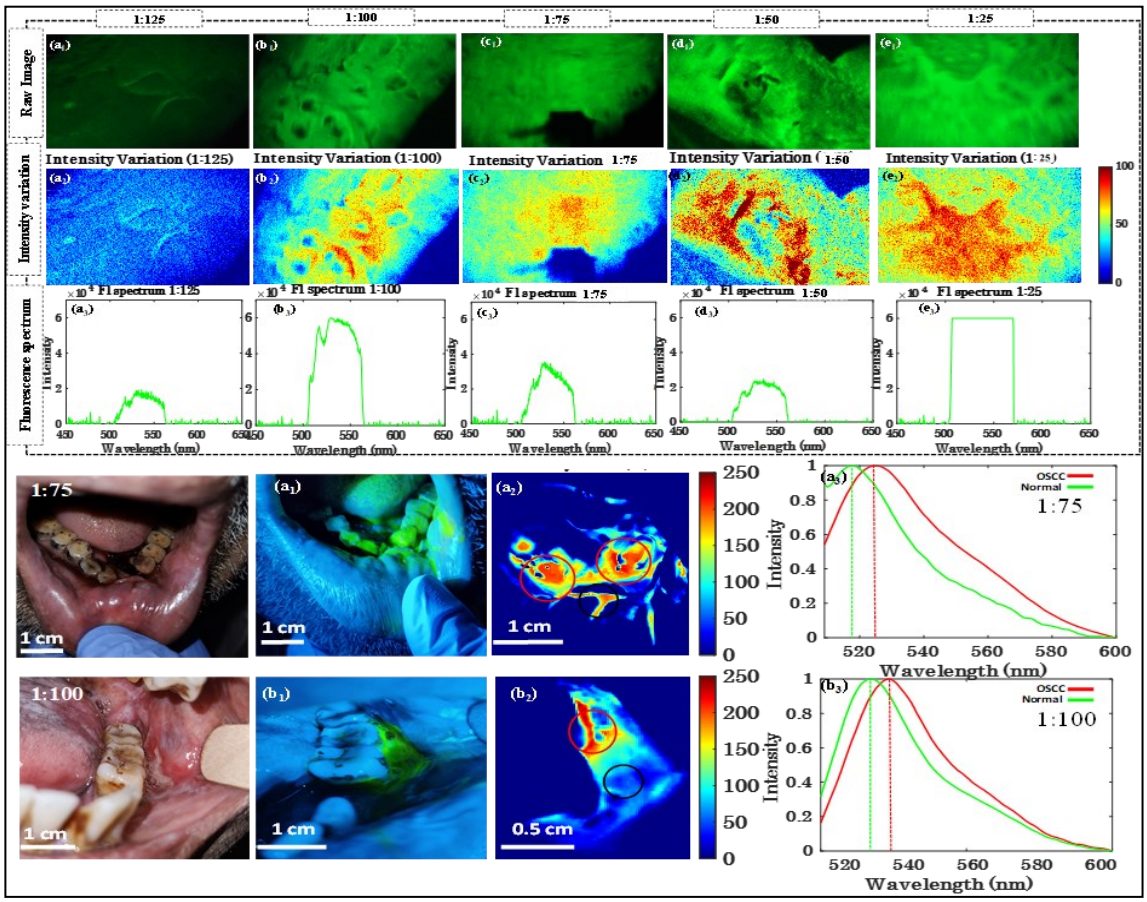

Figure 4. Experimental results of different concentrations on oral cancer tissues and oral cancer patients with FL images and spectra of cancerous and normal tissues.

Two-channel autofluorescence and fluorescence imaging and spectroscopy for renal tissues using micro-spectro-endoscope

This chapter investigates autoimmune diseases through the application of AF and FL techniques. Lupus Nephritis (LN) is one of the autoimmune diseases, and the most typical symptom of LN is proteinuria. Proteinuria is a biological indicator of renal damage and disease activity, and it is counted in indices of lupus disease activity and damage. Chronic kidney disease is brought on by proteinuria, which causes interstitial and renal tubule fibrosis. The chapter employs AF and FL imaging and spectroscopy facilitated by an advanced micro-spectro-endoscope. Specifically, two wavelengths, 370 nm and 405 nm, are employed for AF imaging and spectroscopy, while fluorescein sodium salt, with 488 nm excitation, is utilized for FL imaging and spectroscopy. The study utilizes protein uric kidney samples from the Murphy Roths Large (MRL) strain. The MRL strain has LN, resulting in kidney inflammation and damage. A total of 8 cases, with 12 samples of young (no disease), antibody-positive, and protein uric samples, are studied for AF and FL imaging and spectroscopy. In the case of FL imaging, intensity levels of 1, 1.3, and 1.2 are observed for proteinuria, antibody-positive, and youthful samples, respectively. Conversely, AF imaging exhibits its highest intensity in the antibody-positive group, followed by proteinuria samples and the young. Moreover, AF spectroscopy reveals a novel peak emergence in the antibody-positive group at approximately 468 nm, accompanied by substantial spectral alterations across these three classes. Meanwhile, FL spectroscopy demonstrates notable shifts in spectral profiles within these same groups.

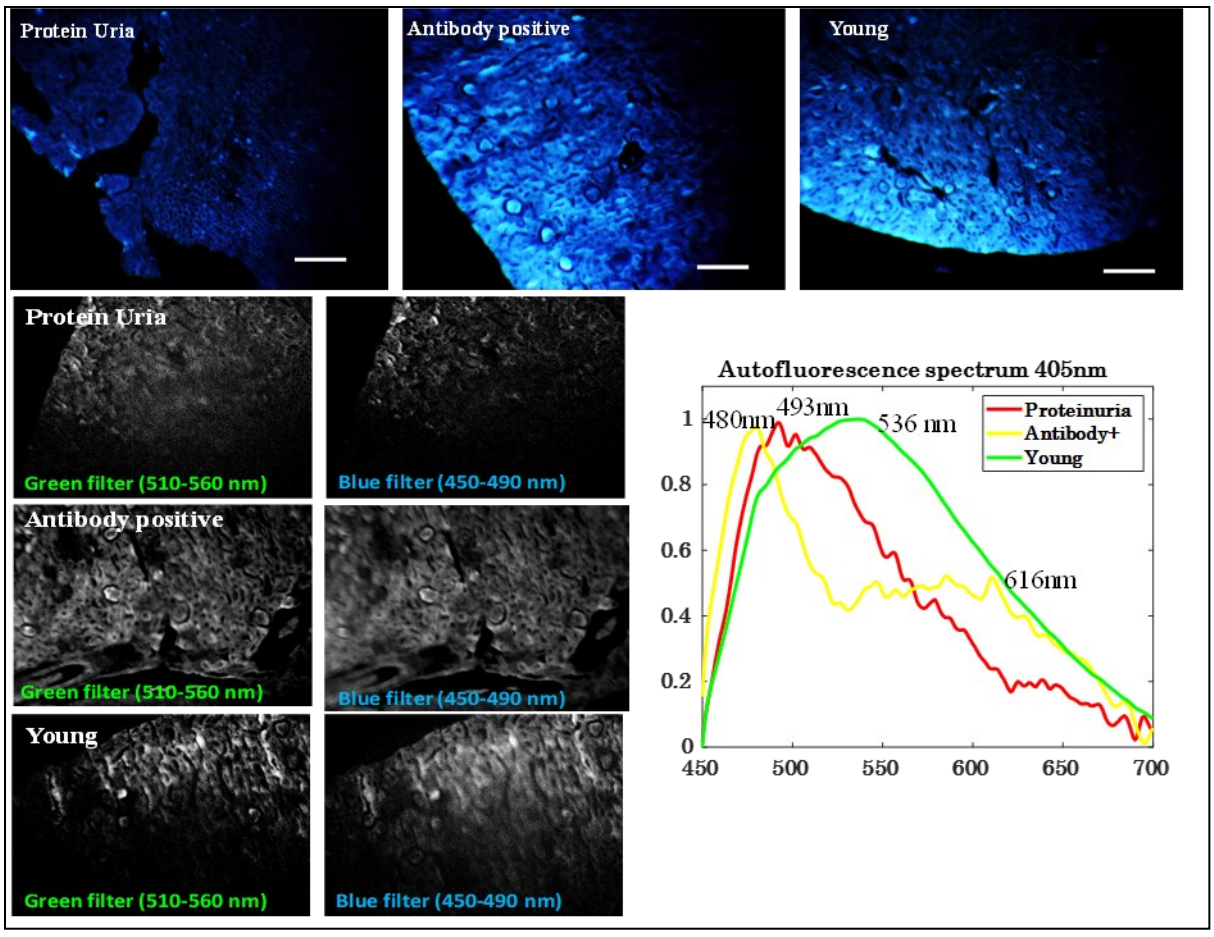

Figure 5. AF images of protein uria, antibody positive, and young renal tissues with simultaneous spectra.

References:

1. Sankaranarayanan, R., *Annals of global health*, 80,412-417 (2014).
2. R. Richards-Kortum et al., *Annual review of physical chemistry*. 47, 555-606 (1996)
3. R. Alfano et. Al., *IEEE Journal of Quantum Electronics.* 20, 1507-1511(1984)
4. J.R. Lakowicz, Principles of fluorescence spectroscopy, Springer (2006).

Development of Scalable and Cost-effective SERS Substrate for Bio-photonic Applications

Sathi Das

Bio-photonics and Green Photonics Laboratory, Indian Institute of Technology Delhi, Hauz-Khas, New Delhi-110016, India

1.1. Introduction

Raman spectroscopy, a technique for probing molecular vibrational and rotational energy levels [1], was first theorized by Austrian physicist Adolf Smekal in 1923 and later experimentally verified by Indian physicist C.V. Raman along with his PhD student K.S. Krishnan in 1928. Dr. C. V. Raman was awarded the Nobel Prize in Physics in 1930 for his discovery of the Raman effect. In the Raman scattering process, incident radiation interacts with a molecule, creating a virtual state. The molecule quickly returns to its initial ground state or a different vibration state. If the initial and final vibrational states match, it results in Rayleigh scattering. Conversely, Raman scattering occurs when the states differ. Stokes Raman scattering arises when a photon excites a molecule from a lower to an upper vibrational state, while Anti-Stokes Raman scattering involves a vibrationally excited molecule returning to the ground state (Fig. 1.) [2].

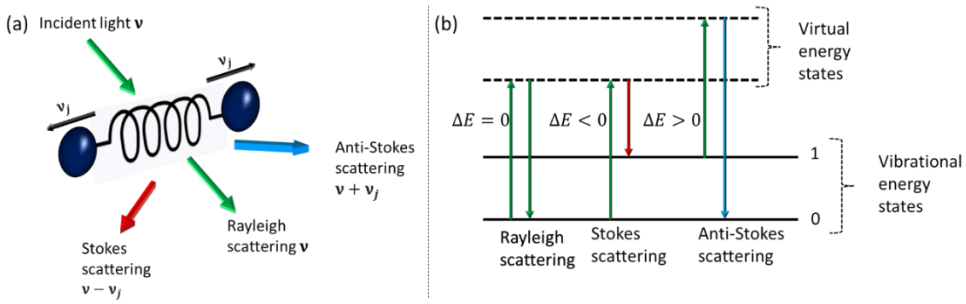

Fig. 1. Principle of Raman scattering. (a) Rayleigh scattering and Raman scattering, (b) Energy diagram of Raman process.

However, the intrinsic Raman scattering cross-section of a molecule is low, resulting in minimal signal intensity, especially for samples with low concentration [3]. To address this limitation, various enhancement techniques have been proposed that includes (a) **Resonant Raman scattering (RRS),** (b) **Coherent Anti-Stokes Raman scattering (CARS),** (c) **Surface-enhanced Raman scattering (SERS)**, etc. [4]. Among other techniques, surface-enhanced Raman scattering (SERS) has gained popularity due to its ability to provide significant enhancement (10^8–10^{10}) in weak Raman signals [3] and is also the focus in the thesis. It offers advantages such as recognition capabilities, non-destructive analysis, minimal sample preparation, measurement in biological fluids, simultaneous detection of different analytes, and on-site analysis with portable instruments.

SERS was first observed in 1974 by Fleischmann et al. [4], who reported a large amount of Raman signal from pyridine absorbed on a roughened silver electrode. The mechanism of SERS enhancement is attributed to electromagnetic and chemical enhancement [5]. Electromagnetic enhancement occurs due to the metal nanostructure, while chemical enhancement occurs due to chemo-adsorption between the metal and analyte molecules. The electromagnetic SERS enhancement of a single molecule can be expressed under the widely used $|E|^4$ approximation, as [5]

$$g_{SERS}^{EM} = \left|\frac{E_{\omega}^{Local}}{E_{\omega}}\right|^2 \left|\frac{E_{\omega'}^{Local}}{E_{\omega'}}\right|^2 \quad (1)$$

Here E_ω and $E_{\omega'}$ represent the electric field generated at incident laser frequency and at Raman frequency, respectively. For small Raman shift, $E_\omega = E_{\omega'}$,

$$g_{SERS}^{EM} = \left|\frac{E_\omega^{Local}}{E_\omega}\right|^4 \quad (2)$$

Thus the $|E|^4$ approximation is valid for small Ramna shifts and if $E_{\omega'}^{Local}$ being not too high.

A "SERS substrate" refers to any nanostructured metallic platform supporting plasmon resonance and enhancing Raman signals significantly. The substrate can be classified with two categories: (a) **Substrates with random morphology:** Irregular substrates with uneven morphologies, such as roughened electrodes, were among the first discovered SERS substrates. (b**) Substrates with periodic nanostructures:** Structured or periodically arranged planar metallic SERS substrates involve arrays of systematically arranged metallic nanotextures on flat substrates, produced through techniques like nanolithography [6]. Fig. 2 depicts the schematic overview of the SERS substrates.

Problems and Challenges in SERS: The current challenges in SERS can be categorised such as: (a) **Fabrication Method:** There is still an open question concerning the facile fabrication method of the SERS substrate that offers cost-effective, and scalable fabrication methods. (b) **Reproducibility, Sensitivity and Selectivity of SERS Signal:** Raman signal enhancement depends on nanostructure dimensions, hotspot distribution, and material plasmonic properties. High-efficiency SERS substrates need spectrum repeatability, sensitivity, and selectivity. Reproducible SERS spectra require uniform intensity distribution across the substrate. The spectrum sensitivity is influenced by the plasmonic enhancement factor, metal-adsorbate interaction, nanoscale roughness, and suitable laser wavelength [7]. (c) **Analysis of Complex Biological Samples:** Biomolecules like bacteria and biological nanocarriers (e.g., DNA) present challenges due to their large, heterogeneous nature. Reproducible spectrum acquisition is more challenging than with single chemical elements. Addressing these challenges is crucial for advancing the effectiveness and applicability of SERS in various fields [8].

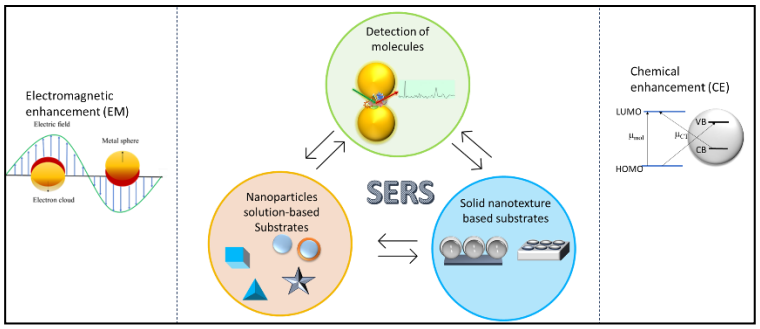

Fig. 2. Overview of SERS substrates.

Thesis overview

The novelty of the work in the thesis is two-fold. The primary aim of the thesis is to develop a novel SERS substrate using a cost-effective and scalable technique. Another primary focus is to detect various hazardous chemicals and biomolecules, such as pathogens and nanocarriers at ultra-low concentrations, analysing their enhanced SERS spectra. One of the significant problems the thesis solves is the ultralow detection and classification of urinary tract infection (UTI) causing bacteria for various species and strains using a SERS substrate fabricated from a scalable and low-cost technique. The tremendous increase in diseases caused by microorganisms in recent years has demanded immediate action from the public healthcare sector. Micro-

organisms can cause serious infections, resulting in significant morbidity and mortality. More than 1.2 million people died from severe bacterial infections in the respiratory, gastrointestinal, and central nervous systems, according to the World Health Organization (WHO) [9]. Consequently, there is a critical requirement to create a rapid and effective testing tool for bacterial infections. Presently, bacterial infections are identified in a clinical environment by isolating bacteria in pure culture and completing biochemical and metabolic studies within 48 − 72 hours. Depending on the conclusion of the diagnostic, professionals may prescribe antibiotics to patients. Hence, the present detection tools are unsuitable for the real-time and fast detection of pathogens at low concentrations to prevent severe infection. This study comprehensively investigates the SERS spectral signature of five distinct UTI-causing pathogens up to 100 colony-forming units/ml (CFU/ml). The acquired spectra of these bacteria were further utilised to for classification using a neural network model that differentiates the SERS spectra of bacterial species with 100% accuracy in strain level. The thesis **"Development of Scalable and Cost-effective SERS Substrates for Bio-photonics Applications"** consists of eight chapters. The overview of the idea is as follows:

Chapter 1: Introduction: In chapter one, the concepts of Raman spectroscopy and SERS have been introduced.

Chapter 2: Fabrication of Ag Nanoparticles using Microwave Irradiation: Chapter 2 briefly describes the synthesis of colloidal spherically shaped silver nanoparticles (Ag NPs) to fabricate the flexible SERS film. The synthesis was done using the microwave technique that produces NPs at a faster reaction rate with controlled heat and pressure. The flexible SERS substrates were utilised to detect various toxic chemicals, such as rhodamine (R6G) and thiram, respectively. to detect pesticides. The NPs were also employed to detect biomolecules, such as bacterial DNA. The incubation of Ag NPs with bacterial genomic content allowed intense SERS spectra of the DNA of two different bacteria species at nanogram concentrations.

Chapter 3: Mesoporous Ag-TiO_2 Nanocage Film as Sensitive and Recyclable Low-cost SERS substrate: In Chapter 3, we explored the heterogeneous nanostructure composed of semiconductor and metal-based nanostructure for SERS applications. In this chapter, we present a facile and cost-effective method for fabricating a highly controllable, low-cost, mesoporous Ag-TiO_2 nanocage (NC) structured film as a SERS substrate. The NC morphology offered additional sites for Ag coating and adsorption of dye molecules. The developed Ag-TiO_2 SERS film exhibited photodegradation activity under UV exposure and was explored for reusable SERS performance up to 5 times. The SERS film was utilised to detect various dye molecules and biomolecules, such as urea, at ultralow concentrations [10] (Chapter Overview: Fig. 3)

Chapter 4: Fabrication of Ag Capped Al Nanorods Array-based SERS Substrate: The chapter explores a cost-effective approach using the glancing angle deposition (GLAD) technique to create patterned NRs on glass plates. The objective is to fabricate a low-cost SERS substrate without compromising signal strength and hotspot distribution. The Ag-capped Al NRs-based SERS substrate, compared to Ag NRs, shows superior enhancement due to the shape anisotropy of Ag nanocap geometry. Optimized for performance, the substrate detects distinct Raman peaks of E. coli bacteria at concentrations as low as 100 CFU/ml using a portable Raman spectrometer [11]. Figure 4 provides a graphical overview of the chapter.

Chapter 5: SERS Nanowire Chip and Machine Learning-Enabled Classification of Wild-Type and Antibiotic-Resistant Bacteria at Species and Strain Levels: In this chapter, a cost-effective and scalable SERS substrate fabrication technique using the metal-assisted chemical etching (MACE), is employed to create silicon nanowire (Si NW) arrays, offering a high-aspect-ratio over a large surface area without the need for expensive vacuum equipment. The optimized Ag-coated Si nanowire SERS chip demonstrated a label-free detection of clinical pathogenic bacterial strains of urinary tract infection disease. The chip, sensitive to concentrations as low as 100 CFU/mL, enables spectral classification using a neural network model. This model successfully distinguishes bacteria at both species and strain levels, showcasing the chip's potential for real-time, molecular-specific bacterial detection. Fig. 3. depicts the bacteria detection scheme using SERS and machine learning [12].

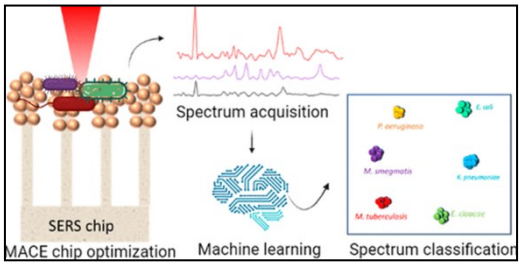

Fig. 3. Overview of chapter 5: The Ag-coated Si nanowire SERS chip and machine learning for the detection and differentiation of clinical pathogens.

Chapter 6: Fabrication of Plasmonic Sculpture Regular Nanostructure using Tuneable Gap Resonance by Nanosphere Lithography: This chapter conducts a thorough exploration of SERS substrate geometry and its impact on enhancement, focusing on nanostructures with regular arrays to achieve periodic hotspots. The study investigates the effect of shape anisotropy on SERS enhancement, developing a highly anisotropic nanosized template. Additionally, the role of the metal-dielectric interface and the thickness of a dielectric layer on a metal-dielectric-metal (MIM) coated nanostructure array is discussed. Crucial factors such as plasmonic tuneability and engineered hotspots through plasmonic modes coupling are briefly explored.

Chapter 7: Plasmonic Nano-bowls for Rapid Capture and Analysis of Liposomes, DNA Micelles, DNA Nanogel in Suspension: Chapter 7 explores a PDMS nano-bowl structure for trapping nanosized biocarriers like liposomes, DNA nanogels, and DNA micelles. These biocompatible nanocarriers, including lipids and nucleic acids, are crucial for developing therapeutics and diagnostic devices, demanding rapid detection for drug delivery applications. SERS, a label-free technique, characterizes these nanocarriers without additional sample preparation in minimal quantities. However, their high Brownian motion in suspension can affect spectrum reproducibility. To address this, we implement surface-topology-assisted trapping in a suspension state, requiring no external force. Unlike the structures in the previous chapter, nanopillars and nanospheres, the proposed nano-bowl substrate passively traps molecules, reducing Brownian motion. The methodology is applied to membrane-modified liposomes, micelles, and DNA gels, with a comprehensive spectral comparison to pure specimens. Fig. 4. provides a schematic overview of this chapter.

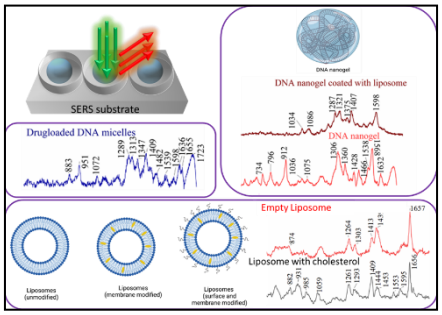

Fig. 4. Overview of chapter 7: Nano-bowl substrate to passively trap nano bio-carriers restricting its Brownian motion.

Chapter 8 provides a conclusive summary of the thesis and outlines future aspects to explore. In conclusion, the thesis is dedicated to nanofabrication and its applications in SERS, proposing a point-of-care, label-free, and accurate technique for biphotonic applications.

References:

1. D. J. Gardiner, 'Introduction to Raman Scattering', in *Practical Raman Spectroscopy*, 1989.
2. U. A. Jayasooriya et al., 'Introduction to Raman Spectroscopy', in *An Introduction to Laser Spectroscopy*, 2002.
3. D. L. Jeanmaire et al., 'Surface raman spectroelectrochemistry', *J Electroanal Chem Interfacial Elec-*

trochem, vol. 84, no. 1, 1977.
4. M. Moskovits, 'Surface-enhanced Raman spectroscopy: A brief retrospective', *Journal of Raman Spectroscopy*, vol. 36, no. 6–7, 2005.
5. P. G. Etchegoin et al., *Basic Electromagnetic Theory of Surface Enhanced Raman Spectroscopy*. 2011.
6. Y. Mandelbaum et al., *Sensors (Switzerland)*, vol. 20, no. 18, pp. 1–21, Sep. 2020.
7. P. Mandal et al., *Surfaces and Interfaces*, vol. 28. 2022.
8. C. Zong *et al.*, *Chemical Reviews*, vol. 118, no. 10. 2018.
9. X. Li *et al.*, *J Clin Med*, vol. 11, no. 10, 2022.
10. S. Das et al., *Opt Mater (Amst)*, vol. 125, 2022.
11. S. Das et al., *Nanotechnology*, vol. 32, no. 49, 2021.
12. S. Das *et al.*, ACS *Appl Mater Interfaces*, vol. 15, no. 20, 2023.

ATOS

ATOSCOPE

ANDOR

Fast ICMOS, EMCCD, CCD & PMT detectors, High resolution imaging spectrographs, Raman, Fluorescence, Micro spectroscopy (UV-VIS-NIR), Plasma spectroscopy

OXFORD INSTRUMENTS

Flow Cryostats for 3K and 77K measurements with ultra low vibration system. Cryogen free cryostats for 4K measurements for optical & transport experiments

CRYOSTATS - OPTICAL/ELECTRICAL/MAGNETIC MEASUREMENTS

4K Closed Cycle Cooling System with ultra low vibration, Custom design

Stinger Cold Edge

ECDL TUNABLE DIODE LASERS LITTROW & LITTMAN, MOPA UP TO 4W

Absorption spectroscopy Rb, Cs, Li & K
Tera Hertz & Quantum Cascade Lasers

Sacher Lasertechnik

IR THERMOGRAPHY CAMERAS

TELEDYNE FLIR
Everywhereyoulook

Temperature Measurement: - 80 °C to 3500 °C
<20mK Sensitivity, World Best calibration

NEW COMPACT FT-IR SPECTROMETERS SOLIDS, LIQUIDS & GASES

AR@ptix
Switzerland

Wide spectral ranges: 900nm - 16µm
High resolution 4cm-1, up to 0.5 cm-1

THE WORLD'S FIRST TRULY TURN-KEY MULTI-PHOTON MICROSCOPE

- Its Portable – No need of an optical table
- Plug & Play – Hassle free of maintenance.
- Inbuilt 700 -1300nm femtosecond fiber laser

PROSPECTIVE

ALL VERSION OF FIBER LASERS

FYLA

3W Supercontinuum VIS-IR white light laser
15 Femtosecond, 950-1150 nm broad band laser

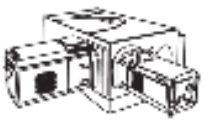

ATOS Instruments Marketing Services

ATOSCOPE Instruments Pvt. Ltd

www.atosindia.com

atos@atosindia.com

LASER OPTICS

Made by Edmund Optics®

24/6 Global Product and Application Support

Live Chat in English is Available 24/6
For Product and Application Guidance

HARRY BASIL
BUSINESS DEVELOPMENT ENGINEER

STEFAAN VANDENDRIESSCHE
DIRECTOR, LASER OPTICS BUSINESS LINE

DEEPTHI SASIKUMAR
TECHNICAL ENGINEERING MANAGGER

Products Categories

Optical Filters

Laser Mirrors

Laser Lenses

Laser Polarizers

Laser Prisms

Laser Beamsplitters

Raman Longpass Edge Filters

Laser Beam Expanders

The **FUTURE** Depends on Optics®

Edmund optics | india

Edmund Optics India Pvt. Ltd.
#267, Greystone Building, Second Floor,
6th Cross Rd, Binnamangala,
Stage 1, Indiranagar, Bengaluru,
Karnataka, India 560038
Phone: +91-80-6845-0000
e-mail: indiasales@edmundoptics.in (Customer Service)
indiatech@edmundoptics.in (Technical Support)
website: **www.edmundoptics.in**

INFRARED OPTICS

Infrared Optics
303C, 3rd Floor, DLF Centre Point, Sector-11,
Mathura road,
Faridabad-121006 (Haryana) India
Phone: +91 9560125000
e-mail: sales@infraredoptics.in
website: **www.infraredoptics.in**

LASER SCIENCE

BRINGING TOMORROW'S TECHNOLOGY TODAY

COHERENT

ASTRELLA: ONE-BOX TI:SAPPHIRE AMPLIFIER

APPLICATIONS

- Time-resolved Spectroscopy
- Multidimensional Spectroscopy

COMPEX: UV EXCIMER LASERS

COHERENT

APPLICATIONS

- PLD – Pulsed Laser Deposition
- Thin Wafer Processing

LIGHT CONVERSION

I-OPA

APPLICATIONS

- 2D Spectroscopy
- Pump-probe spectroscopy

QUANTUM KITS

THORLABS

APPLICATIONS

- Educational Tool to Understand Quantum Cryptography
- Visualizing Quantum Concepts- Demontrate secure communications using quantum technology

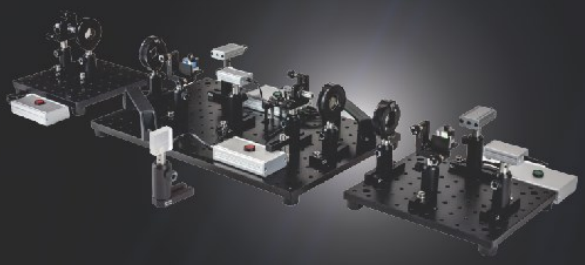

www.laserscience.co.in | sales@laserscience.in | 7710012972 | @laserscienceservices

photonics.cusat.ac.in/optiq-2023